

Molecular and Translational Medicine

*Series Editors:* William B. Coleman · Gregory J. Tsongalis

Robert M. Hoffman *Editor*

# Patient-Derived Mouse Models of Cancer

Patient-Derived Orthotopic Xenografts  
(PDOX)

 Humana Press

---

# Molecular and Translational Medicine

## **Series Editors**

William B. Coleman  
Department of Pathology and Lab Medicine  
University of N.Carolina School of Medicine  
Chapel Hill, North Carolina  
USA

Gregory J. Tsongalis  
Department of Pathology and Lab Medicine  
Dartmouth-Hitchcock Medical Center  
Lebanon, New Hampshire  
USA

As we enter into this new era of molecular medicine with an expanding body of knowledge related to the molecular pathogenesis of human disease and an increasing recognition of the practical implications for improved diagnostics and treatment, there is a need for new resources to inform basic scientists and clinical practitioners of the emerging concepts, useful applications, and continuing challenges related to molecular medicine and personalized treatment of complex human diseases. This series of resource/reference books entitled *Molecular and Translational Medicine* is primarily concerned with the molecular pathogenesis of major human diseases and disease processes, presented in the context of molecular pathology, with implications for translational molecular medicine and personalized patient care.


More information about this series at <http://www.springer.com/series/8176>

---

Robert M. Hoffman  
Editor

# Patient-Derived Mouse Models of Cancer

Patient-Derived Orthotopic  
Xenografts (PDOX)

 Humana Press

*Editor*

Robert M. Hoffman  
University of California and AntiCancer Inc.  
San Diego, California  
USA

ISSN 2197-7852                      ISSN 2197-7860 (electronic)  
Molecular and Translational Medicine  
ISBN 978-3-319-57423-3              ISBN 978-3-319-57424-0 (eBook)  
DOI 10.1007/978-3-319-57424-0

Library of Congress Control Number: 2017949265

© Springer International Publishing AG 2017

This work is subject to copyright. All rights are reserved by the Publisher, whether the whole or part of the material is concerned, specifically the rights of translation, reprinting, reuse of illustrations, recitation, broadcasting, reproduction on microfilms or in any other physical way, and transmission or information storage and retrieval, electronic adaptation, computer software, or by similar or dissimilar methodology now known or hereafter developed.

The use of general descriptive names, registered names, trademarks, service marks, etc. in this publication does not imply, even in the absence of a specific statement, that such names are exempt from the relevant protective laws and regulations and therefore free for general use.

The publisher, the authors and the editors are safe to assume that the advice and information in this book are believed to be true and accurate at the date of publication. Neither the publisher nor the authors or the editors give a warranty, express or implied, with respect to the material contained herein or for any errors or omissions that may have been made. The publisher remains neutral with regard to jurisdictional claims in published maps and institutional affiliations.

Printed on acid-free paper

This Humana Press imprint is published by Springer Nature  
The registered company is Springer International Publishing AG  
The registered company address is: Gewerbestrasse 11, 6330 Cham, Switzerland

*This book is dedicated to the memory  
of A.R. Moossa, M.D., and Sun Lee, M.D.*



Jørgen Rygaard (1934–2016)  
Father of Patient-Derived Mouse Models of Cancer  
and Modern Cancer Research

---

## Preface

Patient-derived xenograft mouse models of cancer are an area of intense research. This field has had a renaissance over the past 10 years after an almost quarter century of being ignored or denigrated as an irrelevant model. The current book gives a perspective on the long history of patient mouse models of cancer since the first paper by Rygaard and Povlsen in 1969. The book provides an overview of the state of the art of the field and especially emphasizes the importance of the use of orthotopic mouse models of patient cancer as these models enable metastasis to occur, which is the essence of clinical cancer. Chapters on patient-derived orthotopic xenograft (PDOX) cover the major cancer types. Other chapters cover important aspects of the use of patient-derived mouse models for cancer research and novel, transformative treatment. The last chapter previews an exciting future where patient-derived models are used for individualized more precise therapy on a routine basis.



---

# Contents

<b>1 In Memoriam: Jørgen Rygaard (1934–2016), Father of Patient-Derived Mouse Models of Cancer and Modern Cancer Research</b> . . . . .	1
Robert M. Hoffman	
<b>2 The Revival of Patient-Derived Xenograft Mouse Models of Cancer: Way Back to the Future.</b> . . . . .	7
Robert M. Hoffman	
<b>3 Patient-Derived Xenograft Models for Human Cancer: The Freiburg Experience</b> . . . . .	13
Heinz-Herbert Fiebig	
<b>4 From Ectopic to Orthotopic Tumor Grafting Sites: Evidence for a Critical Role of the Host Tissue Microenvironment for the Actual Expression of the Malignant Phenotype.</b> . . . . .	43
Bernard C.M. Sordat	
<b>5 The Effects of the Organ Microenvironment on Metastatic Cell Gene Signatures.</b> . . . . .	55
Sun-Jin Kim, Ho Jeong Lee, Hyunkyung Yu, Sung II Choi, John Weinstein, Jing Wang, Yan Qi, and Isaiah J. Fidler	
<b>6 Techniques for Surgical Orthotopic Implantation of Human Tumors to Immunodeficient Mice</b> . . . . .	71
Robert M. Hoffman	
<b>7 The First Patient-Derived Orthotopic Xenograft (PDOX) Mouse Models of Cancer: Cancer of the Colon, Pancreas, Lung, Breast, Ovary, and Mesothelioma</b> . . . . .	79
Robert M. Hoffman	
<b>8 Patient-Derived Xenograft Models of Prostate Cancer.</b> . . . . .	89
R.B. Marques, C.M.A. de Ridder, and W.M. van Weerden	

<b>9</b>	<b>Patient-Derived Mouse Models of Sarcoma</b> . . . . .	113
	Tara A. Russell, Irmina A. Elliott, Arun S. Singh, and Fritz C. Eilber	
<b>10</b>	<b>Cervical Cancer PDOX Models</b> . . . . .	125
	Robert M. Hoffman, Yukihiro Hiroshima, Takashi Murakami, and Takuya Murata	
<b>11</b>	<b>The Use of Pediatric Patient-Derived Xenografts for Identifying Novel Agents and Combinations</b> . . . . .	133
	Raushan T. Kurmasheva and Peter J. Houghton	
<b>12</b>	<b>Development of Orthotopic and Spontaneous Metastatic Human Tumor Xenograft Models for Experimental Therapeutics</b> . . . . .	161
	Marta Paez-Ribes, Raquel Munoz, Eric Guerin, Shan Man, Ping Xu, John Ebos, Christina Lee, Andrew Reynolds, Yuval Shaked, and Robert S. Kerbel	
<b>13</b>	<b>Use of Patient-Derived Orthotopic Xenografts (PDOX) to Evaluate Transformative Cancer Therapeutics</b> . . . . .	183
	Robert M. Hoffman	
<b>14</b>	<b>Fluorescent Protein-Expressing Transgenic Nude Mice as Hosts for Patient Tumors</b> . . . . .	193
	Robert M. Hoffman	
<b>15</b>	<b>Fluorescence Imaging of Tumors in Human Patient-Derived Orthotopic Xenograft (PDOX) Mouse Models</b> . . . . .	207
	Robert M. Hoffman, Atsushi Suetsugu, Tasuku Kiyuna, Shuya Yano, and Michael Bouvet	
<b>16</b>	<b>The Use of Patient-Derived Orthotopic Xenograft (PDOX) Models to Develop Curative Fluorescence-Guided Surgery of Cancer</b> . . . . .	217
	Robert M. Hoffman, Yukihiro Hiroshima, Shuya Yano, Cristina A. Metildi, and Michael Bouvet	
<b>17</b>	<b>Molecular Characteristics of Patient-Derived Tumor Xenografts: Similarities to Patient Tumors and Relevance for Biomarker Discovery</b> . . . . .	227
	Vincent Vuaroqueaux, Anne-Lise Peille, Bruno Zeitouni, Anne-Marie Eades-Perner, and Heinz-Herbert Fiebig	
<b>18</b>	<b>Synergy of Patient-Derived Orthotopic Xenografts (PDOX) Models and Molecular Profiling for Optimal Therapy</b> . . . . .	245
	Robert M. Hoffman, Takashi Murakami, Kei Kawaguchi, Arun S. Singh, and Fritz C. Eilber	

---

<b>19</b>	<b>3D Cell Culture Models</b> .....	<b>251</b>
	David M. Evans and Beverly A. Teicher	
<b>20</b>	<b>Why Patient-Derived Mouse Models Need to Be Orthotopic</b> .....	<b>277</b>
	Robert M. Hoffman	
<b>21</b>	<b>Afterward: The Future of Patient-Derived Models of Cancer</b> .....	<b>285</b>
	Robert M. Hoffman	
	<b>Index</b> .....	<b>291</b>

---

## List of Contributors

**Michael Bouvet** Department of Surgery, University of California, San Diego,  
La Jolla, CA, USA

VA Healthcare System, San Diego, CA, USA

**Sung H Choi** Metastasis Research Laboratory, Department of Cancer Biology,  
University of Texas MD Anderson Cancer Center, Houston, TX, USA

**Anne-Marie Eades-Perner** Oncotest GmbH Am Flughafen 12-1479108,  
Freiburg, Germany

**John Ebos** Roswell Park Cancer Institute, Buffalo, NY, USA

**Fritz C. Eilber** Division of Surgical Oncology, University of California,  
Los Angeles, Los Angeles, CA, USA

UCLA—Jonsson Comprehensive Cancer Center Sarcoma Program, Los Angeles,  
CA, USA

**Irina Elliott** Division of Surgical Oncology, University of California,  
Los Angeles, Los Angeles, CA, USA

**David M. Evans** Leidos Biomedical Research, Inc., Frederick National  
Laboratory for Cancer Research, Frederick, MD, USA

**Isaiah J. Fidler** Metastasis Research Laboratory, Department of Cancer Biology,  
University of Texas MD Anderson Cancer Center, Houston, TX, USA

**Heinz-Herbert Fiebig** 4HF Biotech GmbH Am Flughafen 1479108, Freiburg,  
Germany

Oncotest GmbH Am Flughafen 12-1479108, Freiburg, Germany

**Eric Guerin** Hôpital de Hautepierre - Hôpitaux Universitaires de Strasbourg,  
Strasbourg, France

**Yukihiko Hiroshima** AntiCancer, Inc., San Diego, CA, USA

Department of Surgery, University of California, San Diego, La Jolla, CA, USA

Department of Gastroenterological Surgery, Yokohama City University,  
Yokohama, Japan

**Robert M. Hoffman** AntiCancer, Inc., San Diego, CA, USA

Department of Surgery, University of California, San Diego, La Jolla, CA, USA

**Peter J. Houghton** Greehey Children's Cancer Research Institute, University of Texas Health Science Center, San Antonio (UTHSCSA), San Antonio, TX, USA

**Kei Kawaguchi** AntiCancer, Inc., San Diego, CA, USA

Department of Surgery, University of California, San Diego, La Jolla, CA, USA

Department of Surgery, Tohoku University, Sendai, Japan

**Robert S. Kerbel** Biological Sciences Platform, Sunnybrook Research Institute, Toronto, ON, Canada

Department of Medical Biophysics, University of Toronto, Toronto, ON, Canada

**Sun-Jin Kim** Metastasis Research Laboratory, Department of Cancer Biology, University of Texas MD Anderson Cancer Center, Houston, TX, USA

**Tasuko Kiyuna** AntiCancer, Inc., San Diego, CA, USA

Department of Surgery, University of California, San Diego, La Jolla, CA, USA

Department of Orthopedic Surgery, Graduate School of Medicine, University of the Ryukyus, Okinawa, Japan

**Raushan T. Kurmasheva** Greehey Children's Cancer Research Institute, University of Texas Health Science Center, San Antonio (UTHSCSA), San Antonio, TX, USA

**Ho Jeong Lee** Metastasis Research Laboratory, Department of Cancer Biology, University of Texas MD Anderson Cancer Center, Houston, TX, USA

**Christina Lee** Biological Sciences Platform, Sunnybrook Research Institute, Toronto, ON, Canada

**Shan Man** Biological Sciences Platform, Sunnybrook Research Institute, Toronto, ON, Canada

**Rute B. Marques** Department of Urology, Erasmus MC, Rotterdam, The Netherlands

**Cristina A. Metildi** Department of Surgery, University of California, San Diego, La Jolla, CA, USA

**Raquel Munoz** Departments of Biochemistry, Molecular Biology and Physiology, University of Valladolid, Valladolid, Spain

**Takashi Murakami** AntiCancer, Inc., San Diego, CA, USA

Department of Surgery, University of California, San Diego, La Jolla, CA, USA

Department of Gastroenterological Surgery, Yokohama City University, Yokohama, Japan

**Takuya Murata** Department of Obstetrics and Gynecology, Kawasaki Medical School, Okayama, Japan

**Marta Paez-Ribes** Department of Pathology, University of Cambridge, Cambridge, UK

**Anne-Lise Peille** Oncotest GmbH Flughafen 12-1479108, Freiburg, Germany

**Yan Qi** Department of Bioinformatics and Computational Biology, University of Texas MD Anderson Cancer Center, Houston, TX, USA

**Andrew Reynolds** Tumour Biology Team, The Institute of Cancer Research, London, UK

**Corrina M.A. de Ridder** Department of Urology, Erasmus MC, Rotterdam, The Netherlands

**Tara A. Russell** Division of Surgical Oncology, University of California, Los Angeles, Los Angeles, CA, USA

UCLA – Jonnson Comprehensive Cancer Center Sarcoma Program, Los Angeles, CA, USA

Robert Wood Johnson/Veterans Affairs Clinical Scholars Program, Los Angeles, CA, USA

**Arun S Singh** UCLA – Jonnson Comprehensive Cancer Center Sarcoma Program, Los Angeles, CA, USA

Division of Medical Oncology, University of California, Los Angeles, Los Angeles, CA, USA

Division of Surgical Oncology, University of California, Los Angeles, Los Angeles, CA, USA

**Bernard Sordat** Laboratory of Glycochemistry and Asymmetric Synthesis (LGSA, Prof. P. Vogel), Federal Institute of Technology, Lausanne, Switzerland

**Atsushi Suetsugu** AntiCancer, Inc., San Diego, CA, USA

Department of Surgery, University of California, San Diego, La Jolla, CA, USA  
Gifu University Graduate School of Medicine, Gifu, Japan

**Beverly A. Teicher** Division of Cancer Treatment and Diagnosis, National Cancer Institute, Rockville, MD, USA

Molecular Pharmacology Branch, National Cancer Institute, Bethesda, MD, USA

**Vincent Vuaroqueaux** Oncotest GmbH Flughafen 12-1479108, Freiburg, Germany

**Jing Wang** Department of Bioinformatics and Computational Biology, University of Texas MD Anderson Cancer Center, Houston, TX, USA

**Wyske M. van Weerden** Department of Urology, Erasmus MC, Rotterdam, The Netherlands

**John Weinstein** Department of Bioinformatics and Computational Biology, University of Texas MD Anderson Cancer Center, Houston, TX, USA

**Ping Xu** Biological Sciences Platform, Sunnybrook Research Institute, Toronto, ON, Canada

**Shuya Yano** AntiCancer, Inc., San Diego, CA, USA

Department of Surgery, University of California, San Diego, La Jolla, CA, USA

Department of Gastroenterological Surgery, Graduate School of Medicine, Dentistry and Pharmaceutical Sciences, Okayama University, Okayama, Japan

**Hyunkyung Yu** Metastasis Research Laboratory, Department of Cancer Biology, University of Texas MD Anderson Cancer Center, Houston, TX, USA

**Bruno Zeitouni** Oncotest GmbH Am Flughafen 12-1479108, Freiburg, Germany

---

# In Memoriam: Jørgen Rygaard (1934–2016), Father of Patient-Derived Mouse Models of Cancer and Modern Cancer Research

1

Robert M. Hoffman



---

R.M. Hoffman  
AntiCancer, Inc., 7917 Ostrow Street, San Diego, CA 92111, USA  
Department of Surgery, University of California, San Diego, La Jolla, CA, USA  
e-mail: [all@anticancer.com](mailto:all@anticancer.com)

© Springer International Publishing AG 2017  
R.M. Hoffman (ed.), *Patient-Derived Mouse Models of Cancer*,  
Molecular and Translational Medicine, DOI 10.1007/978-3-319-57424-0\_1

1



The athymic “nude” mouse is possibly the most important tool in cancer research. The nude mouse has enabled the studies of human cancer in the laboratory *in vivo*. Nude mice were first discovered in 1962 in the laboratory of Dr. N. R. Grist at Ruchill Hospital’s Brownlee Virology laboratory in Glasgow. The nude (*nu*) gene behaves as an autosomal recessive. The homozygotes, *nu nu*, are hairless (nude). Other parts of the syndrome initially observed were sulfhydryl group deficiency and abnormal keratinization of hair follicles [1]. All major types of human cancer have been grown and characterized in nude mice.

The nude mouse was first found to be athymic by Pantelourus [2] working in Glasgow, Scotland. Jørgen Rygaard spoke with a colleague in Denmark, Dr. Kresten Work, who had seen the nude mouse in an institute in Glasgow [3]. Rygaard asked Dr. Work what is the nude mouse used for? Work replied, “Nothing...they just keep them in a cage under the lab sink” [3]. Pantelourus observed that the nude mouse was athymic. Pantelourus also observed that blood leucocytes were low in the nude mouse which meant that the nude mouse was T-cell deficient, which explains why foreign tissue is not rejected by nude mice.

Nude mice are unable to mount many types of immune responses, including antibody formation that requires CD4+ helper T cells; cell-mediated immune responses, which require CD4+ and/or CD8+ T cells; delayed-type hypersensitivity responses (require CD4+ T cells); killing of virus-infected or malignant T cells (requires CD8+ cytotoxic T cells); and graft rejection (requires both CD4+ and CD8+ T cells) [1].

Nude mouse females have underdeveloped mammary glands and are unable to effectively nurse their young; therefore, nude males are bred with heterozygous (*nu/+*) females. In controlled, germ-free environments using antibiotic treatment, nude mice can live almost as long as a normal mouse (18 months to 2 years) [1].

Rygaard was able to arrange a shipment of nude mice from Scotland to Copenhagen which were carried in the cockpit of the British Airways plane from Glasgow. Rygaard then bred the nude males with normal NMRI mice from Bomholtgaard and with, brother-sister mating, was producing 50–100 nude mice per week at the SPF animal facility at the Copenhagen Municipal Hospital.

Having established the nude mouse colony, Rygaard asked his colleague Carl Povlsen (1940–1986) to obtain a tumor specimen from a colon-cancer surgery. Povlsen obtained a just-excised adenocarcinoma of the colon from a 74-year-old female. Small pieces from the sterile serosal side of the specimen were implanted subcutaneously into the flank of a nude mouse and the tumor grew. Even though the original donor patient had large metastasis in the liver, the tumor grew encapsulated (noninvasively) in the nude mice, an observation that numerous researchers would make on other subcutaneously-transplanted tumors in nude mice. Only when orthotopic (literally “correct place”) models were developed were tumors able to metastasize in nude mice [3]. The nude mouse-grown tumors maintained the histology of the original patient’s tumors, passage after passage. This is one of the greatest discoveries of cancer research—a patient’s tumor could be grown and replicated indefinitely in a mouse. This discovery made human cancer research a feasible experimental science for the first time.

Rygaard donated breeding colonies of nude mice to NCI in Frederick, MD, to CIEA in Japan and to the Basel Institute for Immunology [3]. The nude mouse changed the paradigm of cancer research. Human tumors and human cancer cell lines could be grown systemically in an animal model for the first time.

Subcutaneous implantation readily allows observation of tumor take and growth. Rygaard's and Povlsen's patient tumor grew in all inoculated animals and reached a considerable size in the longest surviving animals. The mode of growth of the first s.c. human tumor xenograft was characteristic of what was observed later with other human patient tumors [3, 4]. The tumor was a local nodule and was encapsulated in a thin connective tissue capsule. The tumor was found to be mobile and free of the underlying fascia and covered with a network of vessels, both medium-sized and small arteries and veins. Upon histological examination, the tumor appeared to be similar to the patient's tumor. It was a well-differentiated adenocarcinoma [3]. Tumor tissue from this first implanted tumor was serially transferred to other nude mice, again inoculated s.c. and developed in the same manner. The tumor was maintained over 7 years for 76 passages [3, 5].

In 1972, Giovanella et al. [6] successfully transplanted a human melanoma cell line into a nude mouse. Numerous human cancer cell lines have been subsequently transplanted to nude mice. A large group of human patient cancers was transplanted directly from biopsy material into nude mice by Giovanella and his team [6].

Fiebig et al. have developed a very large bank of human patient tumors transplanted directly in nude mice. Initially, Fiebig et al. transplanted 83 human colorectal and 44 stomach cancers subcutaneously in nude mice. Tumor take was observed in 78 and 68%, respectively. Progressive tumor growth was found in 49 and 32%, respectively. Serial passage was performed in 46 colorectal, 17 stomach cancers, and four esophageal cancers. Tumor stage was the most important factor for the take rate. Metastatic tumors of the colon and stomach were grown in nude mice in 89% and 54%, respectively, which was significantly higher than in non-metastatic tumors. The take rate was independent of the degree of differentiation, the amount of fibrous tissue, sex, and tumor localization. The similarity of the xenografts in serial passage in comparison to the donor tumor was shown by histological and immunological examinations. Most of the xenografts were growing more rapidly in the serial passage than in early passages. Drug treatment of the human tumors in nude mice highly correlated with clinical response for the donor patients. Predictions for resistance (100%) and sensitivity (86%) validated the nude mouse for growth of human tumors and drug sensitivity testing (see Chap. 3) [7].

The majority of human tumors were implanted in nude mice in the subcutaneous space, a site which in most cases does not correspond to the anatomical tumor localization in the patient. Discrepancies between the invading and metastasizing abilities of tumors in their natural hosts compared to those of corresponding s.c. xenografts were repeatedly described [8].

The vast majority of human solid tumors, growing as subcutaneous grafts in the nude mouse, exhibited no metastasis which is generally associated with local expansive tumor growth and the presence of circumscribed tumor borders.

Wang and Sordat et al. [9] were among the first to determine whether the growth-regulatory properties of the tissue or organ site might induce changes in the expression of the invasive phenotype. Two human cancer cell lines of colonic origin, a moderately (Co112) and a poorly differentiated (Co115) carcinoma, were implanted as cell suspensions, both subcutaneously and within the descending part of the large bowel of *nu/nu* mice. In contrast to the well-circumscribed, pseudo-encapsulated subcutaneous tumors, Co112 and Co115 displayed a multifocal, micro- and macroinvasive growth pattern when implanted into the colon. Metastases were observed with the Co115 tumor. These were found in mesenteric lymph nodes and could be detected macroscopically. Vascular invasion by colon cancer cells was a constant finding and could be seen both for lymphatics and blood vessels. All these features, including the presence of some alterations of the microvasculature such as dilated thin-walled vessels described in human colorectal tumors, made the histopathology of these xenografts quite similar to the one reported for the original patient tumors. This seminal study indicated that tumor implantation at the orthotopic site, or site corresponding to the origin of the tumor in the patient, allows the tumor to behave in a similar manner as it did in the patient (see Chap. 4).

Subsequent studies from Fidler's laboratory and from others have shown that the implantation of human tumors in the orthotopic sites of nude mice can provide a suitable model of metastasis of human tumors [10].

Our laboratory has developed the technique of surgical orthotopic implantation (SOI) to transplant histologically intact fragments of human cancer, including tumors taken directly from the patient, to the corresponding (orthotopic) organ of immunodeficient rodents. SOI allows the growth and metastatic potential of the transplanted tumors to be expressed and reflects clinical cancer to a greater extent than when a suspension of cancer cells is implanted orthotopically [4, 8].

---

## Patient-Derived Orthotopic Xenografts (PDOX)

Discrepancies have been repeatedly described between the invading and metastasizing abilities of tumors in the patient compared to the benign tumor behavior in the subcutaneous-transplanted xenografts in nude mice as noted above. Human patient tumors rarely metastasize when grown subcutaneously in immunocompromised mice; this includes patient-derived xenograft (PDX) models. However, orthotopic implantation of intact tumor tissue can lead to metastasis that mimics that seen in patients. The patient-derived orthotopic xenograft (PDOX) models better recapitulate human tumors than PDX models. The PDOX nude mouse model was developed with the technique of SOI of intact cancer tissue. A greater extent of metastasis was observed in orthotopic models with implantation of intact tumor tissue compared with orthotopically implanted cell suspensions (e.g., in stomach cancer). This perhaps is due to the intact histology and cancer cell stroma interaction of the orthotopically implanted tumor tissue. PDOX models from patients with colon, pancreatic, breast, ovarian, lung, and stomach cancer and mesothelioma were established in the

early 1990s, resulting in primary and metastatic tumor growth very similar to that of the patient. PDOXS of model cervical cancer and sarcoma were recently developed, and metastasis in the PDOX models in reflects the metastatic pattern in the donor patient (see Chap. 7) [8].

---

## Transgenic Nude Mice Expressing Fluorescent Proteins in Almost All Tissues

We have developed the transgenic green fluorescent protein (GFP) nude mouse with ubiquitous GFP expression [11]. The GFP nude mouse was obtained by crossing non-transgenic nude mice with the transgenic C57/B6 mouse in which the  $\beta$ -actin promoter drives GFP expression in essentially all tissues. A nude mouse expressing red fluorescent protein (RFP) was also developed by our laboratory [12]. The RFP nude mouse was obtained by crossing non-transgenic nude mice with the transgenic C57/B6 mouse in which the  $\beta$ -actin promoter drives RFP (DsRed2) expression in essentially all tissues. The cyan (blue) fluorescent protein (CFP) nude mouse was also developed by our laboratory by crossing non-transgenic nude mice with the transgenic CK/ECFP mouse in which the  $\beta$ -actin promoter drives expression of CFP in almost all tissues (see Chap. 14) [13].

A PDOX pancreatic cancer was passaged orthotopically into transgenic nude mice ubiquitously expressing GFP and subsequently to nude mice ubiquitously expressing RFP. The tumors, with very bright GFP and RFP stroma, were then orthotopically passaged to non-transgenic nude mice. It was possible to image the brightly fluorescent tumors noninvasively longitudinally as they progressed in the non-transgenic nude mice due to the maintenance of the bright stroma throughout passages [14].

The GFP, RFP, and CFP nude mouse models provide unique understanding of the critical interplay between the cancer cells and their microenvironment within tumors especially when implanted with cancer cells expressing a different color fluorescent protein than the mouse.

Rygaard and colleagues also created the first “humanized” mouse. Various fetal tissues were transplanted to the nude mice by Rygaard and his colleagues. These fetal tissues were able to grow including the thymus, lung, pancreas, adrenal glands, kidney, testis, and ovary. The fetal tissues were transplanted subcutaneously [15, 16]. Perhaps if the fetal tissues were transplanted orthotopically, more types would have grown (see Chap. 20).

---

## References

1. Hoffman RM. Nude mouse. In: Giordano A, Pentimalli F, editors. Reference module in life sciences. Elsevier; 2017. Epub ahead of print. doi:10.1016/B978-0-12-809633-8.06825-4.
2. Pantelouris EM. Absence of thymus in a mouse mutant. *Nature*. 1968;217:370–1.
3. Rygaard J, Povlsen CO. Heterotransplantation of a human malignant tumor to ‘nude’ mice. *Acta Pathol Microbiol Scand*. 1969;77:758–60.

4. Hoffman RM. Orthotopic metastatic mouse models for anticancer drug discovery and evaluation: a bridge to the clinic. *Invest New Drugs*. 1999;17:343–59.
5. Rygaard J, Povlsen CO. Heterotransplantation of a human malignant tumour to “nude” mice. 1969. *APMIS*. 2007;115:604–6. discussion 607–8.
6. Giovanella BC, Stehlin JS Jr, Williams U Jr, Lee SS, Shepard RC. Heterotransplantation of human cancers into nude mice: a model system for human cancer chemotherapy. *Cancer*. 1978;42:2269–81.
7. Fiebig HH, Schuchhardt C, Henss H, Fiedler L, Lohr GW. Comparison of tumor response in nude mice and in the patients. *Behring Inst Mitt*. 1984;74:343–52.
8. Hoffman RM. Patient-derived orthotopic xenografts: better mimic of metastasis than subcutaneous xenografts. *Nature Reviews Cancer*. 2015;15:451–2.
9. Wang WR, Sordat B, Piguet D, Sordat M. Human colon tumors in nude mice: implantation site and expression of the invasive phenotype. In: *Immune-deficient animals, 4th international workshop on immune-deficient animals in Exp. Res.*, Chexbres; 1982. p. 239–45 (1984: Karger, Basel).
10. Fidler IJ. Critical factors in the biology of human cancer metastasis: twenty-eighth G.H.A. Clowes memorial award lecture. *Cancer Res*. 1990;50:6130–8.
11. Yang M, Reynoso J, Jiang P, Li L, Moossa AR, Hoffman RM. Transgenic nude mouse with ubiquitous green fluorescent protein expression as a host for human tumors. *Cancer Res*. 2004;64:8651–6.
12. Yang M, Reynoso J, Bouvet M, Hoffman RM. A transgenic red fluorescent protein-expressing nude mouse for color-coded imaging of the tumor microenvironment. *J Cell Biochem*. 2009;106:279–84.
13. Tran Cao HS, Reynoso J, Yang M, Kimura H, Kaushal S, Snyder CS, Hoffman RM, Bouvet M. Development of the transgenic cyan fluorescent protein (CFP)-expressing nude mouse for “Technicolor” cancer imaging. *J Cell Biochem*. 2009;107:328–34.
14. Suetsugu A, Katz M, Fleming J, Truty M, Thomas R, Saji S, Moriwaki H, Bouvet M, Hoffman RM. Non-invasive fluorescent-protein imaging of orthotopic pancreatic-cancer-patient tumor-graft progression in nude mice. *Anticancer Res*. 2012;32:3063–8.
15. Povlsen CO, Skakkebaek NE, Rygaard J, Jensen G. Heterotransplantation of human foetal organs to the mouse mutant nude. *Nature*. 1974;248:247–9.
16. Skakkebaek NE, Jensen G, Povlsen CO, Rygaard J. Heterotransplantation of human foetal testicular and ovarian tissue to the mouse mutant nude. A preliminary study. *Acta Obstet Gynecol Scand Suppl*. 1974;29:73–5.

---

# The Revival of Patient-Derived Xenograft Mouse Models of Cancer: Way Back to the Future

# 2

Robert M. Hoffman

Rygaard and Povlsen established the first patient tumor cancer nude-mouse model with a colon cancer surgical specimen. This was the first use of nude mice to grow a human tumor. During the 1970s and 1980s, there was much worldwide use of nude mice to grow both patient tumors and human cells lines. However, xenograft mouse models went out of fashion for almost 20 years after the introduction of “OncoMouse” in 1984, the first of a long line of transgenic mouse models of cancer. Halfway through the first decade of the present century, there was a revival of xenograft models that were basically the same as Rygaard and Povlsen’s subcutaneous tumor model of 1969, in which the majority of human solid tumors do not metastasize. Orthotopic implantation of tumors enabled metastasis to occur. Although orthotopic metastatic mouse tumor models were first described in 1982 and further developed to be able to mimic metastasis in the patient in 1991, the use of orthotopic model remains limited despite their far superiority to subcutaneous or genetically-engineered mouse models of cancer in current and previous use.

Before the use of the athymic *nu/nu* mouse (nude mouse) for the growth of human tumors in 1969, there was no systematic way to grow human patient tumors in mice. Rygaard and Povlsen [1] implanted tumors in mice from a colon cancer from a 74-year-old patient subcutaneously (s.c.) in nude mice, which grew similar to the donor patient. The tumors grew locally and did not metastasize over 70 passages [1, 2].

Throughout the 1970s and 1980s, many authors noted that despite the metastatic behavior of tumors in the patient, s.c.-transplanted xenografts in nude mice were benign. This is still the case of PDX models today [2–4].

Wang et al. [5] in 1982 transplanted a human colon cancer cell line suspension orthotopically (literally “correct surface”) in nude mice rather than “heterotopically”

---

R.M. Hoffman, Ph.D.

AntiCancer, Inc., 7917 Ostrow Street, San Diego, CA 92111, USA

Department of Surgery, University of California, San Diego, CA, USA

e-mail: [all@anticancer.com](mailto:all@anticancer.com)

(literally “different surface,” such as s.c.). A suspension of colon cancer cells was injected within the descending part of the large bowel of nude mice, resulting in metastases as well as local tumor growth [2]. However, orthotopic implantation of cancer-cell-line suspensions usually resulted in a low frequency of metastasis [2].

Patient-derived orthotopic xenograft (PDOX) models, which were implanted using intact tumor tissue with the technique of surgical orthotopic implantation (SOI) [2, 6], were established from patients with colon [7–9], pancreatic [10–21], breast [22], ovarian [23], lung [24], and stomach cancer [25] and mesothelioma [26] in the early 1990s in our laboratory, resulting in primary and metastatic tumor growth very similar to that of the patient [25]. Recently, PDOX models of sarcoma [27–31] have been developed, cervical cancer [32–34] as well as melanoma [35, 36].

A clinical study of 20 patients having stomach cancers that grew orthotopically in nude mice after SOI showed direct correlation of the metastatic pattern of the patient and mice [25]. In another case, a patient-derived colon cancer lung metastasis grew in the lung, but not in the colon or skin of nude mice [37].

In the 1980s, the Leder group published their famous “OncoMouse” paper [38] describing a transgenic mouse in which the normal mouse *Myc* gene was driven by a hormonally inducible mouse mammary tumor virus promoter to generate spontaneous mammary adenocarcinomas [38]. OncoMouse started the era of transgenic mouse cancer models, which would dominate the cancer mouse model field for almost 25 years. The tumors in these models were usually driven by “oncogenes” constructed with super-active viral promoters. More sophisticated techniques were later developed to establish transgenic tumor mouse models, including homologous recombination and the use of a *Cre-loxP* system for activating “oncogenes” or deactivating (knocking out) “tumor suppressor” genes [2].

The transgenic mouse models of cancer were touted as the “real” mouse models of cancer, and at the same time xenograft models were roundly denigrated and “xenograft” became a taboo word. For example:

Sharpless and Depinho [39] described these two reciprocal phenomena:

Their paper starts out by blaming the lack of effective drugs for cancer on xenograft models:

“Most hold the view that the use of xenograft models in the cancer drug discovery and development process has proved to be problematic, with few predictive achievements and many notable failures.”

Sharpless and Depinho [39] describe the problem:

“Critics who comment on the failure of ‘mouse models’ are being dismissive of xenograft testing in particular” [39].

“This approach [xenograft] has notable flaws, but because of its ease and low cost it has been used extensively in academia and the pharmaceutical industry during the past three decades...” [39]

“The problem with xenograft analyses, however, is that many agents that show consistent and potent anticancer activity in specific xenograft models prove to be of limited use in the therapy of human cancer. This single fact is a major contributor to the low success rate of novel therapeutics when first tested in humans” [39].

“Third, and perhaps most significant, is the fact that these systems [xenograft] model cancer as if it was [sic] a disease of homogeneous rogue cells” [39].

“By failing to recapitulate the complex and evolving tumor-host stroma interactions, which could be further complicated by the immunodeficient state of the animal, xenograft analyses are reductionist and fall short of fully capturing the potent modulating effects of the tumor microenvironment in drug response” [39].

“...xenograft studies typically use only a few human tumor cell lines, the oncogenic profiles of which represent only isolated combinations of the wide spectrum of genetic and epigenetic mutations that are resident in a given tumor type presented in the clinic” [39].

“As the specific genetic profile can alter a tumor’s response to a drug... the inability to predict the outcome of clinical trials probably results in part from a failure to represent the enormous genetic diversity of tumors in patients [by xenografts]” [39].

“...novel inhibitors of angiogenesis (endostatin and angiostatin) showed potent anticancer activity when given alone or in combination against a large variety of xenografted human and murine cell lines, but so far have not demonstrated single-agent activity in human cancers...” [39]

“...by the observation that most compounds entering human clinical testing fail because of lack of efficacy, despite showing promise in preclinical xenograft testing” [39].

These “criticisms” of xenograft models by Sharpless and Depinho were typical of what was said in published scientific papers and in scientific meetings by leaders of the transgenic mouse field. In major meetings on mouse models of cancer, xenograft presentations were discouraged or not allowed. The National Cancer Institute’s “Mouse Models of Human Cancer Program” was funding essentially only grant applications on transgenic mouse models of cancer. Thus, for approximately a quarter century, the great work of mouse xenograft models of cancer, especially human patient tumor xenografts (see later chapters in this book), was ignored or described as worthless and blamed for the failure to find effective drugs for cancer.

In 2006, a “way back to the future” event occurred, all the way back to 1969, Rygaard and Povlsen [1]. The s.c.-transplanted human patient xenograft mouse model was heavily promoted by Hidalgo et al. [40] and his company, Champion’s. At first, the term “tumorgraft” [41] was used so as not to use the taboo term “xenograft” [2].

The reborn s.c. models sometimes used more immunodeficient, such as non-obese diabetic, severe combined immunodeficiency (NOD-SCID) mice. However, the tumors were still s.c. and did not metastasize. In order not to seem to be going back to the 1960s, the born-again s.c.-transplanted mouse models were given even more exotic new names such as “xenopatients” or “avatars” [4] in order to exaggerate their capability and novelty [2]. The October 3, 2014 issue of *Science* had an “avatar” on the cover, which stated: “To make mice better mirrors of human cancer, researchers are building ‘avatars’ with the cancer of a particular patient.... The work marks a sea change in cancer biology and is stirring hope that new mouse models will pave the way to more personalized care” [42]. However, orthotopic patient models are hardly mentioned in the “xenopatient” and “avatar” papers [2, 4, 43]. Patient-derived xenografts, simply referred to as PDX models of cancer, are now the hot fad and “transgenic” cancer models appear to be in eclipse [2].

After 52 years in science, I have seen many scientific fads that come and go and come back again [2, 44]. We are now back to the late 1960s with the so-called patient-derived xenograft “PDX” model. Orthotopic models attained a modicum of popularity in the late 1980s and early 1990s [2], due in large part to the great efforts of Fidler [45]. It seems that most cancer researchers have either forgotten about or



are unaware of orthotopic models [2], especially PDOX models, which are metastatic and resemble the patient's tumors [2]. It is the goal of the present book to give a better appreciation of the history as well as state of the art of patient mouse models of cancer, in particular the patient-derived orthotopic xenograft (PDOX) models.

---

## References

1. Rygaard J, Povlsen CO. Heterotransplantation of a human malignant tumor to 'nude' mice. *Acta Pathol Microbiol Scand*. 1969;77:758–60.
2. Hoffman RM. Patient-derived orthotopic xenografts: better mimic of metastasis than subcutaneous xenografts. *Nat Rev Cancer*. 2015;15:451–2.
3. Zhang Y, Toneri M, Ma H, Yang Z, Bouvet M, Goto Y, Seki N, Hoffman RM. Real-time GFP intravital imaging of the difference in cellular and angiogenic behavior of subcutaneous and orthotopic nude-mouse models of human PC-3 prostate cancer. *J Cell Biochem*. 2016;117:2546–51.
4. Garralda E, Paz K, Lopez-Casas PP, Jones S, Katz A, Kann LM, Lopez-Rios F, Sarno F, Al-Shahrour F, Vasquez D, Bruckheimer E, Angiuoli SV, Calles A, Diaz LA, Velculescu VE, Valencia A, Sidransky D, Hidalgo M. Integrated next-generation sequencing and avatar mouse models for personalized cancer treatment. *Clin Cancer Res*. 2014;20:2476–84.
5. Wang WR, Sordat B, Pigué D, Sordat M. Human colon tumors in nude mice: implantation site and expression of the invasive phenotype. In: Sordat B, editor. *Immune-deficient animals—4th international workshop on immune-deficient animals in experimental research*. Basel: Karger; 1982. p. 239–45.
6. Hoffman RM. Orthotopic metastatic mouse models for anticancer drug discovery and evaluation: a bridge to the clinic. *Invest New Drugs*. 1999;17:343–59.
7. Fu X, Besterman JM, Monosov A, Hoffman RM. Models of human metastatic colon cancer in nude mice orthotopically constructed by using histologically intact patient specimens. *Proc Natl Acad Sci U S A*. 1991;88:9345–9.
8. Metildi CA, Kaushal S, Luiken GA, Talamini MA, Hoffman RM, Bouvet M. Fluorescently-labeled chimeric anti-CEA antibody improves detection and resection of human colon cancer in a patient-derived orthotopic xenograft (PDOX) nude mouse model. *J Surg Oncol*. 2014;109:451–8.
9. Hiroshima Y, Maawy A, Metildi A, Zhang Y, Uehara F, Miwa S, Yano S, Sato S, Murakami T, Momiya M, Chishima T, Tanaka K, Bouvet M, Endo I, Hoffman RM. Successful fluorescence-guided surgery on human colon cancer patient-derived orthotopic xenograft mouse models using a fluorophore-conjugated anti-CEA antibody and a portable imaging system. *J Laparoendosc Adv Surg Tech A*. 2014;24:241–7.
10. Fu X, Guadagni F, Hoffman RM. A metastatic nude-mouse model of human pancreatic cancer constructed orthotopically from histologically intact patient specimens. *Proc Natl Acad Sci U S A*. 1992;89:5645–9.
11. Kaushal S, McElroy MK, Luiken GA, Talamini MA, Moossa AR, Hoffman RM, Bouvet M. Fluorophore-conjugated anti-CEA antibody for the intraoperative imaging of pancreatic and colorectal cancer. *J Gastrointest Surg*. 2008;12:1938–50.
12. Suetsugu A, Katz M, Fleming J, Moriwaki H, Bouvet M, Saji S, Hoffman RM. Multi-color palette of fluorescent proteins for imaging the tumor microenvironment of orthotopic tumor-graft mouse models of clinical pancreatic cancer specimens. *J Cell Biochem*. 2012;113:2290–5.
13. Suetsugu A, Katz M, Fleming J, Truty M, Thomas R, Saji S, Moriwaki H, Bouvet M, Hoffman RM. Imageable fluorescent metastasis resulting in transgenic GFP mice orthotopically implanted with human-patient primary pancreatic cancer specimens. *Anticancer Res*. 2012;32:1175–80.
14. Suetsugu A, Katz M, Fleming J, Truty M, Thomas R, Saji S, Moriwaki H, Bouvet M, Hoffman RM. Non-invasive fluorescent-protein imaging of orthotopic pancreatic-cancer-patient tumor-graft progression in nude mice. *Anticancer Res*. 2012;32:3063–8.

15. Hiroshima Y, Maawy A, Sato S, Murakami T, Uehara F, Miwa S, Yano S, Momiyama M, Chishima T, Tanaka K, Bouvet M, Endo I, Hoffman RM. Hand-held high-resolution fluorescence imaging system for fluorescence-guided surgery of patient and cell-line pancreatic tumors growing orthotopically in nude mice. *J Surg Res*. 2014;187:510–7.
16. Hiroshima Y, Zhao M, Maawy A, Zhang Y, Katz MH, Fleming JB, Uehara F, Miwa S, Yano S, Momiyama M, Suetsugu A, Chishima T, Tanaka K, Bouvet M, Endo I, Hoffman RM. Efficacy of Salmonella typhimurium A1-R versus chemotherapy on a pancreatic cancer patient-derived orthotopic xenograft (PDOX). *J Cell Biochem*. 2014;115:1254–61.
17. Hiroshima Y, Maawy A, Zhang Y, Murakami T, Momiyama M, Mori R, Matsuyama R, Katz MH, Fleming JB, Chishima T, Tanaka K, Ichikawa Y, Endo I, Hoffman RM, Bouvet M. Metastatic recurrence in a pancreatic cancer patient derived orthotopic xenograft (PDOX) nude mouse model is inhibited by neoadjuvant chemotherapy in combination with fluorescence-guided surgery with an anti-CA 19-9-conjugated fluorophore. *PLoS One*. 2014;9:e114310.
18. Hiroshima Y, Zhang Y, Murakami T, Maawy AA, Miwa S, Yamamoto M, Yano S, Sato S, Momiyama M, Mori R, Matsuyama R, Chishima T, Tanaka K, Ichikawa Y, Bouvet M, Endo I, Zhao M, Hoffman RM. Efficacy of tumor-targeting Salmonella typhimurium A1-R in combination with anti-angiogenesis therapy on a pancreatic cancer patient-derived orthotopic xenograft (PDOX) and cell line mouse models. *Oncotarget*. 2014;5:12346–57.
19. Hiroshima Y, Maawy AA, Katz MH, Fleming JB, Bouvet M, Endo I, Hoffman RM. Selective efficacy of zoledronic acid on metastasis in a patient-derived orthotopic xenograft (PDOX) nude-mouse model of human pancreatic cancer. *J Surg Oncol*. 2015;111:311–5.
20. Hiroshima Y, Maawy A, Zhan Y, Murakami T, Momiyama M, Mori R, Matsuyama R, Chishima T, Tanaka K, Ichikawa Y, Endo I, Hoffman RM, Bouvet M. Fluorescence-guided surgery, but not bright-light surgery, prevents local recurrence in a pancreatic cancer patient-derived orthotopic xenograft (PDOX) model resistant to neoadjuvant chemotherapy (NAC). *Pancreatol*. 2015;15:295–301.
21. Yano S, Hiroshima Y, Maawy A, Kishimoto H, Suetsugu A, Miwa S, Toneri M, Yamamoto M, Katz MHG, Fleming JB, Urata Y, Tazawa H, Kagawa S, Bouvet M, Fujiwara T, Hoffman RM. Color-coding cancer and stromal cells with genetic reporters in a patient-derived orthotopic xenograft (PDOX) model of pancreatic cancer enhances fluorescence-guided surgery. *Cancer Gene Ther*. 2015;22:344–50.
22. Fu X, Le P, Hoffman RM. A metastatic-orthotopic transplant nude-mouse model of human patient breast cancer. *Anticancer Res*. 1993;13:901–4.
23. Fu X, Hoffman RM. Human ovarian carcinoma metastatic models constructed in nude mice by orthotopic transplantation of histologically-intact patient specimens. *Anticancer Res*. 1993;13:283–6.
24. Wang X, Fu X, Hoffman RM. A new patient-like metastatic model of human lung cancer constructed orthotopically with intact tissue via thoracotomy in immunodeficient mice. *Int J Cancer*. 1992;51:992–5.
25. Furukawa T, Kubota T, Watanabe M, Kitajima M, Fu X, Hoffman RM. Orthotopic transplantation of histologically intact clinical specimens of stomach cancer to nude mice: correlation of metastatic sites in mouse and individual patient donors. *Int J Cancer*. 1993;53:608–12.
26. Astoul P, Wang X, Colt HG, Boutin C, Hoffman RM. A patient-like human malignant pleural mesothelioma nude-mouse model. *Oncol Rep*. 1996;3:483–7.
27. Hiroshima Y, Zhao M, Zhang Y, Zhang N, Maawy A, Murakami T, Mii S, Uehara F, Yamamoto M, Miwa S, Yano S, Momiyama M, Mori R, Matsuyama R, Chishima T, Tanaka K, Ichikawa Y, Bouvet M, Endo I, Hoffman RM. Tumor-targeting Salmonella typhimurium A1-R arrests a chemo-resistant patient soft-tissue sarcoma in nude mice. *PLoS One*. 2015;10:e0134324.
28. Murakami T, DeLong J, Eilber FC, Zhao M, Zhang Y, Zhang N, Singh A, Russell T, Deng S, Reynoso J, Quan C, Hiroshima Y, Matsuyama R, Chishima T, Tanaka K, Bouvet M, Chawla S, Endo I, Hoffman RM. Tumor-targeting Salmonella typhimurium A1-R in combination with doxorubicin eradicate soft tissue sarcoma in a patient-derived orthotopic xenograft PDOX model. *Oncotarget*. 2016;7:12783–90.
29. Kiyuna T, Murakami T, Tome Y, Kawaguchi K, Igarashi K, Zhang Y, Zhao M, Li Y, Bouvet M, Kanaya F, Singh A, Dry S, Eilber FC, Hoffman RM. High efficacy of tumor-targeting

- Salmonella typhimurium A1-R on a doxorubicin- and dactolisib-resistant follicular dendritic-cell sarcoma in a patient-derived orthotopic xenograft PDOX nude mouse model. *Oncotarget*. 2016;7:33046–54.
30. Murakami T, Singh AS, Kiyuna T, Dry SM, Li Y, James AW, Igarashi K, Kawaguchi K, DeLong JC, Zhang Y, Hiroshima Y, Russell T, Eckardt MA, Yanagawa J, Federman N, Matsuyama R, Chishima T, Tanaka K, Bouvet M, Endo I, Eilber FC, Hoffman RM. Effective molecular targeting of CDK4/6 and IGF-1R in a rare FUS-ERG fusion CDKN2A-deletion doxorubicin-resistant Ewing's sarcoma in a patient-derived orthotopic xenograft (PDOX) nude-mouse model. *Oncotarget*. 2016;7:47556–64.
  31. Kiyuna T, Murakami T, Tome Y, Igarashi K, Kawaguchi K, Russell T, Eckhardt MA, Crompton J, Singh A, Bernthal N, Bukata S, Federman N, Kanaya F, Eilber FC, Hoffman RM. Labeling the stroma of a patient-derived orthotopic xenograft (PDOX) mouse models of undifferentiated pleomorphic soft-tissue sarcoma with red fluorescent protein for rapid non-invasive drug screening. *J Cell Biochem*. 2017;118:361–5.
  32. Hiroshima Y, Zhang Y, Zhang M, Maawy A, Mii S, Yamamoto M, Uehara F, Miwa S, Yano S, Murakami T, Momiyama M, Chishima T, Tanaka K, Ichikawa Y, Bouvet M, Murata T, Endo I, Hoffman RM. Establishment of a patient-derived orthotopic xenograph (PDOX) model of HER-2-positive cervical cancer expressing the clinical metastatic pattern. *PLoS One*. 2015;10:e0117417.
  33. Hiroshima Y, Maawy A, Zhang Y, Zhang N, Murakami T, Chishima T, Tanaka K, Ichikawa Y, Bouvet M, Endo I, Hoffman RM. Patient-derived mouse models of cancer need to be orthotopic in order to evaluate targeted anti-metastatic therapy. *Oncotarget*. 2016;7:71696–702.
  34. Murakami T, Murata T, Kawaguchi K, Kiyuna T, Igarashi K, Hwang HK, Hiroshima Y, Hozumi C, Komatsu S, Kikuchi T, Lwin TM, DeLong JC, Miyake K, Zhang Y, Tanaka K, Bouvet M, Endo I, Hoffman RM. Cervical cancer patient-derived orthotopic xenograft (PDOX) is sensitive to cisplatin and resistant to nab-paclitaxel. *Anticancer Res*. 2017;37:61–5.
  35. Yamamoto M, Zhao M, Hiroshima Y, Zhang Y, Shurell E, Eilber FC, Bouvet M, Noda M, Hoffman RM. Efficacy of tumor-targeting Salmonella typhimurium A1-R on a melanoma patient-derived orthotopic xenograft (PDOX) nude-mouse model. *PLoS One*. 2016;11:e0160882.
  36. Kawaguchi K, Murakami T, Chmielowski B, Igarashi K, Kiyuna T, Unno M, Nelson SD, Russell TA, Dry SM, Li Y, Eilber FC, Hoffman RM. Vemurafenib-resistant BRAF-V600E mutated melanoma is regressed by MEK-targeting drug trametinib, but not cobimetinib in a patient-derived orthotopic xenograft (PDOX) mouse model. *Oncotarget*. 2016;7:71737–43.
  37. Togo S, Wang X, Shimada H, Moossa AR, Hoffman RM. Cancer seed and soil can be highly selective: human-patient colon tumor lung metastasis grows in nude mouse lung but not colon or subcutis. *Anticancer Res*. 1995;15:795–8.
  38. Stewart TA, Pattengale PK, Leder P. Spontaneous mammary adenocarcinomas in transgenic mice that carry and express MTV/myc fusion genes. *Cell*. 1984;38:627–37.
  39. Sharpless NE, Depinho RA. The mighty mouse: genetically engineered mouse models in cancer drug development. *Nat Rev Drug Discov*. 2006;5:741–54.
  40. Rubio-Viqueira B, Jimeno A, Cusatis G, Zhang X, Iacobuzio-Donahue C, Karikari C, Shi C, Danenberg K, Danenberg PV, Kuramochi H, Tanaka K, Singh S, Salimi-Moosavi H, Bouraoud N, Amador ML, Altiock S, Kulesza P, Yeo C, Messersmith W, Eshleman J, Hruban RH, Maitra A, Hidalgo M. An in vivo platform for translational drug development in pancreatic cancer. *Clin Cancer Res*. 2006;12:4652–61.
  41. Garber K. From human to mouse and back: “tumorgraft” models surge in popularity. *J Natl Cancer Inst*. 2009;101:6–8.
  42. Couzin-Frankel J. The littlest patient. *Science*. 2014;346:24–7.
  43. Couzin-Frankel J. Hope in a mouse. *Science*. 2014;346:28–9.
  44. Hoffman RM. Is DNA methylation the new guardian of the genome? *Molecular Cytogenetics* 2017;10:11.
  45. Fidler IJ. Critical factors in the biology of human cancer metastasis: twenty-eighth G.H.A. Clowes memorial award lecture. *Cancer Res*. 1990;50:6130–8.

---

# Patient-Derived Xenograft Models for Human Cancer: The Freiburg Experience

# 3

Heinz-Herbert Fiebig

Since 1969, human patient patient-derived xenograft (PDX) have been grafted into immune-compromised mice, and until today they are the most important model system to evaluate novel compounds against cancer and to study tumor biology. In Freiburg more than 3.000 patient tumors have been transplanted subcutaneously into nude mice from which 450 PDX have been established and selected as permanent tumor models. In 90% of them the molecular profile was determined including gene expression, mutations by WES and copy number variations. 250 models were characterized for their sensitivity against targeted and cytotoxic drugs in-vivo and also in-vitro in 3D cultures. Based on the testing results predictive gene signatures and biomarkers were investigated for small molecules and antibodies. A comprehensive data base of all molecular and sensitivity data allows the selection of suitable tumor models for investigating new drugs.

---

## Historical Aspects of PDX

Since 1969, human PDX models have been developed in immune-suppressed mice, and until today they are the most important model system to evaluate novel compounds against cancer and to study tumor biology. The growth of human tumors in a murine host was only possible when a specific mouse mutant was discovered in Glasgow more than 50 years ago.

---

H.-H. Fiebig  
4HF Biotec GmbH and Oncotest GmbH until Nov. 2015, Am Flughafen 12 - 14, D-79108  
Freiburg, Germany  
e-mail: [fiebig@4hf.eu](mailto:fiebig@4hf.eu)

## Origin and Properties of Nude Mouse

Early in the 1960s, Isaacson and Cattanaach [1] observed in an albino mouse strain a spontaneous mutant which was hairless and had a very short life span. Flanagan described it in 1966 [2]. Because of the hairlessness, he called the mutant “nude” and introduced the symbol “nu.” The mutation was autosomal recessive. Flanagan correlated the nu mutation with known chromosomal markers and found that the mutation nu was located at the chromosomal group VII between the markers Re and Tr. Later on the genes Re-nu-Tr were localized on chromosome 11 of the mouse [3].

The hairlessness was always connected with an aplasia of the thymus [4]. With this discovery, the nude mouse proved to be an excellent model to study the thymus function. The growth of allo- and xenogeneic transplants allowed novel applications in research.

Rygaard and Povlsen reported the first successful transplantation of a human tumor in the nude mouse, namely, an adenocarcinoma of the colon [5]. Other groups transplanted various human tumor types which could also be transferred in serial passage [6, 7]. Also human tumor cell lines being established in tissue culture grew successfully in nude mice; they formed solid tumors after subcutaneous transplantation [8, 9]. The treatment of a Burkitt lymphoma and a melanoma growing in serial passage were reported by the Copenhagen group [10, 11].

Rygaard performed the first xenogeneic transplantation of skin from Wistar rats into nude mice [12]. Further successful transplantations were described with the skin of hamsters and rabbits [13], cats [14], birds [15], and also human skin [16, 17]. The skin of snakes and frogs was not rejected. They showed degenerative changes which were explained by the unphysiological environment [14, 15].

The immunological properties of the nude mouse were further characterized by several research groups. Tumor biologic and therapeutic investigations were also carried out. The findings were presented and summarized at international symposia starting in 1973 in Aarhus, Denmark; 1976 in Tokyo; 1977 in Columbus, USA; and 1979 in London, in Frankfurt, and in Bozeman, Montana, USA [18–22].

The athymic mouse has also opened new possibilities for microbiologic and parasitological studies. Models of lepra and *Pneumocystis carinii* were developed [23–25], and investigations on immune reactions during infections were of special importance. Humoral and cellular mechanisms were studied after infections with *Plasmodium berghei* [26, 27], *Trypanosoma musculi* [28], helminths [29–31], and different virus infections [32].

## Morphologic and Physiologic Characteristics

The nude mutation has a number of consequences of which the aplasia of the thymus is the most important. The initially described complete aplasia of the thymus was not confirmed. Pantelouris and Hair published in 1970 the existence of a rudiment of the thymus, which was confirmed by other groups [33–36]. In the anterior mediastinum, two small lobes with residual components of the thymus were detected [37, 38], and the thymus is much smaller compared to immunocompetent mice [39].

Homo- and heterozygous nude mice have an impaired hematopoiesis. Zipore and Trainin [40] and Holub et al. [41] found that the hematopoietic stem cells have a reduced capability to form colonies. Since also heterozygous mice are defective, Dolenska et al. [42] concluded that these defects are present on stem cells and due to a mesenchymal defect of the mutation and not secondary to the defect of the thymus. Nude mice showed in the peripheral blood a leukopenia of 25–30% of the normal value. In heterozygous mice a reduction to the half of the normal value was already reported by Pantelouris [4]. The leukopenia is caused by lack of mature T lymphocytes [43, 44].

The most obvious effect of the mutation *nu* is the hairlessness. The nude mouse has functional hair follicles, but the keratinization is impaired resulting in braking up of the hair [2]. The hairlessness results in a number of physiological properties. Nude mice have a lower body temperature, a higher metabolic turnover, and lower blood sugar levels compared to heterozygous mice [45–47]. Nude mice have a higher loss of water through the skin and homozygous female drink 2/3 more than heterozygous haired mice [17]. The other organ systems of the nude mouse are developed in a normal way.

## Immunological Properties

Precursors of T lymphocytes are present in the nude mouse, but due to the thymus aplasia, they do not mature into functional T lymphocytes [48–50]. For instance, the lymph of the ductus thoracicus of *nu/nu* mice contains only B lymphocytes, whereas 85% T lymphocytes and 15% B lymphocytes are found in immunocompetent mice [51]. *Nu/nu* mice have an unusual high amount of natural killer cells compared to heterozygous mice or mice without mutation. They are mainly found in the spleen. Natural killer cells seem to play an essential role in the residual immune response of the nude mice, e.g., against the rejection of leukemias and lymphomas. An even higher amount of natural killer cells seen after opportunistic infections can result in a lower take rate and growth of transplanted tumors. Macrophages of the nude mouse have also cytotoxic properties which may play a role in the rejection of tumors [52].

The B-cell population of lymphocytes shows a normal development. The total immunoglobulin concentration is similar to immunocompetent mice. The fractions are slightly different: IgG and IgA are reduced in nude mice and IgM increased [46, 53, 54]. Functional tests showed that the humoral immune reaction is decreased which needs thymus-dependent T helper and T suppressor lymphocytes. A normalization of the humoral and cellular defense occurs after T-cell substitution or thymus transplantation [55, 56], and also large tumor masses were rejected [57].

Due to the missing T lymphocytes, nude mice have a high risk acquiring infection of bacteria or viruses which are not pathogens for immunocompetent strains. Infections have been reported mainly mouse hepatitis virus and noroviruses as well as *Staphylococcus aureus* resulting in skin and eye abscesses.

## **Early Freiburg Experience in the Establishment, Characterization, and Therapeutic Use of PDX from 1978 Until 1988**

I was fascinated by the potential of growing human tumors in a murine host. Over 40 years my group has grafted more than 3,000 patient tumors subcutaneously into nude and in recent years scid mice from which 450 PDX from all solid tumor types have been established and selected as permanent tumor models. When I began my academic career and training as a hematologist and medical oncologist at the University of Freiburg, I initiated a broad systematic program in establishing patient tumors and treated them with registered anticancer drugs. Many of these patients were treated by myself with the standard chemotherapy or with an individualized chemotherapy according to the test result obtained in the nude mouse. The hope was that the testing results could be used to guide and individualize the treatment of the patients.

In 1978 a series of 45 tumors was transplanted subcutaneously in nude mice. Twenty-three tumors grew progressively and were subpassaged. Then a major event occurred: a few tumors were infected by mouse hepatitis virus (MHV), which was very common in those days. When it became evident that it was impossible to eradicate the MHV and that the virus could infect healthy mice via tumor transplantation, it was decided to sacrifice the whole colony of nude mice, and all 18 established tumors were discarded. A restart was done in June 1979. Retrospectively, the MHV was acquired when nude mice were purchased from another breeder.

The restart was done with NMRI outbred nude mice which were obtained from Fortmeyer, Zentrale Tierversuchsanlage, University of Frankfurt/Main as the new breeding stock. During the next 3 years, all nude mice were bred in our facility in Freiburg. Later on, nude mice were purchased for larger studies from the Zentrale Tierversuchsanlage, Medizinische Hochschule Hannover, and Bomholtgard in Denmark. These mice did not show health problems with MHV or other infections.

My research topic was considered highly relevant, and I received two large research grants from the German Ministry of Research and Technology (BMBF) for three funding periods (1980–1988), grants from the EORTC via the NDDO (1985–1992), and the NCI in Bethesda from 1985 to 1998. Pharma companies became more and more interested in the new model system and commissioned *in vivo* and *in vitro* studies allowing to finance the academic program when the large BMBF grant expired. Well before the wave of spin-offs in the Biotech sector, I founded my own company in 1993, Oncotest Institute of Experimental Oncology GmbH, in Freiburg, and transferred my academic program to it. Two buildings were rented and renovated, and the key people from my academic group were hired once their contracts came to term at the university.

I received two prestigious awards: the Vincenz Czerny Prize of the German Society for Hematology and Oncology in 1984 for my PhD thesis [58] and the annual prize for reducing animal experiments (pretesting in the clonogenic assay in 3D tissue culture) by the Ministry of Youth, Family, and Health in 1985. Three scientists from my group were also awarded later on; Dietmar Berger received the annual prize of the AIO of the German Cancer Society in 1995 [59] and Angelika Burger the AIO scientific prize in 2005 [60]. The prize for the outstanding medical

thesis was awarded to Kathrin Schandelmeier in 2003 [61] by the German Society for Hematology and Oncology (tissue microarrays from PDX).

### Take Rate, Growth Behavior, and Drug Response from 1979 Until 1988

In the second series, 205 solid tumors were implanted subcutaneously into NMRI nude mice. Flat tumor slices of  $5 \times 5 \times 1$  mm were implanted bilaterally in the mammary fat pad in the axillary and inguinal region, normally 16 slices into four mice. Initially cell suspensions were injected, but soon it became evident that the implantation of fragments yielded higher take rates.

Table 3.1a summarizes the take rate and growth behavior of the 205 solid tumors [59, 62]. The growth was divided into rapidly and slowly growing tumors and tumors which could be transferred in serial passage for at least three passages. Rapid growth was defined as tumor size calculated by  $a \times b$  of tumor diameters of at least  $60 \text{ mm}^2$  by 90 days after implantation equal to, e.g.,  $8 \times 7.5$  mm in diameter. Slow growth was defined as tumor size  $<60 \text{ mm}^2$  after 90 days. A no-take was defined by no histological evidence of vital tumor cells at the site of implantation. Normally only fast-growing tumors can be transferred in serial passage and are suitable for drug testing. All tumors were studied by histological examination.

Table 3.1b shows a summary of the growth for all solid tumors in the period 1979–1986. Tumor take with rapid growth rates between 45 and 100% was observed for colorectal, gastric, lung squamous cell, esophageal, and skin (squamous cell) cancers

**Table 3.1a** Growth of human tumors in nude mice 1979–1982

Cancer	Total	Rapid growth <sup>a</sup>		Serial passage <sup>b</sup>	
Melanoma	9	4	44%	5	56%
Colorectal	76	37	49%	41	54%
Lung adeno	6	3	50%	3	50%
Sarcoma soft tissue	14	7	50%	6	43%
Esophagus	5	4	80%	2	40%
Lung squamous	18	9	50%	7	39%
Miscellaneous	13	5	38%	5	38%
Wilmstumor	3	2	33%	1	33%
Head and neck	4	1	33%	1	33%
Gastric	37	10	27%	11	30%
Lung small cell	4	1	25%	1	25%
Sarcoma bone	4	1	25%	1	25%
Kidney	5	1	20%	1	20%
Testicular	7	1	14%	0	0%
Total	205	86	42%	85	41%

<sup>a</sup>Rapid growth: tumor size ( $a \times b$ )  $\geq 60 \text{ mm}^2$  90 days after implantation

<sup>b</sup>At least three successful passages



**Table 3.1b** Growth of human tumors in nude mice 1979–1986

Tumor origin	Total	Rapid growth <sup>a</sup>		Serial passage <sup>b</sup>	
		<i>n</i>	%	<i>n</i>	%
Cervix uteri	10	7	70	6	60
Esophagus	10	7	70	6	60
Colorectal	152	88	58	78	51
Corpus uteri	8	4	50	4	50
Lung squamous	106	61	58	50	47
Melanoma	63	39	62	27	43
Lung small cell	39	14	36	16	41
Lung large cell	38	20	53	14	37
Sarcoma	79	36	46	29	37
Ovarian	22	7	32	8	36
Head and neck	47	16	34	16	34
Pancreatic	6	2	33	2	33
Lung adeno	83	37	45	23	28
Miscellaneous	129	42	33	34	26
Gastric	68	17	25	17	25
Testicular	48	14	29	12	25
Pleuramesothelioma	36	14	39	9	25
Bladder	44	17	39	10	23
Renal	124	37	30	24	19
Breast	74	13	18	13	18
Prostate	41	7	17	2	5
Total	1227	499	41	400	33

<sup>a</sup>Rapid growth: tumor size ( $a \times b$ )  $\geq 60 \text{ mm}^2$  90 days after implantation

<sup>b</sup>At least three successful passages and be frozen in liquid nitrogen

as well as soft-tissue sarcomas and melanomas. Tumor take with a growth rate between 20 and 40% was found for gastric, lung small cell, and head and neck renal cancers as well as bone sarcomas. About 80% of them were transferred in serial passage.

This initial experience was summarized in the PhD thesis by the author which was submitted in 1982 to the Medical Faculty of the University of Freiburg [58]. The take rate, model development, and characterization were reported in reference [63] and specifically for soft-tissue sarcomas [62], for gastrointestinal cancers [64, 65], and for small cell lung cancers [66].

A follow-up of the take rates was published in 1991 [67, 68]. Out of 1227 implanted solid tumors, 499 (41%) showed rapid growth and 400 (33%) were established in serial passage [69].

These data confirmed the high take rates observed in the first series. In addition it became evident that breast and prostate cancers are very difficult to establish with an initial take rate of 18 and 17%, respectively. However, only 13 mammary (18%) and two prostate cancers (5%) could be established in serial passage, respectively, despite supplementing the mice with estrogen or dihydrotestosterone.

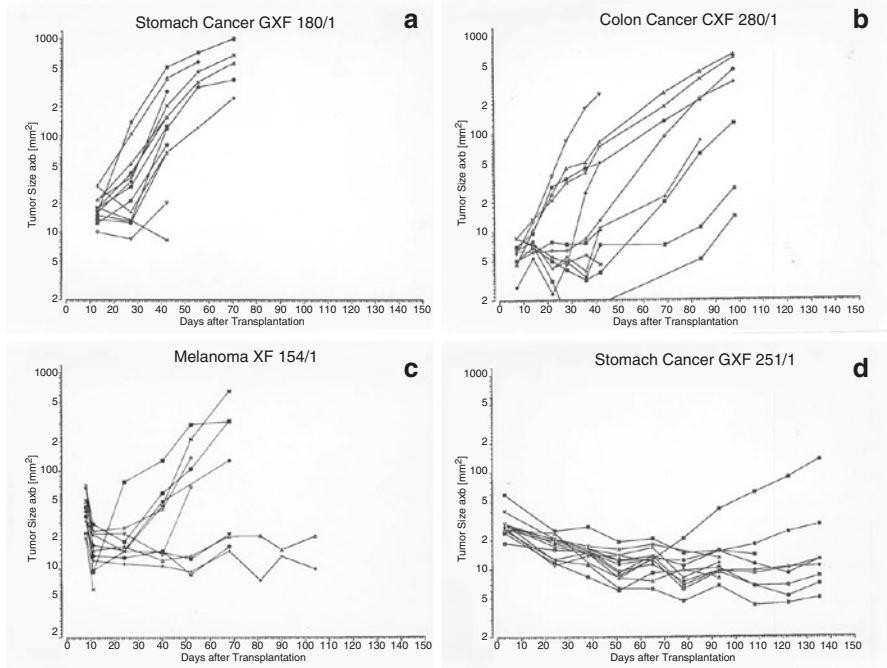


**Fig. 3.1** Growth of individual tumors in the first passage. (a) Gastric cancer GXF180; (b) colorectal cancer CXF280; (c) melanoma MEXF154; (d) gastric cancer GXF 251

The growth behavior of all individual tumors was measured every other week. A huge variation among the different tumors became evident. Figure 3.1 shows an example of all individual tumors from four different patients in the first passage until an observation period up to 150 days for very-slowly growing tumors. Figure 3.1a shows all individual tumors of the very well-growing gastric cancer GXF 180. Such a regular initial growth occurs in less than 10%. All individual tumors grow after an initial lag phase of normally 2–3 weeks. In the colon cancer CXF 280 (Fig. 3.1b), all individual tumors were growing but at quite different intervals up to 100 days. In Fig. 3.1c only half of all individual tumors of melanoma MEXF 154 grew progressively within 2 months (Fig. 3.1c). Gastric cancer GXF 251 showed tumor shrinkage in all individual tumors for 3 months (Fig. 3.1d). Only one tumor started to grow after 2 months, and from this one, a very valuable model with an amplified EGFR was established [58].

The growth of the tumors from a given tumor type also showed a large variation. Figure 3.2 shows an example of 20 successively-implanted colorectal cancers observed for 5 months [67]. A rapid growth was observed in half of them after 2 months, whereas three additional models grew progressively for 4 months and six others always remained stationary.

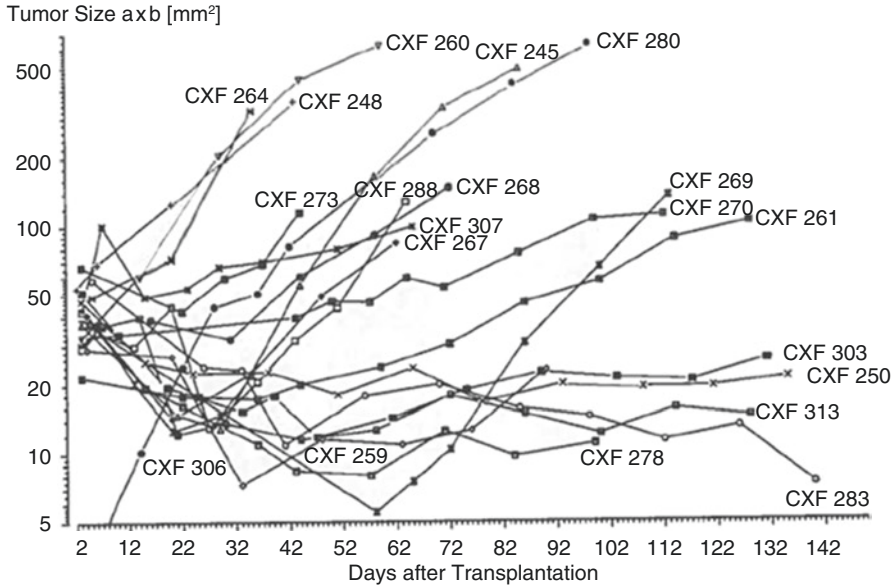


**Fig. 3.2** Growth behavior of 20 successively-transplanted colorectal carcinomas in nude mice

From this growth behavior of the individual tumors originating from individual patients, it is clear that therapeutic studies cannot be performed in the first passages. A more constant growth occurred in passage 3 or sometimes even later, which may take 4–15 months.

### **PDX Take/Growth as a Prognostic Factor for Survival of Cancer Patients**

This question was addressed in colorectal and gastric cancers [58]. For 74 patients with colorectal cancers, mainly localized Dukes' A–C, survival data were recorded after a median time of 2 years after implantation. Patients with tumors showing no growth in nude mice had a statistically significant higher survival rate of 87% compared to 54% for patients with fast-growing tumors in nude mice ( $p = 0.02$ ). A similar trend was observed for 37 patients with gastric cancers (38 vs. 21%); however, the difference was not significant (Table 3.2) [58].

### **PDX Regrowth After Being Frozen in Liquid Nitrogen**

Fast-growing tumors should be passaged after 1–2 months and slowly growing tumors after 3–5 months. Thus, over time, higher passage numbers will occur. Here the risk of selecting subclones and acquiring genetic changes is evident. The same

**Table 3.2** Tumor take as a prognostic factor for survival of patients with colorectal and gastric cancers

Tumor	Behaviour	All patients				Without early deaths <sup>a</sup>			
		Alive	Total	%	Significant	Alive	Total	%	Significant
Colorectal	No growth	13	15	87	$p = 0.02$	13	14	93	$p = 0.01$
	Growth	32	59	54		32	57	56	
	Slow growth	15	23	65	$p = 0.18$ ns	15	22	68	$p = 0.15$ ns
	Rapid growth <sup>b</sup>	17	36	47		17	35	49	
Gastric	No growth	5	13	38	$p = 0.25$ ns	5	9	56	$p = 0.11$ ns
	Growth	5	24	21		5	20	25	
	Slow growth	3	14	21	ns	3	11	27	ns
	Rapid growth	2	10	20		2	9	22	

ns not significant

<sup>a</sup>Without early deaths within 30 days after surgery

<sup>b</sup>Rapid growth, tumor size (a × b) ≥ 60 mm<sup>2</sup> 90 days after implantation

**Table 3.3** Regrowth of PDX after being frozen in liquid nitrogen in 1982

Source	Histology	Take no.	Total	%
Colorectal	Adeno- and undiff. Ca	31	35	89
Gastric	Adeno- and undiff. Ca	9	11	82
Lung	Squamous	6	8	75
	Adeno-Ca	3	3	
	Small cell CA	1	1	
Melanoma	Melanoma	3	3	
Sarcoma	Soft tissue	4	4	
Skin, testicular	Teratoma and embryonal CA	2	3	
Esophagus	Squamous cell	1	1	
Renal	Wilms-Tumor	1	1	
Thyroid	Anaplastic	1	1	
Renal pelvis	Transitional Ca	1	1	
<i>Total</i>		63	72	88

holds true for permanent cancer cell lines. Therefore, it is important to limit the number of passages in order to have a PDX resembling the donor tumor in an always defined genetic state. This can be obtained only by freezing tumors in liquid nitrogen. The earliest PDX of the Freiburg collection was frozen in 1981 and still showed regrowth after 35 years e.g. GXF 97, SXF 81, SXF 117 or CXF 158. This means that frozen PDX can survive indefinitely in liquid nitrogen.

I optimized the freezing process in 1982 and obtained an overall regrowth of 88% (Table 3.3). A higher retake was obtained by freezing tumor fragments compared to tumor cell suspensions. Only fragments resulted in regrowth in squamous cell and small cell lung PDX [58].

## Similarities and Changes of PDX Compared to the Donor Tumor

The growth of cancer cells starts normally at the border of a fragment, whereas the tumor center becomes necrotic and is infiltrated by fibroblasts. After a few weeks—and sometimes months—the viable cancer cells proliferate and the total tumor mass contains vital tumor cells. The stroma, which starts to be organized, depending on the histology, e.g., adenocarcinomas, forms macro- and micro-glands, and squamous cell carcinomas form typical lobules. Breast cancers can either show a solid growth pattern or more glandular structures. Comparing the PDX at different passages, the histology is very similar. The heterogeneity is well preserved. Also typical products like mucus in adeno cancers, keratinization in squamous cell carcinomas, or cysts in bladder cancers can be found. The degree of differentiation changes in serial passages in about 10% of the various PDX. The tumor heterogeneity is in general well preserved in serial passage.

The tumors normally grow as a solid nodule and in most cases with an irregular surface. Sometimes the solid tumor is surrounded by fibrous tissue resembling a pseudo-capsule. Other tumors show a very aggressive behavior infiltrating into the thoracic muscles or into the subcutaneous fat tissue.

Metastases of PDX are very rare after subcutaneous implantation into nude mice. I observed a few cases of lung metastases after several months. Probably the residual immune response and mainly the macrophages of the lung prevent the outgrowth of individual cancer cells to macro-metastases in the lung. A high metastases rate in the bone, liver, etc. was observed by avoiding the passage through the lung capillaries by injection into the left heart ventricle (Shoemaker personal communication 1992).

Another major biological difference between the PDX and the donor tumor is that the tumor stroma is replaced by murine stroma already in the first passage. The tumor cells produce growth factors promoting the growth of fibroblasts as well as a formation of murine capillaries and later on blood vessels.

For the immunotherapy studies, the PDX growing in the nude mice is not a suitable model system since the nude mouse lacks T lymphocytes although natural killer cells and macrophages are present in large numbers.

## Tumor Models Available in 1991

Since it is not possible logistically and financially, to maintain all tumors in vivo in a tumor bank and not all PDX have optimal growth behavior in serial passage, a panel of PDX was selected for therapeutic and biological studies. The goal was to maintain the heterogeneity corresponding to the clinic. Therefore, fast as well as very slowly growing models with different degrees of histology and responsiveness to chemotherapy were selected. In 1991 264 PDX were selected from which 60 were always maintained in the tumor bank in vivo, allowing initiation of therapeutic studies immediately (Tables 3.4 and 3.5) [69].

**Table 3.4** PDX selected as tumor models in nude mice in 1991 and in 2017

Tumor category	Total 1991	Histology cancer	Med. Doubling time [days]	Frozen in N2 take <sup>a</sup> / total	Response/ total <sup>b</sup>	Total 2017 <sup>c</sup>
Lung	20	Adeno	6–19	17/18	3/5	43
Lung	38	Epidermoid	4–18	21/25	7/18	25
Lung	12	Large cell	4–16	12/14	1/3	10
Lung	7	Small cell	6–14	9/12	6/7	9
Colorectal	54	Adeno	4–24	42/44	2/20	70
Pancreas	3	Adeno	6–14	3/3	1/3	47
Stomach	14	Adeno	6–17	14/18	6/13	36
Renal	16	Hypernephrom	7–18	10/11	0/7	35
Melanomas	24	Melanoma	4–23	13/14	1/10	27
Mammary	8	Adeno and solid	8–20	8/9	6/8	18
Ovary	6	Adeno	6–22	5/5	4/5	16
Brain	2	Glioblastoma	5–12	2/2	1/2	11
Sarcoma soft-tissue	17	Miscellaneous	3–16	14/15	3/6	10
Head and neck	7	Squamous	4–15	6/6	3/5	10
Pleuramesotheliomas	6	Mesothelioma	5–16	5/5	0/2	10
Bladder	8	Transitional	4–16	8/8	2/4	10
Liver	4	Hepato and cholangio	5–12	4/4	1/2	10
Uterus cervix and corpus	3	Epidemoid and adeno	5–12	3/3	1/2	6
Sarcoma osteo	4	Osteo	6–15	4/4	1/2	4
Thyroid		Miscellaneous				4
Testis	6	Terato and embryonal	6–16	3/3	4/4	3
GIST		Gastrointestinal stroma				2
Anal		Squamous				2
Prostate <sup>d</sup>	3	Adeno	9–18	0/3	1/3	1
Esophageal	2	Squamous	5–9	2/2	0/0	1
Skin		Squamous				1
Acute leukemias		AML and ALL				7
Lymphoma		Non-hodgkin				7
Total	264		3–24	200/223 90%	54/121 45%	435

For histology, doubling time, regrowth and response data from 1991 are shown

<sup>a</sup>Regrowth freezing down tumor fragments

<sup>b</sup>6–12 cytotoxic anticancer agents tested in each PDX

<sup>c</sup>According Oncotest compendium 2017

<sup>d</sup>All 3 prostate PDX showed no regrowth after being frozen, lost after up to 66 in-vivo passages

**Table 3.5** PDX models grown continuously as in vivo models in nude mice since 1991

Tumor origin	Total	Histology carcinoma	Doubling time (days)	Frozen in N <sub>2</sub> take/total
Colorectal	6	Adeno	4–24	6/6
Gastric	6	Adeno	6–17	6/6
Lung	4	Adeno	6–19	4/4
	4	Squamous cell	4–18	4/4
	2	Large cell	4–16	2/2
	5	Small cell	6–14	5/5
Breast	6	Adeno/solid	8–20	6/6
Melanoma	6	Melanotic/amelanotic	4–23	6/6
Renal	6	Hypernephroma	7–18	6/6
Ovary	5	Adeno	6–22	5/5
Testis	4	Embryonal/terato	6–16	4/4
Miscellaneous	6	Miscellaneous	3–19	6/6
<i>Total</i>	<i>60</i>		<i>3–24</i>	<i>60/60</i>

### Comparison of Drug Response of the Tumor Growing in the Nude Mouse and in the Patient

Fifty comparisons were performed in 1983 [70], and a total of 80 comparisons was published in 1988 [71]. Fifty-five patients were treated with established combinations (43 cases) or with single-agent chemotherapy (37 cases) which were the established standard-of-care therapy of that time. After progression under the initial therapy, a second-line therapy was administered in 25 cases. In the nude mouse, two treatment cycles were given; the patients were treated until progression.

### Experimental Design of Testing

Testing was performed in serial passage, usually between passages 2 and 6, when the tumor growth became constant. Mice were randomized after 3–6 weeks when the average diameters were 8 mm. Tumors with a yellow color, indicating a higher amount of fibrous tissue, were excluded. Using these criteria, spontaneous regression or stationary growth behavior in the untreated control group was never observed after 3–4 weeks, meaning that the model has a reliable growth for in evaluating partial and complete remissions.

### Chemotherapy

Patient follow-up and evaluation of tumor response were performed as in clinical trials. In the nude mouse, the treatment regimen corresponded to clinical schedules

**Table 3.6** Maximum tolerable dose schedules of anticancer drugs in tumor-bearing nude mice

Drug	Dose (mg/kg/day)	Schedule (day)	Route	Day 14		Day 28	
				Death/total	%	Death/total	%
ACNU	20	1	ip	16/134	12	24/134	18
Adriamycin	8	1, 15	iv	22/267	8	58/260	22
CCNU	20	1	ip	33/197	17	50/217	23
Cisplatin	6.4	1, 15	sc	13/143	9	32/143	22
Cyclophosphamide	8	1, 15	sc	19/98	19	30/98	31
DTIC	80	1–4, 15–18	ip	1/50	2	8/50	16
	300–350	1, 15	ip	5/53	9	11/53	21
Etoposid	24	1–3, 15–17	sc	17/123	14	23/123	19
Fluorouracil	40	1–4, 15–18	ip	4/32	13	7/32	22
Mitomycin -C	2	1, 15	iv	15/168	9	48/179	27
Vindesine	1.5	1, 8, 15	iv	15/299	5	33/294	11

with the exception that treatment in mice was repeated usually after 2 weeks and only two treatment cycles were given. Drugs, doses, schedules, and route of administration are shown in Table 3.6. The dose around the LD<sub>20</sub> after 14 days and around the LD<sub>20</sub> after 28 days was considered to be the maximum tolerable dose in nude mice. In combination therapy, 70–80% of the dose of the single agents was given in 2-drug combinations and 50–60% in 3-drug combinations.

## Evaluation Parameters for Tumor Response

The tumors in nude mice were evaluated after maximum tumor regression or after 3–4 weeks in non-regressing tumors in treated compared to control mice. The effect of treatment was classified in the xenograft system and in the patient as *remission* (product of two diameters < 50% of initial value), *minimal regression* (51–75 %), *no change* (76–124 %), and *progression* ( $\geq 125\%$ ). All patients had measurable lesions. Evaluation was usually performed after two treatment cycles or after maximal regression.

## Comparison of Tumor Response

The 55 tumors allowed 80 comparisons between tumor response in nude mice and in the patient. Twenty-four comparisons were carried out in colorectal cancers usually with single-drug chemotherapy with 5-FU or a nitrosourea or a combination. Most of the other tumors were treated with combination therapy. Mammary cancers



were initially treated with tamoxifen and after progression with the combination of cyclophosphamide, methotrexate, and 5-FU. Stomach cancers were treated with the FAM combination (5-FU + adriamycin + mitomycin) and small cell lung cancers with the ACO combination (adriamycin + vincristine + cyclophosphamide) and after progression with cisplatin + VP16.

Table 3.7 shows the overall results. A total of 21 patients went into a remission corresponding to 19 cases in the nude mice. Fifty-nine patients did not respond to the treatment. The same result was obtained in 57/59 cases in the nude mouse. Overall xenografts gave correct predictions for tumor resistance in 97% and for tumor remission in 90%.

Combination chemotherapy was more successful than single-agent chemotherapy. Out of 43 combinations given, 16 (37%) effected a remission in the patients. After single-agent therapy, a remission was obtained in five out of 35

**Table 3.7** Comparison of tumor response in nude mice and in the patient

Mouse	Patient	Total
Remission	Remission	19
No remission	Remission	2
No remission	No remission	57
Remission	No remission	2

Eighty comparisons were obtained in 55 tumors. Xenografts gave a correct prediction for resistance in 57/59 (97%) and for remission in 19/21 (90%)

**Table 3.8a** Comparison of tumor response of human stomach cancers in nude mice and in the patient ( $n = 9$ )

Stomach cancers	Evaluation parameter metastases of	Therapy	Effect	
			Nude mice	Patient
GXF 97	recurrent tumor	FAM	PR	PR
	CEA	CCNU	PR	PR
GXF 180	Liver	FU + BCNU	PR	P
		MITO	NC	NC
		VIND	PR	P
GXF 209	Recurrent tumor, LN	FAM	PR	PR
GXF 236	Recurrent tumor, LN	FAM	P	P
GXF 281	Lymph nodes	FAM	PR	PR
GXF 324	Recurrent tumor, LN	FAM	P	P

FAM 5-FU + adriamycin + mitomycin-C; VIND vindesine; LN lymph node; PR partial response; P progression; NC no change

**Table 3.8b** Comparison of tumor response of human lung cancers in nude mice and in the patient ( $n = 8$ )

Lung cancers	Histology of the carcinomas	Evaluation parameter metastases of	Therapy	Effect	
				Nude mice	Patient
LXFE 66	Epidermoid	Bone, skin	VIND + PLAT	P	P
			CY + CCNU	P	P
LXFE 128	Epidermoid	Bone, skin	MACC-Comb.	P	P
LXFE 247	Epidermoid	Lung, skin	VIND + PLAT	P	P
			VP-16	P	P
LXFA 331	Adeno	Lung, skin	HECNU	P	P
LXFS 177	Small cell	Lymph node	ACO-Comb.	PR	PR
			VP-16 + PLAT	PR	PR

VIND vindesine, MACC-comb MTX + Adriamycin + CY + CCNU, ACO-comb, Adriamycin + CY + VCR, PR partial remission, P progression

(14 %). Examples of the therapies given are shown for stomach and lung cancers in Tables 3.8a and 3.8b, respectively [72].

### Potential of the Nude Mouse System as a Predictive Assay

During the clinical career of the author, great efforts were made to obtain a large number of treatment comparisons. Approximately two-thirds of the tumors were obtained during surgery of the primary tumor with no immediate need to treat the patient with chemotherapy. All efforts were made in order to obtain the testing result in the nude mouse before the patient required treatment. PDX from passages 2–6 were used for the tests. The treatment results became available at the earliest 4 months after surgery for rapidly growing tumors and 1.5 years after surgery in cases of very slow growing tumors [71, 72].

The PDX test results were available before the patient needed chemotherapy in 28 cases. In 18 cases the tumor was treated simultaneously in the nude mouse and in the patient, and in 34 cases the patients were treated first (Table 3.9). The conclusion is that PDX do not have practical significance in determining the patient's treatment [68, 69, 73]. Major limitations are the duration of testing, requiring serial passage, the overall take rate of about 40% (today using NOD-SCID mice, the take rate is approximately 70% and the growth is still very low in some tumor types, e.g., breast and prostatic cancers. In addition, nude mice are very expensive.

In order to overcome these limitations, Fiebig et al. performed chemosensitivity tests in vitro using the clonogenic assay with tumors after being established in the nude mouse [74].

**Table 3.9** Availability of test results in the PDX for patient therapy

Study	No.	%
Prospective <sup>a</sup>	28	35
Simultaneous	18	22.5
Retrospective <sup>b</sup>	34	42.5
Total	80	

<sup>a</sup>Test result from PDX available before patient needed chemotherapy

<sup>b</sup>Patient treated first

## Tumor Clonogenic Assay as a 3D Culture System to Preselect Sensitive Models

The PDX models have the advantage that they grow in 3D culture systems in semi-solid media e.g. in 0.3 – 0.5% agar. Early experience of Fiebig's group goes back to the 1980s [75]. We published the growth of PDX, five murine models, and also human hematopoietic stem cells in 1986 [76]. With more experience, the growth rate for PDX growing in serial passage increased from 20 to 86% using 35 mm Petri dishes. The plating efficiency (number of colonies/number of seeded tumor cells) was low around 0.07% which was similar as observed by others using fresh patient tumors. Human bone marrow stimulated with placenta-conditioned media allowed the growth of granulocyte stem cell colonies (CFU-C). The median plating efficiency was very similar to PDX specimens, 0.08%. The murine leukemia's L1210 and P388 as well as the B16 melanoma, colon carcinoma 38, and the Lewis lung carcinoma grew very well in vitro. The plating efficiency of the murine leukemias and solid tumors was more than 10 times higher compared to PDX specimens (Table 3.10) [77].

Over the years better growth results were obtained with better growth media; the median plating efficiencies increased to 0.37% in the period of 1996–2003 compared with 0.07% during 1985–1987. This improvement allowed the use of 24 multiwell plates with a well diameter of 16 mm [76]. This enabled broader testing's of new experimental drugs and smaller tumor biopsies for patient-oriented sensitivity testing.

In order to validate the clonogenic assay, tumor cells from PDX in low passage were investigated against 13 established drugs and compared to the same drug in vivo in the nude mouse. Sixty-two retrospective correlations were carried out. The clonogenic assay predicted correctly for response in 16/27 (59%) and for resistance in 32/35 cases (91%). These correlations were similar as observed for fresh solid tumors [74]. Stringent quality control parameters were introduced by Berger et al. [78] in order to standardize evaluation of individual experiments and to increase reliability, which was achieved.

Starting in 2008, we were able to run the clonogenic assay in 96 well multiwell plates and introduced broader testing series in 200 PDX. In this way, phase II pre-clinical studies were carried out in order to identify target tumors for clinical phase

**Table 3.10** Growth of human and murine tumors as well as bone marrow in the clonogenic assay in vitro

Origin	Designation	Period	Cells seeded (10E3/mL) <sup>a</sup>	Median	
				Colony number <sup>a</sup>	PE (%) <sup>b</sup>
Human	Different tumors <sup>c</sup>	1996–2003	80–600	112–423	0.37
		1985–1987	200–500	140–350	0.07
Human	Hematopoietic stem cells	2002–2003	42	77	0.18
		1985–1987	300	240	0.08
Mouse	L1210 leukemia	1986–1987	2	640	32
	P388 leukemia		2	240	12
	B16 melanoma		50	650	1.3
	Co38 colon carcinoma		80	624	0.78
	Lewis lung carcinoma		500	300	0.06

<sup>a</sup>Range per year; 1985–1987 cultivated in 35 mm dishes; 1996–2003 cultivated in 16 mm dishes (24 well cell culture microplates); since 2008 cultivated in 96 well plates

<sup>b</sup>Plating efficiency (%); number of colonies/number of vital cells plated  $\times$  100

<sup>c</sup>Derived from xenografts cultivated on nude mice; more than 250 tumors included [77]

II studies. A database of registered agents and also of investigational drugs with known mechanism was established, and with our COMPARE program, we were able to elucidate or to confirm the mechanism of action of novel compounds.

A further application was the search for biomarkers when we had characterized most of the PDX models, in the 1990s for individual oncogene and growth factors, since 2000 a comprehensive molecular characterization was carried out. See Sect. Vuaroqueaux et al. in this book.

## PDX as a Valuable Model System for Tumor Biology Studies

Besides developing anticancer agents, PDX models were very useful for tumor biology studies. The radiosensitivity of PDX was investigated by Hinkelbein et al. [79, 80] in vitro and in vivo and also the combination of radio- and chemotherapy. Different fractionations were studied [80]. Neumann investigated the effects of chemotherapy in combination with hyperthermia in the clonogenic assay in vitro [81, 82], and Wittekind analysed the differentiation of testicular cancers in nude mice. Early in the 1990s, Berger studied the regulation of proliferation by EGF signaling [83] and vascularization by the VEGF [84].

About 10% of PDX cause cachexia in the nude mouse, mainly when tumor burden is high especially by growing two tumors per mouse. Baumgarten studied the molecular mechanism by which the human tumor cells induce body weight loss in the nude mouse. Several cytokines and also hypercalcemia mediated by the parathormone-like peptide were found [85]. The PDX collection was also transferred to tissue microarrays and proteins like HSP90 and angiogenesis-related factors were determined [61, 86, 87].

---

## Combined In Vitro and In Vivo Testing Procedure

Already in the mid-1980s, it was evident that the best use of PDX in anticancer drug testing would be a combined in vitro/in vivo evaluation: the clonogenic assay as a prescreen and the subsequent selection of sensitive models for in vivo studies. Details of the strategy were published in [88], and the tumor models used were described in 1992 [67–69]. This testing strategy, together with the PDX collection, found broad interest and was the basis for collaborative programs with the NCI and the EORTC and for contract research projects from the pharma and biotech industry.

---

## In Vitro and In Vivo Evaluation of Anticancer Agents from a German Drug Development Program, the EORTC and the NCI

Several academic collaborative programs have been carried out from 1980 to 1988 for the German Anticancer Drug Development program which were funded by the German Ministry of Research and Technology. A number of novel nitrosoureas (HECNU) from Eisenbrand et al. [89], platinum derivatives (lobaplatin) from ASTA Medica [90], and numerous compounds from academia were tested. A grant from the NCI from 1985 to 1998 allowed testing of 40 compounds that were in clinical development at the time [91, 92]. Within the EORTC collaboration via the New Drug Development Office, many of the compounds entering clinical trials of the 1990s [93] were studied in Freiburg.

---

## The Concept of Preclinical In Vivo Phase II Studies

Besides the Freiburg group, a number of laboratories in Europe have developed numerous PDX early in the 1990s. Mainly within the EORTC SPG and PAMM groups, a concept was introduced to run multicenter preclinical in vivo studies to identify the tumors for subsequent clinical phase II studies. In vivo studies were carried out in more than 40 PDX selected from different laboratories. These efforts were coordinated by the NDDO [94, 95]. A number of compounds such as novel vinca alkaloids [96], rhizoxin derivatives [97], EO9 [98], or trabectedin [99] were evaluated in the SPG framework, in which Freiburg participated.

In Freiburg also monocenter phase II studies were performed, e.g., the nitrosourea HECNU, mitomycin-C [100], as well as hepsulfan and busulfan [101–103].

---

## Molecular Characterization of the PDX Panel

At the end of the 1980s, the 60 PDX panel used for evaluating cytotoxic and target-directed agents was further characterized [68] and compared when ever possible to the donor tumor. A number of markers such as CEA, NSE, EGFR, hormone receptors, DNA diploidy, as well as chemosensitivity in vitro and in vivo were

investigated. In addition, many oncogenes, tumor suppressor genes, and components of signal transduction were studied.

A major step forward was the advances in high throughput molecular characterization techniques since 2000. Already in 2003 Oncotest initiated a systematic molecular characterization program of PDX. Gene expression profiles were generated with affymetrix HG-U133 plus 2.0 microarrays. Gene copy number variations were investigated with affymetrix SNP6 arrays. Mutations, chromosomal aberrations and gene fusions were determined with the sequenom mass arrays and in recent years with whole exome sequencing and RNAseq. Today, up to 95% of the 450 PDX models are fully characterized. In parallel, a database was developed linking molecular with activity data of known and novel anticancer agents. This database is used for selecting tumor models with the desired target profile and for testing biomarker hypothesis. The molecular data were also extensively used to compare characteristics of tumor models with those of patient tumors. For example, the most frequent mutations were observed for TP53 in 53%, followed by K-ras in 32%, PI3K in 13%, and B-raf in 11% (mainly in melanomas and colon cancers). Details of the characterization are shown in Chap. 7 by Vuaroqueaux et al.

These molecularly characterized PDX models and the potential of biomarker discovery were the basis of strong business development of Oncotest from 2004 to 2012.

---

## Bevacizumab as an Example of the Development of a Predictive Gene Signature

The identification of biomarkers or gene signatures predicting the tumor response to novel targeted and eventually cytotoxic agents will allow individualization of anti-cancer therapy. The EMA and the FDA strongly recommend developing companion diagnostic assays. We investigated the hypothesis that correlating drug response with gene expression in PDX would enable identification of gene signatures which can predict drug response of individual PDX and also for the clinic. The signatures were validated by the leave-one-out cross-validation (LOOCV) in the training set and whenever possible in an independent data set. For Bevacizumab and Cetuximab a retrospective clinical study could be carried out.

When the clinical potential of the VEGFR inhibitor bevacizumab became evident in 2004 we carried out a broad in vivo study in PDX with the support of a grant obtained from the German Ministry of Research & Technology. Seventy-two PDX were treated in vivo with bevacizumab in cancers of the kidney, colon, breast and non-small cell lung, tumor types for which bevacizumab was registered later on. Bevacizumab was administered iv in three weekly injections, starting when the tumors had reached a volume of approximately 100 mm<sup>3</sup>. The cutoff for activity was defined as a T/C 34%. 29% (21/72) of all tumors were sensitive, 12/34 NSCLC, 4/18 colon, 3/10 breast, and 2/10 renal cancers. Long-lasting stable disease (no change) was observed, but no tumor regressions [104]. By randomization, 47/72 PDX were allocated to the training and 25 to an independent validation set. A gene signature of 35 genes was identified of which 21 genes were associated with angiogenesis [105]. The signature was validated with LOOCV in the training set and in the independent set (Figs. 3.3 and 3.4). The number of predicted responders

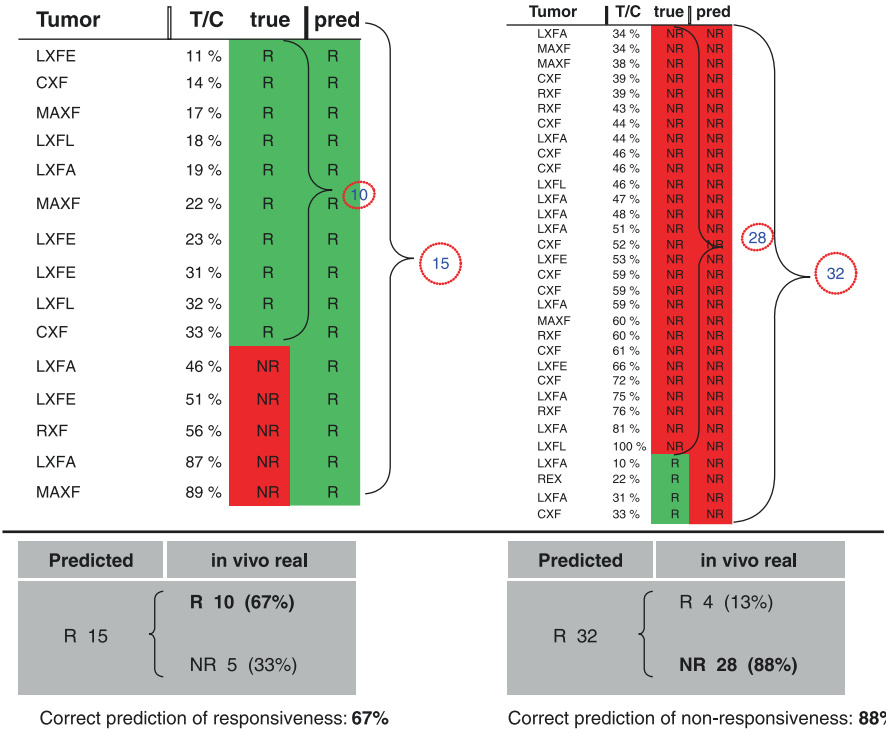
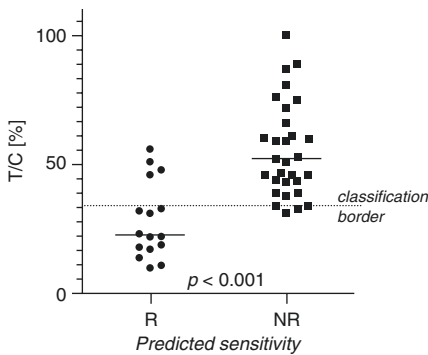


**Fig. 3.3** Validation by leave-one-out cross-validation (LOOCV)

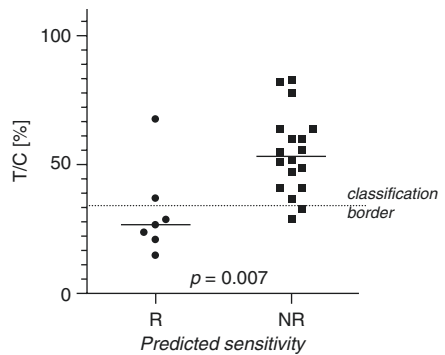
- Leave-one-out cross validation of the training set:  $n = 47$  tumors.



- Median opt. T/C values of predicted tumors

- responsive (R): 22.5 %
- non-responsive (NR): 52.0 %
- 2.3-fold difference,  $p < 0.001$

- Prediction of sensitivity of an independent validation set:  $n = 25$  tumors.



- Median opt. T/C values of predicted tumors

- responsive (R): 27.0 %
- non-responsive (NR): 53.5 %
- 2-fold difference,  $p = 0.007$

**Fig. 3.4** Predicted versus real activity of bevacizumab in LOOCV in the training and independent data set

increased from 30% of the random testings to 67% in the predicted group. From the predicted 32 nonresponders, 28 (88%) were resistant in actual testing. In the independent testing set (25 PDX), the correct prediction rate was 71% for predicted responders and 88% for nonresponders [106].

Figure 3.4 shows the T/C values (tumor volume of test/control) as a measure for activity for the predicted responder and nonresponder. In the training set the median T/C was 22.5% for the predicted responder, compared to 52% ( $p < 0.001$ ) for the nonresponder. In the independent data set, the predicted responders were also more sensitive than the predicted non-responders, T/C were 27 vs. 53.5%, respectively ( $p = 0.007$ ).

The procedure and the signature were patented in 2005, the patents were granted in the USA and in Europe (11/911, 222 and EP 1 869 216 B1, respectively). We tried to interest Genentech and Roche the owner of bevacizumab to license in the patent. Despite the high clinical potential, Genentech and Roche were not interested to license the signature. The main reason was financially, not to decrease revenue by limiting the number of patients which can be treated.

The determination of the 35 genes was optimized, and it was possible to determine the genes by QRT-PCR from fresh frozen and later from FFPE sections from PDX [107] as well as for patient tumors which were in most cases available in the Institutes for Pathology.

In this way, we organized a retrospective clinical study in metastatic colorectal cancer patients who were treated at the Department of Internal Medicine of the University of Freiburg. Sixty patients received the FOLFIRI combination together with bevacizumab. We were able to obtain all data and the corresponding tumor sections from 49 patients. Based on the gene signature, the patients were predicted as responder and nonresponder, and the time to progression was compared. The time to progression of the predicted responder was 16 months compared to 10 months for the predicted nonresponder. Due to the small sample, the difference was not significant. Therefore, a trend with this signature was evident, but the difference was not statistically significant [108]. Of interest the study also revealed that part of the genes forming the gene signature were associated with patient outcome when evaluated individually.

For cetuximab, a predictive signature consisting of 26 genes was also obtained and validated by the LOCCV and by a retrospective clinical study. The published clinical outcome of a phase II study of cetuximab in refractory colorectal cancers and the corresponding gene expression data could be downloaded for each patient [109]. By using the gene expression profiles of this patient cohort, we showed that the predicted responder had a progression-free survival (PFS) of 120 days compared to 59 days for the predicted non-responder [110].

We also evaluated the available activity data of 11 cytotoxic agents in vivo in PDX and compared them with the gene expression profiles [111, 112]. The median cutoff for sensitivity for all drugs was a T/C value of 25%, the range was 11–49%. Using these criteria, on average one-third of the PDX were responders and two-thirds were nonresponders. The bioinformatic analysis yielded predictive gene signatures consisting of 42–129 genes (mean 87). On average, the response rate for the predicted



responders (83%) was 2.45-fold higher than that for all PDX (random testing 34%). Conversely, of the predicted non-responders 94% proved to be nonresponders in the nude mouse. Beyond the LOOCV in the training set, no further validation in independent sets was carried out. Therefore it is unclear if the signature determined only by bioinformatic tools is able to increase the response rate or predict resistance in other sets of PDX and in a clinical trial. At the present time, the majority of cytotoxic agents are generics; there was no interest from pharma industry to sponsor such studies.

## PDX for the Identification of Targeted Therapy, Example: B-raf- Inhibitor Vemurafenib

In the last decade mainly targeted compounds have been selected for clinical trials, and more than ten tyrosine-kinase inhibitors have been registered. Most of them showed a very selective activity in tumor models which over expressed or had a mutated critical target. For example, the B-raf inhibitor vemurafenib is only active in melanomas bearing the V600E mutation. In the clonogenic assay, vemurafenib was active only in V600E-mutated PDX. The  $IC_{70}$  of the sensitive melanomas was about 10 times lesser compared to the mean  $IC_{70}$  of all 67 PDX studied (Fig. 3.5). The in vitro activity was also confirmed by PDX studies in vivo.

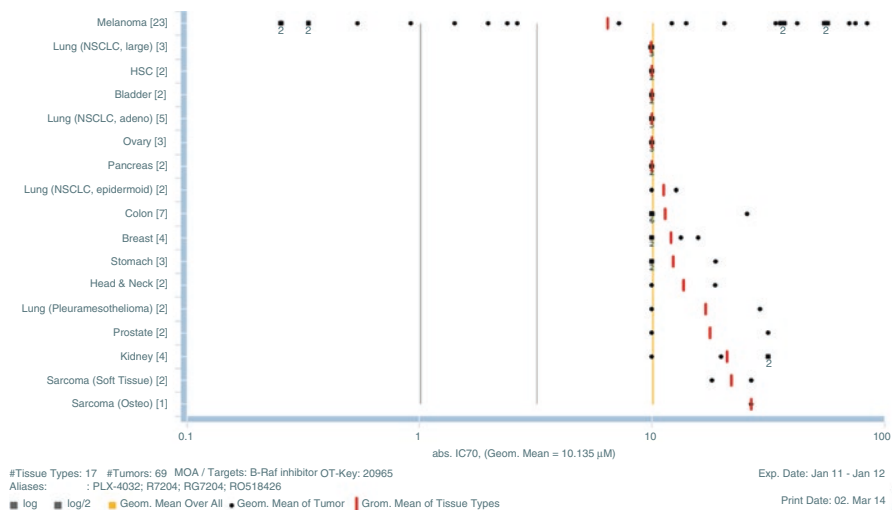


**Fig. 3.5** Efficacy of vemurafenib in the clonogenic assay determined by in-vitro image analysis as read-out in 24 well plates

## Outlook

### PDX for Anticancer Drug Development

Today PDX is considered as the most relevant experimental model system for developing targeted and cytotoxic agents [113]. The high predictivity was confirmed by many groups. Of course if compounds show a different metabolism and pharmacokinetic in mouse and man, false-positive or false-negative predictions may be obtained.

For novel targeted agents registered in combination with cytotoxic agents, synergism was also demonstrated in PDX models. Better understanding of the molecular factors driving the growth of tumors and also the mechanism leading to resistance allow an improved selection of targets and respective inhibitors. Also mechanisms responsible for tumor resistance and the activation of alternative pathways are better understood. This allows development of novel inhibitors active against these secondary resistant tumors.

### PDX for Patient-Oriented Sensitivity Testing

In the last 5 years, transplantation of patient tumors into SCID or NOD-SCID mice were proposed mainly by Hidalgo et al. to predict the sensitivity of patient tumors and to guide the therapy for the patient. For this procedure the term “avatar” was introduced [113, 114]. The concept was also promoted very aggressively in the lay press [115], and high expectations were raised. In addition the patients were charged large amounts of money for testing standard drugs and drugs in clinical development. Today with the use of more immunosuppressed scid and NOD-scid mice compared to nude mice the take rates of tumors from patients are somewhat higher. However, in patients with metastatic disease, therapy is required immediately and they cannot wait until his/her PDX is in passages 3–5 when testing is possible for less than 60% of the patients, depending also on the tumor type. The time factor of 4–15 months clearly shows the limits for the patient benefit. An overview of the value of this procedure was published recently [116].

Thirty years ago we, in Freiburg, have already addressed the question of treating the patient’s tumor in the nude mouse (see Sect. “Potential of the Nude Mouse System as a Predictive Assay”) and concluded that less than 30% of the patients will benefit from the testing [71, 72]. Today molecular profiling of patient tumors, including WES, provides data within weeks and allows complete information about genetic abnormalities to guide and to individualize therapy.

For targeted agents this approach resulted in convincing clinical data, e.g., in melanomas with B-raf inhibitors, NSCL cancers with EGF pathway activation as well as ALK translocations, and in HER-2-positive breast cancers. For classic cytotoxic agents which are mainly administered in combination therapy, there is, however, still a need to determine the a molecular basis of predictors of drug response or resistance. Gene signatures including a larger number of genes from different pathways or a combination of mutations, amplifications, and translocation may be beneficial.

## Summary

In Freiburg, we have implanted more than 2800 human tumors during the last 35 years, and about 450 PDX have been established as tumor models for all major solid tumor types. Two hundred fifty were characterized for their sensitivity against standard agent's in vivo. Their molecular profile is available for gene expression, WES, mutations, and DNA-copy-number variations. Determination of gene signatures predictive for drug response has been carried out.

The response of PDX to standard cytotoxic agents in comparison to the patient tumor was very similar; in sensitive tumors identical results were found in 92% and for resistant tumors in 97%. PDXs retain most of the molecular and pathophysiological characteristics of the patient tumor. They are suitable models to study agents with cytotoxic and targeted mechanism of action.

Many anticancer agents being developed and registered by Pharma and Biotech companies were evaluated in Freiburg, mostly in a combined in vitro/in vivo approach. Since the 1980s, Freiburg was the pioneer in offering PDX for anticancer drug evaluation. In the meantime PDX were more and more accepted, xenograft models were developed in other laboratories, and in the last 10 years, several companies were established in Europe, the USA, and China offering services to perform contract research.

**Acknowledgments** Numerous scientists and technicians have contributed over 35 years to the research summarized in this chapter. I thank mainly Dietmar Berger, Angelika Burger (deceased in 2011), Thomas Metz, Florian Schmidt, and Vincent Vuaroqueaux for their conceptual contributions. This research was supported by grants from the German Ministry of Research and Technology; the National Cancer Institute, Bethesda; and the NDDO of the EORTC and in recent years by a number of contracts from the European Community.

---

## References

1. Isaacson HJ, Cattanach BM. Report. *Mouse News Letter*. 1962;27:31.
2. Flanagan SP. "Nude", a new hairless gene with pleiotropic effects in the mouse. *Genet Res*. 1966;8:295–309.
3. Green MC. Genetic variants and strains of the laboratory mouse. In: Bastert G, Fortmeyer HP, Schmitt-Matthiesen H, editors. *Thymus aplastic nude mice and rats in clinical oncology*. Stuttgart: Fischer; 1981. p. 174–5, 280–1.
4. Pantelouris EM. Absence of the thymus in a mouse mutant. *Nature*. 1968;217:370.
5. Rygaard J, Povlsen CO. Heterotransplantation of a human malignant tumor to the mouse mutant nude. *Acta Pathol Microbiol Scand*. 1969;77:758–66.
6. Sordat B, Tamaoki N, Povlsen CO. List of human tumors transplanted to nude mice. In: Nomura T, et al., editors. *Second international workshop on nude mice*. New York, Stuttgart: Fischer; 1977. p. 587–95.
7. Sordat B, Merenda C, Carrel S. Invasive growth and dissemination of human solid tumors and malignant cell lines grafted subcutaneously to new-born nude mice. In: Nomura T, et al., editors. *Proceedings of the second international workshop on nude mice*. New York, Stuttgart: Fischer; 1977. p. 313–26.
8. Giovanella BC, et al. Development of invasive tumors in the nude mouse after injection of cultured human melanoma cells. *J Natl Cancer Inst*. 1972;48:1531–3.

9. Giovanella BC, Stehlin JS. Assessment of the malignant potential of cultured cells by injection in nude mice. In: Rygaard J, Povlsen CO, editors. Proceedings of the first international workshop on nude mice. Stuttgart: Fischer; 1974. p. 279–84.
10. Povlsen CO, Rygaard J. Effects of cyclophosphamide (EndoxanR) on a Burkitt's lymphoma serially grown in nude mice. In: Rygaard J, Povlsen CO, editors. Proceedings of the first international workshop on nude mice. Stuttgart: Fischer; 1974. p. 285–92.
11. Povlsen CO, Jacobsen GK. Chemotherapy of a human malignant melanoma transplanted in nude mouse. *Cancer Res.* 1975;35:2790–6.
12. Rygaard J. Immunobiology of the mouse mutant "nude". Preliminary investigations. *Acta Pathol Microbiol Scand.* 1969;77:761–2.
13. Shaffer CF, Reed ND, Jutila JW. Comparative survival of skin grafts from several donor species on congenitally athymic mice. *Transplant Proc.* 1973;5:711–2.
14. Manning DD, Reed ND, Shaffer CF. Maintenance of skin xenografts of widely divergent phylogenetic origin on congenitally athymic (nude) mice. *J Exp Med.* 1973;138:488–94.
15. Rygaard J. Skin grafts in nude mice. Third fate of grafts from man and donors of other taxonomic classes. *Acta Pathol Microbiol Scand.* 1974;82:105–12.
16. Reed ND, Manning DD. Long term maintenance of normal human skin on congenitally athymic (nude) mice. *Proc Soc Exp Biol Med.* 1973;143:350.
17. Rygaard J, Friis CW. The husbandry of mice with congenitally absence of the thymus (nude mice). *Z Versuchstierkd.* 1974;16:1–10.
18. Rygaard J, Povlsen CO. Proceedings of the first international workshop on nude mice. Stuttgart: Fischer; 1974.
19. Nomura T, et al. Proceedings of the second international workshop on nude mice. Stuttgart: Fischer; 1978.
20. Sparrow S. Immunodeficient animals in cancer research. London: Macmillan; 1980.
21. Bastert G, Fortmeyer HP, Schmidt-Mathiesen H. Thymus aplastic nude mice and rats in clinical oncology. Stuttgart: Fischer; 1981.
22. Reed ND. Proceedings of the third international workshop on nude mice. Stuttgart: Fischer; 1982.
23. Prabhakaran K, Harris EB, Kirchheimer WF. Hairless mice, human leprosy and thymus-derived lymphocytes. *Experientia.* 1975;31:784.
24. Kohsaka K, et al. Nude mice as a model for chemotherapy of leprosy. In: Reed ND, editor. Proceedings of the third international workshop on nude mice. Stuttgart: Fischer; 1982. p. 59–66.
25. Armstrong D, Walzer P. Experimental infections in the nude mouse. In: Fogh J, Giovanella BC, editors. The nude mouse in experimental and clinical research. New York, San Francisco, London: Academic Press; 1978. p. 477–89.
26. Waki S, Suzuki M. A study of malaria immunobiology using nude mice. In: Nomura T, et al., editors. Proceedings of the second international workshop on nude mice. The potentialities and limitations of the nude mouse. New York, Stuttgart: Fischer; 1977. p. 37–44.
27. Waki S, Suzuki M. T-independent antibody production in nude mice infected with a rodent malaria parasite (*Plasmodium berghei*). In: Reed ND, editor. Proceedings of the first international workshop on nude mice. New York, Stuttgart: Fischer; 1982. p. 91–102.
28. Brooks BO, Reed ND. *Trypanosoma musculi* infections of nude mice. In: Reed ND, editor. Proceedings of the first international workshop on nude mice. New York, Stuttgart: Fischer; 1982. p. 111–22.
29. Jacobsen GK, Reed ND. The immune response of congenitally athymic (nude) mice to the intestinal nematode *Nippostrongylus brasiliensis*. *Proc Soc Exp Biol Med.* 1974;147:667.
30. Mitchell GF, Holmes MC. Nude mice in the study of susceptibility and response to infection with metazoan and protozoan parasites. In: Reed ND, editor. Proceedings of the first international workshop on nude mice. New York, Stuttgart: Fischer; 1981. p. 1–10.
31. Kamiya M, et al. Characteristic responses of nude mice in angiostrongyliasis and echinococcosis. In: Reed ND, editor. Proceedings of the first international workshop on nude mice. New York, Stuttgart: Fischer; 1982. p. 493–504.

32. Fortmeyer HP. Thymusaplastische Maus (nu/nu) - thymusaplastische Ratte (rnu/rnu) - Haltung, Zucht, Versuchsmodelle, vol. 8. Berlin: P. Parey; 1981.
33. Wortis HH, Nehlsen S, Owen JJ. Abnormal development of the thymus in "nude" mice. *J Exp Med.* 1971;134:681-92.
34. Cordier AC. Ciliogenesis and ciliary anomalies in the thymic cysts of "nude" mice. *Cell Tissue Res.* 1974; 148:397-406.
35. Groscurth P, Müntener M, Töndury G. The postnatal development of the thymus in the nude mouse. Light microscopic observations. In: Rygaard J, Povlsen CO, editors. Proceedings of the first international workshop on nude mice. New York, Stuttgart: Fischer; 1974. p. 31-6.
36. Hair J. The morphogenesis of thymus in nude and normal mice. Proceedings of the first international workshop on nude mice. Stuttgart: Fischer; 1974. p. 23-30.
37. Rychter Z, Holub M, Vanecek R. Topical and quantitative analysis of the thymus region in the nude mouse. *Folia Biol (Praha).* 1978;24:414-5.
38. Holub M, Rosmann P, Mandi B. The dysgenetic thymic complex of the nude mouse. *Fol Biol (Praha).* 1978;24:416-8.
39. Scheiff JM, Cordier A. Etude quantitative du thymus de la souris heterozygote pour le gene nu. *Bull Assoc Anat.* 1974;58:163.
40. Zipore BD, Trainin N. Defective capacity of bone marrow from nude mice to restore lethally irradiated recipients. *Blood.* 1973;42:671-8.
41. Holub M, et al. Lymphatic tissues and antibody-forming cells of athymic (nude) mice. *Z Immunitätsforsch Exp Klin Immunol.* 1974;146:322-33.
42. Dolenska S, Holub M, Mandi B. Bone marrow stem cell potential in mice earing the nu gene. *Folia Biol (Praha).* 1978;24:421-3.
43. Raff MC, Wortis HH. Thymus dependence of o-bearing cells in the peripheral lymphoid tissues of mice. *Immunology.* 1970;18:931-42.
44. Yunker VM, Gruntenko EV, Moroskova TS. Leucocyte blood composition in mice C3H/He Nu/Nu, C3H/He. *Fol Biol (Praha).* 1978;24:437.
45. Weihe WH. Effects of air velocity on hairless mice. *J Physiol Paris.* 1971;63:452.
46. Pantelouris EM, Lintern-Moore S. Physiological studies on the nude mouse. In: Fogh J, Giovanella BC, editors. The nude mouse in experimental and clinical research. New York, San Francisco, London: Academic Press; 1978. p. 51-73.
47. Fortmeyer HP, Bastert G. Breeding and maintenance of nu/nu mice and rnu/rnu rats. In: Bastert G, Fortmeyer HP, Schmidt-Matthiesen H, editors. Thymusaplastic nude mice and rats in clinical oncology. Stuttgart: Fischer; 1981. p. 25-38.
48. Loor F, Roelants GE. High frequency of T lineage lymphocytes in nude mouse spleen. *Nature.* 1974;251:229.
49. Loor F, Roelants GE. Immunofluorescence studies of a possible prethymic T-cell differentiation in congenitally athymic (nude) mice. *Ann N Y Acad Sci.* 1975;254:226-41.
50. Sato VL, Waksal SD, Herzenberg LA. Identification and separation of pre-T-cells from nu/nu mice. Differentiation by preculture with thymic reticuloepithelial cells. *Cell Immunol.* 1976;24:173-85.
51. Sprent J. Migration and lifespan of circulating B-lymphocytes. In: Rygaard J, Povlsen CO, editors. Proceedings of the first international workshop on nude mice. New York, Stuttgart: Fischer; 1974. p. 11-12.
52. Meerpohl HG, et al. Cytotoxic capacities of macrophages in nu/nu mice. In: Bastert G, Fortmeyer HP, Schmidt-Matthiesen H, editors. Stuttgart: Fischer; 1981. p. 57-62.
53. Luzzati AL, Jacobson EB. Serum immunoglobulin levels in nude mice. *Eur J Immunol.* 1972;2:473-4.
54. Salomon JC, Bazin H. Low levels of some serum immunoglobulin classes in nude mice. *Rev Eur Etud Clin Biol.* 1972;17:880-2.
55. Kindred B. Antibody response in genetically thymusless nude mice injected with normal thymus cells. *J Immunol.* 1971;107:1291-5.
56. Bloemmen J, Eyssen H. Immunoglobulin levels of sera of genetically thymusless (nude) mice. *Eur J Immunol.* 1973;3:117-8.

57. Jacobsen GK, Povlsen CO, Rygaard J. Effects of thymus grafts in nude mice transplanted with human malignant tumors. In: Reed ND, editor. Proceedings of the third international workshop on nude mice. New York, Stuttgart: Fischer; 1982. p. 493–504.
58. Fiebig HH. Wachstum und Chemotherapie menschlicher Tumoren - vorwiegend Dickdarm-, Magen- und Bronchialkarzinome - in der thymusaplastischen Nacktmaus. Habilitationsschrift, Universität Freiburg; 1983.
59. Berger DP. Proliferation and vascularization humaner solider Tumoren als Grundlage neuer Therapieansätze. Habilitationsschrift, Universität Freiburg; 1995.
60. Burger AM, et al. The G-quadruplex-interactive molecule BRACO-19 inhibits tumor growth, consistent with telomere targeting and interference with telomerase function. *Cancer Res.* 2005;65(4):1489–96.
61. Wirth GJ, et al. Microarrays of 41 human tumor cell lines for the characterization of new molecular targets: expression patterns of Cathepsin B and the transferrin receptor. *Oncology.* 2006;71:86–94.
62. Fiebig HH, Löhr GW. Transplantation of human sarcomas in nude mice and development of tumor models for chemotherapy. *Curr Chemother Immunother.* 1982. p. 1280–2.
63. Fiebig HH, Löhr GW. Wachstum menschlicher Malignome und Entwicklung von Tumormodellen in der thymusaplastischen Nacktmaus. *Med Welt.* 1984;35:52–8, 81–6.
64. Fiebig HH, et al. Biological characterization and chemotherapy of human colorectal, stomach and esophageal cancers growing in nude mice. In: Klein HO, editor. Advances in the chemotherapy of gastrointestinal cancer. Erlangen: Perimed Fachbuch; 1984. p. 53–73.
65. Fiebig HH, et al. Development and characterization of 51 human tumor models for large bowel, stomach and esophageal cancers. *Dig Surg.* 1984;1:225–35.
66. Fiebig HH, Neumann H, et al. Development of 3 human small cell lung cancer models in nude mice. *Recent Results Cancer Res.* 1985;97:77–86.
67. Berger DP, Fiebig HH, Winterhalter BR. Establishment and characterization of human tumor xenograft models in nude mice. In: Fiebig HH, Berger DP, editors. Immunodeficient mice in oncology. Basel: Karger; 1992. p. 23–46.
68. Fiebig HH, et al. Combined in vitro/in vivo test procedure with human tumor xenografts. In: Fiebig HH, Berger DP, editors. Immunodeficient mice in oncology. Basel: Karger; 1992. p. 321–51.
69. Fiebig HH, Dengler WA, Roth T. Human tumor xenografts: Predictivity, characterization and discovery of new anticancer agents. In: Fiebig HH, Burger AM, editors. Relevance of tumor models for anticancer drug development. *Contrib Oncol Basel:* Karger. 1999;54:29–50.
70. Fiebig HH, et al. Biological characterization and chemotherapy of human colorectal comparison of tumor response in nude mice and in the patients. *Behring Inst Mitt.* 1984;74:343–52.
71. Fiebig HH. Comparison of tumor response in nude mice and in the patients. In: Winograd B, Peckham MJ, Pinedo HM, editors. Human tumor xenografts in anticancer drug development. Berlin: Springer; 1988. p. 25–30.
72. Fiebig HH, et al. Comparison of tumor response in nude mice and in the patients. *Behring Inst Mitt.* 1984;74:343–52.
73. Fiebig HH, Winterhalter BR, Scholz CC. Limited potential of the human tumor-nude mouse system for pretherapeutic drug testing. *Zeitschr Antimikrob Antineoplast Chemoth.* 1988;6(1):17–22.
74. Scholz CC, Fiebig HH, Winterhalter BR, Berger DP, Henss H. Correlation of drug response in patients and in the clonogenic assay using solid human tumor xenografts. *Eur J Cancer Clin Oncol.* 1990;26:901–5.
75. Henss H, et al. Clonal growth of human tumor xenografts, first experiences in drug testing. *J Cancer Res Clin Oncol.* 1984;108:233–5.
76. Fiebig HH, et al. Colony assay with human tumor xenografts, murine tumors and human bone marrow. Potential for anticancer drug development. *Eur J Cancer Clin Oncol.* 1987;23:937–48.
77. Fiebig HH, Maier A, Burger AM. Clonogenic assay with established human tumor xenografts: correlation of in vitro to in vivo activity as a basis for anticancer drug discovery. *Eur J Cancer.* 2004;40:802–20.

78. Berger DP, et al. The clonogenic assay with human tumor xenografts. Evaluation, predictive value and application for drug screening. *Ann Oncol.* 1990;1:333–41.
79. Hinkelbein W, et al. Intrinsic thermosensitivity of various human tumors. In: Hinkelbein W, et al., editors. *Preclinical hyperthermia*. Berlin: Springer; 1988;109:198–202.
80. Hinkelbein W, et al. Fractionated irradiation under ambient conditions of human NSCLC transplanted into nude mice. Effect of different fractionation schedules and of radiotherapy and vindesine. *Strahlenther Onkol.* 1989;165:519–20.
81. Neumann HA, Fiebig HH, Engelhardt R. Effect of hyperthermia at 40.5 °C and chemotherapy on various human tumors in vitro. *Recent Results Cancer Res.* 1988;109:224–38.
82. Yamada K, et al. Predicting the sensitivity of human cancers to combined chemotherapy and hyperthermia. *Recent Results Cancer Res.* 1988;109:250–7.
83. Berger DP, et al. Cytotoxicity of TGF- $\alpha$ -PE40 and correlation to expression of epidermal growth factor receptor. *Eur J Cancer.* 1995;31:2067–72.
84. Berger DP, et al. Vascular endothelial growth factor (VEGF) mRNA expression in human tumor models of different histologies. *Ann Oncol.* 1995;6:817–25.
85. Baumgarten AJ, Fiebig HH, Burger AM. Molecular analysis of xenograft models of human cancer cachexia—possibilities for therapeutic intervention. *Cancer Genomics Proteomics.* 2007;4:223–32.
86. Smith V, Wirth GJ, Fiebig HH, Burger AM. Tissue microarrays of human tumor xenografts: characterization of proteins involved in migration and angiogenesis for application in the development of targeted anticancer agents. *Cancer Genomics Proteomics.* 2008;5:263–74.
87. Schandelmaier K, et al. Expression of Hsp90 in a panel of human tumor explants and its relation to response to treatment with the Hsp90 inhibitor 17-AAG. *Cancer Res.* 2005;65(9):104.
88. Fiebig HH, et al. Combined in vitro/in vivo test procedure with human tumor xenografts for anticancer drug development. *Strahlenther Onkol.* 1989;165:22–52.
89. Eisenbrand G, et al. Drug design: nitrosoureas. IARC scientific publications. 1986. p. 281–94.
90. Fiebig HH, et al. Phase I clinical trial of Lobaplatin (D-19466) after intravenous bolus injection. *Onkologie.* 1994;17:142–8.
91. Fiebig HH, et al. In-vitro and in vivo evaluation of US-NCI compounds in human tumor xenografts. *Cancer Treat Rev.* 1990;17:109–17.
92. Berger DP, et al. Präklinische Prüfung von Hepsulfam, Ipomeanol, Oxantrazol, Penclomedin, Pyrazindiazohydroxid und Rapamycin auf antineoplastische Wirksamkeit. In: Zeller WJ, et al., editors. *Germering: W. Zuckschwerdt*; 1992. p. 167–84.
93. Hendriks HR, Berger DP, Fiebig HH. New anticancer drug development: interim results of the cooperative program between the Freiburg preclinical anticancer drug development group and the EORTC new drug development office. In: Arnold 3, Köpf-Maier P, Micheel B, editors. *Immunodeficient animals: Models for cancer research.* *Contrib Oncol.* 1996;51:108–14.
94. Boven E, et al. Phase II preclinical drug screening in human tumor xenografts: a European multicenter collaborative study. *Cancer Res.* 1992;52:5940–7.
95. Langdon SP, et al. Preclinical Phase II studies in human tumor xenografts: a European multicenter follow-up study. *Ann Oncol.* 1994;5:415–22.
96. Hendriks HR, et al. Comparative antitumor activity of Vinblastine-isoleucinate and related vinca alkaloids in human xenografts. *Eur J Cancer.* 1992;28A:767–73.
97. Hendriks HR, et al. Preclinical antitumor activity and animal toxicology studies of rhizoxin, a novel tubulin interacting agent. *Ann Oncol.* 1992;3(9):755–63.
98. Hendriks HR, Pizao PE, Berger DP, et al. E09, a novel bioreductive alkylating indoloquinone with preferential solid tumor activity and lack of bone marrow toxicity in preclinical models. *Eur J Cancer.* 1993;29(6):897–906.
99. Hendriks HR, et al. High antitumour activity of ET743 against human tumour xenografts from melanoma, non-small-cell lung and ovarian cancer. *Ann Oncol.* 1999;10:1233–40.
100. Fiebig HH, et al. Wirksamkeit von Mitomycin-C an 61 menschlichen, in der Nacktmaus wachsenden Tumoren. In: Nagel G, editor. *München: W. Zuckschwerdt*; 1986. vol. 28.

101. Berger DP, Winterhalter BR, Fiebig HH. Chemotherapy: conventional agents. In: Boven W, Winograd W, editors. *The nude mouse in oncology research*. Boca Raton: CRC Press; 1991. p. 165–84.
102. Berger DP, et al. Preclinical activity of Hepsulfam and Busulfan in solid human tumor xenografts and human bone marrow. *Anti-Cancer Drugs*. 1992;3:531–9.
103. Fiebig HH, Berger DP. Preclinical Phase II trials. In: Boven E, Winograd W, editors. *The nude mouse in oncology research*. Amsterdam: CRC Press; 1991. p. 317–26.
104. Fiebig HH, et al. Antitumor activity of Avastin in a panel of 100 patient derived tumor models in vivo in relation to proteomic biomarker profiles. *Mol Cancer Ther*. 2007:A28.
105. Fiebig HH, et al. Determination of a 35 gene signature predictive for the effectiveness of Bevacizumab. *Mol Cancer Ther*. 2007:B10.
106. Fiebig HH, Vuaroqueaux V, et al. Predictive gene signatures for Bevacizumab and Cetuximab as well as cytotoxic agents. *Int J Clin Pharmacol Ther*. 2012;50(1):70–1.
107. Vuaroqueaux V, et al. Identification of tumors responding to Bevacizumab by gene signature using a quantitative RT-PCR from FFPE tumors. *Cancer Res*. 2009;69(9):2567.
108. Promny I. Die Validierung der prädiktiven Marker für das Therapieansprechen auf Bevacizumab bei Patienten mit metastasiertem kolorektalen Karzinom. *Med Thesis*. University of Freiburg. 2011.
109. Khambata-Ford S, et al. Expression of epiregulin and amphiregulin and K-ras mutation status predict disease control in metastatic colorectal cancer patients treated with cetuximab. *J Clin Oncol*. 2007;25:3230–7.
110. Vuaroqueaux V, et al. Clinical validation of a gene expression based signature predicting response to Cetuximab treatment. In: 35th ESMO Congress, vol. 21. 2010.
111. Fiebig HH, et al. Gene signatures developed from patient tumor explants grown in nude mice to predict tumor response to 11 cytotoxic drugs. *Cancer Genomics Proteomics*. 2007;4:187–96.
112. Korrat A, et al. Gene signature-based prediction of tumor response to cyclophosphamide. *Cancer Genomics Proteomics*. 2007;4:187–96.
113. Hidalgo M, et al. A pilot clinical study of treatment guided by personalized tumor grafts in patients with advanced cancer. *Mol Cancer Ther*. 2011;10(8):1311–6.
114. Stebbing J, et al. Patient-derived xenograft models: an emerging platform for translational cancer research. *Cancer*. 2014;120(13):2006–15.
115. Pollack A. Seeking cures, patients enlist mice stand-ins. *Cancer Discov*. 2014:928–1013.
116. Scudellari M. My mighty mouse. Personal drug regimens based on xenograft mice harboring a single patient's tumor still need to prove their true utility medicine. *The Scientist*. 2015. p. 29.



---

# From Ectopic to Orthotopic Tumor Grafting Sites: Evidence for a Critical Role of the Host Tissue Microenvironment for the Actual Expression of the Malignant Phenotype

Bernard C.M. Sordat

*How to search for something whose nature remains unknown and, suppose that you discover it, how will you recognize it as the thing you were looking for?*

*Plato, Meno 80d, 380 B.C.*

*In memory of Jorgen Rygaard and Carl Povlsen  
Initiators to the field and friends*

---

## An Historical Account

From the initial and innovative 1969 report by Jorgen Rygaard and Carl Povlsen describing, for the first time, the heterotransplantation and successful growth of a human solid tumor, a surgical specimen from a colon carcinoma grafted within the subcutaneous space (s.c.) of immune-deficient athymic “nude” mice, it took about 12 years to move to additional and novel experimental grafting conditions which were presented to be more representative of the course and progression of tumors in humans and, potentially, more prone to provide a model with unbiased issues in targeted experimental therapeutic investigations. Following this seminal 1969 report [1] complemented in 1971 [2], abundant data were brought forward by many investigators along three “nude mice workshops” held in Scanticon (Denmark, October 1973) [3], Tokyo (October 1976), [4] and Bozeman (Montana, USA, September 1979) [5], respectively. They included a wealth of results obtained from tumor take and growth rates from a variety of s.c. grafted tumor types, either from *in vitro*

---

B.C.M. Sordat

Laboratory of Glycochemistry and Asymmetric Synthesis (LGSA, Prof. P. Vogel), Federal Institute of Technology, Lausanne, Switzerland  
e-mail: [bernard.sordat@epfl.ch](mailto:bernard.sordat@epfl.ch)

cultured cell lines [6, 7] or patient-derived tumor fragments, mostly carcinomas. It was generally accepted that grafted tumors maintained their original histopathological characteristics such as differentiation grade or expression of some biomarkers during tumor *in vivo* passaging. Attempts were then made to transfer the *nu* allele to standard inbred strains of mice, and a particular attention was taken to improve mice breeding and maintenance in specific pathogen-free (spf) conditions. In brief, the nude mouse became a popular research tool, and interest was rapidly growing to explore and define new robust working protocols for exploiting attractive potentialities of this model in experimental cancer therapeutics.

In the meantime, evidence rapidly accumulated that the subcutaneous (s.c.) space grafting site, later denominated ectopic (from the Greek *ektos*, outside, *topos*, site), proved to be not fully representative of the growth and behavior characteristics observed along the natural history of most human carcinomas: typically slow growing, generally and clinically late symptomatic, micro-/macro-invasive and expressing an overt or discrete metastatic phenotype. In nude mice or in immune-repressed animals (so-called B mice), s.c. solid tumor grafts, such as those from colorectal carcinomas, were found to adopt in most cases, and in contrast to the original patient malignant tumor, an expansive type of growth (designated as “pseudo-benign”) progressing as multi-nodular tumor masses and clearly restrained at graft borders lined by multilayered fibroblastic-like host cells and usually by a lack of or few tumor inflammatory tumor infiltrating cells. As noted by many authors, a tendency of grafted solid tumors to grow more and more rapidly with s.c. passaging may preclude their use in interventional strategies targeting properties or behavior characteristics other than proliferative activity. In fact, solid s.c. tumor grafts rapidly develop hypoxic, pre-necrotic, and necrotic areas, likely due in part to the failure to be sustained by a sufficient and fully functional newly formed vasculature. Accordingly, tumor volume measurements may include a substantial proportion of cell debris affecting the issue of quantitative new drug testing.

Somehow, the s.c. grafting *in vivo* system is reminiscent of the 3-D multicellular tumor spheroids used as an *in vitro* model of nodular carcinoma, a method exposing cells in spinner culture flasks to gradients of oxygen and metabolite concentrations generating within tumor spheroid heterogeneous microenvironments with surface proliferating, underlying quiescent, hypoxic, and pre-necrotic micro-regions. The model exhibits similarities to tumors *in vivo* both in the patient and grown as xenografts in nude mice allowing for combinatorial drug-radiation therapy testing [8].

To initiate and to be able to accomplish the “deadly metastatic cascade,” it has been (over)repeatedly emphasized that malignant cells have to cross multiple and diverse host tissue structures, intravasate, adapt to the blood stream or to the lymphatic fluid, and survive to become a distant intra-vascular cell embolization and then extravasate and find a proper and specific “niche” environment amenable to survival, dormancy, or permissive to *in situ* proliferation. This “cascade” is also relevant to metastases occurring in cases of clinically-unidentified primaries or even metastases from metastases. The notion of accumulated cell-constraining events in the course of this cascade had led Leonard Weiss to elaborate the concept, somewhat paradoxical, of “metastatic inefficiency” [9].

It is perhaps historically valuable to mention here that a “closed” meeting (45 attendants!) was held on June 3–5, 1981, at the University of Saskatchewan, Saskatoon, Canada [10]. Organized by I. Carr, R.S. Kerbel, and P. Scholefield, it covered, for the first time in a meeting, to my knowledge, specific topics such as tumor heterogeneity and phenotypic cancer-cell instability, invasion, and cancer metastasis including tumor xenografting, now recurrent and compulsory themes in popular multi-annual clinical and basic- research workshops and symposia, and welcome in top cancer journals.

Initial micro-invasive processes are thus crucial steps for metastasis to occur. If rapid cell proliferation is privileged in s.c. tumor xenografts and, according to the notion “Go or Grow” issued from basic cell metabolic pathways regulating cycling, migratory, and invasive tumor cell-associated activities, such as proteolytic activities and cell surface integrin-ligand interactions, might be reduced or inhibited temporarily when grafted at ectopic sites, hence a pseudo-benign tumor behavior. Indeed, past work suggested that tumor cell proliferation and invasion were under separate controls.

---

## The Popular Subcutaneous Route

Up until the 1980s, a majority of investigators active in the field of malignant xenografts would consider solid human tumors s.c. grafted in the nude mouse as noninvasive and non- or poorly metastatic. In this context, we contributed data along this line [11] and then reviewed the field in a book chapter published in 1982 [12]. Indeed, with some reported and notable exceptions, the s.c. tissue grafting site, if considered as an experimental primary tumor site in the nude mouse, appeared in most cases to provide no sufficient tissue structure conditions or no site or tumor matrix-associated, yet undefined, factors to restore actual tumor behavior, i.e., invasive and metastatic and eventually to be proposed *in fine* as a model amenable to improving the issues of experimental therapeutics.

Interest moved then to the search and understanding of the reason(s) for the inability of s.c. malignant tumor-grafted nu/nu mice to express a malignant phenotype. Questions were thus addressed to the potential role of the microbiological status of the recipient, the route of cancer- cell or patient-derived tumor fragment inoculation, as well as *a contrario* looking for a possible yet unknown link to some intrinsic properties expressed by defined and rare cell lines shown consistently to invade and disseminate in their host by overwhelming the nude mouse resistance. In brief, metastatic ability appeared dependent on both the microbiological and the genetic status of mice, i.e., for example, spf backcross-mated BALB/c athymic nude s.c.-grafted with a defined tumor showed more propensity to metastasize than conventionally- maintained outbred recipients grafted with the same tumor [13]. When transplanted early in life, nude mice proved to be more permissive for the growth and spreading from the s.c. site of both lymphomyelogenous and carcinoma cell lines, but from day 7 to day 12 after birth, fast-growing tumors stopped to disseminate [14]. Indeed, age, environmental, and genetic factors could determine the level

of natural killer (NK) activity, maturing around 3–5 weeks after birth in nude mice and highest in circulating blood. These and other factors were shown to affect the ability of grafted tumors to metastasize [15].

Regarding alternative routes of tumor cell inoculation [16], we and other investigators have demonstrated that intraperitoneal (i.p.) administration of cancer cells can generate a dose-dependent ascitic carcinosis with mesenteric invasion, mediastinal, and lung metastases. Ascites-forming tumors such as breast, stomach, larynx, and colorectal carcinomas were all diagnosed as poorly-differentiated or undifferentiated cell types. Moreover, it is generally agreed that a majority of carcinoma cells introduced i.v. in the blood compartment will embolize and rapidly be destroyed in the lungs of nude mice, as demonstrated histologically and monitored by  $^{125}\text{I}$ UdR-labeled tumor cell death or survival [17]. More interesting perhaps, and in the perspective to better mimic the post-surgical status of a cancer patient, the removal of locally s.c.-grafted tumor xenografts has been used to follow the long-term tumor behavior in the presence or in the absence of local recurrence, both spontaneous and induced. In our hands, and using the colon carcinoma Co115 cell line, surgical excision of the s.c.-growing xenograft did not increase the presence of lung metastases unless recurrent tumors grew locally, suggesting that post-surgical healing and inflammatory processes at an s.c. site could contribute to extending cancer-cell dissemination from “minimal residual disease.” As reported [18], the extent of tumor deposits in the lungs varied among individual mice, and the number and size of tumor emboli at the time of graft excision might determine their subsequent survival, growth, or death, in the host lung tissue.

Questioning the structural and functional aspects of subcutaneous tissues in the nude mouse, it appears that this route of inoculation is merely a free space easily accessible for a needle containing small cell samples or for a microtrocar loaded with patient-derived solid or disaggregated tumor fragments. The s.c. compartment can develop from *in situ* axillary and inguinal vessels a newly formed and modified vasculature and is drained by regional axillary and inguinal lymph nodes. This space, covered by a hairless skin and easily expandable, is quite convenient for tumor-volume measurements and remains a popular route for pre-clinical drug evaluation despite its reported limited significance in terms of invasive and metastatic ability as an acceptable mimicry of natural tumor behavior. It should not be under-evaluated that, with passaging, the original tumor stroma is replaced by murine tissue supporting the initial establishment and growth of human tumor cells. As discussed above, it became rapidly evident that s.c. environmental tissue conditions presumably lack the proper factors or some stroma-associated cellular and/or structural components able to activate the process of host tissue invasion by malignant cells.

---

## The Orthos Way

In the early days of metastasis research at least, it used to be imperative, perhaps fashionable, to introduce in a communication the historical hypothesis of Stephen Paget (1855–1926) published March 23, 1889, as an article in *The Lancet* (133,

3421, pp. 571–573) and entitled “The distribution of secondary growths in cancer of the breast.” Paget carefully analyzed 735 cases of breast cancer, reviewed the available literature, and went to the conclusion that the distribution of secondary growths cannot be due to chance and proposed the *seed and soil* theory of metastasis. He argued: “When a plant goes to seed, its seeds are carried in all directions but they can only live and growth if they fall on congenial soil.” Moreover, Paget honestly credited an Austrian ophthalmologist, Ernst Fuchs (1851–1930), for his theory of the relation between a cancer embolus and the recipient distant tissue *predisposed* to its specific growth. In addition to the study of the nature of the seeds, Paget, pioneering in the field, concluded “prophetically” that *observations of the properties of the soil may also be useful*.

Therefore, and in view of the well-established fact that the majority of human solid malignant tumors grafted s.c. to the nude mouse adopt a “pseudo-benign” behavior, it became evident that the “soil,” in this case the subcutaneous space and tissue, does not offer the “congenial” properties proper to the full expression by the “seeds” of their invasive and metastatic potential. However and in contrast with the behavior in the s.c. space, we showed, using the same colon Co115 tumor, that the peritoneal cavity of nude mice is permissive for the development of an ascitic carcinoma with free floating and aggregated colonic tumor cells able to adhere to the mesenterium, to grow as multiple foci. and to metastasize to regional lymph nodes and mediastinal and diaphragmatic areas. Furthermore, and in agreement with Paget’s theory, both clinical observations as well as mouse models strongly suggested that specific interactions can take place to promote preferential, non-random, metastatic development. Indeed in 1980, and using murine tumor models, Ian Hart and Isaiah Fidler were able to demonstrate experimentally that i.v. distributed cancer cells (melanoma) could only grow at particular “congenial” sites promoting in situ tissue selectivity for the malignant cells to expand [19].

Time had now come to test for a possible change in the phenotypic tumor behavior using a tissue site in the nude mouse corresponding to the one whereby the original carcinoma grew in the patient. Professor Wu-ru Wang, from the Department of Pathology, Harbin School of Medicine in China, on sabbatical leave at the Institute of Pathology, University of Lausanne, Switzerland, was interested in the project and joined the laboratory at the Cancer Institute (ISREC). Two colonic carcinoma lines established previously in the laboratory from xenografts were used: Coll2, a moderately differentiated, and Co115, a poorly differentiated type. To control for a potential site effect proper to colonic lines only, two melanoma lines were also used. Practice of tumor cell inoculation into the spf nude-mouse gut wall required careful microsurgical work under a laminar flow hood, anesthesia, and mouse body temperature control. Accurate tumorigenic-cell dose ( $1-5 \times 10^6$  in a microliter volume) was difficult to ascertain using an inoculation procedure tangential to the gut wall. Observation time ranged from 20 to 92 days. In the first series of experiments, 11 out of 33 mice showed evidence, macroscopically, of growth within the gut wall. Each case was thus reported as drawings in laboratory notebooks as illustrated in the following Fig. 4.1 by two cases taken at 27 and 37 days after gut implantation.

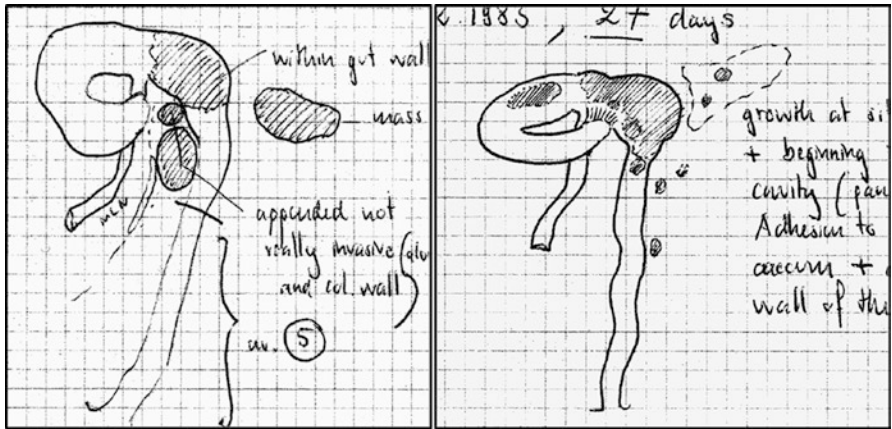


**Fig. 4.1** Two cases illustrating the pattern of human tumor growth within the mouse large bowel wall and extending from implantation site to the caecum (magnif. 1:1 from the original drawings)

Light, electron microscopy and results from autoradiographic analyses were published in 1982 [20]: they were presented as a poster at the fourth International Workshop on Immune-Deficient Animals in Experimental Research that we organized and that was held October 31–November 3, 1982, in Chexbres, near Lausanne.

Clearly, both the gut-implanted Co115 and Co112 colon-cancer cell lines were now able to express a macro- and microinvasive behavior, proliferate, and infiltrate the different layers of the mouse large bowel walls, crossing the muscularis mucosae and the muscularis propria to dissociate smooth muscle layers. Both lymphatics and blood vessels were found to contain intravasated Co115 tumor cells. Moreover, at longer time intervals, tumor foci were found in the serosa and grew as nodular masses in the mesenterium of the peritoneal cavity and distant from the inoculation site. Metastases of Co115 cells only were found in mesenteric lymph nodes. Interestingly, and in contrast to s.c. grafted Co112 and Co115 xenografts, inflammatory cell types were regularly found associated with gut invasive tumors. Four out of seven mice implanted with melanoma cells showed serosal adhesion and implantation and grew preferentially as spheroid-like nodules on the surface of the large bowel wall with limited penetration of the underlying gut layers. These histopathological features obtained with tumor xenografts implanted in an orthotopic (*orthos*, right and straight) site of the nude mouse made them quite similar to those of the Co112 and Co115 original patient tumors.

The content of the poster attracted workshop attendants and abundant questions from invited experts in the metastasis research field: is Paget's "seed and soil" concept applicable to the ecto-orthotopic conversion from "benign" to invasive phenotypes and, for some tumor types, from "pseudo-benign" to invasive and metastatic phenotypes? Is the conversion dependent on structural component(s) of the soil, as suggested by Paget 93 years ago, such as specific constituents of basement membranes of epithelia or of smooth muscle layers? Or is the conversion dependent on

factors diffusible locally or trapped in the stroma or extracellular matrix specific constituents? Is the grade of tumor differentiation, the size of a stem cell population in a tumor of interest, influential since differentiated tumor types appear to need longer time intervals to establish metastatic deposits? Which role or roles do the diverse types of inflammatory cells regularly associated with invasive areas play? Do specific proteolytic activities take direct or indirect part in the process of phenotypic conversion?

As recently underlined by Robert Hoffman [21]: “subsequent studies from Fidler’s laboratory and others have shown that the implantation of many types of human tumours in the orthotopic sites of nude or other immunodeficient mice resulted in metastasis of human tumours.”

At that time and in the context of the interest in the laboratory for proteolytic activities involved in malignant tumor cell behavior, we took advantage of the model to characterize and quantitate plasminogen activators (PAs) expressed by primary colon carcinomas and their respective serial s.c.-grafted xenografts in the nude mouse. Activation of plasminogen to plasmin, a multipotent enzyme, can lead directly to the degradation of major stromal components or, indirectly, by activation of latent metalloproteinases. Patient primary invasive tumors showed high concentrations of PAs, while s.c. xenografts contained very low levels of activity not due to an increase in inhibitors of fibrinolytic activity [22]. A second series of experiments using the ecto-orthotopic conversion cancer-cell system demonstrated that only gut-implanted colonic tumors only could exhibit invasive growth and expressed high tumor cell-secreted PA activity, indicating that fibrinolysis could participate to the complex process of tumor invasion [23].

Another series of experiments allowed us to show that extracellular matrix-cancer cell interactions can regulate growth and migratory, invading, activities *in vivo*. Laminin isoforms are major constituents of basement membranes. The laminin-5 heterotrimer is composed of the alpha-3, beta-3, and gamma-2 subunits and is a primary adhesion protein in the skin and gastrointestinal mucosal epithelia. In colorectal carcinomas, gamma-2 and beta-3 subunits have been found in the cytoplasm of the so-called budding carcinoma cells sprouting out of the neoplastic tubules and invading the tumor stroma [24, 25]. Moreover, the budding phenotype proved to be of prognostic value in patients with colorectal cancer [26]. In our experiments [27], we found that laminin-5-associated budding activity was suppressed when colorectal carcinoma cells grew s.c. but was restored when gut-implanted in the nude mouse, as illustrated in Fig. 4.2.

Previous results using colorectal tumor xenografts support the role of the organ microenvironment in regulating expression of an array of gene products including degradative proteases and growth and inflammation-associated factors [22, 23]. In this context, and since pro-inflammatory cytokines have been shown in human epithelial non-malignant intestinal cells to modulate laminin-5 expression, we tested whether cytokine production *in situ* would affect the level of laminin-5 subunits in HT29 colonic carcinoma cells. Indeed, *in vitro*, preliminary results indicated that TNF-alpha (10 ng/mL) could increase, versus control, up to 5x the level of gamma-2 subunit transcripts and about 2x the levels of alpha3 and beta3 subunit transcripts.

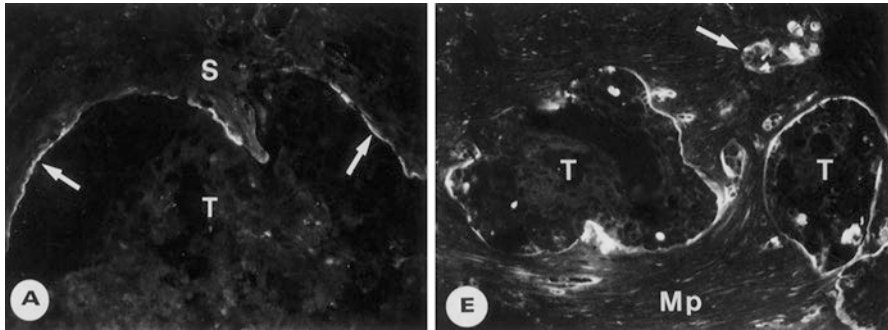


**Fig. 4.2** In A, laminin-5 is extracellular and is confined (*arrows*) to the tumor (T, HT29 colon cells grafted s.c.)—host murine stroma (S) interface. In E, laminin-5 immunoreactivity is now both intra-cytoplasmic in invading HT29 carcinoma cells (*arrow*) and lining tumor nodules (T) infiltrating the mouse muscularis propria (Mp), following gut implantation of HT29 tumor cells (modified from reference [27])

HGF (50 ng/mL) increased 3x the level of the alpha3 subunit only. TGF- $\beta$  (up to 10 ng/mL) did not alter significantly laminin-5 subunit expression under these conditions. A laminin-5-associated pathway could possibly contribute to initiate a process of cancer-cell invasion within the inflammatory context of the orthotopic site of colon carcinoma implantation (Sordat, I. unpublished, 2000).

## Comments in Conclusion

As emphasized above, cancer-cell micro-invasion is a key initial step for metastases to develop in “predisposed” organ environments. Obviously, orthotopic tumor implantation routes in the nude mouse system, specifically the large-bowel gut implantation of human colorectal carcinoma cells (1982) [20], has opened a way from the first subcutaneous ectopic transplantation (1969) [1] to patient-derived orthotopic xenografts (PDOX models) using intact colorectal cancer tissue (1991) [28] where a greater extent of metastasis was observed and presumably due to intact tumor-stroma interactions allowing for malignant micro-invasion at the implantation site. Routes of cancer-cell initial implantation are among the critical factors for metastases to form and further develop non-randomly at distant sites [29]. A variety of tumor types has been established as PDOX models, and clinical relevance in cases of stomach cancer could be observed where a correlation was found between the development of liver metastases both in the patient and in the nude mice orthotopically transplanted with intact tumor tissue [30]. This book updates the present state of knowledge by pioneers in the field of tumor xenografting; see Chaps. 3, 5, 7, and 8. However, mainly due to the failure of pre-clinical mouse tumor models to be better predictive of clinical responses in the patients and as alternatives to human tumor xenografts, transgenic mouse cancer mice systems were developed, rapidly dominating the preclinical research area [21]. In the meantime, more immune-deficient mice strains such as SCID or NOD/SCID as tumor xenograft hosts became



available. In 2006, however, the ectopic s.c. and not the orthotopic human tumor xenograft model as a "back to the future" novelty was revived, and cancer heterotransplants from individual patients were now designated as "xenopatients" [21]!

Robert Kerbel reviewed recently an experience of 10 years of work in his laboratory developing pre-clinical models and pointing out the importance in innovative therapy studies of using and exploiting models of advanced late-stage tumors in mice with spontaneous metastases. A multi-model experimental approach was recommended including the surgical removal of orthotopic tumor grafting followed by *in vivo* selection of more metastatic variant lines [31]. For an update, see Kerbel's Chap. 8 in this book.

A perspective opinion article [32] (42 coauthors) published January 2017 representing a very large multi-institutional platform underlines the ability of patient-derived xenografts (PDXs) to contribute to increasing our knowledge on the role of tumor heterogeneity in the course of drug exposure as well as to plan novel therapeutic strategies or identify malignant biomarkers. PDXs as *in vivo* models are recognized to fulfill certain phenotypic and genotypic criteria but preclude immune-based investigations unless immune-deficient mice as human tumor-grafted hosts can be "humanized" with human specific immunologically- active subpopulations of cells. Surprisingly, the choice of PDXs and not of patient-derived orthotopic xenografts (PDOXs) was done, implying that a full expression of the malignant phenotype as a functional criterion of human tumor murine stroma microenvironmental interactions could not be considered in the study [32]. Certainly, orthotopic implantation routes according to tumor types to be investigated imply technical and financial constraints (microsurgery, imaging, quantitative analysis of drug application strategies, animal maintenance conditions) and necessitate similar protocols to be adopted between each member of the consortium. Moreover, in our experience, there exists a degree of heterogeneity in the success rate of both orthotopic implantation and in the temporal development of the tumor graft in the mouse imposing a relatively large number of tumor recipients. After all, mice (induced) and human beings (spontaneous) express a disease that requires a "personalized" treatment strategy for the potential benefit of one of the two! See citation by Plato under the title of this chapter.

---

## References

1. Rygaard J, Povlsen CO. Heterotransplantation of a human malignant tumor to "nude" mice. *Acta Pathol Microbiol Scand.* 1969;77:758–60.
2. Povlsen CO, Rygaard J. Heterotransplantation of human adenocarcinomas of colon and rectum to the mouse mutant nude. A study of nine consecutive transplantations. *Acta Pathol Microbiol Scand.* 1971;79(2):159–69.
3. Proceedings of the first international workshop on nude mice. In: Jorgen R, Povlsen CO, editors. Stuttgart: Gustav Fischer Verlag; 1974.
4. Proceedings of the second international workshop on nude mice. Tokyo: University of Tokyo Press; Stuttgart: Gustav Fischer Verlag; 1977.
5. Proceedings of the third international workshop on nude mice. Vol. 2. Oncology. In: Norman DR, editor. New York: Gustav Fischer; 1982.

6. Fogh J, Fogh JM, Orfeo T. One hundred and twenty-seven cultured human tumor cell lines producing tumors in nude mice. *J Natl Cancer Inst.* 1977;59:221–5.
7. Giovanella BC, Stehlin JS, Williams IJ Jr. Heterotransplantation of human malignant tumors in “nude” thymusless mice. II. Malignant tumors induced by injection of cell cultures derived from human solid tumors. *J Natl Cancer Inst.* 1974;52:921–30.
8. Sutherland RM, Sordat B, Bamat J, Gabbert H, Bourrat B, Mueller-Klieser W. Oxygenation and differentiation in multicellular spheroids of human colon carcinoma. *Cancer Res.* 1986;46:5320–9.
9. Weiss L. Random and nonrandom processes in metastasis and metastatic inefficiency. *Invasion Metastasis.* 1983;3(4):193–207.
10. Kerbel RS. Meeting report: tumor heterogeneity, invasion and metastasis, June 3–5, Saskatoon, Saskatchewan, Canada. *Invasion Metastasis.* 1982;2(1):61–75.
11. Sordat B, Bogenmann E. Metastatic behaviour of human colon carcinoma in nude mice. In: *Proceedings immunodeficient animals in cancer research.* London: Macmillan; 1980. p. 145–58.
12. Sordat BCM, Ueyama Y, Fogh J. Metastasis of tumor xenografts in the nude mouse. In: Fogh J, Giovanella BC, editors. *The nude mouse in experimental and clinical research, vol. 2.* New York: Academic Press; 1982. p. 95–148.
13. Sordat BCM, Ueyama Y, Fogh J. Metastasis of tumor xenografts in the nude mouse. In: Fogh J, Giovanella BC, editors. *The nude mouse in experimental and clinical research, vol. 2.* New York: Academic Press; 1982. p. 119–20.
14. Sordat B, Merenda C, Carrel S. Invasive growth and dissemination of human solid tumors and malignant cell lines grafted subcutaneously to newborn nude mice. In: *Proceedings of the second international workshop on nude mice.* Tokyo: University of Tokyo Press; Stuttgart: Gustav Fischer Verlag; 1977. p. 313–26.
15. Hanna N, Fidler IJ. The role of natural killer cells in the destruction of circulating tumor emboli. *J Natl Cancer Inst.* 1980;65:801–9.
16. Sordat BCM, Ueyama Y, Fogh J. Metastasis of tumor xenografts in the nude mouse. In: Fogh J, Giovanella BC, editors. *The nude mouse in experimental and clinical research, vol. 2.* New York: Academic Press; 1982. p. 120–5.
17. Sordat B, Lees RK, Bogenmann E, Terres G. The behavior of Co115 human colon carcinoma in nude mice. In: *Proceedings of the third international workshop on nude mice.* New York: Gustav Fischer; 1982. p. 543–55.
18. Sordat BCM, Ueyama Y, Fogh J. Metastasis of tumor xenografts in the nude mouse. In: Fogh J, Giovanella BC, editors. *The nude mouse in experimental and clinical research, vol. 2.* New York: Academic Press; 1982. p. 125–32.
19. Hart IR, Fidler IJ. Role of organ selectivity in the determination of the metastatic patterns of B16 melanoma. *Cancer Res.* 1980;40(7):2281.
20. Wang W-R, Sordat B, Piguët D. Human colon tumors in nude mice: implantation site and expression of the invasive phenotype. In: Sordat B, editor. *Immune-deficient animals in experimental research (formerly Nude Mice Workshop), Chexbres.* Basel, Switzerland: Karger; 1982. p. 239–45.
21. Hoffman RM. Patient-derived orthotopic xenografts: better mimic of metastasis than subcutaneous xenografts. *Nat Rev Cancer.* 2015;15:451–2.
22. Cajot J-F, Sordat B, Bachmann F. Human primary colon carcinomas xenografted into nude mice. I. Characterization of plasminogen activators expressed by primary tumors and their xenografts. *J Natl Cancer Inst.* 1986;77(5):703–12.
23. Cajot J-F, Sordat B, Bachmann F. Human primary colon carcinomas xenografted into nude mice. II. Modulation of tumor plasminogen activator activity by the host tissue environment. *J Natl Cancer Inst.* 1986;77(5):1099–105.
24. Pyke C, Salo S, Ralfkiaer E, Romer J, Dano K, Tryggvason K. Laminin-5 is a marker of invading cancer cells in some human carcinomas and is co-expressed with receptor for urokinase plasminogen activator in budding cancer cells in colon adenocarcinomas. *Cancer Res.* 1995;55:4132–9.

25. Sordat I, Bosman FT, Dorta G, Rousselle P, Aberdam D, Blum A-L, Sordat B. Differential expression of laminin-5 subunits and integrin receptors in human colorectal neoplasia. *J Pathol.* 1998;185:44–52.
26. Hase K, Shatney C, Johnson D, Trollope M, Vierra M. Prognostic value of tumour “budding” in patients with colorectal cancer. *Dis Colon Rectum.* 1993;36:627–35.
27. Sordat I, Rousselle P, Chaubert P, Petermann O, Aberdam D, Bosman FT, Sordat B. Tumor cell budding and laminin-5 expression in colorectal carcinoma can be modulated by the tissue environment. *Int J Cancer.* 2000;88:708–17.
28. Fu X-Y, Besterman JM, Monosov A, Hoffman RM. Models of human metastatic colon cancer in nude mice orthotopically constructed by using histologically intact patient specimens. *Proc Natl Acad Sci U S A.* 1991;88:9345–9.
29. Fidler IJ. Critical factors in the biology of human cancer metastasis: twenty-eight G.H.A. Clowes memorial award lecture. *Cancer Res.* 1990;50(19):6130–8.
30. Furukawa T, Kubota T, Watanabe M, Kitajima M, Hoffman RM. Orthotopic transplantation of histologically intact clinical specimens of stomach cancer to nude mice: correlation of metastatic sites in the mouse and individual patient donors. *Int J Cancer.* 1993;53(4):608–12.
31. Kerbel RS. A decade of experience in developing preclinical models of advanced- or early-stage spontaneous metastasis to study antiangiogenic drugs, metronomic chemotherapy, and the tumor microenvironment. *Cancer J.* 2015;21:274–83.
32. Byrne AT, et al. Interrogating open issues in cancer precision medicine with patient-derived xenografts. *Nat Rev Cancer.* 2017;17:254–68.

---

# The Effects of the Organ Microenvironment on Metastatic Cell Gene Signatures

# 5

Sun-Jin Kim, Ho Jeong Lee, Hyunkyung Yu, Sung Il Choi,  
John Weinstein, Jing Wang, Yan Qi, and Isaiah J. Fidler

---

## Introduction

Most deaths due to cancer are the result of the continued growth of metastases that are refractory to treatment [1]. It is widely recognized that tumors are heterogeneous for metastasis [2] and that most experimental and human metastases are clonal in origin [3, 4]. Clones with increasing metastatic potential tend to have an accelerated rate of spontaneous mutation [5], which causes the molecular landscapes of metastases to differ from those of primary tumors [6, 7]. Moreover, the genetic alterations that take place in metastases may enable the cells to become resistant to therapy [8]. Consequently, much recent investigative effort is directed toward an enhanced understanding of the genetic makeup of cancer metastases.

One notable feature of metastasis is that different types of cancer cells may colonize the same or different organs [9]. The preferred patterns of organ-specific metastasis exhibited by some tumors are governed by several factors, including tissue-specific properties that affect cancer-cell growth, the anatomical route of the circulation from the primary tumor, and selective molecular-adhesive interactions generated between cancer cells and microvascular endothelial cells [10]. The most frequent target organs of disseminating cancer cells are the lung, liver, bone, and brain [11], and reciprocal signaling between cancer cells and normal resident cells in these organs is thought to play a decisive role in determining the fate of metastatic

---

S.-J. Kim • H.J. Lee • H. Yu • S.II. Choi • I.J. Fidler (✉)

Department of Cancer Biology, Metastasis Research Laboratory, Unit 173, University of Texas MD Anderson Cancer Center, 1515 Holcombe Boulevard, Houston, TX 77030, USA  
e-mail: [ifidler@mdanderson.org](mailto:ifidler@mdanderson.org)

J. Weinstein • J. Wang • Y. Qi

Department of Bioinformatics and Computational Biology, University of Texas MD Anderson Cancer Center, Houston, TX, USA

cells [11, 12]. In the following sections, we review how the organ microenvironment influences the patterns of gene expression of cancer cells. We begin the discussion with a brief review of the steps of metastasis.

---

## Process of Metastasis

Metastasis begins when a cancer cell detaches from a primary mass and invades its surrounding tissue. In nontransformed tissues, adjacent epithelial cells are tightly interconnected by several cell-cell adhesion molecules that are responsible for maintaining the structural integrity of the tissue. One of the more widely studied epithelial adhesion proteins is E-cadherin, a member of the cadherin superfamily of proteins [13]. Cancer cells at the invasive front repress E-cadherin expression and begin to display patterns of gene expression that are characteristic of mesenchymal cells. This process is referred to as epithelial-mesenchymal transition (EMT) [14]. Several other epithelial proteins, such as  $\beta$ -catenin and cytokeratin, are also downregulated during EMT. In contrast, mesenchymal-associated proteins, such as N-cadherin, vimentin, and fibronectin, become upregulated during EMT. EMT occurs physiologically during tissue repair processes in the adult, and EMT is also essential for embryonic development [15]. Activation of this developmental program in cancer cells endows the cells with properties that are typically associated with hematopoietic stem cells [16]. Moreover, there is evidence that suggests that activation of the EMT process enables cancer cells to become resistant to therapy [17].

Invading cancer cells first encounter the basement membrane that separates the epithelial compartment from the underlying connective tissue. Cancer cells rely on laminin and integrin receptors to adhere to the basement membrane. Adherent cancer cells activate localized proteolysis at the cancer cell-basement membrane interface [18], and the dissolution of this mechanical barrier represents the transition from a benign carcinoma in situ to an invasive tumor [19]. Cancer cells gain access to the local microcirculation by penetrating postcapillary venules or lymphatic vessels. The structural composition of these thin-walled vessels offers little resistance against invasive cancer cells [1]. Other characteristics of tumor blood vessels render them vulnerable to penetration by cancer cells. Most notably, tumor-associated blood vessels are structurally deficient and hyperpermeable [20]. Pioneer studies in experimental tumor models demonstrated that a significant correlation exists between cancer cell intravasation and the tumor neovascularization process [21].

Once cancer cells gain access to the systemic circulation, they may form homotypic or heterotypic aggregates with other circulating cells. Cancer cells may also circulate independently as single cell entities. However, the ability of cancer cells to generate aggregates with other cancer cells or other circulating cells has been shown to increase their likelihood of forming metastases [22, 23]. Cancer cells may become trapped in the microcirculation of secondary organs due to size restriction (e.g., mechanical trapping), or they may generate selective adhesive interactions with microvascular endothelial cells through mechanisms identical to those used by leukocytes during their trafficking processes.

One of the more extensively studied cancer cell trafficking processes is that of melanoma cells. Several studies have provided a role for the inducible endothelial

glycoprotein, vascular cell adhesion molecule-1 (VCAM-1), in facilitating melanoma brain metastasis. VCAM-1 is negligibly expressed in the microcirculation of most tissues. However, levels of VCAM-1 are dramatically upregulated in response to inflammatory cytokines, such as tumor necrosis factor- $\alpha$ , interleukin-1, and lipopolysaccharide [24]. VCAM-1 is the endothelial counter-receptor for VLA-4 (very late antigen-4 or integrin  $\alpha_4\beta_1$ ), and VCAM-1/VLA-4 interactions normally function to support the adhesion of monocytes, eosinophils, and lymphocytes to the microvascular surface [25]. Clinical investigations of integrin expression in melanoma reported a direct correlation between  $\alpha_4\beta_1$  integrin expression and the occurrence of metastasis, reduced disease-free overall survival, and decreased overall survival [26]. In a spontaneous model of B16-BL6 melanoma metastasis, VCAM-1 expression was downregulated in pulmonary blood vessels, but significantly increased in the cerebral microvasculature [27]. Similarly, recent studies reported marked upregulation of VCAM-1 expression on the tumor-associated vessels in experimental models of breast cancer brain metastasis and on the endothelium of human brain metastasis tissues [28]. Rebhun and coworkers [29] reported that VCAM-1 was constitutively expressed in cell cultures of murine brain endothelial cells and lymphatic endothelial cells and that melanoma cell adhesion to lymphatic endothelial cells was largely VCAM-1 dependent. However, blocking monoclonal antibodies directed against either the integrin  $\alpha_4\beta_1$  expressed on melanoma cells or VCAM-1 expressed on brain endothelial cells had no effect on melanoma cell adhesion to brain endothelial cells. This latter observation suggests the possibility of a separate receptor-ligand pair that can support melanoma cell adhesion to brain endothelial cells.

The abovementioned studies illustrate the variety of technical approaches used to study how cancer cells interact with the tissue microenvironment. Studies are typically initiated in the whole animal and then moved into cell-based systems for detailed mechanistic examinations. Cell-based systems are particularly useful but require rigorous attention to detail. For example, we recently conducted a comparison between MDA-MB-231 breast cancer cells that were 90% confluent in either Minimum Essential Medium (MEM), Dulbecco's Modified Eagle's Medium (DMEM), or Roswell Park Memorial Institute (RPMI)-1640 medium, all containing 10% fetal bovine serum and discovered that almost 9000 genes were differentially expressed [30]. Moreover, genes associated with EMT were among those genes that were differentially modulated by cells grown in these different formulations, and we validated these genes at the protein level [30]. In the next section, we describe another approach that may be used to study how the complex cross talk between cancer cells and resident tissue cells influences patterns of cancer cell gene expression.

---

## Cross-Species Hybridization of Microarrays for Studies of Metastasis

One of the most extensively used approaches to study how the organ microenvironment influences patterns of cancer cell gene expression is through a repeated *in vivo* selection process whereby cancer cells are implanted into recipient mice and allowed to form metastases [31, 32]. Cancer cells harvested from the resulting metastases are frequently compared with the parental cancer cell population in

order to identify candidate genes that may be critical for tissue-specific metastasis. This approach has been exploited on several occasions to study the genetic determinants that allow breast cancer cells to successfully form metastases in secondary target organs [33, 34]. However, such information is generally lacking for other types of cancer cells, and it remains unclear whether different types of tumors that exhibit the same patterns of secondary spread also share overlapping patterns of gene expression.

One factor that has hindered such investigations is that tumors are comprised of so many different cell types that garnering information strictly on cancer cells can prove challenging. Recently, we demonstrated that this hurdle can be overcome by using cross-species hybridization of microarrays, which allows the user to evaluate the stromal (mouse) and cancer cell (human) transcriptomes simultaneously [35]. Other investigators [36] have used the technique to identify patterns of mouse and human gene expression in non-small cell lung cancer (NSCLC) xenografts that had become resistant to bevacizumab therapy. That study was instrumental in identifying the upregulation of the epidermal growth factor receptor (EGFR) and fibroblast growth factor receptor (FGFR)-signaling pathways in the tumor stroma, which restored the revascularization response and allowed tumors to progress while mice were receiving bevacizumab therapy. We applied cross-species hybridization of microarrays to extract the patterns of gene expression of cancer cells and host cells from experimental brain metastases [35]. Analysis of the data sets collected on four different cell lines growing in the brains of nude mice indicated that the cancer cells displayed marked differences in gene expression patterns when compared to the same tumors implanted in either the subcutaneous space or in their primary orthotopic site. That is, the cancer cells growing in the brain no longer exhibited their cell line-specific gene expression program, but rather the cells had acquired neuronal cell characteristics inasmuch as the most enriched gene sets expressed by cancer cells were related to neuronal signaling.

Recently, we decided to expand cross-species hybridization of microarrays in a broader series of experiments in order to examine how patterns of cancer cell gene expression differ between primary tumors and their metastases. We were also interested in comparing the patterns of gene expressions among different types of cancer cells residing in the same secondary organs of metastasis. In the next section, we discuss the technical approach that we used for our gene comparison studies and then review the findings from our experiments.

---

## Experimental Approach

We selected a broad panel of human cancer cells for our studies, including A375 melanoma cells [37], KM12 colon cancer cells [38], MDA-MB-231 breast cancer cells [39], PC-3P prostate cancer cells [40, 41], PC14 lung cancer cells [42], and SN12 renal cancer cells [43]. We then implanted the cancer cells into their equivalent murine organ of origin (primary orthotopic tumors), target organ of metastasis (secondary metastatic tumors), or into an unrelated tissue (ectopic tumor) using methods that we have previously described [44–52].

Four to six weeks after the implantation of cancer cells, we harvested the tumors and processed them for analysis of human and murine transcriptomes. Total RNA was extracted from snap-frozen cancer tissues or cell cultures, and biotin-labeled cRNA samples for hybridization were prepared using Illumina Total Prep RNA Amplification Kits. Individual samples containing 1.5- $\mu$ g of biotinylated cRNAs were hybridized to both Illumina Human-12 BeadChip v.2 and Mouse-6 BeadChip v.1-1 microarrays for analysis of human and murine transcriptomes, respectively. Signals were developed by Amersham fluorolink streptavidin-Cy3, and gene expression data were collected using an Illumina bead array reader confocal scanner. Array data processing and analysis were performed using Illumina BeadStudio software. For our statistical analysis, we used BRB Arraytools Version 3.6 [53] and the R language and normalized the microarray data using the quantile normalization method in the Linear Models for Microarray Data package [54]. A random variance *t*-test was applied to identify any statistical significance between genes when two groups were compared, and one-way ANOVA was performed for multi-group analyses [55]. A Fisher's exact test was applied to genes with expression that was significantly altered ( $P < 0.001$  and a tenfold difference), and cluster analysis was performed. Heat maps were generated using tree view. A K-nearest neighbor imputation method [56] was used to impute missing expression values, followed by log<sub>2</sub>-transformation of the raw data. Quality assessment of the arrays excluded nine sample arrays from the data set due to the extremely low dynamic range measured by interquartile range. Normalization of the dataset ( $n = 72$ ) was performed using quantile normalization, and the bottom 25% probes of mean intensity were filtered out. The discovery dataset was used to identify gene signatures specific for the bone, brain, lung, and skin. A nonparametric Kruskal-Wallis analysis of variance was used to identify differentially expressed genes among all organs, followed by Wilcoxon rank sum test between pairs of organs. The Benjamini-Hochberg method was used to control for false discovery rate at the 0.05 level. The resulting probes were further filtered by a minimal twofold difference in expression value between each organ and any other organ.

Probes that were upregulated in a given organ when compared with any other organ were also identified. Heat maps were generated to compare patterns of gene expression. Genes and samples were clustered using hierarchical clustering with the Pearson correlation metric and average linkage algorithm. Gene ontology analysis of the signature gene was performed using EASE [57]. To eliminate any potential cross-hybridization with mouse tissue, we further filtered the gene signatures by comparing their expression with those in the mouse organ dataset. Signature genes that were also highly expressed in mouse organs were filtered out. In the next several sections, we discuss the results of our studies.

## Cancer Type-Specific Gene Signatures

Class comparisons identified cancer type-specific gene signatures. We obtained common gene signatures of the individual cancer cell lines growing in various organs by comparing the gene signature of each cell line growing in its primary and metastatic organs with those of other cell lines growing in their primary and



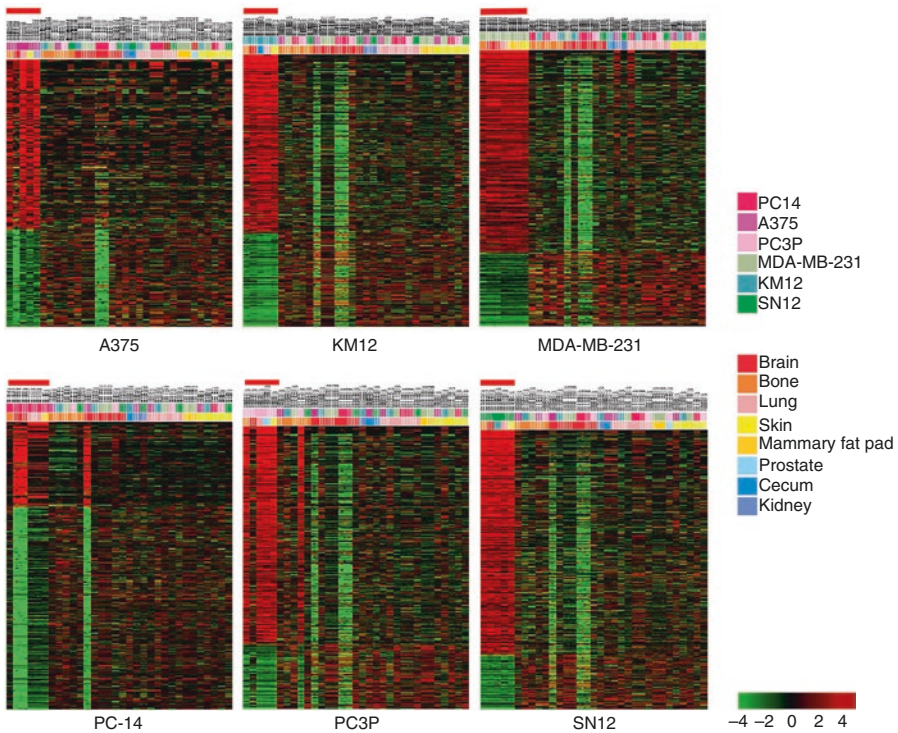


**Fig. 5.1** Cancer cell type-specific gene expression patterns among all organs. Each heat map shows the pattern of differentially expressed genes between each cancer cell type and all other cancer cell types. The data are presented in a matrix format in which rows represent individual genes, and columns represent individual tissues. Each cell in the matrix represents the expression level of a gene in a given tissue. The *red*- and *green*-colored cells reflect relatively high and low expression levels, respectively, as indicated by the scale bar (log<sub>2</sub>-transformed scale) (A375—382; KM12—1667; MDA-MB-231—1546; PC14—2331; PC3P—671; SN12—1428 genes)

metastatic organs. This information provided cancer type-specific common gene signatures for each of the cell lines *in vivo* regardless of where the tumor was located. For example, a cluster of 382 differentially modulated genes was found to distinguish A375 melanoma cells from all other cancer cells that were examined (Fig. 5.1). In the same manner, we determined that clusters of 1667, 1546, 2331, 671, and 1428 genes could identify KM12, MDA-MB-231, PC-14, PC3P, and SN12 cancer cell lines, respectively (Fig. 5.1). We defined these clusters of genes as cancer cell type-specific gene signatures, which provide information regarding the type of cancer cells that the mouse harbors, but not their location in the whole animal.

### Organ Type-Specific Gene Signatures: Effects of the Organ Microenvironment on Cancer Cell Gene Signatures

In order to determine if different types of cancer cells residing in the same organ exhibited unique patterns of gene expression, we compared the gene expression

patterns of A375, KM12, MDA-MB-231, PC3P, PC14, and SN12 cancer cells with those of other cancer cells growing in the same organ (Fig. 5.2). As summarized in Table 5.1, in the bone, 1596, 3232, 2544, 1134, 1118, and 2230 genes were differentially expressed by A375, KM12, MDA-MB-231, PC-14, PC3P, and SN12 cells, respectively. In the brain, 2194, 1078, 2176, 7082, 891, and 1430 genes were differentially expressed by A375, KM12, MDA-MB-231, PC-14, PC3P, and SN12 cells, respectively. In the lung, 1645, 3348, 1694, 3085, 1695, and 2247 genes were differentially expressed by A375, KM12, MDA-MB-231, PC-14, PC3P, and SN12 cells, respectively. In the skin, 1654, 2042, 1752, 1638, 1971, and 1779 genes were differentially expressed by A375, KM12, MDA-MB-231, PC-14, PC3P, and SN12

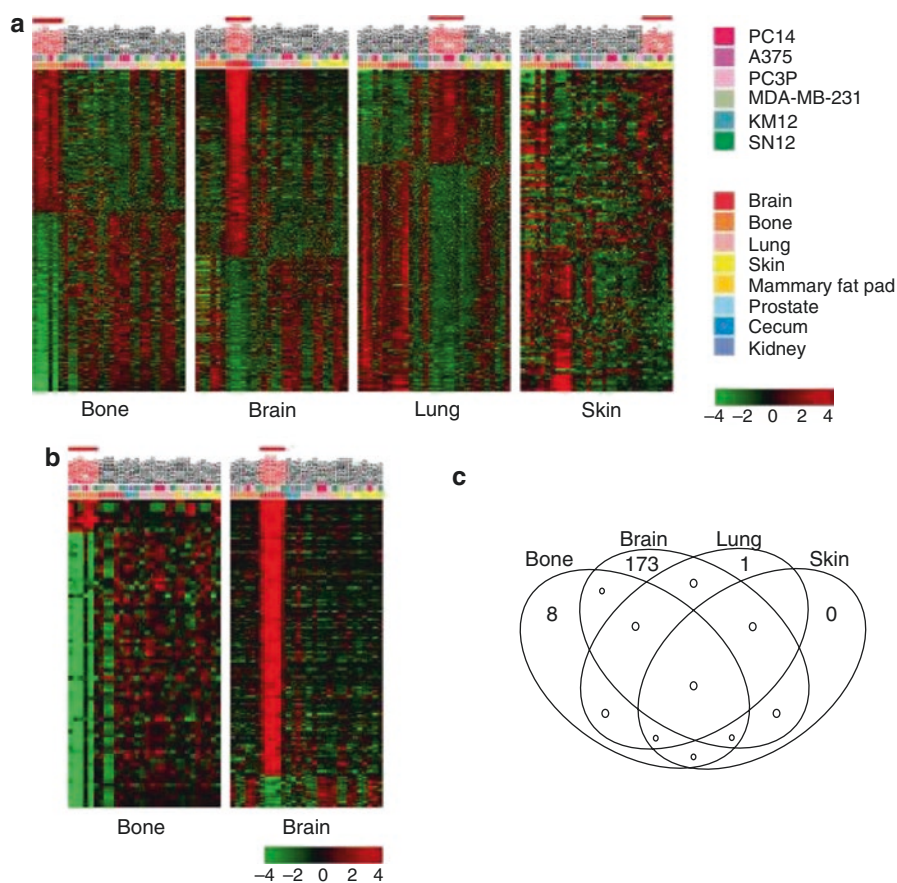


**Fig. 5.2** Organ-specific gene expression patterns among all types of cancer cells. **(a)** Each heat map shows differentially expressed genes in each organ compared with all other organs, with statistical significance (bone 1634; brain 1253; lung 635; skin 173 genes). **(b)** Organ-specific gene expression pattern among all types of cancer with more than twofold changes (bone 75; brain 193; lung 1; skin 0 genes). **(c)** Venn diagram of the genes from each metastatic organ that were significantly and differentially expressed with a twofold change and upregulated compared with other organs. The plot indicates that these genes are unique to each organ

**Table 5.1** Number<sup>a</sup> of genes that were differentially expressed in type of cancer cell compared with all other cancer cell types in the same organ

	A375	KM12	MDA-MB-231	PC-14	PC3P	SN12
Bone	1596	3232	2544	1134	1118	2230
Brain	2194	1078	2176	7082	891	1430
Lung	1645	3348	1694	3085	1695	2247
Skin	1654	2042	1752	1638	1971	1779

<sup>a</sup>Numbers have not been corrected for multiple comparison

**Table 5.2** Number<sup>a</sup> of genes that were differentially expressed with statistical significance (“significant genes”) and with a fold change greater than 2 (“Sig.AND.2FC”) compared with each organs, respectively

	Significant genes	Sig.AND.2FC	Sig.AND.2FC.up	Sig.AND.2FC.down
Bone	1634	75	8	67
Brain	1253	193	173	20
Lung	635	1	1	0
Skin	173	0	0	0

The numbers of genes that were up- and downregulated compared with all other organs among the significant and twofold change genes identified (“Sig.AND.2FC.up” and “Sig.AND.2FC.down”) are also shown

<sup>a</sup>Numbers have not been corrected for multiple comparison

cells, respectively. Overall, we identified 1634, 1253, 635, and 173 genes as the organ-specific signatures in the bone, brain lung, and skin, respectively (Fig. 5.2a). These data indicate that each tumor line expresses a unique pattern of genes when growing in a particular primary organ site. Moreover, metastatic cells from each of the lines under study expressed different sets of gene when growing in different organs of metastasis.

We also investigated whether there were genes that were similarly modulated by different types of cancer cells growing in each organ regardless of the cancer cell types. There were no differentially expressed genes with more than a twofold difference in the skin (Fig. 5.2b, c; Table 5.2). These data demonstrate that gene expression patterns of cancer cells are modulated by the organ microenvironment and that the pattern is similar in all of the six cell lines examined.

## Organ and Cancer Type-Specific Gene Signatures

Class comparison determined the extent that the organ microenvironment modulates patterns of gene expression in cancer cells by comparing patterns of gene expression for the same cancer cells growing in the different organs. For A375 melanoma cells, we found clusters of 78 genes, 221 genes, 8952 genes, and 145 genes that were unique to A375 cells growing in the skin, bone, brain, and lung, respectively (Fig. 5.3). The number of genes differentially expressed in the primary and metastatic organs are summarized in Table 5.3. In brief, clusters of 87, 1672,

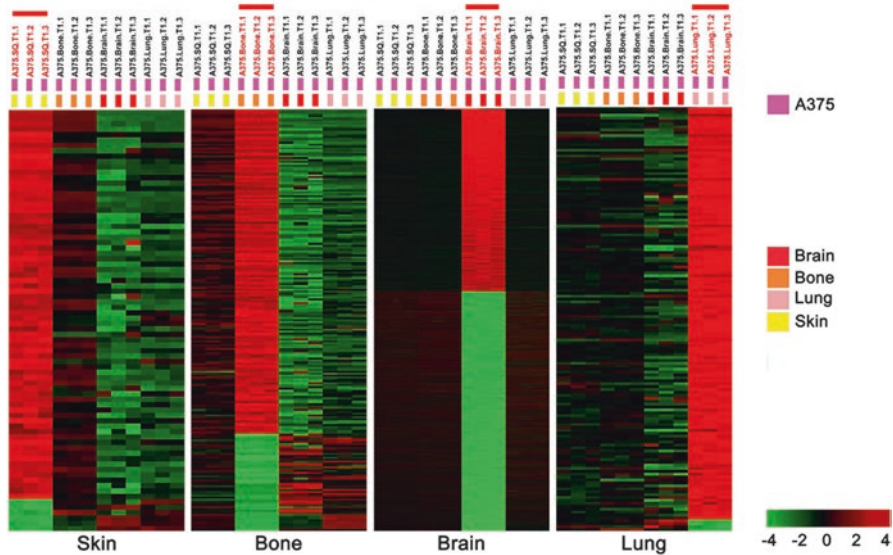


**Fig. 5.3** Organ-specific gene expression patterns of A375 melanoma cells. Each heat map shows the pattern of differentially expressed genes between A375 cells xenografted in each organ and all other organs (skin 78; bone 221; brain 8952; lung 145 genes)

**Table 5.3** Number of genes that were differentially expressed in primary or metastatic organs compared with all other organs

Cell line	Primary site	Bone	Brain	Lung	Skin
A375	(Skin) 78	221	8952	145	–
KM12	(Cecum) 87	1672	395	164	46
MDA-MB-231	(Mammary fat pad) 32	1180	477	42	95
PC-14	(Lung) 351	694	8634	–	56
PC3P	(Prostate) 42	651	2678	15	214
SN12	(Kidney) 141	16	209	871	0

395, 164, and 46 genes were specific to KM12 colon cancer cells growing in the cecum, bone, brain, lung, and skin, respectively. Cluster of 32, 1180, 477, 42, and 95 genes were specific to MDA-MB-231 breast cancer cells growing in the mammary fat pad, bone, brain, lung, and skin, respectively. Clusters of 351, 694, 8634, and 56 genes were specific to PC-14 lung cancer cells growing in the lung, bone, brain, and skin, respectively. Clusters of 42, 651, 2678, 15, and 214 genes were specific to PC3P prostate cancer cells growing in the prostate, bone, brain, lung, and skin, respectively. Clusters of 141, 16, 209, and 871 genes were specific to SN12 renal cancer cells growing in the kidney, bone, brain, and lung, respectively. There were no genes specific to SN12 cells growing in the skin. These data suggest that the organ microenvironment modulates gene expression of each cell line investigated.

Other laboratories have also performed comparative genome-wide expression analyses to provide new information regarding the cellular and molecular mechanisms that promote the recruitment and retention of cancer cells to secondary organs of metastasis. We discuss the results of those studies in the following section.

## **Additional Studies**

One of the more widely used investigative approach to study populations of cancer cells with enhanced metastatic potential is to perform an *in vivo* selection process whereby cancer cells are implanted into recipient mice, and metastasis is allowed to occur. Cancer cells are then isolated from metastases and then expanded in cell culture to establish cancer cell sublines that have higher metastatic potential than the corresponding parental cell line. One of the major drawbacks of this *in vivo* selection process is that it can be time-consuming in as much as it frequently requires several rounds of cycling before one can enrich for a population of cells with enhanced metastatic potential. For example, a total of ten cycles of *in vivo* selection were required to establish the murine B16-F10 melanoma cell line with enhanced metastatic ability to form lung metastases [58]. The B16-BL6 metastatic melanoma variant required six selection cycles before its characterization [59].

Nevertheless, despite this limitation, comparative gene expression profiling of parental cells with their metastatic variants has provided invaluable information concerning the genetic determinants that are critical for tissue-specific metastasis. For example, Bos and coworkers [34] used this approach and identified the cyclooxygenase COX2, the EGFR ligand HB-EGF, and the  $\alpha$ 2,6-sialyltransferase ST6GALNAC5, as critical determinants that allow breast cancer cells to extravasate through the blood-brain barrier. In a similar study, Kang and colleagues [60] created transcriptional profiles on parental MDA-MB-231 breast cancer cells and several metastatic variants and identified an underlying gene signature that explained the organ tropism of the cancer cells for the bone. The bone-colonizing variants expressed significantly more MMP-1, IL-11, osteopontin, connective tissue growth factor, and the chemokine receptor CXCR-4. The concerted expression of this gene set explained the tropisms of these cells to bone (CXCR-4), proteolysis (MMP-1), angiogenesis (connective tissue growth factor), and osteoclastogenesis (IL-11 and osteopontin).

Evidence generated from gene expression arrays also suggests that metastatic cancer cells exhibit a phenotype that is remarkably similar to that of stem cells. Glinsky and coworkers [61] examined the patterns of gene expression in experimental tumors and in human tumors and demonstrated that metastases express an 11-gene molecular signature that is consistent with the gene expression pattern of stem cells. The group also noted that the set of transcripts could predict clinical outcomes in patients with a broad range of tumors.

We [32] grew GI-101A breast cancer cells on a hard (0.9%) agar substrate and discovered that the agar-grown cells, designated GI-AGR, were homogeneous for CD44 and CD133, two markers that have been used to identify stem cells [62]. The GI-AGR cells were five times more invasive than parental GI-101 cells and

formed significantly more experimental brain metastases. We performed comparative gene expression analyses on the GI-AGR cells and found that their patterns of gene expression were markedly distinct from that of parental cells but overlapped with the GI-101A subline GI-BRN, which was generated through repetitive recycling of GI-101A cells in an experimental brain metastasis model.

### Conclusion

Over recent years, it has become increasingly apparent that there are significant phenotypic differences between primary and disseminated cancers [6, 7], suggesting that information garnered from primary tumors may not be ideal for identifying clinically actionable therapeutic targets for patients with systemic disease. Indeed, it is estimated that approximately 90% of cancer deaths are due to progressive growth of metastases that are refractory to therapy [63]. However, very little is known regarding the patterns of gene expression in cancer metastases. Using cross-species hybridization of microarrays to study patterns of gene expression among cancer cells growing in different anatomic regions, we found that:

1. Clusters of cancer cell genes can be used to determine the type of cancer present regardless of its anatomic location
2. Clusters of cancer cell genes can be used to identify the organ that harbors the cancer irrespective of the type of cancer cells that are present (organ-specific gene signature)
3. Clusters of genes can identify both the type of cancer present and its anatomic location (cancer type- and organ-specific gene signature)

While it is widely accepted that the organ microenvironment plays a critical role in mediating tumor progression, metastasis, and response to therapy [11, 12, 64], there is a general lack of knowledge regarding the bidirectional signaling that takes place between cancer cells and resident normal (nontransformed) cells in the microenvironment. One factor that has limited our understanding of the microenvironmental impact on cancer cell gene expression is that separating cancer cells from stroma cells and parenchymal cells still remains a technically challenging procedure. Previously, we demonstrated that this technical limitation could be overcome by applying cross-species hybridization of microarrays to tumor xenografts [35]. The strength of this technique is that it allows the investigator to generate gene expression patterns of cancer cells and stromal cells from a single xenograft tumor by hybridizing its mRNAs to human and mouse microarrays, respectively. When we initially applied competitive cross-species hybridization of microarrays to mice harboring experimental brain metastases, we discovered that the brain microenvironment induces complete reprogramming of the cancer cells to the extent that they gain neuronal cell characteristics and mimic the neurogenesis process observed during development [35].

Here, we found that cancer-cell gene expression was governed intrinsically by the individual cancer cell types themselves and extrinsically by the different organ microenvironments. Recent results from other laboratories have also concluded that regional variations in environmental selection forces contribute to the

molecular diversity of cancer cells in tumors [65]. One of the primary motivations of our study was to test the hypothesis that different types of cancer cells residing in the same secondary tissue express overlapping patterns of gene expression. We confirmed this hypothesis and are currently mining the data to identify candidate therapeutic targets for intervention against fatal metastasis. Continued study of the reciprocal signaling between metastatic cancer cells and the organ microenvironment is likely to provide new opportunities for therapeutic intervention.

**Conflict of Interest** None

---

## References

1. Langley RR, Fidler IJ. Tumor cell-organ microenvironment interactions in the pathogenesis of cancer metastasis. *Endocr Rev.* 2007;3:297–321.
2. Fidler IJ, Kripke ML. Metastasis results from preexisting variant cells within a malignant tumor. *Science.* 1977;197(4306):893–5.
3. Talmadge JE, Wolman SR, Fidler IJ. Evidence for the clonal origin of spontaneous metastases. *Science.* 1982;217(4557):361–3.
4. Wang X, Wang M, MacLennan GT, Abdul-Karim FW, Eble JN, Jones TD, et al. Evidence for common clonal origin of multifocal lung cancers. *J Natl Cancer Inst.* 2009;101(8):560–70.
5. Cifone MA, Fidler IJ. Increasing metastatic potential is associated with increasing genetic instability of clones isolated from murine neoplasms. *Proc Natl Acad Sci U S A.* 1981;78(11):6949–52.
6. Stoecklein NH, Hosch SB, Bezler M, Stern F, Hartmann CH, Vay C, et al. Direct genetic analysis of single disseminated cancer cells for prediction of outcome and therapy selection in esophageal cancer. *Cancer Cell.* 2008;13(5):441–53.
7. Brastianos PK, Carter SL, Santagata S, Cahill DP, Taylor-Weiner A, Jones RT, et al. Genomic characterization of brain metastases reveals branched evolution and potential therapeutic targets. *Cancer Discov.* 2015;11:1164–77.
8. Talmadge JE, Benedict K, Madsen J, Fidler IJ. Development of biological diversity and susceptibility to chemotherapy in murine cancer metastases. *Cancer Res.* 1984;44(9):3801–5.
9. Nguyen DX, Bos PD, Massague J. Metastasis: from dissemination to organ-specific colonization. *Nat Rev Cancer.* 2009;9(4):274–84.
10. Horak CE, Steeg PS. Metastasis gets site specific. *Cancer Cell.* 2005;8(2):93–5.
11. Langley RR, Fidler IJ. The seed and soil hypothesis revisited—the role of tumor-stroma interactions in metastasis to different organs. *Int J Cancer.* 2011;128(11):2527–35.
12. Joyce JA, Pollard JW. Microenvironmental regulation of metastasis. *Nat Rev Cancer.* 2009 Apr;9(4):239–52.
13. van Roy F, Berx G. The cell-cell adhesion molecule E-cadherin. *Cell Mol Life Sci.* 2008;65(23):3756–88.
14. Lamouille S, Xu J, Derynck R. Molecular mechanisms of epithelial-mesenchymal transition. *Nat Rev Mol Cell Biol.* 2014;15(3):178–96.
15. Thiery JP, Acloque H, Huang RY, Nieto MA. Epithelial-mesenchymal transitions in development and disease. *Cell.* 2009;139(5):871–90.
16. Mani SA, Guo W, Liao MJ, Eaton EN, Ayyanan A, Zhou AY, et al. The epithelial-mesenchymal transition generates cells with properties of stem cells. *Cell.* 2008;133(4):704–15.
17. Singh A, Settleman J. EMT, cancer stem cells and drug resistance: an emerging axis of evil in the war on cancer. *Oncogene.* 2010;29(34):4741–51.

18. Liotta LA, Rao NC, Barsky SH, Bryant G. The laminin receptor and basement membrane dissolution: role in tumour metastasis. *Ciba Found Symp.* 1984;108:146–62.
19. Barsky SH, Siegal GP, Jannotta F, Liotta LA. Loss of basement membrane components by invasive tumors but not by their benign counterparts. *Lab Invest.* 1983;49(2):140–7.
20. Dvorak HF. Tumors: wounds that do not heal. Similarities between tumor stroma generation and wound healing. *N Engl J Med.* 1986;315(26):1650–9.
21. Liotta LA, Kleinerman J, Saidel GM. Quantitative relationships of intravascular tumor cells, tumor vessels, and pulmonary metastases following tumor implantation. *Cancer Res.* 1974;34(5):997–1004.
22. Fidler IJ. The relationship of embolic homogeneity, number, size and viability to the incidence of experimental metastasis. *Eur J Cancer.* 1973;9(3):223–7.
23. Liotta LA, Saidel MG, Kleinerman J. The significance of hematogenous tumor cell clumps in the metastatic process. *Cancer Res.* 1976;36(3):889–94.
24. Terry RW, Kwee L, Levine JF, Labow MA. Cytokine induction of an alternatively spliced murine vascular cell adhesion molecule (VCAM) mRNA encoding a glycosylphosphatidylinositol-anchored VCAM protein. *Proc Natl Acad Sci U S A.* 1993;90(13):5919–23.
25. Panes J, Perry M, Granger DN. Leukocyte-endothelial cell adhesion: avenues for therapeutic intervention. *Br J Pharmacol.* 1999;126(3):537–50.
26. Schadendorf D, Heidel J, Gawlik C, Suter L, Czarnetzki BM. Association with clinical outcome of expression of VLA-4 in primary cutaneous malignant melanoma as well as P-selectin and E-selectin on intratumoral vessels. *J Natl Cancer Inst.* 1995;87(5):366–71.
27. Langley RR, Carlisle R, Ma L, Specian RD, Gerritsen ME, Granger DN. Endothelial expression of vascular cell adhesion molecule-1 correlates with metastatic pattern in spontaneous melanoma. *Microcirculation.* 2001;8(5):335–45.
28. Serres S, Soto MS, Hamilton A, McAteer MA, Carbonell WS, Robson MD, et al. Molecular MRI enables early and sensitive detection of brain metastases. *Proc Natl Acad Sci U S A.* 2012;109(17):6674–9.
29. Rebhun RB, Cheng H, Gershenwald JE, Fan D, Fidler IJ, Langley RR. Constitutive expression of the alpha4 integrin correlates with tumorigenicity and lymph node metastasis of the B16 murine melanoma. *Neoplasia.* 2010;12(2):173–82.
30. Kim SW, Kim SJ, Langley RR, Fidler IJ. Modulation of the cancer cell transcriptome by culture media formulations and cell density. *Int J Oncol.* 2015;46(5):2067–75.
31. Cruz-Munoz W, Man S, Xu P, Kerbel RS. Development of a preclinical model of spontaneous human melanoma central nervous system metastasis. *Cancer Res.* 2008;68(12):4500–5.
32. Guo L, Fan D, Zhang F, Price JE, Lee JS, Marchetti D, et al. Selection of brain metastasis-initiating breast cancer cells determined by growth on hard agar. *Am J Pathol.* 2011;178(5):2357–66.
33. Kang Y, He W, Tulley S, Gupta GP, Serganova I, Chen CR, et al. Breast cancer bone metastasis mediated by the Smad tumor suppressor pathway. *Proc Natl Acad Sci U S A.* 2005;102(39):13909–14.
34. Bos PD, Zhang XH, Nadal C, Shu W, Gomis RR, Nguyen DX, et al. Genes that mediate breast cancer metastasis to the brain. *Nature.* 2009;459(7249):1005–9.
35. Park ES, Kim SJ, Kim SW, Yoon SL, Leem SH, Kim SB, et al. Cross-species hybridization of microarrays for studying tumor transcriptome of brain metastasis. *Proc Natl Acad Sci U S A.* 2011;108(42):17456–61.
36. Cascone T, Herynk MH, Xu L, Du Z, Kadara H, Nilsson MB, et al. Upregulated stromal EGFR and vascular remodeling in mouse xenograft models of angiogenesis inhibitor-resistant human lung adenocarcinoma. *J Clin Invest.* 2011;121(4):1313–28.
37. Kozlowski JM, Hart IR, Fidler IJ, Hanna N. A human melanoma line heterogeneous with respect to metastatic capacity in athymic nude mice. *J Natl Cancer Inst.* 1984;72(4):913–7.
38. Morikawa K, Walker SM, Nakajima M, Pathak S, Jessup JM, Fidler IJ. Influence of organ environment on the growth, selection, and metastasis of human colon carcinoma cells in nude mice. *Cancer Res.* 1988;48(23):6863–71.



39. Cailleau R, Young R, Olive M, Reeves Jr WJ. Breast tumor cell lines from pleural effusions. *J Natl Cancer Inst.* 1974;53(3):661–74.
40. Kaighn ME, Narayan KS, Ohnuki Y, Lechner JF, Jones LW. Establishment and characterization of a human prostatic carcinoma cell line (PC-3). *Invest Urol.* 1979;17(1):16–23.
41. Sun JK, Uehara H, Karashima T, McCarty M, Shih N, Fidler IJ. Expression of interleukin-8 correlates with angiogenesis, tumorigenicity, and metastasis of human prostate cancer cells implanted orthotopically in nude mice. *Neoplasia.* 2001;3(1):33–42.
42. Yano S, Nokihara H, Hanibuchi M, Parajuli P, Shinohara T, Kawano T, et al. Model of malignant pleural effusion of human lung adenocarcinoma in SCID mice. *Oncol Res.* 1997;9(11-12):573–9.
43. Naito S, von Eschenbach AC, Fidler IJ. Different growth pattern and biologic behavior of human renal cell carcinoma implanted into different organs of nude mice. *J Natl Cancer Inst.* 1987;78(2):377–85.
44. Killion JJ, Radinsky R, Fidler IJ. Orthotopic models are necessary to predict therapy of transplantable tumors in mice. *Cancer Metastasis Rev.* 1998–1999;17(3):279–84.
45. Huang SF, Kim S-J, Lee AT, Karashima T, Bucana C, Kedar D, et al. Inhibition of growth and metastasis of orthotopic human prostate cancer in athymic mice by combination therapy with pegylated interferon- $\alpha$ -2b and docetaxel. *Cancer Res.* 2002;62(20):5720–6.
46. Schackert G, Fidler IJ. Site-specific metastasis of mouse melanomas and a fibrosarcoma in the brain or meninges of syngeneic animals. *Cancer Res.* 1988;48(12):3478–84.
47. Kim S-J, Kim J-S, Park ES, Lee J-S, Lin Q, Langley RR, et al. Astrocytes upregulate survival genes in tumor cells and induce protection from chemotherapy. *Neoplasia.* 2011;13(3):286–98.
48. Singh RK, Bucana CD, Gutman M, Fan D, Wilson MR, Fidler IJ. Organ site-dependent expression of basic fibroblast growth factor in human renal cell carcinoma cells. *Am J Pathol.* 1994;145(2):365–74.
49. Li L, Price JE, Fan D, Zhang RD, Bucana CD, Fidler IJ. Correlation of growth capacity of human tumor cells in hard agarose with their *in vivo* proliferative capacity at specific metastatic sites. *J Natl Cancer Inst.* 1989;81(18):1406–12.
50. Onn A, Isobe T, Itasaka S, Wu W, O'Reilly MS, Ki Hong W, et al. Development of an orthotopic model to study the biology and therapy of primary human lung cancer in nude mice. *Clin Cancer Res.* 2003;9(15):5532–9.
51. Uehara H, Kim SJ, Karashima T, Shepherd DL, Fan D, Tsan R, et al. Effects of blocking platelet-derived growth factor-receptor signaling in a mouse model of experimental prostate cancer bone metastases. *J Natl Cancer Inst.* 2003;95(6):458–70.
52. Yokoi K, Thaker PH, Yazici S, Rebhun RR, Nam DH, He J, et al. Dual inhibition of epidermal growth factor receptor and vascular endothelial growth factor receptor phosphorylation by AEE788 reduces growth and metastasis of human colon carcinoma in an orthotopic nude mouse model. *Cancer Res.* 2005;65(9):3716–25.
53. Simon R, Lam A, Li M-C, Ngan M, Menendez S, Zhao Y. Analysis of gene expression data using BRB-array tools. *Cancer Inform.* 2007;3:11–7.
54. Bolstad BM, Irizarry RA, Astrand M, Speed TP. A comparison of normalization methods for high density oligonucleotide array data based on variance and bias. *Bioinformatics.* 2003;19(2):185–93.
55. Eisen MB, Spellman PT, Brown PO, Botstein D. Cluster analysis and display of genome-wide expression patterns. *Proc Natl Acad Sci U S A.* 1998;95(25):14863–8.
56. Troyanskaya O, Cantor M, Sherlock G, Brown P, Hastie T, Tibshirani R, et al. Missing value estimation methods for DNA microarrays. *Bioinformatics.* 2001;17(6):520–5.
57. Hosack DA, Dennis Jr G, Sherman BT, Lane HC, Lempicki RA. Identifying biological themes within lists of genes with EASE. *Genome Biol.* 2003;4(10):R70.
58. Fidler IJ, Nicolson GL. Organ selectivity for implantation survival and growth of B16 melanoma variant tumor lines. *J Natl Cancer Inst.* 1976;57(5):1199–202.

59. Poste G, Doll J, Hart IR, Fidler IJ. In vitro selection of murine B16 melanoma variants with enhanced tissue-invasive properties. *Cancer Res.* 1980;40(5):1636–44.
60. Kang Y, Siegel PM, Shu W, Drobnjak M, Kakonen SM, Cordon-Cardo C, et al. A multigenic program mediating breast cancer metastasis to bone. *Cancer Cell.* 2003;3(6):537–49.
61. Glinsky GV, Berezovska O, Glinskii AB. Microarray analysis identifies a death-from-cancer signature predicting therapy failure in patients with multiple types of cancer. *J Clin Invest.* 2005;115(6):1503–21.
62. Clarke MF, Dick JE, Dirks PB, Eaves CJ, Jamieson CH, Jones DL, et al. Cancer stem cells—perspectives on current status and future directions: AACR workshop on cancer stem cells. *Cancer Res.* 2006;66(19):9339–44.
63. Mehlen P, Puisieux A. Metastasis: a question of life or death. *Nat Rev Cancer.* 2006;6(6):449–58.
64. Quail DF, Joyce JA. Microenvironmental regulation of tumor progression and metastasis. *Nat Med.* 2013;19(11):1423–37.
65. Lloyd MC, Cunningham JJ, Bui MM, Gillies RJ, Brown JS, Gatenby RA. Darwinian dynamics of intratumoral heterogeneity: not solely random mutations but also variable environmental selection forces. *Cancer Res.* 2016;76(11):3136–44.

---

# Techniques for Surgical Orthotopic Implantation of Human Tumors to Immunodeficient Mice

# 6

Robert M. Hoffman

---

## Introduction

This chapter is based on [1] and has been updated.

## Early Nude-Mouse Models of Human Cancer

The first nude mouse of human cancer was a subcutaneous implantation of a patient colon tumor in nude mice which grew over 70 passages. However, no metastasis occurred. This was almost always the case with subcutaneous tumor implantation of tumors in immunodeficient mice, even highly malignant tumors [2].

Wang and Sordat showed that disaggregated human colon-cancer cell lines injected into the cecum of nude mice produced tumors that eventually metastasized [3]. Orthotopic injection of cell suspensions was a great improvement over simple subcutaneous implantation. However, the tumors resulting from orthotopic transplantation of cell suspensions often showed relatively low rates of metastasis compared to the original tumor in the patient [1].

## Surgical Orthotopic Implantation (SOI) of Tumor Fragments

The SOI models circumvent the cell disaggregation step used in previous orthotopic models. Instead of injecting cell suspensions into the orthotopic site, we have developed microsurgical technology to transplant tumor fragments

---

R.M. Hoffman, Ph.D.

AntiCancer, Inc., 7917 Ostrow Street, San Diego, CA 92111, USA

Department of Surgery, University of California, San Diego, CA, USA

e-mail: [all@anticancer.com](mailto:all@anticancer.com)

orthotopically [1]. The development of SOI technology led to increased metastatic frequency, and metastatic sites in the transplanted mice which reflect the clinical pattern after SOI [1].

For example, in a head-to-head comparison of SOI with orthotopic transplantation of cell suspensions of stomach cancer, SOI of cancer tissue fragments resulted in metastases in 100% of the nude mice with extensive primary growth. Metastases were found in the regional lymph nodes, liver, and lung as is the clinical characteristic of this cancer [4]. In contrast, orthotopic injection of suspensions of stomach cancer cells to the nude-mouse stomach resulted in lymph node metastases in only 6.7% of those mice with primary tumors and no distant metastases [1].

Theodorescu et al. [5] observed that the RT-4 human bladder carcinoma line is not invasive in nude mice, after orthotopic injection of disaggregated cancer cells. However, when a mutated human *H-ras* gene was transfected into RT-4 so that over-expression of the gene occurred in selected cell lines such as RT-4mr-10 (RT-10), the selected cell line was able to locally invade the bladder after transurethral orthotopic inoculation of disaggregated cancer cells. However, no contiguous or metastatic spread by RT-10 was found in other organs. The parental cell lines and the *ras*-transfectants all produced tumors when inoculated s.c. However, the tumors grew in the s.c. site as pseudo-encapsulated masses without any evidence of tissue invasion. In contrast, when transplanted by SOI, both RT-4 and RT-10 were metastatic to numerous organs [6].

We also compared the metastatic frequency of human renal cell carcinoma SN12C after SOI of tumor tissue and orthotopic injection of cell suspensions in the kidney of nude mice. The primary tumors resulting from SOI were larger and much more locally invasive than primary tumors resulting from orthotopic transplantation of cell suspension and SOI generated higher metastatic frequency than orthotopic transplantation of cell suspensions. The differences in metastatic frequency in the involved organs (the lung, liver, and mediastinal lymph nodes) were two- to three-fold higher in SOI compared to orthotopic transplantation of cell suspensions. Median survival time in the SOI model was 40 days, which was significantly shorter than that of orthotopic transplantation of cell suspensions (68 days). Histological observation of the primary tumors from the SOI model demonstrated a much richer vascular network than the orthotopic transplantation of cell suspension. Lymph node and lung metastases were larger and more cellular in the SOI model compared to the orthotopic transplantation of cell suspension models [1, 7].

SOI models had true time-dependent metastases resulting from clinical-like routes and not due to cells shed in transplantation [1, 8]. These studies directly demonstrate that the implantation of histologically intact tumor tissue orthotopically allows accurate expression of the clinical features of human cancer in nude mice [1].

Colon cancer tissue was transplanted on the serosal layers of the stomach (heterotopic site) and the serosal layers of the colon (orthotopic site) to determine comparison of outcome [9]. Human colon tumor, Co-3, which is well differentiated,

and COL-3-JCK which is poorly differentiated were used for transplantation. After orthotopic transplantation of the human colon tumors on the nude mouse colon, invasive and metastatic behavior resulted. In contrast, after heterotopic transplantation of the human colon tumor on the nude mouse stomach, a large growing tumor resulted but with only limited invasive growth and without serosal spreading lymphatic duct invasion or regional lymph node metastasis. These studies suggest that the original host organ plays a critical role in tumor progression [1, 9].

A correlative clinical trial was carried out to compare the course of stomach tumors in patients and in SOI models after orthotopic transplantation [10]. There was a statistical correlation for both liver metastases and peritoneal involvement between patients and in nude mice after SOI. The histology of both the local and metastatic tumors in the mice closely resembled the original local and metastatic tumors in the patient. These results indicate that the SOI models resemble clinical cancer [1, 10].

---

## Materials and Methods

### General Construction of Models

*Mice:* Four-to-six-week-old outbred nu/nu mice of both sexes are used for the orthotopic transplantation. Other more immunodeficient mice such as SCID, SCID-NOD, SCID-NSG, and SCID-NOG can be used. All animal studies are conducted in accordance with the principles and procedures outlined in the National Institutes of Health Guide for the Care and Use of Laboratory Animals under assurance number A3873-1 [1].

*Specimens:* Fresh surgical specimens from human patients are kept in Earle's MEM at 4 °C and obtained as soon as possible from hospitals. Transplantation should take place within 24 h of surgical excision. Before transplantation, each specimen is inspected, and all necrotic and suspected necrotic tumor tissue is removed [1].

### Examples of Surgical Orthotopic Implantation (SOI) to Establish Patient-Derived Orthotopic Xenograft (PDOX) Mouse Models

#### Colon Cancer PDOX

*Colonic transplantation:* For transplantation, nude mice are anesthetized, and the abdomen is sterilized with iodine and alcohol swabs. A small midline incision is made, and the colorectal part of the intestine is exteriorized. The serosa of the site where tumor pieces are to be implanted is removed. Tumor fragments of one mm<sup>3</sup> size tumor are implanted on the top of the animal intestine. An 8-0 surgical suture is used to penetrate these small tumor pieces and attach them on the wall of the

intestine. The intestine is returned to the abdominal cavity, and the abdominal wall is closed with 7-0 surgical sutures. Animals are kept in a sterile environment. Tumors of all stages and grades can be utilized [1, 11].

*Intrahepatic transplantation:* After anesthesia, an incision is made through the left upper abdominal pararectal line and peritoneum. The left lobe of the liver is carefully exposed, and the liver is cut approximately 3 mm with scissors. Tumor fragments of 1–2 mm<sup>3</sup> size are put on the nude mouse liver and attached immediately with double sutures using 8-0 nylon with an atraumatic needle. After confirmation that no bleeding is occurring, the liver is then returned to the peritoneal cavity. The abdomen and skin are then closed with 6-0 back silk sutures [1, 12].

### **Lung Cancer PDOX**

After anesthesia, the animals are put in a position of right lateral decubitus, with four limbs restrained. A 0.8 cm transverse incision of skin is made in the left chest wall. Chest muscles are separated by sharp dissection and costal and intercostal muscles are exposed. A 0.4–0.5 cm intercostals incision between the third and fourth rib on the chest wall is made, and the chest wall is opened. The left lung is taken up with a forceps, and tumor fragments are sewn promptly into the upper lung with one suture. The lung is then returned into the chest cavity. The incision in the chest wall is closed by a 6-0 surgical suture. The closed condition of the chest wall is examined immediately, and if a leak exists, it is closed by additional sutures. After closing the chest wall, an intrathoracic puncture is made by using a 3-mL syringe and 25G 1/2 needle to withdraw the remaining air in the chest cavity. After the withdrawal of air, a completely inflated lung can be seen through the thin chest wall of the mouse. Then the skin and chest muscle are closed with a 6-0 surgical suture in one layer [1, 13].

### **Pleural Cancer PDOX**

After anesthesia, a 1 cm left transverse thoracotomy via the fourth intercostals space using a sterile #11 scalpel is made. The chest wall and intercostals muscles are separated using sharp and blunt dissection, exposing the intercostals space. A small incision is made to provide access to the pleural space which results in total lung collapse. A sterile 7.0 or 8.0 nylon suture on a cutting needle is inserted into the pleural cavity two intercostals spaces below the incision, and it is removed via the thoracotomy. The tumor fragments are sutured onto the parietal pleura from below and the suture onto the intercostals muscles above. The chest wall incision is closed with a 7.0 nylon suture [14].

If there is any evidence of air leak through the thoracotomy incision, place additional sutures until the incision is completely closed. A sterile 3 cc syringe with an attached 25G 1 1/2 gauge needle (angiocatheter) is inserted into the pleural cavity. Using the attached syringe, air is removed from the closed pleural cavity to actively reinflate the lung. Complete lung re-expansion is verified by observation of an increase in respiratory rate and visualization of the lung through the chest wall of the mouse. Chest muscles and the skin are closed with a single layer

of 6.0 silk suture. All procedures are performed with a 7× magnification microscope [1, 14].

### **Mesothelioma PDOX**

After anesthesia is induced, nude mice are placed in the right lateral position and anesthetized by isoflurane. The chest wall is sterilized with iodine and alcohol swabs. A 1 cm transverse incision is made on the left parietal intercostals space. Another small incision is made to provide access to the pleural cavity which results in total collapse of the left lung. The pleural implantation is performed above [14]. Briefly, a sterile 8.0 nylon suture on a cutting needle is inserted into the pleural cavity two intercostals spaces below the incision and removed via the thoracotomy incision. Tumor fragments ( $1 \text{ mm}^3$ ) are strung over the needle onto the suture. The tumor fragments are sutured onto the parietal pleura from below and onto the intercostals muscles above. The chest wall incision is closed with a 7.0 nylon suture. Air is removed from the closed pleural cavity by a sterile 3 cc syringe with an attached 25 G 11/2 gauge needle. Chest muscles and the skin are then closed [1, 15].

### **Pancreatic Cancer PDOX**

After anesthesia, a left lateral abdominal incision is made, the peritoneum is opened, and the part of the pancreas near the portal area of the spleen is well exposed. Tumor fragments of  $1 \text{ mm}^3$  tumor tissue are transplanted on the pancreas with 8-0 surgical sutures. The peritoneum and the skin are then closed in one layer with a 7-0 surgical suture [1, 16].

### **Breast Cancer PDOX**

After anesthesia, the nude mice are put in a supine position. The second right mammary gland is chosen for orthotopic transplantation because it has anatomical resemblance to the anatomical position of the human breast. The surgical region is sterilized with iodine and alcohol swabs. An incision of about 1.5 cm is made along the medial side of the nipple. After blunt dissection, the fat pad is exposed. A small incision is made on the pad and a small pocket is formed. Fragments of tumor tissue are transplanted into the pocket, and an 8-0 suture is made to close the pocket. The skin layer is closed by 6-0 sutures [1, 17].

### **Ovarian PDOX**

After anesthesia, a midline incision is made in the lower abdomen of the nude mouse, and the peritoneum is opened. One side of the ovary of the nude mouse is exposed. The capsule of the ovary is opened, and fragments of  $1 \text{ mm}^3$  human ovarian tumor tissue are transplanted into the capsule. The capsule is closed with an 8.0 surgical suture. In this way, at maximum, two pieces of tumor tissue can be transplanted orthotopically. In order to transplant more tissue orthotopically, after the opening of the ovarian capsule, more tumor fragments are transplanted with the ovarian capsule left open. After orthotopic transplantation, the nude mouse abdomen is closed with 6-0 surgical sutures on one layer. The procedure takes approximately 10 min [1, 18].

### **Cervical Cancer PDOX**

After anesthesia, a small midline incision (6–10 mm) is made on the lower abdomen of the nude mouse through the skin and peritoneum. The uterus is exposed through this incision, and tumor fragments (1 mm<sup>3</sup>) are sutured to the cervix of the uterus using 8–0 nylon surgical sutures (Ethilon; Ethicon Inc., NJ, USA). On completion, the uterus is returned to the abdomen, and the incision is closed in one layer using 6–0 nylon surgical sutures (Ethilon) [19].

### **Soft-Tissue Sarcoma PDOX**

After nude mice are anesthetized, a 5 mm skin incision is made on the right high thigh into the biceps femoris, which is split to make space for the sarcoma tissue fragments. The wound is closed with a 6-0 nylon suture (Ethilon, Ethicon, Inc., NJ, USA) [20].

### **Metastatic Ewing's Sarcoma PDOX**

A fresh tumor tissue sample from the Ewing's sarcoma from the right chest wall of the patient was obtained. After anesthesia, a 10 mm skin incision is made on the right chest wall of nude mice. The PDOX model is established by implanting single tumor fragments into the layer between the pectoral muscle and intercostal muscle in the right chest wall of the nude mouse. The wound is closed with a 6-0 nylon suture (Ethilon, Ethicon, Inc., NJ) [21].

### **PDOX Model of Melanoma Metastasized to the Chest Wall**

After anesthesia, a 5 mm skin incision is made on the right chest into the chest wall of nude mice, which is split to make space for the melanoma tissue fragment. Tumor fragments are implanted orthotopically into the space to establish the PDOX model. The wound is closed with a 6–0 nylon suture (Ethilon, Ethicon, Inc., NJ, USA) [22].

### **Stomach Cancer PDOX**

After anesthesia is induced, tumor fragments are transplanted orthotopically to the stomach serosa. An incision is made through the left-upper abdominal para-rectal line and peritoneum. The stomach wall is carefully exposed, and the serosal membrane is injured for about 2 mm in the greater curvature of the antrum of the stomach using scissors. Tumor fragments are then fixed on each injured site of the serosal surface with a 6-0 Dexon transmural suture. The stomach is returned into the peritoneal cavity. The abdominal wall and skin is closed with 6-0 Dexon sutures [1, 10].

---

## **References**

1. Hoffman RM. Orthotopic metastatic mouse models for anticancer drug discovery and evaluation: a bridge to the clinic. *Invest New Drugs*. 1999;17:343–59.
2. Rygaard J, Povlsen CO. Heterotransplantation of a human malignant tumor to 'nude' mice. *Acta Pathol Microbiol Scand*. 1969;77:758–60.



3. Wang WR, Sordat B, Piguet D, Sordat M. Human colon tumors in nude mice: implantation site and expression of the invasive phenotype. In: Sordat B, editor. Immune-deficient animals—4th international workshop on immune-deficient animals in experimental research. Basel: Karger; 1982. p. 239–45.
4. Furukawa T, Fu X, Kubota T, Watanabe M, Kitajima M, Hoffman RM. Nude mouse metastatic models of human stomach cancer constructed using orthotopic implantation of histologically intact tissue. *Cancer Res.* 1993;53:1204–8.
5. Theodorescu D, Cornil I, Fernandez BJ, Kerbel RS. Overexpression of normal and mutated forms of HRAS induces orthotopic bladder invasion in a human transitional cell carcinoma. *Proc Natl Acad Sci U S A.* 1990;87:9047–51.
6. Fu X, Hoffman RM. Human RT-4 bladder carcinoma is highly metastatic in nude mice and comparable to *ras*-H-transformed RT-4 when orthotopically onplanted as histologically intact tissue. *Int J Cancer.* 1992;51:989–91.
7. An Z, Jiang P, Wang X, Moossa AR, Hoffman RM. Development of a high metastatic orthotopic model of human renal cell carcinoma in nude mice: benefits of fragment implantation compared to cell-suspension injection. *Clin Exp Metastasis.* 1999;17:265–70.
8. Kuo T-H, Kubota T, Watanabe M, Fujita S, Furukawa T, Teramoto T, Ishibiki K, Kitajima M, Hoffman RM. Early resection of primary orthotopically-growing human colon tumor in nude mouse prevents liver metastasis: further evidence for patient-like hematogenous metastatic route. *Anticancer Res.* 1993;13:293–8.
9. Togo S, Shimada H, Kubota T, Moossa AR, Hoffman RM. Host organ specifically determines cancer progression. *Cancer Res.* 1995;55:681–4.
10. Furukawa T, Kubota T, Watanabe M, Kitajima M, Fu X, Hoffman RM. Orthotopic transplantation of histologically-intact clinical specimens of stomach cancer to nude mice: correlation of metastatic sites in mouse and human. *Int J Cancer.* 1993;53:608–12.
11. Fu X, Besterman JM, Monosov A, Hoffman RM. Models of human metastatic colon cancer in nude mice orthotopically constructed by using histologically-intact patient specimens. *Proc Natl Acad Sci U S A.* 1991;88:9345–9.
12. Kuo T-H, Kubota T, Watanabe M, Furukawa T, Teramoto T, Ishibiki K, Kitajimi M, Moossa AR, Penman S, Hoffman RM. Liver colonization competence governs colon cancer metastasis. *Proc Natl Acad Sci USA.* 1995;92:12085–89.
13. Wang X, Fu X, Hoffman RM. A new patient-like metastatic model of human lung cancer constructed orthotopically with intact tissue via thoracotomy in immunodeficient mice. *Int J Cancer* 1992;51:992–5.
14. Astoul P, Colt HG, Wang X, Hoffman RM. A “patient-like” nude mouse model of parietal pleural human lung adenocarcinoma. *Anticancer Res.* 1994;14:85–91.
15. Astoul P, Wang X, Colt HG, Boutin C, Hoffman RM. A patient-like human malignant pleural mesothelioma nude-mouse model. *Oncol Rep.* 1996;3:483–7.
16. Fu X, Guadagni F, Hoffman RM. A metastatic nude-mouse model of human pancreatic cancer constructed orthotopically with histologically intact patient specimens. *Proc Natl Acad Sci USA* 1992;89:5645–9.
17. Fu X, Le P, Hoffman RM. A metastatic-orthotopic transplant nude-mouse model of human patient breast cancer. *Anticancer Res.* 1993;13:901–4.
18. Fu X, Hoffman RM. Human ovarian carcinoma metastatic models constructed in nude mice by orthotopic transplantation of histologically-intact patient specimens. *Anticancer Res.* 1993;13:283–6.
19. Hiroshima Y, Zhang Y, Zhang M, Maawy A, Mii S, Yamamoto M, Uehara F, Miwa S, Yano S, Murakami T, Momiyama M, Chishima T, Tanaka K, Ichikawa Y, Bouvet M, Murata T, Endo I, Hoffman RM. Establishment of a patient-derived orthotopic xenograph (PDOX) model of HER-2-positive cervical cancer expressing the clinical metastatic pattern. *PLoS One.* 2015;10:e0117417.
20. Murakami T, DeLong J, Eilber FC, Zhao M, Zhang Y, Zhang N, Singh A, Russell T, Deng S, Reynoso J, Quan C, Hiroshima Y, Matsuyama R, Chishima T, Tanaka K, Bouvet M, Chawla S, Endo I, Hoffman RM. Tumor-targeting *Salmonella typhimurium* A1-R in combination with

- doxorubicin eradicate soft tissue sarcoma in a patient-derived orthotopic xenograft PDOX model. *Oncotarget*. 2016;7:12783–90.
21. Murakami T, Singh AS, Kiyuna T, Dry SM, Li Y, James AW, Igarashi K, Kawaguchi K, DeLong JC, Zhang Y, Hiroshima Y, Russell T, Eckardt MA, Yanagawa J, Federman N, Matsuyama R, Chishima T, Tanaka K, Bouvet M, Endo I, Eilber FC, Hoffman RM. Effective molecular targeting of CDK4/6 and IGF-1R in a rare FUS-ERG fusion CDKN2A-deletion doxorubicin-resistant Ewing's sarcoma in a patient-derived orthotopic xenograft (PDOX) nude-mouse model. *Oncotarget*. 2016;7:47556–64.
  22. Kawaguchi K, Murakami T, Chmielowski B, Igarashi K, Kiyuna T, Unno M, Nelson SD, Russell TA, Dry SM, Li Y, Eilber FC, Hoffman RM. Vemurafenib-resistant BRAF-V600E mutated melanoma is regressed by MEK targeting drug trametinib, but not cobimetinib in a patient-derived orthotopic xenograft (PDOX) mouse model. *Oncotarget*. 2016;7:71737–43.

---

# The First Patient-Derived Orthotopic Xenograft (PDOX) Mouse Models of Cancer: Cancer of the Colon, Pancreas, Lung, Breast, Ovary, and Mesothelioma

Robert M. Hoffman

---

## Introduction

The introduction of the athymic *nu/nu* mouse (nude mouse) for the growth of human tumors in 1969 changed the paradigm of basic and applied cancer research. Human tumors could now be grown for the first time in a mouse model due to the nude mouse's lack of a thymus which makes T cells. In 1969, Rygaard and Povlsen [1] implanted a colon cancer from a 74-year-old patient subcutaneously (s.c.) in nude mice, which grew as a well-differentiated adenocarcinoma similar to that from the donor patient. The subcutaneously growing tumors were encapsulated and did not metastasize. The original tumor was maintained over 7 years for 76 passages. The vast majority of human solid tumors, growing s.c. in the nude mouse did not metastasize. The s.c.-transplanted tumors had noninvasive growth [1, 2].

Wang et al. [3] in 1982 were among the first to implant human tumors orthotopically (literally “correct surface”) in nude mice rather than “heterotopically” (literally “different surface,” such as s.c.). Human colon cancer cell suspensions were injected within the descending part of the colon of nude mice, which resulted in occasional metastasis, a big breakthrough. Fidler's laboratory and others have shown that the implantation of many types of human tumors in the orthotopic sites of nude mice resulted in metastasis of human tumors [4].

In order to overcome the low frequency of metastasis observed with orthotopic implantation of cell suspensions, our laboratory pioneered the patient-derived orthotopic xenograft (PDOX) nude mouse model with the technique of surgical orthotopic implantation (SOI) of intact colon cancer tissue [5]. A greater extent of metastasis was observed in PDOX models compared with orthotopically implanted cell suspensions.

---

R.M. Hoffman

AntiCancer, Inc., 7917 Ostrow Street, San Diego, CA 92111, USA

Department of Surgery, University of California, San Diego, San Diego, CA, USA

e-mail: [all@anticancer.com](mailto:all@anticancer.com)

## **The First PDOX Models (1991–1996)**

We developed the first orthotopic metastatic model of patient colon cancer. Histologically intact human colon-cancer specimens derived surgically from patients were implanted orthotopically to the colon or cecum of nude mice. We observed extensive orthotopic growth in 13 of 20 cases of implanted patient colon tumors. These showed various growth patterns with subsequent regional, lymph node, and liver metastasis, as well as general abdominal carcinomatosis [5].

### **Colon-Cancer Local Growth and Abdominal Metastasis**

An example is specimen case 1701, an infiltrating mucinous adenocarcinoma of the right colon (modified Duke's classification C2). Two nude mice with pre-implanted Gelfoam were used for tumor implantation, two nude mice were used for tumor implantation with an internal skin flap, and two nude mice were used for direct implantation of tumor tissue to the cecum. The mice demonstrated extensive primary growth as well as abdominal-wall metastases. All mice showed visible tumor growth in the abdomen. Autopsies were performed 113–139 days after implantation [5].

### **Colon-Cancer Local Growth, Abdominal Metastasis, and Lymph Node Metastasis**

An example is specimen case 1707, an infiltrating adenocarcinoma of the right colon, moderately differentiated (modified Duke's classification D). Two nude mice were used for tumor and normal-surrounding-tissue co-implantation to the cecum, and two nude mice were used for tumor direct implantation to the cecum. Orthotopic primary tumor growth and abdominal metastasis occurred in three mice. A 10 × 10 mm primary tumor and 12 × 14 abdominal-wall metastasis were found at day 175 after implantation in one of the mice (tumor and normal surrounding tissue co-implanted). Lymph node metastases were noted in this animal. The histology of the original tumor and the orthotopically growing tumor both indicated adenocarcinoma [5].

### **Colon-Cancer General Abdominal Carcinomatosis with Extensive Peritoneal Seeding**

An example is specimen case 1935, infiltrating mucinous adenocarcinoma, moderately differentiated. Extensive carcinomatosis was found with small tumors growing all over the peritoneum and abdominal organs [5].

## **Colon-Cancer Liver Metastasis**

One nude mouse with pre-implanted Gelfoam and an orthotopically-implanted colon tumor was found to have extensive primary tumor growth and multiple liver metastasis. Histology studies on the original tumor tissue, abdominal masses, and multiple liver lesions indicated adenocarcinoma [5].

## **Colon-Cancer Sequential Appearance of Primary Tumor and Metastasis**

Laparotomy was performed on day 26 on the nude mouse implanted with patient tumor 1594. Primary tumor growth was observed. No local or distal organ metastases were observed. The animal was returned for further observation on day 78 when the second laparotomy was performed. Primary growth was found. No liver or other distal organ metastasis was found. On day 160, the mouse was sacrificed. Primary tumor growth, local invasion, and liver metastasis were found at autopsy [5].

## **PDOX Model of Lung-Metastatic Colon Cancer**

The human-patient colorectal tumor lung metastasis grew in the lung in 2 out of 2 animals and not in the colon in 4 out of 4 animals nor in the subcutis in 2 out of 2 animals. Histology showed a moderately- differentiated transplanted human colorectal cancer lung metastasis grown on the nude mouse lung. The resected lung metastasis from the patient and the growing lung metastasis in the mouse were both identical histologically to the patient's original rectal tumor from which the lung metastasis occurred [6]. The lung metastasis appeared to be altered to such an extent that it lost the ability to grow in the colon.

## **PDOX Model of Pancreatic Cancer**

We developed the first orthotopic metastatic mouse model of patient pancreatic cancer. Orthotopic transplantation of histologically intact pancreatic-cancer specimens to the nude-mouse pancreas was performed. The results reflected clinical pancreatic cancer including extensive local tumor growth; extension of the locally growing human pancreatic cancer to the nude-mouse stomach and duodenum; metastases to the nude-mouse liver and regional lymph nodes; and distant metastases to the nude-mouse adrenal gland, diaphragm, and mediastinal lymph nodes. In a series of five patient cases, there was a 100% take rate. Of 17 mice transplanted, 15 had tumor growth. Immunohistochemical analysis of the antigenic phenotype of the transplanted human pancreatic tumors showed a similar pattern of expression of two human

tumor-associated antigens, tumor-associated glycoprotein 72, and carcinoembryonic antigen (CEA) in the transplanted tumors, similar to the original surgical biopsy [7].

### **Pancreatic-Cancer Distant Metastasis to Liver**

Metastases to the liver surface were seen in case 2020 [7].

### **Pancreatic-Cancer Very Distant Metastases**

Case number 2020 involved metastasis to mesenteric lymph nodes, and case number 2008 involved distant metastases to the diaphragm, adrenal glands, mesenteric lymph nodes, and mediastinal lymph nodes and iliac lymph nodes. Metastasis to distant sites such as mediastinal lymph nodes demonstrated that actual metastasis occurred in the model, as opposed to just extension or seeding [7].

### **PDOX Model of Lung Cancer**

We developed the first orthotopic metastatic model of patient lung cancer. Poorly differentiated large-cell squamous-cell lung cancer from a patient was transplanted orthotopically to the left lung as histologically-intact tissue directly from surgery. All five implanted mice produced locally grown tumors in an average time of 61 days. Opposite-lung metastases occurred, as well as lymph node metastases. The primary tumor and metastases faithfully maintained its large cell-squamous cell morphology. When grown s.c., this tumor grew only locally in 2 of 4 animals, and no metastases were observed [8].

### **PDOX Model of Mesothelioma**

We developed the first orthotopic metastatic model of patient mesothelioma. Fresh specimens derived from four patients with malignant mesothelioma were implanted on the parietal pleura of nude mice using SOI. All xenografted tumors resulted in locally growing tumors in the mice. The transplants had extensive tumor spread in the ipsilateral and contralateral pleural cavity as well as mediastinal lymph nodes. When the tumors were confined to the ipsilateral parietal pleura, the implanted animals were in good physical condition. The macroscopic features usually found in mesothelioma patients were also found in the implanted animals, such as nodules, masses, and pleural thickness. Histology of the mousegrown tumor was similar to the original tumor [9].

Orthotopic implantation in nude mice of mesothelioma resulted in growth in all four cases attempted. All patient specimens showed regional spread as well as orthotopic primary tumors [9]. Histologic examination as well as immunohistochemical profiling revealed malignant pleural mesothelioma similar to the original

tumor specimen [9]. In case AC 3157, the implanted tumor was located only on the parietal pleura in one mouse, and in the other mouse, the tumor invaded the visceral and mediastinal pleura. Moreover, in one mouse, a huge nodule developed on the chest wall due to tumor invasion from the pleura. Contralateral invasion of the mediastinal pleura as well as ipsilateral metastatic lymph nodes were observed [9]. In case AC 3208, parietal and visceral-pleural involvement was observed in one transplanted mouse without any other signs of tumor-related disease. Macroscopic examination demonstrated tumor involvement of the visceral and mediastinal pleura as well as the diaphragm. The mediastinum was invaded by the tumor, and ipsilateral and contralateral metastatic mediastinal lymph nodes were observed [9]. In case AC 3083, two mice were shown to have tumor spread in the ipsilateral as well as contralateral pleural cavity [9]. Visceral, diaphragmatic, and mediastinal pleura were involved with tumor in the transplanted mice. In some mice, the tumor grew through the mediastinum and invaded the contralateral mediastinal pleura as well as contralateral visceral and parietal pleura. Ipsilateral and contralateral metastatic mediastinal lymph nodes were seen [9]. Orthotopic implantation of patient tumors allowed growth in 100% of the cases. At autopsy, mice were shown to have an extensive tumor spread in the ipsilateral and contralateral pleural cavity as well as mediastinal lymphatic nodes. These results are in agreement with clinical studies showing that mediastinal and visceral-pleural invasion occur in advanced-stage patient cases of mesothelioma [10]. When the lesions were still confined to the ipsilateral parietal pleura, the implanted animals remained in good condition [9].

### **PDOX Model of Ovarian Cancer**

We developed the first orthotopic metastatic model of patient ovarian cancer. Histologically intact patient specimens of ovarian cancer were transplanted by microsurgical techniques under the capsule of the nude mouse ovary. The human tumors grew locally and gave rise to a patient-like metastatic pattern including the parietal peritoneum, colon, omentum, and ascites. Five cases of human ovarian cancer were transplanted into nude mice, two of which gave rise to tumors. In the first case with patient specimen #1943 of stage II cancer, the largest growth was an encapsulated cyst. No rupture or intraperitoneal seeding was observed. This tumor grew with a cystadenocarcinoma growth pattern. In the second case with patient specimen #2443 of stage IV cancer, extensive solid primary tumor growth was observed along with ascites with extensive metastasis to the colon, omentum, and parietal peritoneum of two of the nude mice. It should be noted that in the patient, there was also metastasis to the bowel and omentum [11].

### **PDOX Model of Pleural-Metastatic Ovarian Cancer**

We developed the first orthotopic metastatic model of patient pleural ovarian cancer. Fresh histologically intact patient specimens of human pleural ovarian adenocarcinoma were implanted onto the visceral and parietal pleura of nude mice.

The human tumors grew locally and regionally, mimicking the usual human clinical features of this disease. A pleural adenocarcinoma specimen was obtained from a patient with a metastatic pleural tumor from a primary ovarian cancer. Five tumor pieces were implanted to the visceral pleura of three mice and to the parietal pleura of three others. Tumor growth was noted in all mice at autopsy. Mean average growth time was 65 days. Local and regional spread was observed on macroscopic examination which included involvement of the ipsilateral lung, diaphragm, mediastinum, and pericardium. Enlarged contralateral lymphadenopathies were only observed in mice that were visceral-pleural implanted, corroborating clinical observations that visceral-pleural involvement in pleural cancer represents an advanced-stage disease [12].

### **PDOX Model of Breast Cancer**

We developed the first orthotopic metastatic model of patient breast cancer. Histologically intact patient breast tumor tissue was transplanted as intact tissue to the mammary fat pad of nude mice where the tumor tissue grew extensively and metastasized to the lung. This was the first orthotopic transplant metastatic model of human patient breast cancer [13]. Eight mice were used for orthotopic transplantation, and seven mice were used for subcutaneous transplantation of the breast cancer specimen. All 15 mice had primary tumor growth after transplantation. The subcutaneously growing tumors were encapsulated with no local invasion or distal organ metastasis observed. In contrast, six out of eight (75%) mice in the orthotopic transplantation group had multiple metastatic nodules in the lung [13]. The metastatic nodules in the lung, when examined histopathologically, were seen also to be poorly differentiated and very similar to the locally growing tumor and to the patient's original tumor. In situ hybridization experiments with a human genomic-wide probe were positive for the locally growing tumor and lung metastasis demonstrating their human origin [13].

### **Clinical Correlation of PDOX Model of Stomach Cancer**

We developed the first orthotopic metastatic model of stomach cancer. Fresh surgical specimens derived from 36 patients with advanced stomach cancer were orthotopically transplanted in nude mice using histologically intact tissue. Twenty of thirty-six patient tumors gave rise to locally-growing tumors in the mice. All 20 patients whose stomach tumors resulted in local growth in the nude mice had clinical lymph node involvement. In contrast, only 8 of the other 16 patients whose tumors were rejected had lymph node involvement. Of the 20 cases resulting in local growth in the nude mice, five had clinical liver metastases and all five cases resulted in liver metastases in the nude mice. Of the 15 patients without liver metastases whose primary tumor grew locally in the mice, only one case gave rise to a liver metastasis in a mouse. Of the 20 cases whose tumors grew in nude mice, six had



clinical peritoneal involvement of their tumor and of these five resulted in peritoneal metastasis in the nude mice. Chromosome analysis confirmed the human origin of the tumors grown in nude mice. These results indicate that, after orthotopic transplantation of histologically intact stomach cancers from patients to nude mice, the subsequent metastatic behavior of the tumors in the mice closely correlated with the course of the tumors in the patients [14]. There was a statistical correlation in metastases between patients and mice. The histology both of primary growth and of metastases in the patient were found to be reproduced in the nude mice [14].

## **Pleural Lung Cancer PDOX**

We developed the first orthotopic metastatic model of pleural lung cancer. A patient lung adenocarcinoma was implanted in the parietal pleura of 11 mice [15]. Implantation in the posterior and low part of the parietal pleura was chosen because of the presence of pleural stomas previously described [16]. Such structures are considered to be a gate through which malignant cells are absorbed from the pleural cavity to the lymphatic circulation via sub-mesothelial lymphatic vessels and also have a connection with sub-peritoneal lymphatics [16–18]. All mice were moribund by days 28–31 after surgery. Performance status was stable until shortly before death. Weight loss, however, was constant [15]. Parietal tumor growth was noted on autopsy in all 11 animals transplanted with patient lung cancer on the parietal pleura. All animals had evidence of chest wall invasion. In addition, the lung was also involved in nine, the mediastinum in seven, the diaphragm in six, and the pericardium in four mice. The mouse-grown tumors had similar histology to the original tumor specimens that were derived. Enlarged lymphadenopathy was not observed. Small, ipsilateral pleural effusions were observed in seven mice. No metastases were observed in the kidneys, adrenal glands, liver, or contralateral lung. There was no evidence of abdominal or contralateral lung metastasis. Rapid tumor growth led to cachexia and death in a relatively short time [15]. In another study, both in the visceral- and parietal-pleural implanted groups, tumor grew in all ten mice transplanted in each group. The median survival time was 27.9 days for the visceral-pleural implanted group and 31 days for the parietal-pleural implanted group. The body weights of pleural-implanted mice decreased from the 14th day until day 31 post-transplantation for the mice remaining alive at that time. The visceral-pleural implanted group had the most weight loss. In contrast, no body weight loss was observed in the subcutaneous-implanted group. The mouse-grown tumors had adenocarcinoma histology similar to the original patient tumor specimen that was derived [19]. Although all pleural-implanted animals showed local and regional spread, no macroscopic and microscopic metastases were observed either on ipsi- or contralateral lung as well as in other organs. However, 5/10 visceral-pleural implanted mice developed metastases involving contralateral mediastinal lymph nodes [19]. Thus, visceral-pleural involvement represents an advanced-stage disease with respect to greater tumor metastases as well as a shorter mean survival time than observed in the parietal-pleural implanted group which is an early-stage

disease. These two components of pleural cancer are mimicked in their respective models described here. Moreover, these models contrast with the symptom-free survival of subcutaneous-implanted mice [19].

These early PDOX models were largely forgotten for nearly 20 years as genetically-engineered and subcutaneous cancer models dominated the field. It was not until Nature Reviews Cancer published a comment comparing orthotopic and subcutaneous cancer models did the PDOX model start to make a come back [2].

---

## References

1. Rygaard J, Povlsen CO. Heterotransplantation of a human malignant tumor to 'nude' mice. *Acta Pathol Microbiol Scand.* 1969;77:758–60.
2. Hoffman RM. Patient-derived orthotopic xenografts: better mimic of metastasis than subcutaneous xenografts. *Nat Rev Cancer.* 2015;15:451–2.
3. Wang WR, Sordat B, Piguet D, Sordat M. Human colon tumors in nude mice: implantation site and expression of the invasive phenotype. In: Sordat B, editor. *Immune-deficient animals—4th international workshop on immune-deficient animals in experimental research.* Basel: Karger; 1982. p. 239–45.
4. Fidler IJ. Critical factors in the biology of human cancer metastasis: twenty-eighth G.H.A. Clowes memorial award lecture. *Cancer Res.* 1990;50:6130–8.
5. Fu X, Besterman JM, Monosov A, Hoffman RM. Models of human metastatic colon cancer in nude mice orthotopically constructed by using histologically intact patient specimens. *Proc Natl Acad Sci U S A.* 1991;88:9345–9.
6. Togo S, Wang X, Shimada H, Moossa AR, Hoffman RM. Cancer seed and soil can be highly selective: human-patient colon tumor lung metastasis grows in nude mouse lung but not colon or subcutis. *Anticancer Res.* 1995;15:795–8.
7. Fu X, Guadagni F, Hoffman RM. A metastatic nude-mouse model of human pancreatic cancer constructed orthotopically from histologically intact patient specimens. *Proc Natl Acad Sci U S A.* 1992;89:5645–9.
8. Wang X, Fu X, Hoffman RM. A new patient-like metastatic model of human lung cancer constructed orthotopically with intact tissue via thoracotomy in immunodeficient mice. *Int J Cancer.* 1992;51:992–5.
9. Astoul P, Wang X, Colt HG, Boutin C, Hoffman RM. A patient-like human malignant pleural mesothelioma nude-mouse model. *Oncol Rep.* 1996;3:483–7.
10. Boutin C, Rey F, Gouvernet J, Viallat JR, Astoul P, Ledoray V. Thoracoscopy in pleural malignant mesothelioma: a prospective study of 188 consecutive patients. Part 2: Prognosis and staging. *Cancer.* 1993;72:394–404.
11. Fu X, Hoffman RM. Human ovarian carcinoma metastatic models constructed in nude mice by orthotopic transplantation of histologically-intact patient specimens. *Anticancer Res.* 1993;13:283–6.
12. Astoul P, Colt HG, Wang X, Hoffman RM. Metastatic human pleural ovarian cancer model constructed by orthotopic implantation of fresh histologically-intact patient carcinoma in nude mice. *Anticancer Res.* 1993;13:1999–2002.
13. Fu X, Le P, Hoffman RM. A metastatic-orthotopic transplant nude-mouse model of human patient breast cancer. *Anticancer Res.* 1993;13:901–4.
14. Furukawa T, Kubota T, Watanabe M, Kitajima M, Fu X, Hoffman RM. Orthotopic transplantation of histologically intact clinical specimens of stomach cancer to nude mice: correlation of metastatic sites in mouse and individual patient donors. *Int J Cancer.* 1993;53:608–12.

15. Astoul P, Colt HG, Wang X, Hoffman RM. A “patient-like” nude mouse model of parietal pleural human lung adenocarcinoma. *Anticancer Res.* 1994;14:85–91.
16. Wang NS. The preformed stomas connecting the pleural cavity and the lymphatics in the parietal pleura. *Am Rev Respir Dis.* 1975;111:12–20.
17. Wang NS. Morphological data of pleura. Normal conditions. In: Chretien J, Hirsch A, editors. *Diseases of the pleura.* New York: Masson; 1977. p. 10–24.
18. Feldman GB. Lymphatic obstruction in carcinomatous ascites. *Cancer Res.* 1975;35:325–32.
19. Astoul P, Colt HG, Wang X, Boutin C, Hoffman RM. A “patient-like” nude mouse metastatic model of advanced human pleural cancer. *J Cell Biochem.* 1994;56:9–15.

R.B. Marques, C.M.A. de Ridder, and W.M. van Weerden

---

## Prostate Cancer: An Introduction

Prostate cancer is one of the most commonly diagnosed cancer types in men in western countries. The incidence is strongly related to aging but seems also affected by certain life style factors indicated by geographical variation. The prostate is an endocrine organ and part of the male reproductive system. This small organ is situated around the urethra, at the base of the bladder. It produces prostate fluid that together with sperm constitutes the semen. Prostate-specific antigen (PSA) is one of the factors produced by the prostate. The leakage of PSA into the blood is currently the major biomarker to indicate prostate cancer risk and is being used to monitor disease progression, although PSA plasma levels lack cancer specificity and are also increased in benign prostate conditions [1]. Like the normal prostate, the majority of prostate cancer is dependent on androgens that act via the androgen receptor (AR) [2]. Based on this androgen sensitivity, androgen ablation by surgical or chemical castration has been the mainstay for treatment of advanced, nonlocalized disease since the early 1940s [3]. Prostate cancer dissemination is characterized by a preferential spread to the skeleton. The development of osseous lesions is a clinical hallmark of progressive prostate cancer and is responsible for most of the morbidity experienced by prostate cancer patients [4]. The above-indicated aspects of prostate cancer, i.e., androgen dependence, AR expression, PSA production, and preferential spread to the bone, are crucial aspects for the management of prostate cancer patients. In order to study prostate cancer disease and develop effective treatment options, accurate model systems reflecting these features of clinical cancer are crucial.

---

R.B. Marques • C.M.A. de Ridder • W.M. van Weerden (✉)  
Department of Urology, Erasmus MC, PO Box 2040, 3000 CA Rotterdam, The Netherlands  
e-mail: [w.vanweerden@erasmusmc.nl](mailto:w.vanweerden@erasmusmc.nl)

## Brief History on Animal Models for Prostate Cancer

Prostate cancer research has for long been seriously hampered by the lack of experimental models. First of all, prostate cancer is not a frequent malignancy in mammals. While a small number of dog breeds do develop benign hyperplasia, they very rarely develop prostate cancer, and the disease is rather different from that in men [5]. Some rodent strains, like ACI-Seg rats, develop macroscopic prostate cancer in 30–40% of aging rats [6]. Likewise, spontaneous prostate cancer develops in Lobund Wistar rats with less frequency (10%) but can be increased significantly by testosterone/MNU (N-methyl-N-nitrosourea) treatment [7]. Similarly, in Noble (Nb) rats, prostatic dysplasia and neoplastic lesions can be induced by chronic treatment with both testosterone and estrogen [8]. In 1961, the serially transplantable Dunning rat prostate cancer R3327 model was established from a spontaneous prostate tumor in an aged Copenhagen rat [9]. Following serial passaging in Copenhagen rats, several R3327 sublines were established with different characteristics, including the Dunning R3327-H (Hopkins) subline. These rat models, and the Dunning R3327-H transplantable model in particular, have been instrumental to our understanding of the basic principles of prostate cancer progression, from androgen dependence toward resistance [10, 11]. In more recent years, numerous genetically modified mouse models (GEMMs), such as the transgenic adenocarcinoma of mouse prostate (TRAMP) model and the less aggressive Lady version [12, 13], as well as several *Pten* knockout mouse models, have been established [14, 15]. With the recognition of the involvement of multiple signaling pathways in prostate cancer development, additional genetic lesions have been engineered into the *Pten* null prostate cancer models to study their potential cooperation with *Pten* loss in prostate carcinogenesis [16].

The discovery of the athymic (nude) mice and its recognition as a natural host for human engraftments led to a breakthrough in experimental oncology, with the establishment of the patient-derived xenograft (PDX) model, allowing the study of human tumor tissue in live animals [17].

In this chapter, we will discuss the development of PDX models for prostate cancer, their role in past and current research activities, their contribution to our understanding of prostate cancer, and, finally, novel developments and advancements to secure future use in basic oncology and translational medicine.

---

## Prostate Cancer Patient-Derived Xenografts

The discovery of the athymic (nude) mouse triggered the development of PDXs for all types of cancer. The initial efforts to subcutaneously transplant patient samples from prostate cancer were, however, very poor. One of the very first PDX of prostate cancer was PC82, established in 1977 after numerous unsuccessful attempts [18]. Despite considerable efforts by a few research groups, the success rate remained extremely low (<5%), and only four PDXs were established, from more than 200 primary prostate cancer transplants, over a period of more than 5 years: PC82, PCEW, PC133, and PC135 [18, 19]. In the early 1980s, two additional PDX

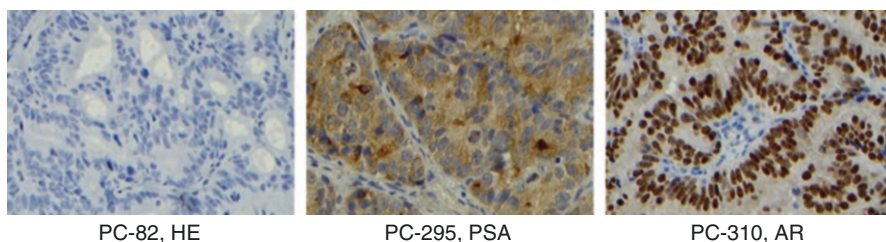


**Fig. 8.1** Three unique PDX models of early-stage, well-differentiated, androgen-responsive prostate cancer, respectively, all expressing AR and PSA [22, 37]

models were established: Honda and the TEN12 model [20, 21]. Continued efforts by the Rotterdam research group finally resulted in a substantial panel of seven new PDXs, established in athymic NMRI nude mice within a relative short period of time and with relative high success rate of 30% (Fig. 8.1) [22]. Inspired by this success, various research groups, predominantly in the USA, took on additional efforts ultimately resulting in additional sets of PDXs, including the CWR series from Case Western Reserve University, Cleveland; the LuCaP series from the University of Washington, Seattle; the MDA-PCa series by MD Anderson, Texas; and the LAPC series of the UCLA [23–28].

The significant expansion of the number of PDXs for prostate cancer by these groups was attributed especially to the significant investments and dedication transplanting large numbers of patient samples to compensate for the general low success rate. In order to understand the high success rates experienced in the NMRI nude mice by the Rotterdam Group, the putative role of (nonpathogenic) murine viruses in triggering PDX establishment has been an interesting suggestion. This hypothesis is supported by the later observation that all newly established PDXs were found to contain murine leukemia virus (MLV). Indeed, we reported on highly activated stroma in these PDXs with increased susceptibility to develop murine lymphomas [29]. Later studies indicated that prostate cancer appeared to have a propensity for infection with murine gamma retroviruses [30], although it remains unclear if infection with these viruses is necessary for the establishment of prostate cancer cell lines and PDXs [31, 32].

In line with the initial rather poor successes to establish PDXs of prostate cancer, a similar difficult development was seen when patient material was directly used for cell cultures. Historically, only a few cell lines were successfully derived from human tissue, namely PC3, DU145, and LNCaP [33–35]. Although only LNCaP shows the important feature of androgen responsiveness (driven by a mutated AR), these cell lines are still among the most frequently used in prostate cancer research. Despite major developments in culture techniques and protocols, only two additional prostate cancer cell lines, i.e., MDA PCa 1 and MDA PCa 2a/b, could be established directly from the patient [36]. More successfully, several cell lines, such as PC346C, VCaP, DUCaP, LAPC4, and CWR22Rv1, could be generated from established PDXs [25, 37–40]. As already indicated above, these PDX-derived cell lines are contaminated with MLV virus, as a result of the original passaging in mice [31, 32].

In an effort to improve growth efficiency, the traditional athymic nude mouse as host for PDX engraftment was replaced by mouse strains that were more immune deficient. Since most nude mice are “leaky” and do have a few T-cells, especially as they age, knockout mice with more complete defects in the immune system have been constructed. In 1983, the severe combined immunodeficient (SCID) mouse was reported, lacking both T-and B-cells [41]. Crossbreeding of SCID and the non-obese diabetic (NOD) mouse, which was characterized by an impaired innate immunity, resulted in NOD-SCID mice, with defects in both innate and adaptive immunity [42]. Later, other knockout mouse strains were developed using genetic engineering to induce specific mutations (*Rag1* and *Rag2*) that prevent mature T- and B-cell development and mutations (*IL-2 $\gamma$* ) preventing natural killer (NK)-cell development. The crossing of *IL-2 $\gamma$* <sup>null</sup> mice with *Rag1*<sup>null</sup>, *Rag2*<sup>null</sup> or NOD/SCID (NSG) mice provided novel mouse strains with even more profound immunological defects, contributing to an increase in the number of PDXs for prostate cancer [25, 43]. Besides the immune deficiency of the host animal, also engraftment site (subcutaneous, orthotopic, or subrenal capsule) may have added to the increased success rates, as was shown by the eminent development of the Vancouver PDX series, using subrenal capsule engraftment [44].

These technological advances are leading the expansion of current PDX collections. In the current PDX series, tumor samples from late-stage disease are over-represented, showing higher take rates than early well-differentiated, androgen-dependent tumors (Fig. 8.2). Moreover, to cover today’s multitude of treatment options for late-stage disease, it is increasingly relevant to include PDX

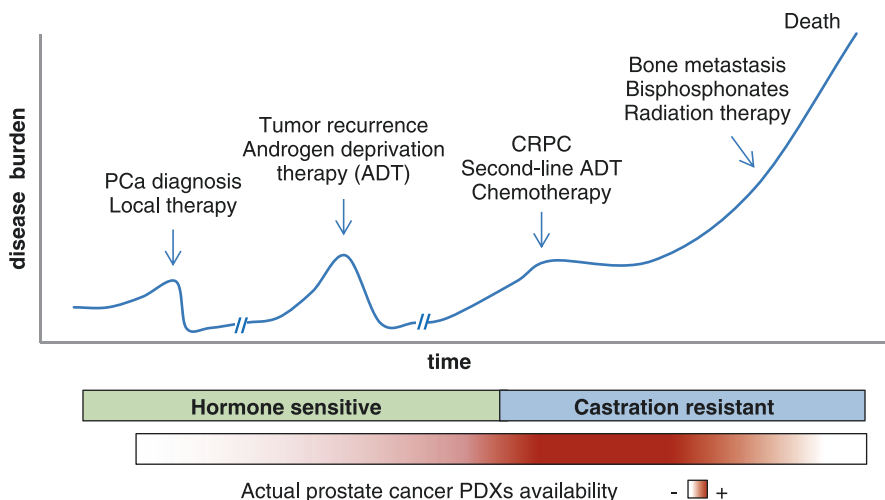


**Fig. 8.2** Typical clinical history and standard treatment of progressive prostate cancer. Most prostate cancer PDX models available are representative of the more advanced castration-resistant stage. There is a lack of well-differentiated, hormone-sensitive models, as well as PDXs that spontaneously metastasize to the bone to represent the earlier and later stages of the disease, respectively. *ADT* androgen deprivation therapy; *CRPC* castration-resistant prostate cancer

models representing resistance toward the various (targeted) therapies. Finally, there is a lack of prostate cancer PDXs that spontaneously metastasize to the bone, the preferential metastatic site in prostate cancer. Ongoing efforts are focused on expanding the PDX assortment to cover the phenotypic spectra of the different stages of prostate cancer disease. Clearly, in order to achieve such a well-balanced panel of prostate cancer PDXs that reflect the current patient population, major dedication and coordinated efforts from both the research center and their clinical partners are essential.

---

## **Do PDX Models Recapitulate the Complexity of Human Prostate Cancer?**

Prostate cancer is a heterogeneous and often multifocal disease [45]. This heterogeneity manifests itself not only in the variability between different patients but also within one patient's tumor, where multiple cancer foci in the prostate may differ in histological grade and/or expression of molecular markers [46–49]. Recent next-generation sequencing studies revealed the presence of multiple clonal populations within a patient's tumor, marked by spatial heterogeneity across different foci and a dynamic clonal composition, that evolves during disease progression and therapy [50–53]. In addition to clonal composition, tumor complexity is also defined by micro-environmental factors, such as extracellular matrix, stroma, and immune cells. Both clonal heterogeneity and complexity are not accurately represented in the conventional *in vitro* cell lines. PDX models are derived directly from patient tumors, without the selective pressure of prior *in vitro* expansion, thereby thought to be a better representation of the original tumor in terms of tissue complexity and clonal heterogeneity.

Overall, we and others have shown that prostate cancer PDXs largely recapitulate the original morphology, androgen sensitivity, and expression of the major biomarkers, such as AR and PSA [22, 23, 54, 55]. Genetic and genomic profiling studies have shown that these prostate cancer PDXs preserve major genetic alterations (e.g., AR, TMPRSS2-ERG, PTEN, and TP53) and global gene expression of the original tumor samples [54–57]. Furthermore, prostate cancer PDX models, depending on their disease stage, reflect the response to conventional systemic therapies, such as androgen deprivation therapy (ADT) and taxane chemotherapy [54, 58, 59]. Knowledge of these phenotypic and genomic characteristics of the xenografts is crucial when choosing the most appropriate preclinical model for the particular research question, and distinctive characteristics should be regularly checked to ensure that the reliability of the model is maintained during extended passaging. In general, prostate cancer PDX characteristics remain relatively stable during serial passage in mice [22, 54, 55].

Inter-patient and intra-tumoral heterogeneity in prostate cancer highlights the need for a broad collection of models to represent the genetic diversity of these tumors at different stages of the disease. Spatial heterogeneity and temporal evolution of clonal composition may be accounted for by taking multiple samples of a



patient's tumor, from different foci within the prostate or from different metastatic lesions or at different time points during the course of disease. Kohli et al. developed a series of PDX models from needle biopsies of a rib metastasis from a prostate cancer patient collected before and after treatment with enzalutamide and found that the PDXs preserved with high fidelity the patient's genomic and transcriptomic alterations [56]. Despite the obvious ethical and practical hurdles, in collecting multiple samples from metastatic lesions at different time points during treatment and establishing prostate cancer PDXs from needle biopsies, this encouraging report demonstrates that modeling clonal evolution during disease progression is feasible using PDXs.

In summary, prostate cancer PDX models reproduce the main characteristics of patient tumors with regard to tissue architecture, genetic alterations, biomarker expression, as well as response to androgen deprivation. Major biomarkers like AR and PSA are essential characteristics that need to be maintained also in late-stage disease to adequately reflect AR-positive progressive castration-resistant prostate cancer (CRPC).

---

## Tumor Micro-environment in Prostate Cancer PDX Models

It is well-recognized that the tumor micro-environment plays a crucial role in regulating tumor growth and metastatic potential of cancer cells. The tumor micro-environment involves the extracellular matrix (ECM) and includes fibroblasts, endothelial cells, mesenchymal stem cells (MSCs), macrophages, and other inflammatory cells to form a highly dynamic heterogeneous cell population with distinct functions. Cancer-associated fibroblasts (CAFs), originating from stromal fibroblasts, local progenitors, and infiltrating bone marrow-derived MSCs, support tumor progression by expressing growth factors and promoting epithelial-mesenchymal transition (EMT) [60]. The ability to adapt the stromal compartment and reprogram fibroblasts into CAFs is vital for the tumor cell to influence and modulate its micro-environment, making it permissive to tumor growth, survival, invasion, and metastasis [61–64]. In PDX models, human stromal cells are lost shortly after subcutaneous tumor engraftment in athymic mice, being replaced within the first mouse passages by murine stroma [65]. The loss of human stroma is considered a major limitation of the PDX model. However, our current understanding of EMT dynamics and tumor-stroma interplay questions the need for human stroma and whether murine fibroblasts cannot be educated to become CAFs with similar properties and function. Indeed, murine fibroblasts and vasculature can efficiently support the overall structure and growth of the engrafted tumor, and it seems that stably established prostate cancer PDXs contain CAFs that are well capable of reprogramming the host (subcutaneous) stroma (van Weerden, unpublished data). However, a consequence of the replacement of human by murine stroma in PDX models is that inter-species incompatibility may compromise the physiological cross talk between some stromal factors and respective receptors on the cancer cells (and vice versa).

Although mice and men share ~83% of homology, some relevant pathways that constitute the intricate tumor-stroma interplay are not reflected in PDX models. For example, species differences have been demonstrated for HGF/cMET and IL6/IL6R, two very relevant pathways implicated in prostate cancer growth and metastasis [66–69].

Clearly, another limitation of PDX models is the requirement for immunodeficient hosts. The lack of a functional immune system has a significant impact on the tumor micro-environment and, obviously, limits the use of PDX models for studies on tumor immunity and immune-modulating therapies. Later in this chapter, we will discuss strategies to tackle this deficiency.

Another determinant aspect in the interaction between tumor and micro-environment is the tissue-specific composition of the stroma and extracellular matrix. Hence, the site of engraftment may influence tumor growth, metastasis, and treatment responses, particularly for drugs directed against tissue-specific targets of the tumor micro-environment. Depending on the research question, orthotopic engraftment into the murine prostate or intraosseous transplantation may be preferable over subcutaneous transplantation. For prostate cancer, the orthotopic model has been especially challenging, not so much because of the small size of the mouse prostate, requiring dedicated microsurgery, but also because of the selection which prostate lobe, dorsolateral or ventral, would be the most appropriate to reflect human prostate tissue. While some research groups inject cells in the ventral prostate for convenience, others argue that based on genomic profiles, the dorsolateral lobe seems to better reflect the human prostate micro-environment [70, 71]. The use of cell line suspensions rather than PDX fragments has also changed the nature of these models into cell line-derived xenograft (CDX) models rather than true PDXs. Although the small size of the mouse prostate makes tumor fragment transplantation troublesome, surgical orthotopic implantation (SOI) was reported to be feasible [72, 73]. Orthotopic models of prostate cancer also demand for alternative methods to accurately monitor tumor-burden plasma PSA may be used as an indicator of tumor burden, although this approach is obviously restricted to PSA-producing xenografts. Transrectal ultrasonography (TRUS) has been established for visualization of the murine prostate [74] (Fig. 8.3). The application of TRUS monitoring of orthotopic prostate cancer has shown to be an excellent noninvasive, reliable, and fast method allowing for intensive monitoring of treatment responses of orthotopic prostate cancer PDXs [75]. New developments in ultrasound imaging include 3D ultrasound combined with photoacoustic imaging that offer longitudinal monitoring of tumor burden as well as displaying tumor vasculature and angiogenesis [76, 77]. Alternative approaches to monitor tumor growth and its micro-environment have been greatly extended by highly dedicated, multimodality small animal imaging applications, including optical imaging using fluorescence and/or bioluminescence and *in vivo* imaging systems (IVIS), MRI, and PET/SPECT [78]. The transfection of cancer cells with multicolor, more intense fluorophores and the establishment of fluorescently tagged transgenic mice to also visualize the murine environment have significantly contributed to our knowledge of tumor behavior and the cross talk with its micro-environment [79, 80].

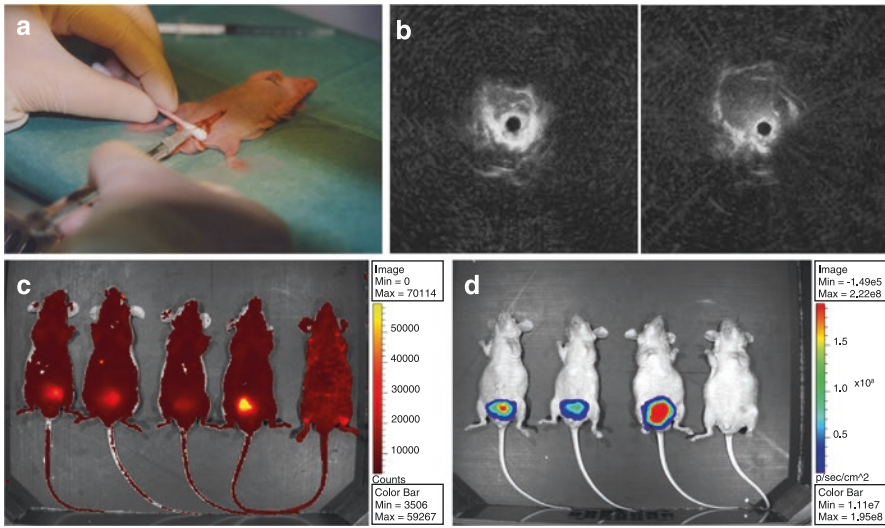


**Fig. 8.3** Prostate cancer orthotopic PDX model. (a) Cell injection into the dorsal mouse prostate. Orthotopic tumor growth can be monitored by (b) rectal ultrasonography, using a dedicated mouse rectal ultrasound probe (adapted from Kraaij et al. 2002 [74]); (c) katushka-fluorescence; or (d) Luc2 bioluminescence

Despite some limitations, PDX models of prostate cancer have shown to recapitulate the complexity of the human disease rather well, providing a substantial contribution to basic and translational research. Techniques to reconstitute human stroma, humanize the immune system, and adapt the hormonal status of the host animal are emerging. These and other innovative strategies in the development of prostate cancer PDX models will be discussed in the last section of this chapter.

## Applications of Prostate Cancer PDX Models

### PDXs in Prostate Cancer Biomarker Research

The introduction of the serum PSA test in the mid-1980s has changed the management of prostate cancer, allowing for early detection when the disease is still curable [81]. A drawback is that physicians are now detecting, and possibly overtreating, insignificant tumors. Furthermore, benign conditions of the prostate may also cause elevated PSA levels, prompting the search for alternative diagnostic biomarkers. Next to screening and diagnostic purposes, serum PSA is being used as a biomarker for monitoring disease progression and response to therapy. However, in the clinical situation, PSA is a modest surrogate of treatment response. Indeed, preclinical studies with the small molecule suramin showed, in the prostate cancer LNCaP CDX model, the inhibition of PSA production without affecting tumor growth, hence illustrating the limited value of PSA as a response biomarker [82, 83]. PDX studies

can be applied to directly correlate tumor growth effects to PSA response and assess whether treatments may directly interfere with PSA production and/or release. Hence, PDX-based studies may provide preclinical validation for the use of PSA as a treatment response biomarker in subsequent clinical trials. Indeed, such PDX studies have been used successfully showing the value of its concept [75, 84, 85].

In the last decade, advances in high-throughput genomic and proteomic profiling led to the discovery of novel prostate cancer biomarkers, including PCA3, TMPRSS2:ERG fusion, and AR splice variant 7 (AR-V7) [86]. Other biomarkers emerging in prostate cancer research include circulating tumor cells (CTCs), microRNAs, and exosomes [87, 88]. These novel biomarkers are still under development and need further validation before being accepted and fully implemented in the clinic. PDXs are particularly suitable preclinical models for biomarker discovery and validation because they constitute a pure source of human tumor tissue that is not contaminated with normal cells. Thus, all alterations in transcripts or proteins detected by genomics or proteomics analyses to be human specific are derived from the tumor and are by definition tumor specific. Genome-wide expression analysis of prostate cancer PDX models has led to the identification of diagnostic and prognostic biomarkers/signatures for prostate cancer. For example, Hendriksen et al. used microarrays to analyze genes affected by castration on a panel of 13 prostate cancer PDXs and identified multiple candidate biomarkers for prognosis. The validation in a small cohort of patient samples showed that low mRNA expression of HERPUD1, STK39, DHCR24, and SOC2 in primary tumors was strongly correlated with the development of metastases after radical prostatectomy [89]. Other studies used next-generation RNA sequencing on paired metastatic/nonmetastatic prostate cancer PDXs to identify microRNAs and long noncoding RNAs, as novel biomarkers associated with metastasis [90, 91]. PDXs are also particularly powerful tools for studies of serum biomarkers, since also here it applies that all human proteins or transcripts detected in the serum of the tumor-bearing mouse are derived from the tumor. Prostate cancer PDXs have been used in combination with proteomics techniques to identify human prostate cancer-secreted proteins and exosomes in the serum of xenograft-bearing mice, as potential diagnostic and prognostic serum markers [92, 93]. In another example, Jansen et al. developed an ingenious PDX-based biomarker discovery method to detect low abundant prostate cancer-derived serum proteins and circumvent the dynamic range limitations of standard patient cohort proteomics comparisons [94]. The authors injected serum from PDX-bearing nude (*nu/nu*) mice in immune-competent (-/+) mice to elicit an antibody response against PDX-derived antigens. These proteins were then identified by probing protein microarrays with serum from the immunized mice and a subset of these potential biomarkers was subsequently validated in serum samples from prostate cancer patients [94].

Predictive biomarkers of treatment response are a developing field in prostate cancer research and becoming increasingly important to identify patients who are most likely to benefit from emerging targeted therapies. A recent study by Beltran et al. illustrated the use of PDX models in the validation of treatment response biomarkers in combination with targeted therapies [95]. Using whole-exome

sequencing, the authors detected a novel alteration involving the DNA repair gene FANCA in a patient with aggressive neuroendocrine prostate cancer, who showed a remarkable clinical response to cisplatin chemotherapy. The authors subsequently established a PDX from a metastatic lesion of this patient, which contained the same gene alteration, allowing a validation of the predictive value of the mutation for cisplatin response [95].

In summary, PDXs are becoming increasingly important in prostate cancer biomarker research. While reflecting the molecular alterations and phenotypic characteristics of human tumors, prostate cancer PDXs provide representative and versatile models for the discovery and validation of diagnostic, prognostic, and therapy response biomarkers.

## PDXs to Investigate Novel Therapies for Prostate Cancer

Until recently, options for medical management of metastatic prostate cancer patients were limited, but the last decade has seen significant advances in the treatment of late-stage prostate cancer with the approval of eight new drugs. Next to the traditional androgen deprivation therapies (ADT), these include the androgen pathway-targeting agents enzalutamide and abiraterone acetate, chemotherapeutics docetaxel and cabazitaxel, bone-targeting agents denosumab and radium-223, and the immunotherapeutic sipuleucel-T [96]. Besides symptom palliation, these novel agents have shown to improve survival in metastatic patients, although resistance to these therapies inevitably develops.

PDX models are valuable tools to test novel drugs for their efficacy, to assess potential interfering pathways, to identify and validate putative tumor biomarkers for response, and to optimize treatment strategies, information that cannot be obtained from *in vitro* studies. Multiple studies have shown that PDX models may predict drug activity in patients remarkably well and are thus useful to generate confirmation and additional information (see above) before or in parallel to clinical trials [97–101]. For prostate cancer, PDX models have shown to recapitulate the clinical response to androgen-targeting agents and docetaxel and are being used increasingly to test novel-targeted agents in combination therapies, particularly with ADT or docetaxel [22, 54, 56, 59]. For example, the combination of PI3K/AKT-targeting drugs with ADT induced durable tumor regression in PTEN-negative prostate cancer PDXs, as compared to either therapy alone, supporting previous reports of a cross talk between PI3K and AR signaling [85, 102, 103]. These promising PDX-based results have paved the way for multiple clinical trials testing combination therapies that target both these pathways simultaneously ([Clinicaltrials.gov](https://clinicaltrials.gov): NCT02407054, NCT01251861, NCT02525068, NCT01485861). Similarly, PDX models of prostate cancer are being used to test co-treatment options in order to improve docetaxel efficacy and delay disease progression. Such studies have tested combinations of docetaxel with various compounds, among which are estramustine (chemotherapeutic), trastuzumab (anti-Her2 antibody), or zoledronic acid (bone-directed agent) [104–106]. Another interesting application of PDX models is

the optimization of the timing and sequence of the different therapies, in order to delay disease progression, as demonstrated in a study by Dahmani et al. that compared four different sequencing schedules of docetaxel and estramustine in a series of prostate cancer PDXs [104]. Finally, prostate cancer PDX models have also been used to evaluate dietary intervention to attempt to delay prostate cancer progression. For example, dietary polyunsaturated fatty acids, protein restriction, lycopene, and vitamin E have been shown to inhibit tumor growth in the CWR22, LuCaP23.1, and PC346C models, respectively [75, 107, 108].

The currently available sets of PDXs for prostate cancer show significant predictive power for clinical response. In the advent of precision medicine, with a multitude of novel-targeted drugs in the pipeline, PDX models will take an important role in the research and development of personalized therapies.

## **PDXs to Understand Mechanisms of Therapy Resistance**

Despite major advances in treatment, metastatic prostate cancer remains a lethal disease, as resistance emerges inevitably to the therapies being currently offered. Knowledge of the mechanisms driving tumor growth and resistance is crucial for designing rational strategies to delay the onset of resistance and for the development of therapies targeting these resistance pathways. While often cell lines are used to establish the resistance phenotype because of convenience, PDX models may be more relevant to mimic the clinical progression and development of treatment resistance. One strategy is to collect tumor biopsies before the initiation of therapy and, again at the time of treatment resistance, to generate pre- and post-therapy PDX models. This approach heavily relies on the successful establishment of such PDXs, which has been shown to be rather challenging for prostate cancer. Also, post-treatment biopsies are not always easy to obtain or readily accessible. An alternative approach is to use treatment-naïve prostate cancer PDXs and establish drug resistance *in vivo* by exposing the host animal to a clinical relevant drug scheme. This approach has the advantage of generating paired treatment-naïve and treatment-resistant models, with the same genetic background [59]. Such PDX pairs are very helpful for molecular-profiling studies, to identify mechanisms and markers of resistance, and for subsequent functional studies, to validate these mechanisms and evaluate treatment options for resistance.

For prostate cancer, the research focus has for long been dedicated toward investigating the mechanisms of resistance to ADT. Hendriksen et al. compared androgen-sensitive with castration-resistant PDX models to characterize the adaptation of the androgen receptor pathway during prostate cancer progression [89]. Other studies in prostate cancer PDX models revealed a novel AR mutation and PI3K/AKT activation as mechanisms of resistance to the anti-androgen bicalutamide [109, 110]. Prostate cancer PDXs have also been used to understand the relevance of the significant intra-tumoral testosterone and dihydrotestosterone (DHT) levels that are maintained in castration-resistant tumors and their potential role in castration-resistant growth. Based on these observations, it was

hypothesized that castration-resistant tumors might be able to produce their own androgens (de novo steroidogenesis) [111] or to maintain intra-tumoral androgen levels by active conversion of adrenal androgens [112, 113]. These potential resistance mechanisms to ADT motivated the development of inhibitors of CYP17A1, a key enzyme in the steroidogenic synthesis, such as abiraterone and ortenorel. Additional studies in castration-resistant PDXs revealed that resistance to abiraterone was associated with the upregulation of CYP17A1 and AR expression, including constitutively active AR splice variants, suggestive of potential mechanisms of abiraterone resistance [114].

For prostate cancer, chemotherapy is almost exclusively dominated by the successful taxane-based therapies. To allow the investigation of mechanisms of taxane-resistance, the discovery of predictive biomarkers of taxane response, and to fill the lack of *in vivo* models for taxane-resistant prostate cancer, novel PDX models of docetaxel resistance have been generated. De Morr e et al. established two docetaxel-resistant PDXs from two independent docetaxel-na ve PDXs, by repeated biweekly administration of docetaxel to tumor-bearing mice [59]. Studies of these PDXs revealed that taxane efficacy was determined by the capacity to accumulate sufficient intra-tumoral drug levels and that resistance was directly related to the inability to achieve this [59]. Other PDX studies were applied to understand the reduced efficacy of docetaxel observed in enzalutamide-resistant patients. These studies demonstrated cross-resistance between these two agents, as docetaxel directly inhibited AR activation in enzalutamide-na ve tumors, but not in enzalutamide-resistant tumors [115]. At the same time, the expanding knowledge of the interactions between taxanes and (hormonal) agents also underscore the importance of defining the best treatment sequence and optimal timing of the treatment.

Altogether, these studies show that PDX models of prostate cancer have contributed to our understanding of mechanisms of therapy resistance and are relevant tools to identify and validate potential therapy resistance biomarkers.

## **PDXs as Translational Tools for Precision Medicine**

The “omics” era has had a profound impact in our understanding of the molecular alterations in prostate cancer, leading to the identification of new disease markers and potential therapeutic targets [50, 116]. This knowledge fueled the development of a new generation of targeted drugs, giving rise to the concept of precision medicine, whereby patients are offered personalized treatment tailored to the molecular characteristics of their tumors. To achieve this, it is essential to improve integration between laboratory research and the clinic, through the use of relevant models that accurately reflect the genetic alterations, disease characteristics, and therapy response of the human tumors. Research and pharmaceutical communities are increasingly turning to PDX models, as a way to recapitulate the complexity of human cancers and improve the predictive power of preclinical research.

Co-clinical trials are a novel trend in the development of targeted therapies, in which PDX studies are conducted in parallel with Phase I/II clinical trials [117, 118]. This concept makes use of genetically-defined PDX models to evaluate drug efficacy, determine patient-selection strategies, identify possible resistance mechanisms, and test drug combination modalities, using real-time integration of PDX and clinical data. This combined approach is assumed to facilitate the selection of treatment strategies for further assessment and to accelerate clinical translation. Taking this concept a step further, a pilot co-clinical study was performed generating personalized tumor grafts from 14 patients with different types of cancer, to evaluate 63 anticancer drugs and guide the selection of individualized patient treatments [98]. Considering the low take rate, long latency, and slow growth of prostate tumors in the mouse, personalized PDX models are unlikely to become feasible tools to aid real-time therapeutic decisions of prostate cancer patients. There are few reports of co-clinical trials in prostate cancer. One of these studies investigated the clinical activity of cabozantinib, a MET/VEGFR2 inhibitor, in 21 metastatic prostate cancer patients in a Phase II trial in parallel to a similar study in three prostate cancer PDXs [119]. Tumor responses in the PDX models closely mimicked the response observed in the patients. The integration of the functional data from the PDX studies brought novel insights into the mechanism of action of cabozantinib, identified potential mechanisms of therapy resistance, and allowed an investigation of the impact of dosing schedules on cabozantinib efficacy [119]. The previously-mentioned study, by Beltran et al, where a PDX was established from the metastatic lesion of a prostate cancer patient to investigate the biological role and predictive value of FANCA deletion on cisplatin sensitivity, provides another example on how PDX models may complement clinical data [95].

Altogether, these studies highlight the potential of integrating PDX-based studies with clinical trials to predict efficacy of novel-targeted agents, investigate mechanisms of drug sensitivity/resistance, and develop patient-stratification strategies, accelerating clinical translation into personalized therapies. To achieve this, access to a broad panel of PDX models representing the range of molecular alterations occurring in prostate cancer is crucial. Such extensive PDX cohorts are currently being assembled, characterized, and annotated to meet this need.

---

## Challenges and Future Directions

### Modeling Inter-Patient Heterogeneity: PDX Clinical Trials

The prediction of clinical efficacy and identification of factors that underlie heterogeneous patient responses are highly relevant for adequate screening and selection of potential candidate therapeutics [120]. To guide screening methods and enhance our ability to predict clinical responses, a novel concept was suggested by Gao et al. [97]. Using an extensive PDX collection, containing ~1000 models with a diverse set of driver mutations, a large-scale *in vivo* compound screen was conducted. This so-called PDX clinical trial (PCT) approach was conducted based on the “one animal per model per treatment” ( $1 \times 1 \times 1$ ) model to reflect inter-patient response heterogeneity and



assess the population responses to various treatments. This novel preclinical concept was demonstrated to be reproducible and reflected, retrospectively, clinical translatability by identifying associations between genotype and drug response, as well as with established mechanisms of resistance [97, 100, 121]. Such an approach clearly requires an extensive set of genomically- characterized PDXs to fully capture the diversity of the disease, a demanding task and major challenge to apply for prostate cancer.

## **Interaction of Tumor Micro-environment: Making the Mouse a Hospitable Host**

The lack of human stroma is considered a major limitation of PDX models. While murine stroma quickly infiltrates the tumor graft, taking over the function of its human counterpart in supporting the overall structure and growth of the tumor, the engraftment site and interspecies compatibility may compromise the interaction between tumor and host micro-environment.

As discussed earlier, orthotopic PDX engraftment in the mouse prostate or in the bone can be used to replicate the micro-environment at the natural sites of local and metastatic prostate cancer, respectively. Advancements in small animal imaging techniques provide noninvasive methods for monitoring of tumor growth and spread and for visualization of the micro-environment [72, 78, 79].

Furthermore, innovative strategies are being developed to reconstruct species-specific interactions in PDX models. These include co-engraftment of patient-matched stroma components or in vitro-expanded human CAFs, and the transplantation of tissue-engineered humanized bone constructs, to serve as homing site for human prostate cancer cells [65, 122, 123]. In addition, humanized mice are being engineered to compensate for species differences in relevant paracrine growth factors and cytokines. Although little is known about the factors involved in the cross talk between tumor and micro-environment and the role of each of these interactions on prostate cancer growth and progression, it is realized that species differences on relevant pathways may hamper a true reflection of the physiological epithelial-stromal interaction within a PDX. This is the case for HGF/cMET and IL6/IL6R, two pathways implicated in CRPC growth and metastasis [66–69]. Engineered SCID mice expressing human HGF have been generated, allowing the investigation of the HGF/cMET axis in relevant PDX models [124]. Also, a humanized IL-6 ligand receptor system has been introduced in mice, although it involves C57BL/6J immune-competent mice and the system still needs translation to immune compromised strains in order to be applicable to PDX models [125].

## **From Immunocompromised Mice to Humanized Immune System**

Inherent to the PDX system is the lack of a functional immune system. With the realization of the important role of the immune system in the regulation and complexity of the tumor micro-environment, and hence in tumor growth and progression,

efforts were undertaken to develop humanized mouse models with a functional immune system. NSG or Rag2<sup>-/-</sup>IL2 $\gamma$ <sup>-/-</sup> triple-negative immunodeficient mice, characterized by profound immunological defects in both innate and adaptive immunity, have been implanted with human hematopoietic stem cells to create a humanized immune-competent tumor micro-environment. The humanized model is based on engraftment of CD34<sup>+</sup> human hematopoietic stem and progenitor cells (HSPCs) isolated from cord blood, bone marrow, or fetal liver and injected intravenously into irradiated immune-deficient mice. Here human T- and B-cells develop from human stem cells engrafted in the mouse, which are tolerant of the mouse host due to negative selection during differentiation into T- and B-cells. An alternative humanization model uses freshly isolated leukocytes, from human peripheral whole blood or spleen, for intravenous or intraperitoneal injection into immune-deficient mice recipient. Because the transferred lymphocytes are functionally mature, this model allows for fast evaluation of immune function, although only for relative short-term (weeks) studies [126, 127]. These humanized models develop a functional human immune system, characterized by T-cell maturation and T-cell-dependent inflammatory responses. NSG mice reconstituted with human immune cells and inoculated with prostate cancer PC-3 cells indeed demonstrated infiltration with tumor-infiltrating lymphocytes (TILs) that were able to affect tumor growth [128]. Since interspecies differences in the specificity of growth factors and cytokines represent a serious hurdle when constructing a human immune system in immunodeficient mice, current developments are directed towards genetically introducing essential human cytokine genes in these mouse models [129].

## Establishing Metastatic Prostate Cancer PDX Models

The tumor micro-environment is a major determinant in the metastatic process and its regulation of the factors that determine shedding of cancer cells and their repopulation into distant organs. The “seed and soil” hypothesis of Paget and popularized by Fidler et al., assuming that the metastatic process can only be faithfully recapitulated by tumors grown in the organ of origin, triggered the development of orthotopic models by Sordat et al. (Chapter 4 in the present volume) and shown to be essential tools to study metastasis and metastatic spread [130–132]. In line with this hypothesis, a recent study using PC-3 cells labeled with green fluorescent protein (GFP) showed improved vascularization and quick metastatic spread after orthotopic transplantation in the prostate, but not when the tumors were transplanted subcutaneously where no cancer-cell invasion was observed over time [133]. The development of orthotopic models and simultaneous advancement in optical imaging technology allowed for the creation of novel PDX models with (distant) metastasis. For prostate cancer, dominated by its preferential spreading to the bone, extensive efforts have been made to create adequate metastatic models. These studies started with the pioneering work by Chung et al. showing the promoting effect of (human) bone fibroblasts on metastatic progression when co-inoculated with human prostate cancer PDXs [134, 135]. Traditionally, prostate cancer

metastasis is investigated by injecting established prostate cancer cells in the left heart ventricle or intra-tibially to generate (bone) metastatic lesions [136–138]. Although highly relevant to understand certain aspects of the metastatic cascade, the major challenge for prostate cancer lies in the establishment of a spontaneous model of osseous metastasis. Orthotopic prostate cancer PDXs generated in NSG mice developed metastatic spread to all relevant organs such as the lymph nodes, lung, and bone as determined by *in vivo* luciferase imaging, although they rarely developed into macroscopic metastatic lesions [139]. Importantly, viable tumor cells could be retrieved from these metastasis-positive organs and reestablished as metastatic sublines (van Zoggel, unpublished data and [139]). The lack of metastatic development was attributed, at least in part, to the decreased life span of the animal as a result of the growing primary orthotopic tumor that could not be removed easily. To circumvent this issue, others implanted fragments in the mouse coagulating gland, as an alternative to the mouse prostate, resulting in (micro) metastasis in the lymph node, lung, and liver, but not in the bone [140]. With the realization that shedding of cells from subcutaneous implanted prostate cancer PDX was not different from that of their orthotopic counterpart, we used the subcutaneous model to allow for debulking of the primary tumor and extend the lifespan of the animal. Indeed, this resulted in metastatic outgrowth in mouse liver, providing the first spontaneous metastatic model for prostate cancer from a subcutaneous PDX (van Zoggel, unpublished data). Although much less frequent than the occurrence of bone (90%) lesions, lung (46%), and liver metastasis are frequent sites (25%) for prostate cancer metastasis, especially in late-stage prostate cancer [141]. Using a similar approach, new dedicated spontaneously models from subcutaneous PDXs with preferential spread toward the lung and bone are currently being developed.

## **Modeling the Endocrine Status of a Patient Under Androgen Deprivation Therapy**

The hormonal status of the host animal is a crucial factor for prostate cancer PDXs, especially for those models that are still driven by androgens and reflect early-stage disease. Since studies show the continued role of the AR even in late-stage, castration-resistant prostate cancer, the presence of AR in these PDXs remains critical. Thus, it is important to aim to achieve a hormonal environment in the host animal that more accurately reflects the patient's endocrine condition. Here, prostate cancer PDXs in (nude) mice are confronted with a limitation [142]. Prostate cancer patients under hormonal therapy have strongly reduced, near-castrate plasma levels of testosterone, but maintain significant levels of the adrenal androgens, androstenedione, and DHEA. Unlike men, rodents do not produce significant levels of these androgens as they lack CYP17A1 expression, a crucial enzyme in the conversion of precursor steroids [143]. In contrast to the clinical situation in patients under ADT, when mice are castrated to reflect ADT, circulating androgens are absent. The conversion of adrenal androgens to testosterone in prostate cancer cells has been shown to fuel castration-resistant growth and is an important mechanism

of resistance to androgen deprivation therapy [112, 113, 144]. CYP17A1 inhibitors that target this mechanism are under development, and abiraterone acetate has been recently approved for the treatment of CRPC [145]. In order to better recapitulate the endocrine environment in CRPC patients, we developed a humanized system where PDX-bearing mice were co-engrafted with tumorigenic human adrenal cells that express physiologically relevant adrenal androgens. This “endocrine-humanized” PDX mouse model allows us to investigate the contribution of adrenal androgens production to prostate cancer growth, and its therapeutic targeting with specific steroid synthesis blockers.

In conclusion, ongoing efforts are focused on expanding the current PDX collections to cover the genotypic and phenotypic spectra of prostate cancer disease. Innovative strategies are being developed to overcome limitations inherent to this system and establish a new generation of PDX models that better represent the complexity of the tumor endocrine, immune, and micro-environment from the patient.

---

## References

1. Stamey TA, Yang N, Hay AR, McNeal JE, Freiha FS, Redwine E. Prostate-specific antigen as a serum marker for adenocarcinoma of the prostate. *N Engl J Med.* 1987;317:909–16.
2. Brinkmann AO. Molecular mechanisms of androgen action—a historical perspective. *Methods Mol Biol.* 2011;776:3–24.
3. Huggins C, Hodges CV. Studies on prostatic cancer: I. The effect of castration, of estrogen and of androgen injection on serum phosphatases in metastatic carcinoma of the prostate. *J Urol.* 2002;168:9–12.
4. Fitzpatrick JM, Bellmunt J, Fizazi K, Heidenreich A, Sternberg CN, Tombal B, et al. Optimal management of metastatic castration-resistant prostate cancer: highlights from a European Expert Consensus Panel. *Eur J Cancer.* 2014;50:1617–27.
5. Polisca A, Troisi A, Fontaine E, Menchetti L, Fontbonne A. A retrospective study of canine prostatic diseases from 2002 to 2009 at the Alfort Veterinary College in France. *Theriogenology.* 2016;85:835–40.
6. Reyes I, Reyes N, Iatropoulos M, Mittelman A, Geliebter J. Aging-associated changes in gene expression in the ACI rat prostate: implications for carcinogenesis. *Prostate.* 2005;63:169–86.
7. Pollard M. The Lobund-Wistar rat model of prostate cancer. *J Cell Biochem Suppl.* 1992;16H:84–8.
8. Yuen M-T, Leung L-K, Wang J, Wong Y-C, Chan FL. Enhanced induction of prostatic dysplasia and carcinoma in Noble rat model by combination of neonatal estrogen exposure and hormonal treatments at adulthood. *Int J Oncol.* 2005;27:1685–95.
9. Voigt W, Dunning WF. In vivo metabolism of testosterone-3H in R-3327, an androgen-sensitive rat prostatic adenocarcinoma. *Cancer Res.* 1974;34:1447–50.
10. Smolev JK, Heston WD, Scott WW, Coffey DS. Characterization of the Dunning R3327H prostatic adenocarcinoma: an appropriate animal model for prostatic cancer. *Cancer Treat Rep.* 1977;61:273–87.
11. Isaacs JT, Weissman RM, Coffey DS, Scott WW. Concepts in prostatic cancer biology: Dunning R-3327 H, HI, and AT tumors. *Prog Clin Biol Res.* 1980;37:311–23.
12. Greenberg NM, DeMayo F, Finegold MJ, Medina D, Tilley WD, Aspinall JO, et al. Prostate cancer in a transgenic mouse. *Proc Natl Acad Sci U S A.* 1995;92:3439–43.
13. Gingrich JR, Barrios RJ, Morton RA, Boyce BF, DeMayo FJ, Finegold MJ, et al. Metastatic prostate cancer in a transgenic mouse. *Cancer Res.* 1996;56:4096–102.

14. Wang S, Gao J, Lei Q, Rozengurt N, Pritchard C, Jiao J, et al. Prostate-specific deletion of the murine Pten tumor suppressor gene leads to metastatic prostate cancer. *Cancer Cell*. 2003;4:209–21.
15. Ma X, Ziel-van der Made AC, Autar B, van der Korput HA, Vermeij M, van Duijn P, et al. Targeted biallelic inactivation of Pten in the mouse prostate leads to prostate cancer accompanied by increased epithelial cell proliferation but not by reduced apoptosis. *Cancer Res*. 2005;65:5730–9.
16. Ittmann M, Huang J, Radaelli E, Martin P, Signoretti S, Sullivan R, et al. Animal models of human prostate cancer: the consensus report of the New York meeting of the Mouse Models of Human Cancers Consortium Prostate Pathology Committee. *Cancer Res*. 2013;73:2718–36.
17. Rygaard J, Povlsen CO. Heterotransplantation of a human malignant tumour to “Nude” mice. *Acta Pathol Microbiol Scand*. 1969;77:758–60.
18. Hoehn W, Schroeder FH, Reimann JF, Joebsis AC, Hermanek P. Human prostatic adenocarcinoma: some characteristics of a serially transplantable line in nude mice (PC 82). *Prostate*. 1980;1:95–104.
19. Wright GL, Haley CL, Csapo Z, van Steenbrugge GJ. Immunohistochemical evaluation of the expression of prostate tumor-association markers in the nude mouse human prostate carcinoma heterotransplant lines PC-82, PC-EW, and PC-EG. *Prostate*. 1990;17:301–16.
20. Ito YZ, Nakazato Y. A new serially transplantable human prostatic cancer (HONDA) in nude mice. *J Urol*. 1984;132:384–7.
21. Harper ME, Goddard L, Smith C, Nicholson RI. Characterization of a transplantable hormone-responsive human prostatic cancer xenograft TEN12 and its androgen-resistant sublines. *Prostate*. 2004;58:13–22.
22. van Weerden WM, de Ridder CM, Verdaasdonk CL, Romijn JC, van der Kwast TH, Schröder FH, et al. Development of seven new human prostate tumor xenograft models and their histopathological characterization. *Am J Pathol*. 1996;149:1055–62.
23. Wainstein MA, He F, Robinson D, Kung HJ, Schwartz S, Giaconia JM, et al. CWR22: androgen-dependent xenograft model derived from a primary human prostatic carcinoma. *Cancer Res*. 1994;54:6049–52.
24. Ellis WJ, Vessella RL, Buhler KR, Bladou F, True LD, Bigler SA, et al. Characterization of a novel androgen-sensitive, prostate-specific antigen-producing prostatic carcinoma xenograft: LuCaP 23. *Clin Cancer Res*. 1996;2:1039–48.
25. Klein KA, Reiter RE, Redula J, Moradi H, Zhu XL, Brothman AR, et al. Progression of metastatic human prostate cancer to androgen independence in immunodeficient SCID mice. *Nat Med*. 1997;3:402–8.
26. Bosland MC, Chung LW, Greenberg NM, Ho SM, Isaacs JT, Lane K, et al. Recent advances in the development of animal and cell culture models for prostate cancer research. A minireview. *Urol Oncol*. 1996;2:99.
27. Navone NM, Logothetis CJ, von Eschenbach AC, Troncoso P. Model systems of prostate cancer: uses and limitations. *Cancer Metastasis Rev*. 1998;17:361–71.
28. Sobel RE, Sadar MD. Cell lines used in prostate cancer research: a compendium of old and new lines—part 2. *J Urol*. 2005;173:360–72.
29. van Weerden WM, Romijn JC, de Ridder CMA, van der Kwast TH, van Steenbrugge GJ, Schröder FH. Frequent occurrence of spontaneous tumors in NMRI athymic nude mice. In: Arnold W, Köpf-Maier P, Michael B, editors. *Immunodeficient animals: models for cancer research*. *Contrib Oncol*. vol. 51. Basel: Karger; 1996. p. 41–4.
30. Aloia AL, Sfanos KS, Isaacs WB, Zheng Q, Maldarelli F, De Marzo AM, et al. XMRV: a new virus in prostate cancer? *Cancer Res*. 2010;70:10028–33.
31. Sfanos KS, Aloia AL, Hicks JL, Esopi DM, Steranka JP, Shao W, et al. Identification of replication competent murine gammaretroviruses in commonly used prostate cancer cell lines. *PLoS One*. 2011;6:e20874.
32. Yang J, Battacharya P, Singhal R, Kandel ES. Xenotropic murine leukemia virus-related virus (XMRV) in prostate cancer cells likely represents a laboratory artifact. *Oncotarget*. 2011;2:358–62.

33. Kaighn ME, Narayan KS, Ohnuki Y, Lechner JF, Jones LW. Establishment and characterization of a human prostatic carcinoma cell line (PC-3). *Invest Urol.* 1979;17:16–23.
34. Stone KR, Mickey DD, Wunderli H, Mickey GH, Paulson DF. Isolation of a human prostate carcinoma cell line (DU 145). *Int J Cancer.* 1978;21:274–81.
35. Horoszewicz JS, Leong SS, Chu TM, Wajzman ZL, Friedman M, Papsidero L, et al. The LNCaP cell line—a new model for studies on human prostatic carcinoma. *Prog Clin Biol Res.* 1980;37:115–32.
36. Navone NM, Olive M, Ozen M, Davis R, Troncoso P, Tu SM, et al. Establishment of two human prostate cancer cell lines derived from a single bone metastasis. *Clin Cancer Res.* 1997;3:2493–500.
37. Marques RB, van Weerden WM, Erkens-Schulze S, de Ridder CM, Bangma CH, Trapman J, et al. The human PC346 xenograft and cell line panel: a model system for prostate cancer progression. *Eur Urol.* 2006;49:245–57.
38. Korenchuk S, Lehr JE, MClean L, Lee YG, Whitney S, Vessella R, et al. VCaP, a cell-based model system of human prostate cancer. *In Vivo.* 2001;15:163–8.
39. Lee YG, Korenchuk S, Lehr J, Whitney S, Vessella R, Pienta KJ. Establishment and characterization of a new human prostatic cancer cell line: DuCaP. *In Vivo.* 2001;15:157–62.
40. Sramkoski RM, Pretlow TG, Giaconia JM, Pretlow TP, Schwartz S, Sy MS, et al. A new human prostate carcinoma cell line, 22Rv1. *In Vitro Cell Dev Biol Anim.* 1999;35:403–9.
41. Bosma GC, Custer RP, Bosma MJ. A severe combined immunodeficiency mutation in the mouse. *Nature.* 1983;301:527–30.
42. Shultz LD, Schweitzer PA, Christianson SW, Gott B, Schweitzer IB, Tennent B, et al. Multiple defects in innate and adaptive immunologic function in NOD/LtSz-scid mice. *J Immunol.* 1995;154:180–91.
43. Maitland NJ, Frame FM, Polson ES, Lewis JL, Collins AT. Prostate cancer stem cells: do they have a basal or luminal phenotype? *Horm Cancer.* 2011;2:47–61.
44. Wang Y, Revelo MP, Sudilovsky D, Cao M, Chen WG, Goetz L, et al. Development and characterization of efficient xenograft models for benign and malignant human prostate tissue. *Prostate.* 2005;64:149–59.
45. Andreou M, Cheng L. Multifocal prostate cancer: biologic, prognostic, and therapeutic implications. *Hum Pathol.* 2010;41:781–93.
46. Arora R, Koch MO, Eble JN, Ulbright TM, Li L, Cheng L. Heterogeneity of Gleason grade in multifocal adenocarcinoma of the prostate. *Cancer.* 2004;100:2362–6.
47. Perner S, Demichelis F, Beroukhim R, Schmidt FH, Mosquera J-M, Setlur S, et al. TMPRSS2:ERG fusion-associated deletions provide insight into the heterogeneity of prostate cancer. *Cancer Res.* 2006;66:8337–41.
48. de Winter JA, Trapman J, Brinkmann AO, Boersma WJ, Mulder E, Schroeder FH, et al. Androgen receptor heterogeneity in human prostatic carcinomas visualized by immunohistochemistry. *J Pathol.* 1990;160:329–32.
49. Qu X, Randhawa G, Friedman C, Kurland BF, Glaskova L, Coleman I, et al. A three-marker FISH panel detects more genetic aberrations of AR, PTEN and TMPRSS2/ERG in castration-resistant or metastatic prostate cancers than in primary prostate tumors. *PLoS One.* 2013;8:e74671.
50. Gundem G, Van Loo P, Kremeyer B, Alexandrov LB, Tubio JMC, Papaemmanuil E, et al. The evolutionary history of lethal metastatic prostate cancer. *Nature.* 2015;520:353–7.
51. Carreira S, Romanel A, Goodall J, Grist E, Ferraldeschi R, Miranda S, et al. Tumor clone dynamics in lethal prostate cancer. *Sci Transl Med.* 2014;6:254ra125.
52. Haffner MC, Mosbrugger T, Esopi DM, Fedor H, Heaphy CM, Walker DA, et al. Tracking the clonal origin of lethal prostate cancer. *J Clin Invest.* 2013;123:4918–22.
53. Hong MKH, Macintyre G, Wedge DC, Van Loo P, Patel K, Lunke S, et al. Tracking the origins and drivers of subclonal metastatic expansion in prostate cancer. *Nat Commun.* 2015;6:6605. Nature Publishing Group.
54. Lin D, Wyatt AW, Xue H, Wang Y, Dong X, Haegert A, et al. High fidelity patient-derived xenografts for accelerating prostate cancer discovery and drug development. *Cancer Res.* 2014;74:1272–83.

55. Aparicio A, Tzelepi V, Araujo JC, Guo CC, Liang S, Troncoso P, et al. Neuroendocrine prostate cancer xenografts with large-cell and small-cell features derived from a single patient's tumor: morphological, immunohistochemical, and gene expression profiles. *Prostate*. 2011;71:846–56.
56. Kohli M, Wang L, Xie F, Sicotte H, Yin P, Dehm SM, et al. Mutational landscapes of sequential prostate metastases and matched patient derived xenografts during enzalutamide therapy. *PLoS One*. 2015;10:1–14.
57. Collins CC, Volik SV, Lapuk AV, Wang Y, Gout PW, Wu C, et al. Next generation sequencing of prostate cancer from a patient identifies a deficiency of methylthioadenosine phosphorylase, an exploitable tumor target. *Mol Cancer Ther*. 2012;11:775–83.
58. van Weerden WM, van Steenbrugge GJ. Human prostate tumor xenografts as representative models for clinical prostate cancer. *Urol Oncol*. 1996;2:122–5.
59. de Morrée E, van Soest R, Aghai A, de Ridder C, de Bruijn P, Ghobadi Moghaddam-Helmantel I, et al. Understanding taxanes in prostate cancer; importance of intratumoral drug accumulation. *Prostate*. 2016;76:927–36.
60. Gandellini P, Andriani F, Merlino G, D'Aiuto F, Roz L, Callari M. Complexity in the tumour microenvironment: cancer associated fibroblast gene expression patterns identify both common and unique features of tumour-stroma crosstalk across cancer types. *Semin Cancer Biol*. 2015;35:96–106.
61. Heneberg P. Paracrine tumor signaling induces transdifferentiation of surrounding fibroblasts. *Crit Rev Oncol Hematol*. 2016;97:303–11.
62. Cunha GR, Hayward SW, Wang YZ, Ricke WA. Role of the stromal microenvironment in carcinogenesis of the prostate. *Int J Cancer*. 2003;107:1–10.
63. Paland N, Kamer I, Kogan-Sakin I, Madar S, Goldfinger N, Rotter V. Differential influence of normal and cancer-associated fibroblasts on the growth of human epithelial cells in an in vitro cocultivation model of prostate cancer. *Mol Cancer Res*. 2009;7:1212–23.
64. van der Pluijm G. Epithelial plasticity, cancer stem cells and bone metastasis formation. *Bone*. 2011;48:37–43.
65. DeRose YS, Wang G, Lin Y-C, Bernard PS, Buys SS, Ebbert MTW, et al. Tumor grafts derived from women with breast cancer authentically reflect tumor pathology, growth, metastasis and disease outcomes. *Nat Med*. 2011;17:1514–20.
66. Jeffers M, Rong S, Vande Woude GF. Hepatocyte growth factor/scatter factor-Met signaling in tumorigenicity and invasion/metastasis. *J Mol Med (Berl)*. 1996;74:505–13.
67. Varkaris A, Corn PG, Gaur S, Dayyani F, Logothetis CJ, Gallick GE. The role of HGF/c-Met signaling in prostate cancer progression and c-Met inhibitors in clinical trials. *Expert Opin Investig Drugs*. 2011;20:1677–84.
68. Hammacher A, Ward LD, Weinstock J, Treutlein H, Yasukawa K, Simpson RJ. Structure-function analysis of human IL-6: identification of two distinct regions that are important for receptor binding. *Protein Sci*. 1994;3:2280–93.
69. Nguyen DP, Li J, Tewari AK. Inflammation and prostate cancer: the role of interleukin 6 (IL-6). *BJU Int*. 2014;113:986–92.
70. Berquin IM, Min Y, Wu R, Wu H, Chen YQ. Expression signature of the mouse prostate. *J Biol Chem*. 2005;280:36442–51.
71. van der Heul-Nieuwenhuijsen L, Hendriksen PJM, van der Kwast TH, Jenster G. Gene expression profiling of the human prostate zones. *BJU Int*. 2006;98:886–97.
72. Fu X, Herrera H, Hoffman RM. Orthotopic growth and metastasis of human prostate carcinoma in nude mice after transplantation of histologically intact tissue. *Int J Cancer*. 1992;52:987–90.
73. Chang XH, Fu YW, Na WL, Wang J, Sun H, Cai L. Improved metastatic animal model of human prostate carcinoma using surgical orthotopic implantation (SOI). *Anticancer Res*. 1999;19:4199–202.
74. Kraaij R, van Weerden WM, de Ridder CMA, Gussenhoven EJ, Honkoop J, Nasu Y, et al. Validation of transrectal ultrasonographic volumetry for orthotopic prostate tumours in mice. *Lab Anim*. 2002;36:165–72.

75. Limpens J, Schröder FH, de Ridder CM, Bolder CA, Wildhagen MF, Obermüller-Jevic UC, et al. Combined lycopene and vitamin E treatment suppresses the growth of PC-346C human prostate cancer cells in nude mice. *J Nutr.* 2006;136:1287–93.
76. Ni J, Cozzi P, Hung T-T, Hao J, Graham P, Li Y. Monitoring prostate tumor growth in an orthotopic mouse model using three-dimensional ultrasound imaging technique. *Transl Oncol.* 2016;9:41–5.
77. Singh S, Pan C, Wood R, Yeh C-R, Yeh S, Sha K, et al. Quantitative volumetric imaging of normal, neoplastic and hyperplastic mouse prostate using ultrasound. *BMC Urol.* 2015;15:97.
78. de Jong M, Essers J, van Weerden WM. Imaging preclinical tumour models: improving translational power. *Nat Rev Cancer.* 2014;14:481–93.
79. Hoffman RM. The multiple uses of fluorescent proteins to visualize cancer in vivo. *Nat Rev Cancer.* 2005;5:796–806.
80. Wu J, Pan D, Chung LWK. Near-infrared fluorescence and nuclear imaging and targeting of prostate cancer. *Transl Androl Urol.* 2013;2:254–64.
81. Lilja H, Ulmert D, Vickers AJ. Prostate-specific antigen and prostate cancer: prediction, detection and monitoring. *Nat Rev Cancer.* 2008;8:268–78.
82. Fleming MT, Morris MJ, Heller G, Scher HI. Post-therapy changes in PSA as an outcome measure in prostate cancer clinical trials. *Nat Clin Pract Oncol.* 2006;3:658–67.
83. Thalmann GN, Sikes RA, Chang SM, Johnston DA, von Eschenbach AC, Chung LW. Suramin-induced decrease in prostate-specific antigen expression with no effect on tumor growth in the LNCaP model of human prostate cancer. *J Natl Cancer Inst.* 1996;88:794–801.
84. van Weerden WM, Schröder FH. The use of PSA as biomarker in nutritional intervention studies of prostate cancer. *Chem Biol Interact.* 2008;171:204–11.
85. Marques RB, Aghai A, de Ridder CMA, Stuurman D, Hoeben S, Boer A, et al. High efficacy of combination therapy using PI3K/AKT inhibitors with androgen deprivation in prostate cancer preclinical models. *Eur Urol.* 2015;67:1177–85.
86. Gaudreau PO, Stagg J, Soulières D, Saad F. The present and future of biomarkers in prostate cancer: proteomics, genomics, and immunology advancements. *Biomark Cancer.* 2016;8(Suppl 2):15–33.
87. Saini S. PSA and beyond: alternative prostate cancer biomarkers. *Cell Oncol.* 2016;39:97–106.
88. Larne O, Martens-Uzunova E, Hagman Z, Edsjö A, Lippolis G, den Berg MSV, et al. miQ—a novel microRNA based diagnostic and prognostic tool for prostate cancer. *Int J Cancer.* 2013;132:2867–75.
89. Hendriksen PJM, Dits NFJ, Kokame K, Veldhoven A, van Weerden WM, Bangma CH, et al. Evolution of the androgen receptor pathway during progression of prostate cancer. *Cancer Res.* 2006;66:5012–20.
90. Watahiki A, Wang Y, Morris J, Dennis K, O'Dwyer HM, Gleave M, et al. MicroRNAs associated with metastatic prostate cancer. *PLoS One.* 2011;6:e24950.
91. Crea F, Watahiki A, Quagliata L, Xue H, Pikor L, Parolia A, et al. Identification of a long non-coding RNA as a novel biomarker and potential therapeutic target for metastatic prostate cancer. *Oncotarget.* 2014;5:764–74.
92. Jansen FH, Krijgsveld J, van Rijswijk A, van den Bemd G-J, van den Berg MS, van Weerden WM, et al. Exosomal secretion of cytoplasmic prostate cancer xenograft-derived proteins. *Mol Cell Proteomics.* 2009;8:1192–205.
93. van den Bemd G-JCM, Krijgsveld J, Luijckx TM, van Rijswijk AL, Demmers JAA, Jenster G. Mass spectrometric identification of human prostate cancer-derived proteins in serum of xenograft-bearing mice. *Mol Cell Proteomics.* 2006;5:1830–9.
94. Jansen FH, van Rijswijk A, Teubel W, van Weerden WM, Reneman S, van den Bemd G-J, et al. Profiling of antibody production against xenograft-released proteins by protein microarrays discovers prostate cancer markers. *J Proteome Res.* 2012;11:728–35.
95. Beltran H, Eng K, Mosquera JM, Sigaras A, Romanel A, Rennett H, et al. Whole-exome sequencing of metastatic cancer and biomarkers of treatment response. *JAMA Oncol.* 2015;1:466.
96. Shiota M, Eto M. Current status of primary pharmacotherapy and future perspectives toward upfront therapy for metastatic hormone-sensitive prostate cancer. *Int J Urol.* 2016;23:360–9.



97. Gao H, Korn JM, Ferretti S, Monahan JE, Wang Y, Singh M, et al. High-throughput screening using patient-derived tumor xenografts to predict clinical trial drug response. *Nat Med*. 2015;21:1318–25.
98. Hidalgo M, Bruckheimer E, Rajeshkumar NV, Garrido-Laguna I, De Oliveira E, Rubio-Viqueira B, et al. A pilot clinical study of treatment guided by personalized tumorgrafts in patients with advanced cancer. *Mol Cancer Ther*. 2011;10:1311–6.
99. Julien S, Merino-Trigo A, Lacroix L, Pocard M, Goefé D, Mariani P, et al. Characterization of a large panel of patient-derived tumor xenografts representing the clinical heterogeneity of human colorectal cancer. *Clin Cancer Res*. 2012;18:5314–28.
100. Bertotti A, Migliardi G, Galimi F, Sassi F, Torti D, Isella C, et al. A molecularly annotated platform of patient-derived xenografts (“xenopatients”) identifies HER2 as an effective therapeutic target in cetuximab-resistant colorectal cancer. *Cancer Discov*. 2011;1:508–23.
101. Hidalgo M, Amant F, Biankin AV, Budinská E, Byrne AT, Caldas C, et al. Patient-derived Xenograft models: an emerging platform for translational cancer research. *Cancer Discov*. 2014;4:998–1013.
102. Wang Y, Kreisberg JI, Ghosh PM. Cross-talk between the androgen receptor and the phosphatidylinositol 3-kinase/Akt pathway in prostate cancer. *Curr Cancer Drug Targets*. 2007;7:591–604.
103. Carver BS, Chapinski C, Wongvipat J, Hieronymus H, Chen Y, Chandralapaty S, et al. Reciprocal feedback regulation of PI3K and androgen receptor signaling in PTEN-deficient prostate cancer. *Cancer Cell*. 2011;19:575–86.
104. Dahmani A, de Plater L, Guyader C, Fontaine J-J, Berniard A, Assayag F, et al. A preclinical therapeutic schedule optimizing docetaxel plus estramustine administration in prostate cancer. *Anticancer Drugs*. 2010;21:927–31.
105. Legrier M-E, Oudard S, Judde J-G, Guyader C, de Pinieux G, Boyé K, et al. Potentiation of antitumour activity of docetaxel by combination with trastuzumab in a human prostate cancer xenograft model and underlying mechanisms. *Br J Cancer*. 2007;96:269–76.
106. Brubaker KD, Brown LG, Vessella RL, Corey E. Administration of zoledronic acid enhances the effects of docetaxel on growth of prostate cancer in the bone environment. *BMC Cancer*. 2006;6:15.
107. McEntee MF, Ziegler C, Reel D, Tomer K, Shoieb A, Ray M, et al. Dietary n-3 polyunsaturated fatty acids enhance hormone ablation therapy in androgen-dependent prostate cancer. *Am J Pathol*. 2008;173:229–41. American Society for Investigative Pathology.
108. Fontana L, Adelaiye RM, Rastelli AL, Marie K, Ciamporcerio E, Longo VD, et al. Dietary protein restriction inhibits tumor growth in human xenograft models of prostate and breast cancer. *Oncotarget*. 2013;4(12):2451–61.
109. Yoshida T, Kinoshita H, Segawa T, Nakamura E, Inoue T, Shimizu Y, et al. Antiandrogen bicalutamide promotes tumor growth in a novel androgen-dependent prostate cancer xenograft model derived from a bicalutamide-treated patient. *Cancer Res*. 2005;65:9611–6.
110. Festuccia C, Gravina GL, Muzi P, Pomante R, Ventura L, Vessella RL, et al. Bicalutamide increases phospho-Akt levels through Her2 in patients with prostate cancer. *Endocr Relat Cancer*. 2007;14:601–11.
111. Montgomery RB, Mostaghel EA, Vessella R, Hess DL, Kalhorn TF, Higano CS, et al. Maintenance of intratumoral androgens in metastatic prostate cancer: a mechanism for castration-resistant tumor growth. *Cancer Res*. 2008;68:4447–54.
112. Mohler JL, Titus MA, Bai S, Kennerley BJ, Lih FB, Tomer KB, et al. Activation of the androgen receptor by intratumoral bioconversion of androstanediol to dihydrotestosterone in prostate cancer. *Cancer Res*. 2011;71:1486–96.
113. Kumagai J, Hofland J, Erkens-Schulze S, Dits NFJ, Steenbergen J, Jenster G, et al. Intratumoral conversion of adrenal androgen precursors drives androgen receptor-activated cell growth in prostate cancer more potently than de novo steroidogenesis. *Prostate*. 2013;73:1636–50.

114. Mostaghel EA, Marck BT, Plymate SR, Vessella RL, Balk S, Matsumoto AM, et al. Resistance to CYP17A1 inhibition with abiraterone in castration-resistant prostate cancer: induction of steroidogenesis and androgen receptor splice variants. *Clin Cancer Res.* 2011;17:5913–25.
115. van Soest RJ, de Morree ES, Kweldam CF, de Ridder CMA, Wiemer EAC, Mathijssen RHJ, et al. Targeting the androgen receptor confers in vivo cross-resistance between enzalutamide and docetaxel, but not cabazitaxel, in castration-resistant prostate cancer. *Eur Urol.* 2015;67:981–5.
116. Grasso CS, Wu Y-M, Robinson DR, Cao X, Dhanasekaran SM, Khan AP, et al. The mutational landscape of lethal castration-resistant prostate cancer. *Nature.* 2012;487:239–43.
117. Nardella C, Lunardi A, Patnaik A, Cantley LC, Pandolfi PP. The APL paradigm and the “co-clinical trial” project. *Cancer Discov.* 2011;1:108–16.
118. Malaney P, Nicosia SV, Davé V. One mouse, one patient paradigm: new avatars of personalized cancer therapy. *Cancer Lett.* 2014;344:1–12.
119. Varkaris A, Corn PG, Parikh NU, Efstathiou E, Song JH, Lee YC, et al. Integrating murine and clinical trials with cabozantinib to understand roles of MET and VEGFR2 as targets for growth inhibition of prostate cancer. *Clin Cancer Res.* 2016;22:107–21.
120. Spratt DE, Zumsteg ZS, Feng FY, Tomlins SA. Translational and clinical implications of the genetic landscape of prostate cancer. *Nat Rev Clin Oncol.* 2016;13(10):597–610.
121. Migliardi G, Sassi F, Torti D, Galimi F, Zanella ER, Buscarino M, et al. Inhibition of MEK and PI3K/mTOR suppresses tumor growth but does not cause tumor regression in patient-derived xenografts of RAS-mutant colorectal carcinomas. *Clin Cancer Res.* 2012;18:2515–25.
122. Cassidy JW, Caldas C, Bruna A. Maintaining tumor heterogeneity in patient-derived tumor xenografts. *Cancer Res.* 2015;75:2963–8.
123. Holzapfel BM, Wagner F, Loessner D, Holzapfel NP, Thibaudeau L, Crawford R, et al. Species-specific homing mechanisms of human prostate cancer metastasis in tissue engineered bone. *Biomaterials.* 2014;35:4108–15.
124. Francone TD, Landmann RG, Chen C-T, Sun MY, Kuntz EJ, Zeng Z, et al. Novel xenograft model expressing human hepatocyte growth factor shows ligand-dependent growth of c-Met-expressing tumors. *Mol Cancer Ther.* 2007;6:1460–6.
125. Ueda O, Tateishi H, Higuchi Y, Fujii E, Kato A, Kawase Y, et al. Novel genetically-humanized mouse model established to evaluate efficacy of therapeutic agents to human interleukin-6 receptor. *Sci Rep.* 2013;3:1196.
126. Pearson T, Greiner DL, Shultz LD. Creation of “humanized” mice to study human immunity. *Curr Protoc Immunol.* 2008.; Chapter 15:Unit 15.21.
127. Sanmamed MF, Chester C, Melero I, Kohrt H. Defining the optimal murine models to investigate immune checkpoint blockers and their combination with other immunotherapies. *Ann Oncol.* 2016;27(7):1190–8.
128. Roth MD, Harui A. Human tumor infiltrating lymphocytes cooperatively regulate prostate tumor growth in a humanized mouse model. *J Immunother Cancer.* 2015;3:12.
129. Shultz LD, Brehm MA, Garcia-Martinez JV, Greiner DL. Humanized mice for immune system investigation: progress, promise and challenges. *Nat Rev Immunol.* 2012;12:786–98.
130. Fidler IJ. Seed and soil revisited: contribution of the organ microenvironment to cancer metastasis. *Surg Oncol Clin N Am.* 2001;10:257–69. vii–viii.
131. Stephenson RA, Dinney CP, Gohji K, Ordóñez NG, Killion JJ, Fidler IJ. Metastatic model for human prostate cancer using orthotopic implantation in nude mice. *J Natl Cancer Inst.* 1992;84:951–7.
132. Hoffman RM. Patient-derived orthotopic xenografts: better mimic of metastasis than subcutaneous xenografts. *Nat Rev Cancer.* 2015;15:451–2.
133. Zhang Y, Toneri M, Ma H, Yang Z, Bouvet M, Goto Y, Seki N, Hoffman RM. Real-time GFP intravital imaging of the difference in cellular and angiogenic behavior of subcutaneous and orthotopic nude-mouse models of human PC-3 prostate cancer. *J Cell Biochem.* 2016;117:2546–51.

134. Gleave M, Hsieh JT, Gao CA, von Eschenbach AC, Chung LW. Acceleration of human prostate cancer growth in vivo by factors produced by prostate and bone fibroblasts. *Cancer Res.* 1991;51:3753–61.
135. Chung LWK. Prostate carcinoma bone-stroma interaction and its biologic and therapeutic implications. *Cancer.* 2003;97:772–8.
136. Corey E, Quinn JE, Bladou F, Brown LG, Roudier MP, Brown JM, et al. Establishment and characterization of osseous prostate cancer models: intra-tibial injection of human prostate cancer cells. *Prostate.* 2002;52:20–33.
137. Miwa S, Toneri M, Igarashi K, Yano S, Kimura H, Hayashi K, et al. Real-time in vivo confocal fluorescence imaging of prostate cancer bone-marrow micrometastasis development at the cellular level in nude mice. *J Cell Biochem.* 2016;117(11):2533–7.
138. Wu TT, Sikes RA, Cui Q, Thalmann GN, Kao C, Murphy CF, et al. Establishing human prostate cancer cell xenografts in bone: induction of osteoblastic reaction by prostate-specific antigen-producing tumors in athymic and SCID/bg mice using LNCaP and lineage-derived metastatic sublines. *Int J Cancer.* 1998;77:887–94.
139. Wang Y, Xue H, Cutz J-C, Bayani J, Mawji NR, Chen WG, et al. An orthotopic metastatic prostate cancer model in SCID mice via grafting of a transplantable human prostate tumor line. *Lab Invest.* 2005;85:1392–404.
140. Corey E, Quinn JE, Vessella RL. A novel method of generating prostate cancer metastases from orthotopic implants. *Prostate.* 2003;56:110–4.
141. Bubendorf L, Schöpfer A, Wagner U, Sauter G, Moch H, Willi N, et al. Metastatic patterns of prostate cancer: an autopsy study of 1,589 patients. *Hum Pathol.* 2000;31:578–83.
142. Michiel Sedelaar JP, Dalrymple SS, Isaacs JT. Of mice and men-warning: intact versus castrated adult male mice as xenograft hosts are equivalent to hypogonadal versus abiraterone treated aging human males, respectively. *Prostate.* 2013;73:1316–25.
143. van Weerden WM, Bierings HG, van Steenbrugge GJ, de Jong FH, Schröder FH. Adrenal glands of mouse and rat do not synthesize androgens. *Life Sci.* 1992;50:857–61.
144. Sharifi N. The 5 $\alpha$ -androstane-3-one pathway to dihydrotestosterone in castration-resistant prostate cancer. *J Invest Med.* 2012;60:504–7.
145. Gomez L, Kovac JR, Lamb DJ. CYP17A1 inhibitors in castration-resistant prostate cancer. *Steroids.* 2015;95:80–7.

---

# Patient-Derived Mouse Models of Sarcoma

# 9

Tara A. Russell, Irmina A. Elliott, Arun S. Singh,  
and Fritz C. Eilber

---

## Introduction

Sarcomas are a rare and heterogeneous group of tumors arising within the soft tissue and bone of patients of all ages. They most commonly arise in the extremities, closely followed by the retroperitoneum and abdomen, but can occur in any anatomical location including the viscera, thorax, head, neck, and central nervous system. Although these mesenchymal malignancies account for only 1% of all adult tumors, they are pathologically diverse and include over 80 different histological subtypes [1, 2].

---

T.A. Russell

Division of Surgical Oncology, University of California Los Angeles, Los Angeles, CA, USA

Jonsson Comprehensive Cancer Center Sarcoma Program, University of California  
Los Angeles, Los Angeles, CA, USA

Robert Wood Johnson/Veterans Affairs Clinical Scholars Program, Los Angeles, CA, USA  
e-mail: [TRussell@mednet.ucla.edu](mailto:TRussell@mednet.ucla.edu)

I.A. Elliott

Division of Surgical Oncology, University of California Los Angeles, Los Angeles, CA, USA

e-mail: [IGawlas@mednet.ucla.edu](mailto:IGawlas@mednet.ucla.edu)

A.S. Singh

Jonsson Comprehensive Cancer Center Sarcoma Program, University of California  
Los Angeles, Los Angeles, CA, USA

Division of Medical Oncology, University of California Los Angeles, Los Angeles, CA, USA  
e-mail: [ASingh@mednet.ucla.edu](mailto:ASingh@mednet.ucla.edu)

F.C. Eilber (✉)

Division of Surgical Oncology, University of California Los Angeles, Los Angeles, CA, USA

Jonsson Comprehensive Cancer Center Sarcoma Program, University of California  
Los Angeles, Los Angeles, CA, USA

e-mail: [fceilber@mednet.ucla.edu](mailto:fceilber@mednet.ucla.edu)

Surgery and radiation therapy is the cornerstone of treatment for primary sarcomas. Proper surgical resection by a sarcoma surgeon in combination with either neoadjuvant or adjuvant radiation can provide excellent local control and functional outcomes, but unfortunately distant metastasis remains a difficult problem. As an example, patients with high-grade extremity sarcomas greater than 5 cm have a 40% risk of developing metastasis despite having local control rates of greater than or equal to 95% with optimal surgery and radiation. In patients with greater than 10 cm high-grade extremity sarcomas, up to 70% will develop metastasis and ultimately die of disease [3, 4]. As a significant proportion of patients with primary disease have subclinical metastases, the only avenue to improve their outcomes is to develop better systemic therapies.

Clinical trials evaluating the efficacy of systemic therapies in sarcoma have been limited due to the rarity and diversity of these tumors. The earliest studies in soft tissue sarcoma focused on the use of doxorubicin and ifosfamide and demonstrated only a modest impact in patients with metastatic and high-risk primary disease [5–8]. Studies in the early 2000s, which explored additional chemotherapeutic regimens, such as epirubicin and ifosfamide [9–11] or the combination of mesna, doxorubicin, ifosfamide, and dacarbazine (MAID) [12], also demonstrated only modest impact with selectively improved response rates, but no overall improvement in survival [8]. Although the overall response rates of soft tissue sarcoma to systemic therapy are relatively low (20–30%), patients that do respond to therapy have significantly improved outcomes [3, 13]. Unfortunately, patients that do not respond do not derive any survival benefit, with outcomes similar to patients who have not received therapy, and incur all of the toxic side effects of treatment [3, 13]. In light of this, identifying optimal systemic therapy for patients with sarcoma continues to be a major focus.

Recent sarcoma research has focused on characterizing the histological subtypes and genetic mutations driving tumorigenesis in order to inform more targeted treatment. Such work has allowed us to progressively understand the molecular biology underlying these diverse malignancies. One success in this arena has been the discovery of mutations in the tyrosine kinase *c-kit* and *PDGFR $\alpha$*  as the driving mutations in gastrointestinal stromal tumors. Mutations in *c-kit*/*PDGFR $\alpha$*  can be targeted by the drug imatinib [2]. Multiple trials of imatinib in patients with both resected and metastatic disease have demonstrated a significant improvement in survival. The success of imatinib provides a glimpse into the potential for targeted therapy; however, the genetic diversity of sarcomas still poses a significant challenge. Continued work evaluating the molecular biology and underlying mechanisms of sarcoma has demonstrated that while approximately one-third of sarcomas possess specific chromosomal translocations or genetic mutations which may be amenable to targeted therapy, two-thirds show a complex karyotype with multiple chromosomal rearrangements, duplications, or deletions [2]. In light of this, identifying additional therapeutic options remains a challenge.

Collectively, the rarity, histologic diversity, high risk of metastasis, and poor response rates to traditional chemotherapy or first-line systemic therapy highlight the rationale and immediate need for more personalized and precise sarcoma therapy. As such, oncologists have started to employ DNA sequencing technologies to identify

novel therapeutic targets and employ targeted therapy for these malignancies. However, even among targeted therapies supported by sequencing data, individual tumor responses are frustratingly low, creating yet another level of complexity.

Patient-derived models, specifically patient-derived orthotopic xenografts (PDOX), which are tumor and patient specific and have demonstrated a high level of correlation with the clinical behavior of the cancer of origin, provide an ideal platform for personalized care in sarcoma. Specifically, these models present the opportunity to test multiple potentially active therapeutic agents (chemotherapy, targeted therapy, etc.) in a preclinical model, shielding patients from the potential toxicity and morbidity of inactive drugs. In an era of increasing promise of novel systemic therapy and personalized medicine, patient-derived models provide an exciting avenue for improving the survival of sarcoma patients.

---

## Mouse Models

Mouse models represent the preclinical model that best approximates human tumors in which therapeutic agents can be tested in an expeditious, cost-effective, and ethical manner. These models came into vogue with the development of immunodeficient mice strains which are able to serve as hosts for patient-derived cell lines and tumors [14]. They have enabled the development of tissue-specific cancer models allowing the study of both the pathogenesis and effect of targeted therapies. Each model system provides unique advantages for evaluating and manipulating tumorigenesis.

## Transgenic Mouse Models

Transgenic mouse models simulate human disease through global or tissue-specific expression of particular oncogene or tumor suppressor mutations. The products of these models are genetically homogenous tumors that enable the study of molecular biology or response to therapy. As such, these models provide an opportunity to study the role of distinct genetic lesions in tumorigenesis. Because they enable the fine-tuning of genetic expression, transgenic mice allow the study of mutations at any stage of development, in any specific tissue, and with the modulation of gene dosage. Moreover, these model systems are immunocompetent, allowing the study of the immune system's interaction with tumor development and progression.

Transgenic mouse models have been developed in varying systems for sarcoma research. The Cre-loxP system has been used to establish soft tissue sarcoma mouse models through the activation of oncogenic *Kras* and inactivation of the tumor suppressor *p53* [15]. This model has been used to preclinically evaluate alterations of the MAPK and PI3K pathways, including radiation and inhibitors of MEK and PI3K [16]. Cre-loxP has been used to generate models of all four liposarcoma subtypes using conditional inactivation of *p53* and *PTEN* [17]. The transgenic approach has also been used to further understand the malignant transformation of malignant peripheral nerve sheath tumors (MPNST) [18]. Gregorian et al. demonstrated that

K-Ras activation in combination with deletion of a single PTEN allele resulted in 100% penetrance of progression of benign neurofibromas to MPNST within a transgenic model. Translation of this finding to the clinical environment demonstrated a similar loss of PTEN in human patients with neurofibromatosis-1-associated MPNST tumors.

While such models have advanced the understanding of the molecular biology of a few sarcoma subtypes, transgenic models have many drawbacks. In particular, development of a transgenic model can be technically challenging and time consuming, as is exemplified by multiple failed attempts at establishing a viable transgenic mouse model for Ewing's sarcoma harboring the EWS-FL1 translocation [19]. In addition, and probably most importantly, transgenic mouse models lack genetic diversity and thus do not capture the genetic heterogeneity and complexity of human patient tumors. This significantly limits the translation of findings in any transgenic mouse model system to a group of patients with a specific sarcoma subtype and is certainly not translatable to an individual patient.

## Patient-Derived Xenograft (PDX) Models

As discussed in previous chapters, patient-derived models have come to the forefront of translational research due to their ability to maintain genetic similarity with, and mimic therapeutic responses of, the patient's primary tumor [20, 21]. The first patient-derived xenografts were published in the late 1960s [14] and focused primarily on colorectal adenocarcinoma. These early models employed subcutaneous implantation of tumor fragments into immunocompromised, athymic mice. The first patient-derived xenograft for sarcoma, a model of pediatric rhabdomyosarcoma, was published in 1982 [20].

Within sarcoma research, subcutaneous models have been established for rhabdomyosarcoma [20, 22], embryonal rhabdomyosarcoma [23], and MPNST [24], among others. PDX models have the ability to replicate the clinical chemosensitivity of the patient's origin tumor. In the earliest sarcoma PDX study, Houghton demonstrated 100% xenograftability in three patient-derived samples and was able to replicate the chemosensitivity profile of the patient's original tumor in the PDX model [20]. In the MPNST sarcoma subtype, Castellsague et al. furthered this translational paradigm by both replicating the histologic and genetic properties of the original tumor and demonstrating parallel efficacy of therapeutic combinations [24]. In addition, PDX models have also advanced our understanding of sarcoma tumor biology, as seen in a single-patient study by Hooper et al., where the authors were able to posthumously identify the probable driving mutation of a parameningeal embryonal rhabdomyosarcoma [23]. It is of note that some researchers have made modifications to the subcutaneous sarcoma. Specifically, Glaser et al. [25] demonstrated the efficacy of an intraperitoneal model for ovarian carcinosarcoma, and Press et al. [26] employed renal capsule implantation for uterine sarcomas. In both of these ectopic models, genetic similarity was demonstrated between the PDX and original tumor through various techniques including comparative genomic

hybridization arrays, immunohistochemistry, and mutation analysis. Collectively these subcutaneous and other ectopic models demonstrate that genetics and chemosensitivity are conserved by these techniques and foreshadow the potential for more personalized translational studies.

In 2014, the first clinical trial of PDX models in sarcoma was published by an international group [27]. Patients with advanced sarcoma of varying subtypes (leiomyosarcoma, liposarcoma, synovial sarcoma, etc.) were enrolled at the time of tumor excision, and subcutaneous PDX models were developed postoperatively for each individual patient. Successfully implanted xenografts were then treated with various chemotherapeutic agents, and mice were monitored for pathologic response. When possible, efficacious agents evaluated in the PDX models were offered as treatment options to the corresponding patients. The study demonstrated an overall engraftment rate of 75.8% (22/29) and reported a correlation between growth of the PDX model and the clinical outcome in 81% (13/16). Additionally, six patients received direct clinical benefit, as they experienced objective response to agents identified to be effective against their PDX model. Although the major findings are promising, this study also demonstrated limitations of translation PDX studies. Specifically, more than 20% of tumors did not produce successful xenografts, and the time required to generate the PDX varied widely from 6 weeks to 6 months. As a consequence of both late-stage enrollment and this variable growth period, nine (39%) patients derived no clinical benefit, as they died of disease prior to their xenograft data becoming available. In spite of these shortcomings, this study, which was the first of its kind for sarcoma, provides a unique glimpse at the potential for PDX models to inform clinical practice, particularly in the setting of rare and genetically diverse malignancies.

PDX models have provided an avenue for individualized mouse models of sarcoma that recapitulate tumor growth kinetics, model clinically observed local disease progression, and mimic tumor-specific chemosensitivity. Yet there have been few PDX models that have been able to replicate advanced disease states, *as subcutaneous models very rarely produce metastatic spread*. As such, there is evidence to suggest that while subcutaneous models allow for the trial of various systemic therapies, they are limited by their inability to assess chemotherapeutic response in advanced or metastatic disease states [28]. Collectively, these limitations have led many researchers to explore additional techniques which may provide the opportunity to simulate advanced disease.

## Patient-Derived Orthotopic Xenograft (PDOX) Models

Due to some of the limitations of subcutaneous implantation, orthotopic xenografts [29–31], in which the patient-derived tissue is implanted into the corresponding anatomical location, have now come to the forefront of sarcoma research. While techniques vary, the best results in this model are obtained when an intact fragment of tumor tissue is directly implanted using microsurgical technique, termed surgical orthotopic implantation (SOI) [32–36]. An example of this technique is illustrated



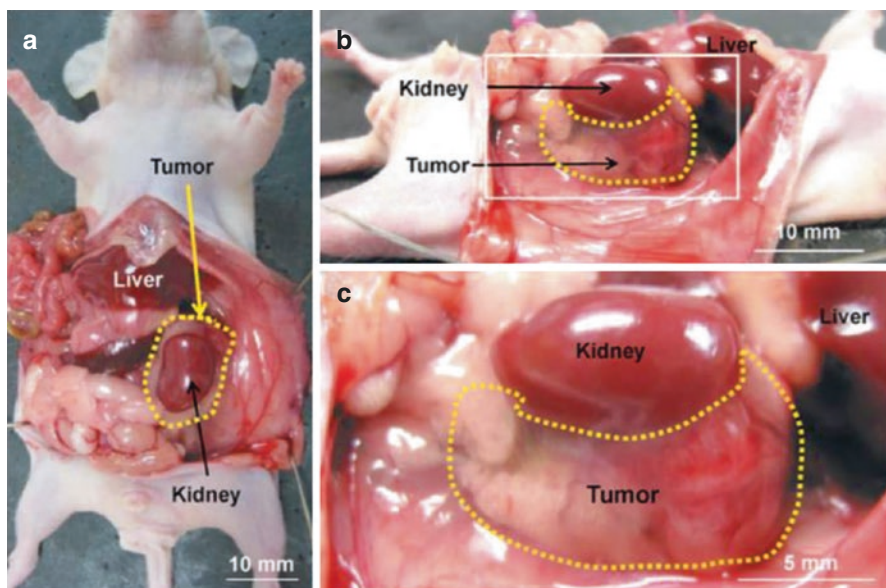


**Fig. 9.1** (a) Laparotomy of the soft tissue sarcoma PDOX model, (b) Lateral view of the laparotomy, (c) High magnification image of b. Patient-derived orthotopic xenograft of a retroperitoneal sarcoma. Tumor growth is observed in the retroperitoneal space, behind the left kidney [1]

in Fig. 9.1 [1]. This method, which has been successfully applied in sarcoma research, has been used previously in other cancers including cervical [37], lung [38], stomach [39, 40], breast [41, 42], ovarian [43], pancreas [33]; mesothelioma [44], and colon cancer [32, 45, 46]. The most significant advantage of this technique is the ability to produce clinically accurate metastatic spread, something that has not been achieved in subcutaneous or other ectopic patient-derived xenografts [34, 35, 47, 48]. In addition to modeling advanced disease, studies have also demonstrated that orthotopic xenografts are superior to subcutaneous xenografts in that they more accurately model therapeutic drug response and produce tumors with even greater histologic similarity [1, 28, 35]. Specifically, Hiroshima et al. found that in a direct comparison of the same retroperitoneal sarcoma implanted in a PDX and PDOX system, the PDOX tumor had greater histologic similarity to the original tumor [1].

To date, the largest published series of PDX models in sarcoma is by Smith et al., which focused on the liposarcoma subtype and included 22 patient-derived subcutaneous tumor mouse models [49]. In this series, which included 13 high-grade, 1 intermediate-grade, and 8 low-grade tumors, the authors reported an engraftment rate of 53.8% among high-grade tumors (no intermediate- or low-grade tumors engrafted). Furthermore, xenograftability correlated with disease-specific survival in liposarcoma patients, such that successfully engrafted tumors were more likely to be derived from aggressive subtypes with a high associated disease-specific mortality.

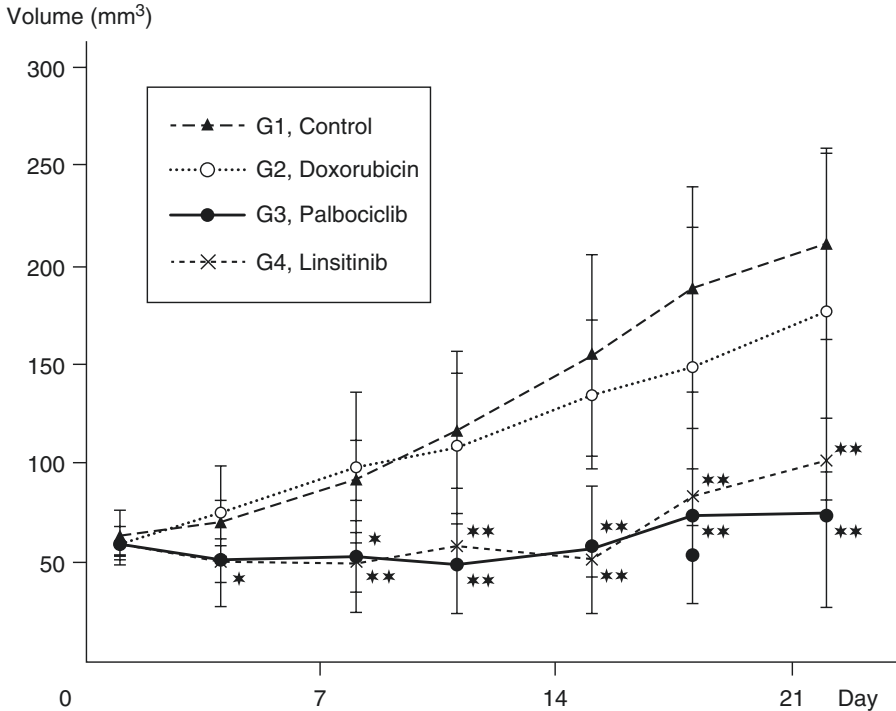


**Fig. 9.2** Example of a translational PDOX model for evaluating potential chemotherapeutic regimens. In this Ewing’s sarcoma PDOX, the model demonstrated doxorubicin resistance in concordance with the resistance seen in the patient’s clinical course. Potential targeted therapies were identified through trials of other chemotherapeutic agents, two of which, palbociclib (CDK4/6 inhibitor) and linsitinib (IGF-1R inhibitor), significantly inhibited tumor growth. \* $P < 0.05$ , \*\* $P < 0.001$ , compared to the untreated control. *CDK* cyclin-dependent kinase, *IGF-1R* insulin-like growth factor-1 receptor [50]

PDOX models in sarcoma have also begun to show promise in the ability to direct patient therapy. In a case study of Ewing’s sarcoma, Murakami et al. tested a series of different chemotherapeutic agents against a PDOX derived from a doxorubicin-resistant tumor. Figure 9.2 shows the PDOX growth curves from this study after treatment with different targeted therapies. The results indicate that the PDOX replicated resistance to doxorubicin seen in the patient and also suggested promising alternative regimens for therapeutic intervention [50]. This study clearly demonstrates the potential for PDOX models to identify individually tailored, effective therapy without exposing the patient to unwarranted therapeutic trials or toxic regimens.

The results from a recently completed UCLA Sarcoma Program PDOX study (Table 9.1), the largest clinical PDOX study ever performed, will further define PDOX’s potential role in sarcoma personalized care [51]. In comparison to the

**Table 9.1** Sarcoma patient-derived xenograft studies to date

Author	Year	Institution	Graft location	Cancer type	Take rate (%)	Sample (n)	Metastases noted in model
Houghton et al.	1982	St. Jude	Subcutaneous	Rhabdomyosarcoma	100	3	No
Monisma et al.	2014	Van Andel Research Inst. (MI)	Subcutaneous	Rhabdomyosarcoma	100	1	No
Hooper et al.	2015	Johns Hopkins	Subcutaneous	Rhabdomyosarcoma	100	1	No
Castellsague et al.	2015	Catalan Inst. of Oncology (Spain)	Subcutaneous	Peripheral nerve sheath tumors	100	4	No
Glaser et al.	2015	Mayo Clinic	Intraperitoneal	Ovarian carcinosarcoma	100	1	No
Press et al.	2008	University of British Columbia	Renal capsule	Uterine sarcoma	100	5	No
Smith et al.	2013	UCLA	Subcutaneous	Liposarcoma	32	22	No
Stebbing et al.	2014	Multi-institution	Subcutaneous	Multiple sarcoma subtypes	76	29	No
Eckardt et al.	2016	UCLA	Orthotopic	Multiple sarcoma subtypes	64	107	Yes

previous translational PDX study, this trial is strengthened by a large volume at a single center, patient enrollment early in the course of disease in order to optimize the window for translating xenograft findings, and application of the PDOX-surgical orthotopic implantation (SOI) technique, which provides the opportunity to model advanced disease. In this focused study, 107 soft tissue sarcomas of varying subtypes were implanted. Similar to the study by Smith et al., there was no successful engraftment of low- or intermediate-grade tumors. Among high-grade tumors, the only factor impacting engraftment and ultimate PDOX establishment was preoperative radiation therapy. Among patients who were treatment-naïve prior to surgical excision, PDOX establishment was successful in over 80%. This trial, which marks the first translational PDOX study in sarcoma and the largest clinical PDOX study ever performed, demonstrates the feasibility of PDOX development in coordination with real-time patient care. In addition, each PDOX model created in this study is being tested with candidate systemic therapies, and the results will be used to help guide treatment decisions in the corresponding patient.

---

### Conclusion

The vast histologic diversity between and within sarcoma subtypes, as well as the low incidence of these malignancies, has hindered the development of evidence-based therapies and execution of large-scale clinical trials to inform treatment of these patients. In this setting, where physicians have few well-validated treatment options, patient-derived orthotopic xenograft (PDOX) models present a unique opportunity to provide patients with specific and tailored treatment options.

---

### References

1. Hiroshima Y, Zhang Y, Zhang N, et al. Patient-derived orthotopic xenograft (PDOX) nude mouse model of soft-tissue sarcoma more closely mimics the patient behavior in contrast to the subcutaneous ectopic model. *Anticancer Res.* 2015;35:697–701.
2. Sampson VB, Kamara DF, Kolb EA. Xenograft and genetically engineered mouse model systems of osteosarcoma and Ewing's sarcoma: tumor models for cancer drug discovery. *Expert Opin Drug Discov.* 2013;8:1181–9. doi:[10.1517/17460441.2013.817988](https://doi.org/10.1517/17460441.2013.817988).
3. Eilber FC, Brennan MF, Eilber FR, et al. Validation of the postoperative nomogram for 12-year sarcoma-specific mortality. *Cancer.* 2004;101(10):2270–5.
4. Eilber FC, Kattan MW. Sarcoma nomogram: validation and a model to evaluate impact of therapy. *J Am Coll Surg.* 2007;205(Suppl 4):S90–5.
5. Antman K, Crowley J, Balcerzak SP, et al. An intergroup phase III randomized study of doxorubicin and dacarbazine with or without ifosfamide and mesna in advanced soft tissue and bone sarcomas. *J Clin Oncol.* 1993;11(7):1276–85.
6. Antman KH. Chemotherapy of advanced sarcomas of bone and soft tissue. *Semin Oncol.* 1992;19(6 Suppl 12):13–20.
7. Antman KH, Ryan L, Elias A, Sherman D, et al. Response to ifosfamide and mesna: 124 previously treated patients with metastatic or unresectable sarcoma. *J Clin Oncol.* 1989;7(1):126–31.
8. Judson I, Verweij J, Gelderblom H, et al. Doxorubicin alone versus intensified doxorubicin plus ifosfamide for first-line treatment of advanced or metastatic soft-tissue sarcoma: a randomised controlled phase 3 trial. *Lancet Oncol.* 2014;15:415–23. doi:[10.1016/S1470-2045\(14\)70063-4](https://doi.org/10.1016/S1470-2045(14)70063-4).

9. Eilber FC, Rosen G, Eckardt J, Forscher C, et al. Treatment-induced pathologic necrosis: a predictor of local recurrence and survival in patients receiving neoadjuvant therapy for high-grade extremity soft tissue sarcomas. *J Clin Oncol.* 2001;19(13):3203–9.
10. Frustaci S, Gherlinzoni F, De Paoli A, et al. Adjuvant chemotherapy for adult soft tissue sarcomas of the extremities and girdles: results of the Italian randomized cooperative trial. *J Clin Oncol.* 2001;19(5):1238–47.
11. Grobmyer SR, Maki RG, Demetri GD, et al. Neo-adjuvant chemotherapy for primary high-grade extremity soft tissue sarcoma. *Ann Oncol.* 2004;15(11):1667–72.
12. Mullen JT, Kobayashi W, Wang JJ, Harmon DC. Long-term follow-up of patients treated with neoadjuvant chemotherapy and radiotherapy for large, extremity soft tissue sarcomas. *Cancer.* 2012;118(15):3758–65.
13. Donahue TR, Kattan MW, Nelson SD, et al. Evaluation of neoadjuvant therapy and histopathologic response in primary, high-grade retroperitoneal sarcomas using the sarcoma nomogram. *Cancer.* 2010;116:3883–91. doi:[10.1002/cncr.25271](https://doi.org/10.1002/cncr.25271).
14. Rygaard J, Povlsen CO. Heterotransplantation of a human malignant tumor to 'nude' mice. *Acta Pathol Microbiol Scand.* 1969;77:758–60.
15. Kirsch DG, Dinulescu DM, Miller JB, et al. A spatially and temporally restricted mouse model of soft tissue sarcoma. *Nat Med.* 2007;13:992–7. doi:[10.1038/nm1602](https://doi.org/10.1038/nm1602).
16. Dodd RD, Añó L, Blum JM, et al. Methods to generate genetically engineered mouse models of soft tissue sarcoma. *Methods Mol Biol.* 2015;1267:283–95.
17. Puzio-Kuter AM, Laddha SV, Castillo-Martin M, et al. Involvement of tumor suppressors PTEN and p53 in the formation of multiple subtypes of liposarcoma. *Cell Death Differ.* 2015;22:1785–91. doi:[10.1038/cdd.2015.27](https://doi.org/10.1038/cdd.2015.27).
18. Gregorian C, Nakashima J, Dry SM, et al. PTEN dosage is essential for neurofibroma development and malignant transformation. *Proc Natl Acad Sci U S A.* 2009;106:19479–84. doi:[10.1073/pnas.0910398106](https://doi.org/10.1073/pnas.0910398106).
19. Minas TZ, Surdez D, Javaheri T, et al. Combined experience of six independent laboratories attempting to create an Ewing sarcoma mouse model. *Oncotarget.* 2016. doi:[10.18632/oncotarget.9388](https://doi.org/10.18632/oncotarget.9388)
20. Houghton JA, Houghton PJ, Green AA. Chemotherapy of childhood rhabdomyosarcomas growing as xenografts in immune-deprived mice. *Cancer Res.* 1982;42:535–9.
21. Izumchenko E, Meir J, Bedi A, et al. Patient-derived xenografts as tools in pharmaceutical development. *Clin Pharmacol Ther.* 2016;99:612–21. doi:[10.1002/cpt.354](https://doi.org/10.1002/cpt.354).
22. Monsma DJ, Cherba DM, Richardson PJ, et al. Using a rhabdomyosarcoma patient-derived xenograft to examine precision medicine approaches and model acquired resistance. *Pediatr Blood Cancer.* 2014;61:1570–7. doi:[10.1002/pbc.25039](https://doi.org/10.1002/pbc.25039).
23. Hooper JE, Cantor EL, Ehlen MS, et al. Research article: a patient-derived xenograft model of parameningeal embryonal rhabdomyosarcoma for preclinical studies. *Sarcoma.* 2015:1–7. doi:[10.1155/2015/826124](https://doi.org/10.1155/2015/826124).
24. Castellsagué J, Gel B, Rodríguez JF, et al. Comprehensive establishment and characterization of orthoxenograft mouse models of malignant peripheral nerve sheath tumors for personalized medicine. *EMBO Mol Med.* 2015;7:608–27. doi:[10.15252/emmm.201404430](https://doi.org/10.15252/emmm.201404430).
25. Glaser G, Weroha SJ, Becker MA, et al. Conventional chemotherapy and oncogenic pathway targeting in ovarian carcinosarcoma using a patient-derived tumorgraft. *PLoS One.* 2015;10:e0126867–15. doi:[10.1371/journal.pone.0126867](https://doi.org/10.1371/journal.pone.0126867).
26. Press JZ, Kenyon JA, Xue H, et al. Xenografts of primary human gynecological tumors grown under the renal capsule of NOD/SCID mice show genetic stability during serial transplantation and respond to cytotoxic chemotherapy. *Gynecol Oncol.* 2008;110:256–64.
27. Stebbing J, Paz K, Schwartz GK, et al. Patient-derived xenografts for individualized care in advanced sarcoma. *Cancer.* 2014;120:2006–15. doi:[10.1002/cncr.28696](https://doi.org/10.1002/cncr.28696).
28. Hiroshima Y, Maawy A, Zhang Y, Zhang N, Murakami T, Chishima T, Tanaka K, Ichikawa Y, Bouvet M, Endo I, Hoffman RM. Patient-derived mouse models of cancer need to be orthotopic in order to evaluate targeted anti-metastatic therapy. *Oncotarget.* 2016;7(44):71696–702.

29. Fidler IJ. Critical factors in the biology of human cancer metastasis: twenty-eighth G. H. A. Clowes Memorial Award Lecture. *Cancer Res.* 1990;50:6130–8.
30. Hoffman RM. Orthotopic is orthodox: why are orthotopic-transplant metastatic models different from all other models? *J Cell Biochem.* 1994;56:1-3.
31. Garber K. Realistic rodents? Debate grows over new mouse models of cancer. *J Natl Cancer Inst.* 2006;98:1176–8.
32. Fu X, Besterman JM, Monosov A, Hoffman RM. Models of human metastatic colon cancer in nude mice orthotopically constructed by using histologically intact patient specimens. *Proc Natl Acad Sci U S A.* 1991;88:9345–9.
33. Fu X, Guadagni F, Hoffman RM. A metastatic nude-mouse model of human pancreatic cancer constructed orthotopically from histologically intact patient specimens. *Proc Natl Acad Sci U S A.* 1992;89:5645–9.
34. Hoffman RM. Orthotopic metastatic mouse models for anticancer drug discovery and evaluation: a bridge to the clinic. *Invest New Drugs.* 1999;17:343–59.
35. Hoffman RM. Patient-derived orthotopic xenografts: better mimic of metastasis than subcutaneous xenografts. *Nat Rev Cancer.* 2015;15:451–2.
36. Manzotti C, Audisio RA, Pratesi G. Importance of orthotopic implantation for human tumors as model systems: relevance to metastasis and invasion. *Clin Exp Metastasis.* 1993;11:5–14. doi:[10.1007/BF00880061](https://doi.org/10.1007/BF00880061).
37. Hiroshima Y, Zhang Y, Zhang N, et al. Establishment of a patient-derived orthotopic xenograft (PDOX) model of HER-2-positive cervical cancer expressing the clinical metastatic pattern. *PLoS One.* 2015;10:e0117417.
38. Wang X, Fu X, Hoffman RM. A new patient-like metastatic model of human lung cancer constructed orthotopically with intact tissue via thoracotomy in immunodeficient mice. *Int J Cancer.* 1992;51:992–5. doi:[10.1002/ijc.2910510626](https://doi.org/10.1002/ijc.2910510626).
39. Furukawa T, Fu X, Kubota T, et al. Nude mouse metastatic models of human stomach cancer constructed using orthotopic implantation of histologically intact tissue. *Cancer Res.* 1993;53:1204–8.
40. Furukawa T, Kubota T, Watanabe M, et al. Orthotopic transplantation of histologically intact clinical specimens of stomach cancer to nude mice: correlation of metastatic sites in mouse and individual patient donors. *Int J Cancer.* 1993;53:608–12. doi:[10.1002/ijc.2910530414](https://doi.org/10.1002/ijc.2910530414).
41. Fu X, Le P, Hoffman RM. A metastatic-orthotopic transplant nude-mouse model of human patient breast cancer. *Anticancer Res.* 1993;13:901–4.
42. DeRose YS, Wang G, Lin Y-C, et al. Tumor grafts derived from women with breast cancer authentically reflect tumor pathology, growth, metastasis and disease outcomes. *Nat Med.* 2011;17:1514–20.
43. Fu X, Hoffman RM. Human ovarian carcinoma metastatic models constructed in nude mice by orthotopic transplantation of histologically-intact patient specimens. *Anticancer Res.* 1993;13:287–91.
44. Astoul P, Wang X, Colt HG, Boutin C, Hoffman RM. A patient-like human malignant pleural mesothelioma nude-mouse model. *Oncol Rep.* 1996;3:483–7.
45. Hiroshima Y, Maawy A, Metildi CA. Successful fluorescence-guided surgery on human colon cancer patient-derived orthotopic xenograft mouse models using a fluorophore-conjugated anti-CEA antibody and a portable imaging system. *J Laparoendosc Adv Surg Tech A.* 2014;24:241–7.
46. Shoji T, Konno H, Tanaka T, et al. Orthotopic implantation of a colon cancer xenograft induces high expression of cyclooxygenase-2. *Cancer Lett.* 2003;195(2):235–41.
47. Hidalgo M, Amant F, Biankin AV, et al. Patient-derived xenograft models: an emerging platform for translational cancer research. *Cancer Discov.* 2014;4:998–1013. doi:[10.1158/2159-8290.CD-14-0001](https://doi.org/10.1158/2159-8290.CD-14-0001).
48. Kubota T. Metastatic models of human cancer xenografted in the nude mouse: the importance of orthotopic transplantation. *J Cell Biochem.* 1994;56(1):4–8.

49. Smith KB, Tran LM, Tam BM, et al. Novel dedifferentiated liposarcoma xenograft models reveal PTEN down-regulation as a malignant signature and response to PI3K pathway inhibition. *Am J Pathol.* 2013;182:1400–11. doi:[10.1016/j.ajpath.2013.01.002](https://doi.org/10.1016/j.ajpath.2013.01.002).
50. Murakami T, Singh AS, Kiyuna T, et al. Effective molecular targeting of CDK4/6 and IGF-1R in a rare FUS-ERG fusion CDKN2A-deletion doxorubicin-resistant Ewing's sarcoma patient-derived orthotopic xenograft (PDOX) nude-mouse model. *Oncotarget.* 2016;7:47556–64. doi:[10.18632/oncotarget.9879](https://doi.org/10.18632/oncotarget.9879).
51. Eckardt M, Russell TA, Murakami T, et al Factors impacting the establishment of individual soft tissue sarcoma patient-derived orthotopic xenograft (PDOX) mouse models: a UCLA Sarcoma Program Prospective Clinical Trial. *Connective Tissue Oncology Society Annual Meeting*, Lisbon, Portugal. 2016.

Robert M. Hoffman, Yukihiro Hiroshima,  
Takashi Murakami, and Takuya Murata

Cervical cancer is worldwide the second most common cancer in women with the majority of squamous cell carcinoma (SCC) [1]. Currently, there are about 454,000 cases and 200,000 deaths per year. Approximately 11,000 new cases and 3,870 deaths occur for cervical carcinoma in the USA [2]. Pelvic lymph nodes, para-aortic lymph nodes, lung, extrapelvic nodes, liver, and bones are frequent metastatic sites [3]. Stage and nodal metastasis are related to overall survival [4].

Chemotherapy drugs used for cervical cancer include paclitaxel, carboplatin, cisplatin, bleomycin, mitomycin C, vincristine, and irinotecan [5]. Retinoids and interferon, in combination with cytotoxic chemotherapy, can be effective in certain cases [6]. However, there is no standard treatment for metastatic cervical cancer. Therefore, a patient-like mouse model of cervical cancer could be very useful.

Patient-derived orthotopic xenograft (PDOX) models [7, 8] from patients with colon [9–11], pancreatic [12–23], breast [24], ovarian [25], lung [26], and stomach cancer [27] and mesothelioma [28] were established in the early 1990s in our laboratory, resulting in primary and metastatic tumor growth very similar to that of the patient [27] (please see Chapter 7 in the present volume). Recently, PDOX models

---

R.M. Hoffman (✉)

AntiCancer, Inc., 7917 Ostrow Street, San Diego, CA 92111, USA

Department of Surgery, University of California, San Diego, La Jolla, CA, USA

e-mail: [all@anticancer.com](mailto:all@anticancer.com)

Y. Hiroshima • T. Murakami

AntiCancer, Inc., 7917 Ostrow Street, San Diego, CA 92111, USA

Department of Surgery, University of California, San Diego, La Jolla, CA, USA

Department of Gastroenterological Surgery, Yokohama City University, Yokohama, Japan

T. Murata

Department of Obstetrics and Gynecology, Kawasaki Medical School, Okayama, Japan



of sarcoma have been developed [29–33] (please see Chapter 9 in the present volume), as well as melanoma [34, 35] (please see Chapter 18 in the present volume).

We recently developed a PDOX model of HER-2-positive cervical cancer [36]. Primary tumors and metastases in the nude mice had histological structures similar to the original tumor and were stained by an anti-HER-2 antibody in the same pattern as the patient's cancer. Primary tumors grew in six out of eight nude mice after orthotopic implantation and metastasis grew in four mice. Metastasis in the nude mice included peritoneal dissemination, liver metastasis, lung metastasis, as well as para-aortic lymph node metastasis. The patient had metastasis in para-aortic lymph nodes, peritoneum, liver, and mesentery. The metastatic pattern, histology, and HER-2 tumor expression of the patient were preserved in the PDOX model. The PDOX model mimicked the patient tumor metastatic pattern. In contrast, the subcutaneous PDX model had no metastasis. The growth rate of the primary tumor was rapid, doubling in 10–15 days during the 36-day observation period. Examples of the sizes and shapes of the various metastasis on various organs were as follows: a roundish liver metastasis (8.5 mm × 8.3 mm), two lung metastases (1.3 mm × 1.0 mm [oval], 1.1 mm × 1.1 mm [round]), and two para-aortic lymph node metastases (4.0 mm × 2.3 mm [oval], 4.6 mm × 2.1 mm [oval]) [14–16, 36].

*Histology of the original tumor is preserved in the mouse:* Sheetlike growth without gland formation and stromal tissue with fibroblastic proliferation, which penetrated into the nests of carcinoma, were observed in the H&E stained sections of the original patient tumor. Oval- to spindle-shaped cancer cells with high nuclear/cytoplasmic ratio were found in high-magnification images. In the immunostained sections with anti-HER-2 antibody, the membrane and the cytoplasm of cancer cells were strongly stained but no staining was found in the stromal tissue. All mouse-grown cervical cancer patient tumors including the metastatic tumors had histological structures similar to the original patient tumor and were stained by anti-human HER-2 antibody, suggesting that the model recapitulates the biological behaviors of the original tumor [36].

*Entinostat did not arrest tumor growth in the subcutaneous model of patient cervical cancer:* Entinostat monotherapy was least effective compared to carboplatin, trastuzumab, and lapatinib in the subcutaneous model [37].

*Entinostat monotherapy was not active on the primary tumor of the PDOX model of cervical cancer:* All regimens tested except entinostat had significant efficacy on the primary tumors compared to the vehicle group (carboplatin, trastuzumab/lapatinib, trastuzumab/lapatinib/entinostat, respectively) compared to entinostat monotherapy [37].

*Entinostat monotherapy was active against metastasis in the PDOX model of cervical cancer:* However, entinostat had efficacy against metastasis in the PDOX model of cervical carcinoma. All other regimens tested also had significant efficacy on metastasis compared to the vehicle group. No metastasis was detected in trastuzumab/lapatinib/entinostat group. All regimens caused body-weight loss, with carboplatin the most toxic Fig. 10.1 [37].

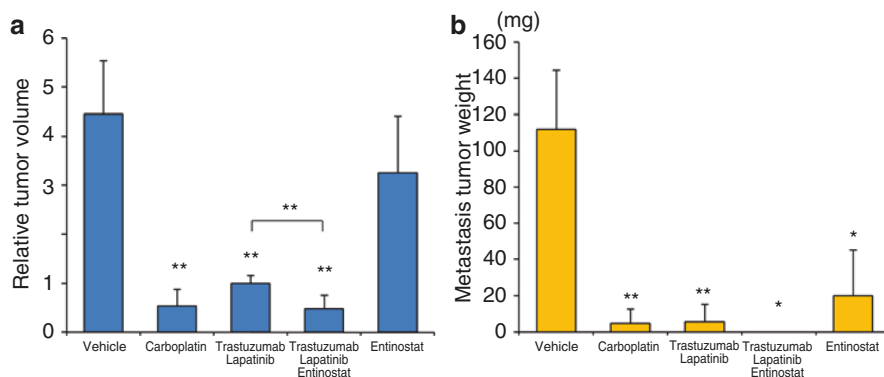


**Fig. 10.1** Drug-efficacy testing in the PDOX model. PDOX nude mice were treated with saline, carboplatin, trastuzumab + lapatinib, trastuzumab + lapatinib + entinostat, or entinostat alone. (a) Bar graphs of the primary tumor weight in each group. (b) Bar graphs of the metastatic tumor weight in each group. (n = 5 for each treatment arm). \*p < 0.05; \*\*p < 0.01

The efficacy of entinostat on the metastasis and not the primary cervical PDOX tumor or subcutaneous tumor is an important example of the critical need of orthotopic models of patient tumors since drugs, such as entinostat, can be evaluated are selectively effective against metastasis only and would have been missed by a subcutaneous model.

PDOX model of squamous cell cervical cancer: The patient was a 57-year-old female with primary cervical cancer. Histology demonstrated squamous cell carcinoma (grade 2). The patient received no previous treatment. A radical hysterectomy was performed with bilateral salpingo-oophorectomy and pelvic lymphadenectomy [38]. Nanoparticle albumin-bound (nab)-paclitaxel (NAB-PTX) is paclitaxel linked to albumin nanoparticles, which makes it soluble. The development of nanotechnology as a delivery system for NAB-PTX has improved the pharmacokinetics and pharmacodynamics of paclitaxel, in part by decreasing its hydrophobicity [38, 39].

In a this study, we compared the efficacy of two first-line drugs for cervical cancer, cisplatin (CDDP), and NAB-PTX [38]. CDDP was highly effective. One tumor treated with CDDP completely regressed. CDDP-treated tumors were significantly smaller (tumor volume ratio,  $0.42 \pm 0.36$ ) than untreated control mice. In contrast, NAB-PTX did not show efficacy on the cervical cancer PDOX model. CDDP-treated tumor weight was significantly less than control. NAB-PTX-treated tumors were not reduced in weight compared to control. There were no significant differences in mouse body weight between groups. Histological evaluation demonstrated that CDDP-treated tumors were fibrotic with scattered squamous cell nests compared to those of control or NAB-PTX-treated [38]. The PDOX model in this case showed that an inexpensive drug, CDDP, was more effective than a very expensive drug.

## Materials and Methods

### Establishment of Patient-Derived Cervical Cancer

Tumor tissues were obtained from the cervical cancer patients at surgery, divided into 3-mm<sup>3</sup> fragments, and transplanted subcutaneously in nude mice [36, 38].

### Orthotopic Tumor Implantation

After the subcutaneous tumors grew in the nude mice, they were harvested and divided into small fragments for orthotopic transplantation which was performed as follows: a small 6–10-mm midline incision was made on the lower abdomen of the nude mouse through the skin and peritoneum. The uterus was exposed through this incision, and a single 3-mm<sup>3</sup> tumor fragment was sutured to the cervix of the uterus using 8-0 nylon surgical sutures (Ethilon, Ethicon Inc., NJ, USA). On completion of tumor implantation, the uterus was returned to the abdomen, and the incision was closed in one layer using 6-0 nylon surgical sutures (Ethilon) [37].

### Treatment

Six weeks after implantation, the mice in the PDX and PDOX models of the HER-2-positive cervical cancer were randomized and treated in the following groups of  $n = 5$ :

1. Saline (vehicle/control, ip, weekly, 5 weeks)
2. Carboplatin (Selleck Chemicals, Houston, TX, USA, 30 mg/kg, ip, weekly, 5 weeks)
3. Trastuzumab (Genentech, Inc., South San Francisco, CA, USA, 20 mg/kg, ip, weekly, 5 weeks) + lapatinib (Selleck Chemicals, 100 mg/kg, orally, daily, 5 weeks)
4. Trastuzumab (20 mg/kg, ip, weekly, 5 weeks) + lapatinib (100 mg/kg, orally, daily, 5 weeks) + entinostat (Selleck Chemicals, 5 mg/kg, orally, daily, 5 weeks)
5. Entinostat (5 mg/kg, orally, daily, 5 weeks)

For the subcutaneous model, tumor size was evaluated every 3 or 4 days by caliper measurements, and the approximate tumor volume was calculated using the formula  $4/3\pi \times (d/2)^2 \times D/2$ , where  $d$  is the minor tumor axis and  $D$  is the major tumor axis [37].

In another PDOX model of cervical cancer, treatment was as follows: treatment protocol (G1, control treated with vehicle (i.v. phosphate buffered saline (PBS), once a week, 3 weeks,  $n = 7$ ); G2, treated with CDDP (i.v., 5 mg/kg, once a week, 3 weeks,  $n = 7$ ); G3, treated with NAB-paclitaxel (NAB-PTX) (i.v., 10 mg/kg,

twice a week, 3 weeks,  $n = 7$ ). Treatment started 4 weeks after orthotopic implantation. Mice were sacrificed on day 22; then tumors were resected for further evaluation. Tumor length and width were measured both on day 0 and day 22. Tumor volume was calculated by the following formula: tumor volume ( $\text{mm}^3$ ) = length (mm)  $\times$  width (mm)  $\times$  width (mm)  $\times$  1/2. Tumor volume ratio was defined as the ratio of volume on day 22 to day 0 [38].

For the orthotopic model, the mice underwent laparotomy 1 week before treatment to confirm the presence of the primary tumor, and its size was evaluated as described above [37].

Relative tumor volume and body weight were calculated by comparison to tumor size before treatment. Animals underwent laparotomy after treatment, and the tumors were photographed with a Canon EOS 60D digital camera with EF-S 18-55 IS lens (Canon, Tokyo, Japan) and weighed and harvested for analysis. Body weight of the mice was measured in a balance once a week [37].

## Tissue Histology

Tumor samples were removed with surrounding normal tissues at the time of resection. Fresh tissue samples were fixed in 10% formalin and embedded in paraffin before sectioning and staining. Tissue sections (3  $\mu\text{m}$ ) were deparaffinized in xylene and rehydrated in an ethanol series. Hematoxylin and eosin (H&E) staining was performed according to standard protocols. For immunohistochemistry, the sections were then treated for 30 min with 0.3% hydrogen peroxide to block endogenous peroxidase activity. The sections were subsequently washed with PBS and incubated in citrate antigen unmasking solution (Mitsubishi Kagaku Iatron, Inc., Tokyo, Japan) in a water bath for 40 min at 98 °C. After incubation with 10% normal goat serum, the sections were incubated with anti-HER-2/ErbB2 antibody (1:100, Cell Signaling Technology, Danvers, MA, USA) at 4 °C overnight. The binding of primary antibodies was detected using anti-mouse secondary antibodies and avidin/biotin/horseradish peroxidase complex (DAKO Cytomation, Kyoto, Japan) for 30 min at room temperature. The labeled antigens were visualized with the DAB kit (DAKO Cytomation). Finally, the sections were counterstained with hematoxylin and examined using an Olympus BH-2 microscope equipped with a INFINITY1 2.0 megapixel CMOS digital camera (Lumenera Corporation, Ottawa, Canada). All images were acquired using INFINITY ANALYZE software (Lumenera Corporation) without post-acquisition processing [37].

## Statistical Analysis

PASW Statistics 18.0 (SPSS, Inc.) was used for all statistical analyses. The Student's *t*-test was used to compare continuous variables between two groups. Analyses of variance models were used to compare multiple groups. A *P*-value of 0.05 was considered statistically significant for all comparisons [37].

## References

1. Wang CW, Wu TI, Yu CT, Wu YC, Teng YH, Chin SY, Lai CH, Chen TC. Usefulness of p16 for differentiating primary pulmonary squamous cell carcinoma from cervical squamous cell carcinoma metastatic to the lung. *Am J Clin Pathol*. 2009;131:715–22.
2. Sabatier R, Roussin C, Riviere JP, Jalaguier A, Jacquemier J, Bertucci F. Breast metastasis of a squamous cell carcinoma of the uterine cervix mimicking inflammatory breast cancer. *Case Rep Oncol*. 2012;5:464–70.
3. Gamez RG, Jessurun J, Berger MJ, Pambuccian SE. Cytology of metastatic cervical squamous cell carcinoma in pleural fluid: report of a case confirmed by human papillomavirus typing. *Diagn Cytopathol*. 2009;37:381–7.
4. Urabe A, Matsumoto T, Kimura M, Sonoue H, Kinoshita K. Grading system of lymphatic invasion according to D2–40 immunostaining is useful for the prediction of nodal metastasis in squamous cell carcinoma of the uterine cervix. *Histopathology*. 2006;49:493–7.
5. Hashimoto K, Yonemori K, Katsumata N, Hirakawa A, Hirata T, Yamamoto H, Shimizu C, Tamura K, Ando M, Fujiwara Y. Use of squamous cell carcinoma antigen as a biomarker of chemotherapy response in patients with metastatic cervical carcinoma. *Eur J Obstet Gynecol Reprod Biol*. 2011;159:394–8.
6. Braud AC, Gonzague L, Bertucci F, Genre D, Camerlo J, Gravis G, Goncalves A, Moutardier V, Viret F, Maraninchi D, Viens P. Retinoids, cisplatin and interferon-alpha in recurrent or metastatic cervical squamous cell carcinoma: clinical results of 2 phase II trials. *Eur Cytokine Netw*. 2002;13:115–20.
7. Hoffman RM. Patient-derived orthotopic xenografts: better mimic of metastasis than subcutaneous xenografts. *Nat Rev Cancer*. 2015;15:451–2.
8. Hoffman RM. Orthotopic metastatic mouse models for anticancer drug discovery and evaluation: a bridge to the clinic. *Invest New Drugs*. 1999;17:343–59.
9. Fu X, Besterman JM, Monosov A, Hoffman RM. Models of human metastatic colon cancer in nude mice orthotopically constructed by using histologically intact patient specimens. *Proc Natl Acad Sci U S A*. 1991;88:9345–9.
10. Metildi CA, Kaushal S, Luiken GA, Talamini MA, Hoffman RM, Bouvet M. Fluorescently-labeled chimeric anti-CEA antibody improves detection and resection of human colon cancer in a patient-derived orthotopic xenograft (PDOX) nude mouse model. *J Surg Oncol*. 2014;109:451–8.
11. Hiroshima Y, Maawy A, Metildi CA, Zhang Y, Uehara F, Miwa S, Yano S, Sato S, Murakami T, Momiyama M, Chishima T, Tanaka K, Bouvet M, Endo I, Hoffman RM. Successful fluorescence-guided surgery on human colon cancer patient-derived orthotopic xenograft mouse models using a fluorophore-conjugated anti-CEA antibody and a portable imaging system. *J Laparoendosc Adv Surg Tech A*. 2014;24:241–7.
12. Fu X, Guadagni F, Hoffman RM. A metastatic nude-mouse model of human pancreatic cancer constructed orthotopically from histologically intact patient specimens. *Proc Natl Acad Sci U S A*. 1992;89:5645–9.
13. Kaushal S, McElroy MK, Luiken GA, Talamini MA, Moossa AR, Hoffman RM, Bouvet M. Fluorophore-conjugated anti-CEA antibody for the intraoperative imaging of pancreatic and colorectal cancer. *J Gastrointest Surg*. 2008;12:1938–50.
14. Suetsugu A, Katz M, Fleming J, Moriwaki H, Bouvet M, Saji S, Hoffman RM. Multi-color palette of fluorescent proteins for imaging the tumor microenvironment of orthotopic tumorgraft mouse models of clinical pancreatic cancer specimens. *J Cell Biochem*. 2012;113:2290–5.
15. Suetsugu A, Katz M, Fleming J, Truty M, Thomas R, Saji S, Moriwaki H, Bouvet M, Hoffman RM. Imageable fluorescent metastasis resulting in transgenic GFP mice orthotopically implanted with human-patient primary pancreatic cancer specimens. *Anticancer Res*. 2012;32:1175–80.
16. Suetsugu A, Katz M, Fleming J, Truty M, Thomas R, Saji S, Moriwaki H, Bouvet M, Hoffman RM. Non-invasive fluorescent-protein imaging of orthotopic pancreatic-cancer-patient tumorgraft progression in nude mice. *Anticancer Res*. 2012;32:3063–8.

17. Hiroshima Y, Maawy A, Sato S, Murakami T, Uehara F, Miwa S, Yano S, Momiyama M, Chishima T, Tanaka K, Bouvet M, Endo I, Hoffman RM. Hand-held high-resolution fluorescence imaging system for fluorescence-guided surgery of patient and cell-line pancreatic tumors growing orthotopically in nude mice. *J Surg Res.* 2014;187:510–7.
18. Hiroshima Y, Zhao M, Maawy A, Zhang Y, Katz MH, Fleming JB, Uehara F, Miwa S, Yano S, Momiyama M, Suetsugu A, Chishima T, Tanaka K, Bouvet M, Endo I, Hoffman RM. Efficacy of *Salmonella typhimurium* A1-R versus chemotherapy on a pancreatic cancer patient-derived orthotopic xenograft (PDOX). *J Cell Biochem.* 2014;115:1254–61.
19. Hiroshima Y, Maawy A, Zhang Y, Murakami T, Momiyama M, Mori R, Matsuyama R, Katz MH, Fleming JB, Chishima T, Tanaka K, Ichikawa Y, Endo I, Hoffman RM, Bouvet M. Metastatic recurrence in a pancreatic cancer patient derived orthotopic xenograft (PDOX) nude mouse model is inhibited by neoadjuvant chemotherapy in combination with fluorescence-guided surgery with an anti-CA 19-9-conjugated fluorophore. *PLoS One.* 2014;9:e114310.
20. Hiroshima Y, Zhang Y, Murakami T, Maawy AA, Miwa S, Yamamoto M, Yano S, Sato S, Momiyama M, Mori R, Matsuyama R, Chishima T, Tanaka K, Ichikawa Y, Bouvet M, Endo I, Zhao M, Hoffman RM. Efficacy of tumor-targeting *Salmonella typhimurium* A1-R in combination with anti-angiogenesis therapy on a pancreatic cancer patient-derived orthotopic xenograft (PDOX) and cell line mouse models. *Oncotarget.* 2014;5:12346–57.
21. Hiroshima Y, Maawy AA, Katz MH, Fleming JB, Bouvet M, Endo I, Hoffman RM. Selective efficacy of zoledronic acid on metastasis in a patient-derived orthotopic xenograft (PDOX) nude-mouse model of human pancreatic cancer. *J Surg Oncol.* 2015;111:311–5.
22. Hiroshima Y, Maawy A, Zhan Y, Murakami T, Momiyama M, Mori R, Matsuyama R, Chishima T, Tanaka K, Ichikawa Y, Endo I, Hoffman RM, Bouvet M. Fluorescence-guided surgery, but not bright-light surgery, prevents local recurrence in a pancreatic cancer patient-derived orthotopic xenograft (PDOX) model resistant to neoadjuvant chemotherapy (NAC). *Pancreatology.* 2015;15:295–301.
23. Yano S, Hiroshima Y, Maawy A, Kishimoto H, Suetsugu A, Miwa S, Toneri M, Yamamoto M, Katz MHG, Fleming JB, Urata Y, Tazawa H, Kagawa S, Bouvet M, Fujiwara T, Hoffman RM. Color-coding cancer and stromal cells with genetic reporters in a patient-derived orthotopic xenograft (PDOX) model of pancreatic cancer enhances fluorescence-guided surgery. *Cancer Gene Ther.* 2015;22:344–50.
24. Fu X, Le P, Hoffman RM. A metastatic-orthotopic transplant nude-mouse model of human patient breast cancer. *Anticancer Res.* 1993;13:901–4.
25. Fu X, Hoffman RM. Human ovarian carcinoma metastatic models constructed in nude mice by orthotopic transplantation of histologically-intact patient specimens. *Anticancer Res.* 1993;13:283–6.
26. Wang X, Fu X, Hoffman RM. A new patient-like metastatic model of human lung cancer constructed orthotopically with intact tissue via thoracotomy in immunodeficient mice. *Int J Cancer.* 1992;51:992–5.
27. Furukawa T, Kubota T, Watanabe M, Kitajima M, Fu X, Hoffman RM. Orthotopic transplantation of histologically intact clinical specimens of stomach cancer to nude mice: correlation of metastatic sites in mouse and individual patient donors. *Int J Cancer.* 1993;53:608–12.
28. Astoul P, Wang X, Colt HG, Boutin C, Hoffman RM. A patient-like human malignant pleural mesothelioma nude-mouse model. *Oncol Rep.* 1996;3:483–7.
29. Hiroshima Y, Zhao M, Zhang Y, Zhang N, Maawy A, Murakami T, Mii S, Uehara F, Yamamoto M, Miwa S, Yano S, Momiyama M, Mori R, Matsuyama R, Chishima T, Tanaka K, Ichikawa Y, Bouvet M, Endo I, Hoffman RM. Tumor-targeting *Salmonella typhimurium* A1-R arrests a chemo-resistant patient soft-tissue sarcoma in nude mice. *PLoS One.* 2015;10:e0134324.
30. Murakami T, DeLong J, Eilber FC, Zhao M, Zhang Y, Zhang N, Singh A, Russell T, Deng S, Reynoso J, Quan C, Hiroshima Y, Matsuyama R, Chishima T, Tanaka K, Bouvet M, Chawla S, Endo I, Hoffman RM. Tumor-targeting *Salmonella typhimurium* A1-R in combination with doxorubicin eradicate soft tissue sarcoma in a patient-derived orthotopic xenograft PDOX model. *Oncotarget.* 2016;7:12783–90.
31. Kiyuna T, Murakami T, Tome Y, Kawaguchi K, Igarashi K, Zhang Y, Zhao M, Li Y, Bouvet M, Kanaya F, Singh A, Dry S, Eilber FC, Hoffman RM. High efficacy of tumor-targeting

- Salmonella typhimurium* A1-R on a doxorubicin- and dactolisib-resistant follicular dendritic-cell sarcoma in a patient-derived orthotopic xenograft PDOX nude mouse model. *Oncotarget*. 2016;7:33046–54.
32. Murakami T, Singh AS, Kiyuna T, Dry SM, Li Y, James AW, Igarashi K, Kawaguchi K, DeLong JC, Zhang Y, Hiroshima Y, Russell T, Eckardt MA, Yanagawa J, Federman N, Matsuyama R, Chishima T, Tanaka K, Bouvet M, Endo I, Eilber FC, Hoffman RM. Effective molecular targeting of *CDK4/6* and *IGF-1R* in a rare *FUS-ERG* fusion *CDKN2A*-deletion doxorubicin-resistant Ewing's sarcoma in a patient-derived orthotopic xenograft (PDOX) nude-mouse model. *Oncotarget*. 2016;7:47556–64.
  33. Kiyuna T, Murakami T, Tome Y, Igarashi K, Kawaguchi K, Russell T, Eckhardt MA, Crompton J, Singh A, Bernthal N, Bukata S, Federman N, Kanaya F, Eilber FC, Hoffman RM. Labeling the stroma of a patient-derived orthotopic xenograft (PDOX) mouse models of undifferentiated pleomorphic soft-tissue sarcoma with red fluorescent protein for rapid non-invasive drug screening. *J Cell Biochem*. 2017;118:361–5.
  34. Yamamoto M, Zhao M, Hiroshima Y, Zhang Y, Shurell E, Eilber FC, Bouvet M, Noda M, Hoffman RM. Efficacy of tumor-targeting *Salmonella typhimurium* A1-R on a melanoma patient-derived orthotopic xenograft (PDOX) nude-mouse model. *PLoS One*. 2016;11:e0160882.
  35. Kawaguchi K, Murakami T, Chmielowski B, Igarashi K, Kiyuna T, Unno M, Nelson SD, Russell TA, Dry SM, Li Y, Eilber FC, Hoffman RM. Vemurafenib-resistant BRAF-V600E mutated melanoma is regressed by MEK targeting drug trametinib, but not cobimetinib in a patient-derived orthotopic xenograft (PDOX) mouse model. *Oncotarget*. 2016;7:71737–43.
  36. Hiroshima Y, Zhang Y, Zhang M, Maawy A, Mii S, Yamamoto M, Uehara F, Miwa S, Yano S, Murakami T, Momiyama M, Chishima T, Tanaka K, Ichikawa Y, Bouvet M, Murata T, Endo I, Hoffman RM. Establishment of a patient-derived orthotopic xenograft (PDOX) model of HER-2-positive cervical cancer expressing the clinical metastatic pattern. *PLoS One*. 2015;10:e0117417.
  37. Hiroshima Y, Maawy A, Zhang Y, Zhang N, Murakami T, Chishima T, Tanaka K, Ichikawa Y, Bouvet M, Endo I, Hoffman RM. Patient-derived mouse models of cancer need to be orthotopic in order to evaluate targeted anti-metastatic therapy. *Oncotarget*. 2016;7:71696–702.
  38. Murakami T, Murata T, Kawaguchi K, Kiyuna T, Igarashi K, Hwang HK, Hiroshima Y, Hozumi C, Komatsu S, Kikuchi T, Lwin TM, DeLong JC, Miyake K, Zhang Y, Tanaka K, Bouvet M, Endo I, Hoffman RM. Cervical cancer patient-derived orthotopic xenograft (PDOX) is sensitive to cisplatin and resistant to nab-paclitaxel. *Anticancer Res*. 2017;37:61–5.
  39. Hoffman RM, Bouvet M. Nanoparticle albumin-bound-paclitaxel: a limited improvement under the current therapeutic paradigm of pancreatic cancer. *Expert Opin Pharmacother*. 2015;16:943–7.

---

# The Use of Pediatric Patient-Derived Xenografts for Identifying Novel Agents and Combinations

11

Raushan T. Kurmasheva and Peter J. Houghton

---

## Historic Perspective

In the USA, approximately 12,500 children and adolescents under the age of 21 are diagnosed annually with cancer. Cytotoxic drug/radiation therapy (RT) has dramatically increased survival over the past 40 years, with 70% cure rate and 5-year event-free survival (EFS) reaching nearly 80%. Further, dose intensification, dose compression, and introduction of new cytotoxic or biologic agents continue to reduce cancer mortality in children [1]. However, the limits of cytotoxic therapy are close to being maximized, and these therapeutic modalities are associated with significant mortality and often long-term debilitating sequelae [2, 3]. Because of the low numbers of patients, and high cure rate, there are relatively few patients eligible for phase I trials. While there remains a need to identify new effective and less toxic therapeutics for treatment of childhood cancer, it is clear that only a very few of the estimated 800 agents being developed as cancer therapeutics can be tested clinically. Clearly, the avenue to more successful treatment of childhood solid tumors lies in understanding the biologic characteristics that confer the malignant phenotype, in the identification of both new targets and novel effective agents, and in the optimization of cytotoxic or molecularly targeted therapy.

Developing new therapies for childhood solid tumors presents certain constraints that are seldom encountered with the neoplastic diseases of adults. Childhood tumors are rare; hence, the numbers of children with a particular diagnosis at any one institution are usually not adequate for large-scale drug evaluation or randomized clinical trials. For example, of the new phase I agents evaluated in adult malignancies, less than 30% receive adequate evaluation in children. Furthermore, the

---

R.T. Kurmasheva, Ph.D. • P.J. Houghton, Ph.D. (✉)  
Greehey Children's Cancer Research Institute,  
University of Texas Health Science Center, San Antonio (UTHSCSA),  
8403 Floyd Curl Drive, MC7784, San Antonio, TX 78229-3000, USA  
e-mail: [Kurmasheva@uthscsa.edu](mailto:Kurmasheva@uthscsa.edu); [houghtonp@uthscsa.edu](mailto:houghtonp@uthscsa.edu)



NCI drug screening strategy focuses on the selection of new anticancer agents with specific activity against adult neoplastic diseases (e.g., colon, lung, breast, etc.), so that agents with specific activity against childhood malignancies might not be identified. This lack of progress in developing more efficacious therapy for many childhood cancers must be attributed in part to the slow rate at which new active compounds reach the clinic and the failure to integrate laboratory and clinical efforts in a way that will generate a steady flow of promising experimental leads that can be used in the design of productive approaches to treatment.

Over the past decade, there has been increasing interest in using patient-derived xenografts (PDX) in oncology drug development (reviewed in [4]). However, establishing PDX models started about 50 years ago using techniques to immunosuppress mice using antithymocyte serum or immune deprivation. However, the discovery that the genetically immunodeficient athymic nude mouse would tolerate human cancer tissue engraftment spurred development of the field [5, 6]. Early studies at the Institute for Cancer Research in the UK focused on growth kinetics and histologic characterization of colon adenocarcinoma PDX models [7–9]. These early studies showed maintenance of histologic integrity and chromosomal stability [10] but also demonstrated increasingly rapid heterograft growth over the first five serial passages in mice [8]. The models were also of value in developing the rationale for combining 5-fluorouracil with leucovorin for treatment of colon cancer [11]. With the exception of hormonally dependent cancers (e.g., breast, prostate), the ability to heterograft patient tumors successfully in different genetically immunodeficient mice is quite high; hence, many PDX models of adult cancers are available.

---

## Rationale for Pediatric PDX (pPDX) Generation

Pediatric cancers are relatively rare, with 70% “cure” rate, and the 5-year event-free survival (EFS) rate is approaching 80%. However, it is estimated that up to 50% of long-term survivors will have life-threatening consequences of their cancer therapy by the time they reach 50 years. While dose intensification and dose compression approaches for chemotherapy are still increasing survivorship, developing effective, but far less toxic treatment for childhood cancer remains a priority. One difficulty in developing novel treatments is the sparse patient resource, due to high rates of cure and high 5-year EFS.

Thus, developing pPDX models becomes important, particularly for rare tumors where it is difficult to accrue sufficient patients to undertake phase II (efficacy) trials. The pPDX models can then be used to identify agents that could be prioritized for these trials. Studies from our group have shown that pPDXs retain histologic and genetic characteristics of patient tumors [12–15]. Some of the first studies to explore the value of xenograft models showed that pPDX models responded to drugs known to be active against clinical disease [16], identified novel drugs [17–21] and drug combinations [21–23], and reported *in situ* development of drug resistance [24, 25]. Probably the first clinical trial developed using pPDX results was

testing of melphalan in pediatric patients with rhabdomyosarcoma at relapse [26]. This trial was informative, as the efficacy of melphalan had been established against PDX models derived from diagnosis tissue [17], whereas, as is typical for phase I/II trials, the clinical population was comprised of relapse patients. Against these patients, melphalan induced an objective response in 1 of 12 patients (hence would be classed as inactive). However, the pharmacokinetics of melphalan in children was very similar to that in mice; hence, it was decided to extend the trial to include patients with poor prognosis (stage 4). In this population, 10 of 13 patients (77%) had objective responses, confirming the utility of the xenograft models for identifying agents that had clinical activity. Of note, testing melphalan against a panel of pPDX models established from patients at relapse confirmed that these were significantly less sensitive to the drug and hence recapitulated the clinical result. Thus, it was clear from these results that the typical phase II population may fail to identify an agent that could have significant activity in a patient at diagnosis.

---

## Prospective Studies

The finding that drugs of known utility were active against the rhabdomyosarcoma panel (vincristine and cyclophosphamide induced  $\geq$  partial responses (PR,  $\geq$ 50% tumor volume regression) in five of ten pPDX models and actinomycin D gave 20% responses) validated these as useful models for drug evaluation. Further, that pPDX models derived from patients at relapse were far less responsive than pPDXs established from diagnosis samples suggested that panels of models recapitulating naive and resistant tumor could be developed. To date, panels of pPDX models representing sarcoma (rhabdomyosarcoma, Ewing sarcoma, osteosarcoma), kidney tumors (Wilms, AT/RT), neuroblastoma, brain tumors (medulloblastoma, ependymoma, glioblastoma, astrocytoma) have been established. Demographic information for many of these models used in the Pediatric Pre-clinical Testing Program (PPTP) is available at <http://gccri.uthscsa.edu/pptp/img/docs/demographics.pdf>.

We identified the camptothecin topoisomerase I poisons, topotecan and irinotecan, as highly active in sarcoma, neuroblastoma, Wilms tumor, and medulloblastoma pPDX models [18, 21], and activity was subsequently confirmed in clinical trials [27–32]. Our studies with camptothecin drugs were integrated with studies of drug pharmacology. For example, understanding the relationship between exposure and tumor response in neuroblastoma PDX models allowed us to test the hypothesis that achieving a specific drug exposure, using pharmacokinetically-guided dosing, would be efficacious in the treatment of clinical neuroblastoma [27]. Understanding the metabolism of irinotecan led to the development of the use of a nonabsorbable cephalosporin to reduce bacterial deconjugation of SN38-glucuronide, and hence ameliorate intestinal toxicity [33], and the use of an EGFR inhibitor to increase the oral bioavailability of irinotecan in mice [34] and patients [35].

Because the current treatment for many pediatric cancers is successful, introduction of new agents involves demonstration of single-agent activity (Phase II clinical trials), usually in patients who relapse on standard therapy; then, if active, the agent

is introduced into high-risk protocols. Thus, our approach to developing the camptothecins was to determine whether there was additive activity when combined with standard-of-care drugs. For many childhood solid tumors, standard protocols include the anti-mitotic agent vincristine and the bifunctional agent cyclophosphamide. For sarcoma, vincristine or cyclophosphamide was selected to combine with topotecan and irinotecan. The combination with vincristine was particularly striking in both sarcoma and neuroblastoma models [20]. Similar synergy was observed with irinotecan, and this combination (vincristine-irinotecan, VI) has shown marked activity in rhabdomyosarcoma [30] and more recently in anaplastic Wilms tumor [36]. The other combination identified in the pPDX models, and currently undergoing clinical evaluation, is irinotecan combined with temozolomide [37–41] or in a three-drug regime with vincristine [42].

---

## Accurate Translation of Pre-clinical Data

For some considerable time, there has been skepticism regarding the value of xenograft-derived data as many drugs active in the pre-clinical studies have shown limited clinical activity [43–46]. In large part, the failure to accurately translate to clinical activity is the result of failing to take into account the pharmacology of the drug [46, 47]. Other reasons are the failure of pre-clinical models to represent the genetic characteristics of human cancers and the use of criteria to assess response in pre-clinical studies that were less stringent than used in clinical trials to assess drug efficacy. There are many examples where drugs tested at the maximum tolerated dose and schedule in mice cause regression of a human cancer xenograft. Early studies using 9-aminocamptothecin “cured” most colon carcinoma xenografts [48]; however, this agent had little activity in patients. A retrospective study showed that minimal drug exposures required to cause xenograft regression could not be achieved in patients [49]. Similarly, MG-114 (irofulven, an analog of the fungal toxin illudin S) was highly active against pre-clinical brain tumor and other PDX models but at doses that produced systemic exposures in mice that greatly exceeded those achieved in patients [50, 51]. Thus, understanding the differential pharmacology of a drug between species appears critical for accurate translation from PDX studies to clinical trials. Indeed, a retrospective study of molecular-targeted agents and cytotoxic drugs by Wong et al. showed a high correlation with clinical efficacy if there was 60% tumor growth inhibition in mice at clinically-relevant drug exposures [52], thus supporting the value of allometric scaling in early drug development [47].

---

## Molecular Validity of Models/Heterogeneity

The original NCI drug screen used cell-derived xenografts and one model representing each disease (MX-1, breast, CX-1 colon, LX-1 lung, etc.) [53]. In part, the use of limited models allowed for high throughput of agents. It is now well recognized that diseases such as breast cancer can be dissected into distinct molecular groups,

as can non-small cell lung cancer, colon carcinoma, and other histotypes. Thus, it is understandable why a single model did not predict for human efficacy—especially when drug pharmacology was largely ignored. Similarly, for many pediatric cancers considered as rather homogeneous, there is clear molecular diversity that can be used to subtype medulloblastoma [54–56], ependymoma [57], neuroblastoma [58], rhabdomyosarcoma [59, 60], and acute leukemias [61]. However for most pediatric cancers the genomic landscape is relatively silent, particularly for Ewing sarcoma [62]. Other tumors, such as atypical teratoid/rhabdoid tumors (AT/RT) of the CNS or kidney, have deletion of *SMARBI* and very few, or any, other gene alterations, whereas osteosarcoma is characterized by extreme karyotype rearrangements yet relatively few mutations. Molecular diversity of osteosarcoma is more readily identified in canine osteosarcoma than in childhood osteosarcoma [63]. In addition to molecular diversity in diagnosis samples, further diversity is apparent at relapse with new characteristics being identified that may be amenable to therapeutic targeting [64]. As will be described later in this review, pPDX models appear to maintain genetic changes characteristic of patient tumor.

---

### Criteria for Tumor Response (Pre-clinical and Clinical)

Another aspect to be considered here that leads to a failure to accurately translate from pre-clinical studies to clinical trials is the disconnect between criteria used for a drug to be regarded as active. For example, a drug may inhibit tumor progression by 80% in a PDX model, but if the tumor increases its volume by >25% during the period of treatment, this is progressive disease by RECIST criteria. Further, in most reports, tumor inhibition data are presented for only a single tumor model to support justification of moving a drug into clinical evaluation against that tumor type. Thus, pre-clinical studies fail in two respects: Firstly, we use criteria to define response that do not have clinical meaning, and secondly, the great majority of studies from academic laboratories report activity in too few models to adequately justify development of an agent. A further point to consider is that, at least in developing new therapies for treating childhood cancer, there are no criteria for what pre-clinical data are required to justify a clinical trial. For example, the anti-metabolite cytosine arabinoside (Ara-C) was tested in children with Ewing sarcoma, and was found not to be active, but induced significant toxicity [65]. The trial was based on Ara-C inducing a similar change in expression profiles as did downregulation of the *EWS-FLI1* oncogene in Ewing sarcoma cells. In vitro Ewing sarcoma cell lines were more sensitive to Ara-C than carcinoma cell lines, and in vivo a single cell-derived Ewing sarcoma xenograft had a partial response to this agent [66]. Subsequent studies showed that Ewing sarcoma cell lines were 25-fold less sensitive to Ara-C than leukemia cell lines, and this drug had minimal activity against only one of six Ewing sarcoma xenograft models, confirming the lack of clinical utility of this agent in Ewing sarcoma [67]. In the situation when patient resources limit the ability to conduct clinical trials, such as pediatric cancer, it seems appropriate to establish criteria that would justify moving an agent into clinical development.

## Development of the Pediatric Pre-clinical Testing Program (PPTP)

PPTP was built upon an understanding that when used intelligently, xenograft models may accurately identify drugs that have significant activity against childhood cancers. With an increasing number of new agents under development for treating cancer, it became imperative that a mechanism should be developed that could accurately identify those agents having the greatest potential to impact those children that have poor outcome with current therapies. Hence, the PPTP's overall goal was to improve the curability of resistant solid tumors and acute lymphoblastic leukemia (ALL) by identifying novel agents that have potential for significant activity and which may be prioritized for clinical evaluation against childhood cancer. During 10 years of its existence, the PPTP successfully tested more than 100 agents using a panel of 83 xenograft cancer models and 23 cell lines. For the primary testing (57 models), 75% of the *in vivo* models were direct grafts from patient to mouse, and 42% of *in vivo* models were derived from drug refractory patients. These models represent most of the more common pediatric solid malignancies and acute lymphoblastic leukemia subtypes, which were molecularly characterized by expression profiles, SNP analysis, and exome sequencing over the last 5 years. Agents (or combinations) that we identified as active that have advanced to clinical testing in children include alisertib in ALL and neuroblastoma (NCT01154816), NTX-010 (NCT01048892), temsirolimus + cyclophosphamide + vinorelbine for rhabdomyosarcoma (NCT01222715), BMN-673 + temozolomide (NCT02116777), and eribulin (NCT02082626).

The demonstration that pPDX models could identify drugs of known utility and identify novel agents and combinations that are active in clinical disease suggested that they could be used as a pre-clinical screen to identify new agents that may have priority for clinical evaluation against pediatric cancers [68]. The screen is depicted

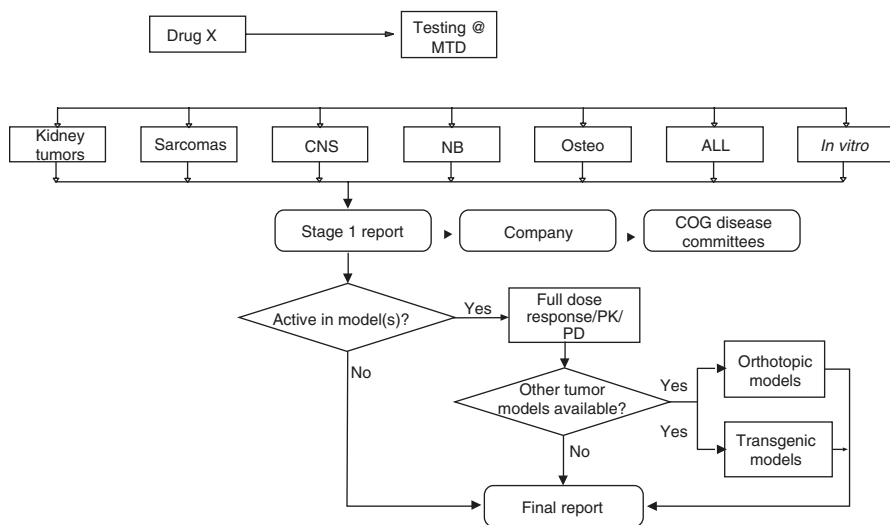


**Fig. 11.1** Schema for testing agents through the Pediatric Pre-clinical Testing Program (PPTP). Adapted from reference [68]



types where they are used as standard-of-care therapy. For example, vincristine, an anti-mitotic tubulin-binding agent, is highly active in ALL models and has activity in pPDX models derived from medulloblastoma, rhabdomyosarcoma, and Wilms tumors. Cyclophosphamide also has broad-spectrum activity, whereas cisplatin has activity in several solid tumor panels, but is poorly active against the ALL models, consistent with its lack of clinical utility in childhood ALL [72]. Topotecan also showed solid tumor and ALL activity consistent with clinical data. The overall objective response rate ( $\geq$ Partial Response) was 39.1% (72/184 tumor/drug studies) and serves as a benchmark for evaluating nonstandard cytotoxic agents.

## Novel Cytotoxic Agents

The activity of 19 novel cytotoxic agents with different mechanisms of action is shown in Fig. 11.3. There were 481 tumor/drug evaluations, and the overall response rate was 25.4%. Most of these agents have not been evaluated in Phase II clinical trials in children, so it is not possible to determine the validity of the pPDX results. However, the proteasome inhibitor, bortezomib, showed activity against only ALL models, and this is consistent with single-agent clinical activity [73]. Two agents are useful for illustrating the value and limitations of pre-clinical xenograft models. The pre-prodrug, PR-104 is activated under hypoxic conditions to 5-hydroxylamine (PR-104H) and amine (PR-104M) to produce DNA interstrand cross-links [74, 75]. This agent was tested at the maximum-tolerated-dose level as, at that time, human pharmacokinetic data were not yet available. The drug demonstrated dramatic broad-spectrum activity (kidney tumors, sarcoma, and ALL). However, it transpired that at the MTD in mice, drug exposures were four- to five-fold above exposures achieved in (adult) patients at the recommended Phase II clinical trial dose level. Subsequent dose response data showed that at dose levels in mice corresponding to human systemic exposures, significant anti-tumor activity was observed only in T-cell ALL models. Of interest, T-cell ALL has very high levels of aldo-keto reductase 1C3 (AKR1C3) that also activates PR-104 [76], suggesting that tumor-selective anabolism in T-cell ALL is responsible for sensitivity to this agent [76].

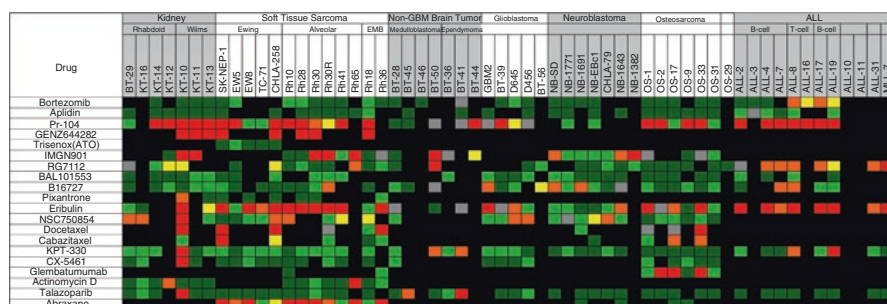


**Fig. 11.3** Heat map representation of anti-tumor activity of novel cytotoxic agents. Tumor panels are arrayed horizontally at the top, and specific PDX and cell-derived xenograft models are shown for each tumor panel. Drugs are listed in the left column. Tumor response classification is as shown in Fig. 11.1

The second agent is the tubulin binder eribulin and can be used to illustrate the positive and negative values of pre-clinical models in developing anti-mitotic agents. This drug has a mode of binding to tubulin that is distinct from vincristine, which for pediatric cancer is the gold standard. In the screen, eribulin showed marked activity in numerous tumor panels at dose levels below the MTD. Notably, eribulin was active in five of six Ewing sarcoma xenograft models, whereas vincristine was not active (see Fig. 11.3). Pharmacokinetic modeling suggests that the systemic exposure to drug in mice is relevant to clinical exposure [77]. However although eribulin caused regression in several osteosarcoma PDX models, it has not shown activity in a Phase II clinical trial in osteosarcoma, suggesting the models overpredict activity. Indeed, vincristine showed activity against osteosarcoma models (Fig. 11.2) but has not been efficacious when added to other combinations in clinical trials. While the models may overpredict activity of anti-mitotic agents, it is of note that the rate of regression in the osteosarcoma models were far slower than in soft tissue models where tumors completely regressed with 1–2 weeks of starting treatment. However, the osteosarcoma results raise the question of whether the PDX models overpredict for the activity of anti-mitotic agents. As shown in Fig. 11.3, cabazitaxel and docetaxel caused tumor regressions but at a dose/schedule that gave exposures per 21-day cycle well above systemic exposures tolerated in patients [78], consistent with the lack of activity of taxane drugs in pediatric cancer. In contrast, another anti-mitotic tubulin binder, BAL101553, showed virtually no anti-tumor activity against either solid tumor or ALL models [79]. The PPTP also tested nanoparticle albumin-bound paclitaxel (nab-paclitaxel; Abraxane) in sarcoma models (Fig. 11.3). Systemic exposures in mice were about 50% higher in mice than patients: (nab-paclitaxel (50 mg/kg) was 36.54  $\mu\text{M}\cdot\text{Hr}$  in mice. In contrast human exposure was 23.80  $\mu\text{M}\cdot\text{Hr}$  in patients receiving 260 mg/m [80]. It is unclear whether plasma exposures are important for this agent as it appears to be concentrated in tumor tissue. Hence tumor drug levels in pPDX models relative to patient tumors may be more relevant. However, that nab-paclitaxel had significant anti-sarcoma activity at drug exposures close to that in patients, in contrast to docetaxel and cabazitaxel, suggests this agent may have activity in Ewing sarcoma and rhabdomyosarcoma.

## Signaling Inhibitors

Twenty-four signaling inhibitors have been evaluated as single agents through the PPTP (Fig. 11.4). These included small-molecule inhibitors and antibodies. Overall there were 1272 drug/tumor data sets that included up to 53 xenograft models. There were 61 objective responses (4.1%), significantly less than observed with the novel cytotoxic agents. Of note, three agents that target the process of mitosis were the most active. GSK923295A, an inhibitor of the centromere kinesin motor protein CENP-E, the Aurora kinase A inhibitor MLN8237 (alisertib), and the polo-like kinase inhibitor BI6727 (volasertib) each showed considerable activity when tested at the MTD. However, for each drug, it is estimated that plasma exposures were fivefold greater than were achieved in patients. For alisertib, the dose-response curve was steep, and at 25% of the MTD, very few pPDX models, other than ALL,



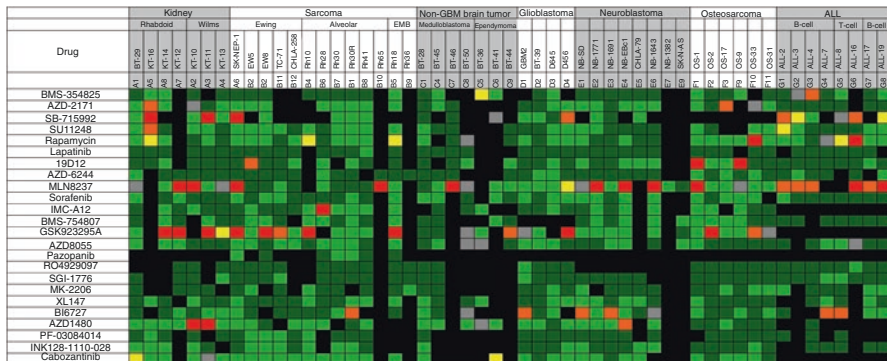


**Fig. 11.4** Heat map representation of anti-tumor activity of signal transduction inhibitors. Tumor panels are arrayed horizontally at the top, and specific PDX and cell-derived xenograft models are shown for each tumor panel. Drugs are listed in the left column. Tumor response classification is as shown in Fig. 11.1

were responsive [81]. GSK923295A was also active only at the mouse MTD [82], and volasertib was not tested at lower dose levels as this agent had limited activity at doses resulting in drug exposures tenfold greater than in adult patients. If responses induced by these three agents are eliminated as being “false positives,” the objective response rate (ORR) for signaling inhibitors decreases to 26/1152 drug/tumor tests (2.25%). This raises the question of whether the PDX/xenograft models overpredict for cytotoxic drugs, but underpredict for signaling inhibitors. Clinical experience shows that for several signaling inhibitors tumor regressions are usually associated with a particular molecular characteristic. Examples are the activity of trastuzumab in *HER2*-amplified breast carcinoma [83], imatinib in *BCR/Abl*-activated chronic myelogenous leukemia [84], erlotinib in *ERBB1*-mutated NSCLC [85], crizotinib and other ALK inhibitors in *EML4-ALK*-translocated NSCLC [86], or BRAF/MEK inhibitors in *BRAF*-mutated melanoma [87]. For pediatric cancers, particularly solid tumors, the frequency of activating mutations that would predispose to drug sensitivity seems to be quite low. One exception is low-grade glioma where activation of *BRAF* occurs through tandem duplication of the *BRAF:KIAA1549* locus [88] or point mutation (usually V600E) in most tumors. In the PPTP screen, the MEK inhibitor selumetinib (AZD6244, Fig. 11.4) had very little activity [89], whereas in secondary screening against two astrocytoma models, it was highly active against the astrocytoma model with a *BRAF*-activating mutation (*BRAF*V600E), but had no activity against the model with wild-type *BRAF* (Fig. 11.5). Of interest, recently, it was reported that at relapse, there was a higher incidence of Ras pathway activation, potentially sensitizing tumors to MEK inhibitors [64]. In the PPTP in vitro screen, RD cells (*NRas* mutant) and NB-EBc1 (*KRas* mutant) were significantly more sensitive to selumetinib. However, NB-EBc1 xenografts were not responsive and neither was the Rh36 embryonal rhabdomyosarcoma PDX that has an *HRas* mutation. Other results that also suggest that the models accurately predict for activity of signaling inhibitors are the sensitivity to sunitinib

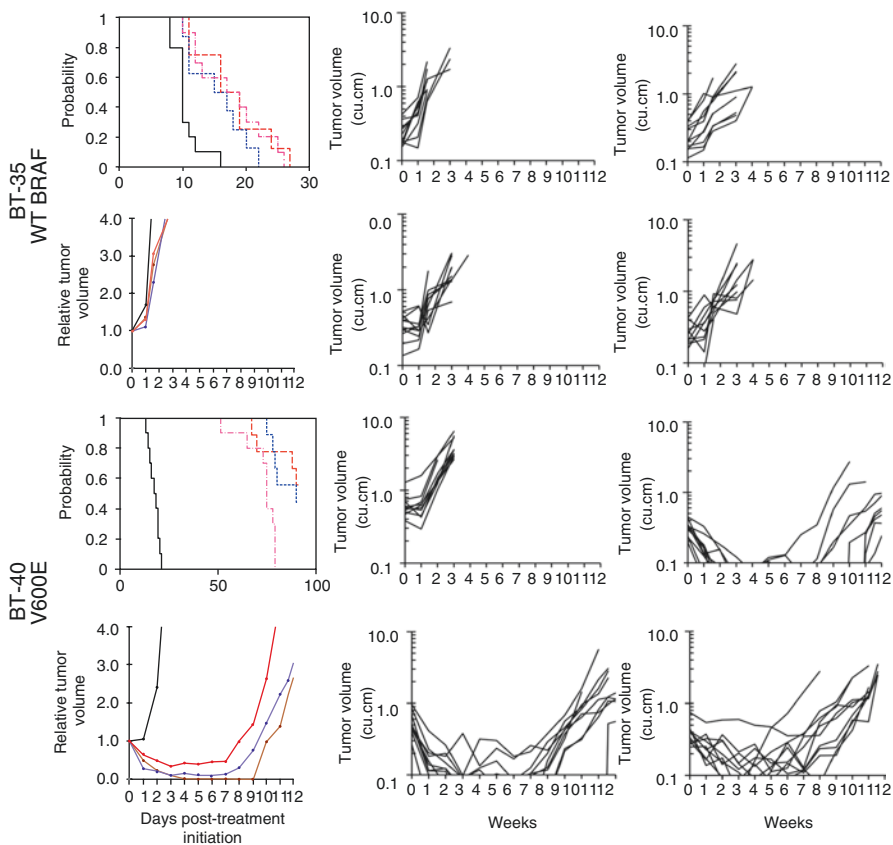


**Fig. 11.5** AZD6244 activity against pilocytic astrocytoma xenografts. Kaplan-Meier curves for EFS, median relative tumor volume graphs, and individual tumor volume graphs are shown for (a): BT-35 and (b) BT-40. Kaplan-Meier curves: controls, *black* solid line; 100 mg/kg BID  $\times$  5/SID  $\times$  2 for 6 consecutive weeks, broken *red* line; 75 mg/kg BID  $\times$  5/SID  $\times$  2 for 6 consecutive weeks, *blue* broken line; 100 mg/kg SID for 6 consecutive weeks, broken *pink* line. Relative tumor volume curves: controls, *black* solid line; 100 mg/kg BID  $\times$  5/SID  $\times$  2 for 6 consecutive weeks, solid *brown* line; 75 mg/kg BID  $\times$  5/SID  $\times$  2 for 6 consecutive weeks, solid *blue* line; 100 mg/kg SID for 6 consecutive weeks, solid *red* line. For individual growth curve plots: upper left panel, control; upper right panel, AZD6244 100 mg/kg BID  $\times$  5/SID  $\times$  2 for 6 consecutive weeks; lower left panel, AZD6244 75 mg/kg BID  $\times$  5/SID  $\times$  2 for 6 consecutive weeks; lower right panel, 100 mg/kg SID for 6 consecutive weeks. Adapted from reference [89]

of ALL-2, a line with *FLT3* mutation (Y572S) [90], sensitivity of NB-1643 with an *ALK* (R1725Q) mutation to the *ALK* inhibitor crizotinib [91], and sensitivity to dasatinib in a Ph+ALL model.

One aspect of translating pre-clinical results is that schedules of administration used in mice may not be possible, or reproduced, in clinical protocols. An example is alisertib that induced objective responses in six of six ALL models at its MTD, in three models at 0.5 MTD, and in two of three at 0.25 MTD using twice daily dosing,

5 days per week for 3 consecutive weeks [81]. In the trial in childhood ALL (NCT01154816), the schedule was amended to once daily for 7 days, due to increased toxicity in pediatric patients. The amended schedule, once daily for 7 days, achieved one response in 33 patients and hence was not considered active. A retrospective study, in two ALL PDX models sensitive to the initial schedule of administration, showed neither models were sensitive to the revised schedule, daily for 7 days [92].

## Combination Testing

Constraints of clinical testing in pediatric cancer include the paucity of patients eligible for experimental drugs, and testing of these agents is usually conducted in a refractory or relapse setting. Consequently, identification of active agents seems to be relatively slow. When we developed the topoisomerase I poisons, topotecan and irinotecan, there was clear evidence for activity in Phase I clinical trials, and these agents were further tested in “upfront window” trials against drug naive patients with advanced disease [29, 30, 93]. In general, a new agent will be added to existing regimens. For example, we evaluated topotecan and irinotecan combination with standard agents, cyclophosphamide and vincristine, used routinely in the treatment of childhood solid tumors [14, 20]. The combination of vincristine and irinotecan (VI) is now incorporated into several protocols for treatment of rhabdomyosarcoma and has recently been shown as highly active in anaplastic Wilms tumor [36]. The mechanism for synergy between camptothecin derivatives such as topotecan and irinotecan and vincristine remains to be elucidated, but this combination seems to be active in several childhood cancers. Similarly, the combination of irinotecan with temozolomide had greater than additive activity in PDX models [37, 94] and has been introduced into several protocols for solid tumors at relapse with or without vincristine [40–42, 95].

The design of drug combination studies is critical, and demonstrating therapeutic synergy requires multiple dose levels of each agent alone or in combination. Many studies, especially those reporting modulation or reversal of multi-drug resistance (MDR), used flawed experimental designs (reviewed in [96]). Essentially, in all published studies (at that time), the MDR modulator + cytotoxic drug was compared to the cytotoxic drug at the same dose used in the combination—despite the combination with the modulator necessitating the reduction of the dose of cytotoxic agent from its optimal dose (maximum tolerated dose level, MTD). For the PPTP, a method was developed to identify “therapeutic enhancement” [23]. Simply stated the combination had to have greater effect than either single agent used at its MTD.

Relatively few combination studies were conducted through the PPTP. Notable were studies with cediranib (AZD2171), a potent small-molecule inhibitor of vascular endothelial growth factor (VEGF) receptors. The cediranib-cyclophosphamide combination was inferior to single-agent cyclophosphamide for both models

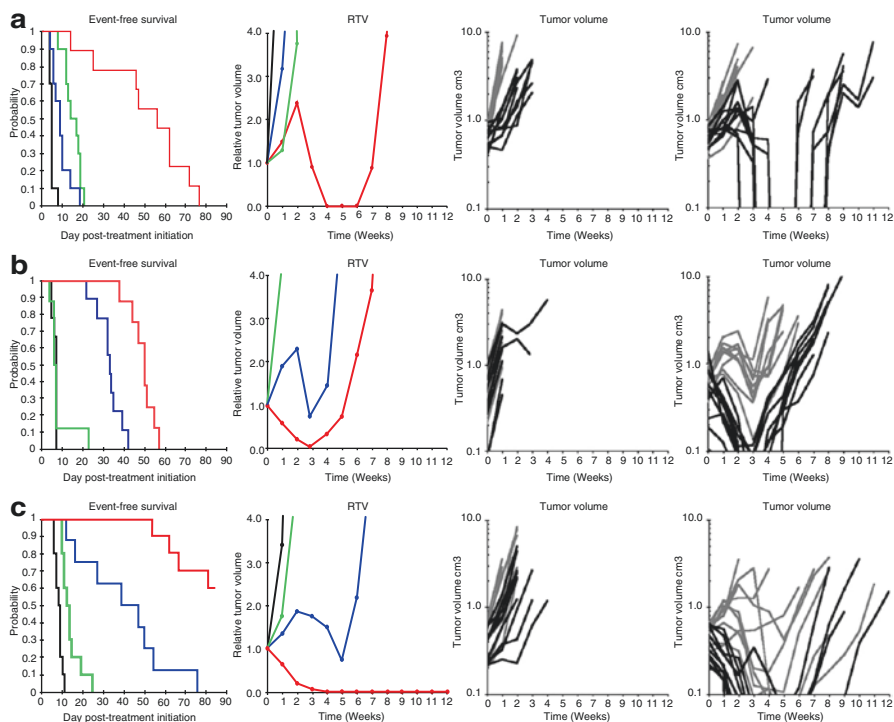


**Fig. 11.6** Rapamycin enhances the therapeutic activity of cyclophosphamide. Tumor-bearing mice were treated with cyclophosphamide at the MTD (150 mg/kg daily dosing 7 days per week for 6 consecutive weeks), rapamycin (5 mg/kg d  $\times$  5 for 6 consecutive weeks), or the combination of cyclophosphamide and rapamycin. Tumor diameters were measured weekly. Panel 1 shows the Kaplan-Meier curves for EFS: control (black), rapamycin (green), cyclophosphamide (blue), or rapamycin + cyclophosphamide (red). Panel 2 shows median relative tumor volumes: control (black), rapamycin (green), cyclophosphamide (blue), or rapamycin + cyclophosphamide (red). Individual tumor-growth curves are shown in panel 3, control (light gray) and rapamycin (dark lines), and panel 4, cyclophosphamide (light gray) and cyclophosphamide + rapamycin (dark lines). (a) D456 glioblastoma; (b) KT-14 rhabdoid tumor of kidney; (c) Rh30 rhabdomyosarcoma

studied and was significantly inferior for one of the models [97]. In contrast, rapamycin enhanced the therapeutic activity of both cyclophosphamide (Fig. 11.6) and vincristine against several PDX models [23]. For treatment of sarcoma at relapse, the Children’s Oncology Group (COG) has adopted an approach where a novel agent is added to a “backbone” therapy for relapsed patients. Using a two-arm design, it is possible to compare the activity of two experimental agents simultaneously (drug A + backbone therapy versus drug B + backbone therapy). The NCT01222715 trial used a backbone of cyclophosphamide + vinorelbine, adding the rapalog temsirolimus to one arm and bevacizumab to the other arm for relapsed rhabdomyosarcoma. The trial was stopped when it became clear that the

temsirolimus arm was significantly superior to that containing bevacizumab. These results seem to parallel the pre-clinical predictions, that is, rapamycins enhance the activity of *Vinca* alkaloids and cyclophosphamide, whereas an inhibitor of VEGF signaling was antagonistic to cyclophosphamide. However, without a control arm (cyclophosphamide + vinorelbine only), it is not possible to determine whether temsirolimus enhanced the activity of backbone therapy or whether bevacizumab antagonized backbone therapy.

Rapamycin also appears to enhance the activity of irinotecan in several PDX models, although, again, the mechanism seems obscure. Indeed, based on the cell cycle-dependent killing by topoisomerase I poisons, one would have anticipated some antagonism as rapamycin causes an increase in G1 fraction, whereas irinotecan (or more precisely the active metabolite SN-38) kills cells only during DNA replication (S phase). In yeast rapamycin potentiates the toxicity of methylmethane sulfonate (MMS)-induced DNA damage, possibly through suppressing damage-induced subunits of ribonucleotide reductase and preventing error-prone translesion bypass repair [98]. Of interest, the combination induced greater kill than did MMS alone but, importantly, suppressed MMS-induced mutations. Thus, because rapalogs enhance the efficacy of DNA-damaging agents such as cyclophosphamide and irinotecan and show therapeutic enhancement in some PDX models, it is proposed to test temsirolimus in a backbone of vincristine-irinotecan in a future COG rhabdomyosarcoma trial.

Interest in developing inhibitors of poly-ADP ribose polymerase (PARP) was largely stimulated following the observation of a synthetic lethal interaction in cell lines lacking homologous recombination through loss of BRCA function [99, 100]. Several PARP inhibitors have demonstrated single-agent activity in patients where BRCA1 or BRCA2 homozygous mutations are tumor specific [101, 102]. Ewing sarcoma cell lines were also reported to be hypersensitive to PARP inhibitors [103, 104], possibly as a result of an interaction between PARP1 and EWS-FLI1. Brenner et al. [104] also reported a dramatic synergy between temozolomide and olaparib in a xenograft model of Ewing sarcoma, although olaparib as a single agent had little activity.

The PARP1/2 inhibitor, talazoparib, was evaluated by PPTP as a single agent, in 44 xenograft models representing childhood solid tumors and ALLs. The result of this testing showed very modest activity among all models. Tumor regressions were observed only in a medulloblastoma and a Wilms tumor PDX [105]. The PPTP data seem to be reflective of clinical activity since continuous high-dose olaparib had no activity in a Phase II clinical trial for Ewing sarcoma patients [106]. There are several pre-clinical studies that provided evidence for combination of PARP inhibitors with DNA damaging agents as chemotherapy with promising activity in xenograft tumor models. This strategy was also supported by the emerging evidence that PARP1 inhibitors are cytotoxic due to PARP trapping initiated by PARP1 binding to DNA with single-strand breaks [107].

Talazoparib showed the highest efficiency at trapping PARP-DNA complexes among all other known PARP inhibitors [108]. Temozolomide contributes to the process by producing N3 and N7 methyl adducts of adenine and guanine, respectively. N7-methylguanine and N3-methyladenine adducts, the most abundant and nonlethal lesions, are repaired by BER, but the process requires PARP to recognize and bind the repair intermediate 5'-deoxyribose phosphate. Thus, PARP inhibitors turn the nonlethal N7-methylguanine and N3-methyladenine into cytotoxic lesions by trapping PARP at 5'-deoxyribose phosphate [109, 110]. Recruitment of additional PARP molecules critical for BER is impaired by inhibition of PARP's catalytic activity; single-stranded breaks become double-stranded breaks, which require homologous recombination for repair. Subsequently, the ability to potentiate temozolomide toxicity aligns with PARP-trapping capacity of PARP inhibitors [107, 108]. Overall, combination of temozolomide with such a potent PARP-trapping inhibitor as talazoparib is a more rational approach than combination of temozolomide with a PARP inhibitor that primarily acts by catalytic inhibition.

In our *in vitro* studies, the low-level damage to DNA induced by temozolomide was potentiated up to 85-fold through inhibition of PARP by talazoparib in the PPTP studies [111]. The potentiation was seen in Ewing sarcoma cell lines as well as ALL cell lines. However, despite significant modulation *in vitro*, the only objective regressions induced by the talazoparib/temozolomide combination were in Ewing sarcoma xenografts, with no activity in ALL. Two dose levels of temozolomide were used in PPTP testing *in vivo*, 30 mg/kg and 12 mg/kg, both administered for 5 consecutive days. Talazoparib was administered at a lower dose with "high"-dose temozolomide. Overall, talazoparib was equally effective when used in a low-dose temozolomide compared to a high-dose temozolomide regimen (Fig. 11.7), which is consistent with the emerging understanding of the role of PARP trapping for talazoparib. Both combinations demonstrated significant activity against five out of ten Ewing sarcoma xenograft models and only modest activity against rhabdomyosarcoma, glioblastoma, and Wilms tumor models, which may suggest that resistance mechanisms in the unresponsive lines exist *de novo*. In the TC-71 Ewing sarcoma model, essentially complete acquired resistance to the combination of talazoparib and temozolomide developed within five transplant generations. Our preliminary data support the mechanism of PARP1/2 trapping on DNA, rather than inhibition of catalytic activity, being responsible for cytotoxicity in Ewing sarcoma models (RTK unpublished).

The PPTP results were used to develop the talazoparib/temozolomide Phase I/II clinical trial through the COG (NCT02116777). As in mice, combination of temozolomide with talazoparib necessitated temozolomide dose reduction to overcome high toxicity of the combination. Early data from the trial indicated thrombocytopenia is limiting when talazoparib (600  $\mu\text{g}/\text{m}^2$ ) is combined with temozolomide (30 mg/m<sup>2</sup>), approximately 15% of the MTD for single-agent temozolomide. This is a similar dose reduction from the MTD for temozolomide, as in mice, when combined with talazoparib.

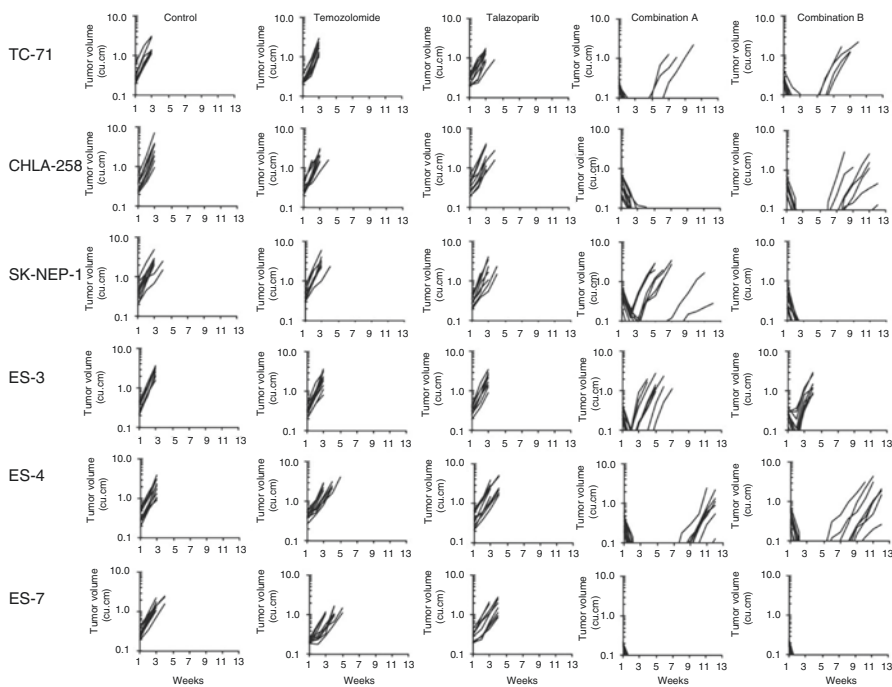


**Fig. 11.7** Responses of ‘sensitive’ Ewing sarcoma xenografts to single-agent therapy or the combination of talazoparib plus temozolomide. Anti-tumor activity of temozolomide (30 mg/kg D $\times$ 5); talazoparib (0.25 mg/kg BID D $\times$ 5); or in combination against ‘sensitive’ Ewing sarcoma models. Combination A (temozolomide 30 mg/kg D $\times$ 5; talazoparib 0.1 mg/kg BID D $\times$ 5); Combination B (temozolomide 12 mg/kg D $\times$ 5; talazoparib 0.25 mg/kg BID D $\times$ 5). Graphs show growth of individual tumors in SCID mice (from reference 111)

## Chemoradiation Combinations

Radiation therapy (RT) remains an essential component of curative therapy for most solid tumors of childhood, yet the long-term consequences of RT, particularly for patients with CNS tumors, can be devastating. For treatment of medulloblastoma, even after reducing the RT dose to 23.4 Gy, neurocognitive outcome data revealed a significant decline of about 1.7 points per year in intellectual functioning over 5 years and an IQ drop of 10–20 points in younger children [112]. The long-term consequences of chemoradiation treatment strategies include neuroendocrine-cognitive deficits, visual deficits, seizure disorders, motor disturbances, vasculopathy, and secondary tumors [113, 114]. Necrotizing leukoencephalopathy [115], a diffuse white matter injury, was first described in children receiving intra-thecal methotrexate [115] with subsequent combined RT and chemotherapy. It has also been observed in adult patients with leukemia [116] and various malignancies that had metastasized to the CNS [117]. The intent for combining RT with molecularly-targeted agents is to increase the cure rate and to reduce the dose of RT through radiosensitization. The

PPTP studies did not include RT or RT combinations. However, in limited studies, following up on PPTP findings, we were able to demonstrate synergistic activity of RT when combined with the MDM2 inhibitor RG7388 [118] in a rhabdomyosarcoma pPDX and with selumetinib (MEK inhibitor) in a heterotopic model of BRAF mutant astrocytoma [119]. Selumetinib enhanced the RT activity by a factor of two- to threefold in this model. The importance of the latter study is that it may be possible to maintain tumor control but reduce the RT dose and hence reduce the long-term CNS toxicities described above. However, it will be critical to demonstrate that inhibition of MEK does not potentiate RT damage to normal brain.

---

## Molecular Subgroup Representation

One of the limitations of the PPTP is that while we evaluated drugs against more than 50 pPDX models, there were limited models representing any one pediatric cancer. For example, the PPTP used eight ALL models, but usually only two models represented ependymoma, medulloblastoma, or Wilms tumor. Clearly this does not represent the clinical heterogeneity of these pediatric tumors. Initially tumor models were compared to clinical samples to determine whether expression profiles were representative of clinical disease [15]. Subsequently, models were characterized by expression profiling and single-nucleotide polymorphisms [120]. Overall, the results suggested that the PDX and xenograft models were similar to the clinical disease from which each was derived. However, to be truly representative of the clinical heterogeneity, further model development is required. Thus, within resource constraints, how can the molecular heterogeneity of pediatric cancer in a pre-clinical screen be accomplished? One approach has been initiated by Novartis, where a large number of melanoma PDX models were developed. Screening used an individual mouse as a “patient.” In this case, 30 melanoma PDX models, each derived from different patients, were grown in a single mouse, and the objective response ( $\geq 50\%$  volume regression) rates (ORR) were assessed for different agents [121]. In part, this would be equivalent in design to a clinical Phase II trial where ORR is determined. The advantage of this approach is that far greater molecular heterogeneity can be encompassed and perhaps gives a more precise estimate of the likely clinical response rate, assuming that the pharmacology of a drug in mice is similar to that in patients. This experimental design identifies drugs that induce a high frequency of tumor regressions, but because no control arm is used, slowing of tumor progression is not identified. The other advantage over the traditional experimental design (more mice/group but fewer tumor lines) is that the potential to identify “exceptional responders” is increased and hence the potential to identify underlying characteristics that would allow clinical stratification in subsequent trials.

In a retrospective analysis of 67 agents tested by the PPTP, we determined whether a single mouse, chosen randomly from each group of a study, predicted the median response for groups of mice with tumor [122]. The individual tumor response from one randomly-chosen mouse was compared to the group median response using criteria developed in the PPTP. A total of 2134 comparisons were




made. The single-tumor response accurately predicted the group median response in 1604 comparisons (75.16%), and the mean-tumor response correct-prediction rate for 1000 single-mouse random samples was 78.09%. Models had a range for correct prediction (60%–87.5%). Allowing for mis-prediction of  $\pm$  one response category, the overall mean-correct single-mouse prediction rate was 95.28%. Further, from the single-mouse data, the predicted overall objective response rates for group data were correct for 66 of 67 drug studies. No differences between pPDX and cell line-derived xenografts were found. Assuming that large treatment effects are targeted, this alternate experimental design has similar predictive value as traditional approaches, allowing for far greater numbers of models to be used that more fully encompass the heterogeneity of disease types. One would anticipate that a “hit” in the single-mouse screen would be confirmed using a traditional experimental design (using 8–10 mice per tumor line).

---

## Development of Drug Resistance

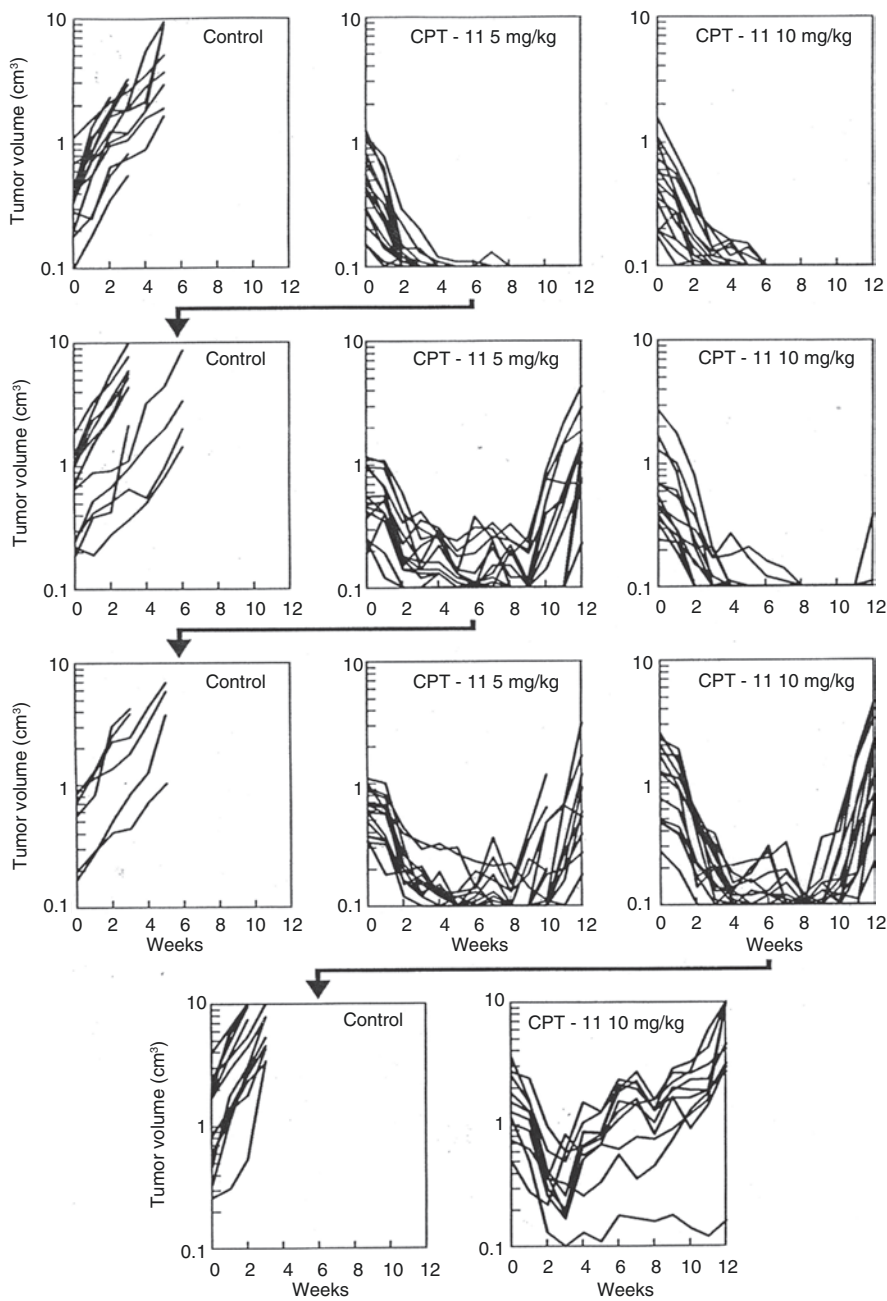
One of the limitations in pediatric oncology is the inability to access patient tumor at relapse, in most instances because of ethical considerations. However, this severely limits the ability to identify drug resistance mechanisms in a cohort of uniformly treated patients receiving protocol therapy. It also limits the ability to develop PDX models from patients at relapse that would more appropriately represent a typical Phase II clinical trial patient population. Such efforts are underway for several adult cancers in so-called co-clinical trials [123, 124]. We have used PDX models to develop drug resistance to vincristine, melphalan, and selumetinib, respectively, in tumor models initially highly sensitive to the individual agent [24, 25, 125]. The approach was to treat tumor-bearing mice with drug at a dose and schedule causing CR, then stopping treatment and allowing tumor to regrow. The tumor with most rapid regrowth was transplanted and the process repeated. This approach was used to select resistance to the talazoparib-temozolomide combination discussed above and for development of resistance to irinotecan (CPT-11) as illustrated in Fig. 11.8. However, the approach is somewhat limited if a traditional experimental design is used (i.e., one would develop

---



**Fig. 11.8** Development of resistance to irinotecan (CPT-11) in NB-1691 xenografts. The schema shows response of parental NB-1691 neuroblastoma to irinotecan (CPT-11). Irinotecan was administered parenterally (IP) 5 days per week for 2 consecutive weeks. Tumor from mice treated at 5 mg/kg was transplanted (*arrow*). Tumor in the subsequent passage was less sensitive to treatment, and again a regrowing tumor from the 5 mg/kg group was transplanted and retested for drug sensitivity. In this passage, a tumor that regrew at the 10 mg/kg dose level was transplanted and its sensitivity tested in the subsequent passage, where it was relatively resistant to this dose of irinotecan

### HxNB 1691



resistance to agents in one or two models). On the other hand, coupled to the “single-mouse” design discussed above, it may be valuable for determining predominant mechanism(s) of action to single agents and combinations in a larger number of PDX models (each derived from a different patient tumor), thus simulating potential mechanisms of clinical drug resistance rather than that developed in vitro under conditions of increasing drug selection pressure.

---

### Conclusions

Our experience with pPDX models suggests that they can be valuable in identifying novel agents and combinations that subsequently show significant clinical activity. However, these models have obvious limitations in overpredicting for drug activity due to host tolerance compared to that in children. Thus, comparing systemic drug exposure in mice at dose levels causing tumor regression and clinically achievable exposures is critical. For most agents, pharmacokinetic parameters in adult patients are available prior to initiating pediatric pre-clinical trials; hence, evaluating these drugs at doses corresponding to clinical exposures is possible. For drugs where there is no clinical pharmacokinetic data, this is more problematic, although these studies should be conducted when such data become available. Our studies have, for the most part, used subcutaneous tumors rather than orthotopic models for drug evaluation, with the exception of the disseminated leukemia models. The use of orthotopic models will be addressed elsewhere. However, for screening purposes, the subcutaneous models appear appropriate and maintain molecular characteristics similar to clinical cancer tissues, which are “orthotopic” by definition. Potentially, secondary screens using orthotopic methods could be useful, particularly for brain tumors, and such approaches have been introduced into the Pediatric Pre-clinical Testing Consortium (PPTC).

Several recent reviews have highlighted deficiencies in the design and execution of cancer pre-clinical studies [126–128]. These articles stressed the need to screen de-identified agents, to insure reproducibility by replicating studies, and to evaluate agents using multiple models, all criteria we used in establishing the PPTC. Current pPDX models do not encompass the clinical heterogeneity (genetic/epigenetic) adequately; hence, additional models need to be developed, carefully characterized, and exchanged freely between laboratories. We have just initiated a project to establish and characterize between 100 and 200 new pPDX models from children in Texas supported through the Cancer Prevention and Research Institute of Texas (CPRIT). These models will be available to all pediatric research laboratories.

---

### References

1. Smith MA, Altekruse SF, Adamson PC, Reaman GH, Seibel NL. Declining childhood and adolescent cancer mortality. *Cancer*. 2014;120(16):2497–506.
2. Oeffinger KC, Mertens AC, Sklar CA, Kawashima T, Hudson MM, Meadows AT, et al. Chronic health conditions in adult survivors of childhood cancer. *N Engl J Med*. 2006;355(15):1572–82.

3. Phillips SM, Padgett LS, Leisenring WM, Stratton KK, Bishop K, Krull KR, et al. Survivors of childhood cancer in the United States: prevalence and burden of morbidity. *Cancer Epidemiol Biomarkers Prev.* 2015;24(4):653–63.
4. Tentler JJ, Tan AC, Weekes CD, Jimeno A, Leong S, Pitts TM, et al. Patient-derived tumour xenografts as models for oncology drug development. *Nat Rev Clin Oncol.* 2012;9(6):338–50.
5. Povlsen CO, Rygaard J. Heterotransplantation of human adenocarcinomas of the colon and rectum to the mouse mutant nude. A study of nine consecutive transplantations. *Acta Pathol Microbiol Scand A.* 1971;79(2):159–69.
6. Povlsen CO, Rygaard J. Heterotransplantation of human epidermoid carcinomas to the mouse mutant nude. *Acta Pathol Microbiol Scand A.* 1972;80(6):713–7.
7. Pickard RG, Cobb LM, Steel GG. The growth kinetics of xenografts of human colorectal tumours in immune deprived mice. *Br J Cancer.* 1975;31(1):36–45.
8. Houghton JA, Taylor DM. Growth characteristics of human colorectal tumours during serial passage in immune-deprived mice. *Br J Cancer.* 1978;37(2):213–23.
9. Houghton JA, Taylor DM. Maintenance of biological and biochemical characteristics of human colorectal tumours during serial passage in immune-deprived mice. *Br J Cancer.* 1978;37(2):199–212.
10. Visfeldt J, Povlsen CO, Rygaard J. Chromosome analyses of human tumours following hetero-transplantation to the mouse mutant nude. *Acta Pathol Microbiol Scand A.* 1972;80(2):169–76.
11. Houghton JA, Maroda Jr SJ, Phillips JO, Houghton PJ. Biochemical determinants of responsiveness to 5-fluorouracil and its derivatives in xenografts of human colorectal adenocarcinomas in mice. *Cancer Res.* 1981;41(1):144–9.
12. Houghton JA, Houghton PJ, Webber BL. Growth and characterization of childhood rhabdomyosarcomas as xenografts. *J Natl Cancer Inst.* 1982;68(3):437–43.
13. Meyer WH, Houghton JA, Houghton PJ, Webber BL, Douglass EC, Look AT. Development and characterization of pediatric osteosarcoma xenografts. *Cancer Res.* 1990;50(9):2781–5.
14. Thompson J, Guichard SM, Cheshire PJ, Richmond LB, Poquette CA, Ragsdale ST, et al. Development, characterization and therapy of a disseminated model of childhood neuroblastoma in SCID mice. *Cancer Chemother Pharmacol.* 2001;47(3):211–21.
15. Whiteford CC, Bilke S, Greer BT, Chen Q, Braunschweig TA, Cenacchi N, et al. Credentialing preclinical pediatric xenograft models using gene expression and tissue microarray analysis. *Cancer Res.* 2007;67(1):32–40.
16. Houghton JA, Houghton PJ, Green AA. Chemotherapy of childhood rhabdomyosarcomas growing as xenografts in immune-deprived mice. *Cancer Res.* 1982;42(2):535–9.
17. Houghton JA, Cook RL, Lutz PJ, Houghton PJ. Melphalan: a potential new agent in the treatment of childhood rhabdomyosarcoma. *Cancer Treat Rep.* 1985;69(1):91–6.
18. Houghton PJ, Cheshire PJ, Myers L, Stewart CF, Synold TW, Houghton JA. Evaluation of 9-dimethylaminomethyl-10-hydroxycamptothecin against xenografts derived from adult and childhood solid tumors. *Cancer Chemother Pharmacol.* 1992;31(3):229–39.
19. Houghton JA, Cook RL, Lutz PJ, Houghton PJ. Childhood rhabdomyosarcoma xenografts: responses to DNA-interacting agents and agents used in current clinical therapy. *Eur J Cancer Clin Oncol.* 1984;20(7):955–60.
20. Thompson J, George EO, Poquette CA, Cheshire PJ, Richmond LB, de Graaf SS, et al. Synergy of topotecan in combination with vincristine for treatment of pediatric solid tumor xenografts. *Clin Cancer Res.* 1999;5(11):3617–31.
21. Houghton PJ, Cheshire PJ, Hallman 2nd JD, Lutz L, Friedman HS, Danks MK, et al. Efficacy of topoisomerase I inhibitors, topotecan and irinotecan, administered at low dose levels in protracted schedules to mice bearing xenografts of human tumors. *Cancer Chemother Pharmacol.* 1995;36(5):393–403.
22. Houghton JA, Houghton PJ. Combinations of 5-FU, hypoxanthine and allopurinol in chemotherapy for human colon adenocarcinoma xenografts. *Cancer Treat Rep.* 1982;66(5):1201–6.

23. Houghton PJ, Morton CL, Gorlick R, Lock RB, Carol H, Reynolds CP, et al. Stage 2 combination testing of rapamycin with cytotoxic agents by the Pediatric Preclinical Testing Program. *Mol Cancer Ther.* 2010;9(1):101–12.
24. Horton JK, Houghton PJ, Houghton JA. Reciprocal cross-resistance in human rhabdomyosarcomas selected in vivo for primary resistance to vincristine and L-phenylalanine mustard. *Cancer Res.* 1987;47(23):6288–93.
25. Houghton JA, Houghton PJ, Brodeur GM, Green AA. Development of resistance to vincristine in a childhood rhabdomyosarcoma growing in immune-deprived mice. *Int J Cancer.* 1981;28(4):409–15.
26. Horowitz ME, Etcubanas E, Christensen ML, Houghton JA, George SL, Green AA, et al. Phase II testing of melphalan in children with newly diagnosed rhabdomyosarcoma: a model for anticancer drug development. *J Clin Oncol.* 1988;6(2):308–14.
27. Santana VM, Furman WL, Billups CA, Hoffer F, Davidoff AM, Houghton PJ, et al. Improved response in high-risk neuroblastoma with protracted topotecan administration using a pharmacokinetically guided dosing approach. *J Clin Oncol.* 2005;23(18):4039–47.
28. Santana VM, Zamboni WC, Kirstein MN, Tan M, Liu T, Gajjar A, et al. A pilot study of protracted topotecan dosing using a pharmacokinetically guided dosing approach in children with solid tumors. *Clin Cancer Res.* 2003;9(2):633–40.
29. Furman WL, Stewart CF, Poquette CA, Pratt CB, Santana VM, Zamboni WC, et al. Direct translation of a protracted irinotecan schedule from a xenograft model to a phase I trial in children. *J Clin Oncol.* 1999;17(6):1815–24.
30. Pappo AS, Lyden E, Breitfeld P, Donaldson SS, Wiener E, Parham D, et al. Two consecutive phase II window trials of irinotecan alone or in combination with vincristine for the treatment of metastatic rhabdomyosarcoma: the Children's Oncology Group. *J Clin Oncol.* 2007;25(4):362–9.
31. Metzger ML, Stewart CF, Freeman 3rd BB, Billups CA, Hoffer FA, Wu J, et al. Topotecan is active against Wilms' tumor: results of a multi-institutional phase II study. *J Clin Oncol.* 2007;25(21):3130–6.
32. Stewart CF, Iacono LC, Chintagumpala M, Kellie SJ, Ashley D, Zamboni WC, et al. Results of a phase II upfront window of pharmacokinetically guided topotecan in high-risk medulloblastoma and supratentorial primitive neuroectodermal tumor. *J Clin Oncol.* 2004;22(16):3357–65.
33. Furman WL, Crews KR, Billups C, Wu J, Gajjar AJ, Daw NC, et al. Cefixime allows greater dose escalation of oral irinotecan: a phase I study in pediatric patients with refractory solid tumors. *J Clin Oncol.* 2006;24(4):563–70.
34. Stewart CF, Leggas M, Schuetz JD, Panetta JC, Cheshire PJ, Peterson J, et al. Gefitinib enhances the antitumor activity and oral bioavailability of irinotecan in mice. *Cancer Res.* 2004;64(20):7491–9.
35. Furman WL, Navid F, Daw NC, McCarville MB, McGregor LM, Spunt SL, et al. Tyrosine kinase inhibitor enhances the bioavailability of oral irinotecan in pediatric patients with refractory solid tumors. *J Clin Oncol.* 2009;27(27):4599–604.
36. Daw NC, Anderson JR, Hoffer FA, Geller JI, Kalapurakal JA, et al. A phase 2 study of vincristine and irinotecan in metastatic diffuse anaplastic Wilms tumor: results from the Children's Oncology Group AREN0321 study. *J Clin Oncol.* 2014;32(5s.) (suppl; abstr 10032).
37. Houghton PJ, Stewart CF, Cheshire PJ, Richmond LB, Kirstein MN, Poquette CA, et al. Antitumor activity of temozolomide combined with irinotecan is partly independent of O6-methylguanine-DNA methyltransferase and mismatch repair phenotypes in xenograft models. *Clin Cancer Res.* 2000;6(10):4110–8.
38. Middlemas DS, Stewart CF, Kirstein MN, Poquette C, Friedman HS, Houghton PJ, et al. Biochemical correlates of temozolomide sensitivity in pediatric solid tumor xenograft models. *Clin Cancer Res.* 2000;6(3):998–1007.
39. Wagner LM, Crews KR, Iacono LC, Houghton PJ, Fuller CE, McCarville MB, et al. Phase I trial of temozolomide and protracted irinotecan in pediatric patients with refractory solid tumors. *Clin Cancer Res.* 2004;10(3):840–8.

40. Wagner LM, McAllister N, Goldsby RE, Rausen AR, McNall-Knapp RY, McCarville MB, et al. Temozolomide and intravenous irinotecan for treatment of advanced Ewing sarcoma. *Pediatr Blood Cancer*. 2007;48(2):132–9.
41. Wagner LM, Villablanca JG, Stewart CF, Crews KR, Groshen S, Reynolds CP, et al. Phase I trial of oral irinotecan and temozolomide for children with relapsed high-risk neuroblastoma: a new approach to neuroblastoma therapy consortium study. *J Clin Oncol*. 2009;27(8):1290–6.
42. Wagner LM, Perentesis JP, Reid JM, Ames MM, Safgren SL, Nelson Jr MD, et al. Phase I trial of two schedules of vincristine, oral irinotecan, and temozolomide (VOIT) for children with relapsed or refractory solid tumors: a Children's Oncology Group phase I consortium study. *Pediatr Blood Cancer*. 2010;54(4):538–45.
43. Johnson JI, Decker S, Zaharevitz D, Rubinstein LV, Venditti JM, Schepartz S, et al. Relationships between drug activity in NCI preclinical in vitro and in vivo models and early clinical trials. *Br J Cancer*. 2001;84(10):1424–31.
44. Gura T. Systems for identifying new drugs are often faulty. *Science*. 1997;278(5340):1041–2.
45. Leaf C. Why we're losing the war on cancer (and how to win it). *Fortune*. 2004;149(6):76–82. 84–6, 88 passim.
46. Sausville EA, Burger AM. Contributions of human tumor xenografts to anticancer drug development. *Cancer Res*. 2006;66(7):3351–4. discussion 54.
47. Peterson JK, Houghton PJ. Integrating pharmacology and in vivo cancer models in preclinical and clinical drug development. *Eur J Cancer*. 2004;40(6):837–44.
48. Giovanella BC, Stehlin JS, Wall ME, Wani MC, Nicholas AW, Liu LF, et al. DNA topoisomerase I—targeted chemotherapy of human colon cancer in xenografts. *Science*. 1989;246(4933):1046–8.
49. Kirstein MN, Houghton PJ, Cheshire PJ, Richmond LB, Smith AK, Hanna SK, et al. Relation between 9-aminocamptothecin systemic exposure and tumor response in human solid tumor xenografts. *Clin Cancer Res*. 2001;7(2):358–66.
50. Leggas M, Stewart CF, Woo MH, Fouladi M, Cheshire PJ, Peterson JK, et al. Relation between Irofulven (MGI-114) systemic exposure and tumor response in human solid tumor xenografts. *Clin Cancer Res*. 2002;8(9):3000–7.
51. Eckhardt SG, Baker SD, Britten CD, Hidalgo M, Siu L, Hammond LA, et al. Phase I and pharmacokinetic study of irofulven, a novel mushroom-derived cytotoxin, administered for five consecutive days every four weeks in patients with advanced solid malignancies. *J Clin Oncol*. 2000;18(24):4086–97.
52. Wong H, Choo EF, Aliche B, Ding X, La H, McNamara E, et al. Antitumor activity of targeted and cytotoxic agents in murine subcutaneous tumor models correlates with clinical response. *Clin Cancer Res*. 2012;18(14):3846–55.
53. Goldin A, Venditti JM, Macdonald JS, Muggia FM, Henney JE, Devita Jr VT. Current results of the screening program at the Division of Cancer Treatment, National Cancer Institute. *Eur J Cancer*. 1981;17(2):129–42.
54. Kool M, Korshunov A, Remke M, Jones DT, Schlanstein M, Northcott PA, et al. Molecular subgroups of medulloblastoma: an international meta-analysis of transcriptome, genetic aberrations, and clinical data of WNT, SHH, Group 3, and Group 4 medulloblastomas. *Acta Neuropathol*. 2012;123(4):473–84.
55. Rausch T, Jones DT, Zapatka M, Stutz AM, Zichner T, Weischenfeldt J, et al. Genome sequencing of pediatric medulloblastoma links catastrophic DNA rearrangements with TP53 mutations. *Cell*. 2012;148(1–2):59–71.
56. Korshunov A, Remke M, Kool M, Hielscher T, Northcott PA, Williamson D, et al. Biological and clinical heterogeneity of MYCN-amplified medulloblastoma. *Acta Neuropathol*. 2012;123(4):515–27.
57. Johnson RA, Wright KD, Poppleton H, Mohankumar KM, Finkelstein D, Pounds SB, et al. Cross-species genomics matches driver mutations and cell compartments to model ependymoma. *Nature*. 2010;466(7306):632–6.

58. Schwab M, Westermann F, Hero B, Berthold F. Neuroblastoma: biology and molecular and chromosomal pathology. *Lancet Oncol.* 2003;4(8):472–80.
59. Davicioni E, Finckenstein FG, Shahbazian V, Buckley JD, Triche TJ, Anderson MJ. Identification of a PAX-FKHR gene expression signature that defines molecular classes and determines the prognosis of alveolar rhabdomyosarcomas. *Cancer Res.* 2006;66(14):6936–46.
60. Shern JF, Chen L, Chmielecki J, Wei JS, Patidar R, Rosenberg M, et al. Comprehensive genomic analysis of rhabdomyosarcoma reveals a landscape of alterations affecting a common genetic axis in fusion-positive and fusion-negative tumors. *Cancer Discov.* 2014;4(2):216–31.
61. Hunger SP, Mullighan CG. Redefining ALL classification: toward detecting high-risk ALL and implementing precision medicine. *Blood.* 2015;125(26):3977–87.
62. Brohl AS, Solomon DA, Chang W, Wang J, Song Y, Sindiri S, et al. The genomic landscape of the Ewing Sarcoma family of tumors reveals recurrent STAG2 mutation. *PLoS Genet.* 2014;10(7):e1004475.
63. Scott MC, Sarver AL, Gavin KJ, Thayanithy V, Getzy DM, Newman RA, et al. Molecular subtypes of osteosarcoma identified by reducing tumor heterogeneity through an interspecies comparative approach. *Bone.* 2011;49(3):356–67.
64. Eleveld TF, Oldridge DA, Bernard V, Koster J, Daage LC, Diskin SJ, et al. Relapsed neuroblastomas show frequent RAS-MAPK pathway mutations. *Nat Genet.* 2015;47(8):864–71.
65. DuBois SG, Krailo MD, Lessnick SL, Smith R, Chen Z, Marina N, et al. Phase II study of intermediate-dose cytarabine in patients with relapsed or refractory Ewing sarcoma: a report from the Children’s Oncology Group. *Pediatr Blood Cancer.* 2009;52(3):324–7.
66. Stegmaier K, Wong JS, Ross KN, Chow KT, Peck D, Wright RD, et al. Signature-based small molecule screening identifies cytosine arabinoside as an EWS/FLI modulator in Ewing sarcoma. *PLoS Med.* 2007;4(4):e122.
67. Houghton PJ, Morton CL, Kang M, Reynolds CP, Billups CA, Favours E, et al. Evaluation of cytarabine against Ewing sarcoma xenografts by the pediatric preclinical testing program. *Pediatr Blood Cancer.* 2010;55(6):1224–6.
68. Houghton PJ, Adamson PC, Blaney S, Fine HA, Gorlick R, Haber M, et al. Testing of new agents in childhood cancer preclinical models: meeting summary. *Clin Cancer Res.* 2002;8(12):3646–57.
69. Houghton PJ, Morton CL, Tucker C, Payne D, Favours E, Cole C, et al. The pediatric preclinical testing program: description of models and early testing results. *Pediatr Blood Cancer.* 2007;49(7):928–40.
70. Carol H, Reynolds CP, Kang MH, Keir ST, Maris JM, Gorlick R, et al. Initial testing of the MDM2 inhibitor RG7112 by the Pediatric Preclinical Testing Program. *Pediatr Blood Cancer.* 2013;60(4):633–41.
71. Richmond J, Carol H, Evans K, High L, Mendo A, Robbins A, et al. Effective targeting of the P53-MDM2 axis in preclinical models of infant MLL-rearranged acute lymphoblastic leukemia. *Clin Cancer Res.* 2015;21(6):1395–405.
72. Tajbakhsh M, Houghton PJ, Morton CL, Kolb EA, Gorlick R, Maris JM, et al. Initial testing of cisplatin by the pediatric preclinical testing program. *Pediatr Blood Cancer.* 2008;50(5):992–1000.
73. Houghton PJ, Morton CL, Kolb EA, Lock R, Carol H, Reynolds CP, et al. Initial testing (stage 1) of the proteasome inhibitor bortezomib by the pediatric preclinical testing program. *Pediatr Blood Cancer.* 2008;50(1):37–45.
74. Houghton PJ, Lock R, Carol H, Morton CL, Phelps D, Gorlick R, et al. Initial testing of the hypoxia-activated prodrug PR-104 by the pediatric preclinical testing program. *Pediatr Blood Cancer.* 2011;57(3):443–53.
75. Gu Y, Guise CP, Patel K, Abbattista MR, Li J, Sun X, et al. Reductive metabolism of the dinitrobenzamide mustard anticancer prodrug PR-104 in mice. *Cancer Chemother Pharmacol.* 2011;67(3):543–55.

76. Moradi Manesh D, El-Hoss J, Evans K, Richmond J, Toscan CE, Bracken LS, et al. AKR1C3 is a biomarker of sensitivity to PR-104 in preclinical models of T-cell acute lymphoblastic leukemia. *Blood*. 2015;126(10):1193–202.
77. Kolb EA, Gorlick R, Reynolds CP, Kang MH, Carol H, Lock R, et al. Initial testing (stage 1) of eribulin, a novel tubulin binding agent, by the pediatric preclinical testing program. *Pediatr Blood Cancer*. 2013;60(8):1325–32.
78. Reynolds CP, Kang MH, Maris JM, Kolb EA, Gorlick R, Wu J, et al. Initial testing (stage 1) of the anti-microtubule agents cabazitaxel and docetaxel, by the pediatric preclinical testing program. *Pediatr Blood Cancer*. 2015;62(11):1897–905.
79. Kolb EA, Gorlick R, Keir ST, Maris JM, Kang MH, Reynolds CP, et al. Initial testing (stage 1) of BAL101553, a novel tubulin binding agent, by the pediatric preclinical testing program. *Pediatr Blood Cancer*. 2015;62(6):1106–9.
80. Gardner ER, Dahut WL, Scripture CD, Jones J, Aragon-Ching JB, Desai N, et al. Randomized crossover pharmacokinetic study of solvent-based paclitaxel and nab-paclitaxel. *Clin Cancer Res*. 2008;14(13):4200–5.
81. Carol H, Boehm I, Reynolds CP, Kang MH, Maris JM, Morton CL, et al. Efficacy and pharmacokinetic/pharmacodynamic evaluation of the Aurora kinase A inhibitor MLN8237 against preclinical models of pediatric cancer. *Cancer Chemother Pharmacol*. 2011;68(5):1291–304.
82. Lock RB, Carol H, Morton CL, Keir ST, Reynolds CP, Kang MH, et al. Initial testing of the CENP-E inhibitor GSK923295A by the pediatric preclinical testing program. *Pediatr Blood Cancer*. 2012;58(6):916–23.
83. Puglisi F, Fontanella C, Amoroso V, Bianchi GV, Bisagni G, Falci C, et al. Current challenges in HER2-positive breast cancer. *Crit Rev Oncol Hematol*. 2016;98:211–21.
84. Fava C, Morotti A, Dogliotti I, Saglio G, Rege-Cambrin G. Update on emerging treatments for chronic myeloid leukemia. *Expert Opin Emerg Drugs*. 2015;20(2):183–96.
85. Russo A, Franchina T, Ricciardi GR, Picone A, Ferraro G, Zanghi M, et al. A decade of EGFR inhibition in EGFR-mutated non small cell lung cancer (NSCLC): old successes and future perspectives. *Oncotarget*. 2015;6(29):26814–25.
86. Sullivan I, Planchard D. Treatment modalities for advanced ALK-rearranged non-small-cell lung cancer. *Future Oncol*. 2016;12(7):945–61.
87. Robert C, Karaszewska B, Schachter J, Rutkowski P, Mackiewicz A, Stroiakovski D, et al. Improved overall survival in melanoma with combined dabrafenib and trametinib. *N Engl J Med*. 2015;372(1):30–9.
88. Jones DT, Kocialkowski S, Liu L, Pearson DM, Backlund LM, Ichimura K, et al. Tandem duplication producing a novel oncogenic BRAF fusion gene defines the majority of pilocytic astrocytomas. *Cancer Res*. 2008;68(21):8673–7.
89. Kolb EA, Gorlick R, Houghton PJ, Morton CL, Neale G, Keir ST, et al. Initial testing (stage 1) of AZD6244 (ARRY-142886) by the Pediatric Preclinical Testing Program. *Pediatr Blood Cancer*. 2010;55(4):668–77.
90. Maris JM, Courtright J, Houghton PJ, Morton CL, Kolb EA, Lock R, et al. Initial testing (stage 1) of sunitinib by the pediatric preclinical testing program. *Pediatr Blood Cancer*. 2008;51(1):42–8.
91. Bresler SC, Wood AC, Haglund EA, Courtright J, Belcastro LT, Plegaria JS, et al. Differential inhibitor sensitivity of anaplastic lymphoma kinase variants found in neuroblastoma. *Sci Transl Med*. 2011;3(108):108ra14.
92. Jones L, Carol H, Evans K, Richmond J, Houghton PJ, Smith MA, et al. A review of new agents evaluated against pediatric acute lymphoblastic leukemia by the pediatric preclinical testing program. *Leukemia*. 2016;30(11):2133–41.
93. Rodriguez-Galindo C, Radomski K, Stewart CF, Furman W, Santana VM, Houghton PJ. Clinical use of topoisomerase I inhibitors in anticancer treatment. *Med Pediatr Oncol*. 2000;35(4):385–402.



94. Patel VJ, Elion GB, Houghton PJ, Keir S, Pegg AE, Johnson SP, et al. Schedule-dependent activity of temozolomide plus CPT-11 against a human central nervous system tumor-derived xenograft. *Clin Cancer Res.* 2000;6(10):4154–7.
95. Bagatell R, London WB, Wagner LM, Voss SD, Stewart CF, Maris JM, et al. Phase II study of irinotecan and temozolomide in children with relapsed or refractory neuroblastoma: a Children's Oncology Group study. *J Clin Oncol.* 2011;29(2):208–13.
96. Tew KD, Houghton JA, Houghton PJ. Pharmacology of drugs that alter multidrug resistance in cancer. *Pharmacol Rev.* 1993;42:155–99.
97. Morton CL, Maris JM, Keir ST, Gorlick R, Kolb EA, Billups CA, et al. Combination testing of cediranib (AZD2171) against childhood cancer models by the pediatric preclinical testing program. *Pediatr Blood Cancer.* 2012;58(4):566–71.
98. Shen C, Lancaster CS, Shi B, Guo H, Thimmaiah P, Bjornsti MA. TOR signaling is a determinant of cell survival in response to DNA damage. *Mol Cell Biol.* 2007;27(20):7007–17.
99. Bryant HE, Schultz N, Thomas HD, Parker KM, Flower D, Lopez E, et al. Specific killing of BRCA2-deficient tumours with inhibitors of poly(ADP-ribose) polymerase. *Nature.* 2005;434(7035):913–7.
100. Farmer H, McCabe N, Lord CJ, Tutt AN, Johnson DA, Richardson TB, et al. Targeting the DNA repair defect in BRCA mutant cells as a therapeutic strategy. *Nature.* 2005;434(7035):917–21.
101. Kaufman B, Shapira-Frommer R, Schmutzler RK, Audeh MW, Friedlander M, Balmana J, et al. Olaparib monotherapy in patients with advanced cancer and a germline BRCA1/2 mutation. *J Clin Oncol.* 2015;33(3):244–50.
102. Sandhu SK, Schelman WR, Wilding G, Moreno V, Baird RD, Miranda S, et al. The poly(ADP-ribose) polymerase inhibitor niraparib (MK4827) in BRCA mutation carriers and patients with sporadic cancer: a phase I dose-escalation trial. *Lancet Oncol.* 2013;14(9):882–92.
103. Garnett MJ, Edelman EJ, Heidorn SJ, Greenman CD, Dastur A, Lau KW, et al. Systematic identification of genomic markers of drug sensitivity in cancer cells. *Nature.* 2012;483(7391):570–5.
104. Brenner JC, Feng FY, Han S, Patel S, Goyal SV, Bou-Maroun LM, et al. PARP-1 inhibition as a targeted strategy to treat Ewing's sarcoma. *Cancer Res.* 2012;72(7):1608–13.
105. Smith MA, Hampton OA, Reynolds CP, Kang MH, Maris JM, Gorlick R, et al. Initial testing (stage 1) of the PARP inhibitor BMN 673 by the pediatric preclinical testing program: PALB2 mutation predicts exceptional in vivo response to BMN 673. *Pediatr Blood Cancer.* 2015;62(1):91–8.
106. Choy E, Butrynski JE, Harmon DC, Morgan JA, George S, Wagner AJ, et al. Phase II study of olaparib in patients with refractory Ewing sarcoma following failure of standard chemotherapy. *BMC Cancer.* 2014;14:813.
107. Murai J, Huang SY, Das BB, Renaud A, Zhang Y, Doroshow JH, et al. Trapping of PARP1 and PARP2 by clinical PARP inhibitors. *Cancer Res.* 2012;72(21):5588–99.
108. Shen Y, Rehman FL, Feng Y, Boshuizen J, Bajrami I, Elliott R, et al. BMN 673, a novel and highly potent PARP1/2 inhibitor for the treatment of human cancers with DNA repair deficiency. *Clin Cancer Res.* 2013;19(18):5003–15.
109. Cistulli C, Lavrik OI, Prasad R, Hou E, Wilson SH. AP endonuclease and poly(ADP-ribose) polymerase-1 interact with the same base excision repair intermediate. *DNA Repair.* 2004;3(6):581–91.
110. Horton JK, Wilson SH. Strategic combination of DNA-damaging agent and PARP inhibitor results in enhanced cytotoxicity. *Front Oncol.* 2013;3:257.
111. Smith MA, Reynolds CP, Kang MH, Kolb EA, Gorlick R, Carol H, et al. Synergistic activity of PARP inhibition by talazoparib (BMN 673) with temozolomide in pediatric cancer models in the pediatric preclinical testing program. *Clin Cancer Res.* 2015;21(4):819–32.
112. Ris MD, Walsh K, Wallace D, Armstrong FD, Holmes E, Gajjar A, et al. Intellectual and academic outcome following two chemotherapy regimens and radiotherapy for average-risk medulloblastoma: COG A9961. *Pediatr Blood Cancer.* 2013;60(8):1350–7.

113. Sharif S, Ferner R, Birch JM, Gillespie JE, Gattamaneni HR, Baser ME, et al. Second primary tumors in neurofibromatosis 1 patients treated for optic glioma: substantial risks after radiotherapy. *J Clin Oncol.* 2006;24(16):2570–5.
114. Donahue B. Short- and long-term complications of radiation therapy for pediatric brain tumors. *Pediatr Neurosurg.* 1992;18(4):207–17.
115. Kay HE, Knapton PJ, O’Sullivan JP, Wells DG, Harris RF, Innes EM, et al. Encephalopathy in acute leukaemia associated with methotrexate therapy. *Arch Dis Child.* 1972;47(253):344–54.
116. Rubinstein LJ, Herman MM, Long TF, Wilbur JR. Disseminated necrotizing leukoencephalopathy: a complication of treated central nervous system leukemia and lymphoma. *Cancer.* 1975;35(2):291–305.
117. Norrell H, Wilson CB, Slagel DE, Clark DB. Leukoencephalopathy following the administration of methotrexate into the cerebrospinal fluid in the treatment of primary brain tumors. *Cancer.* 1974;33(4):923–32.
118. Phelps D, Bondra K, Seum S, Chronowski C, Leasure J, Kurmasheva RT, et al. Inhibition of MDM2 by RG7388 confers hypersensitivity to X-radiation in xenograft models of childhood sarcoma. *Pediatr Blood Cancer.* 2015;62(8):1345–52.
119. Studebaker A, Bondra K, Seum S, Shen C, Phelps DA, Chronowski C, et al. Inhibition of MEK confers hypersensitivity to X-radiation in the context of BRAF mutation in a model of childhood astrocytoma. *Pediatr Blood Cancer.* 2015;62(10):1768–74.
120. Neale G, Su X, Morton CL, Phelps D, Gorlick R, Lock RB, et al. Molecular characterization of the pediatric preclinical testing panel. *Clin Cancer Res.* 2008;14(14):4572–83.
121. Gao H, Korn JM, Ferretti S, Monahan JE, Wang Y, Singh M, et al. High-throughput screening using patient-derived tumor xenografts to predict clinical trial drug response. *Nat Med.* 2015;21(11):1318–25.
122. Murphy B, Yin H, Maris J, Kolb E, Gorlick R, Reynolds C, et al. Evaluation of alternative in vivo drug screening methodology: a single mouse analysis. *Cancer Res.* 2016;76(19):5798–809.
123. Aparicio S, Hidalgo M, Kung AL. Examining the utility of patient-derived xenograft mouse models. *Nat Rev Cancer.* 2015;15(5):311–6.
124. Hidalgo M, Amant F, Biankin AV, Budinska E, Byrne AT, Caldas C, et al. Patient-derived xenograft models: an emerging platform for translational cancer research. *Cancer Discov.* 2014;4(9):998–1013.
125. Bid HK, Kibler A, Phelps DA, Manap S, Xiao L, Lin J, et al. Development, characterization, and reversal of acquired resistance to the MEK1 inhibitor selumetinib (AZD6244) in an in vivo model of childhood astrocytoma. *Clin Cancer Res.* 2013;19(24):6716–29.
126. Begley CG, Ioannidis JP. Reproducibility in science: improving the standard for basic and preclinical research. *Circ Res.* 2015;116(1):116–26.
127. Begley CG, Ellis LM. Drug development: raise standards for preclinical cancer research. *Nature.* 2012;483(7391):531–3.
128. Begley CG. An unappreciated challenge to oncology drug discovery: pitfalls in preclinical research. *Am Soc Clin Oncol Educ Book.* 2013:466–8.

---

# Development of Orthotopic and Spontaneous Metastatic Human Tumor Xenograft Models for Experimental Therapeutics

# 12

Marta Paez-Ribes, Raquel Munoz, Eric Guerin, Shan Man, Ping Xu, John Ebos, Christina Lee, Andrew Reynolds, Yuval Shaked, and Robert S. Kerbel

---

## Developing Translational Models of Metastatic Cancer, Including Breast Cancer for Experimental Therapeutics

For decades a recurring problem in cancer research has been the poor reliability of pre-clinical experimental therapy studies undertaken in mice to predict subsequent clinical activity, at least at randomized Phase III clinical trial level [1, 2]. A common problem is overprediction, i.e., the reporting of results in mice which turn out to

---

M. Paez-Ribes

Department of Pathology, University of Cambridge, Cambridge, UK

R. Munoz

Departments of Biochemistry, Molecular Biology and Physiology, University of Valladolid, Valladolid, Spain

E. Guerin

Hôpital de Hautepierre, Hôpitaux Universitaires de Strasbourg, Strasbourg, France

S. Man • P. Xu • C. Lee

Biological Sciences Platform, Sunnybrook Research Institute, Toronto, ON, Canada

J. Ebos

Roswell Park Cancer Institute, Buffalo, NY, USA

A. Reynolds

Tumour Biology Team, The Institute of Cancer Research, London, UK

Y. Shaked

Department of Cell Biology and Cancer Science, Technion – Israel Institute of Technology, Haifa, Israel

R.S. Kerbel (✉)

Biological Sciences Platform, Sunnybrook Research Institute, Toronto, ON, Canada

Department of Medical Biophysics, University of Toronto, Toronto, ON, Canada

e-mail: [robert.kerbel@sw.ca](mailto:robert.kerbel@sw.ca)

be false positives, as it is not uncommon for even spectacular results observed in mice to be followed later by complete failure in Phase III clinical trials. Indeed, over 60% of randomized phase III trials in oncology fail despite earlier Phase II and pre-clinical results which looked positive [3, 4]. As a result, there has been a significant effort over the last 20 years to try and improve the predictive power of pre-clinical mouse therapy models. The two most significant initiatives in this regard have been the use of spontaneous tumors arising in genetically engineered mouse models (GEMMs) or patient-derived xenografts (PDXs)—as opposed to the use of tumors generated by direct transplantation of tumor cells into either immune deficient mice (when using human tumor cells) or in immunocompetent mice (when using mouse tumor cell lines). It is still not clear how much of an improvement in terms of clinical predictive potential the GEMM or PDX approaches have made, or are making, compared to models involving direct transplantation of cancer cells, usually obtained from cell culture of established cell lines.

In 2004 we initiated a program evaluating a different approach aimed at developing improved, more clinically relevant, and predictive cancer therapy models in mice, namely, treatment of spontaneous metastatic disease, especially advanced metastatic disease (but also early-stage micrometastatic disease for adjuvant therapy studies) using human tumor xenografts [2, 5]. The rationale for undertaking this initiative is as follows. The vast majority of pre-clinical mouse therapy studies involve treatment of established primary tumors, and this is true not only for transplanted tumors but also for GEMMs and PDXs. The two latter approaches are generally associated with very low incidence of overt spontaneous visceral metastatic disease [6], although there are some notable exceptions, some with GEMMs [7–10] and others involving orthotopic implantation of patient-derived surgical specimens of human tumors called “PDOX,” patient-derived orthotopic xenografts, using a technique called “SOI,” surgical orthotopic implantation [11–19]. Metastatic disease, especially when advanced in nature, is a far more difficult clinical circumstance to successfully and meaningfully treat. Indeed, in this circumstance, most treatments are palliative in nature, whereas in the neoadjuvant or adjuvant circumstances, treatments can sometimes be curative. Thus, with the aim of improving the predictive/translational power of pre-clinical mouse models, a program was initiated to recapitulate in mice treatment of advanced metastatic disease [2] and then later of early-stage micrometastatic disease [20–22]. A number of models of metastatic cancer have been developed, beginning with human breast cancer in immune-deficient mice [23] but also including human colorectal [24], renal [25], and ovarian [26] carcinoma as well as malignant melanoma [27] and locally advanced orthotopic HCC [28].

The methodology used for developing these metastatic models, in most cases, involved orthotopic transplantation and serial selection of metastases *in vivo* [2, 5]. For example, using the established MDA-MB-231 triple-negative human breast cancer cell line (which is probably used widely more than any other breast cancer cell line for pre-clinical studies), cultured cancer cells are injected into the mammary fat pads of female immunosuppressed SCID mice [23]. Orthotopic transplantation is a known method of promoting distant spontaneous metastatic spread [2]. However, detection of such metastases may necessitate surgical resection (mastectomy) of the primary tumor to allow sufficient time for overt metastases to develop in such sites as the lungs or liver. We found that detecting by the naked eye such distant metastases

took between 4 and 6 months [23]. Such overt metastases, mostly found in the lungs, were pooled and a cell line was established called LM1. The LM1 cells were then injected into mammary fat pads and the procedure repeated one more time in a second group of recipient SCID mice [23]. This second *in vivo* selection resulted in accelerated and more robust metastatic disease after surgical resection of the primary tumor, and these metastases occurred not only in the lungs but sometimes in extrapulmonary sites such as the liver and lymph nodes [23]. A single lung metastasis was selected and a cell line established from it, called LM2-4. This line was then used for experimental therapy studies usually involving orthotopic transplantation, surgical resection, and then initiating therapy approximately 1 month later when mice develop, albeit in a heterogeneous fashion, distant metastatic disease. An example of a mouse with postsurgical advanced metastatic disease is shown in Fig. 12.1a [23].

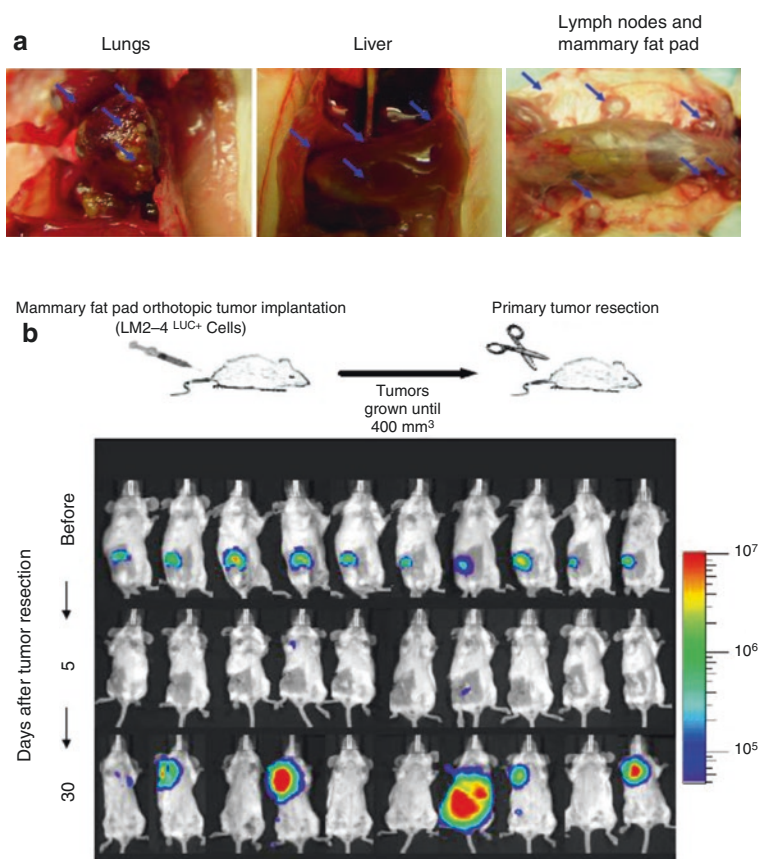


**Fig. 12.1** Panel (a) illustrates the pattern of spontaneous systemic metastases that can arise heterogeneously in mice within a month or more after surgical resection of an established primary orthotopic tumor using a metastatic variant (called LM2-4) selected *in vivo* from the MDA-MB-231 human breast cancer cell line. The majority of metastases are detected in the lungs but extrapulmonary metastases can sometimes also be found, e.g., in the liver and lymph nodes. Recurrence of tumor growth at the surgical resection site can also occur [23]. Panel (b) illustrates whole body bioluminescence imaging of LM2-4 tumors before primary tumor resection (“before”) or 5 or 30 days after mastectomy. Panel (a) is taken from Munoz et al. [23]; Panel (b) adapted from Ebos et al. [20]

Importantly, the variant metastatic cells can be easily tagged with an imageable biomarker, e.g., luciferase, enabling whole body optical bioluminescence imaging to monitor disease progression and therapeutic response of metastatic disease [20]. An example of the luciferase tagging is shown in Fig. 12.1b where orthotopic primary tumors are imaged in the upper panel and mice imaged 5 or 30 days after surgical resection of the primary tumors. This illustrates how initiating therapy within a few days of primary tumor resection would constitute a version of adjuvant therapy of early-stage (micrometastatic) disease in this model, whereas waiting a month after resection until initiating therapy would constitute treatment of overt metastatic disease. Examples are described below of how therapeutic outcomes can be very different depending on what stage of disease progression therapy is initiated. We have also utilized this serial selection approach to generate models of HER-2-positive metastatic breast cancer where mice are treated with a drug such as trastuzumab (Herceptin) [29, 30]. An obvious question is whether these metastatic models better reflect clinical outcomes compared to the conventional approach of treating established primary tumors. A number of examples follow which suggest this may be the case.

### **Emergence of Brain Metastases in Therapy-Induced Long-Term Survivors and Establishment of Spontaneous Brain Metastasizing Cell Lines**

We recapitulated a common and important clinical therapeutic outcome of growing importance, namely, the emergence of spontaneous brain metastases in mice that had no evidence of such brain metastases when a successful treatment was first initiated in mice with systemic visceral metastases [27]. Presumably, as the result of extending the survival times of mice with such overt visceral metastatic disease, allowed what were asymptomatic microscopic brain metastases more time to develop into overt lesions [31, 32]. This brain metastasis “sanctuary” phenomenon, as it is known, is a discouraging observation in women with metastatic HER-2-positive cancer treated with trastuzumab-based therapy, i.e., they can experience a higher rate of relapse involving brain metastases [32]. The brain metastasis model we developed arose from treating mice with advanced systemic malignant melanoma with a chemotherapy protocol that extended survival [27]. When brain metastases were detected, they were isolated and cell lines were established from the lesions. The isolated variants were then analyzed for their ability to spontaneously metastasize to the brain from primary (and then resected) tumors after subdermal injection of the cells—but without any therapeutic intervention to extend survival. We found that, indeed, the cells were capable of such heritable spontaneous brain metastases [27]. Subsequent studies revealed possible molecular mediators of spontaneous metastasis, e.g., endothelins 1 and 3 and endothelin receptor B [33].

## Recapitulating the Phase III Clinical Trial Failure of Anti-Angiogenic Drugs in Mouse Models with Metastasis

We undertook a comparative analysis of the therapeutic effects of an antiangiogenic drug—testing three different antiangiogenic agents—in the conventional circumstance of established primary orthotopic tumors, on the one hand, versus established visceral metastatic disease after primary tumor resection, on the other. An example of this is shown in Fig. 12.2. We found that oral anti-angiogenic TKIs

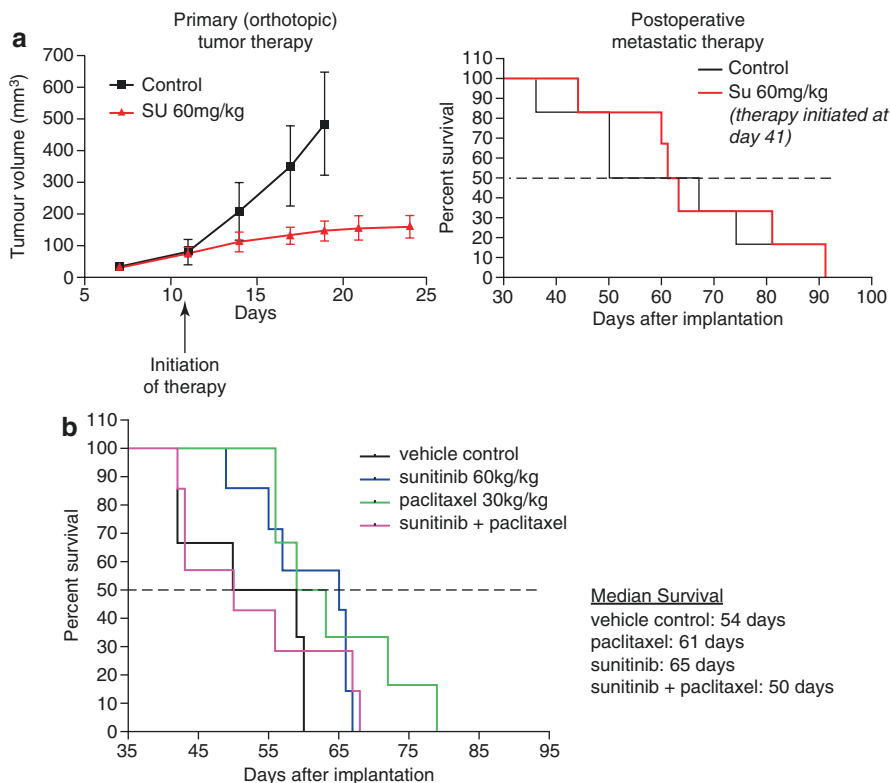


**Fig. 12.2** Panel (a), *left side*, shows the positive efficacy impact of daily anti-angiogenic therapy using the anti-angiogenic TKI sunitinib on established orthotopic primary human breast cancer xenografts of the LM2-4 variant obtained from the MDA-MB-231 cell line, versus the lack of therapeutic impact (*right side*) of the same therapy when initiated in mice with established metastatic disease approximately a month after surgical resection of the primary tumor. Similar results to sunitinib were obtained with pazopanib and DC101, an anti-VEGFR-2 antibody when treating primary tumors. Panel (b) shows the therapeutic impact of sunitinib with paclitaxel chemotherapy in the metastatic setting where a lack of efficacy is observed in contrast to the primary tumor treatment setting. Taken from Guerin et al. [34]

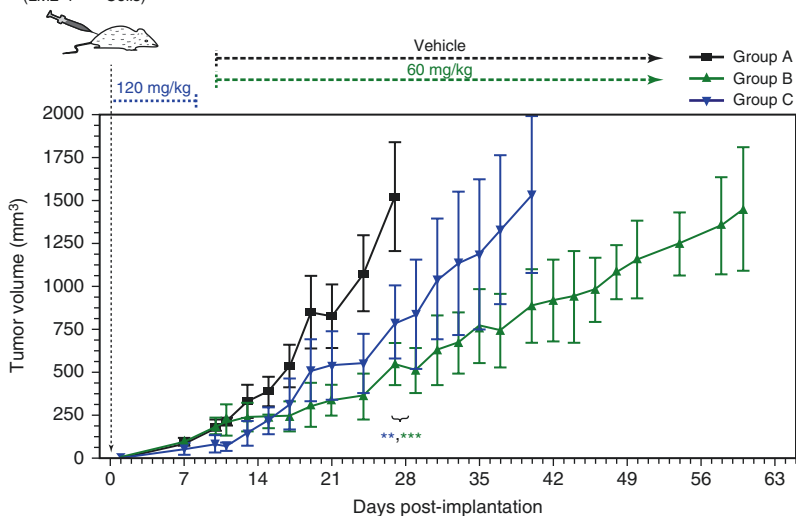
such as sunitinib or pazopanib, as well as an antibody to mouse VEGFR-2 (called DC101), all caused primary antitumor growth delay. The results using sunitinib are shown in Fig. 12.2a (*left panel*) [34]. In contrast, no such efficacy was detected when treating overt metastatic disease (which was mainly confined to the lungs) as shown in Fig. 12.2a (*right panel*). Moreover, when sunitinib was combined with standard paclitaxel chemotherapy, again no efficacy was noted in the metastatic-treatment setting compared to other treatment groups, as also shown in Fig. 12.2b. These pre-clinical results, using the metastatic model, recapitulated the negative results of four failed randomized phase III clinical trials assessing sunitinib alone or combined with chemotherapy in women with metastatic breast cancer [35–38]. Furthermore, we also reported results that foreshadowed the subsequent failure of adjuvant anti-angiogenic therapy for the treatment of early-stage micrometastatic disease [20], including breast cancer, e.g., the adjuvant breast cancer “BEATRICE” [39], “BETH,” and ECOG-5103 adjuvant trials [21, 39]. This is shown in Fig. 12.3. Thus, as already described, treatment of mice with sunitinib was effective in the primary tumor treatment setting, as shown in Fig. 12.3a. However, in complete contrast when the primary LM2-4 breast cancer was resected and adjuvant treatment initiated immediately, using a short course of high dose sunitinib, the therapeutic outcome (as shown in Fig. 12.3b) was actually worse in the treated mice compared to the vehicle control [20].

In the discussion of this published adjuvant therapy breast cancer study in 2009 [20], we cautioned that the clinical assessment of anti-angiogenic therapy in the adjuvant setting should perhaps be postponed until more information was known about the use of these agents in early-stage disease settings based on our pre-clinical results [20]. Subsequently, more than 12 randomized adjuvant trials involving bevacizumab plus chemotherapy or a TKI monotherapy have been undertaken in breast, colorectal, renal, lung and liver cancers, and all failed to meet their primary endpoint (reviewed in the Supplemental section of ref. 21). Although none showed a worse outcome with one exception (a colorectal trial called AVANT), it is notable that all the bevacizumab trials involved bevacizumab plus chemotherapy followed by maintenance bevacizumab. It is thus possible that the addition of chemotherapy may have prevented any potential pro-invasive/metastatic effect induced by the anti-angiogenic drug treatment. Indeed, we recently published evidence in tentative support of this hypothesis. In brief, we found that DC101 (a VEGFR-2 antibody) or sunitinib could increase local invasion of orthotopic primary breast tumors, and moreover, this undesirable effect could be prevented by the addition of concurrent chemotherapy, using either paclitaxel or cyclophosphamide [40], as shown in Fig. 12.4. In this same study, we also showed that a sequenced combination of neoadjuvant followed by adjuvant anti-angiogenic-based therapy could bring about an overall survival effect (shown in Fig. 12.5). Interestingly, this limited study result recapitulates a secondary analysis of a recent adjuvant Phase III clinical trial outcome in breast cancer (NSABP-B-40) involving neoadjuvant chemotherapy followed by adjuvant bevacizumab therapy, showing an overall survival benefit [41].



Mammary fat pad orthotopic tumor implantation  
(LM2-4<sup>LUC+</sup> Cells)

**a**



**b**

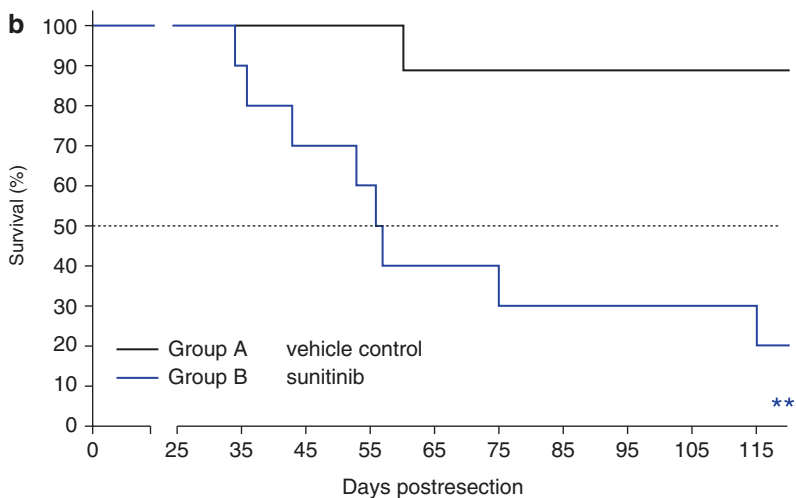


**Fig. 12.3** Panel (a) illustrates the therapeutic impact of sunitinib on established primary orthotopic breast cancer xenografts using the LM2-4 metastatic variant of MDA-MB-231 human breast cancer cells and two different doses and schedules of the drug. An antitumor benefit is caused by either protocol. In contrast a short course (1 week) therapy using the high dose of sunitinib (Group B) causes a decrease in survival in the postsurgical adjuvant treatment setting compared to Group A (vehicle control) where therapy was initiated a day after surgical resection of established primary tumors. Taken from Ebos et al. [20]

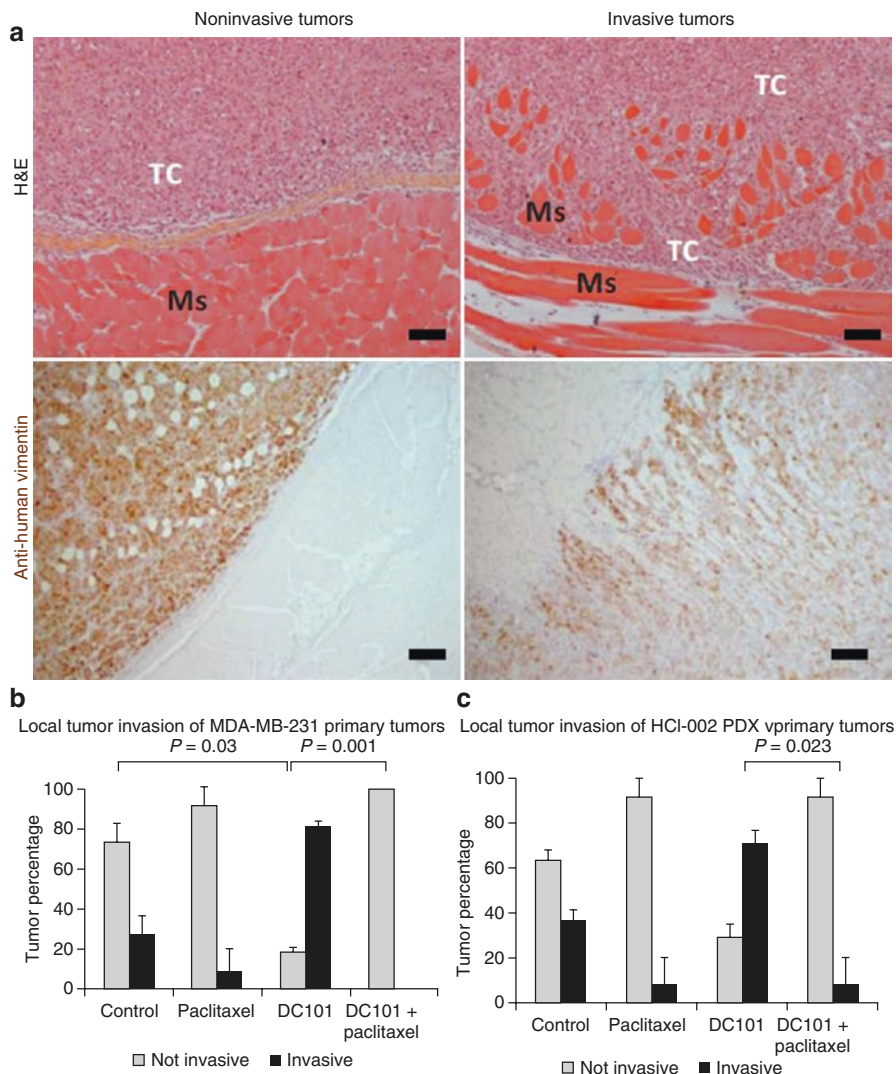
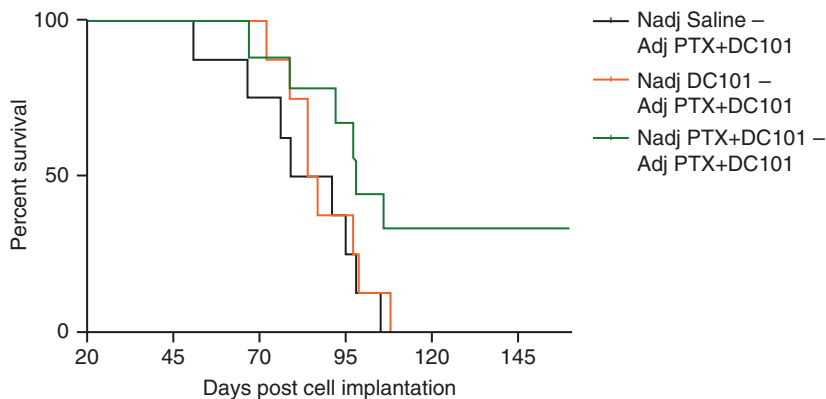


**Fig. 12.4** Increase in local invasion after anti-angiogenic therapy and blockade of this effect by concurrent chemotherapy. MDA-MB-231 breast cancer cells and the triple-negative PDX breast cancer HCI-002 were orthotopically implanted in the mammary fat pads of SCID mice. When tumor volumes reached 150 mm<sup>3</sup>, therapy was started with vehicle, DC101 (a VEGFR-2 antibody), paclitaxel (30 mg/kg once every 2 weeks), or the combination of the two. **(a)** Tumors are considered invasive when tumor cells encroached into the adjacent muscular fibers of the abdominal wall. *Left panels* show a noninvasive MDA-MB-231 tumor stained for H&E (*upper panel*) and human vimentin antibody (*lower panel*, cells in brown). *Right panels* show invasive tumors stained for H&E (*upper panel*) and anti-human vimentin (*lower panel*). *Ms* muscle cells of the abdominal wall, *TC* tumor cells. Scale bars, 150  $\mu$ m. **(b, c)** Graphs showing the percentage of invasive and noninvasive tumors in MDA-MB-231 **(b)** and PDX HCI-002 **(c)** breast tumors. \* $p < 0.05$  by Mann-Whitney test. Error bars indicate  $\pm$ SD. In all groups  $n \geq 6$ . Results taken from Paez-Ribes et al. [40]



Therapy group	Median survival (days)	p value vs Control
Nadj Saline – Adj PTX+DC101	85	-
Nadj DC101 – Adj PTX+DC101	85.5	0.5235
Nadj PTX+DC101 – Adj PTX+DC101	98	0.0377

**Fig. 12.5** Neoadjuvant + adjuvant therapy with DC101, the VEGFR-2 antibody, and paclitaxel increases survival and reduces toxicity. Mice were implanted with the metastatic variant LM2-4, and therapy was started when tumor volumes reached 150 mm<sup>3</sup> and maintained for 10 days [DC101 (800 µg twice a week)] or the combination of DC101 and paclitaxel (30 mg/kg every other week). Tumors were resected when they reached 500 mm<sup>3</sup>, and 5 days later therapy with DC101 and paclitaxel protocol was started in all mice for 4 weeks. The Kaplan-Meier survival curve shows the overall survival of mice after receiving neoadjuvant + adjuvant therapy. The log-rank test was used for statistics. Taken from Paez-Ribes et al. [40]. This result superficially recapitulates the secondary analysis of an overall survival benefit in the NSABP-B-40 neoadjuvant/adjuvant trial of bevacizumab plus chemotherapy in early-stage breast cancer [41]

### Comparing Orthotopic Primary Tumors vs. Spontaneous Metastases Reveals Evidence for Non-angiogenic “Vessel Co-option” in Lung Metastases

With these previous published anti-angiogenic therapy results in mind, we subsequently focused on another important question using our orthotopic primary tumor or postsurgical human tumor xenograft models. We asked why it is that the primary orthotopic breast cancers in our studies are sensitive to an anti-angiogenic drug treatment, whereas distant metastases, found mainly in the lungs, are apparently not. To address this question, we analyzed the nature of the tumor vasculature populating primary tumors versus lung metastases and did so in collaboration with several investigators—Dr. Harold Dvorak in Boston; Dr. Andrew Reynolds in London, UK; and Dr. Peter Vermeulen in Antwerp, Belgium [42]. We found that whereas the primary tumors are highly angiogenic, based on histopathologic criteria, the lung metastases are not. Instead, as shown in Fig. 12.6, we found evidence of what is known as “vessel co-option.” This refers to the property of tumor cells to hijack, i.e., co-opt, the existing abundant vasculature in a particular organ site such as the lungs.

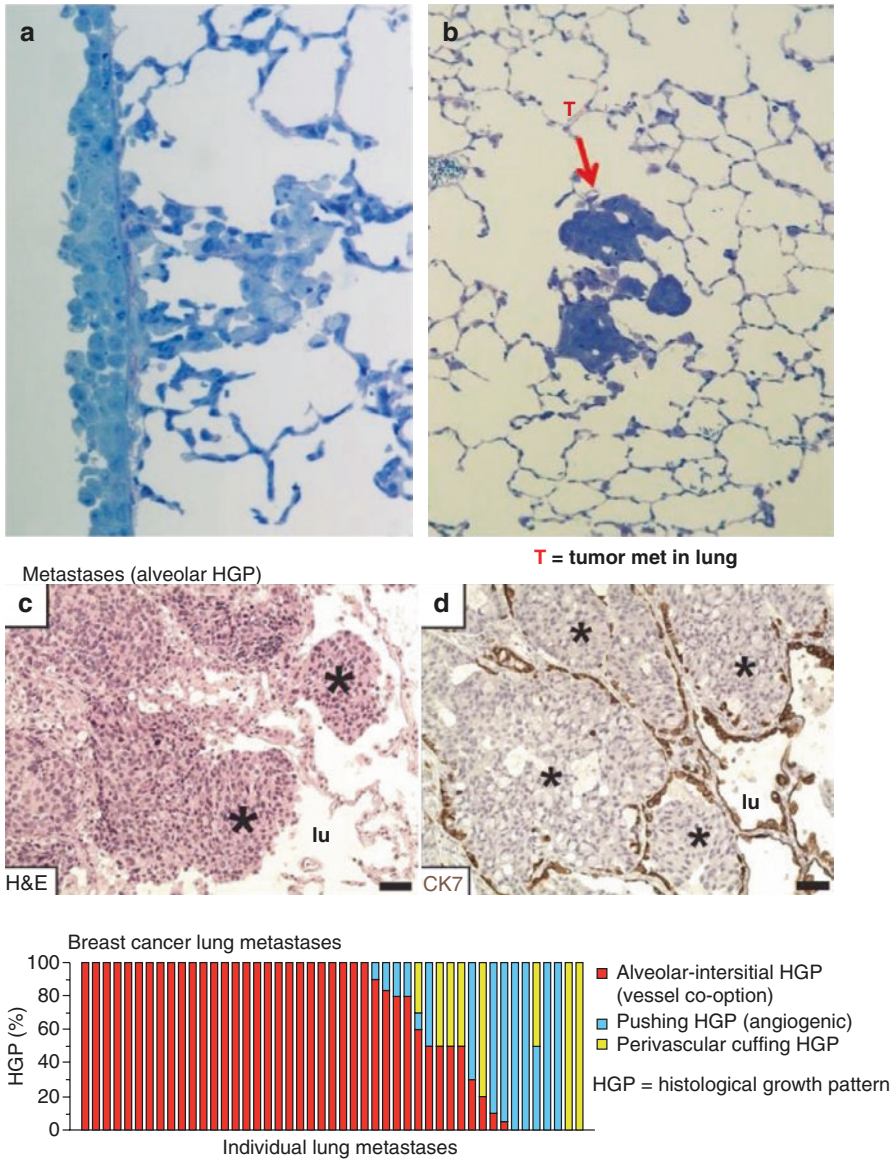


**Fig. 12.6** (a) illustrates “cuffing” of tumor cells around the membranes surrounding lung alveolar air sacs of spontaneous lung metastases in the LM2-4 metastatic model, while (b) shows metastatic tumor (*T*) cells of a spontaneous polyoma middle T-driven breast cancer “GEMM” filling up the air sacs. (c, d) illustrate vessel co-option in human breast cancer lung metastases, and the *bottom panel* illustrates the extent of such vessel co-option detected in multiple, individual human breast cancer metastases (red bars in *bottom panel*). (c, d) and *bottom panel* taken from Bridgeman et al. [42]. \* indicates aveolar sacs filled with cancer cells

For example, the alveolar spaces/air sacs can become filled with cancer cells and simply utilize the existing extensive blood vessel network in the membranes surrounding the air sacs [42], or alternatively, the cancer cells can “cuff” the membranes and parasitize their existing blood vessels. In either circumstance, as tumors in the lungs grow and expand, there is little or even no need to induce new blood vessel formation, i.e., sprouting neoangiogenesis. Previous pre-clinical work by Szabo et al. also showed lack of angiogenesis in lung metastases, where vessel co-option was dominant in a variety of lung metastasis models in mice [43].

Vessel co-option was first reported in the modern literature in 1996 by Francesco Pezzella and colleagues when studying human non-small cell lung cancer [44, 45]. Both primary tumors and metastases growing in lung tissue often show minimal or no sprouting angiogenesis. Instead, they show evidence of vessel co-option. These observations have been confirmed by an examination of over 164 human lung metastasis cases, including cases of lung metastasis derived from breast, colorectal, and renal cancer patients [42]. As such, this could readily explain the modest effects or even the absence of a therapeutic effect when utilizing an anti-angiogenic drug to treat lung metastases. Moreover, vessel co-option has also been described in liver metastases of colorectal cancer by Peter Vermeulen and colleagues [46].

The vessel co-option results described above could readily account for some of the modest effects of anti-angiogenic drugs, in general, and for treatment of metastatic breast cancer in particular. Moreover, they may also account for some instances of acquired/evasive resistance to such drugs. Indeed, we recently published results utilizing a model of orthotopic HCC using the anti-angiogenic TKI called sorafenib [47]—which is approved for HCC patients—showing that it is initially effective in blunting the growth of the HCC tumors during which time tumor angiogenesis can be detected. However, within about a month, the sorafenib treatment begins to lose its efficacy, and this coincides with a switch by the tumors from relying on angiogenesis to exploiting vessel co-option. The switch to vessel co-option is preceded by a marked invasion (migration) of the sorafenib-treated cancer cells into the liver and eventually replacing the liver parenchyma so that the tumor comes to co-opt the pre-existing liver vasculature [47]. Of considerable interest is that similar results showing a switch to co-option was reported clinically in liver metastases of colorectal cancer patients receiving a bevacizumab-based therapy [48].

These vessel co-option results have raised a critical question, namely, can co-opted blood vessels in tumors be therapeutically targeted in a safe manner by an anti-vascular therapy that is independent of inhibiting angiogenesis? If so, this could open up a new therapeutic era involving targeting of the tumor vasculature. In this regard, there is a basis for speculating that co-opted tumor vessels are not completely normal. For example, blood vessels in metastatic sites often show evidence of hyperpermeability, i.e., “vascular leak,” and this physiologic abnormality along with their structural abnormalities (e.g., as a result of extensive cancer cell compression and high interstitial fluid pressures) and the fact that they are enveloped by cancer cells secreting various growth factors, cytokines, and enzymes make it likely that they express various abnormalities. These abnormalities may, in some cases, be therapeutically exploited so as to render them vulnerable while sparing the normal (tumor-free) vasculature in the same organ or other organs/tissues elsewhere in the body.

## Studies with Patient-Derived Xenografts (PDXs)

All of the aforementioned work, as well as other studies not summarized here involving human orthotopic and metastatic colorectal cancer [24] and renal cell carcinoma [25] xenografts, involved the use of long-term-established human cell lines. We asked whether the basic approach could be adapted and extended to PDXs by evaluating whether spontaneous metastasis PDX models could be developed utilizing a similar approach for successfully establishing such models using established cell lines [2]. We also undertook some comparisons of the response to a particular therapy using primary tumors, established from human tumor cell lines on the one hand, versus PDXs on the other [49]. With respect to the first initiative, the results were disappointing. We analyzed several different triple-negative human breast cancer PDXs, e.g., HCI-001 and HCI-002, among three others, that were obtained from Dr. Alana Welm, Huntsman Cancer Institute, Utah [50]. The tumors were orthotopically transplanted and then surgically resected. A total of 144 SCID mice were used as recipients for these tumor transplantations.

Unfortunately detection of distant overt metastases visible upon gross inspection was exceedingly rare with only three lung metastases detected among the 144 transplanted mice [6]. The protocol used and results are summarized in Fig. 12.7 and Table 12.1. Moreover, when a metastasis was transplanted orthotopically as a histologically intact tissue mass, no evidence of increased metastatic aggressiveness was noted—in marked contrast to the results we obtained using an established human tumor cell line, e.g., MDA-MB-231, to select metastatic variants [23]. Although a number of tumors outside the transplant site were noted, they turned out, with rare exception, to be *de novo* mouse thymomas [6]. The reasons for the failure to obtain distant overt metastatic disease using PDXs in this study are unknown, but several possibilities come to mind. For example, we used SCID mice as the recipients for these studies and it is known that mice with greater degrees of immune deficiency such as NOD-SCID-IL-2 $\gamma$ R<sup>-/-</sup> NSG/NOG mice are more prone to developing metastatic disease (reviewed in ref. 50). Indeed, we undertook a previous comparative analysis of the metastatic aggressiveness of MDA-MB-231 cells and the LM2-4 variant selected from MDA-MB-231 in SCID, NOD-SCID, and NSG mice after orthotopic injection of tumor cells followed by surgical resection of the primary tumors [51]. The results highlighted the much greater metastatic aggressiveness in NSG mice [51]. In fact, even the “poorly metastatic” parental MDA-MB-231 tumor cell line was highly metastatic in NSG mice which suggests metastatic spread may be strongly restricted by cellular elements of the innate immune system that are missing or deficient in the NSG mice [51]. In addition, most PDXs are obtained from primary tumors or malignant effusions, as opposed to distant isolated metastases. Using PDXs derived from metastases may result in a greater chance of detecting distant metastases in recipient mice. What is intriguing about our preliminary inability to develop models of metastatic disease, or to detect metastases with any frequency using PDXs, is that these results stand in marked contrast to an impressive body of literature from the group led by Robert Hoffman reporting that surgical orthotopic implantation (SOI) to develop “PDOXs” (patient-derived orthotopic xenografts) resulted in clinically relevant patterns of metastatic disease

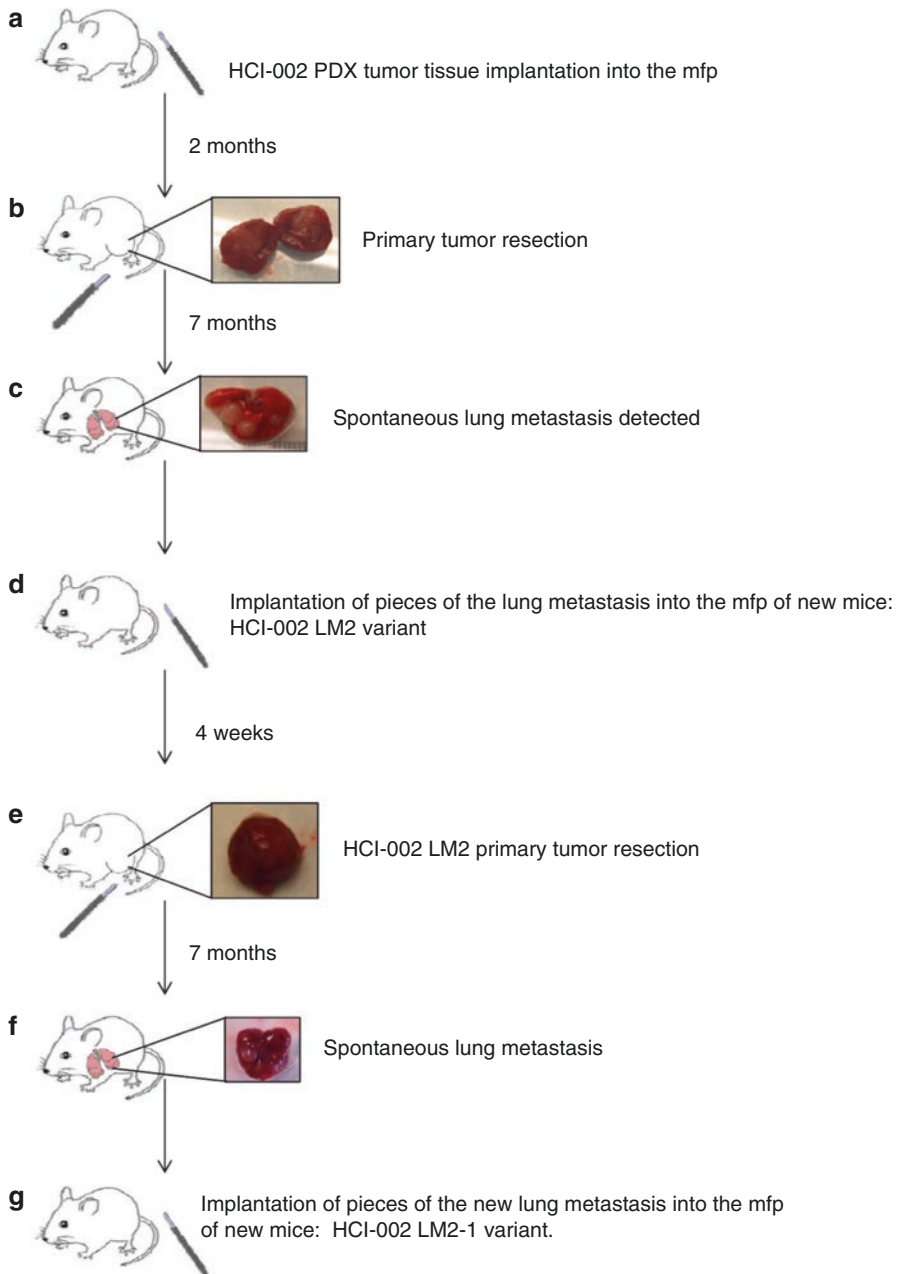


**Fig. 12.7** Flow diagram of methodology used to try and generate spontaneous metastases from a primary resected breast cancer PDX called HCI-002. *mfp* mammary fat pad. Taken from Paez-Ribes et al. [6]

**Table 12.1** Summary of secondary tumor detection after orthotopic primary tumor resection detected in SCID mice transplanted with triple-negative human breast cancer PDXs

Tumor type	Metastases of human origin	Tumors of mouse origin (%) <sup>a</sup>	Total mice implanted
HCI-001	1	6 (15.3)	39
HCI-002	2	9 (15)	60
HCI-004	0	2 (13.3)	15
HCI-008	0	3 (20)	15
HCI-009	0	3 (20)	15
All tumors	3	23 (15.9)	144

<sup>a</sup>Mouse tumor detected are de novo thymomas. Taken from Paez-Ribes et al. [6]

when studying a very broad spectrum of human tumor types [11–19] as cited earlier. Moreover, these experiments were mostly undertaken using athymic nude mice as recipients. The reasons for the discrepancy in these results and ours remain to be determined but may reveal important factors involved in metastatic efficiency in addition to host-mediated control mechanisms of metastatic disease and responsiveness to therapy [6]. We should also acknowledge some recent results by the group of Dr. Zena Werb, i.e., Lawson et al, “Single-cell analysis reveals a stem-cell program in human metastatic breast cancer cells” *Nature* 526:131–135, 2015, which would appear to be a variance with ours. These authors reported that by using molecular markers such as antibodies to human CD298 (ATP1B3) for immunohistochemistry or FACS based assays, that metastatic PDX-derived cells could be detected in peripheral tissues (e.g. lung, liver, brain, bone, marrow, lymph node) in 70% of mice that had undergone surgical resection of a primary orthotopic PDX breast cancer. NOD-SCID mice showed evidence of either “low burden” or “high burden” disease, though high burden disease seemed to consist of microscopic or small nodules in greater numbers. Thus imaging and detailed molecular detection may reveal evidence of spontaneous metastatic disease using PDXs; however, the extent of overt life-threatening overt metastatic disease that develops in this study remains unclear.

## Studies of Metronomic Chemotherapy

In addition to studying the therapeutic impact of anti-angiogenic drugs in the orthotopic/metastatic xenograft models discussed above, a series of investigations were undertaken to assess an investigational form of chemotherapy known as “metronomic” chemotherapy [23–26]. This refers to the administration of conventional chemotherapy drugs in an unconventional fashion, namely, low to relatively low doses well below the maximum tolerated dose (MTD), on a frequent regular administration schedule (e.g., daily) with no prolonged breaks between each successive treatment [52, 53]. As such, the majority of metronomic chemotherapy studies and clinical trial investigations involve oral chemotherapy agents such as cyclophosphamide, methotrexate, and 5-FU prodrugs such as capecitabine or UFT, i.e., tegafur plus uracil [54, 55]. The mechanisms involved in causing efficacy using metronomic chemotherapy are multi-faceted and



complex; include anti-vascular effects, e.g. angiogenesis inhibition [52], stimulation of immunity [56], possibly direct tumor cell killing [57], and effects on the stromal fibroblast compartment of tumors [58]. One of the surprising findings when testing metronomic chemotherapy pre-clinically, is that in contrast to various targeted agents such as anti-angiogenic drugs, metronomic chemotherapy regimens can cause surprisingly potent efficacy when treating advanced metastatic disease, at least when utilizing human tumor xenografts for such studies [23, 25, 26]. An example is shown in Fig. 12.8 which involves oral metronomic

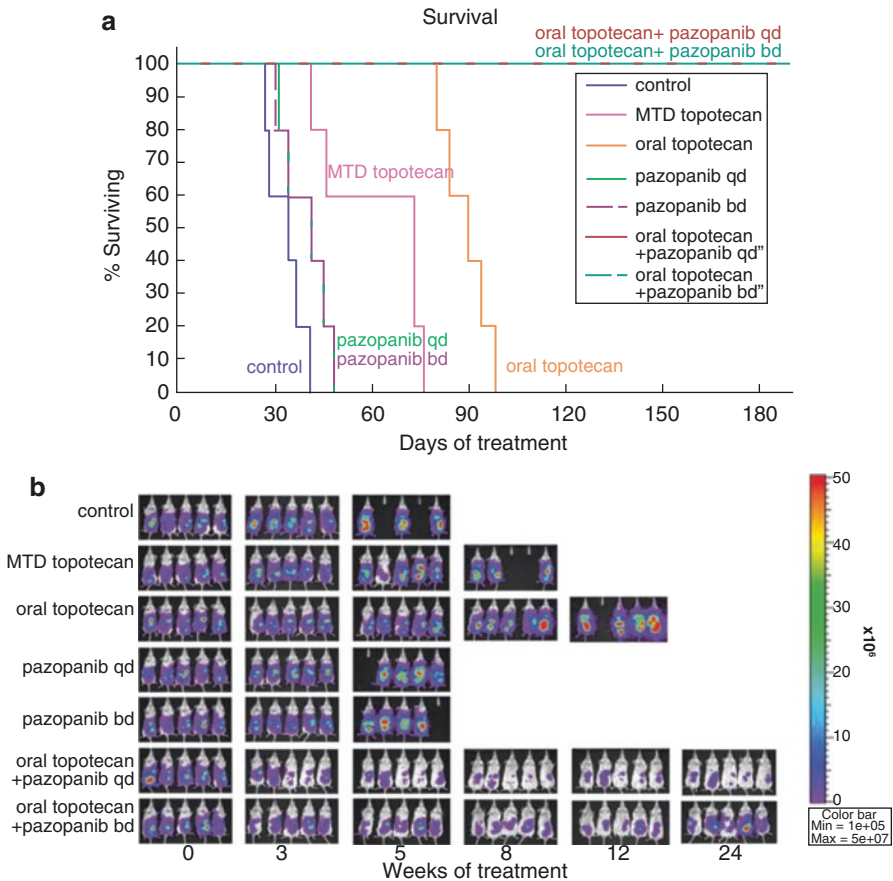


**Fig. 12.8** Therapeutic impact on survival of low-dose daily metronomic or maximum tolerated dose (MTD) topotecan chemotherapy with or without oral pazopanib, an anti-angiogenic tyrosine kinase inhibitor (TKI) on advanced intraperitoneal metastatic human ovarian cancer (using the SKOV-3-13 metastatic variant of SKOV-3) in SCID mice. Panel (a) shows the survival analysis which illustrates superiority of the metronomic topotecan protocol over the MTD protocol and the lack of pazopanib monotherapy efficacy. However, addition of pazopanib substantially enhances the efficacy of the oral metronomic topotecan protocol. Panel (b) shows responses to the various therapies as assessed by whole body bioluminescence imaging based on luciferase tagging of the SKOV-3-13 variant. Adapted and taken from Hashimoto et al. [26]

topotecan used alone or when combined with an anti-angiogenic TKI drug (pazopanib). This model involved treatment of advanced ovarian cancer [26], whereas another (not shown here) involved renal cell carcinoma [25]. In addition, prior studies indicated that a combination of metronomic cyclophosphamide, administered daily through the drinking water, with daily UFT administered by gavage, was remarkably effective in treating mice with advanced metastatic disease using the postsurgical LM2-4 breast cancer xenograft model [23]. The efficacy of this regimen in the metastatic setting stands in marked contrast to the results obtained with anti-angiogenic drugs where little or no efficacy was detected in the metastatic setting, as described above and shown in Fig. 12.2.

Such encouraging results, among others, have helped contribute to the rationale of undertaking clinical trials assessing versions of oral metronomic chemotherapy used either alone [55] or combined with a targeted agent such as the VEGF antibody bevacizumab [59]. Some of the results obtained in randomized Phase III trials are encouraging, at least when the metronomic chemotherapy regimens are used as a long-term maintenance treatment strategy [55, 59]. There remain some indisputable handicaps to further the successful clinical translation of metronomic chemotherapy such as determining the optimal dose and schedule when not using a standard MTD regimen. Nevertheless, the pre-clinical results combined with the results of some of the first randomized Phase III clinical trials together make a case for further clinical assessment of this therapeutic concept in patients. If successful, this would be particularly beneficial in low- and middle-income countries [60] when using inexpensive off-patent oral chemotherapy drugs [61], which can be taken outside of a hospital setting. Finally, one other aspect of our metronomic chemotherapy results that needs comment concerns an aspect of the mechanisms involved, specifically as they relate to an advantage over conventional MTD chemotherapy, namely, that metronomic chemotherapy is less likely to provoke various reactive host responses that act as protective or even growth promoting mechanisms for cancer cells, and which can be induced by MTD chemotherapy [62, 63]. Thus, MTD chemotherapy can cause a rapid increase in bone marrow derived pro-angiogenic cells e.g., circulating endothelial progenitor cells (EPCs), accompanied by an acute systemic induction of several growth factors and cytokines known to support tumor growth [62]. However, if the same drugs are given metronomically, the levels of such cells (and growth factors) are not changed and little or no pro-tumorigenic effects are found [62]. Myeloid-derived suppressor cells (MDSCs) are suppressed in response to metronomic gemcitabine therapy when compared to MTD chemotherapy (shown in Fig. 12.9). In addition, they also showed that pancreatic cancer cells cultured in the presence of plasma from mice treated with MTD gemcitabine resulted in increased invasion and migration when compared to the same cells cultured in the presence of plasma from mice treated with metronomic gemcitabine. This suggests that such host effects induced after MTD chemotherapy are diminished when the same drug is administered using metronomic chemotherapy.

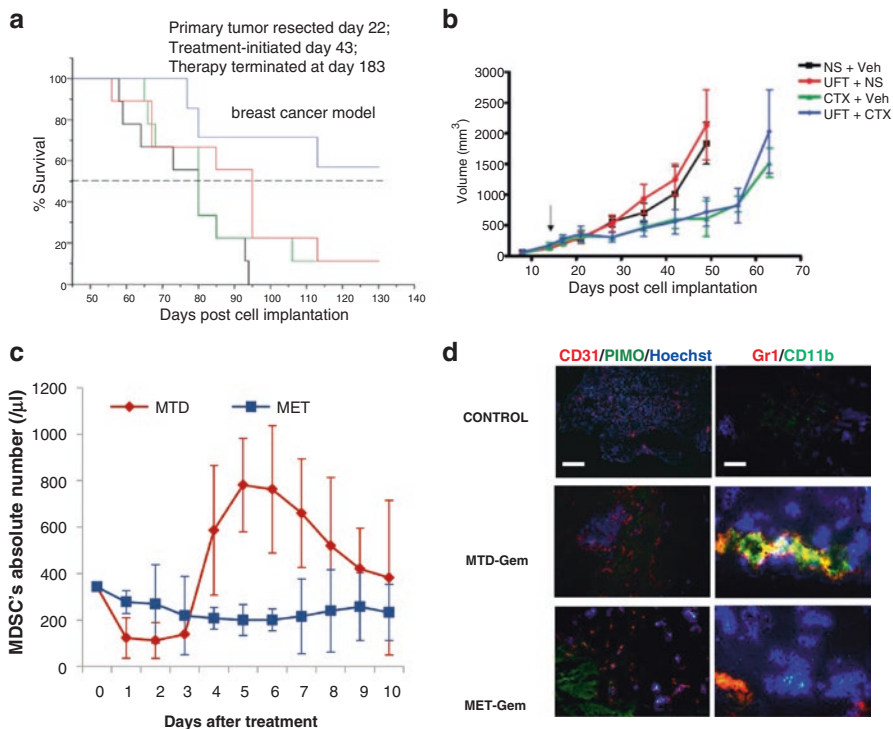


**Fig. 12.9** (a, b) Impact of combination metronomic chemotherapy using two oral drugs administered concurrently on survival times of mice with advanced visceral metastatic cancer or only primary tumors at the time treatment was initiated. The drugs used were cyclophosphamide (CTX), administered daily through the drinking water, and UFT (an oral 5-FU prodrug comprised of uracil and tegafur) administered daily by gavage. (a) shows results when treating established metastatic disease after primary orthotopic tumor resection of the MDA-MB-231/LM2-4 human breast cancer. (b) shows the results on tumor volume when the response of only primary tumors were assessed in a control group of mice ( $n=8$ ), where only a modest growth delay was observed, and which was due only to the CTX treatment. Taken from Munoz et al, *Cancer Res* 2006 (14). (c) C57Bl/6 mice were treated with MTD or metronomic chemotherapy (MET) gemcitabine regimens. Blood was sampled on a daily basis for 10 sequential days. The number of MDSCs in the peripheral blood was evaluated by flow cytometry (using CD11b+ and Gr1+ surface markers). (d) Pancreatic tumor (Panc-02) bearing mice (orthotopically implanted) were treated with MTD or metronomic chemotherapy (MET) gemcitabine regimens. After 21 days of treatment, mice were sacrificed, and tumors were removed. Left panel: Tumor sections from all treatment groups were stained for CD31 representing endothelial cells (in red), hypoxia using hypoxic probe (PIMO, in green), and Hoechst for assessment of perfusion (in blue). Right panel: To visualize MDSCs within the tumor, the sections were immunostained with anti-Gr1 (red) and anti-CD11b (green) antibodies. Nuclei were stained with 4',6-diamidino-2-phenylindole (DAPI) (blue); scale bar, 200  $\mu\text{m}$ . The results in C&D demonstrate that following MTD but not metronomic chemotherapy of gemcitabine, MDSCs are mobilized to the peripheral blood (c) and colonize treated tumors, hence contributing to tumor angiogenesis (d). Modified from Hasnis et al, *Neoplasia* 2014 [63]

## Summary

Taken together the results summarized herein illustrate a number of significant benefits that can be gained by utilizing translational orthotopic/metastatic human tumor xenograft models for experimental therapeutics. This approach can be extended to the use of mouse tumors grown in immunocompetent mice allowing assessment of immune-based therapies, e.g., using immune checkpoint inhibitors, not only in the primary-tumor-treatment setting but also in the adjuvant-and metastatic-treatment settings [21]. Clearly, metastatic treatment models are not practical for rapid routine screening of large numbers of new drug or therapies, but they could be used to help make a more informed decision regarding future clinical development of a particular drug or therapy after apparent successful testing in conventional primary tumor treatment models, whether these involve transplanted tumors, PDXs, or GEMMs. Considering the enormous cost of a single randomized Phase III clinical trial, a case can be made for the inclusion of either adjuvant or metastatic therapy models in mice before making a final “go–no go” decision regarding clinical development. In addition these models can be very informative with respect to acquiring a better understanding of the biology of tumors, especially metastatic disease, as the vessel co-option and brain metastasis discoveries described above illustrate.

**Acknowledgments** Dr. Kerbel’s studies summarized in this review chapter have been supported by multiple academic grants since 2004, as well as several sponsored research agreements with companies. Sources of academic grants include the Canadian Cancer Society Research Institute (CCSRI), the Canadian Institutes of Health Research (CIHR), the Ontario Institute for Cancer Research (OICR), the Canadian Breast Cancer Foundation (CBCF), the Worldwide Cancer Research (WCR), and the National Institutes of Health (NIH), USA. Sponsored Research Agreements include ImClone Systems, GlaxoSmithKline, and Cerulean Pharma. In addition a donation from Dr. Rena & Michael Buckstein administered through the Israel Cancer Research Fund (ICRF) to support studies of metronomic chemotherapy is gratefully acknowledged.

---

## References

1. Kamb A. What’s wrong with our cancer models? *Nat Rev Drug Discov.* 2005;4(2):161–5.
2. Francia G, Cruz-Munoz W, Man S, Xu P, Kerbel RS. Mouse models of advanced spontaneous metastasis for experimental therapeutics. *Nat Rev Cancer.* 2011;11:135–41.
3. Amiri-Kordestani L, Fojo T. Why do phase III clinical trials in oncology fail so often? *J Natl Cancer Inst.* 2012;104(8):568–9.
4. Grignolo A, Pretorius S. Phase III trial failures: costly, but preventable. [www.appliedclinical-trialsonline.com](http://www.appliedclinical-trialsonline.com), 2016;25(8).
5. Kerbel RS, Guerin E, Francia G, Xu P, Lee CR, Ebos JML, Man S. Evaluating outcomes of antiangiogenic and chemotherapy in preclinical mouse models mimicking postsurgical adjuvant or metastatic breast cancer therapy. *Breast.* 2013;22:S57–65.
6. Paez-Ribes M, Man S, Xu P, Kerbel RS. Development of patient derived Xenograft models of overt spontaneous breast cancer metastasis: a cautionary note. *PLoS One.* 2016;11(6):e0158034.
7. Kerbel RS, Paez-Ribes M, Man S, Xu P, Guerin E, Cruz-Munoz W, Ebos JML. Modelling therapy of late or early stage metastatic disease in mice. In: Holland-Frei Cancer Medicine, 9th Edition, Eds. Bast Jr., Croce, Hait et al. 2017; p. 199–205.

8. Rampetsreiter P, Casanova E, Eferi R. Genetically modified mouse models of cancer invasion and metastasis. *Drug Discov Today Dis Models*. 2011;9:67–74.
9. Saxena M, Christofori G. Rebuilding cancer metastasis in the mouse. *Mol Oncol*. 2013;7(2):283–96.
10. Cho H, Herzka T, Zheng W, Qi J, Wilkinson JE, Bradner JE, Robinson BD, Castillo-Martin M, Cordon-Cardo C, Trotman LC. RapidCaP, a novel GEM model for metastatic prostate cancer analysis and therapy, reveals myc as a driver of Pten-mutant metastasis. *Cancer Discov*. 2014;4(3):318–33.
11. Hoffman RM. Orthotopic metastatic mouse models for anticancer drug discovery and evaluation: a bridge to the clinic. *Invest New Drugs*. 1999;17(4):343–59.
12. Hoffman RM. Patient-derived orthotopic xenografts: better mimic of metastasis than subcutaneous xenografts. *Nat Rev Cancer*. 2015;15(8):451–2.
13. Furukawa T, Kubota T, Watanabe M, Kitajima M, Hoffman RM. Orthotopic transplantation of histologically intact clinical specimens of stomach cancer to nude mice: correlation of metastatic sites in mouse and individual patient donors. *Int J Cancer*. 1993;53(4):608–12.
14. Fu X, Guadagni F, Hoffman RM. A metastatic nude-mouse model of human pancreatic cancer constructed orthotopically with histologically intact patient specimens. *Proc Natl Acad Sci U S A*. 1992;89(12):5645–9.
15. Hiroshima Y, Zhang Y, Zhang N, Maawy A, Mii S, Yamamoto M, Uehara F, Miwa S, Yano S, Murakami T, Momiyama M, Chishima T, Tanaka K, Ichikawa Y, Bouvet M, Murata T, Endo I, Hoffman RM. Establishment of a patient-derived orthotopic xenograft (PDOX) model of HER-2-positive cervical cancer expressing the clinical metastatic pattern. *PLoS One*. 2015;10(2):e0117417.
16. An Z, Jiang P, Wang X, Moossa AR, Hoffman RM. Development of a high metastatic orthotopic model of human renal cell carcinoma in nude mice: benefits of fragment implantation compared to cell-suspension injection. *Clin Exp Metastasis*. 1999;17(3):265–70.
17. Fu XY, Besterman JM, Monosov A, Hoffman RM. Models of human metastatic colon cancer in nude mice orthotopically constructed by using histologically intact patient specimens. *Proc Natl Acad Sci U S A*. 1991;88(20):9345–9.
18. Wang X, Fu X, Kubota T, Hoffman RM. A new patient-like metastatic model of human small-cell lung cancer constructed orthotopically with intact tissue via thoracotomy in nude mice. *Anticancer Res*. 1992;12(5):1403–6.
19. Fu X, Le P, Hoffman RM. A metastatic orthotopic-transplant nude-mouse model of human patient breast cancer. *Anticancer Res*. 1993;13(4):901–4.
20. Ebos JML, Lee CR, Cruz-Munoz W, Bjarnason GA, Christensen JG, Kerbel RS. Accelerated metastasis after short-term treatment with a potent inhibitor of tumor angiogenesis. *Cancer Cell*. 2009;15:232–9.
21. Wu FT, Man S, Xu P, Chow A, Paez-Ribes M, Lee CR, Pirie-Shepherd SR, Emmenegger U, Kerbel RS. Efficacy of cotargeting angiopoietin-2 and the VEGF pathway in the adjuvant post-surgical setting for early breast, colorectal, and renal cancers. *Cancer Res*. 2016;76(23):6988–7000.
22. Wu FT, Paez-Ribes M, Xu P, Man S, Bogdanovic E, Thurston G, Kerbel RS. Aflibercept and Ang1 supplementation improve neoadjuvant or adjuvant chemotherapy in a preclinical model of resectable breast cancer. *Sci Rep*. 2016;6:36694.
23. Munoz R, Man S, Shaked Y, Lee C, Wong J, Francia G, Kerbel RS. Highly efficacious non-toxic treatment for advanced metastatic breast cancer using combination UFT-cyclophosphamide metronomic chemotherapy. *Cancer Res*. 2006;66:3386–91.
24. Hackl C, Man S, Francia G, Xu P, Kerbel RS. Metronomic oral topotecan prolongs survival and reduces liver metastasis in improved preclinical orthotopic and adjuvant therapy colon cancer models. *Gut*. 2013;62:259–71.
25. Jedeszko C, Paez-Ribes M, Di Desidero T, Bocci G, Man S, Lee CR, Xu P, Bjarnason GA, Kerbel RS. Orthotopic primary and postsurgical adjuvant or metastatic renal cell carcinoma therapy models reveal potent anti-tumor activity of minimally toxic metronomic oral topotecan with pazopanib. *Sci Transl Med*. 2015;7(282):282ra250.

26. Hashimoto K, Man S, Xu P, Cruz-Munoz W, Tang T, Kumar R, Kerbel RS. Potent preclinical impact of metronomic low-dose oral topotecan combined with the antiangiogenic drug pazopanib for the treatment of ovarian cancer. *Mol Cancer Ther.* 2010;9:996–1006.
27. Cruz-Munoz W, Man S, Xu P, Kerbel RS. Development of a preclinical model of spontaneous human melanoma CNS metastasis. *Cancer Res.* 2008;68:4500–5.
28. Tang TC, Man S, Lee CR, Xu P, Kerbel RS. Impact of UFT/cyclophosphamide metronomic chemotherapy and antiangiogenic drug assessed in a new preclinical model of locally advanced orthotopic hepatocellular carcinoma. *Neoplasia.* 2010;12:264–74.
29. Francia G, Emmenegger U, Lee CR, Shaked Y, Folkins C, Mossoba M, Medin JA, Man S, Zhu Z, Witte L, Kerbel RS. Long term progression and therapeutic response of visceral metastatic disease non-invasively monitored in mouse urine using beta-hCG choriogonadotropin secreting tumor cell lines. *Mol Cancer Ther.* 2008;7:3452–9.
30. Francia G, Man S, Lee C-J, Lee CR, Xu P, Mossoba ME, Emmenegger U, Medin JA, Kerbel RS. Comparative impact of trastuzumab and cyclophosphamide on HER-2 positive human breast cancer xenografts. *Clin Cancer Res.* 2009;15:6358–66.
31. Palmieri D, Chambers AF, Felding-Habermann B, Huang S, Steeg PS. The biology of metastasis to a sanctuary site. *Clin Cancer Res.* 2007;13(6):1656–62.
32. Lin NU, Winer EP. Brain metastases: the HER2 paradigm. *Clin Cancer Res.* 2007;13(6):1648–55.
33. Cruz-Munoz W, Jaramillo ML, Man S, Xu P, Banville M, Collins C, Nantel A, Francia G, Morgan SS, Cranmer LD, O'Connor-McCourt MD, Kerbel RS. Roles for endothelin receptor B and BCL2A1 in spontaneous CNS metastasis of melanoma. *Cancer Res.* 2012;72(19):4909–19.
34. Guerin E, Man S, Xu P, Kerbel RS. A model of postsurgical advanced metastatic breast cancer more accurately replicates the clinical efficacy of antiangiogenic drugs. *Cancer Res.* 2013;73:2743–8.
35. Barrios CH, Liu MC, Lee SC, Vanlemmens L, Ferrero JM, Tabei T, Pivot X, Iwata H, Aogi K, Lugo-Quintana R, Harbeck N, Brickman MJ, Zhang K, Kern KA, Martin M. Phase III randomized trial of sunitinib versus capecitabine in patients with previously treated HER2-negative advanced breast cancer. *Breast Cancer Res Treat.* 2010;121(1):121–31.
36. Bergh J, Bondarenko IM, Lichinitser MR, Liljegren A, Greil R, Voytko NL, Makhson AN, Cortes J, Lortholary A, Bischoff J, Chan A, Delaloge S, Huang X, Kern KA, Giorgetti C. First-line treatment of advanced breast cancer with sunitinib in combination with docetaxel versus docetaxel alone: results of a prospective, randomized phase III study. *J Clin Oncol.* 2012;30(9):921–9.
37. Crown JP, Dieras V, Staroslawska E, Yardley DA, Bachelot T, Davidson N, Wildiers H, Fasching PA, Capitain O, Ramos M, Greil R, Cognetti F, Fountzilias G, Blasinska-Morawiec M, Liedtke C, Kreienberg R, Miller WH, Jr, Tassell V, Huang X, Paolini J, Kern KA, Romieu G. Phase III trial of sunitinib in combination with capecitabine versus capecitabine monotherapy for the treatment of patients with pretreated metastatic breast cancer. *J Clin Oncol* 2013;31(23):2870–2878.
38. Robert NJ, Saleh MN, Paul D, Generali D, Gressot L, Copur MS, Brufsky AM, Minton SE, Giguere JK, Smith JW, Richards PD, Gernhardt D, Huang X, Liau KF, Kern KA, Davis J. Sunitinib plus paclitaxel versus bevacizumab plus paclitaxel for first-line treatment of patients with advanced breast cancer: a phase III, randomized, open-label trial. *Clin Breast Cancer.* 2011;11(2):82–92.
39. Cameron D, Brown J, Dent R, Jackisch C, Mackey J, Pivot X, Steger GG, Suter TM, Toi M, Parmar M, Laeufle R, Im YH, Romieu G, Harvey V, Lipatov O, Pienkowski T, Cottu P, Chan A, Im SA, Hall PS, Bubuteishvili-Pacaud L, Henschel V, Deurloo RJ, Pallaud C, Bell R. Adjuvant bevacizumab-containing therapy in triple-negative breast cancer (BEATRICE): primary results of a randomised, phase 3 trial. *Lancet Oncol.* 2013;14(10):933–42.
40. Paez-Ribes M, Man S, Xu P, Kerbel RS. Potential pro-invasive or metastatic effects of preclinical antiangiogenic therapy are prevented by concurrent chemotherapy. *Clin Cancer Res.* 2015;21:5488–98.
41. Bear HD, Tang G, Rastogi P, Geyer CE, Jr, Liu Q, Robidoux A, Baez-Diaz L, Brufsky AM, Mehta RS, Fehrenbacher L, Young JA, Senecal FM, Gaur R, Margolese RG, Adams PT, Gross

- HM, Costantino JP, Paik S, Swain SM, Mamounas EP, Wolmark N. Neoadjuvant plus adjuvant bevacizumab in early breast cancer (NSABP B-40 [NRG Oncology]): secondary outcomes of a phase 3, randomised controlled trial. *Lancet Oncol* 2015;16(9):1037–1048.
42. Bridgeman VL, Vermeulen PB, Foo S, Bilecz A, Kostaras L, Daley F, Nathan M, Wan E, Frentzas S, Schweiger T, Hegedus B, Renyi-Vamos F, Vasudev N, Larkin J, Gore M, Dvorak HF, Paku S, Kerbel RS, Dome B, Reynolds AR. Vessel co-option is common in human lung metastases and mediates resistance to anti-angiogenic therapy in preclinical lung metastasis models. *J Pathol*. 2016;241(3):362–74. doi:[10.1002/path.4845](https://doi.org/10.1002/path.4845). Epub ahead of print.
  43. Szabo V, Bugyik E, Dezso K, Ecker N, Nagy P, Timar J, Tovari J, Laszlo V, Bridgeman VL, Wan E, Frentzas S, Vermeulen PB, Reynolds AR, Dome B, Paku S. Mechanism of tumour vascularisation in experimental lung metastases. *J Pathol*. 2015;235(3):384–96.
  44. Donnem T, Hu J, Ferguson M, Adighibe O, Snell C, Harris AL, Gatter KC, Pezzella F. Vessel co-option in primary human tumors and metastases: an obstacle to effective anti-angiogenic treatment? *Cancer Med*. 2013;2(4):427–36.
  45. Pezzella F, Di BA, Andreola S, Nicholson AG, Pastorino U, Harris AL. Angiogenesis in primary lung cancer and lung secondaries. *Eur J Cancer*. 1996;32A(14):2494–500.
  46. Vermeulen PB, Colpaert C, Salgado R, Royers R, Hellemans H, Van den Heuvel E, Goovaerts G, Dirix LY, Van ME. Liver metastases from colorectal adenocarcinomas grow in three patterns with different angiogenesis and desmoplasia. *J Pathol*. 2001;195(3):336–42.
  47. Kuczynski EA, Yin M, Bar-Zion A, Lee CR, Butz H, Man S, Daley F, Vermeulen P, Yousef G, Foster FS, Reynolds AR, Kerbel RS. Co-option of liver vessels and not sprouting angiogenesis drives acquired sorafenib resistance in hepatocellular carcinoma. *J Natl Cancer Inst* 2016;108(8). pii:djw030. doi:[10.1093/jnci/djw030](https://doi.org/10.1093/jnci/djw030).
  48. Frentzas S, Bridgeman VL, Simoneau E, Vermeulen PB, Foo S, Wotherspoon A, Gao Z-H, Lachapelle J, Van den Eynden G, Salman A, Lazaris A, Daley F, Gazinska P, Berg TJ, Eltahir Z, Peckitt C, Ritsma L, Van Rheenen J, Khashper A, Brown G, Nystrom H, Sund M, Loyer E, Dirix L, Metrakos P, Cunningham D, Reynolds AR. Vessel co-option mediates resistance to antiangiogenic therapy in liver metastases. *Nat Med*. 2016;22(11):1294–302.
  49. Pham E, Yin M, Peters CG, Lee CR, Brown D, Xu P, Man S, Jayaraman L, Rohde E, Chow A, Lazarus D, Eliasof S, Foster FS, Kerbel RS. Preclinical efficacy of bevacizumab with CRLX101, an investigational nanoparticle-drug conjugate, in treatment of metastatic triple-negative breast cancer. *Cancer Res*. 2016;76(15):4493–503. doi:[10.1158/0008-5472](https://doi.org/10.1158/0008-5472).
  50. DeRose YS, Wang G, Lin YC, Bernard PS, Buys SS, Ebbert MT, Factor R, Matsen C, Milash BA, Nelson E, Neumayer L, Randall RL, Stijleman IJ, Welm BE, Welm AL. Tumor grafts derived from women with breast cancer authentically reflect tumor pathology, growth, metastasis and disease outcomes. *Nat Med*. 2011;17(11):1514–20.
  51. Milsom CC, Lee CR, Hackl C, Man S, Kerbel RS. Differential post-surgical metastasis and survival in SCID, NOD-SCID and NOD-SCID-IL-2R $\gamma$  null mice with parental and subline variants of human breast cancer: implications for host defense mechanisms regulating metastasis. *PLoS One*. 2013;8(8):e71270.
  52. Kerbel RS, Kamen BA. Antiangiogenic basis of low-dose metronomic chemotherapy. *Nat Rev Cancer*. 2004;4:423–36.
  53. Pasquier E, Kavallaris M, Andre N. Metronomic chemotherapy: new rationale for new directions. *Nat Rev Clin Oncol*. 2010;7(8):455–65.
  54. Kato H, Ichinose Y, Ohta M, Hata E, Tsubota N, Tada H, Watanabe Y, Wada H, Tsuboi M, Hamajima N, Ohta M. A randomized trial of adjuvant chemotherapy with uracil-tegafur for adenocarcinoma of the lung. *N Engl J Med*. 2004;350(17):1713–21.
  55. Colleoni M, Gray KP, Gelber S, Lang I, Thurlimann B, Gianni L, Abdi EA, Gomez HL, Linderholm BK, Puglisi F, Tondini C, Kralidis E, Eniu A, Cagossi K, Rauch D, Chirgwin J, Gelber RD, Regan MM, Coates AS, Price KN, Viale G, Goldhirsch A. Low-dose oral cyclophosphamide and methotrexate maintenance for hormone receptor-negative early breast cancer: International Breast Cancer Study Group Trial 22-00. *J Clin Oncol*. 2016;34(28):3400–8.
  56. Ghiringhelli F, Larmonier N, Schmitt E, Parcellier A, Cathelin D, Garrido C, Chauffert B, Solary E, Bonnotte B, Martin F. CD4+CD25+ regulatory T cells suppress tumor immunity but

- are sensitive to cyclophosphamide which allows immunotherapy of established tumors to be curative. *Eur J Immunol.* 2004;34(2):336–44.
57. Folkins C, Man S, Shaked Y, Xu P, Hicklin DJ, Kerbel RS. Anti-cancer therapies combining antiangiogenic and tumor cell cytotoxic effects reduce the tumor stem-like cell fraction in glioma xenograft tumors. *Cancer Res.* 2007;67:3560–4.
  58. Chan T-S, Hsu C-C, Pai VC, Liao W-Y, Huang S-S, Tan K-T, Yen C-J, Hsu S-C, Chen W-Y, Shan Y-S, Li C-R, Lee MT, Jiang K-Y, Chu J-M, Lien G-S, Weaver VM, Tsai KK. Metronomic chemotherapy prevents therapy-induced stromal activation and induction of tumor-initiating cells. *J Exp Med.* 2016;213(13):2967–88.
  59. Simkens LHJ, van Tinteren H, May A, Ten Tije AJ, Creemers G-JM, Loosveld OJL, de Jongh FE, FLG E, Erjavec Z, van der Torren AME, Tol J, HJJ B, Nieboer P, van der Hoeven JJM, Haasjes JG, RLH J, Wals J, Cats A, Derleyn VA, Honkoop AH, Mol L, CJA P, Koopman M. Maintenance treatment with capecitabine and bevacizumab in metastatic colorectal cancer, the phase 3 CAIRO3 study of the Dutch Colorectal Cancer Group (DCCG). *Lancet.* 2015;385:1843–52.
  60. Andre N, Banavali S, Snihur Y, Pasquier E. Has the time come for metronomics in low-income and middle-income countries? *Lancet Oncol.* 2013;14(6):e239–48.
  61. Bocci G, Tuccori M, Emmenegger U, Liguori V, Kerbel RS, Del Tacca M. Cyclophosphamide-methotrexate “metronomic” chemotherapy for the palliative treatment of metastatic breast cancer. A comparative pharmacoeconomic evaluation. *Ann Oncol.* 2004;16:1243–52.
  62. Shaked Y. Balancing efficacy of and host immune responses to cancer therapy: the yin and yang effects. *Nat Rev Clin Oncol.* 2016;13(10):611–26.
  63. Hasnis E, Alishekevitz D, Gingis-Veltski S, Bril R, Fremder E, Voloshin T, Raviv Z, Karban A, Shaked Y. Anti-Bv8 antibody and metronomic gemcitabine improve pancreatic adenocarcinoma treatment outcome following weekly gemcitabine therapy. *Neoplasia.* 2014;16(6):501–10.



---

# Use of Patient-Derived Orthotopic Xenografts (PDOX) to Evaluate Transformative Cancer Therapeutics

# 13

Robert M. Hoffman

---

## Introduction

Our laboratory pioneered the patient-derived orthotopic xenograft (PDOX) nude mouse model with the technique of surgical orthotopic implantation (SOI) [1, 2], including pancreatic [3–14], breast [15], ovarian [16], lung [17], cervical [18–20], colon [21–23], and stomach [24] cancer, sarcoma [25–31], and melanoma [32–34].

The tumor-targeting *Salmonella typhimurium* A1-R (*S. typhimurium* A1-R) strain was developed by our laboratory [35, 36]. *S. typhimurium* A1-R is auxotrophic for Leu-Arg, which prevents it from mounting a continuous infection in normal tissues. *S. typhimurium* A1-R was able to inhibit or eradicate primary and metastatic tumors as monotherapy in nude mouse models of major cancers [37], including prostate [35, 38], breast [39–41], lung [42, 43], pancreatic [9, 11, 44–46], ovarian [47, 48] stomach [49], and cervical cancer [50], as well as sarcoma cell lines [26, 51–53] and glioma [54], all of which are highly aggressive tumor models.

---

R.M. Hoffman

AntiCancer, Inc., 7917 Ostrow Street, San Diego, CA 92111, USA

Department of Surgery, University of California, San Diego, San Diego, CA, USA

e-mail: [all@anticancer.com](mailto:all@anticancer.com)

© Springer International Publishing AG 2017

R.M. Hoffman (ed.), *Patient-Derived Mouse Models of Cancer*,

Molecular and Translational Medicine, DOI 10.1007/978-3-319-57424-0\_13

183

## PDOX Models to Evaluate Bacterial Therapy with *Salmonella* typhimurium A1-R

### Sarcoma PDOX

A patient high-grade undifferentiated pleomorphic soft-tissue sarcoma (UPS) from a striated muscle was grown orthotopically in the right biceps femoris muscle of nude mice to establish a PDOX model. Histological examination demonstrated eradication of the PDOX tumor with *S. typhimurium* A1-R followed by doxorubicin (DOX) [26] (Fig. 13.1a).

Follicular dendritic cell sarcoma (FDCS) is a rare and recalcitrant disease. A PDOX mouse model of FDCS was established in the biceps muscle of nude mice. The FDCS PDOX was resistant to both DOX and NVP-BEZ235, dactolisib

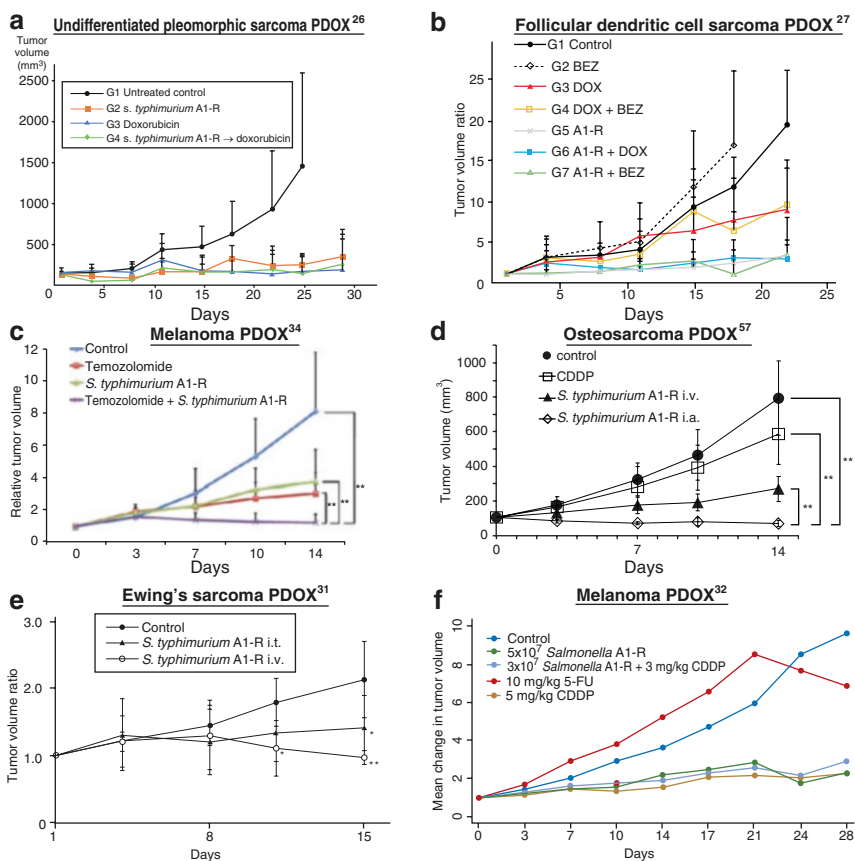


**Fig. 13.1** Patient sarcomas and melanomas were obtained at surgery, established in nude mice and subsequently implanted orthotopically in nude mice and treated with drugs indicated [26, 27, 30–34, 57]. DOX doxorubicin; CDDP cisplatin; BEZ dactolisib; A1-R *S. typhimurium* A1-R; 5-FU 5-fluorouracil

(BEZ), a dual pan-phosphoinositide 3-kinase-mammalian target of rapamycin inhibitor. In contrast to DOX and BEZ, the FDCS PDOX was sensitive to *S. typhimurium* A1-R. The combination of *S. typhimurium* A1-R and either DOX or BEZ did not increase the antitumor efficacy of *S. typhimurium* A1-R, indicating that DOX and BEZ were not active in this PDOX model. *S. typhimurium* A1-R was effective in a PDOX model of FDCS. The patient failed first-line DOX therapy, as did the PDOX model, which was sensitive to *S. typhimurium* A1-R [27] (Fig. 13.1b).

A PDOX model of osteosarcoma, established in the nude mouse distal femur with a lung metastasis, was resistant to CDDP as was the patient donor. The osteosarcoma PDOX model was sensitive to *S. typhimurium* A1-R administered intravenously (i.v.), but even more sensitive to *S. typhimurium* A1-R when administered intra-arterially, which caused regression of the tumor. Intra-arterial *S. typhimurium* A1-R was significantly more efficacious than when administered i.v. [57] (Fig. 13.1d).

A tumor from a patient with soft-tissue Ewing's sarcoma, who failed DOX therapy, was implanted in nude mice to establish a PDOX model. The PDOX model faithfully replicated the DOX resistance the Ewing's sarcoma had in the patient. *S. typhimurium* A1-R converted the Ewing's sarcoma from DOX resistant to sensitive. *S. typhimurium* A1-R administered intra-tumorally (i.t.) arrested the growth of the Ewing's sarcoma PDOX and *S. typhimurium* A1-R administered i.v. regressed the tumor [31] (Fig. 13.1e).

## Melanoma PDOX

*S. typhimurium* A1-R highly and selectively colonized a PDOX melanoma and significantly suppressed tumor growth. The combination of *Salmonella* A1-R and cisplatin (CDDP), both at low-dose, also significantly suppressed the growth of the melanoma PDOX [32], suggesting a role for *S. typhimurium* A1-R in combination therapy at low doses (Fig. 13.1f).

A melanoma, expressing the BRAF-V600E mutation, obtained from the right chest wall of a patient was grown orthotopically in the right chest wall of nude mice to establish a PDOX model. Temozolomide (TEM) combined with *S. typhimurium* was significantly more effective than either *S. typhimurium* A1-R alone or TEM alone. TEM combined with *S. typhimurium* A1-R could regress the melanoma in the PDOX model, again suggesting a role of *S. typhimurium* A1-R in combination chemotherapy [34] (Fig. 13.1c).

## Pancreatic Cancer PDOX

A pancreatic cancer PDOX was transplanted by SOI in transgenic nude RFP mice so that the PDOX stably acquired RFP-expressing stroma for the purpose of imaging the tumor after passage to non-transgenic nude mice in order to visualize the tumor growth and drug efficacy [7, 29] (See Chap. 7 and 15). The nude

mice with human pancreatic PDOX were treated with *S. typhimurium* A1-R or standard chemotherapy, including gemcitabine (GEM), which is a first-line therapy for pancreatic cancer, for comparison of efficacy. *S. typhimurium* A1-R treatment significantly reduced tumor weight, as well as tumor fluorescence area, compared to untreated control, with comparable efficacy of GEM, CDDP, and 5-fluorouracil (5-FU). Histopathological response to treatment was defined according to Evans's criteria, which showed *S. typhimurium* A1-R had increased efficacy compared to standard chemotherapy [9].

A pancreatic cancer PDOX that was VEGF-positive and an orthotopic VEGF-positive human pancreatic cancer cell line (MiaPaCa-2-GFP) as well as a VEGF-negative cell line (Panc-1) were evaluated for sensitivity to *S. typhimurium* A1-R in combination with anti-angiogenic agents. Nude mice with these tumors were treated with GEM, bevacizumab (BEV), and *S. typhimurium* A1-R. BEV/GEM followed by *S. typhimurium* A1-R significantly reduced tumor weight compared to BEV/GEM treatment alone in the PDOX and MiaPaCa-2 models. Neither treatment was as effective in the VEGF-negative model as in the VEGF-positive models. These results demonstrate that *S. typhimurium* A1-R following antiangiogenic therapy is effective on pancreatic cancer including the PDOX model [11].

## **PDOX Models to Determine Efficacy and Distinguish Similar Molecular-Targeting Drugs**

Ewing's sarcoma is a rare and aggressive malignancy. A chest-wall metastasis from a patient with Ewing's sarcoma with cyclin-dependent kinase inhibitor 2A/B (*CDKN2A/B*) loss and *FUS-ERG* fusion was implanted in the right chest wall of nude mice to establish a PDOX model. Tumor growth was significantly suppressed by CDK 4/6 inhibitor (palbociclib) and an IGF-1R inhibitor (linsitinib). In contrast, first-line therapy DOX did not inhibit tumor growth at any time point, which is consistent with the failure of DOX in the patient. The PDOX model identifies effective targeted molecular therapy of a recalcitrant DOX-resistant Ewing's sarcoma with specific genetic alterations [28].

The BRAF-V600E-mutant melanoma PDOX grown orthotopically in the right chest wall of nude mice described above was also tested with the molecularly targeting drug. Trametinib (TRA), an MEK inhibitor, was the only agent of the four tested that caused tumor regression. In contrast, another MEK inhibitor, cobimetinib (COB), could slow but not arrest growth or cause regression of the melanoma. First-line therapy temozolomide (TEM) could slow but not arrest tumor growth or cause regression. The BRAF-V600E-mutant melanoma was a candidate for vemurafenib (VEM) since VEM targets this mutation. However, VEM was not effective. The PDOX model thus helped identify the very high efficacy of TRA against the melanoma PDOX which was superior to COB even though they both target MEK. Genomic analysis alone was not sufficient for determining drug efficacy as the PDOX failed VEM and responded well to one MEK inhibitor and not another [33].

## Use of PDOX Models to Evaluate Anti-metastatic Agents

We evaluated the efficacy of zoledronic acid (ZA) on primary tumor growth and metastasis in a PDOX nude mouse model of pancreatic cancer. ZA alone did not significantly suppress tumor growth. The primary tumor weight of GEM + ZA-treated mice was significantly decreased compared to GEM alone-treated mice. No metastasis was detected in combination GEM + ZA-treated mice compared to the control group. In contrast, GEM alone could not suppress metastasis. The results indicate that ZA can selectively target metastasis in a pancreatic cancer PDOX model [12].

A subcutaneous nude mouse model of HER-2-expressing cervical carcinoma was not sensitive to entinostat (a benzamide histone deacetylase inhibitor). Entinostat also did not inhibit primary tumor growth in a PDOX model of this tumor. However, in the PDOX model, entinostat alone significantly reduced the metastatic tumor burden, compared to the control. Thus, only the PDOX model could be used to discover the antimetastatic activity of entinostat for this tumor. The results indicate the importance of using mouse models that can recapitulate metastatic cancer for precisely individualizing cancer therapy [19].

---

## Materials and Methods

### Mice

Use athymic *nu/nu* nude mice (AntiCancer Inc., San Diego, CA), 4–6-weeks-old. Conduct all animal studies with an AntiCancer Institutional Animal Care and Use Committee (IACUC) protocol specifically approved for this study and in accordance with the principles and procedures outlined in the National Institute of Health Guide for the Care and Use of Animals under Assurance Number A3873-1.

### Preparation and Administration of *S. typhimurium* A1-R

GFP-expressing *S. typhimurium* A1-R bacteria (AntiCancer, Inc., San Diego, CA, USA) were grown overnight on LB medium, and then diluted 1:10 in LB medium. The bacteria were harvested at late-log phase, wash with PBS, and then diluted in PBS. *S. typhimurium* A1-R was administered intratumorally or intravenously in PBS to each tumor [9, 11, 26, 27, 32, 34].

### Culture of GFP-Labeled *S. typhimurium* A1-R Bacteria from Tumor and Normal Organs

PDOX tumor tissues as well as normal organs (liver, spleen, and blood) were minced and diluted in 1:1, 1:10 and 1:100 with 100  $\mu$ L PBS, respectively. Each

dilution (10  $\mu$ l) were spotted on an LB agar plate containing 50  $\mu$ g/mL ampicillin, and incubated at 37 °C for 24 h. Colonies are visualized by GFP expression and quantitated per mg of tissue [32].

## Imaging of *S. typhimurium* A1-R in Tumors

An FV1000 confocal microscope (Olympus) [55] or equivalent was used to image resected tumors for the presence of *S. typhimurium* A1-R-GFP. An OV100 (Olympus) variable-magnification fluorescence imager [56] or equivalent was used to image colonies of *S. typhimurium* A1-R grown from resected tumors.

## Histological Analysis

Tumor samples in 10% formalin were embedded in paraffin before sectioning and staining. Tissue sections (5  $\mu$ m) were deparaffinized in xylene and rehydrated in an ethanol series. Hematoxylin and eosin (H & E) staining was performed according to standard protocol [26].

---

## References

1. Hoffman RM. Patient-derived orthotopic xenografts: better mimic of metastasis than subcutaneous xenografts. *Nat Rev Cancer*. 2015;15:451–2.
2. Hoffman RM. Orthotopic metastatic mouse models for anticancer drug discovery and evaluation: a bridge to the clinic. *Invest New Drugs*. 1999;17:343–59.
3. Fu X, Guadagni F, Hoffman RM. A metastatic nude-mouse model of human pancreatic cancer constructed orthotopically from histologically intact patient specimens. *Proc Natl Acad Sci U S A*. 1992;89:5645–9.
4. Kaushal S, McElroy MK, Luiken GA, Talamini MA, Moossa AR, Hoffman RM, Bouvet M. Fluorophore-conjugated anti-CEA antibody for the intraoperative imaging of pancreatic and colorectal cancer. *J Gastrointest Surg*. 2008;12:1938–50.
5. Suetsugu A, Katz M, Fleming J, Moriwaki H, Bouvet M, Saji S, Hoffman RM. Multi-color palette of fluorescent proteins for imaging the tumor microenvironment of orthotopic tumorgraft mouse models of clinical pancreatic cancer specimens. *J Cell Biochem*. 2012;113:2290–5.
6. Suetsugu A, Katz M, Fleming J, Truty M, Thomas R, Saji S, Moriwaki H, Bouvet M, Hoffman RM. Imageable fluorescent metastasis resulting in transgenic GFP mice orthotopically implanted with human-patient primary pancreatic cancer specimens. *Anticancer Res*. 2012;32:1175–80.
7. Suetsugu A, Katz M, Fleming J, Truty M, Thomas R, Saji S, Moriwaki H, Bouvet M, Hoffman RM. Non-invasive fluorescent-protein imaging of orthotopic pancreatic-cancer-patient tumorgraft progression in nude mice. *Anticancer Res*. 2012;32:3063–8.
8. Hiroshima Y, Maawy A, Sato S, Murakami T, Uehara F, Miwa S, Yano S, Momiyama M, Chishima T, Tanaka K, Bouvet M, Endo I, Hoffman RM. Hand-held high-resolution fluorescence imaging system for fluorescence-guided surgery of patient and cell-line pancreatic tumors growing orthotopically in nude mice. *J Surg Res*. 2014;187:510–7.
9. Hiroshima Y, Zhao M, Maawy A, Zhang Y, Katz MH, Fleming JB, Uehara F, Miwa S, Yano S, Momiyama M, Suetsugu A, Chishima T, Tanaka K, Bouvet M, Endo I, Hoffman RM. Efficacy of *Salmonella typhimurium* A1-R versus chemotherapy on a pancreatic cancer patient-derived orthotopic xenograft (PDOX). *J Cell Biochem*. 2014;115:1254–61.

10. Hiroshima Y, Maawy A, Zhang Y, Murakami T, Momiyama M, Mori R, Matsuyama R, Katz MH, Fleming JB, Chishima T, Tanaka K, Ichikawa Y, Endo I, Hoffman RM, Bouvet M. Metastatic recurrence in a pancreatic cancer patient derived orthotopic xenograft (PDOX) nude mouse model is inhibited by neoadjuvant chemotherapy in combination with fluorescence-guided surgery with an anti-CA 19-9-conjugated fluorophore. *PLoS One*. 2014;9:e114310.
11. Hiroshima Y, Zhang Y, Murakami T, Maawy AA, Miwa S, Yamamoto M, Yano S, Sato S, Momiyama M, Mori R, Matsuyama R, Chishima T, Tanaka K, Ichikawa Y, Bouvet M, Endo I, Zhao M, Hoffman RM. Efficacy of tumor-targeting *Salmonella typhimurium* A1-R in combination with anti-angiogenesis therapy on a pancreatic cancer patient-derived orthotopic xenograft (PDOX) and cell line mouse models. *Oncotarget*. 2014;5:12346–57.
12. Hiroshima Y, Maawy AA, Katz MH, Fleming JB, Bouvet M, Endo I, Hoffman RM. Selective efficacy of zoledronic acid on metastasis in a patient-derived orthotopic xenograft (PDOX) nude-mouse model of human pancreatic cancer. *J Surg Oncol*. 2015;111:311–5.
13. Hiroshima Y, Maawy A, Zhan Y, Murakami T, Momiyama M, Mori R, Matsuyama R, Chishima T, Tanaka K, Ichikawa Y, Endo I, Hoffman RM, Bouvet M. Fluorescence-guided surgery, but not bright-light surgery, prevents local recurrence in a pancreatic cancer patient-derived orthotopic xenograft (PDOX) model resistant to neoadjuvant chemotherapy (NAC). *Pancreatology*. 2015;15:295–301.
14. Yano S, Hiroshima Y, Maawy A, Kishimoto H, Suetsugu A, Miwa S, Toneri M, Yamamoto M, Katz MHG, Fleming JB, Urata Y, Tazawa H, Kagawa S, Bouvet M, Fujiwara T, Hoffman RM. Color-coding cancer and stromal cells with genetic reporters in a patient-derived orthotopic xenograft (PDOX) model of pancreatic cancer enhances fluorescence-guided surgery. *Cancer Gene Ther*. 2015;22:344–50.
15. Fu X, Le P, Hoffman RM. A metastatic-orthotopic transplant nude-mouse model of human patient breast cancer. *Anticancer Res*. 1993;13:901–4.
16. Fu X, Hoffman RM. Human ovarian carcinoma metastatic models constructed in nude mice by orthotopic transplantation of histologically-intact patient specimens. *Anticancer Res*. 1993;13:283–6.
17. Wang X, Fu X, Hoffman RM. A new patient-like metastatic model of human lung cancer constructed orthotopically with intact tissue via thoracotomy in immunodeficient mice. *Int J Cancer*. 1992;51:992–5.
18. Hiroshima Y, Zhang Y, Zhang M, Maawy A, Mii S, Yamamoto M, Uehara F, Miwa S, Yano S, Murakami T, Momiyama M, Chishima T, Tanaka K, Ichikawa Y, Bouvet M, Murata T, Endo I, Hoffman RM. Establishment of a patient-derived orthotopic xenograft (PDOX) model of HER-2-positive cervical cancer expressing the clinical metastatic pattern. *PLoS One*. 2015;10:e0117417.
19. Hiroshima Y, Maawy A, Zhang Y, Zhang N, Murakami T, Chishima T, Tanaka K, Ichikawa Y, Bouvet M, Endo I, Hoffman RM. Patient-derived mouse models of cancer need to be orthotopic in order to evaluate targeted anti-metastatic therapy. *Oncotarget*. 2016;7:71696–702.
20. Murakami T, Murata T, Kawaguchi K, Kiyuna T, Igarashi K, Hwang HK, Hiroshima Y, Hozumi C, Komatsu S, Kikuchi T, Lwin TM, Delong JC, Miyake K, Zhang Y, Tanaka K, Bouvet M, Endo I, Hoffman RM. Cervical cancer patient-derived orthotopic xenograft (PDOX) is sensitive to cisplatinum and resistant to nab-paclitaxel. *Anticancer Res*. 2017;37:61–5.
21. Fu X, Besterman JM, Monosov A, Hoffman RM. Models of human metastatic colon cancer in nude mice orthotopically constructed by using histologically intact patient specimens. *Proc Natl Acad Sci U S A*. 1991;88:9345–9.
22. Metildi CA, Kaushal S, Luiken GA, Talamini MA, Hoffman RM, Bouvet M. Fluorescently-labeled chimeric anti-CEA antibody improves detection and resection of human colon cancer in a patient-derived orthotopic xenograft (PDOX) nude mouse model. *J Surg Oncol*. 2014;109:451–8.
23. Hiroshima Y, Maawy A, Metildi CA, Zhang Y, Uehara F, Miwa S, Yano S, Sato S, Murakami T, Momiyama M, Chishima T, Tanaka K, Bouvet M, Endo I, Hoffman RM. Successful fluorescence-guided surgery on human colon cancer patient-derived orthotopic xenograft mouse models using a fluorophore-conjugated anti-CEA antibody and a portable imaging system. *J Laparoendosc Adv Surg Tech A*. 2014;24:241–7.

24. Furukawa T, Kubota T, Watanabe M, Kitajima M, Fu X, Hoffman RM. Orthotopic transplantation of histologically intact clinical specimens of stomach cancer to nude mice: correlation of metastatic sites in mouse and individual patient donors. *Int J Cancer*. 1993;53:608–12.
25. Hiroshima Y, Zhao M, Zhang Y, Zhang N, Maawy A, Murakami T, Mii S, Uehara F, Yamamoto M, Miwa S, Yano S, Momiyama M, Mori R, Matsuyama R, Chishima T, Tanaka K, Ichikawa Y, Bouvet M, Endo I, Hoffman RM. Tumor-targeting *Salmonella typhimurium* A1-R arrests a chemo-resistant patient soft-tissue sarcoma in nude mice. *PLoS One*. 2015;10:e0134324.
26. Murakami T, DeLong J, Eilber FC, Zhao M, Zhang Y, Zhang N, Singh A, Russell T, Deng S, Reynoso J, Quan C, Hiroshima Y, Matsuyama R, Chishima T, Tanaka K, Bouvet M, Chawla S, Endo I, Hoffman RM. Tumor-targeting *Salmonella typhimurium* A1-R in combination with doxorubicin eradicate soft tissue sarcoma in a patient-derived orthotopic xenograft PDOX model. *Oncotarget*. 2016;7:12783–90.
27. Kiyuna T, Murakami T, Tome Y, Kawaguchi K, Igarashi K, Zhang Y, Zhao M, Li Y, Bouvet M, Kanaya F, Singh A, Dry S, Eilber FC, Hoffman RM. High efficacy of tumor-targeting *Salmonella typhimurium* A1-R on a doxorubicin- and dactolisib-resistant follicular dendritic-cell sarcoma in a patient-derived orthotopic xenograft PDOX nude mouse model. *Oncotarget*. 2016;7:33046–54.
28. Murakami T, Singh AS, Kiyuna T, Dry SM, Li Y, James AW, Igarashi K, Kawaguchi K, DeLong JC, Zhang Y, Hiroshima Y, Russell T, Eckardt MA, Yanagawa J, Federman N, Matsuyama R, Chishima T, Tanaka K, Bouvet M, Endo I, Eilber FC, Hoffman RM. Effective molecular targeting of *CDK4/6* and *IGF-1R* in a rare *FUS-ERG* fusion *CDKN2A*-deletion doxorubicin-resistant Ewing's sarcoma in a patient-derived orthotopic xenograft (PDOX) nude-mouse model. *Oncotarget*. 2016;7:47556–64.
29. Kiyuna T, Murakami T, Tome Y, Igarashi K, Kawaguchi K, Russell T, Eckhardt MA, Crompton J, Singh A, Bernthal N, Bukata S, Federman N, Kanaya F, Eilber FC, Hoffman RM. Labeling the stroma of a patient-derived orthotopic xenograft (PDOX) mouse models of undifferentiated pleomorphic soft-tissue sarcoma with red fluorescent protein for rapid non-invasive drug screening. *J Cell Biochem*. 2017;118(2):361–5.
30. Igarashi K, Kawaguchi K, Kiyuna T, Murakami T, Miwa S, Nelson SD, Dry SM, Li Y, Singh A, Kimura H, Hayashi K, Yamamoto N, Tsuchiya H, Eilber FC, Hoffman RM. Temozolomide combined with irinotecan caused regression in an adult pleomorphic rhabdomyosarcoma patient-derived orthotopic xenograft (PDOX) nude-mouse model. *Oncotarget* in press. doi: [10.18632/oncotarget.16548](https://doi.org/10.18632/oncotarget.16548)
31. Murakami T, Kiyuna T, Kawaguchi K, Igarashi K, Singh AS, Hiroshima Y, Zhang Y, Zhao M, Miyake K, Nelson SD, Dry SM, Li Y, DeLong JC, Lwin TM, Chishima T, Tanaka K, Bouvet M, Endo I, Eilber FC, Hoffman RM. The irony of highly-effective bacterial therapy of a patient-derived mouse model of Ewing's sarcoma, which was blocked by Ewing himself 80 years ago. *Cell Cycle* 2017;16:1046–52.
32. Yamamoto M, Zhao M, Hiroshima Y, Zhang Y, Shurell E, Eilber FC, Bouvet M, Noda M, Hoffman RM. Efficacy of tumor-targeting *Salmonella typhimurium* A1-R on a melanoma patient-derived orthotopic xenograft (PDOX) nude-mouse model. *PLoS One*. 2016;11:e0160882.
33. Kawaguchi K, Murakami T, Chmielowski B, Igarashi K, Kiyuna T, Unno M, Nelson SD, Russell TA, Dry SM, Li Y, Eilber FC, Hoffman RM. Vemurafenib-resistant BRAF-V600E mutated melanoma is regressed by MEK targeting drug trametinib, but not cobimetinib in a patient-derived orthotopic xenograft (PDOX) mouse model. *Oncotarget*. 2016;7:71731–43.
34. Kawaguchi K, Igarashi K, Murakami T, Chmielowski B, Kiyuna T, Zhao M, Zhang Y, Singh A, Unno M, Nelson SD, Russell T, Dry SM, Li Y, Eilber FC, Hoffman RM. Tumor-targeting *Salmonella typhimurium* A1-R combined with temozolomide regresses malignant melanoma with a BRAF-V600E mutation in a patient-derived orthotopic xenograft (PDOX) model. *Oncotarget*. 2016;7:85929–36.
35. Zhao M, Yang M, Li X-M, Jiang P, Baranov E, Li S, Xu M, Penman S, Hoffman RM. Tumor-targeting bacterial therapy with amino acid auxotrophs of GFP-expressing *Salmonella typhimurium*. *Proc Natl Acad Sci U S A*. 2005;102:755–60.



36. Zhang Y, Zhang N, Zhao M, Hoffman RM. Comparison of the selective targeting efficacy of *Salmonella typhimurium* A1-R and VNP20009 on the Lewis lung carcinoma in nude mice. *Oncotarget*. 2015;6:14625–31.
37. Hoffman RM, editor. Bacterial therapy of cancer: methods and protocols. *Methods in Molecular Biology* 1409 (Walker JM, series editor). New York: Humana Press (Springer Science+Business Media); 2016.
38. Zhao M, Geller J, Ma H, Yang M, Penman S, Hoffman RM. Monotherapy with a tumor-targeting mutant of *Salmonella typhimurium* cures orthotopic metastatic mouse models of human prostate cancer. *Proc Natl Acad Sci U S A*. 2007;104:10170–4.
39. Zhao M, Yang M, Ma H, Li X, Tan X, Li S, Yang Z, Hoffman RM. Targeted therapy with a *Salmonella typhimurium* leucine-arginine auxotroph cures orthotopic human breast tumors in nude mice. *Cancer Res*. 2006;66:7647–52.
40. Zhang Y, Tome Y, Suetsugu A, Zhang L, Zhang N, Hoffman RM, Zhao M. Determination of the optimal route of administration of *Salmonella typhimurium* A1-R to target breast cancer in nude mice. *Anticancer Res*. 2012;32:2501–8.
41. Zhang Y, Miwa S, Zhang N, Hoffman RM, Zhao M. Tumor-targeting *Salmonella typhimurium* A1-R arrests growth of breast-cancer brain metastasis. *Oncotarget*. 2015;6:2615–22.
42. Uchugonova A, Zhao M, Zhang Y, Weinigel M, König K, Hoffman RM. Cancer-cell killing by engineered *Salmonella* imaged by multiphoton tomography in live mice. *Anticancer Res*. 2012;32:4331–9.
43. Liu F, Zhang L, Hoffman RM, Zhao M. Vessel destruction by tumor-targeting *Salmonella typhimurium* A1-R is enhanced by high tumor vascularity. *Cell Cycle*. 2010;9:4518–24.
44. Nagakura C, Hayashi K, Zhao M, Yamauchi K, Yamamoto N, Tsuchiya H, Tomita K, Bouvet M, Hoffman RM. Efficacy of a genetically modified *Salmonella typhimurium* in an orthotopic human pancreatic cancer in nude mice. *Anticancer Res*. 2009;29:1873–8.
45. Yam C, Zhao M, Hayashi K, Ma H, Kishimoto H, McElroy M, Bouvet M, Hoffman RM. Monotherapy with a tumor-targeting mutant of *S. typhimurium* inhibits liver metastasis in a mouse model of pancreatic cancer. *J Sur Res*. 2010;164:248–55.
46. Hiroshima Y, Zhao M, Zhang Y, Maawy A, Hassanein MK, Uehara F, Miwa S, Yano S, Momiyama M, Suetsugu A, Chishima T, Tanaka K, Bouvet M, Endo I, Hoffman RM. Comparison of efficacy of *Salmonella typhimurium* A1-R and chemotherapy on stem-like and non-stem human pancreatic cancer cells. *Cell Cycle*. 2013;12:2774–80.
47. Matsumoto Y, Miwa S, Zhang Y, Hiroshima Y, Yano S, Uehara F, Yamamoto M, Toneri M, Bouvet M, Matsubara H, Hoffman RM, Zhao M. Efficacy of tumor-targeting *Salmonella typhimurium* A1-R on nude mouse models of metastatic and disseminated human ovarian cancer. *J Cell Biochem*. 2014;115:1996–2003.
48. Matsumoto Y, Miwa S, Zhang Y, Zhao M, Yano S, Uehara F, Yamamoto M, Hiroshima Y, Toneri M, Bouvet M, Matsubara H, Tsuchiya H, Hoffman RM. Intraperitoneal administration of tumor-targeting *Salmonella typhimurium* A1-R inhibits disseminated human ovarian cancer and extends survival in nude mice. *Oncotarget*. 2015;6:11369–77.
49. Yano S, Zhang Y, Zhao M, Hiroshima Y, Miwa S, Uehara F, Kishimoto H, Tazawa H, Bouvet M, Fujiwara T, Hoffman RM. Tumortargeting *Salmonella typhimurium* A1-R decoys quiescent cancer cells to cycle as visualized by FUCCI imaging and become sensitive to chemotherapy. *Cell Cycle*. 2014;13:3958–63.
50. Hiroshima Y, Zhang Y, Zhao M, Zhang N, Murakami T, Maawy A, Mii S, Uehara F, Yamamoto M, Miwa S, Yano S, Momiyama M, Mori R, Matsuyama R, Chishima T, Tanaka K, Ichikawa Y, Bouvet M, Endo I, Hoffman RM. Tumor-targeting *Salmonella typhimurium* A1-R in combination with Trastuzumab eradicates HER-2-positive cervical cancer cells in patient-derived mouse models. *PLoS One*. 2015;10:e0120358.
51. Hayashi K, Zhao M, Yamauchi K, Yamamoto N, Tsuchiya H, Tomita K, Hoffman RM. Cancer metastasis directly eradicated by targeted therapy with a modified *Salmonella typhimurium*. *J Cell Biochem*. 2009;106:992–8.
52. Hayashi K, Zhao M, Yamauchi K, Yamamoto N, Tsuchiya H, Tomita K, Kishimoto H, Bouvet M, Hoffman RM. Systemic targeting of primary bone tumor and lung metastasis of high-grade

- osteosarcoma in nude mice with a tumor-selective strain of *Salmonella typhimurium*. *Cell Cycle*. 2009;8:870–5.
53. Miwa S, Zhang Y, Baek K-E, Uehara F, Yano S, Yamamoto M, Hiroshima Y, Matsumoto Y, Kimura H, Hayashi K, Yamamoto N, Bouvet M, Tsuchiya H, Hoffman RM, Zhao M. Inhibition of spontaneous and experimental lung metastasis of soft-tissue sarcoma by tumortargeting *Salmonella typhimurium* A1-R. *Oncotarget*. 2014;5:12849–61.
  54. Momiyama M, Zhao M, Kimura H, Tran B, Chishima T, Bouvet M, Endo I, Hoffman RM. Inhibition and eradication of human glioma with tumor-targeting *Salmonella typhimurium* in an orthotopic nude-mouse model. *Cell Cycle*. 2012;11:628–32.
  55. Uchugonova A, Duong J, Zhang N, König K, Hoffman RM. The bulge area is the origin of nestin-expressing pluripotent stem cells of the hair follicle. *J Cell Biochem*. 2011;112:2046–50.
  56. Yamauchi K, Yang M, Jiang P, Xu M, Yamamoto N, Tsuchiya H, Tomita K, Moossa AR, Bouvet M, Hoffman RM. Development of real-time subcellular dynamic multicolor imaging of cancer-cell trafficking in live mice with a variable-magnification whole-mouse imaging system. *Cancer Res*. 2006;66:4208–14.
  57. Igarashi K, Kawaguchi K, Murakami T, Kiyuna T, Miyake K, Nelson SD, Dry SM, Li Y, Yanagawa J, Russell TA, Singh A, Yamamoto N, Hayashi K, Kimura H, Miwa S, Tsuchiya H, Eilber FC, Hoffman RM. Intra-arterial administration of tumor-targeting *Salmonella typhimurium* A1-R regresses a cisplatin-resistant relapsed osteosarcoma in a patient-derived orthotopic xenograft (PDOX) mouse model. *Cell Cycle* 2017;16:1164–70.

---

# Fluorescent Protein-Expressing Transgenic Nude Mice as Hosts for Patient Tumors

# 14

Robert M. Hoffman

---

## Introduction

Patient-derived xenografts (PDX) have made important contributions to our understanding and treatment of cancer. The initial PDX model in 1969 [1] (please see Chap. 1), and the model which is still predominant, comprises subcutaneously-transplanted patient tumors in immuno-deficient mice. Since subcutaneous tumors rarely metastasize, tumor growth is easily measured with calipers. However, the orthotopic PDX model, which we have termed patient-derived orthotopic xenograft (PDOX), has tumors growing and metastasizing on internal organs. Therefore, internal tumor growth and metastasis require an external means of monitoring. The use of nude mice ubiquitously expressing bright fluorescent proteins offers an opportunity to image the orthotopic tumors by contrast or by labeling the PDOX tumor with fluorescent stroma (please see Chap. 15).

## GFP Nude Mouse

Okabe et al. [2] produced transgenic mice with GFP under the control of a chicken  $\beta$ -actin promoter and cytomegalovirus enhancer. All of the tissues from these transgenic mice, with the exception of erythrocytes and hair, fluoresce green. In the parental immuno-competent GFP mouse, red fluorescent protein (RFP)-expressing murine cancer cells were transplanted [3–5], enabling color-coded fluorescence

---

R.M. Hoffman

AntiCancer, Inc., 7917 Ostrow Street, San Diego, CA 92111, USA

Department of Surgery, University of California, San Diego, San Diego, CA, USA

e-mail: [all@anticancer.com](mailto:all@anticancer.com)

imaging of the tumor–host interaction in the living state, including tumor angiogenesis and immunology [4].

In order to visualize the tumor microenvironment (TME) of human tumors, we developed and characterized the transgenic GFP nude mouse with ubiquitous GFP expression. The GFP nude mouse, which is a unique construct, was obtained by crossing non-transgenic nude mice with transgenic GFP C57/B6 mice described above. The GFP nude mouse was used to visualize the growth, metastasis, and tumor–host interaction of human cancer cell lines or patient tumors expressing RFP [5–8].

## RFP Nude Mouse

Nagy's group developed an RFP variant, DsRed.T3, enabling them to produce a transgenic RFP mouse with DsRed.T3 driven by the  $\beta$ -actin promoter [9]. Using this mouse, we developed a transgenic RFP nude mouse by crossing non-transgenic nude mice with the RFP transgenic mouse. The RFP transgenic mouse serves as a host for GFP or GFP-RFP-labeled human cancer cells [10] or patient tumors [6–8].

## CFP Nude Mouse

The transgenic cyan fluorescent protein CK6/ECFP mouse was also developed by Nagy [11]. We crossed non-fluorescent nude mice with the transgenic CK6/ECFP mouse to obtain the CFP nude mouse. The CFP nude mouse exhibited the same fluorescence pattern that we previously described in the wild-type CK6/ECFP mouse [9]. The CFP nude mouse expresses blue fluorescence in nearly all its tissues but at much different intensities. Among internal organs, the pancreas displays the strongest CFP blue fluorescence signal [12].

## Nestin-Dependent (ND) GFP Nude Mouse

We crossed the ND-GFP-C57/B6 mouse onto the nude background to obtain ND-GFP nude mice. The ND-GFP mouse brightly expresses GFP in nascent blood vessels among other organs. Dual-color fluorescence imaging visualized nascent tumor angiogenesis of various human and mouse cancer cell lines expressing RFP transplanted in the ND-GFP nude mouse [13].

---

## Materials and Methods

### Transgenic Green Fluorescent Protein (GFP) Nude Mice

1. Cross 6-week-old transgenic GFP female C57/B6 mice with 6- to 8-week-old *nu/nu* male mice (Harlan, Indianapolis, IN).
2. Cross male F<sub>1</sub> mice with female F<sub>1</sub> C57/B6 GFP mice.

3. Cross female F<sub>2</sub> immunocompetent GFP *nu/+* mice with male GFP nude mice, or back-cross F<sub>2</sub> GFP male nude mice with female F<sub>1</sub> immunocompetent GFP mice to obtain approximately 50% of the offspring as GFP nude mice.
4. GFP nude mice can be consistently produced by the methods described above.

### **Transgenic Red Fluorescent Protein (RFP) Nude Mice**

1. Cross 6-week-old transgenic RFP female mice with both 6- to 8-week-old *nu/nu* male mice (Harlan, Indianapolis, IN).
2. Cross male F<sub>1</sub> mice with female F<sub>1</sub> immunocompetent RFP mice.
3. Cross female F<sub>2</sub> immunocompetent RFP mice with male RFP nude mice, or back-cross F<sub>2</sub> RFP nude male to female F<sub>1</sub> immunocompetent RFP *nu/+* mice to obtain approximately 50% of their offspring as RFP nude mice.
4. RFP nude mice were then consistently produced using the methods described above.

### **Transgenic Cyan Fluorescent Protein (CFP) Nude Mice**

1. Cross 6-week-old transgenic CFP female mice with 6- to 8-week-old *nu/nu* male mice (Harlan, Indianapolis, IN).
2. Cross male F<sub>1</sub> mice with female F<sub>1</sub> immunocompetent CFP mice.
3. Cross male F<sub>2</sub> *nu/nu* CFP immunocompetent mice with female F<sub>1</sub> or F<sub>2</sub> *nu/+* CFP immunocompetent mice to obtain approximately 50% of their offspring as CFP nude mice.

### **Transgenic Nestin-Driven Green Fluorescent Protein (ND-GFP) Nude Mice**

1. Cross 6-week-old transgenic ND-GFP female C57/B6 mice with 6- to 8-week-old *nu/nu* male mice (Harlan, Indianapolis, IN).
2. Cross male F<sub>1</sub> nude mice with female F<sub>1</sub> C57/B6 ND-GFP mice.
3. Cross female F<sub>2</sub> immunocompetent ND-GFP *nu/+* mice with male ND-GFP nude mice, or back-cross F<sub>2</sub> ND-GFP nude male mice with female F<sub>1</sub> immunocompetent ND-GFP mice to obtain approximately 50% of the offspring as ND-GFP nude mice.

### **Whole-Body Imaging**

The Olympus OV100 whole-mouse imaging system (Olympus Corp., Tokyo, Japan), containing an MT-20 light source (Olympus Biosystems, Planegg, Germany) and DP70 CCD camera (Olympus), was used for subcellular imaging in live mice. The optics of the OV100 fluorescence imaging system have been specially developed for macro-imaging as well as micro-imaging with high light-gathering capacity. The

instrument incorporates a unique combination of high-numerical aperture and long working distance. Multiple individually-optimized objective lenses, parcentered and parfocal, provide a 105-fold magnification range for seamless imaging of the entire body down to the subcellular level without disturbing the animal. The OV100 has the lenses mounted on an automated turret with a high magnification range of  $\times 1.6$  to  $\times 16$  and a field of view ranging from 6.9 to 0.69 mm. The optics and anti-reflective coatings ensure optimal imaging of multiplexed fluorescent reporters in small animals. High-resolution images were captured directly on a PC (Fujitsu Siemens, Munich, Germany). Images were processed for contrast and brightness and analyzed with the use of Paint Shop Pro 8 and Cell<sup>®</sup> (Olympus Biosystems) [14].

## Scanning Laser Imaging

The Olympus IV100 microscope is a scanning laser microscope. A 488 nm argon laser was used. The novel stick objectives (as small as 1.3 mm) were designed specifically for this laser scanning microscope. The very narrow objectives deliver very high resolution images. A PC computer running FluoView software (Olympus Corp.) was used to control the microscope. All images were recorded and stored as proprietary multilayer 16-bit Tagged Image File Format files [15].

## Confocal Microscopy

Confocal two-photon microscopy (FluoView FV1000, Olympus Corp., Tokyo, Japan) was used for two- ( $x,y$ ) and three-dimensional (3D,  $x,y,z$ ) high-resolution imaging. A cw semiconductor laser at 473 nm for GFP excitation and a tunable Mai Tai HP femtosecond laser emitting at 700–1020 nm (Newport Spectra-Physics, Irvine, CA) can be used for deep tissue imaging of autofluorescence and GFP. Fluorescence images were obtained using the 20  $\times/0.50$  UPlan FLN and 40  $\times/1.3$  Oil Olympus UPLAN FLN objectives [16].

---

## Results and Discussion

### Characterization of the Green Fluorescent Protein (GFP) Nude Mouse

In crosses between *nu/nu* GFP male mice and *nu/+* GFP female mice, the resultant embryos were green, apparently at the single-cell stage. Newborn mice and adult mice were very bright green. Green fluorescence could be detected with a simple blue-light-emitting diode flashlight with a central peak of 470 nm and a bypass emission filter (Chroma Technology) [5]. In the adult mice, the organs all brightly expressed GFP, including the heart, lungs, spleen, pancreas, esophagus, stomach, adrenal gland, kidney, and duodenum (Fig. 14.1). The entire digestive system was

dissected out from tongue to anus and could be seen to fluoresce brilliant green upon blue-light excitation. The male and female reproductive systems were dissected out, and all components fluoresced bright green on blue-light excitation. The dissected brain and spinal cord also had brilliant GFP fluorescence. The dissected-out circulatory system, including the heart and major arteries and veins, had a brilliant green fluorescence. The skinned skeleton highly expressed GFP. Pancreatic islets showed GFP fluorescence. The spleen cells were also GFP positive [5].

The GFP nude mice appear to have a life span similar to that of non-GFP nude mice, such that long-term tumor growth and metastasis studies can be carried out. The normal life span of the GFP nude and immunocompetent mice demonstrates

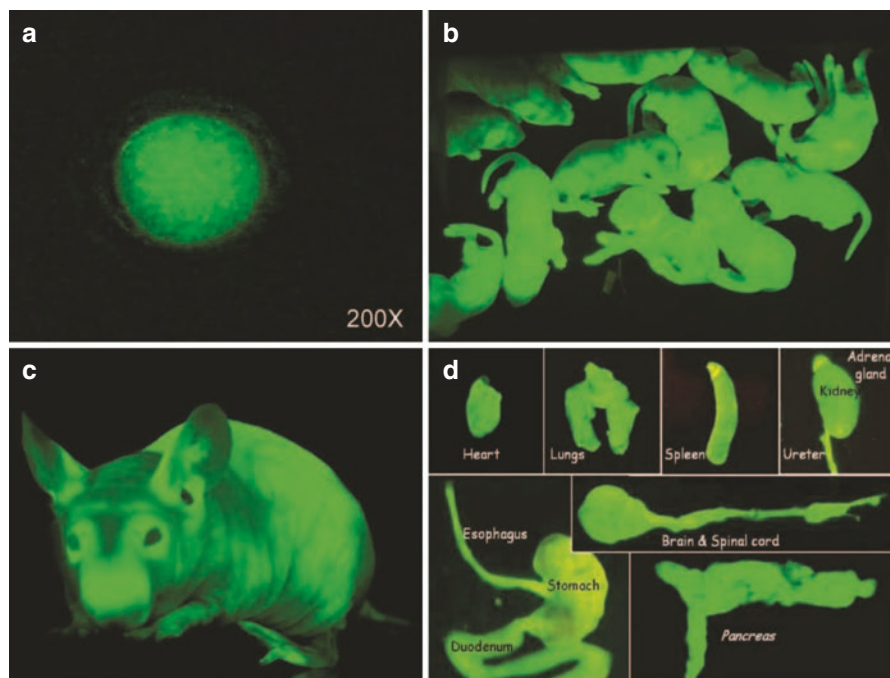


**Fig. 14.1** GFP expression in the tissues and cells of the transgenic GFP nude mouse. (a) An embryo expresses GFP at the single-cell stage. Magnification, x200. (b) and (c) Newborn and adult mice fluoresce brilliant, bright green under blue light excitation. The fluorescence could be detected with a simple blue-light-emitting diode flashlight with a central peak of 470 nm and a bypass emission filter. (d) The panel shows GFP expressed in major internal organs including the heart, lungs, spleen, adrenal gland, kidney, esophagus, stomach, duodenum, pancreas, brain, and spinal cord on blue-light excitation. (e) The entire digestive system was dissected out from tongue to anus and fluoresces brilliant green on blue-light excitation. (f) and (g) The male and female reproductive systems were dissected out, and all components fluoresced bright green on blue-light excitation. (h) The dissected circulatory system, including the heart and major arteries and veins, had brilliant green fluorescence on blue-light excitation. (i) The entire skeleton was dissected and could be seen to fluoresce brilliant green upon blue-light excitation. (j) Pancreatic islets had brilliant green fluorescence. (k) Spleen cells also could be seen to fluoresce brilliant green upon blue-light excitation [5]

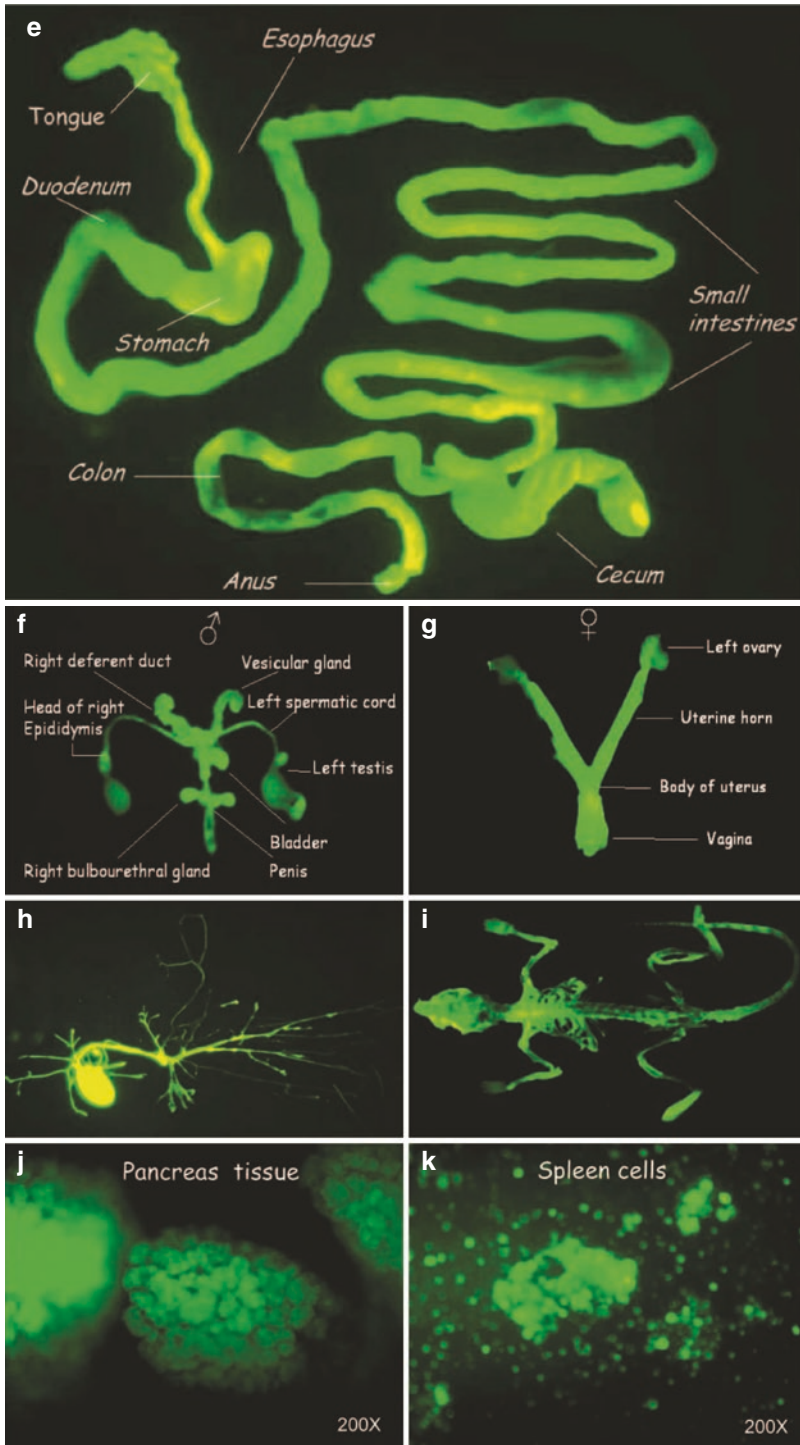


**Fig. 14.1** (continued)



that GFP expression is not toxic. The GFP nude mouse has a critical advantage over the GFP C57/B6 immunocompetent mouse in that human tumors can grow in the GFP nude mouse. In addition, the lack of hair in the GFP nude mouse makes imaging more facile [5]. RFP-expressing human cancer cells growing in GFP nude mice can allow color-coded imaging of the tumor microenvironment (TME) to visualize cancer-cell stroma-cell interaction [5, 17].

## Characterization of the Transgenic RFP Nude Mouse

### Development of the Transgenic RFP Nude Mouse

We have developed the RFP nude mouse, a new strain of transgenic nude mice, by crossing non-transgenic nude mice with the transgenic RFP C57/B6 mouse as described above [10].

### The RFP Nude Mouse Expresses RFP Essentially in All Tissues

After sacrifice of the RFP transgenic nude mouse, organs including the brain, heart and lungs, liver, uterus and ovary, pancreas, kidney, and spleen and the circulatory system were harvested and imaged (Fig. 14.2 and 14.3). All of the tissues from this

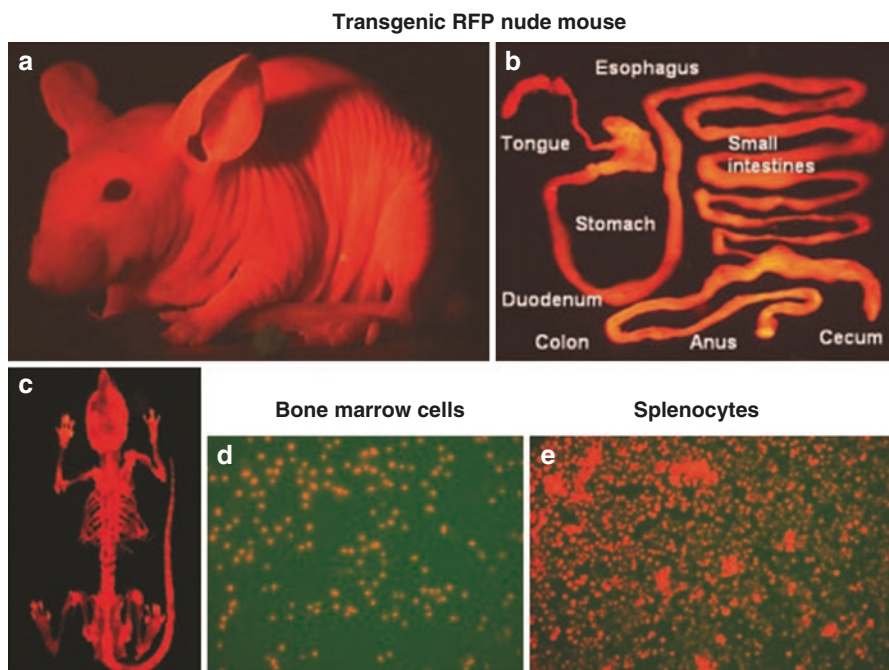


**Fig. 14.2** Transgenic RFP nude mouse. (a) Whole-body image of transgenic RFP nude mouse. (b) Digestive tract of RFP nude mice. (c) Whole skeleton of RFP nude mouse. (d) Bone marrow cells of the RFP nude mouse. (e) Splenocytes of the RFP nude mouse. Images were taken with a Hamamatsu C5810 tree-chip CCD camera (a) and an Olympus IMT-2 inverted fluorescence microscope (b–e) [10]

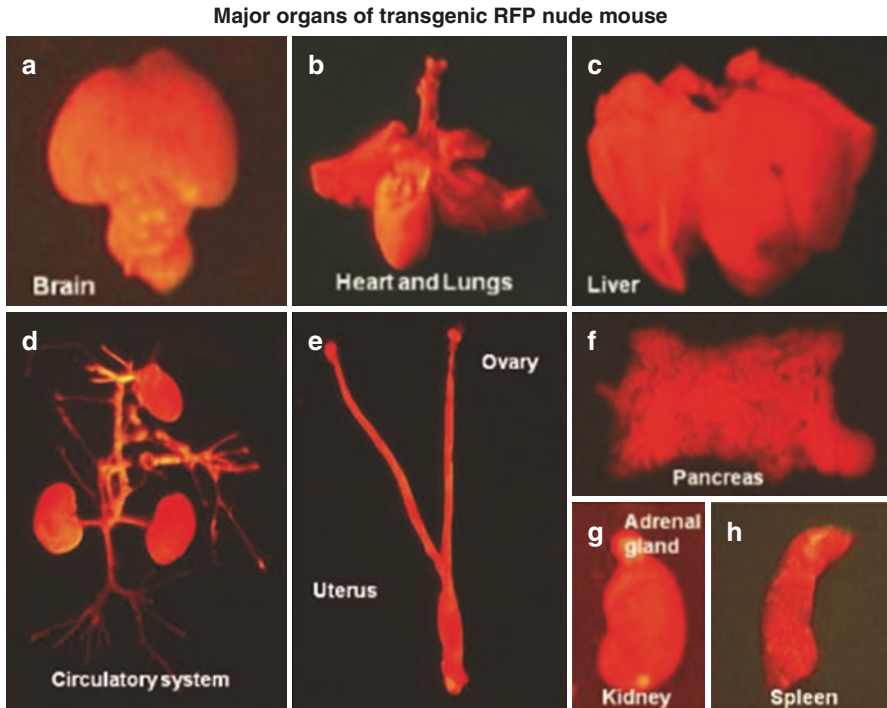


**Fig. 14.3** Major organs of transgenic RFP nude mouse. All of the major organs and tissues are red under fluorescence excitation with blue light. (a) Brain. (b) Heart and Lungs. (c) Liver. (d) Circulatory system. (e) Uterus and ovary. (f) Pancreas. (g) Kidney and adrenal gland. (h) Spleen. All images were taken with the Indec Biosystems FluorVivo imaging system [10]

transgenic line, with the exception of erythrocytes, were red fluorescent under appropriate excitation light [10].

### **Whole-Body Imaging of Cancer Cells Labeled with GFP Orthotopically Transplanted in RFP Nude Mice**

GFP-expressing human cancer cell lines, including HCT116-GFP human colon and MDA-MB-435-GFP human breast, were orthotopically transplanted in the RFP nude mice. The GFP-expressing tumors were noninvasively imaged. These human tumors had similar growth rates of the tumors growing in the non-transgenic nude mouse [10].

### **Tumor–Host Interaction and Tumor Microenvironment (TME) of GFP-Expressing Cancer Cells in RFP Transgenic Mice**

Dual-color fluorescence imaging enabled visualization of PC-3-GFP human prostate cancer and B16F10 mouse melanoma cells expressing GFP in the nucleus and RFP in the cytoplasm, interacting with RFP-expressing host cells. RFP-expressing tumor vasculature in viable tumor tissue and necrotic tumor tissue in the same tumor mass were visualized. RFP-expressing tumor vasculature were readily identified in



**Fig. 14.4** Non-invasive imaging of a fluorescent tumor from a patient with pancreatic cancer growing in a patient-derived orthotopic xenograft (PDOX) nude mouse model. Whole-body non-invasive imaging with the OV100 of human pancreatic cancer PDOX in a non-transgenic nude mouse. The mouse was non-invasively imaged at day-21 (*left panel*), day-30 (*middle panel*) and day-74 (*right panel*) [8]

the area where the tumor tissue maintained good viability. However, only remnants of RFP-expressing vasculature could be visualized in the necrotic area. GFP-expressing PC-3 cancer cells were visualized in the lung of RFP nude mouse 8 weeks after orthotopic tumor implantation. Numerous dying B16F10-dual-color melanoma cancer cells were visualized in the area where the tumor vasculature was lacking. Numerous well-developed, host-derived RFP-expressing blood vessels were visualized in the GFP-expressing mouse melanoma 2 weeks after subcutaneous injection of B16F10-dual-color melanoma cells in the transgenic RFP mouse [10].

### RFP Mouse as Host for Patient Tumors to Label Their Stroma

Human patient tumors, such as pancreatic cancer [6–8] and sarcoma [18], which acquired RFP labeled stroma during growth in RFP transgenic mice which are stably associated with the tumor as it grew in non-colored nude mice as visualized by non-invasive fluorescence imaging (Fig. 14.4) [8].

### Characterization of the Transgenic Cyan Fluorescent Protein (CFP) Nude Mouse

The CFP nude mouse exhibits the same fluorescence pattern that was described in the wild-type CK6/ECFP mouse [12]. The CFP nude mouse expresses blue fluorescence in nearly all its tissues but at much different intensities. Among internal organs, the pancreas displays the strongest CFP blue fluorescent signal [12].

In addition to intravital imaging, all organs were harvested and individually imaged under the CFP filter of the UVP iBox imaging machine. The musculoskeletal system displayed strong blue fluorescence. Internal organs expressed varying levels of CFP expression. The lungs, cardiovascular system, kidneys, and adrenals glands, as well as the neurological system, were very weakly fluorescent. Likewise, the liver required a prolonged exposure time (5 s) to display a fairly low level of blue fluorescence. In contrast, both female and male reproductive organs brightly fluoresced blue after 1 s

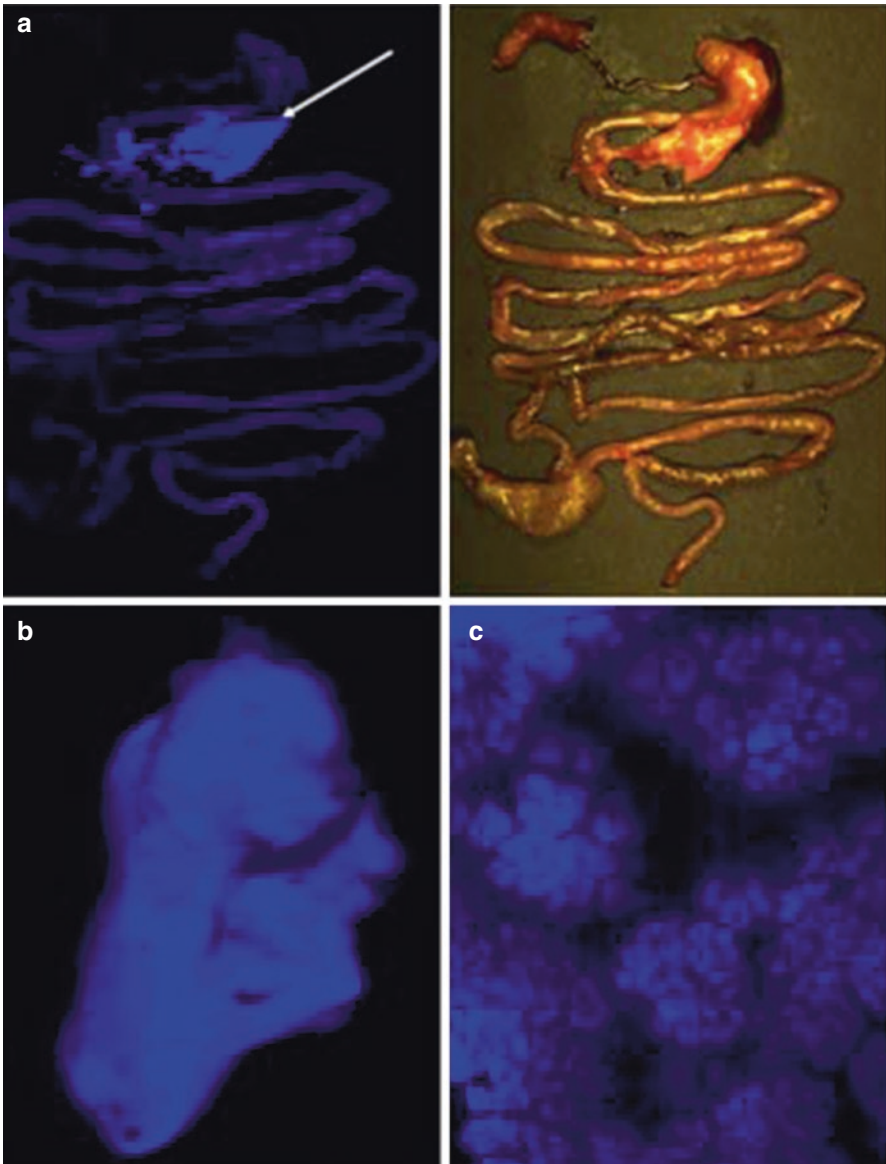


**Fig. 14.5** Imaging the pancreas and gastrointestinal tract. The GI tract was dissected en bloc, from the tongue to the rectum. (a) The fluorescence of the pancreas (*arrow*) was much stronger than that of the rest of the GI tract. Exposure time of 1.5 s was used. A brightfield image is also shown. (b) The pancreas was isolated from the rest of the GI tract and imaged individually. (c) Examination under the microscope at 10 $\times$  revealed clearly the glandular nature of the pancreas [12]

exposure. Within the gastrointestinal tract, the brilliant fluorescence of the pancreas stood out in sharp contrast to the relatively weak fluorescence signal of the rest of the tract. When the pancreas was isolated and examined under higher magnification, the glandular nature of the organ became evident [12] (Fig. 14.5).

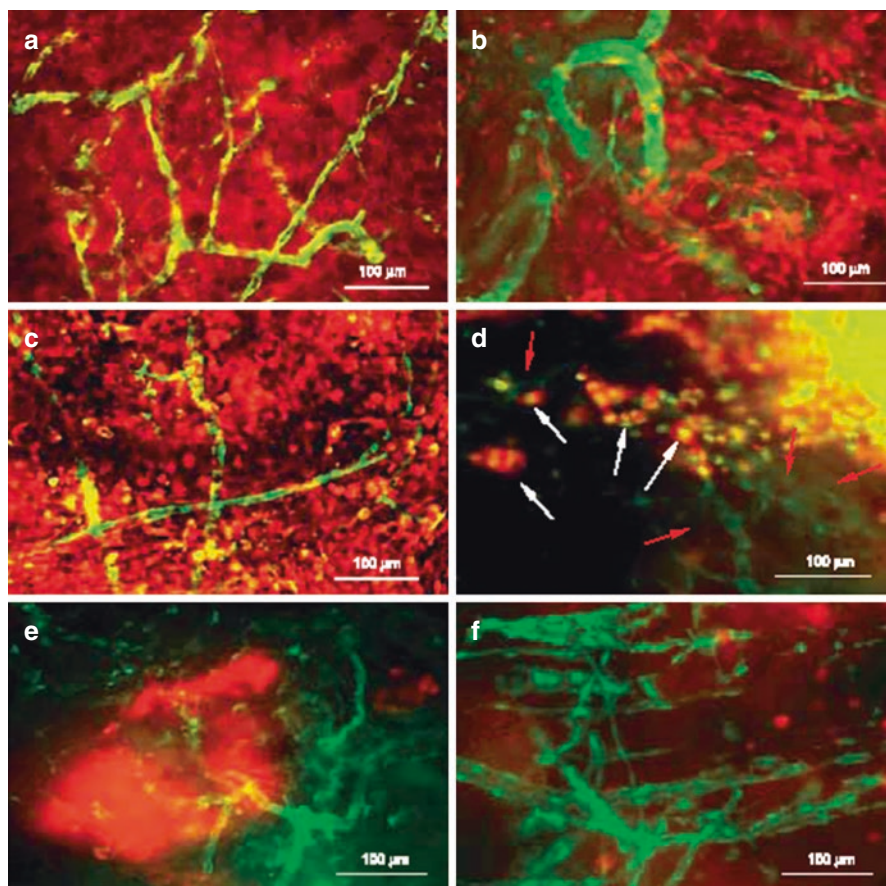


**Fig. 14.6** Fluorescence imaging of tumor angiogenesis in transgenic ND-GFP nude mice. (a) RFP-expressing mouse B16F10 melanoma cells growing in a nestin-GFP transgenic nude mouse. Host-derived ND-GFP-expressing blood vessels were visualized in the RFP-expressing mouse melanoma on day 10 after s.c. injection of B16F10-RFP cells in the transgenic ND-GFP nude mouse. Bar, 100  $\mu\text{m}$ . (b) Numerous host-derived ND-GFP-expressing blood vessels were visualized in the RFP-expressing mouse mammary tumor on day 14 after orthotopic implantation of mouse MTT-060562-RFP mammary cancer cells. Bar, 100  $\mu\text{m}$ . (c) RFP-expressing U87 human glioma cells growing in the ND-GFP transgenic nude mouse. ND-GFP-expressing blood vessels were visualized in the RFP-expressing human glioma on day 14 after subcutaneous implantation of U87-RFP cells. Bar, 100  $\mu\text{m}$ . (d) Human HT1080 fibrosarcoma on day 14 after implantation. Dual-color tumor cells expressing GFP in the nucleus and RFP in the cytoplasm are polarized towards ND-GFP-expressing blood vessels (white arrows). Bar, 100  $\mu\text{m}$ . (e) RFP-expressing Bx-PC-3 human pancreatic tumor vascularized with ND-GFP vessels on day 14 after orthotopic implantation. Bar, 100  $\mu\text{m}$ . (f) RFP-expressing human HCT-116 colon tumor vascularized with ND-GFP vessels on day 14 after orthotopic implantation. Bar, 100  $\mu\text{m}$ . (g) Extensive ND-GFP-expressing blood vessels were visualized in the RFP-expressing human fibrosarcoma 8 days after implantation of HT1080 RFP cells. Only ND-GFP vessels are visualized. Bar, 100  $\mu\text{m}$ . (h) Extensive inhibition of ND-GFP-expressing blood vessel formation in the RFP-expressing HT-1080 human fibrosarcoma by doxorubicin on days 0, 1, and 2. Bar, 100  $\mu\text{m}$  [13]

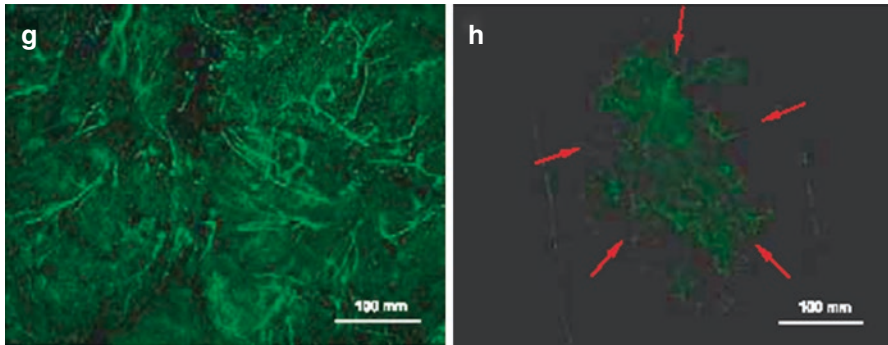


**Fig. 14.6** (continued)

### Characterization of the ND-GFP Nude Mouse

ND-GFP was expressed in the brain, spinal cord, pancreas, stomach, esophagus, heart, blood vessels of glomeruli, blood vessels of skeletal muscle, testes, hair follicles, and blood vessel network in the skin of the ND-GFP mouse [13].

### Nascent Angiogenesis of Human Fibrosarcoma Subcutaneously Implanted in the ND-GFP Nude Mouse

HT1080 human fibrosarcoma cells, expressing histone H2B-GFP in the nucleus and RFP in the cytoplasm [19], were implanted into the subcutis of the ND-GFP nude mice. On day 14 after implantation of the cancer cells, ND-GFP-expressing nascent blood vessels were visualized growing into the dual-color tumor mass. The dual-color cancer cells became polarized toward the ND-GFP-expressing nascent blood vessels [13].

### Nascent Angiogenesis of Murine Melanoma Implanted in the ND-GFP Nude Mouse

B16F10-RFP cells growing in the skin had numerous GFP-expressing ND-GFP vessels within the tumor. The extensive vascularization was striking (Fig. 14.6) when only the GFP vessels were visualized. Doxorubicin inhibited the formation of ND-GFP vessels in the B16F10 tumor by ~85% [13].

### Nascent Angiogenesis of Orthotopically Implanted Human Pancreatic Tumor in the ND-GFP Nude Mouse

ND-GFP-expressing nascent blood vessels vascularized the orthotopically-transplanted RFP-expressing Bx-PC-3 and MiaPaCa human pancreatic tumors. The endothelial cell marker CD31 and ND-GFP fluorescence were both expressed in the newly-formed blood vessels growing into the pancreatic tumors [13].

### **ND-GFP-Expressing Nascent Blood Vessels Vascularize Orthotopically Implanted Human RFP Colon Tumor in the ND-GFP Mouse**

ND-GFP-expressing nascent blood vessels vascularized human colon tumor HCT-116-RFP. CD31 and ND-GFP fluorescence were coexpressed in the newly-formed ND-GFP-expressing blood vessels in the colon tumor [13].

### **ND-GFP-Expressing Blood Vessels Vascularize Orthotopically-Implanted Murine Mammary Tumor**

ND-GFP expressing blood vessels vascularized orthotopically-implanted murine mammary tumor MMT060562-RFP. The vessels showed extensive tortuosity and heterogeneity [13].

### **ND-GFP-Expressing Blood Vessels Vascularize Orthotopically Implanted Human Brain Tumor**

Extensive vascularization by ND-GFP-expressing blood vessels of the orthotopically implanted U87-RFP human glioma was visualized. Many RFP-expressing tumor cells seemed to grow closely associated with the ND-GFP vessels after implantation [13].

The four transgenic fluorescent-protein-expressing nude mice described in this chapter, GFP, RFP, CFP, and ND-GFP, provide the basis to revolutionize our understanding of the tumor microenvironment (TME) using color-coded imaging [17, 20]. The fluorescent protein-expressing transgenic mice will be important for the growth of PDOX tumors to visualize and characterize their TME.

---

## **References**

1. Rygaard J, Povlsen CO. Heterotransplantation of a human malignant tumor to 'nude' mice. *Acta Pathol Microbiol Scand.* 1969;77:758–60.
2. Okabe M, Ikawa M, Kominami K, Nakanishi T, Nishimune Y. “Green mice” as a source of ubiquitous green cells. *FEBS Lett.* 1997;407:313–9.
3. Hoffman R. Green fluorescent protein imaging of tumour growth, metastasis, and angiogenesis in mouse models. *Lancet Oncol.* 2002;3:546–56.
4. Yang M, Li L, Jiang P, Moossa AR, Penman S, Hoffman RM. Dual-color fluorescence imaging distinguishes tumor cells from induced host angiogenic vessels and stromal cells. *Proc Natl Acad Sci U S A.* 2003;100:14259–62.
5. Yang M, Reynoso J, Jiang P, Li L, Moossa AR, Hoffman RM. Transgenic nude mouse with ubiquitous green fluorescent protein expression as a host for human tumors. *Cancer Res.* 2004;64:8651–6.
6. Suetsugu A, Katz M, Fleming J, Moriwaki H, Bouvet M, Saji S, Hoffman RM. Multi-color palette of fluorescent proteins for imaging the tumor microenvironment of orthotopic tumorigraft mouse models of clinical pancreatic cancer specimens. *J Cell Biochem.* 2012;113:2290–5.
7. Suetsugu A, Katz M, Fleming J, Truty M, Thomas R, Saji S, Moriwaki H, Bouvet M, Hoffman RM. Imageable fluorescent metastasis resulting in transgenic GFP mice orthotopically implanted with human-patient primary pancreatic cancer specimens. *Anticancer Res.* 2012;32:1175–80.

8. Suetsugu A, Katz M, Fleming J, Truty M, Thomas R, Saji S, Moriwaki H, Bouvet M, Hoffman RM. Non-invasive fluorescent-protein imaging of orthotopic pancreatic-cancer-patient tumor-graft progression in nude mice. *Anticancer Res.* 2012;32:3063–8.
9. Vintersten K, Monetti C, Gertsenstein M, Zhang P, Laszlo L, Biechele S, Nagy A. Mouse in red: red fluorescent protein expression in mouse ES cells, embryos, and adult animals. *Genesis.* 2004;40:241–6.
10. Yang M, Reynoso J, Bouvet M, Hoffman RM. A transgenic red fluorescent protein-expressing nude mouse for color-coded imaging of the tumor microenvironment. *J Cell Biochem.* 2009;106:279–84.
11. Hadjantonakis AK, Macmaster S, Nagy A. Embryonic stem cells and mice expressing different GFP variants for multiple non-invasive reporter usage within a single animal. *BMC Biotechnol.* 2002;2:11.
12. Tran Cao HS, Reynoso J, Yang M, Kimura H, Kaushal S, Snyder CS, Hoffman RM, Bouvet M. Development of the transgenic cyan fluorescent protein (CFP)-expressing nude mouse for “Technicolor” cancer imaging. *J Cell Biochem.* 2009;107:328–34.
13. Amoh Y, Yang M, Li L, Reynoso J, Bouvet M, Moossa AR, Katsuoka K, Hoffman RM. Nestin-linked green fluorescent protein transgenic nude mouse for imaging human tumor angiogenesis. *Cancer Res.* 2005;65:5352–7.
14. Yamauchi K, Yang M, Jiang P, Xu M, Yamamoto N, Tsuchiya H, Tomita K, Moossa AR, Bouvet M, Hoffman RM. Development of real-time subcellular dynamic multicolor imaging of cancer-cell trafficking in live mice with a variable-magnification whole-mouse imaging system. *Cancer Res.* 2006;66:4208–14.
15. Yang M, Jiang P, Hoffman RM. Whole-body subcellular multicolor imaging of tumor-host interaction and drug response in real time. *Cancer Res.* 2007;67:5195–200.
16. Uchugonova A, Duong J, Zhang N, König K, Hoffman RM. The bulge area is the origin of nestin-expressing pluripotent stem cells of the hair follicle. *J Cell Biochem.* 2011;112:2046–50.
17. Hoffman RM, Yang M. Color-coded fluorescence imaging of tumor-host interactions. *Nat Protoc.* 2006;1:928–35.
18. Kiyuna T, Murakami T, Tome Y, Igarashi K, Kawaguchi K, Russell T, Eckhardt MA, Crompton J, Singh A, Bernthal N, Bukata S, Federman N, Kanaya F, Eilber FC, Hoffman RM. Labeling the stroma of a patient-derived orthotopic xenograft (PDOX) mouse models of undifferentiated pleomorphic soft-tissue sarcoma with red fluorescent protein for rapid non-invasive drug screening. *J Cell Biochem.* 2017;118:361–5.
19. Yamamoto N, Jiang P, Yang M, Xu M, Yamauchi K, Tsuchiya H, Tomita K, Wahl GM, Moossa AR, Hoffman RM. Cellular dynamics visualized in live cells in vitro and in vivo by differential dual-color nuclear-cytoplasmic fluorescent-protein expression. *Cancer Res.* 2004;64:4251–6.
20. Hoffman RM, Bouvet M. Imaging the microenvironment of pancreatic cancer patient-derived orthotopic xenografts (PDOX) growing in transgenic nude mice expressing GFP, RFP, or CFP. *Cancer Lett.* 2016;380:349–55.



---

# Fluorescence Imaging of Tumors in Human Patient-Derived Orthotopic Xenograft (PDOX) Mouse Models

# 15

Robert M. Hoffman, Atsushi Suetsugu, Tasuku Kiyuna,  
Shuya Yano, and Michael Bouvet

---

## Introduction

Our laboratory pioneered patient-derived orthotopic xenograft (PDOX) mouse tumor models in the early 1990s [1–13]. The PDOX models are much more patient-like than ectopic subcutaneous-transplant tumor models. However, in orthotopic models, it is difficult to visualize tumor growth and metastasis.

---

R.M. Hoffman (✉)

AntiCancer, Inc., 7917 Ostrow Street, San Diego, CA 92111, USA

Department of Surgery, University of California, San Diego, CA, USA

e-mail: [all@anticancer.com](mailto:all@anticancer.com)

A. Suetsugu

AntiCancer, Inc., 7917 Ostrow Street, San Diego, CA 92111, USA

Department of Surgery, University of California, San Diego, CA, USA

Graduate School of Medicine, Gifu University, Gifu, Japan

T. Kiyuna

AntiCancer, Inc., 7917 Ostrow Street, San Diego, CA 92111, USA

Department of Surgery, University of California, San Diego, CA, USA

Department of Orthopedic Surgery, Graduate School of Medicine,

University of the Ryukyus, Okinawa, Japan

S. Yano

AntiCancer, Inc., 7917 Ostrow Street, San Diego, CA 92111, USA

Department of Surgery, University of California, San Diego, CA, USA

Department of Gastroenterological Surgery, Graduate School of Medicine,  
Dentistry and Pharmaceutical Sciences, Okayama University, Okayama, Japan

M. Bouvet

Department of Surgery, University of California, San Diego, CA, USA

VA Healthcare System, San Diego, CA, USA

© Springer International Publishing AG 2017

R.M. Hoffman (ed.), *Patient-Derived Mouse Models of Cancer*,

Molecular and Translational Medicine, DOI 10.1007/978-3-319-57424-0\_15

207

To address this problem of imaging PDOX models, we have recently developed the technology to introduce fluorescent protein-expressing stroma [14–20] into tumors by passaging PDOX models through transgenic nude mice ubiquitously expressing fluorescent proteins. The tumors were passaged in transgenic nude mice ubiquitously expressing either red fluorescent protein (RFP), green fluorescent protein (GFP), or cyan fluorescent protein (CFP), whereby the tumor acquired RFP, GFP, and CFP stroma, respectively [21].

In subsequent experiments, the primary patient tumors, passaged in transgenic GFP-expressing nude mice, acquired GFP-expressing stroma and subsequently metastasized to the liver and also formed disseminated peritoneal metastases. The metastases maintained the GFP stroma from the primary tumor, and apparently acquired stroma from the metastatic site, resulting in their very bright fluorescence [22].

Pancreatic cancer PDOX tumors were passaged orthotopically into transgenic nude mice ubiquitously expressing GFP and subsequently to nude mice ubiquitously expressing RFP. The tumors, with very bright GFP and RFP stroma, were then orthotopically passaged to non-transgenic nude mice. It was possible to image the brightly fluorescent tumors non-invasively longitudinally as they progressed in the non-transgenic nude mice [21].

We subsequently demonstrated a non-invasive imageable soft tissue sarcoma PDOX model, established with brightly labeled RFP-expressing sarcoma by only a single passage through an RFP transgenic nude mouse [27].

We initially selectively labeled tumors with GFP using a telomerase-dependent adenovirus (OBP-401) that expresses the *gfp* gene only in cancer cells. The labeled tumors could then be resected under fluorescence guidance [23]. Tumors that recurred after fluorescence-guided surgery (FGS) maintained GFP expression, demonstrating the stability of OBP-401-GFP labeling [24–26].

We labeled cancer cells in a pancreatic cancer PDOX model with GFP using OBP-401 and labeled stroma in the PDOX with RFP by previous growth in RFP transgenic mice. This color-coded model of cancer and stromal cells within a tumor enabled precise fluorescence-guided surgery [26].

---

## Materials and Methods

### Mice

Transgenic GFP and RFP nude mice [16] are from AntiCancer, Inc. (San Diego, CA). The nude mice express GFP or RFP under the control of the chicken  $\beta$ -actin promoter and cytomegalovirus enhancer. All of the tissues from this transgenic line, with the exception of erythrocytes and hair, fluoresce green under excitation light.

### Animal Care

Transgenic GFP nude mice [16–18] are bred and maintained in a HEPA-filtered environment with cages, food, and bedding sterilized by autoclaving. Animal diets were obtained from Harlan Teklad (Madison, WI, USA). Ampicillin (5.0%, w/v; Sigma,

St. Louis, MO, USA) was added to the autoclaved drinking water. All surgical procedures and imaging were performed with the animal anesthetized by intramuscular injection of 0.02 mL of a solution of 50% ketamine, 38% xylazine, and 12% acepromazine maleate. All animal studies were conducted in accordance with the principles of and procedures outlined in the NIH Guide for the Care and Use of Laboratory Animals [22].

## **Establishment of a PDOX Model of Patient Tumors**

Tumor tissue from patients was obtained at surgery with informed consent and cut into 3 mm<sup>3</sup> fragments and transplanted subcutaneously into nude or SCID mice [28, 29].

## **Orthotopic Transgenic Fluorescent Protein-Expressing Nude Mice**

Intact pancreatic cancer tissue fragments were orthotopically transplanted into four 6-week-old transgenic GFP or RFP nude mice using surgical orthotopic implantation (SOI). A small 6–10 mm transverse incision was made on the left flank of the mouse through the skin and peritoneum. The tail of the pancreas was exposed through this incision, and a single 3 mm [2, 13] tumor fragment from subcutaneous tumors was sutured to the tail of the pancreas using 8-0 nylon surgical sutures (Ethilon; Ethicon Inc., NJ, USA). On completion, the tail of the pancreas was returned to the abdomen, and the incision is closed in one layer using 6-0 nylon surgical sutures (Ethilon) [2, 13, 30].

## **Establishment of a PDOX Model of Soft Tissue Sarcoma**

A PDOX model of soft tissue sarcoma was established by making a 5 mm skin incision on the right high thigh into the biceps femoris. The muscle was then split to make space for the patient sarcoma tissue fragment. A single tumor fragment was implanted orthotopically into the space to establish the PDOX model. The wound was closed with a 6-0 nylon suture (Ethilon) [31].

## **Fluorescence Imaging**

Mice were imaged with an Olympus OV100 whole-mouse fluorescence imaging system with a sensitive CCD camera and four objective lenses, parcentered and parfocal, enabling imaging from macrocellular to subcellular [32] or equivalent.

## **Confocal Microscopy**

Confocal two-photon microscopy (FluoView FV1000, Olympus Corp., Tokyo, Japan) was used for two- (x,y) and three-dimensional (3D, x,y,z) high-resolution

imaging. A cw semiconductor laser at 473 nm for GFP excitation and a tunable Mai Tai HP femtosecond laser emitting at 700–1020 nm (Newport Spectra-Physics, Irvine, CA) can be used for deep tissue imaging of autofluorescence and GFP. Fluorescence images were obtained using the 20 ×/0.50 UPlan FLN and 40 ×/1.3 Oil Olympus UPLAN FLN objectives [33].

## Histological Analysis

The primary tumor, liver metastases, and disseminated peritoneal metastases were sectioned at a thickness of 8 μm using frozen sections for fluorescence imaging and paraffin-embedded tissue for staining using hematoxylin and eosin for microscopic analysis [22].

## GFP-Expressing Telomerase-Specific Adenovirus

The adenovirus OBP-401 contains a promoter element of the human telomerase reverse transcriptase (*hTERT*) gene which drives the expression of E1A and E1B genes linked to an internal ribosome entry site. OBP-401 also contains the GFP gene which is driven by the CMV promoter. The virus only replicates in cancer cells, labeling them with the GFP gene [23, 26].

## OBP-401-GFP Labeling of an RFP-Expressing PDOX

The PDOX tumor exposed and OBP-401 ( $1 \times 10^8$  PFU/tumor) is injected into the exposed tumor [26].

---

## Results and Discussion

### GFP Host Stromal Cells Infiltrate a Pancreatic Cancer PDOX

Human patient pancreatic cancer was transplanted orthotopically into 6-week-old transgenic GFP nude mice. After 110 days, primary tumors were observed using the OV100 imaging system. The GFP stromal cells from the GFP host mouse had migrated into the orthotopic pancreatic tumor, causing the tumors to fluoresce bright green [34]. Both GFP cancer-associated fibroblasts (CAFs) and tumor-associated macrophages (TAMs) were observed in the primary tumor. Histological examination at 110 days of tumor growth revealed pancreatic tubular adenocarcinoma [26] (Fig. 15.1).

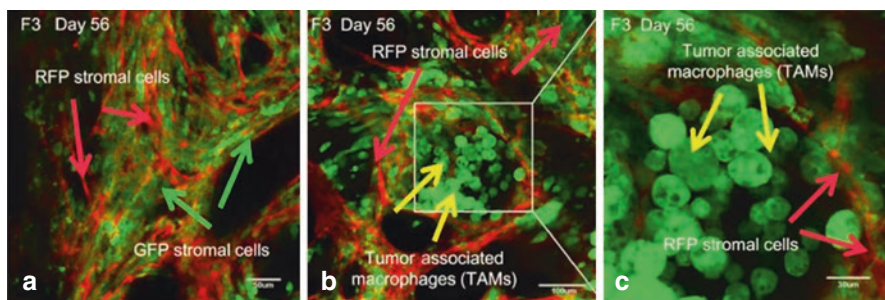


**Fig. 15.1** (a) Human pancreatic-cancer-patient tumor with RFP and GFP stromal cells. Image was obtained with the Olympus FV1000. Green arrows indicate GFP stromal cells from GFP mouse. Red arrows indicate RFP stromal cells from RFP mouse. (Bar=50  $\mu\text{m}$ ). (b) Human pancreatic-cancer-patient tumor with RFP stromal cells and GFP TAMs. (Bar=100  $\mu\text{m}$ ). Image taken with the Olympus FV1000. (c) High magnification image of (b). RFP stromal cells and GFP-TAMs are readily observed. (Bar=30  $\mu\text{m}$ ). Image obtained with the Olympus FV1000 [34]

### GFP Host Stromal Cells Infiltrate Peritoneal Disseminated Metastases of Pancreatic Cancer PDOX

The GFP stromal cells from the GFP host mouse formed a capsule around the disseminated peritoneal metastases. Both GFP-labeled CAFs and TAMs were observed in the disseminated peritoneal metastases. Histological examination at 110 days of tumor growth demonstrated pancreatic tubular adenocarcinoma, similar to the primary tumor [26].

### GFP Host Stromal Cells Infiltrate Liver Metastases of Pancreatic Cancer PDOX

High-magnification fluorescence imaging showed extensive GFP fluorescence in the liver metastasis. Both GFP CAFs and TAMs were observed in the liver metastasis. Histological examination of the liver metastasis demonstrated pancreatic tubular adenocarcinoma [26].

### RFP Host Stromal Cells Infiltrate Pancreatic Cancer PDOX

Patient pancreatic cancer was transplanted orthotopically in 6-week-old transgenic RFP nude mice. After 30 days, tumors were imaged using the OV100. The RFP stromal cells from the RFP host mice formed a capsule around the tumor and infiltrated into the central part of the tumor as well. RFP-expressing TAMs could be visualized in the tumor [34].

### GFP Host Stromal Cells Infiltrate Pancreatic PDOX Labeled with RFP Stroma to Form a Two-Color Stroma Model

Tumors were grown in RFP transgenic nude mice and subsequently in GFP nude mice, after which the human pancreatic-cancer PDOX contained both RFP and GFP stromal cells. The RFP stromal cells still persisted after passage to GFP transgenic mice. Under confocal microscopy with the FV1000, RFP and GFP stromal cells were clearly visualized in the tumor including GFP and RFP CAFs and TAMs in the central part of the tumor [34].

### CFP Host Stromal Cells Infiltrate Pancreatic Cancer PDOX Previously Grown in RFP and GFP Transgenic Nude Mice to Form a Three-Color Stroma Model

Pancreatic cancer previously grown in RFP and GFP transgenic mice were orthotopically implanted in 6-week-old nude CFP mice. The tumors were excised and observed with the FV1000 confocal microscope. RFP-, GFP-, and CFP-expressing stromal cells were observed in the human pancreatic-cancer patient tumor. The RFP stroma persisted after two passages and GFP stroma persisted after one passage in CFP mice. RFP TAMs and CAFs and GFP blood vessels still persisted in the human pancreatic-cancer patient tumor after one and two passages, respectively [34] (Fig. 15.2).

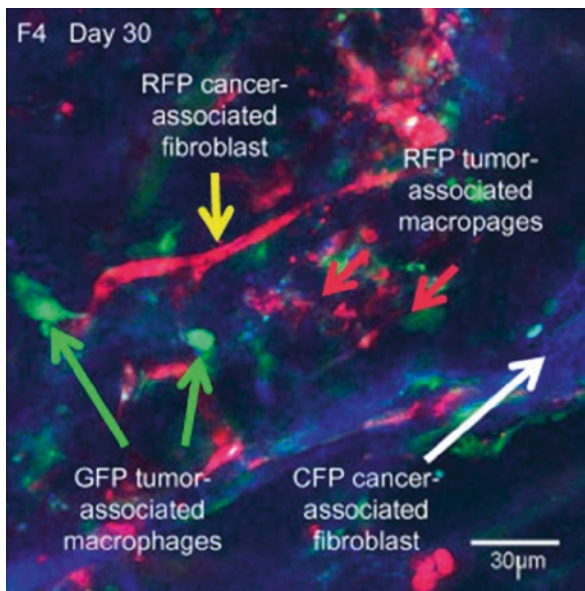


**Fig. 15.2** Human pancreatic-cancer-patient PDOX tumor growing in CFP nude-mouse-host after previous growth in RFP and GFP nude-mouse-hosts. RFP CAFs (*yellow arrow*) and GFP TAMs (*green arrows*) in the PDOX tumor. White arrow indicates CFP CAFs. (Bar=30  $\mu$ m). Image was obtained with the FV1000 confocal microscope [34]

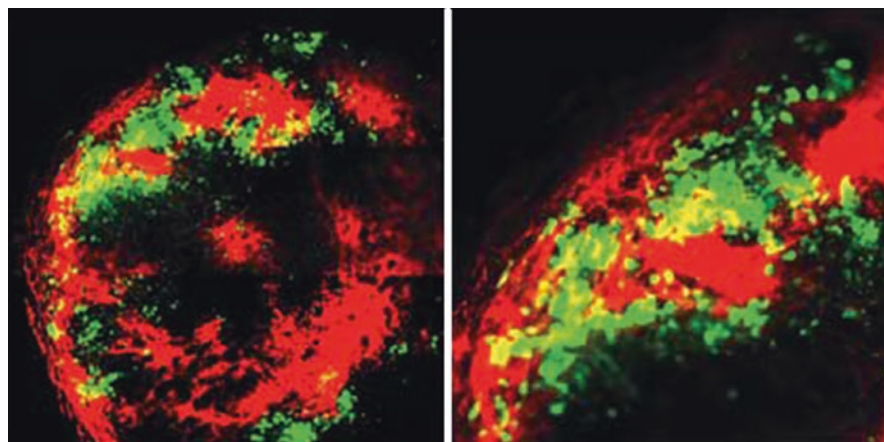


**Fig. 15.3** FGS of a pancreatic cancer PDOX with GFP-labeled cancer cells and RFP-labeled stroma. RFP-stroma were acquired by previous growth of the PDOX in RFP transgenic nude mice. GFP-cancer cells were obtained from infection with OBP-401-GFP. Representative images of a cross-section of the resected dual-color tumor. Images were acquired with the FV1000 confocal laser imaging system [26]

### **OBP-401-GFP Labeling of Cancer Cells in Pancreatic Cancer PDOX with RFP-Expressing Stroma**

OBP-401 selectively labeled cancer cells with GFP in the pancreatic cancer PDOX containing RFP-expressing stroma obtained from previous growth in RFP transgenic nude mice. The double-labeled PDOX enabled precise visualization of color-coded cancer and stromal cells [26] (Fig. 15.3).

### **Noninvasive Imaging of Pancreatic Cancer PDOX with Labeled Stromal Cells**

Noninvasive imaging at days 21, 30, and 74 demonstrated extensive orthotopic growth of the pancreatic cancer PDOX, labeled with RFP and GFP stroma, on the nude mouse pancreas [21] (Fig. 15.4).

### **Noninvasive Imaging of a PDOX Sarcoma in Non-colored Nude Mouse After a Single Passage in RFP Nude Mice**

A patient soft tissue sarcoma (STS) was grown orthotopically in the right biceps femoris of an RFP-expressing nude mouse. The PDOX tumor in the RFP-expressing nude mouse became brightly fluorescent. The resected PDOX tumor from the RFP transgenic nude mouse was also brightly fluorescent. The RFP-expressing PDOX tumor was passed orthotopically to the right biceps femoris of non-fluorescent

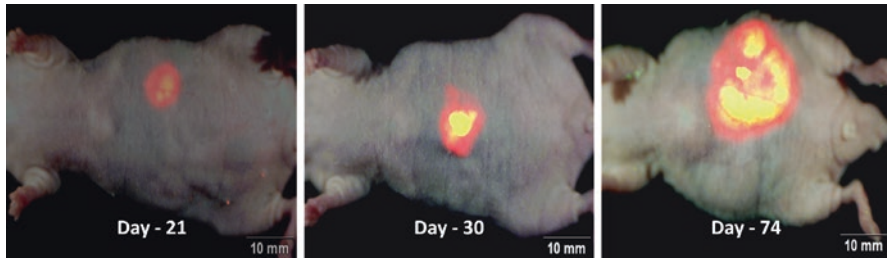


**Fig. 15.4** Non-invasive imaging of fluorescent tumor from a patient with pancreatic cancer growing in a PDOX model in non-transgenic nude mice. The PDOX was previously grown in transgenic RFP and transgenic GFP nude mice where the PDOX acquired RFP and GFP stroma, respectively. Whole-body non-invasive imaging with the OV100 of human pancreatic cancer PDOX in non-transgenic nude mice. Mice were non-invasively imaged at day-21 (*left panel*), day-30 (*middle panel*) and day-74 (*right panel*) [21]

nude mice to establish a noninvasively imageable PDOX model. The bright RFP-expressing STS PDOX was readily visible without opening the skin. The STS PDOX tumor in the nontransgenic nude mouse was then exposed by a skin flap. Tumor RFP expression was very bright when imaged through the skin flap. The resected RFP-expressing PDOX was also very bright [27].

FV1000 confocal laser microscopy imaging visualized RFP-expressing tumor stroma in the STS PDOX derived from RFP-expressing nude mice, after passage to a nontransgenic nude mouse. The PDOX tumors had bright and diffusely distributed RFP-expressing stroma with fibroblast-like cells and lymphocyte-like cells [27].

The results in this chapter demonstrate the feasibility of labeling PDOX mouse models with fluorescent proteins. Cancer cells as well as stroma can be differentially labeled. The color-coded tumor stroma model is a powerful measure to simultaneously visualize the two types of cells within the PDOX tumors and how they may differentially respond to approved and experimental therapeutics agents. In addition, the stroma acquired by the PDOX appears stable and able to grow in parallel with the cancer cells of the PDOX. The labeling with adenovirus OBP-401-GFP also appears stable.

## References

1. Fu X, Besterman JM, Monosov A, Hoffman RM. Models of human metastatic colon cancer in nude mice orthotopically constructed by using histologically intact patient specimens. *Proc Natl Acad Sci U S A*. 1991;88:9345–9.
2. Fu X, Guadagni F, Hoffman RM. A metastatic nude-mouse model of human pancreatic cancer constructed orthotopically from histologically intact patient specimens. *Proc Natl Acad Sci U S A*. 1992;89:5645–9.
3. Wang X, Fu X, Hoffman RM. A new patient-like metastatic model of human lung cancer constructed orthotopically with intact tissue via thoracotomy in immunodeficient mice. *Int J Cancer*. 1992;51:992–5.



4. Fu X, Hoffman RM. Human ovarian carcinoma metastatic models constructed in nude mice by orthotopic transplantation of histologically-intact patient specimens. *Anticancer Res.* 1993;13:283–6.
5. Fu X, Le P, Hoffman RM. A metastatic-orthotopic transplant nude-mouse model of human patient breast cancer. *Anticancer Res.* 1993;13:901–4.
6. Furukawa T, Kubota T, Watanabe M, Kitajima M, Fu X, Hoffman RM. Orthotopic transplantation of histologically intact clinical specimens of stomach cancer to nude mice: correlation of metastatic sites in mouse and individual patient donors. *Int J Cancer.* 1993;53:608–12.
7. Astoul P, Colt HG, Wang X, Hoffman RM. Metastatic human pleural ovarian cancer model constructed by orthotopic implantation of fresh histologically-intact patient carcinoma in nude mice. *Anticancer Res.* 1993;13:1999–2002.
8. Astoul P, Wang X, Hoffman RM. “Patient-like” nude- and SCID-mouse models of human lung and pleural cancer (Review). *Int J Oncol.* 1993;3:713–8.
9. Astoul P, Colt HG, Wang X, Hoffman RM. A “patient-like” nude mouse model of parietal pleural human lung adenocarcinoma. *Anticancer Res.* 1994;14:85–91.
10. Astoul P, Colt HG, Wang X, Boutin C, Hoffman RM. “Patient-like” nude mouse metastatic model of advanced human pleural cancer. *J Cell Biochem.* 1994;56:9–15.
11. Togo S, Wang X, Shimada H, Moossa AR, Hoffman RM. Cancer seed and soil can be highly selective: human-patient colon tumor lung metastasis grows in nude mouse lung but not colon or subcutis. *Anticancer Res.* 1995;15:795–8.
12. Astoul P, Wang X, Colt HG, Boutin C, Hoffman RM. A patient-like human malignant pleural mesothelioma nude-mouse model. *Oncol Rep.* 1996;3:483–7.
13. Hoffman RM. Orthotopic metastatic mouse models for anticancer drug discovery and evaluation: a bridge to the clinic. *Invest New Drugs.* 1999;17:343–59.
14. McElroy M, Kaushal S, Bouvet M, Hoffman RM. Color-coded imaging of splenocyte-pancreatic cancer cell interactions in the tumor microenvironment. *Cell Cycle.* 2008;7:2916–21.
15. Yang M, Li L, Jiang P, Moossa AR, Penman S, Hoffman RM. Dual-color fluorescence imaging distinguishes tumor cells from induced host angiogenic vessels and stromal cells. *Proc Natl Acad Sci U S A.* 2003;100:14259–62.
16. Yang M, Reynoso J, Jiang P, Li L, Moossa AR, Hoffman RM. Transgenic nude mouse with ubiquitous green fluorescent protein expression as a host for human tumors. *Cancer Res.* 2004;64:8651–6.
17. Yang M, Reynoso J, Bouvet M, Hoffman RM. A transgenic red fluorescent protein-expressing nude mouse for color-coded imaging of the tumor microenvironment. *J Cell Biochem.* 2009;106:279–84.
18. Tran Cao HS, Reynoso J, Yang M, Kimura H, Kaushal S, Snyder CS, Hoffman RM, Bouvet M. Development of the transgenic cyan fluorescent protein (CFP)-expressing nude mouse for “Technicolor” cancer imaging. *J Cell Biochem.* 2009;107:328–34.
19. Suetsugu A, Hassanein MK, Reynoso J, Osawa Y, Nagaki M, Moriwaki H, Saji S, Bouvet M, Hoffman RM. The cyan fluorescent protein nude mouse as a host for multicolor-coded imaging models of primary and metastatic tumor microenvironments. *Anticancer Res.* 2012;32:31–8.
20. Hoffman RM, Yang M. Color-coded fluorescence imaging of tumor-host interactions. *Nat Protoc.* 2006;1:928–35.
21. Suetsugu A, Katz M, Fleming J, Truty M, Thomas R, Saji S, Moriwaki H, Bouvet M, Hoffman RM. Non-invasive fluorescent-protein imaging of orthotopic pancreatic-cancer-patient tumor-graft progression in nude mice. *Anticancer Res.* 2012;32:3063–8.
22. Suetsugu A, Katz M, Fleming J, Truty M, Thomas R, Saji S, Moriwaki H, Bouvet M, Hoffman RM. Imageable fluorescent metastasis resulting in transgenic GFP mice orthotopically implanted with human-patient primary pancreatic cancer specimens. *Anticancer Res.* 2012;32:1175–80.
23. Kishimoto H, Zhao M, Hayashi K, Urata Y, Tanaka N, Fujiwara T, Penman S, Hoffman RM. In vivo internal tumor illumination by telomerase-dependent adenoviral GFP for precise surgical navigation. *Proc Natl Acad Sci U S A.* 2009;106:14514–7.

24. Kishimoto H, Aki R, Urata Y, Bouvet M, Momiyama M, Tanaka N, Fujiwara T, Hoffman RM. Tumor-selective adenoviral-mediated GFP genetic labeling of human cancer in the live mouse reports future recurrence after resection. *Cell Cycle*. 2011;10:2737–41.
25. Bouvet M, Hoffman RM. Glowing tumors make for better detection and resection. *Sci Transl Med*. 2011;3:110sf10.
26. Yano S, Hiroshima Y, Maawy A, Kishimoto H, Suetsugu A, Miwa S, Toneri M, Yamamoto M, Katz MHG, Fleming JB, Urata Y, Tazawa H, Kagawa S, Bouvet M, Fujiwara T, Hoffman RM. Color-coding cancer and stromal cells with genetic reporters in a patient-derived orthotopic xenograft (PDOX) model of pancreatic cancer enhances fluorescence-guided surgery. *Cancer Gene Ther*. 2015;22:344–50.
27. Kiyuna T, Murakami T, Tome Y, Igarashi K, Kawaguchi K, Russell T, Eckhardt MA, Crompton J, Singh A, Bernthal N, Bukata S, Federman N, Kanaya F, Eilber FC, Hoffman RM. Labeling the stroma of a patient-derived orthotopic xenograft (PDOX) mouse models of undifferentiated pleomorphic soft-tissue sarcoma with red fluorescent protein for rapid non-invasive drug screening. *J Cell Biochem*. 2017;118:361–5.
28. Kim MP, Evans DB, Wang H, Abbruzzese JL, Fleming JB, Gallick GE. Generation of orthotopic and heterotopic human pancreatic cancer xenografts in immunodeficient mice. *Nat Protoc*. 2009;4:1670–80.
29. Kim MP, Truty MJ, Choi W, Kang Y, Chopin-Lally X, Gallick GE, Wang H, McConkey DJ, Hwang R, Logsdon C, Abbruzzese J, Fleming JB. Molecular profiling of direct xenograft tumors established from human pancreatic adenocarcinoma after neoadjuvant therapy. *Ann Surg Oncol*. 2012;19(Suppl 3):S395–403.
30. Hiroshima Y, Maawy A, Zhan Y, Murakami T, Momiyama M, Mori R, Matsuyama R, Chishima T, Tanaka K, Ichikawa Y, Endo I, Hoffman RM, Bouvet M. Fluorescence-guided surgery, but not bright-light surgery, prevents local recurrence in a pancreatic cancer patient-derived orthotopic xenograft (PDOX) model resistant to neoadjuvant chemotherapy (NAC). *Pancreatol*. 2015;15:295–301.
31. Murakami T, DeLong J, Eilber FC, Zhao M, Zhang Y, Zhang N, Singh A, Russell T, Deng S, Reynoso J, Quan C, Hiroshima Y, Matsuyama R, Chishima T, Tanaka K, Bouvet M, Chawla S, Endo I, Hoffman RM. Tumor-targeting *Salmonella typhimurium* A1-R in combination with doxorubicin eradicate soft tissue sarcoma in a patient-derived orthotopic xenograft PDOX model. *Oncotarget*. 2016;7:12783–90.
32. Yamauchi K, Yang M, Jiang P, Xu M, Yamamoto N, Tsuchiya H, Tomita K, Moossa AR, Bouvet M, Hoffman RM. Development of real-time subcellular dynamic multicolor imaging of cancer cell trafficking in live mice with a variable-magnification whole-mouse imaging system. *Cancer Res*. 2006;66:4208–14.
33. Uchugonova A, Duong J, Zhang N, König K, Hoffman RM. The bulge area is the origin of nestin-expressing pluripotent stem cells of the hair follicle. *J Cell Biochem*. 2011;112:2046–50.
34. Suetsugu A, Katz M, Fleming J, Moriwaki H, Bouvet M, Saji S, Hoffman RM. Multi-color palette of fluorescent proteins for imaging the tumor microenvironment of orthotopic tumor-graft mouse models of clinical pancreatic cancer specimens. *J Cell Biochem*. 2012;113:2290–5.

---

# The Use of Patient-Derived Orthotopic Xenograft (PDOX) Models to Develop Curative Fluorescence-Guided Surgery of Cancer

# 16

Robert M. Hoffman, Yukihiro Hiroshima, Shuya Yano, Cristina A. Metildi, and Michael Bouvet

---

## Introduction

Curative surgery of cancer requires accurate visualization of tumor margins. Fluorescence imaging is appropriate for intra-operative cancer navigation and offers much higher resolution and sensitivity compared to radiological imaging or to visual inspection and palpation during surgery [1].

Genetic labeling of tumors in situ with green fluorescent protein (GFP) has been used for fluorescence-guided surgery (FGS). Kishimoto et al. [2, 3] were the first to selectively and accurately label tumors in mice with GFP with a telomerase-dependent adenovirus (OBP-401) that expresses the *gfp* gene only in cancer cells, which, in contrast to normal cells, express the telomerase enzyme. The labeled tumors were resected under fluorescence guidance.

---

R.M. Hoffman (✉)

AntiCancer, Inc., 7917 Ostrow Street, San Diego, CA 92111, USA

Department of Surgery, University of California, San Diego, CA, USA

e-mail: [all@anticancer.com](mailto:all@anticancer.com)

Y. Hiroshima

AntiCancer, Inc., 7917 Ostrow Street, San Diego, CA 92111, USA

Department of Surgery, University of California, San Diego, CA, USA

Department of Gastroenterological Surgery, Yokohama City University, Yokohama, Japan

S. Yano

AntiCancer, Inc., 7917 Ostrow Street, San Diego, CA 92111, USA

Department of Surgery, University of California, San Diego, CA, USA

Department of Gastroenterological Surgery, Graduate School of Medicine, Dentistry and Pharmaceutical Sciences, Okayama University, Okayama, Japan

C.A. Metildi • M. Bouvet

Department of Surgery, University of California, San Diego, CA, USA

Since almost all tumors express telomerase, the genetic labeling method that uses the telomerase-dependent adenovirus OBP-401 to deliver GFP offers the potential of widespread application. This genetically-stable label also allows detection of cancer recurrence [2, 3].

Also promising are the tumor-labeling methods that use fluorescent tumor-specific antibodies, which also may have wide applicability. However, this method is limited to only those cancers for which tumor-specific antigens have been characterized. Since fluorescent antibodies are not genetic reporters, they will not label recurrent tumors, unless readministered to the patient [4–9].

Patient-derived orthotopic xenografts (PDOX) models from patients with colon [7, 8, 10], pancreatic [5, 11–21], breast [22], ovarian [23], lung [24] and stomach cancer [25], and mesothelioma [26] were established in the early 1990s in our laboratory, resulting in primary and metastatic tumor growth very similar to that of the patient [25]. Recently, PDOX models have been developed for cervical cancer [27–29], sarcoma [30–36], and melanoma [37–41].

This present chapter demonstrates the utility of PDOX models to develop FGS.

---

## Materials and Methods

### GFP-Expressing Telomerase-Specific Adenovirus

In OBP-401, the promoter element of the human telomerase reverse transcriptase (*hTERT*) gene drives the expression of E1A and E1B genes, linked by an internal ribosome entry site. This construction confers selective replication of this virus only in cancer cells. The *GFP* gene is driven by the CMV promoter inserted in OBP-401 [42].

### Mouse Experiments

Athymic (*nu/nu*) nude mice (AntiCancer, Inc., San Diego) are kept in a barrier facility under HEPA filtration. Feed mice with an autoclaved laboratory rodent diet (Teklad LM-485, Western Research Products). All animal studies were in accordance with the principles and procedures outlined in the National Institutes of Health Guide for the Care and Use of Laboratory Animals under Assurance Number A3873-01 [43].

### Surgical Orthotopic Implantation of Pancreatic Cancer PDOX

Under ketamine anesthesia (an injection of a 0.02 mL solution of 80–100 mg/kg ketamine, 10 mg/kg xylazine, and 3 mg/kg acepromazine maleate 10 min before surgery), a small 6–10 mm transverse incision on the left flank of the nude mouse is made through the skin and peritoneum. The tail of the pancreas is pulled through this incision in order to suture a single 1 mm<sup>3</sup> tumor fragment using 8-0 nylon surgical sutures (Ethilon; Ethicon, Somerville, NJ, USA). On completion, the tail of the pancreas is returned to the abdomen and the incision is closed in one layer using 6-0 nylon surgical sutures (Ethilon) [5, 11–21].

## **Surgical Orthotopic Implantation of Colon Cancer PDOX**

Colon cancer PDOX models are established in nude mice by direct surgical implantation of single 1 mm<sup>3</sup> tumor fragments from previously subcutaneous-xenografted tumors. The cecum is delivered through a small 6–10 mm midline abdominal incision. The tumor fragment is sutured to the mesenteric border of the cecal wall using 8-0 nylon surgical sutures. Upon completion, the cecum is returned to the abdomen and the incision is closed in two layers using 6.0 Ethibond nonabsorbable sutures (Ethicon, Inc., Somerville, NJ) [7, 10].

## **Neoadjuvant Chemotherapy**

After confirmation of tumor engraftment, pancreatic PDOX mice are randomized to four groups: bright-light surgery (BLS) only, BLS + neoadjuvant chemotherapy (NAC), FGS only, and FGS + NAC. For NAC treatment, administer 80 mg/kg gemcitabine (GEM) (Eli Lilly and Company, Indianapolis, IN, USA). Inject GEM i.p. on day 8, 15, and 22 [17].

## **OBP-401 Labeling of the PDOX Cancer Cells**

The PDOX tumor is labeled in the stroma with red fluorescent protein (RFP) by growth in an RFP transgenic nude mouse. For viral GFP labeling, the tumor is exposed in the peritoneal cavity during laparotomy. OBP-401 ( $1 \times 10^8$  PFU/tumor) is then injected into the exposed tumor [21].

## **Imaging**

PDOX tumors labeled with GFP in the cancer cells and RFP in the stroma, are imaged with a laser scanning imaging system (IV100; Olympus, Tokyo, Japan) [44] or a confocal laser scanning imaging system (FV1000; Olympus) [45] or an OV100 Olympus Small Animal Imaging System (Olympus) [46].

## **Fluorescence-Guided Surgery**

### **OBP-401-Based Fluorescence-Guided Surgery (OBP-401-FGS) of a Pancreatic Cancer PDOX**

FGS procedures are performed under anesthesia using s.c. administration of a ketamine mixture. PDOX tumors labeled with genetic reporters are visualized with noninvasive fluorescence imaging (OV100) before FGS is performed [43].

A Dino-Lite mobile imaging system or equivalent is used for imaging during FGS. The portable system has seven filtered (480 nm) blue LEDs for excitation lighting, a 510 nm emission filter, a white LED switched by software, and a 1.3 megapixel

sensor. This digital camera can magnify from  $\times 30$  up to  $\times 200$  and can readily take both pictures and videos of magnified green fluorescent objects. The camera's dimensions are  $10.5 \times 3.2$  cm and the weight is only 105 g. This all-in-one compact digital camera makes the Dino-Lite imaging system easily transportable and thereby suitable for FGS [15].

A 20 mm incision at the lateral midline of the abdomen is made to expose the pancreatic tumor. Either under bright light or fluorescence, the tumor is resected using a scalpel and forceps. The Dino-Lite visualized residual GFP cancer cells or RFP stroma remaining FGS. The resected area of the pancreas is closed with a 6-0 suture. After surgery, the abdominal wall is closed with a 6-0 suture [21].

### **Labeling of Colon Cancer PDOX with Fluorescent Antibodies**

Chimeric anti-CEA-Alexa 488 (75  $\mu\text{g}$ ) is injected i.v. 24 h prior to planned resection of the colon tumor. This allows for accurate assessment of pre-operative tumor burden for comparison among surgical groups [7].

### **FGS of a Colon Cancer PDOX Using Fluorescent Antibodies**

After anesthesia, the cecum is delivered through a midline incision to expose the colon tumor. The tumor is pre-operatively imaged with an OV100 (Olympus Corp., Tokyo, Japan), under both standard bright field and fluorescence illumination [46]. The primary colon tumor is imaged intra-operatively using an MVX-10 fluorescence dissecting microscope (Olympus Corp.) [47] with a GFP filter (excitation HQ 470/10 m, emission 525/50 m) or with the Dino-Lite [15]. After removal of the tumor under fluorescence guidance with a scalpel and forceps, the cecal stump is sutured in a running fashion with 8-0 nylon surgical sutures [48]. The surgical resection bed is imaged with the OV100 under both standard bright-field and fluorescence illumination to assess completeness of surgical resection [7, 8].

### **FGS of a Pancreatic Cancer PDOX Using Fluorescent Antibodies**

A 15 mm transverse incision on the left flank of the mouse is made through the skin and peritoneum and kept open with a retractor. The tail of the pancreas is exposed through this incision. Anti-CA19-9 antibody, conjugated to DyLight 650 ((50  $\mu\text{g}$ ) is coinjected, via the tail vein in the mice in the FGS group 24 h before surgery. A MINI MAGLITE LED PRO flashlight (MAG INSTRUMENT, Ontario, CA, USA) coupled to an excitation filter (ET 640/30X, Chroma Technology Corporation, Bellows Falls, VT, USA) is used as the excitation light source. A Canon EOS 60D digital camera with an EF-S 18-55 IS lens (Canon, Tokyo, Japan) coupled with an emission filter (HQ700/75 M-HCAR, Chroma Technology Corporation) is used as a real-time image capturing device for FGS. The tumor is removed under fluorescence guidance with a scalpel and forceps. After completion of surgery, the incision is closed in one layer using 6-0 nylon surgical sutures [17].

### **Postsurgical Animal Imaging**

In order to assess for recurrence and to follow tumor progression postoperatively, the mice are injected with an anti-CEA antibody conjugated to Alexa 647. The mice are imaged at 2 weeks, then at 1 month, post-operatively, and monthly thereafter.

Imaging was done 24 and 48 h after tail vein injection of the chimeric antibody conjugate with the OV100 [46]. The mice are followed for 6 months post-operatively or until pre-morbid, whichever occurs first, at which point the mice are sacrificed 24 h after intravenous injection of the chimeric anti-CEA-647 antibody. Intravital and ex vivo images are also obtained to evaluate the presence of local and/or distant recurrence. Pre-morbidity was determined by the degree of ascites, cachexia, and/or mobility on a scale of 0–4. When ascites and cachexia and/or mobility reach a grade of 4, the mouse is sacrificed. All images were analyzed with Image J v1.440 (National Institutes of Health, Bethesda, MD).

### **Tissue Histology**

Tumor samples with surrounding normal tissues are resected. Fresh tissue samples are fixed in Bouin solution and regions of interest embedded in paraffin prior to sectioning and staining with H&E for standard light microscopy. H&E-stained permanent sections are examined using a BX41 microscope (Olympus Corp.) equipped with a MicroPublisher 3.3 RTV camera (QImaging, Surrey, B.C., Canada). Images are acquired using QCapture software (QImaging) without post-acquisition processing.

### **Statistical Analysis**

PASW Statistics 18.0 (SPSS, Armonk, NY, USA) is used for all statistical analyses. Data are shown as mean  $\pm$  s.d. For comparison between two groups, determine significant differences using the Student's *t*-test. *P*-values of  $<0.05$  is considered significant [21].

Anti-CEA antibody administered as a single intravenous dose 24 h before laparotomy selectively labeled cancer cells in the colon cancer PDOX, and tumor fluorescence was present for at least 1 week [8].

---

## **Results and Discussion**

### **Labeling of the Pancreatic Cancer PDOX with RFP Stroma with OBP-401-GFP**

The pancreatic cancer PDOX model, labeled with RFP stroma from previous growth in an RFP-expressing nude mouse, was double labeled by OBP-401 in the cancer cells 3 days after OBP-401 infection. OBP-401-GFP-labeled cancer cells along with the RFP-expressing stromal cells remained sufficiently bright to perform FGS 6 days after infection [21]. The margin between the tumor and pancreas was very unclear under bright light. In contrast, OBP-401 made the tumor margin much clearer. The Dino-Lite fluorescence digital camera system, imaged during FGS, the margin between tumor and normal sufficiently clearly for successful resection of the pancreatic tumor. Whole-tumor and cross-sectional imaging demonstrated that OBP-401 labeled the whole tumor [21]. The color-coded PDOX model with OBP-401-GFP labeled cancer cells and RFP-labeled stromal cells enabled FGS to completely resect the pancreatic tumors including stroma. Dual-colored FGS significantly prevented local recurrence, which BLS or single-color FGS could not [21] (Fig. 16.1).

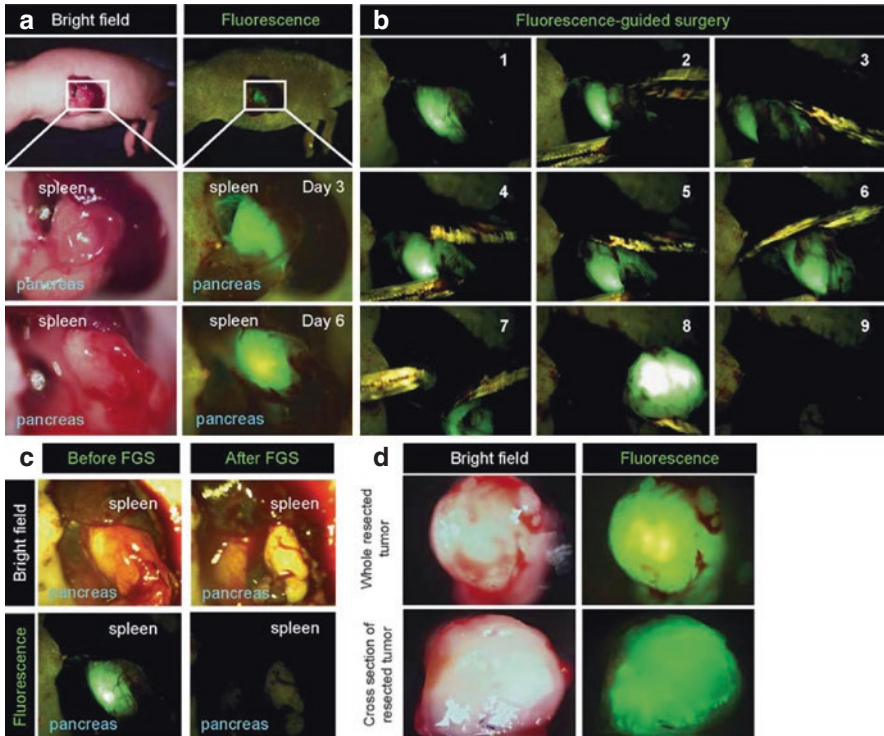


**Fig. 16.1** OBP-401-based FGS of a pancreatic cancer patient-derived orthotopic xenograft (PDOX). (a) Representative intravital images of a pancreatic cancer PDOX labeled with OBP-401-GFP 3 days after infection (upper and middle panels) and 6 days after infection (lower panels). (b) FGS of GFP-labeled PDOX was performed with a Dino-Lite hand-held fluorescence scope. The tumor was resected under fluorescence guidance in steps shown in 1–7. The resected tumor is shown in panel 8. Panel 9 shows no tumor remaining after resection. (c) Representative intravital images before and after FGS. (d) Representative images of resected tumor (upper) and cross-section (lower). Images were acquired with the OV100 fluorescence imaging system. FGS, fluorescence-guided surgery; GFP, green fluorescent protein [21]

### Fluorescence-Guided Surgery of a Colon Cancer PDOX Labeled with a Fluorescent Chimeric Antibody

A chimeric mouse-human anti-CEA antibody conjugated to Alexa 488 demonstrated accurate and specific labeling of a colon tumor PDOX model. The labeled antibody permitted visualization of submillimeter tumor deposits along the wall of the cecum that were not visible in bright field images. A complete resection was evident by the absence of fluorescence in post-operative images. The improved visualization and real-time detection of the fluorescently-labeled tumor resulted in an increase in complete resection rates, compared to standard bright-light surgery, from 85.7 to 95.5% [7].



In another FGS study with an anti-CEA antibody labeled with Alexa Fluor 468, a colon tumor PDOX was successfully resected with FGS using the Dino-Lite. OV100 imaging demonstrated a complete absence of tumor fluorescence after FGS [8].

### **Effect of Neoadjuvant Chemotherapy (NAC) on Pancreatic Cancer PDOX Recurrence with Bright-Light Surgery (BLS) or FGS**

In a pancreatic cancer PDOX labeled with fluorescent anti-CA19-9, the metastatic recurrence rate after FGS + NAC was significantly less than after BLS + NAC. FGS + NAC significantly reduced the metastatic recurrence frequency to one of eight mice compared to FGS only where metastasis recurred in six out of eight mice and BLS + NAC where it occurred in seven out of eight mice [17].

A NAC-resistant pancreatic cancer PDOX was brightly labeled with a fluorescent anti-CEA antibody. Only one of eight mice had local recurrence in the FGS group, and none of eight had recurrence in the FGS + NAC group compared to BLS or BLS + NAC, where six of eight mice recurred in each group [20].

---

## **References**

1. Bouvet M, Hoffman RM. Glowing tumors make for better detection and resection. *Sci Transl Med.* 2011;3:110fs10.
2. Kishimoto H, Zhao M, Hayashi K, Urata Y, Tanaka N, Fujiwara T, Penman S, Hoffman RM. In vivo internal tumor illumination by telomerase-dependent adenoviral GFP for precise surgical navigation. *Proc Natl Acad Sci U S A.* 2009;106:14514–7.
3. Kishimoto H, Aki R, Urata Y, Bouvet M, Momiyama M, Tanaka N, Fujiwara T, Hoffman RM. Tumor-selective adenoviral-mediated GFP genetic labeling of human cancer in the live mouse reports future recurrence after resection. *Cell Cycle* 2011;10:2737–41.
4. McElroy M, Kaushal S, Luiken G, Moossa AR, Hoffman RM, Bouvet M. Imaging of primary and metastatic pancreatic cancer using a fluorophore-conjugated anti-CA19-9 antibody for surgical navigation. *World J Surg.* 2008;32:1057–66.
5. Kaushal S, McElroy MK, Luiken GA, Talamini MA, Moossa AR, Hoffman RM, Bouvet M. Fluorophore-conjugated anti-CEA antibody for the intraoperative imaging of pancreatic and colorectal cancer. *J Gastrointest Surg.* 2008;12:1938–50.
6. Metildi CA, Kaushal S, Pu M, Messer KA, Luiken GA, Moossa AR, Hoffman RM, Bouvet M. Fluorescence-guided surgery with a fluorophore-conjugated antibody to carcinoembryonic antigen (CEA), that highlights the tumor, improves surgical resection and increases survival in orthotopic mouse models of human pancreatic cancer. *Ann Surg Oncol.* 2014;21:1405–11.
7. Metildi CA, Kaushal S, Luiken GA, Talamini MA, Hoffman RM, Bouvet M. Fluorescently-labeled chimeric anti-CEA antibody improves detection and resection of human colon cancer in a patient-derived orthotopic xenograft (PDOX) nude mouse model. *J Surg Oncol.* 2014;109:451–8.
8. Hiroshima Y, Maawy A, Metildi CA, Zhang Y, Uehara F, Miwa S, Yano S, Sato S, Murakami T, Momiyama M, Chishima T, Tanaka K, Bouvet M, Endo I, Hoffman RM. Successful fluorescence-guided surgery on human colon cancer patient-derived orthotopic xenograft mouse models using a fluorophore-conjugated anti-CEA antibody and a portable imaging system. *J Laparoendosc Adv Surg Tech A.* 2014;24:241–7.

9. Metildi CA, Kaushal S, Luiken GA, Hoffman RM, Bouvet M. Advantages of fluorescence-guided laparoscopic surgery of pancreatic cancer labeled with fluorescent anti-carcinoembryonic antigen antibodies in an orthotopic mouse model. *J Am Coll Surg.* 2014;219:132–41.
10. Fu X, Besterman JM, Monosov A, Hoffman RM. Models of human metastatic colon cancer in nude mice orthotopically constructed by using histologically intact patient specimens. *Proc Natl Acad Sci U S A.* 1991;88:9345–9.
11. Fu X, Guadagni F, Hoffman RM. A metastatic nude-mouse model of human pancreatic cancer constructed orthotopically from histologically intact patient specimens. *Proc Natl Acad Sci U S A.* 1992;89:5645–9.
12. Suetsugu A, Katz M, Fleming J, Moriwaki H, Bouvet M, Saji S, Hoffman RM. Multi-color palette of fluorescent proteins for imaging the tumor microenvironment of orthotopic tumorgraft mouse models of clinical pancreatic cancer specimens. *J Cell Biochem.* 2012;113:2290–5.
13. Suetsugu A, Katz M, Fleming J, Truty M, Thomas R, Saji S, Moriwaki H, Bouvet M, Hoffman RM. Imageable fluorescent metastasis resulting in transgenic GFP mice orthotopically implanted with human-patient primary pancreatic cancer specimens. *Anticancer Res.* 2012;32:1175–80.
14. Suetsugu A, Katz M, Fleming J, Truty M, Thomas R, Saji S, Moriwaki H, Bouvet M, Hoffman RM. Non-invasive fluorescent-protein imaging of orthotopic pancreatic-cancer-patient tumorgraft progression in nude mice. *Anticancer Res.* 2012;32:3063–8.
15. Hiroshima Y, Maawy A, Sato S, Murakami T, Uehara F, Miwa S, Yano S, Momiyama M, Chishima T, Tanaka K, Bouvet M, Endo I, Hoffman RM. Hand-held high-resolution fluorescence imaging system for fluorescence-guided surgery of patient and cell-line pancreatic tumors growing orthotopically in nude mice. *J Surg Res.* 2014;187:510–7.
16. Hiroshima Y, Zhao M, Maawy A, Zhang Y, Katz MH, Fleming JB, Uehara F, Miwa S, Yano S, Momiyama M, Suetsugu A, Chishima T, Tanaka K, Bouvet M, Endo I, Hoffman RM. Efficacy of *Salmonella typhimurium* A1-R versus chemotherapy on a pancreatic cancer patient-derived orthotopic xenograft (PDOX). *J Cell Biochem.* 2014;115:1254–61.
17. Hiroshima Y, Maawy A, Zhang Y, Murakami T, Momiyama M, Mori R, Matsuyama R, Katz MH, Fleming JB, Chishima T, Tanaka K, Ichikawa Y, Endo I, Hoffman RM, Bouvet M. Metastatic recurrence in a pancreatic cancer patient derived orthotopic xenograft (PDOX) nude mouse model is inhibited by neoadjuvant chemotherapy in combination with fluorescence-guided surgery with an anti-CA 19-9-conjugated fluorophore. *PLoS One.* 2014;9:e114310.
18. Hiroshima Y, Zhang Y, Murakami T, Maawy AA, Miwa S, Yamamoto M, Yano S, Sato S, Momiyama M, Mori R, Matsuyama R, Chishima T, Tanaka K, Ichikawa Y, Bouvet M, Endo I, Zhao M, Hoffman RM. Efficacy of tumor-targeting *Salmonella typhimurium* A1-R in combination with anti-angiogenesis therapy on a pancreatic cancer patient-derived orthotopic xenograft (PDOX) and cell line mouse models. *Oncotarget.* 2014;5:12346–57.
19. Hiroshima Y, Maawy AA, Katz MH, Fleming JB, Bouvet M, Endo I, Hoffman RM. Selective efficacy of zoledronic acid on metastasis in a patient-derived orthotopic xenograft (PDOX) nude-mouse model of human pancreatic cancer. *J Surg Oncol.* 2015;111:311–5.
20. Hiroshima Y, Maawy A, Zhan Y, Murakami T, Momiyama M, Mori R, Matsuyama R, Chishima T, Tanaka K, Ichikawa Y, Endo I, Hoffman RM, Bouvet M. Fluorescence-guided surgery, but not bright-light surgery, prevents local recurrence in a pancreatic cancer patient-derived orthotopic xenograft (PDOX) model resistant to neoadjuvant chemotherapy (NAC). *Pancreatol.* 2015;15:295–301.
21. Yano S, Hiroshima Y, Maawy A, Kishimoto H, Suetsugu A, Miwa S, Toneri M, Yamamoto M, Katz MHG, Fleming JB, Urata Y, Tazawa H, Kagawa S, Bouvet M, Fujiwara T, Hoffman RM. Color-coding cancer and stromal cells with genetic reporters in a patient-derived orthotopic xenograft (PDOX) model of pancreatic cancer enhances fluorescence-guided surgery. *Cancer Gene Ther.* 2015;22:344–50.
22. Fu X, Le P, Hoffman RM. A metastatic-orthotopic transplant nude-mouse model of human patient breast cancer. *Anticancer Res.* 1993;13:901–4.

23. Fu X, Hoffman RM. Human ovarian carcinoma metastatic models constructed in nude mice by orthotopic transplantation of histologically-intact patient specimens. *Anticancer Res.* 1993;13:283–6.
24. Wang X, Fu X, Hoffman RM. A new patient-like metastatic model of human lung cancer constructed orthotopically with intact tissue via thoracotomy in immunodeficient mice. *Int J Cancer.* 1992;51:992–5.
25. Furukawa T, Kubota T, Watanabe M, Kitajima M, Fu X, Hoffman RM. Orthotopic transplantation of histologically intact clinical specimens of stomach cancer to nude mice: correlation of metastatic sites in mouse and individual patient donors. *Int J Cancer.* 1993;53:608–12.
26. Astoul P, Wang X, Colt HG, Boutin C, Hoffman RM. A patient-like human malignant pleural mesothelioma nude-mouse model. *Oncol Rep.* 1996;3:483–7.
27. Hiroshima Y, Zhang Y, Zhang M, Maawy A, Mii S, Yamamoto M, Uehara F, Miwa S, Yano S, Murakami T, Momiyama M, Chishima T, Tanaka K, Ichikawa Y, Bouvet M, Murata T, Endo I, Hoffman RM. Establishment of a patient-derived orthotopic xenograph (PDOX) model of HER-2-positive cervical cancer expressing the clinical metastatic pattern. *PLoS One.* 2015;10:e0117417.
28. Hiroshima Y, Maawy A, Zhang Y, Zhang N, Murakami T, Chishima T, Tanaka K, Ichikawa Y, Bouvet M, Endo I, Hoffman RM. Patient-derived mouse models of cancer need to be orthotopic in order to evaluate targeted anti-metastatic therapy. *Oncotarget.* 2016;7:71696–702.
29. Murakami T, Murata T, Kawaguchi K, Kiyuna T, Igarashi K, Hwang HK, Hiroshima Y, Hozumi C, Komatsu S, Kikuchi T, Lwin TM, DeLong JC, Miyake K, Zhang Y, Tanaka K, Bouvet M, Endo I, Hoffman RM. Cervical cancer patient-derived orthotopic xenograft (PDOX) is sensitive to cisplatin and resistant to nab-paclitaxel. *Anticancer Res.* 2017;37:61–6.
30. Hiroshima Y, Zhao M, Zhang Y, Zhang N, Maawy A, Murakami T, Mii S, Uehara F, Yamamoto M, Miwa S, Yano S, Momiyama M, Mori R, Matsuyama R, Chishima T, Tanaka K, Ichikawa Y, Bouvet M, Endo I, Hoffman RM. Tumor-targeting *Salmonella typhimurium* A1-R arrests a chemo-resistant patient soft-tissue sarcoma in nude mice. *PLoS One.* 2015;10:e0134324.
31. Murakami T, DeLong J, Eilber FC, Zhao M, Zhang Y, Zhang N, Singh A, Russell T, Deng S, Reynoso J, Quan C, Hiroshima Y, Matsuyama R, Chishima T, Tanaka K, Bouvet M, Chawla S, Endo I, Hoffman RM. Tumor-targeting *Salmonella typhimurium* A1-R in combination with doxorubicin eradicate soft tissue sarcoma in a patient-derived orthotopic xenograft PDOX model. *Oncotarget.* 2016;7:12783–90.
32. Kiyuna T, Murakami T, Tome Y, Kawaguchi K, Igarashi K, Zhang Y, Zhao M, Li Y, Bouvet M, Kanaya F, Singh A, Dry S, Eilber FC, Hoffman RM. High efficacy of tumor-targeting *Salmonella typhimurium* A1-R on a doxorubicin- and dactolisib-resistant follicular dendritic-cell sarcoma in a patient-derived orthotopic xenograft PDOX nude mouse model. *Oncotarget.* 2016;7:33046–54.
33. Murakami T, Singh AS, Kiyuna T, Dry SM, Li Y, James AW, Igarashi K, Kawaguchi K, DeLong JC, Zhang Y, Hiroshima Y, Russell T, Eckardt MA, Yanagawa J, Federman N, Matsuyama R, Chishima T, Tanaka K, Bouvet M, Endo I, Eilber FC, Hoffman RM. Effective molecular targeting of *CDK4/6* and *IGF-1R* in a rare *FUS-ERG* fusion *CDKN2A*-deletion doxorubicin-resistant Ewing's sarcoma in a patient-derived orthotopic xenograft (PDOX) nude-mouse model. *Oncotarget.* 2016;7:47556–64.
34. Kiyuna T, Murakami T, Tome Y, Igarashi K, Kawaguchi K, Russell T, Eckhardt MA, Crompton J, Singh A, Bernthal N, Bukata S, Federman N, Kanaya F, Eilber FC, Hoffman RM. Labeling the stroma of a patient-derived orthotopic xenograft (PDOX) mouse models of undifferentiated pleomorphic soft-tissue sarcoma with red fluorescent protein for rapid non-invasive drug screening. *J Cell Biochem.* 2017;118:361–5.
35. Murakami T, Igarashi K, Kawaguchi K, Kiyuna T, Zhang Y, Zhao M, Hiroshima Y, Nelson SD, Dry SM, Li Y, Yanagawa J, Russell T, Federman N, Singh A, Elliott I, Matsuyama R, Chishima T, Tanaka K, Endo I, Eilber FC, Hoffman RM. Tumor-targeting *Salmonella typhimurium* A1-R regresses an osteosarcoma in a patient-derived xenograph model resistant to a molecular-targeting drug. *Oncotarget* 2017;8:8035–42.

36. Igarashi K, Kawaguchi K, Kiyuna T, Murakami T, Miwa S, Nelson SD, Dry SM, Li Y, Singh A, Kimura H, Hayashi K, Yamamoto N, Tsuchiya H, Eilber FC, Hoffman RM. Patient-derived orthotopic xenograft (PDOX) mouse model of adult rhabdomyosarcoma invades and recurs after resection in contrast to the subcutaneous ectopic model. *Cell Cycle* 2017;16:91–94.
37. Yamamoto M, Zhao M, Hiroshima Y, Zhang Y, Shurell E, Eilber FC, Bouvet M, Noda M, Hoffman RM. Efficacy of tumor-targeting *Salmonella typhimurium* A1-R on a melanoma patient-derived orthotopic xenograft (PDOX) nude-mouse model. *PLoS One*. 2016;11:e0160882.
38. Kawaguchi K, Murakami T, Chmielowski B, Igarashi K, Kiyuna T, Unno M, Nelson SD, Russell TA, Dry SM, Li Y, Eilber FC, Hoffman RM. Vemurafenib-resistant BRAF-V600E mutated melanoma is regressed by MEK targeting drug trametinib, but not cobimetinib in a patient-derived orthotopic xenograft (PDOX) mouse model. *Oncotarget*. 2016;7:71737–43.
39. Kawaguchi K, Igarashi K, Murakami T, Chmielowski B, Kiyuna T, Zhao M, Zhang Y, Singh A, Unno M, Nelson SD, Russell T, Dry SM, Li Y, Eilber FC, Hoffman RM. Tumor-targeting *Salmonella typhimurium* A1-R combined with Temozolomide regresses malignant melanoma with a BRAF-V600 mutation in a patient-derived orthotopic xenograft (PDOX) model. *Oncotarget* 2016;7:85929–36.
40. Kawaguchi K, Igarashi K, Murakami T, Zhao M, Zhang Y, Chmielowski B, Kiyuna T, Nelson SD, Russell TA, Dry SM, Li Y, Unno M, Eilber FC, Hoffman RM. Tumor-targeting *Salmonella typhimurium* A1-R sensitizes melanoma with a BRAF-V600E mutation to vemurafenib in a patient-derived orthotopic xenograft (PDOX) nude mouse model. *J Cell Biochem.*, Epub ahead of print. DOI:10.1002/jcb.25886.
41. Kawaguchi K, Igarashi K, Chmielowski B, Murakami T, Kiyuna T, Zhao M, Zhang Y, Nelson SD, Russell TA, Dry SM, Singh AS, Li Y, Unno M, Eilber FC, Hoffman RM. *Salmonella typhimurium* A1-R targeting of a chemotherapy resistant BRAF-V600E melanoma in a patient-derived orthotopic xenograft (PDOX) model is enhanced in combination with either vemurafenib-temozolomide. *Cell Cycle*, in press.
42. Kishimoto H, Kojima T, Watanabe Y, Kagawa S, Fujiwara T, Uno F, Teraishi F, Kyo S, Mizuguchi H, Hashimoto Y, Urata Y, Tanaka N, Fujiwara T. In vivo imaging of lymph node metastasis with telomerase-specific replication-selective adenovirus. *Nat Med*. 2006;12:1213–9.
43. Yano S, Miwa S, Kishimoto H, Uehara F, Tazawa H, Toneri M, Hiroshima Y, Yamamoto M, Urata Y, Kagawa S, Bouvet M, Fujiwara T, Hoffman RM. Targeting tumors with a killer-reporter adenovirus for curative fluorescence-guided surgery of soft-tissue sarcoma. *Oncotarget*. 2015;6:13133–48.
44. Yang M, Jiang P, Hoffman RM. Whole-body subcellular multicolor imaging of tumor-host interaction and drug response in real time. *Cancer Res*. 2007;67:5195–200.
45. Uchugonova A, Duong J, Zhang N, König K, Hoffman RM. The bulge area is the origin of nestin-expressing pluripotent stem cells of the hair follicle. *J Cell Biochem*. 2011;112:2046–50.
46. Yamauchi K, Yang M, Jiang P, Xu M, Yamamoto N, Tsuchiya H, Tomita K, Moossa AR, Bouvet M, Hoffman RM. Development of real-time subcellular dynamic multicolor imaging of cancer-cell trafficking in live mice with a variable-magnification whole-mouse imaging system. *Cancer Res*. 2006;66:4208–14.
47. Kimura H, Momiyama M, Tomita K, Tsuchiya H, Hoffman RM. Long-working-distance fluorescence microscope with high-numerical-aperture objectives for variable-magnification imaging in live mice from macro- to subcellular. *J Biomed Opt*. 2010;15(6):066029.
48. Metildi CA, Kaushal S, Snyder CS, Hoffman RM, Bouvet M. Fluorescence-guided surgery of human colon cancer increases complete resection resulting in cures in an orthotopic nude mouse model. *J Surg Res*. 2013;179:87–93.

---

# Molecular Characteristics of Patient-Derived Tumor Xenografts: Similarities to Patient Tumors and Relevance for Biomarker Discovery

# 17

Vincent Vuaroqueaux, Anne-Lise Peille, Bruno Zeitouni, Anne-Marie Eades-Perner, and Heinz-Herbert Fiebig

---

## Background

The concept of using human tumor xenografts for anticancer drug development programs was already suggested as early as 1969 [1, 2]. PDXs have re-emerged and become attractive preclinical models within the last 10 years as more researchers realize their resemblance to patient tumors [3–7]. PDXs have been shown to be particularly suitable to test the efficacy of anticancer agents because they enable solid tumor growth within a microenvironment comprising stromal cells and blood vessels which better reflects the clinical situation [8]. Additionally, PDXs were shown to well preserve histological features, such as cell differentiation and architecture, and to have more cellular heterogeneity compared to cancer cell lines [8]. Overall, these characteristics allow PDXs to mimic the patient tumor response to therapies particularly well [2, 7, 9, 10].

We and others have developed large collections of PDXs [11, 12] and several thousand PDX models are currently available for oncology research. Worldwide efforts on PDX development have demonstrated that not all models can be engrafted with equal success. While pancreatic, colon, or lung cancers have an engraftment rate close to 60–90% ensuring to well cover the tumor diversity seen in the clinic, others such as hormone-dependent breast, and prostate, or gastric tumors have much lower success rates and remain particularly challenging to establish [6, 7, 13].

In parallel, the recent efforts for cancer molecular characterization (e.g., The Cancer Genome Atlas) have revealed the huge diversity of tumors [14–16]. Tumors were found to have a high heterogeneity of genomic alteration loads, mutational profiles, mutated genes, chromosome aberrations (gene losses/gains, fusions) and expression profiles. Integrative analyses demonstrated that these alterations occur in

---

V. Vuaroqueaux (✉) • A.-L. Peille • B. Zeitouni • A.-M. Eades-Perner • H.-H. Fiebig  
Oncotest GmbH, Am Flughafen 12-14, 79108 Freiburg, Germany  
e-mail: [vincent.vuaroqueaux@4hf.eu](mailto:vincent.vuaroqueaux@4hf.eu)

infinite combinations. As a consequence, although there may be similarities between individual tumors, none have identical genomic alteration profiles, thus explaining their disparity in drug responses.

In this context, the detailed analysis of PDX molecular features has become crucial for their optimal use in translational research, with the need to address the questions of genomic and transcriptomic resemblance with patient tumors and whether existing collections cover cancer diversity.

---

## **PDX Characterization**

We established a collection that currently comprises more than 450 PDXs encompassing up to 20 different histological types. After stable establishment (over four passages), PDXs are routinely analyzed for tumor histological features including grade, stroma content, necrotic area content, and vasculature. In addition, PDX materials are collected for molecular characterization: (1) by whole exome sequencing (WES) to reveal mutations, (2) by Affymetrix SNP6.0 microarrays to assess somatic copy number variations and large chromosome aberrations, and (3) by microarray Affymetrix HGU133 Plus 2.0 and/or by RNAseq to determine transcript expression, mutations, and gene fusions. For designated PDX models, the analysis is completed by assessment of clinical biomarkers such as MLH1 loss or ERBB2, EGFR, or MET overexpression/amplification.

---

## **Genomic Alterations Detected in PDXs Are Highly Similar to Those Found in Patient Tumors**

While the fidelity of PDXs with regard to histology and drug response has been largely demonstrated [2, 8], their similarities with patient tumors regarding genomic features have been questioned. To assess this, we compared the exome mutational profiles of 268 of our PDXs with those of patient tumors from publicly available databases of The Cancer Genome Atlas (TCGA) [17]. First we showed that PDXs presented typical signatures of mutational processes observed in patient tumors [18]. For example, we found that part of the lung cancer PDXs displayed a mutational signature associated with smoking history. The melanoma PDXs presented a signature typical of UV-light exposure. Some colon, gastric, and pancreatic PDXs shared typical signatures of DNA mismatch repair (MMR) deficiency and aging. We observed furthermore that PDX mutational loads and distribution across histological types were very similar to those reported in patient tumors. The analysis revealed both heavily mutated tumor types such as melanoma, lung, or colon cancer PDXs and others usually displaying lower mutation loads such as glioblastoma, renal, or pancreatic tumors.

By focusing on genomic alterations in a given tumor type, we showed, for example, that non-small cell lung cancer (NSCLC) PDXs were heavily mutated with mutation loads of 4.3–26.8 mutations/megabase per model [19] (Fig. 17.1a). We observed furthermore that genomic alteration patterns were associated with histologic subtypes of NSCLC PDXs. For example, the mutation prevalence and the

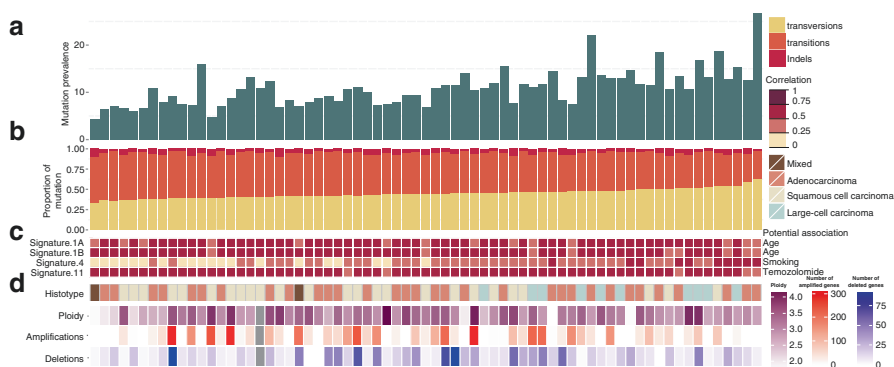


**Fig. 17.1** Landscape of genomic alterations in NSCLC PDXs. **(a)** Barplot showing mutation prevalence in mutations per megabase (WES). **(b)** Proportions of transversions ( $A > C$ ,  $A > T$ ,  $G > C$ ,  $G > T$ ), transitions ( $A > G$  &  $C > T$ ), and indels (WES). **(c)** Matrix showing the correlations between the mutational signatures (proportions of 96 possible trinucleotide substitutions) of the NSCLC PDXs and the 21 mutational signatures published by Alexandrov et al. [18]. **(d)** Heatmaps showing histotypes, ploidy, the number of gene amplifications (Affymetrix SNP6.0 PICNIC  $\geq 8$ ), and gene deletions (Affymetrix SNP6.0 PICNIC = 0) [77] in NSCLC PDXs sorted by increasing proportion of transversions and the gene alterations among the 22 chromosomes

proportions of transversions, often reflecting smoking history of the patients, were significantly higher in the large-cell carcinomas than in adenocarcinoma and squamous NSCLC PDXs ( $p = 0.03$  and  $p = 0.002$ , respectively, Fig. 17.1b). Of interest, other signatures of mutational processes known to be associated with aging and temozolomide sensitivity were also found throughout the NSCLC PDX collection (Fig. 17.1c). Accompanying these mutations, we observed additionally that the NSCLC PDXs presented high chromosomal instability with frequent polyploidy, high number of gene amplifications, and homozygous deletions (Fig. 17.1d).

In accordance with previous analyses of patient tumors [20–22], detailed examination of cancer-related genes in NSCLC PDXs revealed that alterations of the RAS/RAF pathway and MET amplification occurred frequently in adenocarcinoma and large-cell carcinoma models, explaining the frequent resistance to anti-EGFR therapy (Fig. 17.2a–d). In contrast, we found that squamous cell carcinoma PDXs had, as seen in patient tumors [23], frequent alterations in TP53, PIK3CA, and PTEN genes and high expression of TP63 and FGFR3 mRNA (Fig. 17.2c). In line with their distinct genomic backgrounds, the different NSCLC PDX histological subtypes exhibited differences in drug sensitivity (Fig. 17.2d). Squamous-cell cancer PDXs were the most sensitive to cis-platinum, whereas adenocarcinoma PDXs were the most resistant ( $p = 0.003$ ). In contrast, squamous-cell carcinoma and adenocarcinoma PDXs were more sensitive to paclitaxel than large-cell cancer PDXs ( $p = 0.03$ ). Among adenocarcinoma and large-cell cancer PDXs, we identified three models with EGFR mutations, one of which contained the codon insertion EGFR<sup>A767\_S768InsSVA</sup> associated with a strong sensitivity toward cetuximab, but not to erlotinib [19]. Therefore, these investigations confirm that the genomic alterations in PDXs are highly similar to those found in patient tumors of the corresponding histological type. These alterations determine modalities of tumor growth behavior and drug sensitivity of each model.

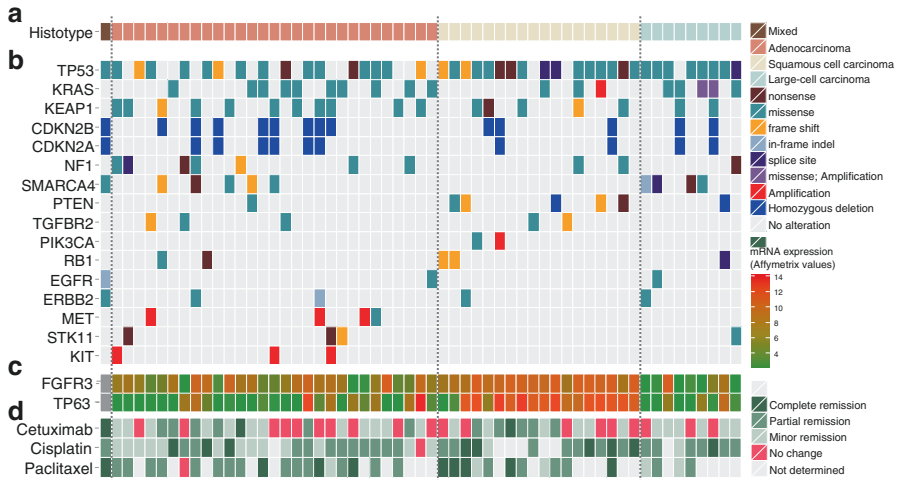


**Fig. 17.2** Landscape of cancer-related genes alterations in NSCLC PDXs and sensitivity to selected compounds. (a) Heatmap showing the histotypes of NSCLC PDXs. (b) Heatmap showing the types of genomic alterations in cancer-related genes for each NSCLC PDX. (c) Level of mRNA expression of *FGFR3* and *TP63* (Affymetrix HGU133 Plus2.0 data) for each NSCLC PDX. (d) Heatmap showing the responses to *in vivo* therapies. (*In vivo* activity: complete remission,  $T/C < 10\%$ ; partial remission,  $10\% \geq T/C > 50\%$ ; minor remission,  $50\% \geq T/C > 75\%$ ; no change,  $T/C \geq 75\%$ )

## PDX Models Retain the Transcriptomic Profiles of Patient Tumors

We aimed to investigate whether transcriptomic profiles of patient tumors were retained in PDXs. First, concurring with the results reported by Martinez-Garcia et al. [24], an internal study showed that newly established pancreatic ductal adenocarcinoma (PDAC) PDXs at passages 1, 2, and 3 shared high similarities in their gene expression profiles with those of corresponding parental patient tumors (results not shown). This confirms to some extent that transcriptomic profiles are largely conditioned by genetic imprint and that growth of the cancer cells in the mouse host does not dramatically modify gene expression profiles during the first passages. Differences were however found for genes expressed in human tumor stroma that were not detectable after passage 2 due to its replacement by murine stroma.

In line with results recently reviewed by Hidalgo et al. and the study of Guo et al. [7, 25], we found that the transcriptomic profiles of PDXs were largely related to the histological tumor type. The PDXs were shown to cluster mainly by tissue origin when they are analyzed by using unsupervised hierarchical clustering with the most differentially expressed genes (Fig. 17.3a). The colon and PDAC PDXs (CXF, PAXF) presented very different profiles compared to mammary (MAXF), lung (LXF), or renal models (RXF). Moreover, for a given tumor type, we observed that PDX transcriptomic profiles were also dependent on histological subtypes. For example, among the NSCLC PDXs, adeno (LXFA), squamous cell (LXFE), or large-cell carcinoma subtypes (LXFL) all exhibited distinct patterns of gene



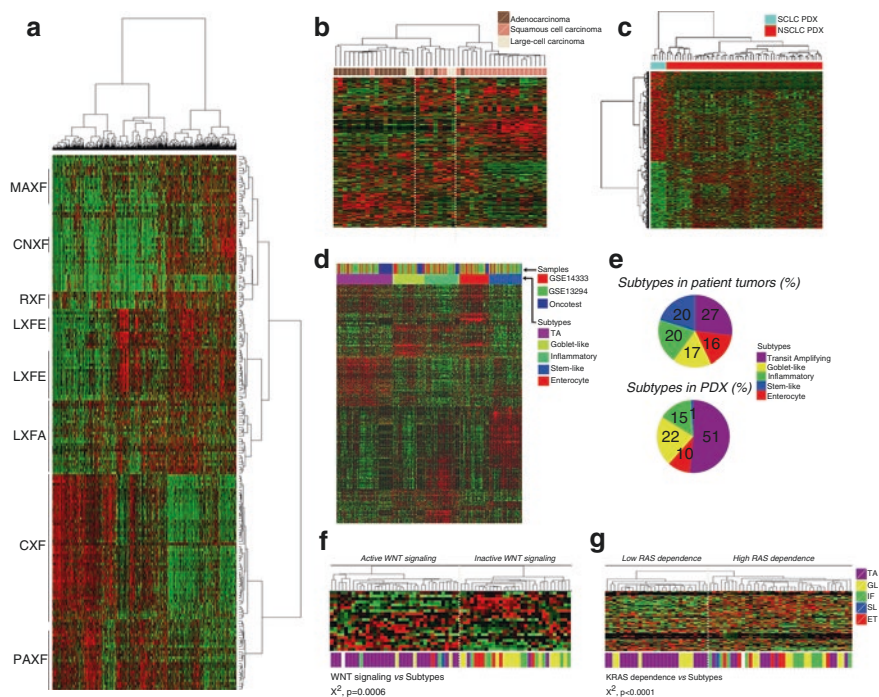


**Fig. 17.3** Transcriptomic profiles of PDX tumor models. **(a)** Heatmap with the 1000 most variant genes among 188 PDX samples of different histological types. **(b)** Heatmap showing the 1000 most differentially expressed genes in the adenocarcinoma, squamous cell, and large cell NSCLC PDXs. **(c)** Heatmap showing the 2912 genes differentially expressed between SCLC and NSCLC PDX tumor models (*right panel*). **(d)** Heatmap showing molecular subtypes from merged core datasets GSE13294 ( $n = 135$ ) and GSE14333 ( $n = 252$ ) of CRC patient tumors with regard to 786 gene-expression profiles. Data were merged using distance-weighted discrimination as described by Sadanandam et al. [31]. **(e)** Pie charts comparing the distribution of the subtypes retrieved in patient colon tumors with that in Oncotest colon PDXs. **(f)** Unsupervised hierarchical clusters showing the association of the Sadanandam classification to the WNT activation signature. **(g)** Unsupervised hierarchical clusters showing the association of the Sadanandam classification to the RAS-pathway-dependence signature

expression (Fig. 17.3b) [19]. Similarly, we found that SCLC PDXs retained a very strong distinctive signature compared to NSCLC PDXs with a notably high expression of neuroendocrine markers including ASCL1, DLK1, GRP, or CHGA (Fig. 17.3c) [26, 27].

In tumor types such as colorectal cancers, extensive analysis of the transcriptome revealed that tumors can be classified by using gene-expression signatures with prognostic and predictive implications [28–32]. A detailed meta-analysis showed that these signatures strongly overlapped and were largely dependent on cancer cell origin (crypt top or base) and genomic alterations and related to pathway activation [32, 33]. Similarly, we aimed to determine whether we could classify our colon tumor PDX collection into subtypes [34]. We used for example, the five transcriptomic subtypes proposed by Sadanandam et al. (transit amplifying (TA), stem-like (SL),

goblet-like (GL), inflammatory (IF), and enterocyte (ET)) [33]. For this, we merged gene expression profiles of colon PDXs with core datasets (GSE13294,  $n = 135$ ) and (GSE14333,  $n = 252$ ) of patient colon tumors using the distance-weighted discrimination method and analyzed the samples for a 786-gene expression signature (Fig. 17.3d). By this approach, the PDXs classified into the goblet-like (22% vs. 17%), inflammatory (15% vs. 20%), and enterocyte (10% vs. 16%) subtypes with similar proportions as for patient tumors (Fig. 17.3e). The stem-like PDXs were however not identified due to a signature mostly related to stroma-expressed genes [35] and, conversely, transit-amplifying PDXs were overrepresented (51% vs. 27% in patient tumors). These results suggested that part of stem-like PDXs were misclassified as transit amplifying, most probably due to marked transcriptomic profile similarities linked to a common basal crypt origin. Supporting this hypothesis, we observed that the PDXs classified as transit amplifying share, similar to stem-like tumors, a gene expression signature indicative of *WNT*-signaling pathway activation [36] in contrast to most of enterocyte, goblet-like, or inflammatory PDXs (Fig. 17.3f). We also observed that transit-amplifying PDXs were predominant among tumors with low RAS pathway dependence (Fig. 17.3g) [37]. In addition to the tumor origin, we showed that the transcriptomic profiles of PDXs were related to their genomic-alteration profiles (Fig. 17.4a, b). Notably, we observed that inflammatory and goblet-like subtypes comprised heavily mutated PDXs including notably those with MMR deficiency. In contrast, the transit-amplifying PDXs were frequently seen with lower mutation loads and less frequent alterations in genes of the RAS pathway which determine cetuximab sensitivity (Fig. 17.4c). In agreement

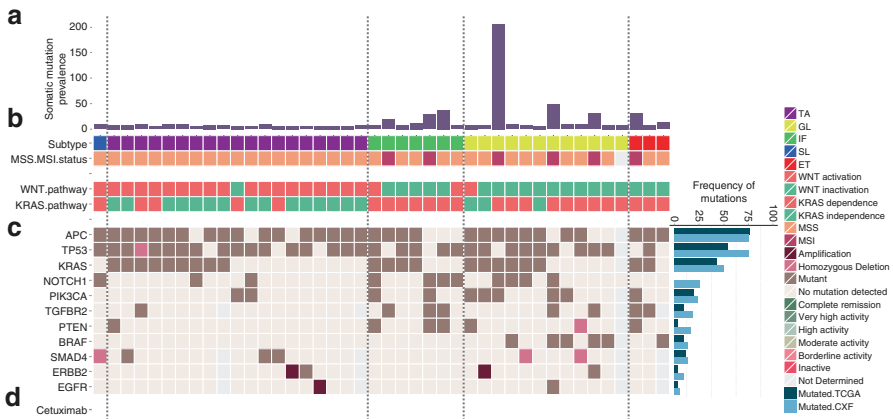


**Fig. 17.4** Landscape of genomic alterations in colon PDXs. **(a)** Barplot showing the mutation prevalence in mutations per megabase (WES). **(b)** Heatmap showing the PDX transcriptomic subtypes according to the Sadanandam classification, the microsatellite instability status, WNT pathway activation, and RAS dependence. **(c)** Heatmap showing the genomic alterations of selected cancer-related genes within the colon PDX collection and the comparison of mutation frequencies with patient tumors from the TCGA (right barplot). **(d)** Response to in vivo cetuximab therapy. In vivo activity: complete remission,  $T/C < 5\%$ ; very high activity,  $5\% \geq T/C > 10\%$ ; high activity,  $10\% \geq T/C > 25\%$ ; moderate activity,  $25\% \geq T/C > 50\%$ ; borderline activity,  $50\% \geq T/C > 65\%$ ; and inactive,  $T/C \geq 65\%$

with other studies [38–40], these results confirm the strong implications of genetic alterations in the transcriptomic profile of PDXs and consequently the representativeness of PDXs at the transcriptome level.

---

## The Microenvironment of PDXs Has Certain Similarities with Patient Tumors

Another aspect of the preferred use of PDXs over tumor cell lines in drug development is the capability of solid tumor growth within a microenvironment comprising an extracellular matrix with lymphatic and blood vessels, fibroblasts, as well as a variety of signaling molecules. It implies that during replacement of human stroma by murine stroma, a paracrine communication between human cancer cells and the host enable to promote neovascularization and to mobilize surrounding fibroblasts still exist. In human tumors, cancer-associated fibroblasts (CAFs) have been shown to be drivers of tumor progression, cell proliferation, invasion, epithelial to mesenchymal transition, cancer-cell survival after chemotherapy, and tumor growth via secretion of multiple growth factors [41]. In PDXs, human CAFs and murine fibroblasts are found around tumor cells and their implications for growth and response to anticancer drugs have been suggested [8]. However the exact interrelation between tumor and stroma cells in PDX still remains obscure.

To know more about the PDX stroma environment and fibroblast interactions, we focused on PDAC PDXs, which presented various levels of stroma content and differentiation stages (Fig. 17.5a, b). With a relatively high engraftment success rate (65%) which correlates closely to poor patient outcome [42, 43], we have established over the years a collection comprising today more than 40 models [44]. By following models during the early stages of development, we found that the replacement of human stroma by murine stroma occurred during the first two passages. We also observed that PDAC PDXs develop various stroma contents that can range from 5 to up to 60%, and that frequently correlated with those of respective parental tumors (Fig. 17.5c). These results suggest that cancer cells may dictate the amount of stroma in the tumor. In addition, evidence for activated fibroblasts with changed morphology (small spindle, thin and wavy body structure, and a symmetric/parallel orientation) was found in some PDAC PDXs (Fig. 17.5d) [43]. Similarly to the recent findings in patient PDAC tumors [45], our results suggested that these activated fibroblasts may play a role in the PDX model growth.

Next, we analyzed whether stroma content and fibroblast activation were associated with particular molecular subtypes of PDAC PDX [43]. Using the gene-expression signature proposed by Collisson et al. [46], PDAC PDXs were classified as classical (52%), quasi-mesenchymal (QM-PDA) (36%), and exocrine-like subtypes (12%) comparable to the proportion observed for patient tumors (Fig. 17.6a). As previously reported for PDAC [47, 48], integrative analysis revealed that the PDAC PDX stroma content and fibroblast activation were both associated with transcriptomic subtypes and tumor grades (Fig. 17.6b). The quasi-mesenchymal PDAC PDXs frequently had activated fibroblasts and lower stroma contents in contrast to classical subtypes.

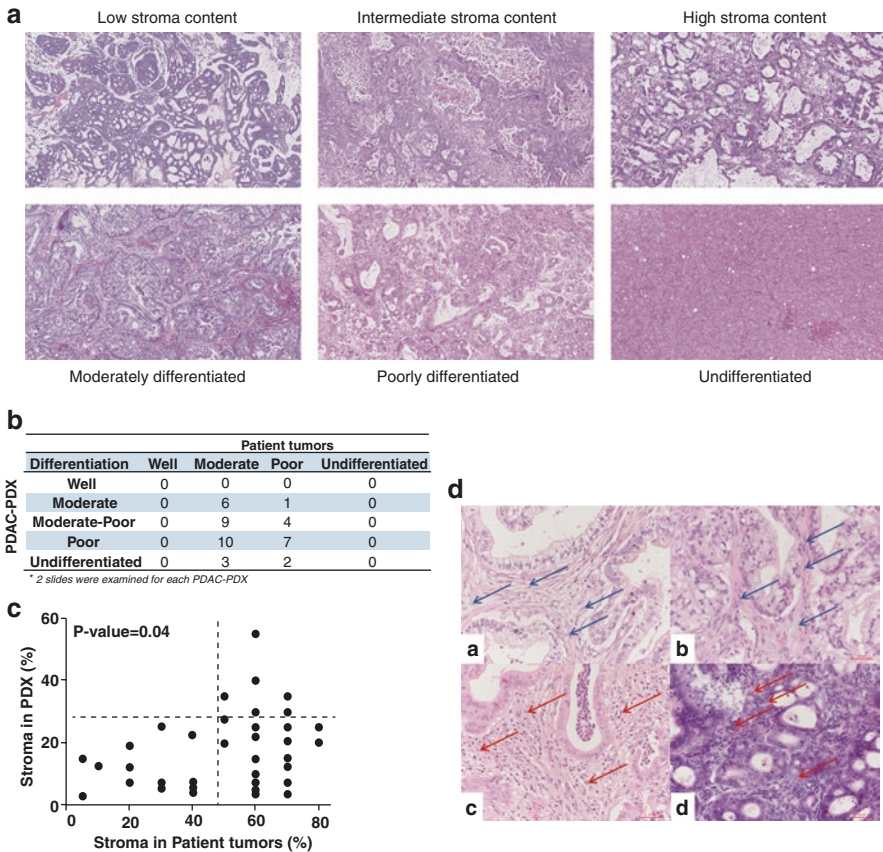


**Fig. 17.5** Histology features of PDAC PDXs. (a) Representative photomicrographs of hematoxylin and eosin (H&E)-stained slides of PDAC PDXs with different differentiation and stroma content. (b) Contingency table comparing PDAC PDX grade with those of parental tumors and (c) correlation between the stroma content of patient tumors and the PDAC PDXs. (d) Activated stroma in patient tumors (a, c) and PDX tumors (b, d) according to the Ha et al. classification [76]. Activated tumor stroma is defined by fibroblasts with small spindle-cell morphology, a thin and wavy body structure, and a symmetric/parallel orientation (a, b; blue arrows). By comparison, inactivated tumor stroma features fibroblasts with plump spindle-shaped cell morphology, a prominent nucleus and nucleoli and with a random spatial orientation (c, d; red arrows)

Analyzing the PDAC PDX collection for genomic subtypes (chromosomal-instable CIN, genomic stable GS or mismatch repair deficient MMR) and mutated genes, we observed, similar to patient tumors [49], KRAS (93%), TP53 (74%), CDKN2A (67%), and TGFBR2/SMAD4 (69%) among the most frequently altered genes (Fig. 17.6c). However, we did not observe any association between genomic patterns and transcriptomic subtypes or tumor-model stroma features. Together these results suggest that the molecular subtype of PDAC PDXs determines its own microenvironment characteristics via mutual communication between cancer cells and murine stroma cells. The hedgehog-signaling pathway appears to be a good

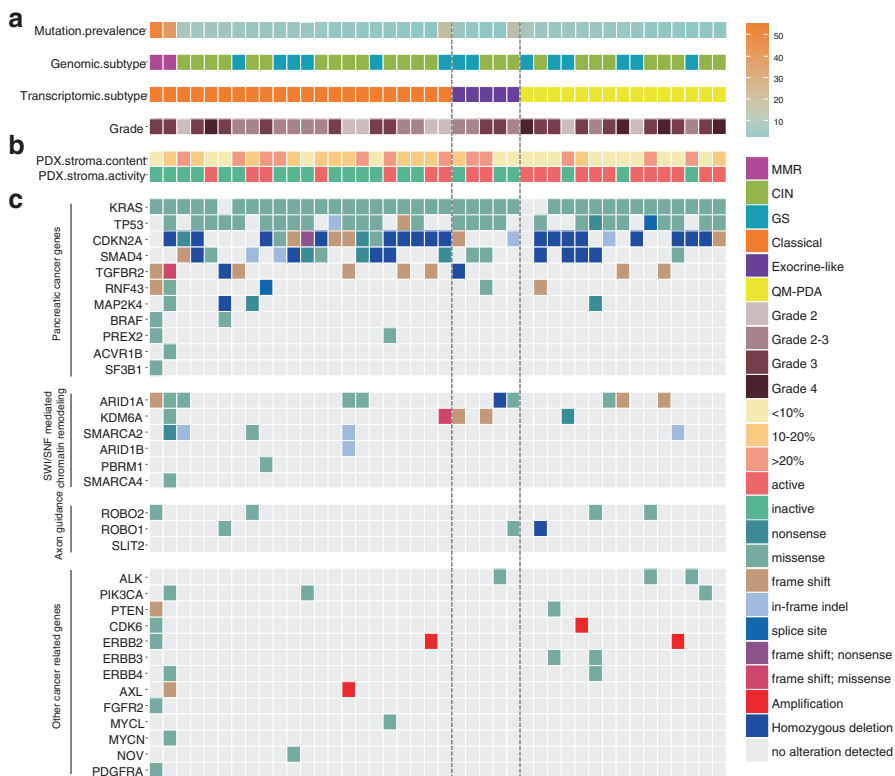


**Fig. 17.6** Landscape of genomic alterations in PDAC PDXs. (a) Heatmap showing the mutation prevalence, genomic subtypes, transcriptomic subtypes, and grades. (b) Heatmap showing the stroma content and activation. (c) Heatmap showing the genomic alterations of cancer-related genes

candidate to drive such interaction [50, 51], since previous investigations demonstrated that the ligands sonic hedgehog (SHH) and Indian hedgehog (IHH) were expressed in cancer cells, whereas the PTCH1 receptors and downstream signaling molecules Gli 1 to 3 were expressed by murine stroma cell [52]. This could be investigated in more detail in PDXs by RNA-seq analysis, which would identify human and mouse transcripts simultaneously.

## Tumor Molecular Subtypes Are Determinants of Successful Engraftment

It soon became obvious that not all tumors and tumor types can be equally successfully established as PDXs. Establishment of breast and prostate cancer models, with an engraftment success rate below 30%, was found to be particularly challenging, mostly because of the hormone dependence of the tumors [53–55]. We and others have only been able to establish a limited number of breast PDXs [56, 57], mostly estrogen-receptor-negative (triple negative and ERBB2-positive) PDXs. Only a few

estrogen-receptor-positive tumors have been successfully grown in mice, these tumors growing, however, independently of estrogen [58]. The supplementation with estrogen pellets was shown to enhance the stable xenograft take rate. However, successful establishment remains only around 20% [59], and a recent study showed that breast tumors undergo a strong selection pressure when implanted in nude mice [60]. Similarly, campaigns for development of prostate cancer PDXs resulted in a disappointing failure rate [61]. The process of prostate cancer PDX establishment is additionally complicated by the very low tumor-growth rate. Only very few PDXs originating from prostate cancer patient tumors were developed, and those established were very aggressive.

A more surprising example of a histological type engrafted with a low success rate was recently highlighted with campaigns for establishment of gastric-cancer PDX models. While developing gastric PDX tumors models from cancer patients of Asian ethnicity, only 27 stable PDXs were established from a total of 100 tumors (manuscript under preparation). Other groups observed similar low engraftment success rates [62, 63]. However, a collaborative Japanese-American study carried out in Keio University demonstrated nude mouse engraftment of 20 of 36 cases in nude mice [64]. The high engraftment rate in this study may have been due to the orthotopic transplantation of the tumors.

In agreement with recent data of Choi et al [62], a detailed analysis of our collection showed strong histological and molecular feature selections with intestinal subtype (74%) being more frequently established than diffuse or mixed subtypes (15 and 11%, respectively). By following the gastric cancer classification subtypes proposed by the TCGA [65], we found that the gastric PDX collection comprised mainly models with marked MMR deficiency due to MLH1 loss (52%) and models with high chromosomal instability (41%) with notably five models with ERBB2 gene amplification [66]. Only two gastric PDXs were found with genomic stability and none with EBV infection. The analysis of the molecular subtypes of parental tumors revealed the representativeness of the cohort and confirmed a strong bias in PDX establishment associated with subtypes. We noticed however a good concordance between subtypes of PDX and corresponding parental tumors ( $p < 0.0001$ ). While we have demonstrated a high resemblance of PDXs with parental tumors with regard to histology, genomic, and transcriptomic subtypes, we also highlighted the bias in the collections. Thus a detailed molecular analysis of PDX is essential for optimal use. We still have to determine whether selection during PDX establishment is associated with selection of preexisting clones, rather than generation of new clones as recently suggested [67].

---

## **PDX Allows Early Identification of Predictive Clinical Biomarkers**

Our PDX collection has been used for the identification of biomarkers and for the development of predictive gene signatures for sensitivity to chemotherapeutics and targeted therapies such as Avastin and cetuximab [68, 69]. As proof of principle, we further validated our cetuximab-sensitivity gene signature by demonstrating its

ability to predict clinical response in publicly-available datasets [70], consisting of metastatic colorectal cancers treated with cetuximab as second-line monotherapy [71].

The PDX collection and related molecular data have been also largely used to investigate the ability of individual biomarkers to predict response to targeted therapies. For example, we validated KRAS mutations or PTEN alterations as predictors of resistance to anti-EGFR therapy [72] and ERBB2 and MET amplification or BRAF<sup>V600E</sup> mutation as predictors of sensitivity to Herceptin, PF-04217903, or vemurafenib-targeted therapies, respectively [34, 64, 73]. Whereas PDX characteristics and molecular data have been shown to be particularly appropriate for early biomarker identification, the size and genetic diversity of PDX cohorts are important for statistical analyses. Drug-sensitivity investigations of PDXs using an ex vivo 3D clonogenic assay allow the assessment of compounds in a reasonable time and at a reasonable cost, simultaneously covering the large diversity of cancer and obtaining sufficient data for statistical analyses [74, 75]. Such biomarker discovery programs performed at an early stage should facilitate the enrollment of appropriate patients into clinical trials and make it feasible to individualize and, thereby, improve the effectiveness of anticancer therapy.

---

## Conclusions and Further Steps

The extensive characterization of PDXs has confirmed their close resemblance to patient tumor genomic alterations and gene expression profiles. PDXs additionally were shown to recapitulate part of the stroma component, with some evidence of cross talk between human cancer cells and the host microenvironment. This contributes to their high relevance to mimic patient tumor responses to anticancer agents. In this respect, some challenges need to be overcome, such as the development of PDX growing in hosts containing immune cells and the microbiome or decrease of bias in the establishment of specific histological or molecular subtypes.

For optimal use of PDXs, we strongly encourage the more frequent monitoring of molecular characteristics of PDXs over time and passages. Although models were shown to have a relative genomic stability, evolution of molecular features over time will occur in every PDX. The decreased cost of high-throughput genomic analyses should help to obtain molecular data at the same time as analysis for compound sensitivity. The development of molecular-based methods to assess clonal heterogeneity of PDX should also provide important information for better-modeled tumor response to anticancer agents.

**Acknowledgments** We would like to thank Anke Behnke, Stefanie Klingel, Volker Knauff, and Sandra Pimenta for their technical assistance. We are indebted to Dr. Manuel Landesfeind for his helpful support in bioinformatics data analyses and Dr. Peter Bronsert for the histology review of the PDX collection. We thank Dr. Hanz Hendriks and Dr. Thomas Metz for their advice in the manuscript preparation.

**Disclosure** A-LP, BZ and A-ME-P are employed by Oncotest, Charles River Discovery. HHH and VV are employed by 4HF Biotec GmbH.

## References

1. Rygaard J, Povlsen CO. Heterotransplantation of a human malignant tumor to the mouse mutant nude. *Acta Pathol Microbiol Scand.* 1969;77:758–66.
2. Fiebig HH, Schuchhardt C, Henss H, Fiedler L, Lohr GW. Comparison of tumor response in nude mice and in the patients. *Behring Inst Mitt.* 1984;74:343–52.
3. Sausville EA, Burger AM. Contributions of human tumor xenografts to anticancer drug development. *Cancer Res.* 2006;66:3351–4. discussion 3354.
4. Tentler JJ, Tan AC, Weekes CD, Jimeno A, Leong S, Pitts TM, Arcaroli JJ, Messersmith WA, Eckhardt SG. Patient-derived tumour xenografts as models for oncology drug development. *Nat Rev Clin Oncol.* 2012;9:338–50.
5. Siolas D, Hannon GJ. Patient-derived tumor xenografts: transforming clinical samples into mouse models. *Cancer Res.* 2013;73:5315–9.
6. Williams SA, Anderson WC, Santaguida MT, Dylla SJ. Patient-derived xenografts, the cancer stem cell paradigm, and cancer pathobiology in the 21st century. *Lab Invest.* 2013;93:970–82.
7. Hidalgo M, Amant F, Biankin AV, Budinska E, Byrne AT, Caldas C, Clarke RB, de Jong S, Jonkers J, Maelandsmo GM, Roman-Roman S, Seoane J, Trusolino L, Villanueva A. Patient-derived xenograft models: an emerging platform for translational cancer research. *Cancer Discov.* 2014;4:998–1013.
8. Choi SY, Lin D, Gout PW, Collins CC, Xu Y, Wang Y. Lessons from patient-derived xenografts for better in vitro modeling of human cancer. *Adv Drug Deliv Rev.* 2014;79–80:222–37.
9. Burger AM, Fiebig H-H. Preclinical screening for anticancer agents. In: Rudek MA, Chau CH, Figg W, McLeod HL, editors. *Handbook of anticancer pharmacokinetics and pharmacodynamics.* Cancer Drug Discovery and Development. New York: Springer-Verlag; 2014. p. 836.
10. Rosfjord E, Lucas J, Li G, Gerber HP. Advances in patient-derived tumor xenografts: from target identification to predicting clinical response rates in oncology. *Biochem Pharmacol.* 2014;91:135–43.
11. Gao H, Korn JM, Ferretti S, Monahan JE, Wang Y, Singh M, Zhang C, Schnell C, Yang G, Zhang Y, Balbin OA, Barbe S, Cai H, Casey F, Chatterjee S, Chiang DY, Chuai S, Cogan SM, Collins SD, Dammassa E, Ebel N, Embry M, Green J, Kauffmann A, Kowal C, Leary RJ, Lehar J, Liang Y, Loo A, Lorenzana E, Robert McDonald III E, McLaughlin ME, Merkin J, Meyer R, Naylor TL, Patawaran M, Reddy A, Roelli C, Ruddy DA, Salangsang F, Santacroce F, Singh AP, Tang Y, Tinetto W, Tobler S, Velazquez R, Venkatesan K, Von Arx F, Wang HQ, Wang Z, Wiesmann M, Wyss D, Xu F, Bitter H, Atadja P, Lees E, Hofmann F, Li E, Keen N, Cozens R, Jensen MR, Pryer NK, Williams JA, Sellers WR. High-throughput screening using patient-derived tumor xenografts to predict clinical trial drug response. *Nat Med.* 2015;21:1318–25.
12. Krumbach R, Virayah J, Metcalfe T, Fiebig HH, Vuaroqueaux V. A functional mutational profile of a compendium of 350 patient-derived tumor xenografts (PDXs). In: *Proceedings of the AACR-NCI-EORTC International Conference: Molecular Targets and Cancer Therapeutics,* Boston, MA. 2013.
13. Cho SY, Kang W, Han JY, Min S, Kang J, Lee A, Kwon JY, Lee C, Park H. An integrative approach to precision cancer medicine using patient-derived xenografts. *Mol Cells.* 2016;39:77–86.
14. Mardis ER. Genome sequencing and cancer. *Curr Opin Genet Dev.* 2012;22:245–50.
15. Tomasetti C, Vogelstein B, Parmigiani G. Half or more of the somatic mutations in cancers of self-renewing tissues originate prior to tumor initiation. *Proc Natl Acad Sci U S A.* 2013;110:1999–2004.
16. Vandin F, Upfal E, Raphael BJ. De novo discovery of mutated driver pathways in cancer. *Genome Res.* 2012;22:375–85.
17. Foucault F, Kiefer F, Zeitouni B, Virayah J, Metcalfe T, Vuaroqueaux V, Fiebig, HH. Whole-exome sequencing analysis across 23 histotypes of patient-derived tumor xenografts reveals their similarities with TCGA patient tumors. In: *Proceedings of the 105th Annual Meeting of the American Association for Cancer Research,* Philadelphia, PA. 2014.



18. Alexandrov LB, Nik-Zainal S, Wedge DC, Aparicio SA, Behjati S, Biankin AV, Bignell GR, Bolli N, Borg A, Borresen-Dale AL, Boyault S, Burkhardt B, Butler AP, Caldas C, Davies HR, Desmedt C, Eils R, Eyfjord JE, Foekens JA, Greaves M, Hosoda F, Hutter B, Illicic T, Imbeaud S, Imielinski M, Jager N, Jones DT, Jones D, Knappskog S, Kool M, Lakhani SR, Lopez-Otin C, Martin S, Munshi NC, Nakamura H, Northcott PA, Pajic M, Papaemmanuil E, Paradiso A, Pearson JV, Puente XS, Raine K, Ramakrishna M, Richardson AL, Richter J, Rosenstiel P, Schlesner M, Schumacher TN, Span PN, Teague JW, Totoki Y, Tutt AN, Valdes-Mas R, van Buuren MM, van 't Veer L, Vincent-Salomon A, Waddell N, Yates LR, Australian Pancreatic Cancer Genome Initiative, ICGC Breast Cancer Consortium, ICGC MMML-Seq Consortium, ICGC PedBrain, Zucman-Rossi J, Futreal PA, McDermott U, Lichter P, Meyerson M, Grimmond SM, Siebert R, Campo E, Shibata T, Pfister SM, Campbell PJ, Stratton MR. Signatures of mutational processes in human cancer. *Nature*. 2013;500:415–21.
19. Peille AL, Zeitouni B, Fiebig V, Fiebig HH, Vuaroqueaux V. Molecular profiling of a non-small cell lung PDX collection by whole exome sequencing and RNAseq revealed subtype specificities with therapeutic implications. In: Proceedings of the AACR-NCI-EORTC International Conference: Molecular Targets and Cancer Therapeutics, Boston, MA. 2015.
20. Krumbach R, Schuler J, Hofmann M, Gieseemann T, Fiebig HH, Beckers T. Primary resistance to cetuximab in a panel of patient-derived tumour xenograft models: activation of MET as one mechanism for drug resistance. *Eur J Cancer*. 2011;47:1231–43.
21. Smith MA, Hall R, Fisher K, Haake SM, Khalil F, Schabath MB, Vuaroqueaux V, Fiebig HH, Altioik S, Chen YA, Haura EB. Annotation of human cancers with EGFR signaling-associated protein complexes using proximity ligation assays. *Sci Signal*. 2015;8:ra4.
22. Cancer Genome Atlas Research Network. Comprehensive molecular profiling of lung adenocarcinoma. *Nature*. 2014;511:543–50.
23. Cancer Genome Atlas Research Network. Comprehensive genomic characterization of squamous cell lung cancers. *Nature*. 2012;489:519–25.
24. Martinez-Garcia R, Lopez-Casas PP, Rico D, Valencia A, Hidalgo M. Colorectal cancer classification based on gene expression is not associated with FOLFIRI response. *Nat Med*. 2014;20:1230–1.
25. Guo S, Qian W, Cai J, Zhang L, Wery JP, Li QX. Molecular pathology of patient tumors, patient-derived xenografts, and cancer cell lines. *Cancer Res*. 2016;76:4619–26.
26. Vuaroqueaux V, Peille AL, Zeitouni B, Fiebig V, Fiebig HH. Comprehensive genomic profile analyses of small cell lung cancer patient-derived xenografts for pharmacogenomics. In: Proceedings of the AACR-NCI-EORTC International Conference: Molecular Targets and Cancer Therapeutics, Boston, MA. 2015.
27. George J, Lim JS, Jang SJ, Cun Y, Ozretic L, Kong G, Leenders F, Lu X, Fernandez-Cuesta L, Bosco G, Muller C, Dahmen I, Jahchan NS, Park KS, Yang D, Karnezis AN, Vaka D, Torres A, Wang MS, Korbel JO, Menon R, Chun SM, Kim D, Wilkerson M, Hayes N, Engelmann D, Putzer B, Bos M, Michels S, Vlastic I, Seidel D, Pinther B, Schaub P, Becker C, Altmuller J, Yokota J, Kohno T, Iwakawa R, Tsuta K, Noguchi M, Muley T, Hoffmann H, Schnabel PA, Petersen I, Chen Y, Soltermann A, Tischler V, Choi CM, Kim YH, Massion PP, Zou Y, Jovanovic D, Kontic M, Wright GM, Russell PA, Solomon B, Koch I, Lindner M, Muscarella LA, la Torre A, Field JK, Jakopovic M, Knezevic J, Castanos-Velez E, Roz L, Pastorino U, Brustugun OT, Lund-Iversen M, Thunnissen E, Kohler J, Schuler M, Botling J, Sandelin M, Sanchez-Cespedes M, Salvesen HB, Achter V, Lang U, Bogus M, Schneider PM, Zander T, Ansen S, Hallek M, Wolf J, Vingron M, Yatabe Y, Travis WD, Nurnberg P, Reinhardt C, Perner S, Heukamp L, Buttner R, Haas SA, Brambilla E, Peifer M, Sage J, Thomas RK. Comprehensive genomic profiles of small cell lung cancer. *Nature*. 2015;524:47–53.
28. Budinska E, Popovici V, Tejpar S, D'Ario G, Lapique N, Sikora KO, Di Narzo AF, Yan P, Hodgson JG, Weinrich S, Bosman F, Roth A, Delorenzi M. Gene expression patterns unveil a new level of molecular heterogeneity in colorectal cancer. *J Pathol*. 2013;231:63–76.
29. De Sousa EMF, Wang X, Jansen M, Fessler E, Trinh A, de Rooij LP, de Jong JH, de Boer OJ, van Leersum R, Bijlsma MF, Rodermond H, van der Heijden M, van Noesel CJ, Tuijnman JB, Dekker E, Markowitz F, Medema JP, Vermeulen L. Poor-prognosis colon cancer is defined

- by a molecularly distinct subtype and develops from serrated precursor lesions. *Nat Med*. 2013;19:614–8.
30. Marisa L, de Reynies A, Duval A, Selves J, Gaub MP, Vescovo L, Etienne-Grimaldi MC, Schiappa R, Guenot D, Ayadi M, Kirzin S, Chazal M, Flejou JF, Benchimol D, Berger A, Lagarde A, Pencreach E, Piard F, Elias D, Parc Y, Olschwang S, Milano G, Laurent-Puig P, Boige V. Gene expression classification of colon cancer into molecular subtypes: characterization, validation, and prognostic value. *PLoS Med*. 2013;10:e1001453.
  31. Sadanandam A, Lyssiotis CA, Homicsko K, Collisson EA, Gibb WJ, Wullschleger S, Ostos LC, Lannon WA, Grotzinger C, Del Rio M, Lhermitte B, Olshen AB, Wiedenmann B, Cantley LC, Gray JW, Hanahan D. A colorectal cancer classification system that associates cellular phenotype and responses to therapy. *Nat Med*. 2013;19:619–25.
  32. Guinney J, Ferte C, Dry J, McEwen R, Manceau G, Kao KJ, Chang KM, Bendtsen C, Hudson K, Huang E, Dougherty B, Ducreux M, Soria JC, Friend S, Derry J, Laurent-Puig P. Modeling RAS phenotype in colorectal cancer uncovers novel molecular traits of RAS dependency and improves prediction of response to targeted agents in patients. *Clin Cancer Res*. 2014;20:265–72.
  33. Sadanandam A, Wang X, de Sousa EMF, Gray JW, Vermeulen L, Hanahan D, Medema JP. Reconciliation of classification systems defining molecular subtypes of colorectal cancer: interrelationships and clinical implications. *Cell Cycle*. 2014;13:353–7.
  34. Vuaroqueaux V, Gieseemann T, Tornillo L, Maier A, Krumbach R, Peille AL, Kees T, Guo J, Foucault F, Amalou Z, Eppenberger S, Terracciano L, Fiebig HH. The use of a patient derived tumor xenograft collection to assess different Met and HGF detection methods and their predictive values for therapy response. In: *Proceedings of the AACR-NCI-EORTC International Conference: Molecular Targets and Cancer Therapeutics*, Boston, MA. 2013.
  35. Isella C, Terrasi A, Bellomo SE, Petti C, Galatola G, Muratore A, Mellano A, Senetta R, Cassenti A, Sonetto C, Inghirami G, Trusolino L, Fekete Z, De Ridder M, Cassoni P, Storme G, Bertotti A, Medico E. Stromal contribution to the colorectal cancer transcriptome. *Nat Genet*. 2015;47:312–9.
  36. Vermeulen L, De Sousa EMF, van der Heijden M, Cameron K, de Jong JH, Borovski T, Tuynman JB, Todaro M, Merz C, Rodermond H, Sprick MR, Kemper K, Richel DJ, Stassi G, Medema JP. Wnt activity defines colon cancer stem cells and is regulated by the microenvironment. *Nat Cell Biol*. 2010;12:468–76.
  37. Loboda A, Nebozhyn M, Klinghoffer R, Frazier J, Chastain M, Arthur W, Roberts B, Zhang T, Chenard M, Haines B, Andersen J, Nagashima K, Paweletz C, Lynch B, Feldman I, Dai H, Huang P, Watters J. A gene expression signature of RAS pathway dependence predicts response to PI3K and RAS pathway inhibitors and expands the population of RAS pathway activated tumors. *BMC Med Genet*. 2010;3:26.
  38. Brown KM, Xue A, Mittal A, Samra JS, Smith R, Hugh TJ. Patient-derived xenograft models of colorectal cancer in pre-clinical research: a systematic review. *Oncotarget*. 2016;7(40):66212–66225.
  39. Chou J, Fitzgibbon MP, Mortales CL, Towler AM, Upton MP, Yeung RS, McIntosh MW, Warren EH. Phenotypic and transcriptional fidelity of patient-derived colon cancer xenografts in immune-deficient mice. *PLoS One*. 2013;8:e79874.
  40. Julien S, Merino-Trigo A, Lacroix L, Pocard M, Goere D, Mariani P, Landron S, Bigot L, Nemati F, Dartigues P, Weiswald LB, Lantuas D, Morgand L, Pham E, Gonin P, Dangles-Marie V, Job B, Dessen P, Bruno A, Pierre A, De The H, Soliman H, Nunes M, Lardier G, Calvet L, Demers B, Prevost G, Vrignaud P, Roman-Roman S, Duchamp O, Berthet C. Characterization of a large panel of patient-derived tumor xenografts representing the clinical heterogeneity of human colorectal cancer. *Clin Cancer Res*. 2012;18:5314–28.
  41. Ostman A, Augsten M. Cancer-associated fibroblasts and tumor growth—bystanders turning into key players. *Curr Opin Genet Dev*. 2009;19:67–73.
  42. Garrido-Laguna I, Uson M, Rajeshkumar NV, Tan AC, de Oliveira E, Karikari C, Villaroel MC, Salomon A, Taylor G, Sharma R, Hruban RH, Maitra A, Laheru D, Rubio-Viqueira B,

- Jimeno A, Hidalgo M. Tumor engraftment in nude mice and enrichment in stroma-related gene pathways predict poor survival and resistance to gemcitabine in patients with pancreatic cancer. *Clin Cancer Res*. 2011;17:5793–800.
43. Bronsert P, Kees T, Zeitouni B, Peille AL, Landesfeind M, Fiebig HH, Küsters S, Vuaroqueaux V. Subtyping of pancreatic cancer patient-derived xenograft tumors and implications for anti-cancer agent testing. In: *Proceedings of the 107th Annual Meeting of the American Association for Cancer Research*, New Orleans, LA. 2016.
  44. Beckers T, Maier A, Schüler J, Giesemann T, Hopt U, Haller T, Fiebig HH, Küsters S. Comprehensive characterization of a newly established patient-derived pancreatic adenocarcinoma xenograft collection. In *AACR 101st Annual Meeting 2010 for Cancer Research*, Washington, DC. 2010.
  45. Mei L, Du W, Ma WW. Targeting stromal microenvironment in pancreatic ductal adenocarcinoma: controversies and promises. *J Gastrointest Oncol*. 2016;7:487–94.
  46. Collisson EA, Sadanandam A, Olson P, Gibb WJ, Truitt M, Gu S, Cooc J, Weinkle J, Kim GE, Jakkula L, Feiler HS, Ko AH, Olshen AB, Danenberg KL, Tempero MA, Spellman PT, Hanahan D, Gray JW. Subtypes of pancreatic ductal adenocarcinoma and their differing responses to therapy. *Nat Med*. 2011;17:500–3.
  47. Moffitt RA, Marayati R, Flate EL, Volmar KE, Loeza SG, Hoadley KA, Rashid NU, Williams LA, Eaton SC, Chung AH, Smyla JK, Anderson JM, Kim HJ, Bentrem DJ, Talamonti MS, Iacobuzio-Donahue CA, Hollingsworth MA, Yeh JJ. Virtual microdissection identifies distinct tumor- and stroma-specific subtypes of pancreatic ductal adenocarcinoma. *Nat Genet*. 2015;47:1168–78.
  48. Bailey P, Chang DK, Nones K, Johns AL, Patch AM, Gingras MC, Miller DK, Christ AN, Bruxner TJ, Quinn MC, Nourse C, Murtaugh LC, Harliwong I, Idrisoglu S, Manning S, Nourbakhsh E, Wani S, Fink L, Holmes O, Chin V, Anderson MJ, Kazakoff S, Leonard C, Newell F, Waddell N, Wood S, Xu Q, Wilson PJ, Cloonan N, Kassahn KS, Taylor D, Quek K, Robertson A, Pantano L, Mincarelli L, Sanchez LN, Evers L, Wu J, Pinese M, Cowley MJ, Jones MD, Colvin EK, Nagrial AM, Humphrey ES, Chantrill LA, Mawson A, Humphris J, Chou A, Pajic M, Scarlett CJ, Pinho AV, Giry-Laterriere M, Rooman I, Samra JS, Kench JG, Lovell JA, Merrett ND, Toon CW, Epari K, Nguyen NQ, Barbour A, Zeps N, Moran-Jones K, Jamieson NB, Graham JS, Duthie F, Oien K, Hair J, Grutzmann R, Maitra A, Iacobuzio-Donahue CA, Wolfgang CL, Morgan RA, Lawlor RT, Corbo V, Bassi C, Rusev B, Capelli P, Salvia R, Tortora G, Mukhopadhyay D, Petersen GM, Australian Pancreatic Cancer Genome Initiative, Munzy DM, Fisher WE, Karim SA, Eshleman JR, Hruban RH, Pilarsky C, Morton JP, Sansom OJ, Scarpa A, Musgrove EA, Bailey UM, Hofmann O, Sutherland RL, Wheeler DA, Gill AJ, Gibbs RA, Pearson JV, Waddell N, Biankin AV, Grimmond SM. Genomic analyses identify molecular subtypes of pancreatic cancer. *Nature*. 2016;531:47–52.
  49. Waddell N, Pajic M, Patch AM, Chang DK, Kassahn KS, Bailey P, Johns AL, Miller D, Nones K, Quek K, Quinn MC, Robertson AJ, Fadlullah MZ, Bruxner TJ, Christ AN, Harliwong I, Idrisoglu S, Manning S, Nourse C, Nourbakhsh E, Wani S, Wilson PJ, Markham E, Cloonan N, Anderson MJ, Fink JL, Holmes O, Kazakoff SH, Leonard C, Newell F, Poudel B, Song S, Taylor D, Waddell N, Wood S, Xu Q, Wu J, Pinese M, Cowley MJ, Lee HC, Jones MD, Nagrial AM, Humphris J, Chantrill LA, Chin V, Steinmann AM, Mawson A, Humphrey ES, Colvin EK, Chou A, Scarlett CJ, Pinho AV, Giry-Laterriere M, Rooman I, Samra JS, Kench JG, Pettitt JA, Merrett ND, Toon C, Epari K, Nguyen NQ, Barbour A, Zeps N, Jamieson NB, Graham JS, Niclou SP, Bjerkvig R, Grutzmann R, Aust D, Hruban RH, Maitra A, Iacobuzio-Donahue CA, Wolfgang CL, Morgan RA, Lawlor RT, Corbo V, Bassi C, Falconi M, Zamboni G, Tortora G, Tempero MA, Australian Pancreatic Cancer Genome Initiative, Gill AJ, Eshleman JR, Pilarsky C, Scarpa A, Musgrove EA, Pearson JV, Biankin AV, Grimmond SM. Whole genomes redefine the mutational landscape of pancreatic cancer. *Nature*. 2015;518:495–501.
  50. Li X, Ma Q, Duan W, Liu H, Xu H, Wu E. Paracrine sonic hedgehog signaling derived from tumor epithelial cells: a key regulator in the pancreatic tumor microenvironment. *Crit Rev Eukaryot Gene Expr*. 2012;22:97–108.

51. Merchant JL, Saqui-Salces M. Inhibition of Hedgehog signaling in the gastrointestinal tract: targeting the cancer microenvironment. *Cancer Treat Rev.* 2014;40:12–21.
52. Vuaroqueaux V, Küsters S, Fiebig HH, Foucault F, Beckers T. Expression of Hedgehog pathway molecules in patient-derived pancreatic adenocarcinoma xenograft models. In: Proceedings of the 102nd Annual Meeting of the American Association for Cancer Research, Orlando, FL. 2011.
53. Marangoni E, Poupon MF. Patient-derived tumour xenografts as models for breast cancer drug development. *Curr Opin Oncol.* 2014;26:556–61.
54. Risbridger GP, Taylor RA. Patient-derived prostate cancer: from basic science to the clinic. *Horm Cancer.* 2016;7:236–40.
55. Whittle JR, Lewis MT, Lindeman GJ, Visvader JE. Patient-derived xenograft models of breast cancer and their predictive power. *Breast Cancer Res.* 2015;17:17.
56. Giesemann T, Krumbach R, Schüller J, Vuaroqueaux V, Hofmann M, Liu N, Haegebarth A, Beckers T, Fiebig HH. Molecular characterization of a panel of patient-derived breast cancer xenografts. In: Proceedings of the 101st Annual Meeting of the American Association for Cancer Research, Washington, DC. 2010.
57. DeRose YS, Wang G, Lin YC, Bernard PS, Buys SS, Ebbert MT, Factor R, Matsen C, Milash BA, Nelson E, Neumayer L, Randall RL, Stijleman IJ, Welm BE, Welm AL. Tumor grafts derived from women with breast cancer authentically reflect tumor pathology, growth, metastasis and disease outcomes. *Nat Med.* 2011;17:1514–20.
58. Kanaya N, Somlo G, Wu J, Frankel P, Kai M, Liu X, Wu SV, Nguyen D, Chan N, Hsieh MY, Kirschenbaum M, Kruper L, Vito C, Badie B, Yim JH, Yuan Y, Hurria A, Peiguo C, Mortimer J, Chen S. Characterization of patient-derived tumor xenografts (PDXs) as models for estrogen receptor positive (ER+HER2- and ER+HER2+) breast cancers. *J Steroid Biochem Mol Biol.* 2016; doi:10.1016/j.jsbmb.2016.05.001.
59. Zhang X, Claeherout S, Prat A, Dobrolecki LE, Petrovic I, Lai Q, Landis MD, Wiechmann L, Schiff R, Giuliano M, Wong H, Fuqua SW, Contreras A, Gutierrez C, Huang J, Mao S, Pavlick AC, Froehlich AM, Wu MF, Tsimelzon A, Hilsenbeck SG, Chen ES, Zuloaga P, Shaw CA, Rimawi MF, Perou CM, Mills GB, Chang JC, Lewis MT. A renewable tissue resource of phenotypically stable, biologically and ethnically diverse, patient-derived human breast cancer xenograft models. *Cancer Res.* 2013;73:4885–97.
60. Eirew P, Steif A, Khattri J, Ha G, Yap D, Farahani H, Gelmon K, Chia S, Mar C, Wan A, Laks E, Biele J, Shumansky K, Rosner J, McPherson A, Nielsen C, Roth AJ, Lefebvre C, Bashashati A, de Souza C, Siu C, Aniba R, Brimhall J, Oloumi A, Osako T, Bruna A, Sandoval JL, Algara T, Greenwood W, Leung K, Cheng H, Xue H, Wang Y, Lin D, Mungall AJ, Moore R, Zhao Y, Lorette J, Nguyen L, Huntsman D, Eaves CJ, Hansen C, Marra MA, Caldas C, Shah SP, Aparicio S. Dynamics of genomic clones in breast cancer patient xenografts at single-cell resolution. *Nature.* 2015;518:422–6.
61. Wetterauer C, Vljajnic T, Schuler J, Gsponer JR, Thalman GN, Cecchini M, Schneider J, Zellweger T, Pueschel H, Bachmann A, Ruiz C, Dirnhofer S, Bubendorf L, Rentsch CA. Early development of human lymphomas in a prostate cancer xenograft program using triple knock-out immunocompromised mice. *Prostate.* 2015;75:585–92.
62. Choi YY, Lee JE, Kim H, Sim MH, Kim KK, Lee G, Kim HI, An JY, Hyung WJ, Kim CB, Noh SH, Kim S, Cheong JH. Establishment and characterisation of patient-derived xenografts as preclinical models for gastric cancer. *Sci Rep.* 2016;6:22172.
63. Zhu Y, Tian T, Li Z, Tang Z, Wang L, Wu J, Li Y, Dong B, Li Y, Li N, Zou J, Gao J, Shen L. Establishment and characterization of patient-derived tumor xenograft using gastroscopic biopsies in gastric cancer. *Sci Rep.* 2015;5:8542.
64. Furukawa T, Kubota T, Watanabe M, Kitajima M, Fu X, Hoffman RM. Orthotopic transplantation of histologically intact clinical specimens of stomach cancer to nude mice: correlation of metastatic sites in mouse and individual patient donors. *Int J Cancer.* 1993;53:608–12.
65. Cancer Genome Atlas Research Network. Comprehensive molecular characterization of gastric adenocarcinoma. *Nature.* 2014;513:202–9.

66. Vuaroqueaux V, Ackermann A, Guo J, Peille AL, Krumbach R, Foucault F, Metz T, Fiebig HH. The molecular determinants of sensitivity to HER2 targeted therapy in Patient Derived Xenograft gastric tumor models from Caucasian and Eastern Asian patients. In: Proceedings of the 104th Annual Meeting of the American Association for Cancer Research, Washington, DC. 2013.
67. Aparicio S, Hidalgo M, Kung AL. Examining the utility of patient-derived xenograft mouse models. *Nat Rev Cancer*. 2015;15:311–6.
68. Fiebig HH, Schuler J, Bausch N, Hofmann M, Metz T, Korrat A. Gene signatures developed from patient tumor explants grown in nude mice to predict tumor response to 11 cytotoxic drugs. *Cancer Genomics Proteomics*. 2007;4:197–209.
69. Fiebig HH, Vuaroqueaux V, Korrat A, Foucault F, Beckers T. Predictive gene signatures for bevacizumab and cetuximab as well as cytotoxic agents. *Int J Clin Pharmacol Ther*. 2012;50:70–1.
70. Khambata-Ford S, Garrett CR, Meropol NJ, Basik M, Harbison CT, Wu S, Wong TW, Huang X, Takimoto CH, Godwin AK, Tan BR, Krishnamurthi SS, Burris III HA, Poplin EA, Hidalgo M, Baselga J, Clark EA, Mauro DJ. Expression of epiregulin and amphiregulin and K-ras mutation status predict disease control in metastatic colorectal cancer patients treated with cetuximab. *J Clin Oncol*. 2007;25:3230–7.
71. Vuaroqueaux V, Korrat A, Foucault F, Beckers T, Fiebig HH. Clinical validation of a 26-gene signature predicting response to Cetuximab in wild type K-ras metastatic colorectal cancer. In: ESMO, Milano, Italy. 2010.
72. Vuaroqueaux V, Ackermann A, Krumbach R, Tillmann HC, Foucault F, Schuler J, Metz T, Fiebig HH. PTEN/PTENP1 transcripts expression and alterations in a large panel of human tumor xenograft in nude mice: implication for resistance to targeted therapies involving EGFR/PI3K/PTEN pathways. In: AACR-NCI-EORTC International Conference: Molecular Targets and Cancer Therapeutics, San Francisco, CA. 2011.
73. Kelter G, Krumbach R, Maier A, Giesemann T, Vuaroqueaux V, Foucault F, Virayah J, Metz T, Metcalfe T, Fiebig HH. Mutation and chemosensitivity profiling of 18 human melanoma cell lines. In Proceedings: AACR 103rd Annual Meeting 2012–Mar 31–Apr 4, 2012; Chicago, IL.
74. Zeitouni B, Peille AL, Amalou Z, Metz T, Fiebig HH, Vuaroqueaux V. A systematic patient-derived xenograft based solution for preclinical biomarker discovery. In Proceedings of the AACR-NCI-EORTC International Conference: Molecular Targets and Cancer Therapeutics, Boston, MA. 2015.
75. Fiebig HH, Maier A, Burger AM. Clonogenic assay with established human tumour xenografts: correlation of in vitro to in vivo activity as a basis for anticancer drug discovery. *Eur J Cancer*. 2004;40:802–20.
76. Ha SY, Yeo SY, Xuan YH, Kim SH. The prognostic significance of cancer-associated fibroblasts in esophageal squamous cell carcinoma. *PLoS One*. 2014;9:e99955.
77. Greenman CD, Bignell G, Butler A, Edkins S, Hinton J, Beare D, Swamy S, Santarius T, Chen L, Widaa S, Futreal PA, Stratton MR. PICNIC: an algorithm to predict absolute allelic copy number variation with microarray cancer data. *Biostatistics*. 2009;11(1):164–175.

---

# Synergy of Patient-Derived Orthotopic Xenografts (PDOX) Models and Molecular Profiling for Optimal Therapy

# 18

Robert M. Hoffman, Takashi Murakami, Kei Kawaguchi,  
Arun S. Singh, and Fritz C. Eilber

Clinically-relevant mouse models of patient tumors can permit evaluation of individualized targeted molecular therapy based on the genetic alternations of the patient's tumor.

Our laboratory pioneered the patient-derived orthotopic xenograft (PDOX) nude mouse model with the technique of surgical orthotopic implantation (SOI). Our laboratory has developed PDOX models of all major tumor types including pancreatic [1–5], breast [6], ovarian [7], lung [8], cervical [9–11], colon [12–14], and stomach cancer [15] as well as mesothelioma [16] and sarcoma [17–20].

*Palbociclib (PD0332991, CDK4/6 inhibitor) and linsitinib (OSI-906, IGF-1R inhibitor) significantly inhibited tumor growth in the Ewing's sarcoma PDOX model.* Palbociclib (PD0332991), a CDK4/6 inhibitor, has shown treatment efficacy for ovarian cancer, glioblastoma, and chordoma cell lines with *CDKN2A* loss [21–23]. Palbociclib has also been used for patients with metastatic breast cancer with *CDKN2A* loss and for liposarcoma with *CDK4* amplification [24, 25].

Linsitinib, a kinase inhibitor of both insulin receptor (IR) and insulin growth factor receptor (IGF-1R) [26], was previously used to treat osteosarcoma cells and Ewing's sarcoma cells [27] and tested in a Phase III clinical trial in adrenocortical carcinoma and in a Phase I/II clinical trial in ovarian cancer [28].

---

R.M. Hoffman (✉) • T. Murakami • K. Kawaguchi  
AntiCancer, Inc., 7917 Ostrow Street, San Diego, CA 92111, USA

Department of Surgery, University of California, San Diego, CA, USA  
e-mail: [all@anticancer.com](mailto:all@anticancer.com)

A.S. Singh  
Division of Hematology-Oncology, University of California,  
Los Angeles, CA, USA

F.C. Eilber  
Division of Surgical Oncology, University of California,  
Los Angeles, CA, USA

A PDOX model of Ewing's sarcoma patient with both *FUS-ERG* fusion [29, 30] and *CDKN2A/B* loss was established. This is the first patient described with both these genetic alterations in a tumor. Therefore, CDK4/6 and IGF-1R inhibitors described above were tested on this patient's tumor in the PDOX model [25].

Ewing's sarcoma PDOX nude-mouse models were randomized into the following groups when tumor volume reached 50 mm<sup>3</sup>: untreated control; doxorubicin (DOX) (intraperitoneal (i.p.) injection, weekly, for 2 weeks); CDK4/6 inhibitor (palbociclib, PD0332991, peroral (p.o.), daily, for 14 days); and G4, IGF-1R inhibitor (linsitinib, OSI-906, p.o., daily, for 14 days). DOX did not inhibit tumor growth, which is consistent with the failure of DOX to control tumor growth in the patient. Palbociclib significantly inhibited tumor growth compared to untreated control from day 8 to 22. Linsitinib also significantly inhibited tumor growth compared to control from day 4 to 22 [25] (Fig. 18.1).

Palbociclib, a CDK4/6 inhibitor, was predicted to be active in the Ewing's sarcoma PDOX. The palbociclib treatment efficacy was previously observed in Ewing's sarcoma and was possibly through suppression of the CDK4/6 pathway which was activated by *CDKN2A* loss [25].

Currently there are no therapies that have been developed that reliably inhibit ERG fusion proteins. In the Ewing's sarcoma PDOX, the IGF-R inhibitor linsitinib essentially arrested the Ewing's sarcoma and may be useful in other cases with a *FUS-ERG* fusion [25].

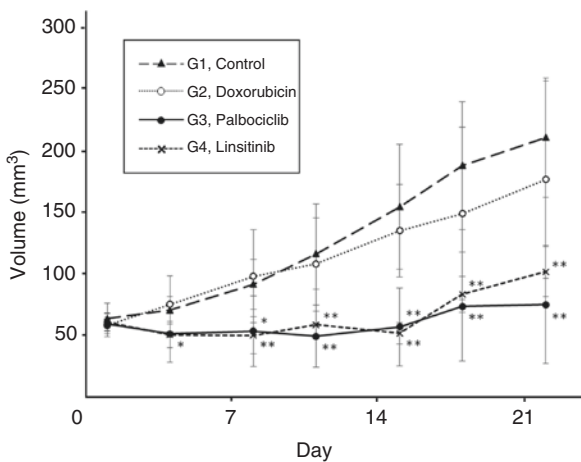


**Fig. 18.1** A Ewing's sarcoma PDOX with a *FUS-ERG* fusion *CDKN2A*-deletion mutation was treated with a CDK4/6 inhibitor, Palbociclib, and a IGF-1R inhibitor, linsitinib, as well as first-line therapy doxorubicin (DOX). Tumor volume was measured as a function of time. \* $P < 0.05$ . \*\* $P < 0.01$  compared to untreated control. Error bars:  $\pm 1$  SD. CDK: cyclin-dependent kinase; IGF-1R: insulin-like growth factor-1 receptor; PDOX: patient-derived orthotopic xenograft [25]

We established a PDOX model of BRAF-V600E-mutant melanoma to test sensitivity to three molecularly targeted drugs and one standard chemotherapeutic. The melanoma obtained from the right chest wall of a patient and implanted orthotopically in the right chest wall of nude mice to establish a PDOX model. Two weeks after implantation, 50 PDOX nude mice were divided into five groups: control without treatment; vemurafenib (VEM) (30 mg/kg); temozolomide (TEM) (25 mg/kg); trametinib (TRA) (0.3 mg/kg); and cobimetinib (COB) (5 mg/kg). Each drug was administered orally, daily for 14 consecutive days. Tumor sizes were measured with calipers twice a week. On day 14 from initiation of treatment, TRA, an MEK inhibitor, was the only agent of the four tested that caused tumor regression. Another MEK inhibitor, COB, could slow but not arrest growth or cause regression of the melanoma. First-line therapy TEM could slow but not arrest tumor growth or cause regression. Since the patient in this study had a BRAF-V600E-mutant melanoma, the patient would be considered to be a candidate for VEM as first-line therapy, since it targets this mutation, but VEM was not effective. The PDOX model thus helped identify the very high efficacy of TRA and is a promising drug for this patient. These results demonstrate the powerful precision of the PDOX model for cancer therapy, not achievable by genomic analysis alone [31] (Fig. 18.2).

Our results demonstrated that drug response testing in the PDOX model can distinguish efficacy of drugs on individual tumors that have similar molecular targets. The results suggest that molecular profiling alone may not predict drug response [31].

More studies combining molecular profiling of tumors and their establishment in PDOX models will be a major factor in developing effective individualized therapy for cancer patients.

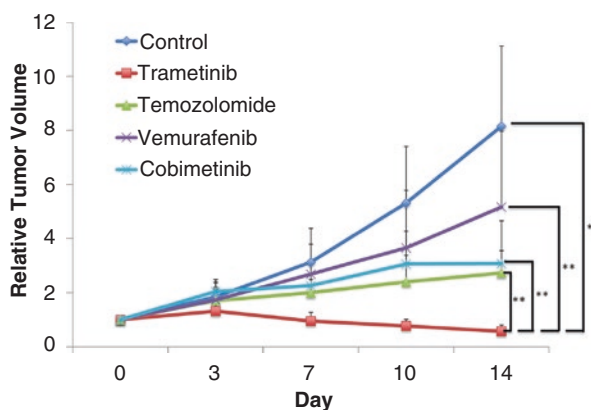


**Fig. 18.2** A melanoma PDOX with a BRAF-V600E mutation was tested with vemurafenib (VEM), temozolomide (TEM), trametinib (TRA) and cobimetinib (COB). Tumor volume was measured as a function of time.  $P \leq 0.0001$ . Error bars:  $\pm$  SD [31]



## References

1. Fu X, Guadagni F, Hoffman RM. A metastatic nude-mouse model of human pancreatic cancer constructed orthotopically from histologically intact patient specimens. *Proc Natl Acad Sci U S A*. 1992;89:5645–9.
2. Hiroshima Y, Zhao M, Maawy A, Zhang Y, Katz MH, Fleming JB, Uehara F, Miwa S, Yano S, Momiyama M, Suetsugu A, Chishima T, Tanaka K, Bouvet M, Endo I, Hoffman RM. Efficacy of *Salmonella typhimurium* A1-R versus chemotherapy on a pancreatic cancer patient-derived orthotopic xenograft (PDOX). *J Cell Biochem*. 2014;115:1254–61.
3. Hiroshima Y, Maawy A, Zhang Y, Murakami T, Momiyama M, Mori R, Matsuyama R, Katz MH, Fleming JB, Chishima T, Tanaka K, Ichikawa Y, Endo I, Hoffman RM, Bouvet M. Metastatic recurrence in a pancreatic cancer patient derived orthotopic xenograft (PDOX) nude mouse model is inhibited by neoadjuvant chemotherapy in combination with fluorescence-guided surgery with an anti-CA 19-9-conjugated fluorophore. *PLoS One*. 2014;9:e114310.
4. Hiroshima Y, Zhang Y, Murakami T, Maawy AA, Miwa S, Yamamoto M, Yano S, Sato S, Momiyama M, Mori R, Matsuyama R, Chishima T, Tanaka K, Ichikawa Y, Bouvet M, Endo I, Zhao M, Hoffman RM. Efficacy of tumor-targeting *Salmonella typhimurium* A1-R in combination with anti-angiogenesis therapy on a pancreatic cancer patient-derived orthotopic xenograft (PDOX) and cell line mouse models. *Oncotarget*. 2014;5:12346–57.
5. Hiroshima Y, Maawy AA, Katz MH, Fleming JB, Bouvet M, Endo I, Hoffman RM. Selective efficacy of zoledronic acid on metastasis in a patient-derived orthotopic xenograft (PDOX) nude-mouse model of human pancreatic cancer. *J Surg Oncol*. 2015;111:311–5.
6. Fu X, Le P, Hoffman RM. A metastatic-orthotopic transplant nude-mouse model of human patient breast cancer. *Anticancer Res*. 1993;13:901–4.
7. Fu X, Hoffman RM. Human ovarian carcinoma metastatic models constructed in nude mice by orthotopic transplantation of histologically-intact patient specimens. *Anticancer Res*. 1993;13:283–6.
8. Wang X, Fu X, Hoffman RM. A new patient-like metastatic model of human lung cancer constructed orthotopically with intact tissue via thoracotomy in immunodeficient mice. *Int J Cancer*. 1992;51:992–5.
9. Hiroshima Y, Zhang Y, Zhang M, Maawy A, Mii S, Yamamoto M, Uehara F, Miwa S, Yano S, Murakami T, Momiyama M, Chishima T, Tanaka K, Ichikawa Y, Bouvet M, Murata T, Endo I, Hoffman RM. Establishment of a patient-derived orthotopic xenograft (PDOX) model of HER-2-positive cervical cancer expressing the clinical metastatic pattern. *PLoS One*. 2015;10:e0117417.
10. Murakami T, Murata T, Kawaguchi K, Kiyuna T, Igarashi K, Hwang HK, Hiroshima Y, Hozumi C, Komatsu S, Kikuchi T, Lwin TM, Delong JC, Miyake K, Zhang Y, Tanaka K, Bouvet M, Endo I, Hoffman RM. Cervical cancer patient-derived orthotopic xenograft (PDOX) is sensitive to cisplatin and resistant to nab-paclitaxel. *Anticancer Res*. 2017;37:61–6.
11. Hiroshima Y, Maawy A, Zhang Y, Zhang N, Murakami T, Chishima T, Tanaka K, Ichikawa Y, Bouvet M, Endo I, Hoffman RM. Patient-derived mouse models of cancer need to be orthotopic in order to evaluate targeted anti-metastatic therapy. *Oncotarget*. 2016;7(44):71696–702.
12. Fu X, Besterman JM, Monosov A, Hoffman RM. Models of human metastatic colon cancer in nude mice orthotopically constructed by using histologically intact patient specimens. *Proc Natl Acad Sci U S A*. 1991;88:9345–9.
13. Metildi CA, Kaushal S, Luiken GA, Talamini MA, Hoffman RM, Bouvet M. Fluorescently-labeled chimeric anti-CEA antibody improves detection and resection of human colon cancer in a patient-derived orthotopic xenograft (PDOX) nude mouse model. *J Surg Oncol*. 2014;109:451–8.
14. Hiroshima Y, Maawy A, Metildi CA, Zhang Y, Uehara F, Miwa S, Yano S, Sato S, Murakami T, Momiyama M, Chishima T, Tanaka K, Bouvet M, Endo I, Hoffman RM. Successful fluorescence-guided surgery on human colon cancer patient-derived orthotopic xenograft mouse models using a fluorophore-conjugated anti-CEA antibody and a portable imaging system. *J Laparoendosc Adv Surg Tech A*. 2014;24:241–7.

15. Furukawa T, Kubota T, Watanabe M, Kitajima M, Fu X, Hoffman RM. Orthotopic transplantation of histologically intact clinical specimens of stomach cancer to nude mice: correlation of metastatic sites in mouse and individual patient donors. *Int J Cancer*. 1993;53:608–12.
16. Astoul P, Wang X, Colt HG, Boutin C, Hoffman RM. A patient-like human malignant pleural mesothelioma nude-mouse model. *Oncol Rep*. 1996;3:483–7.
17. Murakami T, DeLong J, Eilber FC, Zhao M, Zhang Y, Zhang N, Singh A, Russell T, Deng S, Reynoso J, Quan C, Hiroshima Y, Matsuyama R, Chishima T, Tanaka K, Bouvet M, Chawla S, Endo I, Hoffman RM. Tumor-targeting *Salmonella typhimurium* A1-R in combination with doxorubicin eradicate soft tissue sarcoma in a patient-derived orthotopic xenograft PDOX model. *Oncotarget*. 2016;7:12783–90.
18. Hiroshima Y, Zhang Y, Zhang N, Uehara F, Maawy A, Murakami T, Mii S, Yamamoto M, Miwa S, Yano S, Momiyama M, Mori R, Matsuyama R, Chishima T, Tanaka K, Ichikawa Y, Bouvet M, Endo I, Hoffman RM. Patient-derived orthotopic xenograft (PDOX) nude mouse model of soft-tissue sarcoma more closely mimics the patient behavior in contrast to the subcutaneous ectopic model. *Anticancer Res*. 2015;35:697–701.
19. Hiroshima Y, Zhao M, Zhang Y, Zhang N, Maawy A, Murakami T, Mii S, Uehara F, Yamamoto M, Miwa S, Yano S, Momiyama M, Mori R, Matsuyama R, Chishima T, Tanaka K, Ichikawa Y, Bouvet M, Endo I, Hoffman RM. Tumor-targeting *Salmonella typhimurium* A1-R arrests a chemo-resistant patient soft-tissue sarcoma in nude mice. *PLoS One*. 2015;10:e0134324.
20. Kiyuna T, Murakami T, Tome Y, Kawaguchi K, Igarashi K, Zhang Y, Zhao M, Li Y, Bouvet M, Kanaya F, Singh A, Dry S, Eilber FC, Hoffman RM. High efficacy of tumor-targeting *Salmonella typhimurium* A1-R on a doxorubicin- and dactolisib-resistant follicular dendritic-cell sarcoma in a patient-derived orthotopic xenograft nude mouse model. *Oncotarget*. 2016;7:33046–54.
21. Konecny GE, Winterhoff B, Kolarova T, Qi J, Manivong K, Dering J, Yang G, Chalukya M, Wang HJ, Anderson L, Kalli KR, Finn RS, Ginther C, Jones S, Velculescu VE, Riehle D, Cliby WA, Randolph S, Koehler M, Hartmann LC, Slamon DJ. Expression of p16 and retinoblastoma determines response to CDK4/6 inhibition in ovarian cancer. *Clin Cancer Res*. 2011;17:1591–602.
22. Cen L, Carlson BL, Schroeder MA, Ostrem JL, Kitange GJ, Mladek AC, Fink SR, Decker PA, Wu W, Kim JS, Waldman T, Jenkins RB, Sarkaria JN. p16-Cdk4-Rb axis controls sensitivity to a cyclin-dependent kinase inhibitor PD0332991 in glioblastoma xenograft cells. *Neuro-Oncology*. 2012;14:870–81.
23. von Witzleben A, Goertler LT, Marienfeld R, Barth H, Lechel A, Mellert K, Böhm M, Kornmann M, Mayer-Steinacker R, von Baer A, Schultheiss M, Flanagan AM, Möller P, Brüderlein S, Barth TF. Preclinical characterization of novel chordoma cell systems and their targeting by pharmacological inhibitors of the CDK4/6 cell-cycle pathway. *Cancer Res*. 2015;75:3823–31.
24. Dickson MA, Tap WD, Keohan ML, D'Angelo SP, Gounder MM, Antonescu CR, Landa J, Qin LX, Rathbone DD, Condy MM, Ustoyev Y, Crago AM, Singer S, Schwartz GK. Phase II trial of the CDK4 inhibitor PD0332991 in patients with advanced CDK4-amplified well-differentiated or dedifferentiated liposarcoma. *J Clin Oncol*. 2013;31:2024–8.
25. Murakami T, Singh AS, Kiyuna T, Dry SM, Li Y, James AW, Igarashi K, Kawaguchi K, DeLong JC, Zhang Y, Hiroshima Y, Russell T, Eckardt MA, Yanagawa J, Federman N, Matsuyama R, Chishima T, Tanaka K, Bouvet M, Endo I, Eilber FC, Hoffman RM. Effective molecular targeting of *CDK4/6* and *IGF-1R* in a rare *FUS-ERG* fusion *CDKN2A*-deletion doxorubicin-resistant Ewing's sarcoma in a patient-derived orthotopic xenograft (PDOX) nude-mouse model. *Oncotarget*. 2016;7:47556–64.
26. Mulvihill MJ, Cooke A, Rosenfeld-Franklin M, Buck E, Foreman K, Landfair D, O'Connor M, Pirritt C, Sun Y, Yao Y, Arnold LD, Gibson NW, Ji QS. Discovery of OSI-906: a selective and orally efficacious dual inhibitor of the IGF-1 receptor and insulin receptor. *Future Med Chem*. 2009;1:1153–71.
27. Garofalo C, Manara MC, Nicoletti G, Marino MT, Lollini PL, Astolfi A, Pandini G, Lopez-Guerrero JA, Schaefer KL, Belfiore A, Picci P, Scotlandi K. Efficacy of and resistance to anti-IGF-1R therapies in Ewing's sarcoma is dependent on insulin receptor signaling. *Oncogene*. 2011;30:2730–40.

28. Kuijjer ML, Peterse EF, van den Akker BE, Briaire-de Bruijn IH, Serra M, Meza-Zepeda LA, Myklebost O, Hassan AB, Hogendoorn PC, Cleton-Jansen AM. IR/IGF1R signaling as potential target for treatment of high-grade osteosarcoma. *BMC Cancer*. 2013;13:245.
29. Shing DC, McMullan DJ, Roberts P, Smith K, Chin SF, Nicholson J, Tillman RM, Ramani P, Cullinane C, Coleman N. FUS/ERG gene fusions in Ewing's tumors. *Cancer Res*. 2003;63:4568–76.
30. Chen S, Deniz K, Sung YS, Zhang L, Dry S, Antonescu CR. Ewing sarcoma with ERG gene rearrangements: a molecular study focusing on the prevalence of FUS-ERG and common pitfalls in detecting EWSR1-ERG fusions by FISH. *Genes Chromosomes Cancer*. 2016;55:340–9.
31. Kawaguchi K, Murakami T, Chmielowski B, Igarashi K, Kiyuna T, Unno M, Nelson SD, Russell TA, Dry SM, Li Y, Eilber FC, Hoffman RM. Vemurafenib-resistant BRAF-V600E mutated melanoma is regressed by MEK targeting drug trametinib, but not cobimetinib in a patient-derived orthotopic xenograft (PDOX) mouse model. *Oncotarget*. 2016;7(44):71737–43.

David M. Evans and Beverly A. Teicher

---

### The Historical Perspective

Cell culture methods developed in the 1950s and 1960s for growing cells in suspension and in mono-layer quickly became a widely-used standard technique in biology laboratories studying normal tissue function and diseases. In the late 1960s, a scientist studying the effects of radiation on solid tumors was searching for a technique that would facilitate understanding of the effects of radiation in a well-controlled setting representing the heterogeneity of solid tumors. In 1971, Sutherland et al. reported that multi-cell spheroids grown in culture could serve as a model for nodular carcinomas [1]. The group noted that Chinese hamster V79 lung cells grown in suspension culture formed multicell spheroids that resembled subcutaneous tumors grown in mice and carcinomas in patients. The V79 multicell spheroids grew to 370 microns in diameter in less than 2 weeks. The spheroids exhibited an outer zone with many cells undergoing cell division, an intermediate zone with few cells in mitosis, and a central zone that was necrotic—common features now identified in spheroids [1, 2]. The multi-cell spheroid appeared to be an in vitro tumor model that could be studied under well-controlled conditions.

V79 cells grown as spheroids were less sensitive to radiation than the same cells exposed to radiation as single cells [3–5]. It was observed that upon exposure to ionizing radiation, the pattern of cell survival varied with the size of the spheroid. The multi-component radiation survival curves included radio-sensitive

---

D.M. Evans

Leidos Biomedical Research, Inc., Frederick National Laboratory for Cancer Research,  
Frederick, MD 21702, USA

B.A. Teicher (✉)

Division of Cancer Treatment and Diagnosis, National Cancer Institute,  
Rockville, MD 20852, USA

Molecular Pharmacology Branch, National Cancer Institute,  
RM 4-W602, MSC 9735, 9609 Medical Center Drive, Bethesda, MD 20892, USA  
e-mail: [beverly.teicher@nih.gov](mailto:beverly.teicher@nih.gov); [teicherba@mail.nih.gov](mailto:teicherba@mail.nih.gov)

G1-like non-cycling cells, more resistant asynchronously cycling cells, and highly radio-resistant hypoxic internal non-cycling cells [6]. The G1-like non-cycling sub-population of spheroids was similar to stationary/plateau-phase cells grown in mono-layer [7]. After exposure to a single dose of radiation, spheroids were either disaggregated by exposure to trypsin and plated for colony formation or were plated as whole spheroids. In both situations, surviving cells were found that could proliferate to form colonies. The internal chronically-hypoxic cells were capable of proliferation even when the spheroid was not reduced to single cells for plating after irradiation [8, 9].

Spheroids were also found to be useful targets for *in vitro* immuno-therapy studies. When EMT6 Balb/C mouse mammary-tumor-line spheroids were incubated with normal spleen cells or alloimmune spleen cells generated *in vitro* in mixed leukocyte cultures [10], there was a 60–80% decrease in colony formation by EMT6 cell spheroids exposed to immune lymphocytes compared with EMT6 cell spheroids exposed to normal lymphocytes.

EMT6 mouse mammary tumor cell spheroids were markedly less sensitive to a concentration range of doxorubicin than either exponentially growing or stationary-phase mono-layers of the same cells [11]. Exposure of spheroids and mono-layers, exponentially growing or plateau phase, to 1 mM doxorubicin for 1 h resulted in a surviving fractions of 0.3 and 0.001, respectively. High concentrations of hypoxic-cell radio-sensitizers, known to be cyto-toxic toward hypoxic cells, were cyto-toxic toward EMT6 spheroids maintained at low-oxygen concentrations and toward internal cells of large spheroids [12]. In addition, exposure of EMT6 spheroids to doxorubicin immediately after exposure to misonidazole, a hypoxic cell sensitizer, resulted in apparent supra-additive tumor cell killing. The EMT6 spheroids could be trypsinized in layers by exposure to dilute trypsin solution at room temperature. Cells were released only from the outer spheroid layer, then the process was repeated. The cell volume, membrane integrity, and clonogenic capacity decreased for cells in the inner spheroid regions [13]. Due to the marked gradient of doxorubicin distribution from the outer surface to the core of multicell spheroids, the survival of spheroid cells after exposure to doxorubicin was greater than the survival of the same cells grown in mono-layer and exposed to doxorubicin. Growth in 3D resulted in apparent doxorubicin resistance compared with the same cells grown in mono-layer, in that equal toxicity required higher intra-cellular doxorubicin concentrations be present in the spheroid cultures [14]. Although the penetration of anthracyclines into xenograft tumor and spheroids was poor, these remain very useful drugs in the human clinic. The slow delivery of anthracyclines to the inner cells of spheroids caused by rapid binding of drug in the cells in outer layer cells suggested that keeping the spheroid or tumor intact could result in increased cyto-toxicity [15]. Similarly, Hoechst 33342 staining of multicell spheroids results in a marked gradient in the dye concentration, which is time-dependent and reproducible. Thus, fluorescence-activated cell sorting can be used to separate outer layer cells from inner core cells [16]. After staining EMT6 spheroids with acridine orange, flow cytometry followed by centrifugal elutriation was used to isolate a quiescent/non-proliferating sub-population of cells. The quiescent cells were of interest, because they tend to be less responsive to chemotherapy and to radiation therapy [17]. Chinese hamster V79 cell spheroids were used as a tumor model to

investigate the cyto-toxicity of combinations of doxorubicin and radiation on spheroid sub-populations [18]. Fluorescence-activated cell sorting was used to isolate the sub-population of cells least responsive to each single agent, and then combinations were tested. The most effective combination was exposure to doxorubicin first followed by radiation—potentially due to drug-induced spheroid re-oxygenation.

Spheroids enabled the abnormal heterogeneous micro-physiology of tumors to be examined under well-controlled conditions [19]. Consequently, a variety of new techniques were developed to determine the characteristics of these micro-regions in spheroids and to study the interactions of cells with each other and with the micro-environment. During EMT6 tumor cell spheroid growth, a large number of cells were shed into the medium. Cells were released from the spheroid during mitosis and re-aggregated after mitosis [20]. A model describing the rate of expansion of spheroid diameter, cell doubling time in a spheroid, and parameters responsible for growth saturation in large spheroids was developed [21]. Spheroids, like tumors, have a decreasing growth fraction and develop quiescent sub-populations as they enlarge [2, 22] (Fig. 19.1). The re-growth/re-population kinetics in spheroids after exposure to cisplatin and etoposide suggest that “drug resistance” in spheroids may be a kinetic as well as a genetic issue. Repair and re-population kinetics are major factors when spheroids are exposed to fractionated radiation [23–25]. Oxygen tension ( $pO_2$ ) was determined in EMT6 spheroids using recessed micro-electrodes and correlated with the diameter of the spheroids tested. The oxygen profiles were characterized by a diffusion-depleted zone at the spheroid surface, a

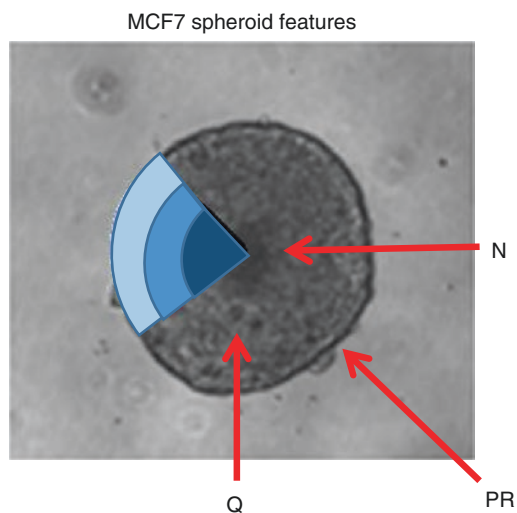


**Fig. 19.1** Representative image of a spheroid showing the key features. MCF7 cells seeded at 5000 cells per well in a 96-well ULA plate exhibited a tight spheroid after 96 h. The necrotic core (N), proliferating region (PR), and the quiescent cell layer (Q) are shown along with an overlay showing the relative distribution of gas ( $O_2$ ) and nutrients (e.g., glucose) across the spheroid (adapted from [2]). In the gradient the lighter color represents highest gas and nutrient concentrations, while darker colors represent lowest amounts

steep decrease within 200–250  $\mu\text{M}$  from the outer edge, and a plateau in the central core of spheroids  $>500 \mu\text{M}$  in diameter [26–28]. The effects of oxygen and glucose concentrations on the growth of EMT6 spheroids were examined by growing spheroids in either 20 or 5% oxygen atmospheres in the presence of 16.5, 5.5, 1.7, or 0.8 mM glucose [29, 30]. At first, the growth of spheroids was similar under all test conditions; however, over time the largest spheroids were observed in the cultures maintained under 20% oxygen and 16.5 mM glucose, and the smallest spheroids were in the cultures maintained under 5% oxygen and 0.8 mM glucose. Oxygenation and development of necrosis were assessed in spheroids of human HT-29 colon carcinoma cells and human Col12 colon-carcinoma cells. Spheroids were grown up to 2800  $\mu\text{M}$  diameter after 5 weeks in culture. Col12 spheroids had a pseudo-glandular structure with lumens similar to the original tumor specimen. Both HT-29 and Col12 spheroids had steep  $\text{pO}_2$  gradients in spheroids  $>600 \mu\text{M}$  in diameter. Overall, the more differentiated Col12 spheroids were more hypoxic than the spheroids from poorly-differentiated HT-29 cells [31]. The effective diffusivity of glucose was determined in EMT6 mouse mammary carcinoma spheroids, in three human colon carcinoma (HT-29, Col12, WiDr) cell-line spheroids, and in two human squamous-carcinoma cell-line spheroids (CaSki and A431). The glucose diffusion coefficients were determined by measuring the efflux of tracer tritium-labeled L-glucose from spheroids into label-free medium. The values indicated that a significant glucose concentration gradient might exist in spheroids [32]. A mathematical model was built to predict EMT6 spheroid growth and micro-environment based upon diffusion/reaction of oxygen, glucose, lactate, carbon dioxide, bicarbonate, chlorine, and pH. However, the model could not predict accurately the onset of necrosis, observed decreases in oxygen and glucose metabolism seen over time, or the observed growth plateau. Thus, other factors such as cell-cell contact must be considered in 3D growth [33, 34]. The growth and response to radiation were examined for multi-cell spheroids of the human MLS ovarian carcinoma cell line [35]. The MLS spheroids were grown in spinner flasks and grew up to  $>2000 \mu\text{M}$  in diameter. Histologically, the MLS spheroids had pseudo-glandular structures with lumens and were slightly less differentiated than the same cells grown as xenografts in mice. The similarity between the response of MLS spheroids of different sizes and MLS xenograft tumors to radiation indicated MLS spheroids may be a useful *in vitro* model for studies of human-tumor radiation biology and related physiological processes.

By 1990, spheroids were being used to study drug combinations with clinical potential [36]. Drugs such as topoisomerase II inhibitors (etoposide), topoisomerase I inhibitors (camptothecin), and cell cycle-specific agents (5-fluorouracil) were studied in V79 cell spheroids in comparison with V79 cell mono-layers. Only the topoisomerase II inhibitor etoposide was equally cyto-toxic to the cells grown in both formats, while the spheroids were less responsive to the other drugs [37]. A series of bio-reductive hypoxic cell-selective agents including misonidazole, mitomycin C, porfiro-mycin, and tirapazamine (SR-4233) produced less cyto-toxicity toward spheroid inner cells than expected from hypoxic mono-layer experiments [38]. This was likely due to poor penetration into the spheroid core or to rapid metabolism by the cells.

EMT6 mouse mammary carcinoma tumors were made resistant to cisplatin, carboplatin, cyclophosphamide, or thiotepa *in vivo* by treatment of

tumor-bearing mice with the drug over a 6-month period [39]. Although the tumors were highly resistant *in vivo*, the cells from the resistant tumors were not resistant to the drugs when grown as monolayers. In the absence of treatment, the drug resistance of the cancer-cell lines decreased over 3–6 months, indicating that resistance was not due to a permanent genetic change. When the drug-resistant cancer cells were grown as spheroids, the drug resistance was partially retained, indicating the cell-cell contact of the 3D spheroid structure provided more of the environment of tumors *in vivo* than did mono-layer cultures [40, 41]. In a study using the EMT6 mouse mammary tumor and *in vivo* alkylating agent-resistant sublines of EMT6, there were clear gene expression differences between the cells grown in mono-layer and the same cells grown as spheroids [42]. Decreased DNA mismatch repair appeared to be a factor in the reversible multi-cellular resistance in the *in-vivo* resistant lines.

Further emphasizing that cell-cell contact is an important factor in response, small spheroids exposed to ionizing radiation, hyper-thermia, photo-dynamic therapy, or topoisomerase II inhibitors are less responsive than the same cells in mono-layer [43]. Four human ovarian cancer cell lines were used to compare the effects of paclitaxel and cisplatin when the cells were grown as spheroids or mono-layers [44]. While cisplatin was equally cyto-toxic to the cells grown as spheroids or as mono-layers, the cancer-cell spheroids were less responsive to paclitaxel than were the same cells exposed to the drug in mono-layer. In the mono-layer cultures, paclitaxel exposure resulted in accumulation of cells in G<sub>2</sub>-M phases and apoptosis. However, this was not seen in the spheroid cultures. The proteasome-inhibitor bortezomib was tested in the same four ovarian carcinoma cell lines and had equal or greater activity in the cells grown as spheroids than in the cells grown as mono-layers [45].

Angiogenesis is an important factor in tumor growth, and vascular-endothelial growth factor (VEGF) is a major pro-angiogenic growth factor *in vivo*. Human HT-29 colon carcinoma cells grown as spheroids were examined for hypoxia and for the expression of VEGF [46, 47]. VEGF expression was localized mainly to interior spheroid cells that were hypoxic, as determined by staining with the bio-reductive probe EF5. When the longevity of hypoxic tumor cells was examined in spheroids, a range of 3–5 days was observed; while in human tumor xenografts, the range was 4–10 days, indicating that in both models, the hypoxic cells live long enough to be a therapeutic problem [48]. The von Hippel-Lindau (VHL) tumor-suppressor gene is mutated in most renal-cell carcinoma tumors and cell lines. When grown as spheroids, human 786-0 renal cell carcinoma cells (which have a mutant VHL gene) form compact, cohesive clusters. When the same cells were genetically engineered to produce normal VHL, the cells grew more slowly and produced spheroids that were more loosely aggregated [49].

---

## 3D Cell-Based Models for Drug Discovery

There is a need for cell-based assays that can be used to determine the activity of compounds that can translate into leads and candidates for clinical use in cancer. The National Cancer Institute has had the NCI-60 screen in place for the past 20+ years to screen compounds for cyto-toxicity toward cancer cells. The NCI-60 assay uses



cells in mono-layer (or suspension) to evaluate the effect of submitted compounds on viability. The 60-cell line panel includes nine cancer histologies (non-small cell lung, breast, prostate, colorectal, ovarian, renal, CNS, melanoma, and leukemia/lymphoma) [50]. While similar assays have been used in biotechnology companies, pharmaceutical companies, and elsewhere, it has become clear that these mono-layer cell-based assays may not be optimal for compound selection. For drug discovery, screening compounds in 3D-culture models rather than mono-layer culture is an effort to move to a model closer to the patient. Many essential cellular functions that are present in tissues are absent in mono-layer cultures, thus limiting the usefulness of mono-layer cultures in the drug discovery process. However, it has been difficult to adapt multi-cellular spheroids to high-throughput screening [51]. Mayer et al. grew 17 gastric cancer cell lines from varied gastric cancer subtypes and found that 12 out of the 17 cell lines recapitulated some of the complexity of the parental tumors and expressed molecular markers consistent with the tumor of origin [52]. Growth-factor signaling pathways, proliferation, and differentiation operate better in 3D culture models than in mono-layer cultures [53]. It is preferable to observe 3D cultures over a time course to determine responses to compounds. Technologies have been adapted to examine changes in the size/diameter of spheroids either in suspension in gels or soft agar media and/or with use of dyes or stains [54]. The recognition that the gene expression in 3D spheroid cultures is more similar to that of tumor tissues than is gene expression of mono-layer cultures provided impetus for the pharmaceutical industry to establish spheroid-based compound screening platforms and protocols. The NCI-60 cell line panel representing the nine tumor types was one of the first cell-line panels integrated into a large-scale 3D spheroid screen [55]. The screening protocol from spheroid initiation, compound exposure, and endpoint determination was 7 days. With longer times, spheroid growth delay and re-growth could be observed. However, while utilization of 3D spheroids for compound screening is more complicated than screening with 2D mono-layers [56], 3D cell-spheroid models can now be applied to high-throughput assays due to the availability of hardware and consumables to readily support growth and analysis of cell-spheroids exposed to test compounds. Several spheroid-generation technologies have been developed including hanging-drop technologies, ultra-low attachment (ULA) plates, hydro-gel seeding, suspension growth, and micro-fluidic approaches [reviewed in 2].

Vinci et al. described a 3D spheroid high-throughput protocol involving the growth of a single spheroid per well in suspension culture in a 96- or 384-well format and using high-content imaging to assess the diameter of the spheroid and staining to determine viability of the cells [57]. In a similar protocol, single spheroids embedded in Matrigel™ allowed determination of the migration and invasion of cells as the spheroids increased in size or decreased in diameter due to treatment. Future challenges for large-scale integration of 3D spheroid models into high-throughput screening programs include growth of the spheroids, data collection, and availability of suitable endpoints, e.g., using high-content imaging [58]. However, while the driving force for pursuit of this approach is that 3D cell-based models, especially those including co-culture with stromal cells, may be more representative of the in-vivo tumor micro-environment and provide more robust data, reports on the use of such co-culture models are still limited.

In the early study of spheroids in the 1970s and 1980s, the effect of spheroid size (cell number per spheroid) on oxygenation, proliferation, drug penetration, and end-point validity was recognized as a critically important variable. The effects of spheroid size differed from cell line to cell line depending upon the tightness of the cell clusters. In the high-throughput setting with many cell lines being screened, a single-time point post-plating of the cells is often selected. While many types of data including spheroid diameter, cell number per spheroid, and regional viability of cells in the spheroid can be collected in focused studies, it is difficult to apply these methods in the high-throughput setting, and the screen endpoint is most often an average ATP determination per well, limiting inferences on the cell sub-populations within the spheroid. Larger spheroids are more difficult to image using high-content imaging scanners due to limited light penetration and may require immunohistochemical methods to visualize effects throughout the spheroid.

Among the normal processes in tumor growth is angiogenesis. Although much of tumor growth involves co-opting existing blood vessels, neo-angiogenesis is also common in tumors but is difficult to incorporate into cell models used in high-throughput screening programs. Varied substrates have been applied to mimicking the growth of blood vessels in 3D culture systems [59, 60]. In addition, tumor-immune system interactions have been investigated in 3D spheroid culture models [61]. 3D bio-printing of cells into 3D structures is being investigated at several centers for varied applications [62]. 3D bio-printing has been used to fabricate vasculature with a tight-confluent endothelial lining capable of supporting the viability of cells up to 5 mm away. Tumor cells and matrix can be printed around the vessel.

Most 3D cell-based screens have used well-established cell lines that were previously used as mono-layer screens. However, these cell lines may not provide sufficiently diverse genetic backgrounds to represent the heterogeneity of clinical disease. There is a drive to utilize early-passage cells derived from patients, in screens to determine whether more predictive models—be it mono-layer culture, mono-layer co-culture (e.g., with fibroblasts), or a spheroid model (cancer cells alone or as a co-culture with stromal cells)—can be developed. Empirical studies aimed at examining the power to predict activity in tumor-bearing mice of the same early-passage cell lines in mono-layer versus 3D cultures are required to determine which assay format is most applicable for use in future screening. Cell lines recently derived from tumors have been applied to screens and drug selection in both 2D and 3D assays [63]. Drug-resistant sublines prepared in cell culture (by exposing the cells in mono-layer to increasing concentrations of drug) have been compared with cell lines derived from the tumors of patients who have stopped responding to the same drug. Orlandi et al. showed that human breast cancer cell lines (MCF7) differed in response to idarubicin, a doxorubicin derivative, and its active metabolite when studied in 3D cultures versus 2D [64]. There were an apparent decrease in potency of the compound and the need for prolonged exposure in the 3D model. Friedrich et al. showed that the response of the human HT-29 colon-cancer cell line to irinotecan was different in 3D spheroid culture than in mono-layer culture, with the  $IC_{50}$  of the drug increasing >100-fold in the 3D model [55]. Furthermore, other antic-ancer drugs had reduced efficacy because of slow drug penetration into the spheroid or so-called “multi-cellular” resistance [11, 42, 65].

Some of the changes in drug sensitivity observed may be due to the extra-cellular matrix and microenvironment surrounding the cells. Multi-cellular tumor spheroids derived from human TC32 and TC71 Ewing's-sarcoma cells varied in their response to the compound LY294002 and anti-cancer drugs based on the expression of a dominant-negative form of E-cadherin or the wild-type protein [66]. In human SKOV3 serous ovarian-carcinoma cells, increased expression of two transcripts of Kallikrein-related peptidase (KLK7) enhanced spheroid formation through integrin-mediated adhesion. Spheroids of the SKOV3 subline over-expressing KLK7 were less sensitive to paclitaxel than parental SKOV3 spheroids [67]. In other studies, the ratio of pannexins (Pannx1 to Pannx2; a class of gap-junction proteins) may determine the degree of compaction of cell aggregates by remodeling the actin cytoskeleton, and this structural alteration may modulate drug sensitivity [68].

---

## Newer Cell Lines: Patient-Derived Xenograft (PDX) Cells

Many early 3D models used in high-throughput screening programs were developed with well-established cell lines that had traditionally been grown in mono-layer culture [50]. While these 2D and 3D culture models provided well-controlled experimental systems to determine the effects of the change in cell culture format on compound response, the well-established cell lines were not sufficient to represent the heterogeneity of human cancers [55]. To address this issue, there have been several large efforts to develop new cell lines recently derived from patients and to develop new xenograft models recently derived from patients. Because patient-derived xenografts (PDX) and patient-derived cell lines have a shorter history in mice or cell culture, they maintain more of the genetic variations exhibited in the clinical disease and may be models that can successfully inform the best therapeutic option for treatment of the tumor type from which they were derived [69–74].

---

## 3D Assays Allow Extended Compound Exposure

While many DNA- and tubulin-interactive agents exert cyto-toxic effects on cells during short exposure times (48–72 h), many targeted drugs and compounds require multiple cell doublings to manifest their cytotoxicity. Examples include the epigenetic modifiers that alter DNA methylation. To accurately assess the effects of these agents in a high-throughput screen requires that the cells be exposed to the compounds for 5–10 days (depending upon cell doubling time). In a mono-layer culture system, well-established cell lines frequently have doubling times between 17 and 36 h. Since many high-throughput screening assays are performed in flat-bottomed multi-well plates, long compound-exposure times can result in over-confluent cell growth in control wells, resulting in invalid endpoint readings. While initial seeding density can be reduced, for assays which extend >10 days, after ~ 10 doublings slight variations in the initial cell plating number can result in marked variations in the cell number at assay endpoint, resulting in highly variable data that is difficult to

interpret. Indeed, depending on spheroid size, it is sometimes necessary to extend the compound exposure time of spheroids to achieve a response similar to that observed in 2D cultures of the same cells [55, 64].

Spheroid models may more closely mimic the tumor micro-environment than mono-layer cultures. Depending on spheroid size and the lipophilicity of the test compound, reduced drug penetration can occur in these models. Similarly, contact-induced multi-drug resistance, hypoxia, and glycolytic metabolism may also be observed in spheroids [75, 76]. Furthermore, since it is well established that cellular gene expression profiles in 3D spheroids more closely mimic those in tumor specimens than do 2D mono-layers, 3D spheroids may be better models for compound testing [77–80].

Spheroid cell number, volume, and tightness are important variables in compound testing [81]. Erlanson et al. examined drug penetration, distribution, and retention in spheroids of a human glioma line and a human colon carcinoma line after 15–30 min exposure to drugs [65]. Properties of the drug, the spheroids, and the cells affected the uptake and retention of doxorubicin, actinomycin D, and cytosine arabinoside (ara-C) in the spheroids. In some cases, compounds accumulated in the spheroids [65]. 3D tumor spheroids differ in sensitivity to cytotoxic agents such as 5-fluorouracil, cisplatin, and doxorubicin depending upon cell type and propensity to form a dense extracellular matrix [40, 42, 82, 83]. Because of these features of multicell spheroids, the hope is that 3D cell culture models applied in high-throughput screening drug discovery programs will be better predictors of compounds likely to have activity in human tumor models and thus improve upon the current success rates of cancer drug discovery. However, these models require an appropriate assay format to identify compound activities of interest.

---

### 3D Assay Endpoints

Many 2D mono-layer culture screens for compound testing relied on measures of viability to determine activity. Sulforhodamine B (used in the NC-I60 screen) is not readily applicable to 3D multicell spheroid models [84]. Fluorescent dyes such as MTT may be of limited use since, depending upon spheroid size, the dye may not reliably penetrate all of the cells during the time course of the assay [85]. Furthermore, the fluorescence intensity of vital fluorescent dyes can be affected by the penetration of the dye into the spheroid. Similarly, depending upon the intensity of the light source, spheroid density may reduce uniform access of excitation light in the spheroid as well as the amount of emitted light. Luminescence assays (e.g., measurement of ATP levels using Cell Titer-Glo (Promega, Madison, WI) or ATPlite (PE, Waltham, MA)) provide useful measures of cell viability in 2D culture systems, and with a suitable detection system, the wide dynamic range of these techniques provides a robust output at very low numbers of viable cells [86]. Recently, the Cell Titer-Glo assay was adapted for use in 3D spheroids (Cell Titer-Glo 3D). Increasing the cell-lysis capability of the assay solution and increasing the concentration of the luminescence substrate (to efficiently measure released intracellular

ATP) allowed this assay to be used for quantitation in spheroid models [87, 88]. However, the assay is limited by producing a single average reading per well; thus, information regarding sub-populations of cells in the spheroid is lost. In co-culture models, an average reading per well does not differentiate between different cell types, and in the presence of high numbers of stromal cells, the killing of cancer cells may be missed. Consequently, cancer cells and stromal cells have been genetically engineered to express molecular markers such as luciferase to distinguish between them [89]. In addition, high-content imaging can be used to examine parameters such as morphology changes in the cells upon compound exposure, and these techniques may prove valuable when applied in parallel with viability endpoints, making screens with 3D multicell spheroids more complex than traditional 2D mono-layer culture screens but more informative regarding cell fate [55, 58]. In publications examining spheroids using these high-content screening approaches, it was evident that 3D spheroids may actually exhibit greater sensitivity to some compounds than could be observed in 2D cultures of the same cells [56, 88, 90, 91]. However, by pre-selecting spheroids of a given size prior to compound addition, it is possible to obtain useful information from cytotoxicity data alone [81, 88].

---

## Fibroblast and Stromal Effects on Sensitivity to Drugs

Fibroblasts are an essential component of the stromal cell population, and they may affect cancer cell sensitivity to therapeutic compounds in a number of ways. Fibroblasts secrete collagen and other proteins that are part of the extra-cellular matrix (ECM) surrounding cells. Extra-cellular matrix proteins provide a barrier for access to cancer cells by potential therapeutics. In addition, fibroblasts secrete growth factors that can alter drug sensitivity through paracrine signaling between the fibroblasts and the cancer cells [92]. To better replicate the tumor micro-environment in cell-based assays, several studies examined inclusion of fibroblasts and other stromal components in 3D multi-cell spheroid assays. Spheroids formed from human mesenchymal stem cells and human umbilical-vein endothelial cells (HUVEC) can develop primitive vascular structures. Drug sensitivity in these complex spheroid models compared favorably with the drug sensitivity of the same cells grown as human tumor xenografts [93].

Interest in 3D cell-based assays is being driven by the recognition that compound failure in moving from mono-layer cell-based assays to human tumor xenograft assays was high. To allow implementation of 3D cell-based screens in high throughput, manufacturers have developed varied proprietary plasticware options so that 3D spheroids can be grown and/or assayed using a variety of endpoints. Plasticware that allows cancer cells and/or stromal cells to be grown as spheroids in 384-well hanging-drop plates has demonstrated utility in testing compounds for potential oncology applications [56, 94]. Hydro-gel-based systems (including agarose and alginate scaffolds) allow capture of cells in micro-droplets of the matrices, and micro-wells punched into an agarose scaffold promote spheroid formation [95, 96]. The agarose and alginate micro-spheres are transparent and, at very small

diameters, allow diffusion of compounds and detection reagents into the multi-cell spheroids. In the agarose micro-wells, spheroids with differing size demonstrated varying sensitivity to test compounds, with larger spheroids being less responsive than smaller spheroids.

High-content imaging agents could readily be applied in both of these systems [95, 96]. Ultra-low attachment U-bottomed plates (96- or 384-well) coated with polyHEMA, or a similar hydrophobic matrix, allow 3D multi-cell spheroid generation and automated compound testing, since the plates conform to a standard Society for Biomolecular Screening (SBS) compliant format and are compatible with high-throughput screening instrumentation such as cell dispensers, plate washers, and plate readers. ULA plates have been used to categorize the morphologies of spheroids and to compare compound sensitivities of cells in 3D versus the same cells as mono-layer cultures [97]. Other methods for spheroid production include bioreactor technologies applied to generation of large numbers of spheroids, as well as microfluidic technologies that can generate and test very small spheroids [2, 95].

The success of the multi-cell spheroid models in predicting response to a test compound in human tumor xenografts depends on several factors: spheroid growth (size at time of compound addition and percent of cells actively dividing), duration of compound exposure, and appropriate endpoint and data analysis. Results obtained from a 3D multi-cell spheroid screen are only as valuable as the representative nature of the cells and other components used in generating the spheroids and the assay endpoints. Well-established cell lines such as the NCI-60 cell line panel can provide valuable information on compound response in 3D assays and can provide a valuable bridge between 2D and 3D assays to elucidate the strengths and weaknesses of each assay format [97]. The NCI-60 cell lines can be propagated in routine cell culture flasks and have been extensively characterized at the level of DNA for mutations, methylation, and copy number, at the level of RNA for gene expression and microRNA expression and at the protein level. Furthermore, a large database of assay results (from compounds tested in the classic 2D mono-layer culture screen using the sulforhodamine B readout) has been developed over a considerable time [50]. Consequently, the NCI-60 cell lines have been grown as spheroids in 96-well U-bottomed ULA plates [97]. Spheroid growth is critically dependent upon the number of cells plated at time zero. MCF7 human breast carcinoma cells and HT-29 human colon carcinoma cells plated at numbers from 50 cells to 10,000 cells per well grow widely-varying spheroids in 72 h (Fig. 19.2). Spheroids can be tightly adhered spheres or loose clusters. Cell lines from each of the nine tumor types represented in the NCI-60 cell line panel develop spheroids of varying tightness. The spheroids grown from the NCI-60 cell lines have been classified into groups depending upon the characteristic growth pattern of that cell line (Fig. 19.3a, b). There is no tumor-type panel that produced uniform spheroids; thus, heterogeneity in the spheroid growth characteristics does not depend upon the tumor of origin but varies from cell line to cell line in each of the nine tumor panels (Fig. 19.3c). To examine the differential sensitivity of HT-29 human colon carcinoma cells grown in mono-layer and grown as spheroids to an anticancer agent, the topoisomerase 1 inhibitor topotecan was tested. The concentration response curve for HT-29 cells exposed to

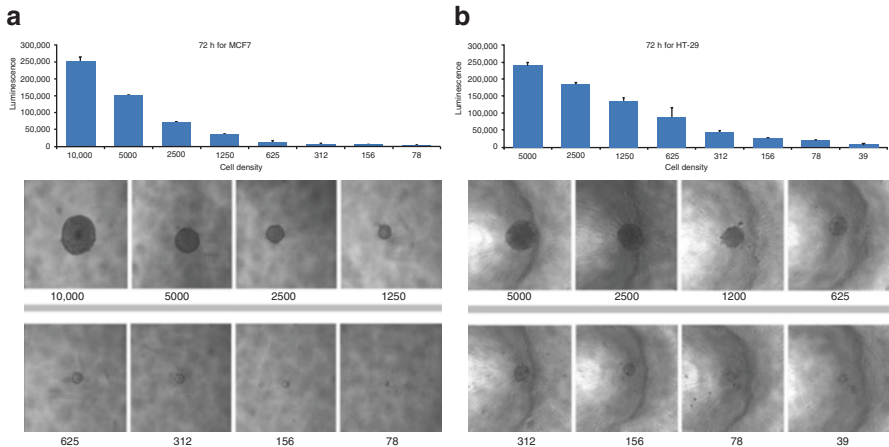


**Fig. 19.2** Spheroid images for MCF7 human breast cancer cells panel (a) and HT-29 human colon carcinoma cells panel (b) showing spheroids initiated with varied cell numbers after 72 h of incubation. Cells were plated into 96-well U-bottomed ultra-low attachment plates, and spheroids were allowed to grow for 72 h. Cell numbers plated are below each image. After 72 h, the ATP content of each well was determined using Cell Titer-Glo 3D (Promega). ATP content was measured as luminescence. Error bars are the SD from four independent determinations

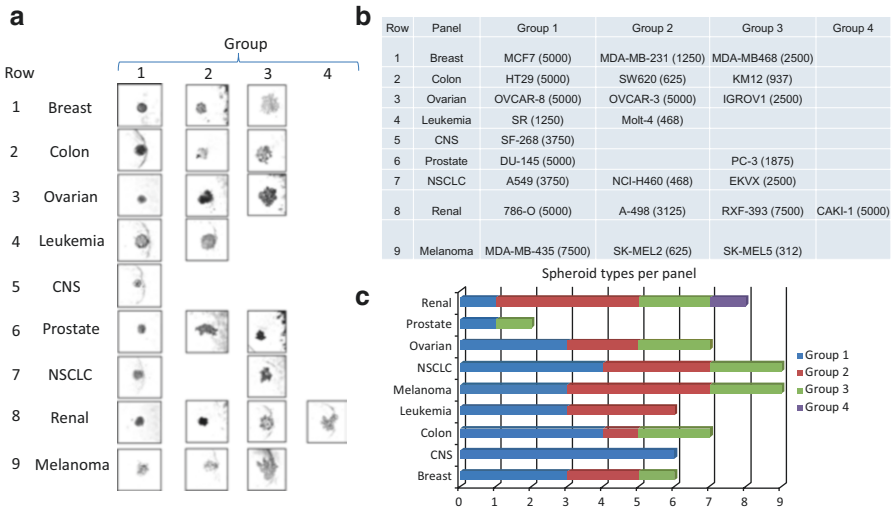


**Fig. 19.3** NCI-60 cell line panel spheroid morphologies and classification based upon tightness of the cell cluster. Panel (a): examples of spheroids from NCI-60 cell lines representing each of the nine tumor types covered by the panel classified into groups by spheroid tightness. Panel (b): table showing the cell line (cell number) and group classification for the spheroids shown in panel (a). Panel (c): bar chart showing the distribution of spheroids classified by tightness for the NCI-60 cell panel for the nine tumor types covered by the panel

topotecan for 72 h in mono-layers gave an  $IC_{50}$  of 0.11  $\mu\text{M}$  (Fig. 19.4a). However, the same cells grown as spheroids had an  $IC_{50}$  of 0.9  $\mu\text{M}$ , a nearly ninefold decrease in sensitivity. The HT-29 colon carcinoma spheroids were tracked over a time course for response to topotecan plus/minus the ATR inhibitor VE-821 (1  $\mu\text{M}$ ) using calcein AM to mark the live cells and ethidium homodimer to mark the dead regions of the spheroid (Fig. 19.4b). The fluorescent images show that with increasing concentrations of topotecan and longer duration of exposure, the cells in the interior and the periphery of the spheroids are dying. VE-821 further increased the degree of cell killing observed, and this was validated by data on cell viability measured using Cell Titer-Glo 3D [where exposure to the combination demonstrated a substantial decrease in luminescence (Fig. 19.4c)].

However, while many of the NCI-60 cell lines form xenograft tumors in immune-deficient mice, 60 human cell lines are not sufficient to represent the heterogeneity of human malignant disease. Consequently, to better replicate clinical

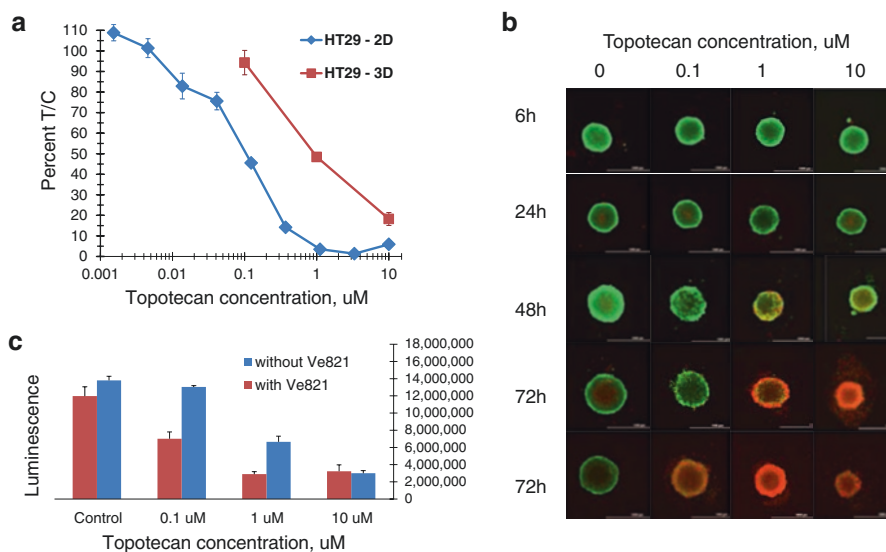


**Fig. 19.4** Panel (a): concentration response curves for HT-29 human colon carcinoma cells grown in mono-layer (2D) or as spheroids (3D) exposed for 72 h to varied concentrations of topotecan. The experimental endpoint was ATP determination using Cell Titer-Glo. Panel (b): fluorescent images of HT-29 human colon carcinoma cells grown as spheroids for 72 h and then exposed to varied concentrations of topotecan plus 1  $\mu\text{M}$  of the ATR inhibitor VE-821 over a time course from 6 to 72 h. At the selected time points, cells were exposed to calcein AM and ethidium homodimer (live/dead stain; Invitrogen). Live cells take up calcein AM which fluoresces green in the presence of calcium. Ethidium homodimer cannot penetrate intact cell membranes and fluoresces red when bound to cell-free DNA indicating dead cells. At increasing topotecan concentrations and with increasing time, there is increased killing of the HT-29 cells by topotecan. Panel (c): Cell Titer-Glo 3D was used to assess cell killing by topotecan plus 1  $\mu\text{M}$  ATR inhibitor VE-821 after 72 h exposure to the combination



disease, there has been a great effort devoted to using materials recently derived from patients' tumors in experimental models to identify optimal therapeutic regimens. Biopsy samples from a primary tumor, metastatic disease, or circulating tumor cells from a patient can be implanted into NSG severely immune-deficient mice and propagate as patient-derived xenograft (PDX) tumor nodules [69–74]. PDX tumors are composed of a patient's cancer cells and, thus, have the genetic abnormalities that define and drive the patient's tumor. By examining the response of a wide array of PDX models to FDA-approved and investigational agents, the sensitivity of each tumor to specific therapeutic agents, alone or in combinations, can be determined [98–101].

---

## Development and Propagation of PD Cell Lines

PDX tumor specimens are routinely implanted subcutaneously in the flank of NSG mice or orthotopically in a mouse organ corresponding to the tissue of origin of the tumor [102]. Orthotopic transplants may better mimic the genotypic and histological characteristics from the tumor [103].

The usefulness of human tumor xenografts as a source of cells for cell-based screening in the cloning assays has been explored. This strategy offers the opportunity to correlate gene expression profiles within a tumor with sensitivity to therapeutic agents. The application of the tumor clonogenic assay (TCA) to chemosensitivity testing of clinical tumors and xenografts and for assessments within drug discovery was examined [104, 105]. Comparison between the responses of human tumors (well established as xenografts in nude mice) in the tumor clonogenic assay in vitro to that of the clinical response in mice indicated that 62% of the comparisons for drug sensitivity and 92% of the comparisons for drug resistance were correct. The same percentage of true/false observations was found when tumors were tested in the tumor clonogenic assay in vitro after serial passage in nude mice and their response was compared to in vivo activity in corresponding xenografts (60% and 90%, respectively). Furthermore, PDX responses to chemotherapeutic agents have been suggested to resemble the response rates of mono-therapy in clinical trials [69–74, 103], making cells derived from them a potential model of interest for use in high-throughput screening assays.

---

## Cell-Based Screens Using PD Cells

While patient-derived xenografts (PDX) implanted into severely immune-deficient mice (NSG, NOD SCID, SCID, or nude) may be of value in identifying efficacious agents for treatment of specific tumor types, the cost in time, and money, and the complexity of performing these tests has resulted in an effort to generate cell-based patient-derived models. Cell-based models have the advantage of being amenable to automation, thus allowing increased throughput at reduced costs and with an improvement in time to result. To facilitate development of an immortal cell line,

the Rock-II kinase inhibitor, Y27632, is sometimes included to chemically produce a mutant RAS-like cell metabolic state [106]. There is a distinction between patient-derived cell lines which are cancer cells adapted to growth in cell culture and organoid cultures which are minceates of patient tumor tissue dissected to remove fatty and necrotic tissue, treated to remove red blood cells, then prepared as a heterogeneous mixture of small clusters of cells which can grow in short-term culture [107]. Generating organoid models can occur in a time frame of several weeks, while development of cancer cell lines and the generation of patient-derived xenografts usually require more time. The organoid model could potentially facilitate sampling of patient populations that had previously been difficult to model using traditional approaches and may allow identification of therapeutic strategies for specific patients. The development of organoid culture methods from human tumors is one avenue that may provide robust, stage-specific, cellular models that will be a valuable resource for the field [108]. Another approach is the use of PDX tumor-bearing mice in a screening mode.

Over the course of several years, Gao et al. utilized ~1000 PDX models exhibiting a wide variety of driver mutations to explore several compounds with potential anticancer activity [109]. When the RECIST criteria and the response categories (complete response, partial response, stable disease) were combined into a single “responder” category, the response calls made on a single mouse were consistent with the majority response 95% of the time, which strongly supported the rationale of using one animal to reflect the true response. Thus, a  $1 \times 1 \times 1$  experimental approach was used, facilitating efficient assessment of compound response of the 1000 xenografts to determine population-based response rates. Thirty-eight unique small molecules were screened either as single agents [38] or in combination [26], and model responses were categorized. Associations between PDX genotype and compound response were observed. The data confirmed earlier work that PDX models may be useful in selecting compounds with clinical potential.

Stromal cells play an important role in some cancer types through paracrine signaling and may regulate a tumor’s response to drug treatment [89, 110, 111]. Furthermore, stromal cells can contribute biomarkers that may be predictive of treatment regimen and/or response to treatment [112]. Lung cancer PDX and prostate cancer PDX have been applied in cell-based assays after transfer of tumor cells to culture. Lung cancer cells mixed with fibroblasts from lung cancer surgical specimens were embedded in Cultrex basement membrane extract as a 3D cell-based screen model, and prostate cancer cells mixed with human osteoblasts were embedded in a hydro-gel as a 3D cell-based screen model [113, 114]. The 3D hydro-gel system used to co-culture prostate cancer cells with osteoblast cells mimicked the prostate cancer cell-osteoblast in the bone metastatic microenvironment. The cancer cells and fibroblasts were embedded in the matrix which allowed paracrine signaling between the cells. Furthermore, this 3D model allowed culture of prostate cancer cells that tend to be difficult to grow as mono-layers. When dovitinib, a receptor tyrosine kinase inhibitor of FGFR and VEGFR, was tested in the 3D prostate cancer-osteoblast model, it exhibited activity when prostate cancer cells and osteoblast cells were co-cultured and with either cell type alone [114].

This type of 3D cell culture assay has been applied to colorectal cancer metastases and primary tumors, esophageal cancer, as well as pancreatic cancer. Inclusion of carcinoma-associated fibroblasts in co-culture with cancer cells resulted in decreased  $IC_{50}$  values for cisplatin and vinorelbine as single agents but not when the drugs were used in combination. While an increase in  $IC_{50}$  with HDAC inhibitors was seen upon inclusion of carcinoma-associated fibroblasts in the 3D Cultrex cell culture assay, many lung-cancer cell lines remained more sensitive, and HDAC inhibitors were shown to sensitize select cancer-cell-types to standard-care drugs such as cisplatin, vinorelbine, and gemcitabine. Based on these results, including stromal cells in 3D cell-culture screening models will likely provide a better model for selecting compounds for further testing than will assays using cancer cells alone.

Recently, patient-derived cell culture models have been validated in automated screening workflows. Boehnke et al. used a 3D model in 384-well plates to demonstrate the utility and reproducibility of the model in compound screening using colon cancer cells derived from organoid cultures [106]. Patient-derived colon cancer cells were embedded in an extracellular matrix as single cells, and in some cases the cells self-organized into organoid/vesicle structures within 4 days. Patient-derived organoid samples were cultured and expanded in Matrigel droplets in 12-well plates and were then disaggregated into single-cell suspensions into growth factor-reduced Matrigel and seeded into 384-well plates. Compound treatment was initiated after a culture period of 4 days, and cell viability was analyzed after culture for two population-doubling times. In some cases, single cells seeded into 384-well plates subsequently formed 3D vesicle structures after 4 days of culture. Viability assays after exposure to various agents were monitored using Cell Titer-Glo, which measures released ATP in a luminescent reaction that can be quantitated using a luminescence plate reader. The Z values for the assay were between 0.62 and 0.83 [115], suggesting a robust assay and indicating that PDX-derived cells can be utilized in automated assays.

However, patient-derived cell-based models cannot be examined in drug response assays in isolation. Baseline data in response to the standard of care must be established, and molecular data including DNA sequence, mRNA expression, DNA methylation, copy number variation, microRNA, and lncRNA must be considered in understanding response to treatment with targeted therapeutics. To fully evaluate the prognostic power of this approach, a large number of well-characterized models from diverse tumors must be developed and characterized. Furthermore, cancer cells in isolation may exhibit different responses than those co-cultured with appropriate stromal cells [106], and therefore examination of the contribution of cancer-associated fibroblasts (CAFs), endothelial cells, and infiltrating cells is required in models representative of the heterogeneity of the human disease in order to increase our understanding of the variables involved in determination of response [106, 114].

Organoid cultures may exhibit a closer association with the initial patient-derived tumor sample; however, unless propagated in a way that maintains the cellular heterogeneity, these preparations drift rapidly [107, 116–118]. In high-throughput screening assays, test compounds are usually added at time zero, and cells are exposed to the compound continuously. 3D multi-cell spheroid models are well suited to prolonged compound exposure studies without over-confluency in the well

of the assay plate [88]. Prolonged compound exposure can be important to fully manifest the activity of epigenetic inhibitors and other targeted agents. Prolonged exposures (>12 days) also open up the possibility to perform combination studies to more closely mimic clinical regimens with either sequential or alternating compound exposure. High-throughput screening experiments aimed at mimicking clinical regimens may require media exchange on the spheroids after each drug exposure and sufficient exposure time to mimic the PD/PK, metabolism, and excretion of compound(s) in a patient over time.

As improved high-throughput screening assay techniques are developed and widely adopted to mimic clinical disease response to known therapeutics, these models can be applied to test investigational agents to improve the selection of compounds that move forward toward clinical trial. Patient-derived models may also provide insight into suitable biomarkers to use in identifying patients most likely to benefit from a targeted therapeutic, to indicate response in patients to guide therapy to a positive outcome, or to enable rapid use of alternative treatment options. Eventually, it may be possible to start with a small amount of tumor tissue from a biopsy or surgical resection, generate cancer organoids, expand the organoid cultures using specific growth factors and matrices, and in a matter of days or weeks, use the expanded cultures to select a therapeutic option or combination therapies that may benefit the patient. The time between biopsy or surgery, expansion in culture, and use in such a small-scale drug screen will depend on the expansion/growth rate of the organoids, the number of compounds to be tested, and the sensitivity of the assay endpoint.

Currently, large volumes of data are being generated from patient-derived models that have been molecularly characterized (DNA mutations, methylation, gene copy number, mRNA, microRNA, and lncRNA), and databases have been established to correlate the drug response of the models with these and other molecular characteristics. Compared with well-established cell line xenografts, recent patient-derived models may be superior because they retain greater molecular similarity to the patient's tumor [119–125]. However, many patient-derived cell lines have not been extensively studied in cell-based screening systems primarily due to the complexity and high cost of obtaining and validating the models. Since patient-derived cell lines are expensive to produce and are widely diverse, their application in routine drug discovery efforts is still limited. However, retrospective analyses have demonstrated that patient-derived cell lines have predictive capability for treatment selection [107, 116–118]. Such patient-derived models included samples from 34 patients with solid tumors that were tested to determine efficacy of approved cancer agents. *In vivo*, a PDX response correlated with a response in patients 12 out of 13 times (92%). A lack of response was also predictive in the PDX models (36/37 times; 97%) [73, 74]. In another example [71], PDX models correctly predicted response in 19 out of 21 cases (90%) and resistance in 57 out of 59 cases (97%). These studies used antibodies such as bevacizumab and cetuximab, and additional studies in 85 metastatic colorectal PDX models treated with cetuximab showed results that also closely correlated with the clinical observations [126, 127] suggesting that such assays are not restricted to small molecules.

## Assay Endpoints for PD Cell Line Models

In recent studies, patient-derived cells used in mono-layer cultures or in 3D multi-cell spheroid assays, endpoints have included viability measurements such as Alamar Blue [113] and Cell Titer-Glo [106, 114]. Other assays have focused on the use of high-content imaging (with and without stains) to determine cell viability in live/dead assays or (in the case of 3D spheroids) in parallel with measurement of the size of the spheroid [55, 58]. It is possible that rationally selecting a suitable therapy for a patient may rely on a cell-based screen using an early passage of patient-derived cells. To improve the ability to treat a patient with the optimal therapy, a select subset of clinically relevant compounds may be chosen based on the gene profile, mutational status of select targets, and other analyses of the tumor sample or after an early amplification of the cancer cells as a xenograft or in culture. If good correlative power is demonstrated between a cell-based assay using a recent patient-derived cell line and *in vivo* efficacy using the patient-derived cells grown as a xenograft in repeated drug tests, it may be possible to justify using the cell-based screen to select the best treatment for the patient without lengthy *in vivo* testing, thus speeding up the process of choosing the treatment most appropriate to the current stage and genomic profile of the tumor with an option for different treatment regimens being implemented over time. However, until a high level of confidence can be achieved that cell-based screens are predictive of *in vivo* results, there will be a need to follow up with a xenograft model.

### Conclusion

Patient-derived cell models are expensive to produce and maintain, but these cultures are being adapted for use in miniaturized assays that are demonstrating utility in the identification of growth-inhibitory compounds that may have potential to become drugs. As suitable cell culture models that more closely mimic the response of cancer cells *in vivo* are developed and as the number of cells required for an assay is reduced through miniaturization, it is expected that patient-derived cells will be used more widely in the primary screening operations to identify potential therapeutic compounds.

Such models could have greater prognostic power and decrease the attrition rate as compounds move forward through the discovery and development pipeline toward the clinic. Patient-derived cells may be used to identify the optimal therapeutics for a specific patient or to increase understanding of molecular biomarkers that predict response. Consequently, such use of patient-derived cells and patient-derived cell lines may assist in converting cancers into a clinically manageable disease.

To this end, drug testing on 3D fragments of the patient original tumor has turned out to be predictive of patient outcome [128, 129, 130, 131, 132]. In the future, it would be informative to compare data from direct tumor fragment culture and cell lines derived from them in 3D culture, to validate their utility in the drug discovery process.

## References

1. Sutherland RM, McCredie JA, Inch WR. Growth of multicell spheroids in tissue culture as a model of nodular carcinomas. *J Natl Cancer Inst.* 1971;46:113–20.
2. Hirschhaeuser F, Menne H, Dittfield C, West J, Mueller-Klieser W, Kunz-Schugart LA. Multicellular tumor spheroids: an underestimated tool is catching up again. *J Biotechnol.* 2010;148(1):3–15.
3. Durand RE. Radiation-resistant tumor cells may be more sensitive in vitro. *Cancer Res.* 1972;32:2587–8.
4. Sutherland RM. Cell contact as a possible contribution to radiation resistance of some tumors. *Br J Radiol.* 1972;45(538):788–9.
5. Durand RE, Sutherland RM. Effects of intercellular contact on repair of radiation damage. *Exp Cell Res.* 1972;71:75–80.
6. Durand RE, Sutherland RM. Dependence of the radiation response of an in vitro tumor model on cell cycle effects. *Cancer Res.* 1973;33:213–9.
7. Durand RE. Isolation of cell subpopulations from in vitro tumor models according to sedimentation velocity. *Cancer Res.* 1975;35:1295–300.
8. Durand RE. Cure, regression and cell survival: a comparison of common radiobiological endpoints using an in vitro tumor model. *Br J Radiol.* 1975;48:556–71.
9. Sutherland RM, Durand RE. Radiation response of multicell spheroids – an in vitro tumor model. *Curr Top Radiat Res Q.* 1976;11:87–139.
10. Sutherland RM, MacDonald HR, Howell RL. Multicellular spheroids: a new model target for in vitro studies of immunity to solid tumor allografts. *J Natl Cancer Inst.* 1977;58:1849–53.
11. Sutherland RM, Eddy HA, Bareham B, Reich K, Van Antwerp D. Resistance to adriamycin in multicellular spheroids. *Int J Radiat Oncol Biol Phys.* 1979;5:1225–30.
12. Sutherland RM, Bareham BJ, Reich KA. Cytotoxicity of hypoxic cell sensitizers in multicell spheroids. *Cancer Clin Trials.* 1980;3:73–83.
13. Freyer JP, Sutherland RM. Selective dissociation and characterization of cells from different regions of multicell tumor spheroids. *Cancer Res.* 1980;40:3956–65.
14. Durand RE. Flow cytometry studies of intracellular adriamycin in multicell spheroids in vitro. *Cancer Res.* 1981;41:3495–8.
15. Durand RE. Slow penetration of anthracyclines into spheroids and tumors: a therapeutic advantage? *Cancer Chemother Pharmacol.* 1990;26:198–204.
16. Durand RE. Use of Hoechst 33342 for cell selection from multicell systems. *J Histochem Cytochem.* 1982;30:117–22.
17. Bauer KD, Keng PC, Sutherland RM. Isolation of quiescent cells from multicellular tumor spheroids using centrifugal elutriation. *Cancer Res.* 1982;42:72–8.
18. Durand RE, Vanderbyl SL. Sequencing radiation and Adriamycin exposures in spheroids to maximize therapeutic gain. *Int J Radiat Oncol Biol Phys.* 1989;17:345–50.
19. Sutherland RM. Cell and environment interactions in tumor microregions: the multicell spheroid model. *Science.* 1988;240:177–84.
20. Landry J, Freyer JP, Sutherland RM. Shedding of mitotic cells from the surface of multicell spheroids during growth. *J Cell Physiol.* 1981;106:23–32.
21. Landry J, Freyer JP, Sutherland RM. A model for the growth of multicellular spheroids. *Cell Tissue Kinet.* 1982;15:585–94.
22. Durand RE. Multicell spheroids as a model for cell kinetic studies. *Cell Tissue Kinet.* 1990;23:141–59.
23. Brown RC, Durand RE. Repair, redistribution and repopulation of V79 spheroids during multifraction irradiation. *Cell Prolif.* 1994;27:343–54.
24. Durand RE. Chemosensitivity testing in V79 spheroids: drug delivery and cellular microenvironment. *J Natl Cancer Inst.* 1986;77:247–52.
25. Rasey JS, Grunbaum Z, Magee S, Nelson NJ, Olive PL, Durand RE, Krohn KA. Characterization of radio labeled fluoromisonidazole as a probe for hypoxic cells. *Radiat Res.* 1987;111:292–304.

26. Mueller-Klieser WF, Sutherland RM. Influence of convection in the growth medium on oxygen tensions in multicellular tumor spheroids. *Cancer Res.* 1982;42:237–42.
27. Durand RE. Oxygen enhancement ratio in V79 spheroids. *Radiat Res.* 1983;96:322–34.
28. Durand RE. Repair during multifraction exposures: spheroids versus monolayers. *Br J Cancer Suppl.* 1984;6:203–6.
29. Sutherland RM, Durand RE. Growth and cellular characteristics of multicell spheroids. *Recent Results Cancer Res.* 1984;95:24–49.
30. Freyer JP, Sutherland RM. Regulation of growth saturation and development of necrosis in EMT6/Ro multicellular spheroids by the glucose and oxygen supply. *Cancer Res.* 1986;46:3504–12.
31. Sutherland RM, Sordat B, Bamat J, Gabbert H, Bournat B, Mueller-Klieser W. Oxygenation and differentiation in multicellular spheroids of human colon carcinoma. *Cancer Res.* 1986;46:5320–9.
32. Casciari JJ, Sotirchos SV, Sutherland RM. Glucose diffusivity in multicellular tumor spheroids. *Cancer Res.* 1988;48:3905–9.
33. Casciari JJ, Sotirchos SV, Sutherland RM. Mathematical modelling of microenvironment and growth in EMT6/Ro multicellular tumor spheroids. *Cell Prolif.* 1992;25:1–22.
34. Durand RE, Vanderbyl SL. Response of cell subpopulations in spheroids to radiation-drug combinations. *NCI Monogr.* 1988;6:95–100.
35. Rofstad EK, Sutherland RM. Growth and radiation sensitivity of the MLS human ovarian carcinoma cell line grown as multicellular spheroids and xenografted tumors. *Br J Cancer.* 1989;59:28–35.
36. Durand RE. Cisplatin and CCNU synergism in spheroid cell subpopulations. *Br J Cancer.* 1990;62:947–53.
37. Olive PL, Durand RE, Banath JP, Evans HH. Etoposide sensitivity and topoisomerase II activity in Chinese hamster V79 monolayers and small spheroids. *Int J Radiat Biol.* 1991;60:453–66.
38. Durand RE, Olive PL. Evaluation of bioreductive drugs in multicell spheroids. *Int J Radiat Oncol Biol Phys.* 1992;22:689–92.
39. Teicher BA, Herman TS, Holden SA, Wang YY, Pfeffer MR, Crawford JW, Frei E. Tumor resistance to alkylating agents conferred by mechanisms operative only in vivo. *Science.* 1990;247:1457–61.
40. Kobayashi H, Man S, Graham CH, Kapitain SJ, Teicher BA, Kerbel RS. Acquired multicellular-mediated resistance to alkylating agents in cancer. *Proc Natl Acad Sci U S A.* 1993;90:3294–8.
41. St Croix B, Florenes VA, Rak JW, Flanagan M, Bhattacharya N, Slingerland JM, Kerbel RS. Impact of the cyclin-dependent kinase inhibitor p27Kip1 on resistance of tumor cells to anticancer agents. *Nat Med.* 1996;2:1204–10.
42. Francia G, Man S, Teicher B, Grasso L, Kerbel RS. Gene expression analysis of tumor spheroids reveals a role for suppressed DNA mismatch repair in multicellular resistance to alkylating agents. *Mol Cell Biol.* 2004;24:6837–49.
43. Olive PL, Durand RE. Drug and radiation resistance in spheroids: cell contact and kinetics. *Cancer Metastasis Rev.* 1994;13:121–38.
44. Frankel A, Buckman R, Kerbel RS. Abrogation of taxol-induced G2-M arrest and apoptosis in human ovarian cancer cells grown as multicellular tumor spheroids. *Cancer Res.* 1997;57:2388–93.
45. Frankel A, Man S, Elliott P, Adams J, Kerbel RS. Lack of multicellular drug resistance observed in human ovarian and prostate carcinoma treated with the proteasome inhibitor PS-341. *Clin Cancer Res.* 2000;6:3719–28.
46. Waleh NS, Brody MD, Knapp MA, Mendonca HL, Lord EM, Koch CJ, Laderoute KR, Sutherland RM. Mapping of the vascular endothelial growth factor-producing hypoxic cells in multicellular tumor spheroids using a hypoxia-specific marker. *Cancer Res.* 1995;55:6222–6.
47. Rak J, Mitsushashi Y, Sheehan C, Krestow JK, Florenes VA, Filmus J, Kerbel RS. Collateral expression of proangiogenic and tumorigenic properties in intestinal epithelial cell variants selected for resistance to anoikis. *Neoplasia.* 1999;1:23–30.

48. Durand RE, Sham E. The lifetime of hypoxic human tumor cells. *Int J Radiat Oncol Biol Phys.* 1998;42:711–5.
49. Lieubeau-Teillet B, Rak J, Jothy S, Iliopoulos O, Kaelin W, Kerbel RS. Von Hippel-Lindau gene-mediated suppression and induction of differentiation in renal cell carcinoma cells grown as multicellular tumor spheroids. *Cancer Res.* 1998;58:4957–62.
50. Shoemaker RH. The NCI60 human tumour cell line anticancer drug screen. *Nat Rev Cancer.* 2006;6:813–23.
51. Pampaloni F, Reynaud EG, Stelzer EHK. The third dimension bridges the gap between cell culture and live tissue. *Nat Rev Mol Cell Biol.* 2007;8:839–45.
52. Mayer B, Klement G, Kaneko M, Man S, Jothy S, Rak J, Kerbel RS. Multicellular gastric cancer spheroids recapitulate growth pattern and differentiation phenotype of human gastric carcinomas. *Gastroenterology.* 2001;121:839–52.
53. Carlson MW, Alt-Holland A, Egles C, Garlick JA. Three-dimensional tissue models of normal and diseased skin. *Curr Protoc Cell Biol.* 2008.; Chapter: Unit 19.9. doi:[10.1002/0471143030.cb1909s41](https://doi.org/10.1002/0471143030.cb1909s41).
54. Kajiwarra Y, Panchabhai S, Levin VA. A new preclinical 3-dimensional agarose colony formation assay. *Technol Cancer Res Treat.* 2008;7:329–34.
55. Friedrich J, Seidel C, Ebner R, Kunz-Schughart LA. Spheroid-based drug screen: considerations and practical approach. *Nat Protoc.* 2009;4:309–24.
56. Tung YC, Hsiao AY, Allen SG, Torisawa Y, Ho M, Takayama S. High throughput 3D spheroid culture and drug testing using 384 hanging drop array. *Analyst.* 2011;136:473–8.
57. Vinci M, Gowan S, Boxall F, Patterson L, Zimmermann M, Court W, Lomas C, Mendiola M, Hardisson D, Eccles SA. Advances in establishment and analysis of three-dimensional tumor spheroid-based functional assays for target validation and drug evaluation. *BMC Biol.* 2012;10:29. doi:[10.1186/1741-7007-10-29](https://doi.org/10.1186/1741-7007-10-29).
58. LaBarbera DV, Reid BG, Yoo BH. The multicellular tumor spheroid model for high-throughput cancer drug discovery. *Expert Opin Drug Discov.* 2012;7:819–30.
59. Chwalek K, Bray LJ, Werner C. Tissue-engineered 3D tumor angiogenesis models: potential technologies for anti-cancer drug discovery. *Adv Drug Deliv Rev.* 2014;79–80:30–9.
60. Song HHG, Park KM, Gerecht S. Hydrogels to model 3D in vitro microenvironment of tumor vascularization. *Adv Drug Deliv Rev.* 2014;79–80:19–29.
61. Hirt C, Papadimitropoulos A, Mele V, Muraro MG, Mengus C, Iezzi G, Terracciano L, Martin I, Spagnoli GC. “In vitro” 3D models of tumor-immune system interaction. *Adv Drug Deliv Rev.* 2014;79–80:145–54.
62. Lee VK, Kim DY, Ngo H, Lee Y, Seo L, Yoo SS, Vincent PA, Dai G. Creating perfused functional vascular channels using 3D bio-printing technology. *Biomaterials.* 2014;35:8092–102.
63. Crystal AS, Shaw AT, Sequist LV, Friboulet L, Niederst MJ, Lockerman EL, Frias RL, Gainor JF, Amzallag A, et al. Patient-derived models of acquired resistance can identify effective drug combinations for cancer. *Science.* 2014;346:1480–6.
64. Orlandi P, Barbara C, Bocci G, Fioravanti A, Di Paolo A, Del Tacca M, Danesi R. Idarubicin and idarubicinol effects on breast cancer multicellular spheroids. *J Chemother.* 2005;17:663–7.
65. Erlanson M, Daniel-Szolgay E, Carlsson J. Relations between the penetration, binding and average concentration of cytostatic drugs in human tumour spheroids. *Cancer Chemother Pharmacol.* 1992;29:343–53.
66. Kang HG, Jenabi JM, Zhang J, Keshelava N, Shimada H, May WA, Ng T, Reynolds CP, Triche TJ, Sorensen PHB. E-Cadherin cell-cell adhesion in ewing tumor cells mediates suppression of anoikis through activation of the ErbB4 tyrosine kinase. *Cancer Res.* 2007;67:3094–105.
67. Dong Y, Tan OL, Loessner D, Stephens C, Walpole C, Boyle GM, Parsons PG, Clements JA. Kallikrein-related peptidase 7 promotes multicellular aggregation via the alpha(5)beta(1) integrin pathway and paclitaxel chemoresistance in serous epithelial ovarian carcinoma. *Cancer Res.* 2010;70:2624–33.
68. Bao BA, Lai CP, Naus CC, Morgan JR. Pannexin 1 drives multicellular aggregate compaction via a signaling cascade that remodels the actin cytoskeleton. *J Biol Chem.* 2012;287:8407–16.



69. Fichtner I, Rolff J, Soong R, Hoffmann J, Hammer S, Sommer A, et al. Establishment of patient derived non-small cell lung cancer xenografts as models for the identification of predictive biomarkers. *Clin Cancer Res.* 2008;14:6456–68.
70. Fichtner I, Slisow W, Gill J, Becker M, Elbe B, Hillebrand T, et al. Anticancer drug response and expression of molecular markers in early-passage xenotransplanted colon carcinomas. *Eur J Cancer.* 2004;40:298–307.
71. Fiebig HH, Dengler WA, Roth T. Human tumor xenografts: predictivity, characterization and discovery of new anticancer agents. In: Fiebig HH, Burger AM, editors. *Relevance of tumor models for anticancer drug development.* Basel: Karger; 1999. p. 29–50.
72. Fiebig HH, Maier A, Burger AM. Clonogenic assay with established human tumour xenografts: correlation of in vitro to in vivo activity as a basis for anticancer drug discovery. *Eur J Cancer.* 2004;40:802–20.
73. Fiebig HH, Schuchhardt C, Henss H, Fiedler L, Lohr GW. Comparison of tumor response in nude mice and in the patients. *Behring Inst Mitt.* 1984;74:343–52.
74. Fiebig HH, Vuaroqueaux V, Korrat A, Foucault F, Beckers T. Predictive gene signatures for bevacizumab and cetuximab as well as cytotoxic agents. *Int J Clin Pharmacol Ther.* 2012;50:70–1.
75. Kunz-Schughart LA, Groebe K, Mueller-Klieser W. Three-dimensional cell culture induces novel proliferative and metabolic alterations associated with oncogenic transformation. *Int J Cancer.* 1996;66:578–86.
76. Wartenberg M, Hoffmann E, Schwindt H, Grunheck F, Petros J, Arnold JR, Hescheler J, Sauer H. Reactive oxygen species-linked regulation of the multidrug resistance transporter P-glycoprotein in Nox-1 overexpressing prostate tumor spheroids. *FEBS Lett.* 2005;579:4541–9.
77. Oloumi A, Lam W, Banath JP, Olive PL. Identification of genes differentially expressed in V79 cells grown as multicell spheroids. *Int J Radiat Biol.* 2002;78:483–92.
78. Shiras A, Bhosale A, Patekar A, Shepal V, Shastry P. Differential expression of CD44(S) and variant isoforms v3, v10 in three-dimensional cultures of mouse melanoma cell lines. *Clin Exp Metastasis.* 2002;19:445–55.
79. Zietarska M, Maugard CM, Filali-Mouhim A, Alam-Fahmy M, Tonin PN, Provencher DM, Mes-Masson AM. Molecular description of a 3D in vitro model for the study of epithelial ovarian cancer (EOC). *Mol Carcinog.* 2007;46:872–85.
80. L'Esperance S, Bachvarova M, Tetu B, Mes-Masson AM, Bachvarov D. Global gene expression analysis of early response to chemotherapy treatment in ovarian cancer spheroids. *BMC Genomics.* 2008;9:99.
81. Zanoni M, Piccinini F, Arienti C, Zamagni A, Santi S, Polico R, Bevilacqua A, Tesei A. 3D tumor spheroid models for in vitro therapeutic screening: a systematic approach to enhance the biological relevance of data obtained. *Sci Rep.* 2016;6:19103. doi:10.1038/srep19103.
82. Kerr DJ, Wheldon TE, Kerr AM, Freshney RI, Kaye SB. The effect of adriamycin and 4'-deoxydoxorubicin on cell survival of human lung tumour cells grown in monolayer and as spheroids. *Br J Cancer.* 1986;54:423–9.
83. Longati P, Jia X, Eimer J, Wagman A, Witt MR, Rehnmark S, Verbeke C, Toftgard R, Lohr M, Heuchel RL. 3D pancreatic carcinoma spheroids induce a matrix-rich chemoresistant phenotype offering a better model for drug testing. *BMC Cancer.* 2013;13:95.
84. Vichai V, Kirtikara K. Sulforhodamine B colorimetric assay for cytotoxicity screening. *Nat Protoc.* 2006;1:1112–8.
85. Liu Y, Peterson DA, Kimura H, Schubert D. Mechanism of cellular 3-(4,5-dimethylthiazol-2-yl)-2,5-diphenyltetrazolium bromide (MTT) reduction. *J Neurochem.* 1997;69:581–93.
86. Riss TL, Moravec RA, Niles AL, et al. Cell viability assays. [2013 May 1 (Updated 2016 Jul 1)]. In: Sittampalam GS, Coussens NP, Nelson H, et al., editors. *Assay guidance manual* [Internet]. Bethesda, MD: Eli Lilly & Company and the National Center for Advancing Translational Sciences; 2004. <http://www.ncbi.nlm.nih.gov/books/NBK144065/>

87. Kijanska M, Kelm J. In vitro 3D spheroids and microtissues: ATP-based cell viability and toxicity assays [2016 Jan 21]. In: Sittampalam GS, Coussens NP, Nelson H, et al., editors. *Assay guidance manual* [Internet]. Bethesda, MD: Eli Lilly & Company and the National Center for Advancing Translational Sciences; 2004. <http://www.ncbi.nlm.nih.gov/books/NBK343426/>
88. McMillin DW, Negri JM, Mitsiades CS. The role of tumour–stromal interactions in modifying drug response: challenges and opportunities. *Nat Rev Drug Discov*. 2013;12:217–28.
89. McMillin DW, Delmore J, Weisberg E, Negri JM, Geer DC, Klippel S, Mitsiades N, Schlossman RL, Munshi NC, Kung AL, Griffin JD, Richardson PG, Anderson KC, Mitsiades C. Tumor cell-specific bioluminescence platform to identify stroma-induced changes to anticancer drug activity. *Nat Med*. 2010;16:483–90.
90. Wenzel C, Riefke B, Grundemann S, Krebs A, Christian S, Prinz F, Osterland M, Golfier S, Rase S, et al. 3D high-content screening for the identification of compounds that target cells in dormant tumor spheroid regions. *Exp Cell Res*. 2014;323:131–43.
91. Howes AL, Chaing GG, Lang ES, Ho CB, Powis G, Vuori K, Abraham RT. The phosphatidylinositol 3-kinase inhibitor, PX-866, is a potent inhibitor of cancer cell motility and growth in three-dimensional cultures. *Mol Cancer Ther*. 2007;6:2505–14.
92. Buchsbaum RJ, Oh SY. Breast cancer-associated fibroblasts: where we are and where we need to go. *Cancers*. 2016;8:19.
93. Fennema E, Rivron N, Rouwkema J, van Blitterswijk C, de Boer J. Spheroid culture as a tool for creating 3D complex tissues. *Trends Biotechnol*. 2013;31:108–15.
94. Breslin S, O'Driscoll L. Three-dimensional cell culture: the missing link in drug discovery. *Drug Discov Today*. 2013;18:240–9.
95. Stock K, Estrada MF, Vidic S, Gjerde K, Rudisch A, Santo VE, Barbier M, Blom S, Arundkar SC, et al. Capturing tumor complexity in vitro: comparative analysis of 2D and 3D tumor models for drug discovery. *Sci Rep*. 2016;6:28951. doi:10.1038/srep28951.
96. Gong X, Lin C, Cheng J, Su J, Zhao H, Liu T, Wen X, Zhao P. Generation of multicellular tumor spheroids with microwell-based agarose scaffolds for drug testing. *PLoS One*. 2015;10:e0130348.
97. Selby MH, Delosh R, Laudeman J, Ogle C, Reinhart R, Silvers T, Lawrence S, Kinders R, Parchment R, Teicher BA, Evans DM. 3D models of the NCI60 cell lines for screening oncology compounds. *SLAS Discov*. 2017;1–11. doi:10.1177/2472555217697434.
98. Tentler JJ, Tan AC, Weekes CD, Jimeno A, Leong S, Pitts TM, Arcaroli JJ, Messersmith WA, Eckhardt SG. Patient-derived tumour xenografts as models for oncology drug development. *Nat Rev Clin Oncol*. 2012;9:338–50.
99. Fiebig HH, Burger AM. Human tumor xenografts and explants. In: Teicher BA, editor. *Tumor models in cancer research*. New York:Humana Press (Springer Science+Business Media); 2002. p. 113–37.
100. Uronis JM, Osada T, McCall S, Yang XY, Mantyh C, Morse MA, Lyerly HK, Clary BM, Hsu DS. Histological and molecular evaluation of patient-derived colorectal cancer explants. *PLoS One*. 2012;7(6):e38422.
101. Jin K, Teng L, Shen Y, He K, Xu Z, Li G. Patient-derived human tumour tissue xenografts in immunodeficient mice: a systematic review. *Clin Transl Oncol*. 2010;12(7):473–80.
102. Hoffman, RM. Orthotopic metastatic mouse models for anticancer drug discovery and evaluation: a bridge to the clinic. *Investigational New Drugs* 1999;17:343–59.
103. Hoffman, RM. Patient-derived orthotopic xenografts: better mimic of metastasis than subcutaneous xenografts. *Nature Reviews Cancer* 2015;15:451–52.
104. Von Hoff DD. Activity of gemcitabine in a human tumor cloning assay as a basis for clinical trials with gemcitabine. San Antonio Drug Development Team. *Invest New Drugs*. 1996;14:265–70.
105. Hanauske AR, Hilsenbeck SG, Von Hoff DD. Human tumor screening. In: Teicher BA, editor. *Anticancer drug development guide*. New York: Humana Press (Springer Science+Business Media); 1997. p. 43–58.

106. Boehnke K, Iversen PW, Schumacher D, Lallena MJ, Haro R, Amat J, Haybaeck J, Liebs S, et al. Assay establishment and validation of a high throughput screening platform for three-dimensional patient derived colon cancer organoid cultures. *J Biomol Screen*. 2016;21(9):931–41.
107. Van de Wetering M, Francies HE, Francis JM, Bounova G, Iorio F, Pronk A, van Houdt W, van Gorp J, Taylor-Weiner A, Kester L, McLaren-Douglas A, et al. Prospective derivation of a living organoid biobank of colorectal cancer patients. *Cell*. 2015;161:933–45.
108. Boj SF, Hwang C, Baker LA, Engle DD, Tuveson DA, Clevers H. Model organoids provide new research opportunities for ductal pancreatic cancer. *Mol Cell Oncol*. 2016;3:e1014757.
109. Gao H, Korn JM, Ferretti S, Monahan JE, Wang Y, Singh M, Zhang C, Schnell C, Yang G, Zhang Y, Balbin OA, Barbe S, Cai H, et al. High-throughput screening patient-derived tumor xenografts to predict clinical trial drug response. *Nat Med*. 2015;21:1318–25.
110. Joyce JA, Pollard JW. Microenvironment regulation of metastasis. *Nat Rev Cancer*. 2009;9:239–52.
111. Quail DF, Joyce JA. Microenvironmental regulation of tumor progression and metastasis. *Nat Med*. 2013;19:1423–37.
112. Bradford JR, Wappett M, Beran G, Logie A, Delpuech O, Brown H, Boros J, Camp NJ, McEwen R, Mazzola AM, et al. Whole transcriptome profiling of patient derived xenograft models as a tool to identify both tumor and stromal specific biomarkers. *Oncotarget*. 2016;7:20773–87.
113. Onion D, Argent R, Reece-Smith AM, Craze ML, Pineda RG, Clarke PA, Ratan HL, Parsons SL, Lobo DN, et al. 3-dimensional patient derived lung cancer assays reveal resistance to standards-of-care promoted by stromal cells but sensitivity to histone deacetylase inhibitors. *Mol Cancer Ther*. 2016;15:753–63.
114. Fong ELS, Wan X, Yang J, Morgado M, Mikos AG, Harrington DA, Navone NM, Farach-Carson MC. A 3D in vitro model of patient derived prostate cancer xenograft for controlled interrogation of in vivo tumor-stromal interactions. *Biomaterials*. 2016;77:164–72.
115. Zhang JH, Chung TD, Oldenburg KR. A simple statistical parameter for use in evaluation and validation of high throughput screening assays. *J Biomol Screen*. 1999;4:67–73.
116. Shroyer NF. Tumor organoids fill the niche. *Cell Stem Cell*. 2016;18:686–8.
117. Fujii M, Shimokawa M, Date S, Takano A, Matano M, Nanki K, Ohta Y, Toshimitsu K, Nakazato Y, et al. A colorectal tumor organoid library demonstrates progressive loss of niche factor requirements during tumorigenesis. *Cell Stem Cell*. 2016;18:827–38.
118. Zhang X, Lewis MT. Establishment of Patient-Derived Xenograft (PDX) models of human breast cancer. *Curr Protoc Mouse Biol*. 2013;3:21–9.
119. Bogner PN, Patnaik SK, Pitoniak R, Kannisto E, Repasky E, Hylander B, Yendamuri S, Ramnath N. Lung cancer xenografting alters microRNA profile but not immunophenotype. *Biochem Biophys Res Commun*. 2009;386:305–10.
120. DeRose YS, Wang G, Lin YC, Bernard PS, Buys SS, Ebbert MT, Factor R, Matsen C, Milash BA, Nelson E, Neumayer L, Randall RL, Stijleman IJ, Welm BE, Welm AL. Tumor grafts derived from women with breast cancer authentically reflect tumor pathology, growth, metastasis and disease outcomes. *Nat Med*. 2011;17:1514–20.
121. Loukopoulos P, Kanetaka K, Takamura M, Shibata T, Sakamoto M, Hirohashi S. Orthotopic transplantation models of pancreatic adenocarcinoma derived from cell lines and primary tumors and displaying varying metastatic activity. *Pancreas*. 2004;29:193–203.
122. McEvoy J, Ulyanov A, Brennan R, Wu G, Pounds S, Zhang J, Dyer MA. Analysis of MDM2 and MDM4 single nucleotide polymorphisms, mRNA splicing and protein expression in retinoblastoma. *PLoS One*. 2012;7:e42739.
123. Morton CL, Houghton PJ. Establishment of human tumor xenografts in immunodeficient mice. *Nat Protoc*. 2007;2:247–50.
124. Reyat F, Guyader C, Decraene C, Lucchesi C, Auger N, Assayag F, De Plater L, Gentien D, Poupon MF, Cottu P, De Cremoux P, Gestraud P, et al. Molecular profiling of patient-derived breast cancer xenografts. *Breast Cancer Res*. 2012;14:R11.

125. Zhao X, Liu Z, Yu L, Zhang Y, Baxter P, Voicu H, Gurusiddappa S, Luan J, Su JM, Leung HC, Li XN. Global gene expression profiling confirms the molecular fidelity of primary tumor-based orthotopic xenograft mouse models of medulloblastoma. *Neuro Oncol.* 2012;14:574–83.
126. Bertotti A, Migliardi C, Galimi F, Sassi F, Torti D, Isella C, et al. A molecularly annotated platform of patient-derived xenografts (“xenopatients”) identifies HER2 as an effective therapeutic target in cetuximab-resistant colorectal cancer. *Cancer Discov.* 2011;1:508–23.
127. Cunningham D, Humblet Y, Siena S, Khayat D, Bleiburg H, Santoro A, et al. Cetuximab monotherapy and cetuximab plus irinotecan in irinotecan-refractory metastatic colorectal cancer. *N Engl J Med.* 2004;351:337–45.
128. Furukawa T, Kubota T, Hoffman RM. Clinical applications of the histoculture drug response assay. *Clin Cancer Res.* 1995;1:305–11.
129. Kubota T, Sasano N, Abe O, Nakao I, Kawamura E, Saito T, Endo M, Kimura K, Demura H, Sasano H, Nagura H, Ogawa N, Hoffman RM. Potential of the histoculture drug response assay to contribute to cancer patient survival. *Clin Cancer Res.* 1995;1:1537–43.
130. Singh B, Li R, Xu L, Poluri A, Patel S, Shaha AR, Pfister D, Sherman E, Hoffman RM, Shah J. Prediction of survival in patients with head and neck cancer using the histoculture drug response assay. *Head Neck.* 2002;24:437–42.
131. Jung PS, Kim DY, Kim MB, Lee SW, Kim JH, Kim YM, Kim YT, Hoffman RM, Nam JH. Progression-free survival is accurately predicted in patients treated with chemotherapy for epithelial ovarian cancer by the histoculture drug response assay in a prospective correlative clinical trial at a single institution. *Anticancer Res.* 2013;33:1029–34.
132. Robbins KT, Connors KM, Storniolo AM, Hanchett C, Hoffman RM. Sponge-gel-supported histoculture drug-response assay for head and neck cancer. Correlations with clinical response to cisplatin. *Arch Otolaryngol Head Neck Surg.* 1994;120:288–92.

---

# Why Patient-Derived Mouse Models Need to Be Orthotopic

# 20

Robert M. Hoffman

Patient-derived xenograft (PDX) mouse models of cancer were first established by Rygaard and Povlsen in 1969 [1] in athymic nude mice, a few years after their discovery of the nude mouse [2]. The first nude mouse PDX models were established by sub-cutaneous tumor transplantation. The PDX models were popular world-wide in the 1970s and 1980s until transgenic mouse models of cancer were developed and PDX models went into a 20-year decline in popularity. PDX models now are reemerging as a potential component of personalized precision cancer therapy. However, most PDX models currently offered to patients still have their tumors subcutaneously transplanted in immunodeficient mice, which rarely metastasize [3]. Discrepancies have been described for decades between the invasive and metastatic behavior of tumors in the patient compared to their benign behavior in the s.c.-transplanted xenografts in immunocompetent mice [1]. In contrast, orthotopic-transplant patient-derived models, termed patient-derived orthotopic xenografts (PDOX), usually metastasize as in the patient. Orthotopic models are important for the patient, since primary and metastatic tumors developed in an orthotopic model can have differential chemosensitivity, which may not be detectable in standard subcutaneous tumor models. In the present chapter, we review first studies of cancer cell lines which have different drug response patterns at the orthotopic and subcutaneous sites in mouse models. We then review a subcutaneous nude mouse model of patient HER-2 expressing cervical carcinoma that was not sensitive to entinostat (a benzamide histone deacetylase inhibitor). In the PDOX model of this cervical carcinoma, entinostat was not active against the primary tumor. However, in the PDOX model, entinostat significantly reduced the metastatic tumor burden, compared to the primary tumor. Thus, only the PDOX model could be used to discover

---

R.M. Hoffman

AntiCancer, Inc., 7917 Ostrow Street, San Diego, CA 92111, USA

Department of Surgery, University of California, San Diego, CA, USA

e-mail: [all@anticancer.com](mailto:all@anticancer.com)

© Springer International Publishing AG 2017

R.M. Hoffman (ed.), *Patient-Derived Mouse Models of Cancer*,

Molecular and Translational Medicine, DOI 10.1007/978-3-319-57424-0\_20

277

the anti-metastatic activity of entinostat for this patient. We emphasize the importance of using mouse models that can accurately recapitulate metastatic cancer for precisely individualizing cancer therapy [4].

Wang et al. [5] in 1982 were among the first to implant human tumors orthotopically (literally “correct place”) in nude mice, using colon-cancer cell suspensions, rather than “heterotopically” (literally “different place,” such as s.c.) [5]. Metastases as well as local tumor growth occurred in the orthotopic model, a very important advance (please see Chap. 4 in the present volume).

Fidler’s group determined the response of murine CT-26 colon carcinoma cells to chemotherapeutic agents. CT-26 cells were injected either i.v. to produce experimental lung metastasis, subcutaneously, or into the cecal wall and into the spleen to produce spleen and liver metastasis. Doxorubicin (DOX), 5-fluorouracil (5-FU), and saline (control) were tested. Colon cancer cells growing subcutaneously were most sensitive to DOX. Colon cancer cells growing in the spleen and cecum were most sensitive to 5-FU and less sensitive to DOX. Colon cancer cells in the liver were very resistant to both drugs. Experimental lung metastases were sensitive to 5-FU and resistant to DOX. Drug distribution was similar at all sites. The authors stated that the organ environment modulates chemosensitivity of the cancer cells and that the organ environment has greatly affected the response of cancer cells to chemotherapy [6] (please see Chap. 5 in the present volume).

Our laboratory pioneered the PDOX nude mouse model with the technique of surgical orthotopic implantation (SOI) of intact colon cancer tissue [7, 8]. A greater extent of metastasis was observed in orthotopic models with implanted intact tumor tissue compared with orthotopically implanted cell suspensions of the same tumor [9]. This perhaps is due to the intact histology and cancer cell-stroma interaction of the orthotopically-implanted tumor tissue.

We have established an orthotopic metastatic model of the human gastric cancer cell line, SC-1-NU, by SOI in nude mice. Liver metastasis occurred in this model. We tested the efficacy of OK-432, a bacterial product, 5-FU, and mitomycin C (MMC). Low doses of 5-FU and MMC resulted in a significant reduction of primary stomach tumor growth. However, liver metastases were not reduced. High doses of 5-FU and MMC, combined with OK-432 reduced liver metastases, with synergistic reduction of primary stomach tumor growth. NK-cell activity was possibly stimulated by OK-432. This metastatic model of human stomach cancer demonstrated again that primary and metastatic tumors may have different chemosensitivities [10].

Our laboratory established, beginning in the early 1990s PDOX models from patients’ tumors including pancreatic [11–14], breast [15], ovarian [16], lung [17], cervical [18], colon [7, 8, 19], stomach [20], sarcoma [21–28], mesothelioma [29], and melanoma [30–34].

We previously established a PDOX model of HER-2-positive cervical cancer. Metastasis in nude mice included peritoneal dissemination, liver metastasis, lung metastasis, as well as lymph node metastasis, reflecting the metastatic pattern in the donor patient. Primary tumors and metastases in the nude mice had histological

structures similar to those in the original tumor and were stained by a HER2-specific antibody in the same pattern as was the patient's original cancer [18].

We observed that the benzamide histone deacetylase inhibitor, entinostat, was not active in a subcutaneous nude mouse model of the HER-2 expressing cervical carcinoma nor did entinostat prevent primary tumor growth in the PDOX model of the same tumor. In contrast, in the PDOX model, entinostat significantly reduced the metastatic tumor burden compared to the control [4]:

Entinostat monotherapy was least effective compared to carboplatin, trastuzumab, and lapatinib in the subcutaneous nude mouse model of this patient cervical cancer [4].

In the PDOX model of the cervical carcinoma, all regimens tested, except entinostat alone, had significant efficacy on the primary tumors compared to the vehicle control groups, including carboplatin, trastuzumab/lapatinib, and trastuzumab/lapatinib/entinostat [4]. However, entinostat alone had efficacy against metastasis in the PDOX model of cervical carcinoma. The other drugs tested also had significant efficacy on metastasis. No metastasis was detected in the mice treated with trastuzumab/lapatinib/entinostat group. All regimens caused body weight loss, with carboplatin the most toxic [4] (Fig. 20.1).

These results are another important example of how the tumor site can have a major effect on drug sensitivity. In particular, primary and metastatic tumors may have dramatically opposite patterns of drug sensitivity. Orthotopic, rather than sub-cutaneous mouse models of cancer, since they can metastasize, are necessary to determine accurate drug response, especially when used for designing patient treatment.

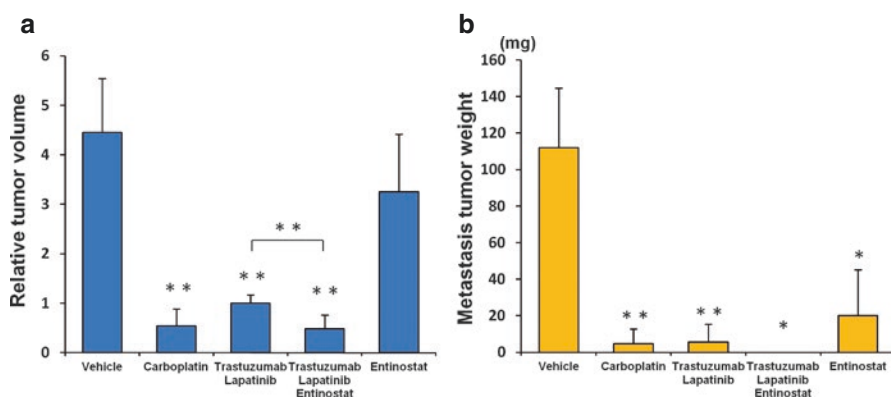


**Fig. 20.1** Drug efficacy testing in the PDOX model of HER-2-expressing cervical carcinoma. PDOX nude mice were treated with saline, carboplatin, trastuzumab + lapatinib, trastuzumab + lapatinib + entinostat, or entinostat alone. (a) Bar graphs of the primary tumor volume in each group. (b) Bar graphs of the metastatic tumor weight in each group ( $n = 5$  for each treatment arm). \* $p < 0.05$ ; \*\* $p < 0.01$  [4]

## Materials and Methods

### Tumor Implantation

For the cervical cancer model, subcutaneous tumors grown in nude mice, were harvested and divided into small fragments for orthotopic transplantation. A small 6–10 mm midline incision was made on the lower abdomen of the nude mouse through the skin and peritoneum. The uterus was exposed through this incision, and a single 3 mm<sup>3</sup> tumor fragment was sutured to the cervix of the uterus using 8-0 nylon surgical sutures (Ethilon; Ethicon Inc., NJ, USA). On completion of tumor implantation, the uterus was returned to the abdomen, and the incision was closed in one layer using 6-0 nylon surgical sutures (Ethilon) [18] (see Chap. 10 in the present volume).

For the CT26 model, Wilmanns et al. [6] produced s.c. tumors by injecting ( $2.5 \times 10^4$ ) CT-26 cancer cells in 0.05 ml HBSS with a 27-G needle into the lateral flank. Wilmanns et al. [6] produced spleen tumors and experimental liver metastasis in anesthetized mice by making a small incision in the body wall to examine the spleen. CT-26 cancer cells ( $2 \times 10^4$ ) were injected with a 27-G needle into the spleen parenchyma. Wilmanns et al. [6] produced cecal wall tumors after methoxyflurane anesthesia by making a small incision to exteriorize the cecum and injecting CT-26 cells between the submucosa and the subserosa. Wilmanns et al. [6] produced experimental lung metastasis by injecting in the tail vein  $2 \times 10^4$  CT-26 cells in 0.2 ml HBSS [6].

Furukawa et al. [10] orthotopically transplanted gastric tumor-tissue pieces of approximately  $3 \times 3 \times 3$  mm in nude mice. Mice were anesthetized with a 2.5% solution of a mixture of 2,2,2-tribromoethanol (Sigma-Aldrich) and *tert*-amyl alcohol (1:1). An incision through the left upper abdominal pararectal line and peritoneum was made. The stomach was exposed and a part of the serosal membrane on the middle of the greater curvature of the glandular stomach (2 mm) was mechanically injured with scissors. Tumor pieces were fixed on injured sites of the serosal surface with 6-0 Dexon transmural sutures [10].

---

## Treatment

### Treatment Protocol for the Cervical Cancer Subcutaneous and PDOX Models

Six weeks after implantation, the mice in the PDX and PDOX models were randomized and treated in the following groups of  $n = 5$ : (1) saline control, (ip, weekly, 5 weeks); (2) carboplatin (Selleck Chemicals, Houston, TX, USA, 30 mg/kg, ip, weekly, 5 weeks); (3) trastuzumab (Genentech, Inc., South San Francisco, CA, USA, 20 mg/kg, ip, weekly, 5 weeks) + lapatinib (Selleck Chemicals, 100 mg/kg, orally, daily, 5 weeks); (4) trastuzumab (20 mg/kg, ip, weekly, 5 weeks) + lapatinib



(100 mg/kg, orally, daily, 5 weeks) + entinostat (Selleck Chemicals, 5 mg/kg, orally, daily, 5 weeks); and (5) entinostat (5 mg/kg, orally, daily, 5 weeks) [4].

## Treatment Protocol for the Orthotopic Colon Cancer Model

Wilmanns et al. [6] administered doxorubicin (DOX) in the lateral tail vein on days 7 and 16 after tumor cell injection at a dose of 10 mg/kg body weight. Wilmanns et al. [6] dissolved 5-FU in PBS to a concentration of 2 mg/ml which was injected at a dose of 20 mg/kg body weight in the lateral tail vein. Wilmanns et al. [6] administered 5-FU in five daily injections followed by weekly injection.

## Treatment Protocol for the Orthotopic Gastric-Cancer Model

Furukawa et al. [10] dissolved 5-FU and MCC in a physiological saline solution and administered the drugs i.p. as a bolus. 5-FU was administered at 180, 90, and 45 mg/kg and MMC was administered at 6, 3, and 1.5 mg/kg which were equivalent to maximum tolerated doses (MTDs), half MTDs, and quarter MTDs in nude mice. Furukawa et al. [10] administered OK-432 i.p. everyday for 5 days from day 5 to day 9 at a dose of 1 Klinische Einheit (KE) per mouse.

### Conclusions

The early Fidler et al. [6] and Furukawa et al. [10] papers showed that primary and metastatic tumors can have differential chemosensitivity. In the cervical cancer PDOX model, entinostat monotherapy significantly inhibited the metastasis of HER-2-positive cervical cancer even though there was no efficacy of this agent on the primary tumor or on the subcutaneous model. The efficacy of entinostat would not have been detected in a subcutaneous PDX model of this tumor [4]. These results emphasize that patient mouse models of cancer should be orthotopic.

## References

1. Rygaard J, Povlsen CO. Heterotransplantation of a human malignant tumour to "nude" mice. *Acta Pathol Microbiol Scand.* 1969;77:758–60.
2. Pantelouris EM. Absence of thymus in a mouse mutant. *Nature.* 1968;217:370–1.
3. Hoffman RM. Patient-derived orthotopic xenografts: better mimic of metastasis than subcutaneous xenografts. *Nat Rev Cancer.* 2015;15:451–2.
4. Hiroshima Y, Maawy A, Zhang Y, Zhang N, Murakami T, Chishima T, Tanaka K, Ichikawa Y, Bouvet M, Endo I, Hoffman RM. Patient-derived mouse models of cancer need to be orthotopic in order to evaluate targeted anti-metastatic therapy. *Oncotarget.* 2016;7:71696–702.
5. Wang WR, Sordat B, Piguat D, Sordat M. Human colon tumors in nude mice: implantation site expression of the invasiveness phenotype. In: *Immune-deficient animals—4th international workshop on immune-deficient animals in experimental research*, Chexbres, 1982. Basel: Karger, 1984; p. 239–44.

6. Wilmanns C, Fan D, O'Brian CA, Bucana CD, Fidler IJ. Orthotopic and ectopic organ environments differentially influence the sensitivity of murine colon carcinoma cells to doxorubicin and 5-fluorouracil. *Int J Cancer*. 1992;52:98–104.
7. Fu XY, Besterman JM, Monosov A, Hoffman RM. Models of human metastatic colon cancer in nude mice orthotopically constructed by using histologically intact patient specimens. *Proc Natl Acad Sci U S A*. 1991;88:9345–9.
8. Metildi CA, Kaushal S, Luiken GA, Talamini MA, Hoffman RM, Bouvet M. Fluorescently-labeled chimeric anti-CEA antibody improves detection and resection of human colon cancer in a patient-derived orthotopic xenograft (PDOX) nude mouse model. *J Surg Oncol*. 2014;109:451–8.
9. Furukawa T, Fu X, Kubota T, Watanabe M, Kitajima M, Hoffman RM. Nude mouse metastatic models of human stomach cancer constructed using orthotopic implantation of histologically intact tissue. *Cancer Res*. 1993;53:1204–8.
10. Furukawa T, Kubota T, Watanabe M, Kuo T-H, Kitajima M, Hoffman RM. Differential chemosensitivity of local and metastatic human gastric cancer after orthotopic transplantation of histologically intact tumor tissue in nude mice. *Int J Cancer*. 1993;54:397–401.
11. Hiroshima Y, Zhang Y, Murakami T, Maawy AA, Miwa S, Yamamoto M, Yano S, Sato S, Momiyama M, Mori R, Matsuyama R, Chishima T, Tanaka K, et al. Efficacy of tumor-targeting *Salmonella typhimurium* A1-R in combination with anti-angiogenesis therapy on a pancreatic cancer patient-derived orthotopic xenograft (PDOX) and cell line mouse models. *Oncotarget*. 2014;5:12346–57.
12. Fu X, Guadagni F, Hoffman RM. A metastatic nude-mouse model of human pancreatic cancer constructed orthotopically with histologically intact patient specimens. *Proc Natl Acad Sci U S A*. 1992;89:5645–9.
13. Hiroshima Y, Maawy A, Zhang Y, Murakami T, Momiyama M, Mori R, Matsuyama R, Katz MH, Fleming JB, Chishima T, Tanaka K, Ichikawa Y, Endo I, et al. Metastatic recurrence in a pancreatic cancer patient derived orthotopic xenograft (PDOX) nude mouse model is inhibited by neoadjuvant chemotherapy in combination with fluorescence-guided surgery with an anti-CA 19–9-conjugated fluorophore. *PLoS One*. 2014;9:e114310.
14. Hiroshima Y, Maawy AA, Katz MH, Fleming JB, Bouvet M, Endo I, Hoffman RM. Selective efficacy of zoledronic acid on metastasis in a patient-derived orthotopic xenograft (PDOX) nude-mouse model of human pancreatic cancer. *J Surg Oncol*. 2015;111:311–5.
15. Fu X, Le P, Hoffman RM. A metastatic-orthotopic transplant nude-mouse model of human patient breast cancer. *Anticancer Res*. 1993;13:901–4.
16. Fu X, Hoffman RM. Human ovarian carcinoma metastatic models constructed in nude mice by orthotopic transplantation of histologically intact patient specimens. *Anticancer Res*. 1993;13:283–6.
17. Wang X, Fu X, Hoffman RM. A new patient-like metastatic model of human lung cancer constructed orthotopically with intact tissue via thoracotomy in immunodeficient mice. *Int J Cancer*. 1992;51:992–5.
18. Hiroshima Y, Zhang Y, Zhang M, Maawy A, Mii S, Yamamoto M, Uehara F, Miwa S, Yano S, Murakami T, Momiyama M, Chishima T, Tanaka K, et al. Establishment of a patient-derived orthotopic xenograft (PDOX) model of HER-2-positive cervical cancer expressing the clinical metastatic pattern. *PLoS One*. 2015;10:e0117417.
19. Hiroshima Y, Maawy A, Metildi CA, Zhang Y, Uehara F, Miwa S, Yano S, Sato S, Murakami T, Momiyama M, Chishima T, Tanaka K, Bouvet M, et al. Successful fluorescence-guided surgery on human colon cancer patient-derived orthotopic xenograft mouse models using a fluorophore-conjugated anti-CEA antibody and a portable imaging system. *J Laparoendosc Adv Surg Tech A*. 2014;24:241–7.
20. Furukawa T, Kubota T, Watanabe M, Kitajima M, Fu X, Hoffman RM. Orthotopic transplantation of histologically intact clinical specimens of stomach cancer to nude mice: correlation of metastatic sites in mouse and individual patient donors. *Int J Cancer*. 1993;53:608–12.

21. Murakami T, DeLong J, Eilber FC, Zhao M, Zhang Y, Zhang N, Singh A, Russell T, Deng S, Reynoso J, Quan C, Hiroshima Y, Matsuyama R, et al. Tumor-targeting *Salmonella typhimurium* A1-R in combination with doxorubicin eradicate soft tissue sarcoma in a patient-derived orthotopic xenograft PDOX model. *Oncotarget*. 2016;7:12783–90.
22. Hiroshima Y, Zhao M, Zhang Y, Zhang N, Maawy A, Murakami T, Mii S, Uehara F, Yamamoto M, Miwa S, Yano S, Momiyama M, Mori R, et al. Tumor-targeting *Salmonella typhimurium* A1-R arrests a chemo-resistant patient soft-tissue sarcoma in nude mice. *PLoS One*. 2015;10:e0134324.
23. Kiyuna T, Murakami T, Tome Y, Kawaguchi K, Igarashi K, Zhang Y, Zhao M, Li Y, Bouvet M, Kanaya F, Singh A, Dry S, Eilber FC, et al. High efficacy of tumor-targeting *Salmonella typhimurium* A1-R on a doxorubicin- and dactolisib-resistant follicular dendritic-cell sarcoma in a patient-derived orthotopic xenograft PDOX nude mouse model. *Oncotarget*. 2016;7:33046–54.
24. Murakami T, Singh AS, Kiyuna T, Dry SM, Li Y, James AW, Igarashi K, Kawaguchi K, DeLong JC, Zhang Y, Hiroshima Y, Russell T, Eckardt MA, et al. Effective molecular targeting of CDK4/6 and IGF-1R in a rare FUS-ERG fusion CDKN2A-deletion doxorubicin-resistant Ewing's sarcoma in a patient-derived orthotopic xenograft (PDOX) nude-mouse model. *Oncotarget*. 2016;7:47556–64.
25. Hiroshima Y, Zhang Y, Zhang N, Uehara F, Maawy A, Murakami T, Mii S, Yamamoto M, Miwa S, Yano S, Momiyama M, Mori R, Matsuyama R, et al. Patient-derived orthotopic xenograft (PDOX) nude mouse model of soft-tissue sarcoma more closely mimics the patient behavior in contrast to the subcutaneous ectopic model. *Anticancer Res*. 2015;35:697–701.
26. Kiyuna T, Murakami T, Tome Y, Igarashi K, Kawaguchi K, Russell T, Eckhardt MA, Crompton J, Singh A, Bernthal N, Bukata S, Federman N, Kanaya F, Eilber FC, Hoffman RM. Labeling the stroma of a patient derived orthotopic xenograft (PDOX) mouse models of undifferentiated pleomorphic soft tissue sarcoma with red fluorescent protein for rapid noninvasive drug screening. *J Cell Biochem*. 2017;118:361–5.
27. Igarashi K, Kawaguchi K, Kiyuna T, Murakami T, Miwa S, Nelson SD, Dry SM, Li Y, Singh A, Kimura H, Hayashi K, Yamamoto N, Tsuchiya H, Eilber FC, Hoffman RM. Temozolomide combined with irinotecan caused regression in an adult pleomorphic rhabdomyosarcoma patient derived orthotopic xenograft (PDOX) nude mouse model. *Oncotarget* in press.
28. Murakami T, Kiyuna T, Kawaguchi K, Igarashi K, Singh AS, Hiroshima Y, Zhang Y, Zhao M, Miyake K, Nelson SD, Dry SM, Li Y, DeLong JC, Lwin TM, Chishima T, Tanaka K, Bouvet M, Endo I, Eilber FC, Hoffman RM. The irony of highly effective bacterial therapy of a patient derived mouse model of Ewing's sarcoma, which was blocked by Ewing himself 80 years ago. *Cell Cycle*, in press.
29. Astoul P, Wang X, Colt HG, Boutin C, Hoffman RM. A patient-like human malignant pleural mesothelioma nude-mouse model. *Oncol Rep*. 1996;3:483–7.
30. Yamamoto M, Zhao M, Hiroshima Y, Zhang Y, Shurell E, Eilber FC, Bouvet M, Noda M, Hoffman RM. Efficacy of tumor-targeting *Salmonella typhimurium* A1-R on a melanoma patient-derived orthotopic xenograft (PDOX) nude-mouse model. *PLoS One*. 2016;11:e0160882.
31. Kawaguchi K, Murakami T, Chmielowski B, Igarashi K, Kiyuna T, Unno M, Nelson SD, Russell TA, Dry SM, Li Y, Eilber FC, Hoffman RM. Vemurafenib-resistant BRAF-V600E mutated melanoma is regressed by MEK targeting drug trametinib, but not cobimetinib in a patient-derived orthotopic xenograft (PDOX) mouse model. *Oncotarget*. 2016;7:71737–43.
32. Kawaguchi K, Igarashi K, Murakami T, Chmielowski B, Kiyuna T, Zhao M, Zhang Y, Singh A, Unno M, Nelson SD, Russell T, Dry SM, Li Y, et al. Tumor-targeting *Salmonella typhimurium* A1-R combined with Temozolomide regresses malignant melanoma with a BRAF-V600 mutation in a patient-derived orthotopic xenograft (PDOX) model. *Oncotarget*. 2016;7:85929–36.
33. Kawaguchi K, Igarashi K, Chmielowski B, Murakami T, Kiyuna T, Zhao M, Zhang Y, Nelson SD, Russell TA, Dry SM, Singh AS, Li Y, Unno M, Eilber FC, Hoffman RM. *Salmonella*

typhimurium A1-R targeting of a chemotherapy resistant BRAF-V600E melanoma in a patient-derived orthotopic xenograft (PDOX) model is enhanced in combination with either vemurafenib-temozolomide. *Cell Cycle*, in press.

34. Kawaguchi K, Igarashi K, Murakami T, Zhao M, Zhang Y, Chmielowski B, Kiyuna T, Nelson SD, Russell TA, Dry SM, Li Y, Unno M, Eilber FC, Hoffman RM. Tumor-targeting Salmonella typhimurium A1-R sensitizes melanoma with a BRAF-V600E mutation to vemurafenib in a patient-derived orthotopic xenograft (PDOX) nude mouse model. *J Cell Biochem.*, Epub ahead of print. DOI: 10.1002/jcb.25886.

Robert M. Hoffman

---

## Use of Patient-Derived Mouse Models for Individualized Precision Therapy

Metastatic cancer is almost as deadly as it was a half century ago. Although, there are many more FDA-approved cancer drugs than before, and the medical oncologist is presented with a much wider choice of therapy for each patient.

Most teaching hospitals and other large hospitals have a “tumor board” meeting of cancer doctors of the particular hospital, as well as guest doctors. Usually the meetings are weekly and the status of many different cancer patients are presented with advanced disease, along with various radiological scans and other data. A pathologist may present the tumor’s histological information. The surgeon may present findings at surgery, and the medical oncologist may present the prior treatment if any and an opinion of the current treatment plan. At this point, doctors in the audience also present their ideas for treatment, as well as ask questions among the presenting doctors. The treatment plans offered by the medical oncologist in charge and doctors in the audience may vary greatly. Watching such a spectacle is frustrating and disheartening and evokes great sympathy for the poor patient. After these brief discussions, the next patient is brought up and the above cycle is repeated.

The patient-derived mouse models described in the present volume offer a solution to this seemingly intractable problem of effective treatment of metastatic cancer. Various attempts have been made to use the patient-derived models to design individual therapy. However, most models currently offered to patients

---

R.M. Hoffman

AntiCancer, Inc., 7917 Ostrow Street, San Diego, CA 92111, USA

Department of Surgery, University of California, San Diego, CA, USA

e-mail: [all@anticancer.com](mailto:all@anticancer.com)

have their tumors sub-cutaneously transplanted in immuno-deficient mice, which rarely metastasize. In contrast, orthotopic-transplant patient-derived models, termed patient-derived orthotopic xenografts (PDOX), usually metastasize as in the patient [1]. In addition, the drug response pattern of the tumor can vary significantly in the same tumor depending on whether the tumor is growing sub-cutaneously or orthotopically. In addition, the same mouse's primary and orthotopic tumors can have a different drug response pattern (see Chap. 20 in the present volume).

There are important issues for patient-derived mouse models to be useful for individualized therapy:

Gastrointestinal tumors, sarcomas, melanoma, glioblastomas, and some lung cancer types have a greater chance for establishment in mouse models. Higher-stage and higher-grade tumors also establish more readily in mouse models. X-ray treatment decreases the tumor's chance for establishment in mice. Drugs should be tested at doses that could be achieved in the patient (Please see Chap. 9 in the present volume).

In the early days of patient-derived models, chemotherapy response on human patient cancer xenografts in nude mice was directly compared with clinical response to the same chemotherapy in the patients. Single-drug treatment of an investigational agent resulted in inhibition of tumor growth in the xenograft model and to the donor patient. Chemotherapy in three other xenografts produced no significant response, which corresponds to the clinical response to other donor patients [2].

Fiebig (Chap. 3 in the present volume) and Houghton (Chap. 11 in the present volume) also found good correlations between patient mouse models and the patient. The drug response of patient breast cancer was concordant with that of the patient's in five of seven analyzable cases. The panel of breast cancer xenografts included mostly triple-negative but also ER positive and ERBB2 positive [3].

A correlation between the patient-derived mouse models and clinical outcome was observed in 13 of 16 (81%) of sarcoma patients [4].

Non-small-cell lung carcinoma (NSCLC) patient tumors were implanted into nonobese diabetic severe combined immune-deficient (NOD-SCID) mice and treated with epidermal growth factor receptor (EGFR) tyrosine kinase inhibitors (TKIs). The patient models had variable sensitivity to first- and second-generation EGFR TKIs and the monoclonal antibody cetuximab. All EGFR-mutant NSCLC patient models studied recapitulated their corresponding patient tumor phenotype and clinical course, including response pattern to EGFR TKIs [5].

A tumor from a patient with advanced, gemcitabine-resistant, pancreatic cancer was established in immunodeficient mice. Mitomycin C, identified on the basis of its efficacy in the patient's xenograft models, resulted in a more than 3-year tumor response [6].

These studies, although they have taken place over approximately 40 years, are just a beginning of the use of patient-derived xenografts for individualized precision cancer therapy. Perhaps the biggest obstacle for their further development and use to improve treatment outcome is the attitude of the treating physician.

## “Humanized” Patient-Derived Mouse Models

Current “humanized” mouse models are based on severe combined immunodeficient (SCID) mice with mutations in the interleukin-2 receptor common  $\gamma$ -chain locus. This mutation leads to highly deficient T, B, and NK cells in the mice. These engineered mouse strains support the engraftment of functional human immune cells [7].

A nonobese diabetic SCID (NOD/SCID) mouse line with a complete null mutation of the interleukin-2 receptor immune  $\gamma$  chain (NOD/SCID/interleukin 2 receptor [IL2r]  $\gamma$ (null) (NSG mice) enabled development of functional human hemato-lymphopoiesis. Purified human CD34<sup>+</sup> or hCD34<sup>+</sup> hCD38<sup>-</sup> cord blood cells were transplanted into NOD/SCID/IL2r  $\gamma$ (null) newborn mice. Functional hematopoietic cells were reconstituted in 70% of the animals [8]. NOD/SCID mice with a mutation in the IL-2 receptor that lack the intra-cytoplasmic chain were also developed (NOG mice) [7].

NSG and NOG mice that can be transplanted with fetal thymus/liver fragments in the subrenal capsule have been shown to be optimal for generating human immune systems, but these mice can develop graft-versus-host disease [9].

NOD/SCID IL-2R $\gamma$  null mice were transplanted with human cord blood CD34<sup>+</sup> cells, which developed human T cells in their thymus which migrated into peripheral lymphoid organs [10]. NSG mice had a greater rate of engraftment of human immune cells than NOG mice [7].

NSG mice also had a greater engraftment rate of human primary colon tumor fragments than NOD [11].

These “humanized” mouse models can be used to evaluate immune checkpoint blockers such as anti-PD-1 and PD-L1 antibodies for cancer treatment [12].

Ovarian cancer biopsy specimens were transplanted intraperitoneally (i.p.) into NSG mice. Tumors grew in the omentum, ovaries, liver, spleen, uterus, and pancreas, with subsequent development of ascites, spontaneous metastasis to the lung. Increasing serum and ascites levels of CA125 were observed. Cancer-associated human fibroblasts and lymphocytes were retained and remained functional and responsive to cytokines [13].

---

## Circulating Tumor Cells (CTCs) for Production of Patient Xenografts

Circulating tumor cell (CTC)-derived xenografts (CDX) were established from melanoma patients [14].

Primary human luminal breast cancer CTCs were used to establish patient xenografts which give rise to bone, lung, and liver metastases in mice [15].

CTCs from patients with small-cell lung carcinoma (SCLC) were tumorigenic in immunocompromised mice. The CTC-derived xenografts reproduced the donor patient’s response to platinum and etoposide chemotherapy [16].

---

## Establishment of Cell Lines from Patient-Derived Xenografts

Human cancer cell lines were successfully derived from patient-derived xenografts [17].

The intra-tumor clonal mutations in the original breast cancers were mostly preserved upon serial passaging in xenografts and in short-term cultures derived from the xenografts [18].

---

## Use of Patient Models to Develop New Treatment Strategies

Continuous vemurafenib administration of a BRAF V600E-mutant melanoma xenograft resulted in drug-dependent continued proliferation, and cessation of drug administration led to regression of the drug-resistant tumors. Thus drug-resistant cells may also develop drug dependency and that altered dosing is needed to prevent the emergence of drug resistance [19]. PDOX models of BRAF V600E-mutant melanoma have led to identification of unexpected effective therapy [20–23] (see also Chap. 18).

---

## Use of Patient-Derived Models to Study Tumor Heterogeneity

DNA copy number profiling, sequencing, and lentiviral lineage tracking and the repopulation dynamics of 150 single lentivirus-marked lineages from 10 human colorectal cancers were followed through serial xenograft passages in mice. Individual clones were thereby distinguished and shown to remain stable upon serial transplantation. However, chemotherapy tolerance of lentivirally-marked lineages were variable within each clone. Chemotherapy could promote the dominance of previously minor or dormant lineages [24].

---

## Single-Mouse Studies for Drug Evaluation

Approximately 1000 patient-derived tumor xenograft models were established. Compound screens used a single mouse for 62 treatments for six tumor types [25]. The single mouse human tumor response accurately predicted the group median response in 1604 comparisons (75.16%) [26].

The EurOPDX has undertaken an international initiative devoted to PDX-based research which may lead to many new applications for precision medicine [27].

---

## References

1. Hoffman RM. Patient-derived orthotopic xenografts: better mimic of metastasis than subcutaneous xenografts. *Nature Reviews Cancer*. 2015;15:451–2.
2. Fujita M, Hayata S, Taguchi T. Relationship of chemotherapy on human cancer xenografts in nude mice to clinical response in donor patient. *J Surg Oncol*. 1980;15:211–9.



3. Marangoni E, Vincent-Salomon A, Auger N, Degeorges A, Assayag F, de Cremoux P, de Plater L, Guyader C, De Pinieux G, Judde JG, Rebutti M, Tran-Perennou C, Sastre-Garau X, Sigal-Zafrani B, Delattre O, Diéras V, Poupon MF. A new model of patient tumor-derived breast cancer xenografts for preclinical assays. *Clin Cancer Res.* 2007;13:3989–98.
4. Stebbing J, Paz K, Schwartz GK, Wexler LH, Maki R, Pollock RE, Morris R, Cohen R, Shankar A, Blackman G, Harding V, Vasquez D, Krell J, Zacharoulis S, Ciznadija D, Katz A, Sidransky D. Patient-derived xenografts for individualized care in advanced sarcoma. *Cancer.* 2014;120:2006–15.
5. Stewart EL, Mascaux C, Pham NA, Sakashita S, Sykes J, Kim L, Yanagawa N, Allo G, Ishizawa K, Wang D, Zhu CQ, Li M, Ng C, Liu N, Pintilie M, Martin P, John T, Jurisica I, Leigh NB, Neel BG, Waddell TK, Shepherd FA, Liu G, Tsao MS. Clinical utility of patient-derived xenografts to determine biomarkers of prognosis and map resistance pathways in EGFR-mutant lung adenocarcinoma. *J Clin Oncol.* 2015;33:2472–80.
6. Villarroel MC, Rajeshkumar NV, Garrido-Laguna I, De Jesus-Acosta A, Jones S, Maitra A, Hruban RH, Eshleman JR, Klein A, Laheru D, Donehower R, Hidalgo M. Personalizing cancer treatment in the age of global genomic analyses: PALB2 gene mutations and the response to DNA damaging agents in pancreatic cancer. *Mol Cancer Ther.* 2011;10:3–8.
7. Shultz LD, Brehm MA, Garcia-Martinez JV, Greiner DL. Humanized mice for immune system investigation: progress, promise and challenges. *Nat Rev Immunol.* 2012;12:786–98.
8. Ishikawa F, Yasukawa M, Lyons B, Yoshida S, Miyamoto T, Yoshimoto G, Watanabe T, Akashi K, Shultz LD, Harada M. Development of functional human blood and immune systems in NOD/SCID/IL2 receptor  $\gamma$  chain(null) mice. *Blood.* 2005;106:1565–73.
9. Covassin L, Jangalwe S, Jovet N, Laning J, Burzenski L, Shultz LD, Brehm MA. Human immune system development and survival of nonobese diabetic (NOD)-scid IL2r $\gamma$ (null) (NSG) mice engrafted with human thymus and autologous haematopoietic stem cells. *Clin Exp Immunol.* 2013;174:372–88.
10. Yahata T, Ando K, Nakamura Y, Ueyama Y, Shimamura K, Tamaoki N, Kato S, Hotta T. Functional human T lymphocyte development from cord blood CD34+ cells in nonobese diabetic/Shi-scid, IL-2 receptor gamma null mice. *J Immunol.* 2002;169:204–9.
11. Maykel J, Liu JH, Li H, Shultz LD, Greiner DL, Houghton J. NOD-scidIl2rg (tm1Wjl) and NOD-Rag1 (null) Il2rg (tm1Wjl): a model for stromal cell-tumor cell interaction for human colon cancer. *Dig Dis Sci.* 2014;59:1169–79.
12. Sanmamed MF, Chester C, Melero I, Kohrt H. Defining the optimal murine models to investigate immune checkpoint blockers and their combination with other immunotherapies. *Ann Oncol.* 2016;27:1190–8.
13. Bankert RB, Balu-Iyer SV, Odunsi K, Shultz LD, Kelleher Jr RJ, Barnas JL, Simpson-Abelson M, Parsons R, Yokota SJ. Humanized mouse model of ovarian cancer recapitulates patient solid tumor progression, ascites formation, and metastasis. *PLoS One.* 2011;6:e24420.
14. Girotti MR, Gremel G, Lee R, Galvani E, Rothwell D, Viros A, Mandal AK, Lim KH, Saturno G, Furney SJ, Baenke F, Pedersen M, Rogan J, Swan J, Smith M, Fusi A, Oudit D, Dhomen N, Brady G, Lorigan P, Dive C, Marais R. Application of sequencing, liquid biopsies, and patient-derived xenografts for personalized medicine in melanoma. *Cancer Discov.* 2016;6:286–99.
15. Baccelli I, Schneeweiss A, Riethdorf S, Stenzinger A, Schillert A, Vogel V, Klein C, Saini M, Bäuerle T, Wallwiener M, Holland-Letz T, Höfner T, Sprick M, Scharpf M, Marmé F, Sinn HP, Pantel K, Weichert W, Trumpp A. Identification of a population of blood circulating tumor cells from breast cancer patients that initiates metastasis in a xenograft assay. *Nat Biotechnol.* 2013;31:539–44.
16. Hodgkinson CL, Morrow CJ, Li Y, Metcalf RL, Rothwell DG, Trapani F, Polanski R, Burt DJ, Simpson KL, Morris K, Pepper SD, Nonaka D, Greystoke A, Kelly P, Bola B, Krebs MG, Antonello J, Ayub M, Faulkner S, Priest L, Carter L, Tate C, Miller CJ, Blackhall F, Brady G, Dive C. Tumorigenicity and genetic profiling of circulating tumor cells in small-cell lung cancer. *Nat Med.* 2014;20:897–903.
17. Dangles-Marie V, Pocard M, Richon S, Weiswald LB, Assayag F, Saulnier P, Judde JG, Janneau JL, Auger N, Validire P, Dutrillaux B, Praz F, Bellet D, Poupon MF. Establishment of

- human colon cancer cell lines from fresh tumors versus xenografts: comparison of success rate and cell line features. *Cancer Res.* 2007;67:398–407.
18. Bruna A, Rueda OM, Greenwood W, Batra AS, Callari M, Batra RN, Pogrebniak K, Sandoval J, Cassidy JW, Tufegdžic-Vidakovic A, Sammut SJ, Jones L, Provenzano E, Baird R, Eirew P, Hadfield J, Eldridge M, McLaren-Douglas A, Barthorpe A, Lightfoot H, O'Connor MJ, Gray J, Cortes J, Baselga J, Marangoni E, Welm AL, Aparicio S, Serra V, Garnett MJ, Caldas C. A biobank of breast cancer explants with preserved intra-tumor heterogeneity to screen anticancer compounds. *Cell.* 2016;167:260–74.
  19. Das Thakur M, Salangsang F, Landman AS, Sellers WR, Pryer NK, Levesque MP, Dummer R, McMahon M, Stuart DD. Modelling vemurafenib resistance in melanoma reveals a strategy to forestall drug resistance. *Nature.* 2013;494:251–5.
  20. Kawaguchi K, Murakami T, Chmielowski B, Igarashi K, Kiyuna T, Unno M, Nelson SD, Russell TA, Dry SM, Li Y, Eilber FC, Hoffman RM. Vemurafenib-resistant BRAF-V600E mutated melanoma is regressed by MEK targeting drug trametinib, but not cobimetinib in a patient-derived orthotopic xenograft (PDOX) mouse model. *Oncotarget* 2016;7:71737–43.
  21. Kawaguchi K, Igarashi K, Murakami T, Chmielowski B, Kiyuna T, Zhao M, Zhang Y, Singh A, Unno M, Nelson SD, Russell T, Dry SM, Li Y, Eilber FC, Hoffman RM. Tumor-targeting Salmonella typhimurium A1-R combined with Temozolomide regresses malignant melanoma with a BRAF-V600 mutation in a patient-derived orthotopic xenograft (PDOX) model. *Oncotarget* 2016;7:85929–36.
  22. Kawaguchi K, Igarashi K, Murakami T, Zhao M, Zhang Y, Chmielowski B, Kiyuna T, Nelson S,D, Russell TA, Dry SM, Li Y, Unno M, Eilber FC, Hoffman RM. Tumor-targeting Salmonella typhimurium A1-R sensitizes melanoma with a BRAF-V600E mutation to vemurafenib in a patient-derived orthotopic xenograft (PDOX) nude mouse model. *J. Cell. Biochem., Epub ahead of print.* DOI: 10.1002/jcb.25886.
  23. Kawaguchi K, Igarashi K, Chmielowski B, Murakami T, Kiyuna T, Zhao M, Zhang Y, Nelson SD, Russell TA, Dry SM, Singh AS, Li Y, Unno M, Eilber FC, Hoffman RM. Salmonella typhimurium A1-R targeting of a chemotherapy resistant BRAF-V600E melanoma in a patient-derived orthotopic xenograft (PDOX) model is enhanced in combination with either vemurafenib-temozolomide. *Cell Cycle*, in press.
  24. Kreso A, O'Brien CA, van Galen P, Gan OI, Notta F, Brown AM, Ng K, Ma J, Wienholds E, Dunant C, Pollett A, Gallinger S, McPherson J, Mullighan CG, Shibata D, Dick JE. Variable clonal repopulation dynamics influence chemotherapy response in colorectal cancer. *Science.* 2013;339:543–8.
  25. Gao H, Korn JM, Ferretti S, Monahan JE, Wang Y, Singh M, Zhang C, Schnell C, Yang G, Zhang Y, Balbin OA, Barbe S, Cai H, Casey F, Chatterjee S, Chiang DY, Chuai S, Cogan SM, Collins SD, Dammassa E, Ebel N, Embry M, Green J, Kauffmann A, Kowal C, Leary RJ, Lehar J, Liang Y, Loo A, Lorenzana E, Robert McDonald III E, McLaughlin ME, Merkin J, Meyer R, Naylor TL, Patawaran M, Reddy A, Röelli C, Ruddy DA, Salangsang F, Santacroce F, Singh AP, Tang Y, Tinetto W, Tobler S, Velazquez R, Venkatesan K, Von Arx F, Wang HQ, Wang Z, Wiesmann M, Wyss D, Xu F, Bitter H, Atadja P, Lees E, Hofmann F, Li E, Keen N, Cozens R, Jensen MR, Pryer NK, Williams JA, Sellers WR. High-throughput screening using patient-derived tumor xenografts to predict clinical trial drug response. *Nat Med.* 2015;21:1318–25.
  26. Murphy B, Yin H, Maris JM, Kolb EA, Gorlick R, Reynolds CP, Kang MH, Keir ST, Kurmasheva RT, Dvorchik I, Wu J, Billups CA, Boateng N, Smith MA, Lock RB, Houghton PJ. Evaluation of alternative in vivo drug screening methodology: a single mouse analysis. *Cancer Res.* 2016;76:5798–809.
  27. Byrne AT, Alférez DG, Amant F, Annibaldi D, Arribas J, Biankin AV, Bruna A, Budinská E, Caldas C, Chang DK, Clarke RB, Clevers H, Coukos G, Dangles-Marie V, Eckhardt SG, Gonzalez-Suarez E, Hermans E, Hidalgo M, Jarzabek MA, de Jong S, Jonkers J, Kemper K, Lanfrancone L, Mælandsmo GM, Marangoni E, Marine JC, Medico E, Norum JH, Palmer HG, Peeper DS, Pelicci PG, Piris-Gimenez A, Roman-Roman S, Rueda OM, Seoane J, Serra V, Soucek L, Vanhecke D, Villanueva A, Vinolo E, Bertotti A, Trusolino L. Interrogating open issues in cancer precision medicine with patient-derived xenografts. *Nat Rev Cancer.* 2017; doi: 10.1038/nrc.2016.140.

---

# Index

## A

- Androgen deprivation therapy (ADT), 93, 104–105
- Androgen-responsive prostate cancer, 91
- Antiangiogenic drugs, 165–169
- Anticancer agents
  - drug development, 35
  - in vitro and in vivo evaluation, 30
  - PDX models, 31
  - tumor biology studies, 29
- Anti-CEA antibody, 222
- Anti-metastatic agents evaluation, 187
- Athymic nude mouse, 2
- AZD6244 activity, 143

## B

- Bevacizumab, 31–34
- B-raf inhibitor vemurafenib, 34
- Brain metastases, 164
- Breast cancer
  - PDOX models, 84
  - surgical orthotopic implantation, 75

## C

- Cancer type-specific gene signatures, 59–60
- Cell culture models
  - 3D assays
    - endpoints, 259–260
    - extended compound exposure, 258–259
  - for drug discovery, 255–258
  - EMT6 mouse mammary carcinoma tumors, 253–255
  - fibroblast and stromal effects, 260–264
  - growth in, 252
  - PD cell lines

- assay endpoints, 268
- cell-based screens, 264–267
- development and propagation, 264
- PDX cells, 258
- spheroids, 252–253
- Cervical cancer, PDOX models
  - CDDP, 127
  - drug-efficacy testing, 127
  - establishment of patient-derived, 128
  - NAB-PTX, 127
  - orthotopic tumor implantation, 128
  - SOI, 76
  - squamous cell, 127
  - statistical analysis, 129
  - subcutaneous, 280–281
  - tissue histology, 129
  - treatment, 128–129
- Chemoradiation combinations, 148–149
- Circulating tumor cells (CTCs), 287
- Colon cancer
  - fluorescence-guided surgery of cancer, 219, 220
  - lung-metastatic, 81
  - surgical orthotopic implantation, 73–74
  - treatment protocol and PDOX models, 281
- Cyan fluorescent protein (CFP)
  - characterization, 201–202
  - nude mouse, 194
  - transgenic, 195

## D

- 3D cell culture models
  - 3D assays
    - endpoints, 259–260
    - extended compound exposure, 258–259
  - for drug discovery, 255–258
  - EMT6 mouse mammary carcinoma tumors, 254–255

3D cell culture models (*cont.*)  
 fibroblast and stromal effects, 260–264  
 growth in, 252  
 PD cell lines  
 assay endpoints, 268  
 cell-based screens, 264–267  
 development and propagation, 264  
 PDX cells, 258  
 spheroids, 252–253  
 Doxorubicin (DOX), 278  
 Drug efficacy testing, 279

## E

E-cadherin, 56  
 EMT6 mouse  
 mammary carcinoma tumors, 254–255  
 mammary tumor cell spheroids, 252  
 Entinostat monotherapy, 279  
 Epidermal growth factor receptor (EGFR), 58  
 Epithelial-mesenchymal transition (EMT), 56  
 EurOPDX, 288  
 Event-free survival (EFS), 133  
 Ewing's sarcoma, 244

## F

Fibroblast effects, 260–264  
 Fibroblast growth factor receptor (FGFR)-  
 signaling pathways, 58  
 Fluorescence imaging of tumors, PDOX  
 models  
 animal care, 208–209  
 confocal microscopy, 209–210  
 GFP-expressing telomerase-specific  
 adenovirus, 210  
 histological analysis, 210  
 mice, 208  
 noninvasive imaging, 213  
 OBP-401-GFP labeling, 210  
 orthotopic transgenic fluorescent protein-  
 expressing nude mice, 209  
 pancreatic cancer, 210–213  
 patient tumors, 209  
 soft tissue sarcoma, 209  
 Fluorescent protein-expressing transgenic  
 nude mice  
 confocal microscopy, 196  
 cyan fluorescent protein  
 characterization, 201–202  
 nude mouse, 194  
 transgenic, 195

green fluorescent protein  
 characterization, 196–199, 204–205  
 nestin-dependent, 194  
 nude mouse, 5, 193–194  
 transgenic, 194–195  
 red fluorescent protein  
 characterization, 199–201  
 nude mouse, 194  
 transgenic, 195  
 scanning laser imaging, 196  
 whole-body imaging, 195–196  
 5-Fluorouracil (5-FU), 278  
 Freiburg experience. *See also* Patient-derived  
 xenograft (PDX) models  
 donor tumor, similarities and changes, 22  
 drug response, 17  
 growth behavior, 17, 20  
 human tumors growth, nude mice, 17–18  
 mouse hepatitis virus (MHV), 16  
 PDX regrowth after freezing, 20–21  
 survival of patients, 20  
 PDX take/growth, 20  
 tumor models available in 1991, 22–24

## G

Gastric cancer, 281  
 Genetically engineered mouse models  
 (GEMMs), 162  
 Grafting  
 ectopic sites, 45  
 in vivo system, 44  
*Orthos* way, 46–50  
 orthotopic sites, 48, 50  
 sites, 43  
 subcutaneous route, 45–46  
 Green fluorescent protein (GFP)  
 characterization, 196–199  
 nestin-dependent, 194  
 characterization, 204–205  
 nude mouse, 5, 193–194  
 transgenic, 194–195

## H

“Humanized” patient-derived mouse  
 models, 287  
 cell lines establishment, 288  
 individualized precision therapy,  
 285–286  
 study tumor heterogeneity, 288  
 treatment strategies, 288

**L**

- Leave-one-out cross-validation (LOOCV), 31
- Linsitinib, 245
- Lung cancer, PDOX models, 82

**M**

- Metastasis
  - cancer cell types, 55
  - cancer type-specific gene signatures, 59–60
  - experimental approach, 58–59
  - microarrays, cross-species hybridization of, 57–58
  - organ and cancer type-specific gene signatures, 62–64
  - organ type-specific gene signatures, 60–62
  - process of, 55–57
- Metronomic chemotherapy, 174–177
- Microarrays, cross-species hybridization of, 57–58

**N**

- Nanoparticle albumin-bound (nab)-paclitaxel (NAB-PTX), 127
- Nestin-dependent (ND) GFP nude mouse, 194
- Nonobese diabetic, severe combined immunodeficiency (NOD-SCID) mice, 9
- Non-small cell lung cancer (NSCLC) xenografts, 58
- Nude mouse, 2
  - athymic, 2
  - vs. drug response
    - chemotherapy, 24–25
    - experimental design of testing, 24
    - tumor response, 24–27
  - females, 2
  - green fluorescent protein, 5
  - human melanoma cell line transplantation, 33
  - immunological properties, 15
  - morphologic and physiologic characteristics, 14–15
  - origin and properties of, 14
    - as predictive assay, 27
    - progressive tumor growth, 3
    - transgenic, 55

**O**

- OBP-401-GFP labeling, 210
- OncoMouse, 7
- Organ and cancer type-specific gene signatures, 62–64
- Organ microenvironment, metastatic cell gene signatures
  - cancer cell types, 55
  - cancer type-specific gene signatures, 59–60
  - experimental approach, 58–59
  - microarrays, cross-species hybridization of, 57–58
  - organ and cancer type-specific gene signatures, 62–64
  - organ type-specific gene signatures, 60–62
  - process of, 55–57
- Ovarian cancer, 83

**P**

- Palbociclib, 243, 244
- Pancreatic cancer
  - fluorescence imaging of tumors, 210–213
  - PDOX models, 218–220
  - surgical orthotopic implantation, 75
- Pancreatic ductal adenocarcinoma (PDAC) PDXs, 227
  - genomic alterations in, 235
  - genomic subtypes, 234
  - histology features, 234
- Patient-derived orthotopic xenografts (PDOX) models, 4–5
  - anti-CEA antibody, 220
  - anti-metastatic agents evaluation, 187
  - bacterial therapy with *Salmonella typhimurium* A1-R, 184–186
  - breast cancer, 84
  - cervical cancer
    - CDDP, 127
    - drug-efficacy testing, 127
    - establishment of patient-derived, 128
    - NAB-PTX, 127
    - orthotopic tumor implantation, 128
    - squamous cell, 127
    - statistical analysis, 129
    - tissue histology, 129
    - treatment, 128–129
  - colon-cancer
    - liver metastasis, 81
    - local growth and abdominal metastasis, 80

- Patient-derived orthotopic xenografts (PDOX) models (*cont.*)
- determine efficacy and distinguish similar molecular-targeting drugs, 186
  - Ewing's sarcoma, 246
  - extensive peritoneal seeding, 80
  - first models (1991–1996), 78
  - fluorescence-guided surgery of cancer
    - colon cancer, 219, 220
    - GFP-expressing telomerase-specific adenovirus, 218
    - imaging, 219
    - mouse experiments, 218
    - neoadjuvant chemotherapy, 219
    - OBP-401 labeling, 219–220
    - pancreatic cancer, 218–220
    - postsurgical animal imaging, 220–221
    - statistical analysis, 221
    - tissue histology, 221
  - fluorescence imaging of tumors
    - animal care, 208–209
    - confocal microscopy, 209–210
    - GFP-expressing telomerase-specific adenovirus, 210
    - histological analysis, 210
    - mice, 208
    - noninvasive imaging, 213
    - OBP-401-GFP labeling, 210
    - orthotopic transgenic fluorescent protein-expressing nude mice, 209
    - pancreatic cancer, 210–212
    - patient tumors, 209
    - soft tissue sarcoma, 209
  - lung cancer, 82
  - lung-metastatic colon cancer, 81
  - lymph node metastasis, 80
  - mesothelioma, 82–83
  - mice, 187
  - neoadjuvant chemotherapy, 223
  - ovarian cancer, 83
  - pancreatic cancer, 81–82
  - pleural lung cancer, 85–86
  - pleural-metastatic ovarian cancer, 83–84
  - primary tumor and metastasis, 81
  - Salmonella typhimurium* A1-R
    - bacterial therapy with, 184–187
    - culture of GFP-labeled, 187–188
    - histological analysis, 188
    - preparation and administration, 187
    - in tumors, 188
  - of sarcoma, 7, 117–121
  - stomach cancer, 84–85
  - surgical orthotopic implantation, 8
    - breast cancer cancer, 75
    - cervical cancer, 76
    - colon cancer, 73–74
    - lung cancer, 74
    - melanoma metastasized to chest wall, 76
    - mesothelioma, 75
    - metastatic Ewing's sarcoma, 76
    - ovarian cancer, 75
    - pancreatic cancer, 75
    - pleural cancer, 74–75
    - soft-tissue sarcoma, 76
    - stomach cancer, 76
  - transformative cancer therapeutics, 183
- Patient-derived xenograft (PDX) models, 4
- for human cancer
    - anticancer agents, 30
    - anticancer drug development, 35
    - bevacizumab, 31–34
    - B-raf inhibitor vemurafenib, 34
    - combined in vitro and in vivo testing procedure, 30
    - historical aspects, 13
    - molecular characterization, 30–31
    - patient-oriented sensitivity testing, 35
    - preclinical in vivo phase II studies, 30
    - tumor biology studies, valuable model system, 29
    - tumor clonogenic assay, 28–29
  - molecular characteristics
    - characterization, 226
    - genomic alterations, 228–230
    - microenvironment, 233–235
    - predictive clinical biomarkers, 236–237
    - subtypes, 235–236
    - transcriptomic profiles, patient tumors, 230–233
  - novel agents and combinations, 133
    - chemoradiation combinations, 148–149
    - combination testing, 144–148
    - drug resistance development, 150–152
    - models/heterogeneity, molecular validity, 136–137
    - molecular subgroup representation, 149–150
    - novel cytotoxic agents, 140–141
    - PPTP, 138–139
    - preclinical data, accurate translation, 136
    - prospective studies, 135–136

- signaling inhibitors, 141–144
    - standard cytotoxic agents, 139–140
    - tumor response criteria, 137
  - pediatric cancers, 134–135
  - of prostate cancer
    - androgen deprivation therapy, 104–105
    - androgen-responsive prostate cancer, 91
    - applications, 94–101
    - biomarker research, 96–98
    - clinical history, 92
    - complexity, 93–94
    - early-stage, 91
    - establishing metastatic, 103–104
    - history on animal models for, 90
    - immunocompromised mice to humanized immune system, 102–103
    - incidence, 89
    - mechanisms of therapy resistance, 99–100
    - modeling inter-patient heterogeneity, 101–102
    - non-obese diabetic mouse, 92
    - novel therapies investigation, 98–99
    - severe combined immunodeficient mouse, 92
    - standard treatment, 92
    - translational tools, precision medicine, 100–101
    - tumor microenvironment, 94–96
    - tumor microenvironment interaction, 102
    - well-differentiated, 91
  - of sarcoma, 116–117
  - studies with, 172–174
  - Patient-oriented sensitivity testing, 35
  - Pediatric cancers, 134–135
  - Pediatric PDX (pPDX) generation
    - prospective studies, 135–136
    - rationale for, 134–135
  - Pediatric preclinical testing program (PPTP), 138–139
  - Plasminogen activators (PAs), 49
  - Progression-free survival (PFS), 33
  - Prostate cancer, PDX models
    - androgen deprivation therapy, 104–105
    - androgen-responsive prostate cancer, 91
    - applications, 96–101
    - biomarker research, 96–98
    - clinical history, 92
    - complexity, 93–94
    - early-stage, 91
    - establishing metastatic, 103–104
    - history on animal models for, 90
    - immunocompromised mice to humanized immune system, 102–103
    - incidence, 89
    - mechanisms of therapy resistance, 99–100
    - modeling inter-patient heterogeneity, 101–102
    - non-obese diabetic mouse, 92
    - novel therapies investigation, 98–99
    - severe combined immunodeficient mouse, 92
    - standard treatment, 92
    - translational tools, precision medicine, 100–101
    - tumor microenvironment, 94–96
    - tumor microenvironment interaction, 102
    - well-differentiated, 91
  - Prostate-specific antigen (PSA), 89
- R**
- Rapamycin, 146
  - Red fluorescent protein (RFP)
    - characterization, 199–201
    - nude mouse, 194
    - transgenic, 195
  - Rygaard, Jørgen, 1–4
- S**
- Salmonella typhimurium* A1-R
    - bacterial therapy with, 184–187
    - culture of GFP-labeled, 187–188
    - histological analysis, 188
    - preparation and administration, 187
    - in tumors, 188
  - Sarcoma
    - PDOX models, 117–121
    - PDX models, 116–117
    - transgenic mouse models, 115–116
  - Single-mouse studies, drug evaluation, 288
  - Spheroids, 252
  - Spontaneous brain metastasizing cell lines, 164
  - Spontaneous metastases vs. orthotopic primary tumors, 169–171

Stomach cancer, 84–85  
Stromal effects, 260–264  
Surgical orthotopic implantation (SOI), 4  
  construction of models, 73  
  early nude-mouse models, human  
    cancer, 71  
  PDOX mouse models  
    breast cancer, 75  
    cervical cancer, 76  
    colon cancer, 73–74  
    lung cancer, 74  
    melanoma metastasized to chest  
      wall, 76  
    mesothelioma, 75  
    metastatic Ewing's sarcoma, 76  
    ovarian cancer, 75  
    pancreatic cancer, 75  
    pleural cancer, 74–75  
    soft-tissue sarcoma, 76  
    stomach cancer, 76  
of tumor fragments, 71–73

**T**

Talazoparib, 147  
Transcriptomic profiles  
  of patient tumors, 230  
  PDX tumor model, 231  
Transgenic mouse models, 8  
  sarcoma, 115–116  
Tumor biology studies, valuable model  
  system, 29  
Tumor clonogenic assay, 28–29  
Tumor implantation, 280  
Tumor microenvironment  
  interaction, 102  
  prostate cancer, PDX models, 94–96

**V**

Vascular cell adhesion molecule-1  
  (VCAM-1), 57  
V79 cells, 251  
Vemurafenib, 34